FINE BLANKING OF METALS

By

Mohammad Najafi-Sani B.Sc.(Eng.), M.Sc., D.I.C.

October 1980

A thesis submitted for the degree
of Doctor of Philosophy of the
University of London

Department of Mechanical Engineering
Imperial College of Science and Technology
London, S.W.7.

To

Imam Khomeini

"Blessed are those who are persecuted for
righteousness sake, for thiers is the
Kingdom of heaven"

(Mathew 5:11)

To

my late beloved father

To

my mother, brothers and sisters

SUMMARY

A comprehensive survey concerning different methods of blank production such as conventional blanking, finish blanking, the smooth shearing process and fine blanking is first given. The subject of this investigation is fine blanking which is the process highly favoured in the production of blanks with smooth edge surface finishes. The method is similar to conventional blanking except for the use of a much smaller punch/die clearance together with a clamping force and back-load.

During the course of this work the effect of clamping force, clamp diameter and back-load on the load/displacement characteristics and blank edge surface finish is experimentally examined when fine blanking different thicknesses of mild steel and the results are presented. The experimental findings indicate that the load/displacement curve is almost independent of clamping force, clamp diameter and back-load. An increase in the clamping force increases the smooth sheared surface area of the blank edge and an optimum clamp diameter exists which, for any given value of clamping force gives the minimum fractured surface area.

To identify the highly deformed regions during conventional blanking and fine blanking a hardness survey across the partially blanked parts is performed. The results indicate the existence of a severely deformed zone in the region of the clearance between the punch and die.

Partly blanked, sectioned and etched specimens are examined to establish the effect of the blank-holder and blank-holder diameter on the mode of deformation.

An elastic-plastic finite element program is developed to examine the condition under which a change of fracture from fibrous to pure

shear in fine blanking on the surface finish of the blank edge occurs. As a preliminary study the experimental and theoretical load/displacement curves are compared to check the validity of the computer program. The distribution of the normal force and shear load per unit length along the punch and die faces are presented. The normal forces can be used as an indication of the pressure distribution, and the shear loads can identify the direction of material flow at the vicinity of these surfaces. The maximum normal load per unit length occurs at the punch and die edges, indicating the highest pressures in these two regions. The material on the die face moves away from the shear line in conventional blanking, which indicates that the blank-holder helps to raise the compressive stresses in the shearing zone not only by compression but also by blocking the outward flow of the material.

The effect of hydrostatic pressure on the ductility of different materials is reviewed and its effect on different metal forming processes is examined. Using these findings conclusions are drawn from the theoretical increase in the hydrostatic component of stress and decrease in the maximum principal stress in the shearing zone in fine blanking when using a clamping force and back-load. These effects are suggested as the likely cause of transition from fibrous fracture to pure shear.

The effect of clamping force, back-load, clamp diameter, punch/die clearance and material thickness on the hydrostatic component of stress and corresponding maximum principal stress on the shear line is demonstrated and a possible explanation for the existence of an optimum clamp diameter is presented. Finally the results are discussed and conclusions are drawn concerning the different aspects of fine blanking.

ACKNOWLEDGEMENTS

I sincerely express my deepest gratitude to Dr. B. Lengyel for suggesting the topic and for his guidance and invaluable advice throughout this work without which this project would have not been completed.
I also would like to thank professor J. M. Alexander for his kind permission to use the metal working facilities in the course of experiments.

Thanks are also due to Mr. H. Ramsey for his kind permission to use the work-shop facilities and his assistance in making the tools.
Special thanks are also due to Mr. G. Yantian for reading the text and to Miss. P. J. Campbell who patiently typed the manuscript

Financial support from the University of Tabriz is gratefully acknowledged and highly appreciated.

Last but not least the constant encouragement and support of my late father and also of my mother, and brother Mr. Hussein Najafi-Sani, is acknowledged and greatly appreciated.

Mohammad Najafi-Sani

October 1980.

CONTENTS

NOTATION

k	Shear flow stress
PR	Punch diameter
CR	Clamp diameter
CF	Clamping force
BP	Back-load
BF	Blanking force
PP	Punch penetration
$\{\ \}$	A column vector
$[\ ]$	Rectangular or square matrix
$[\ ]^T, \{\ \}^T$	Transpose of a matrix or vector
$[\ ]^{-1}$	Inverse of a square matrix
det$[\ ]$	Determinant of a square matrix
$\partial(\ )/\partial$	Indicates partial differentiation
$d(\ )$	Infinitesimal increment of a variable
$\Delta(\ )$	Finite increment of a variable
E, ν	Elastic modulus and poisson's ratio of an isotropic material
G	Shear modulus
t	Thickness of a member
AREA	Area of an element
u_i, v_i	Nodal point displacement (at nodal point i) in r and z direction
U_i, V_i	Nodal point forces (at nodal point i) in r and z direction
$\{\delta\}^e$	Element nodal point displacements
$\{F\}^e$	Element nodal point forces
$\{\delta\}$	Structural nodal point displacement
$\{F\}$	Structural nodal point forces
$\{P\}$	Distributed force, applied at the structure boundary

$\{\sigma\}$, $\{\varepsilon\}$	Stresses and strains
$\{\sigma_0\}$, $\{\varepsilon_0\}$	Initial stresses and strains
$[D^e]$	Elastic stress-strain relation $\{\sigma\} = [D]\{\varepsilon\}$ for $\{\varepsilon_0\} = 0$
$[D^{ep}]$	Elastic-plastic stress strain matrix $d\{\sigma\} = [D^{ep}]\ d\{\varepsilon\}$
$\{f\}$	The vector representing displacements at every point within the elements
$[N]$	Shape function matrix $\{f\} = [N]\{\delta\}^e$
$[B]$	Strain displacement matrix $\{\varepsilon\} = [B]\{\delta\}^e$
$[\bar{B}]$	Strain displacement matrix at centroid (for triangular elements)
$[k^e]$	Elastic element stiffness matrix
$[k^{ep}]$	Elastic plastic element stiffness matrix
$[K^{ep}]$	Overall stiffness matrix of the structure
$[J]$	Jacobian matrix
$\bar{\sigma}$	Equivalent stress
$\bar{\varepsilon}$	Equivalent total strain
$\bar{\varepsilon}^e$	Elastic component of effective strain
$\bar{\varepsilon}^p$	Plastic component of effective strain
$\bar{r}$, $\bar{z}$	Coordinates of the centroid of a triangle
ξ, η	Natural coordinates
$\bar{r}$	Nodal force in direction r (for triangular ring elements)
$\bar{z}$	Nodal force in direction z (for triangular ring elements)
σ'	Hydrostatic component of stresses
ETA	Rating factor
$\bar{\sigma}_y$	Uniaxial yield stress of the material
$\{\varepsilon^p\}$	Plastic strains

CHAPTER 1

LITERATURE SURVEY OF BLANKING

1.1 Introduction

Conventional blanking which consists of a punch and die with moderate clearance together with a stripper plate, is a commercially important process for medium to large batch production of components from sheet and strip material.

The terms associated with the study of an axi-symmetric blanking operation are adequately defined by reference to Fig. 1-1. To blank a specimen conventionally the specimen material is placed between the punch and die and the operation begins by advancing the punch towards the die. The specimen is indented and pressed into the die-hole and the operation is completed when the punch cuts through the whole thickness of the material. After the blanking operation is completed the specimen is stripped off the punch by means of the stripper plate, the blank is removed and a new blanking operation can be started.

In conventional blanking, at the early stages of the process the material undergoes a pure shear deformation, giving rise to a bright burnished section on the blank surface finish. As the process continues cracks develop at the punch and die edges and propagate towards one another. When the cracks from the punch and die edges meet the blank separates from the specimen. Part of the blank surface finish caused by the crack propagation appears ragged and very rough. This is in direct contrast to the surface finish caused by pure shear deformation which is bright and burnished.

The main limitation of the conventional blanking process is poor

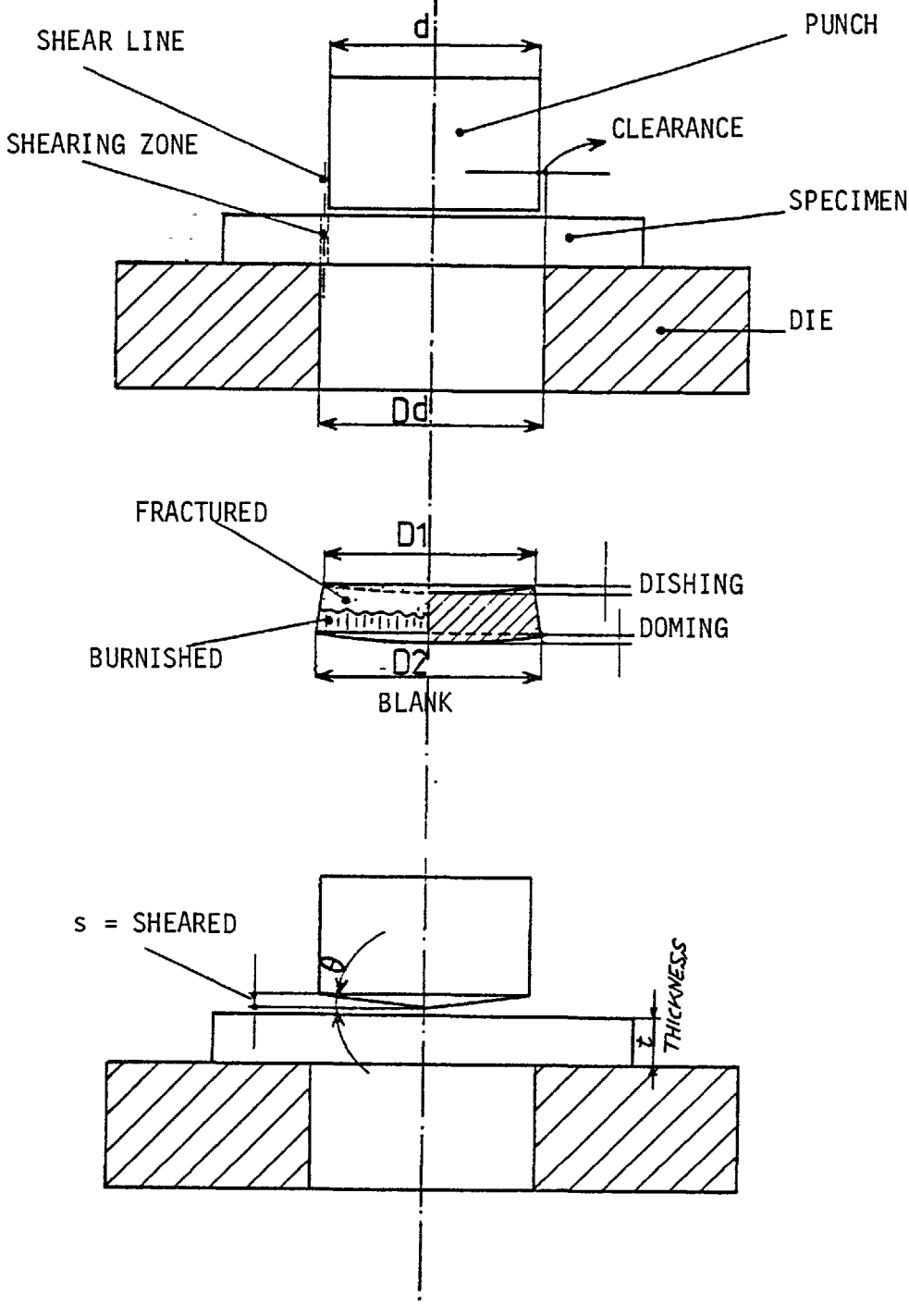

SHEAR PERCENTAGE = s/t

D1 = PUNCH SIDE DIAMETER

D2 = DIE SIDE DIAMETER

D2 - D1 = EDGE TAPER

Fig. 1-1.

dimensional accuracy due to the presence of one or more separation cracks on the edge of the blanks and distortion of the component in the through thickness direction exhibited as dishing and doming.

The disadvantage associated with edge cracking of the components may be overcome when the conventional blanking process is combined with one or more shaving or machining operations. However, due to the introduction of relatively lengthy handling, the cost of component production rises sharply with the number of operations.

The Production Engineering Research Association of Great Britain have shown (1,2,3) that the regions of cracking on the component edge may be eliminated by the use of their finish blanking process, which involves the use of a radius or chamfer on the cutting edge of the die and a smaller radial punch/die clearance than in conventional blanking. However, dishing of the component produced by the finish blanking process may be more pronounced than in conventional blanking.

The fine blanking process which makes use of a blank-holder and a counter-punch together with a very small radial punch/die clearance eliminates both cracking on the blank edge and dishing of the component. Fine blanked parts have advantages of no dishing as well as the square and clean sheared surfaces. Furthermore, parts with complicated geometrical form and sheet metal with low deformability can be fine blanked successfully.

As there are many important factors inherent in different shearing operations such as, finish blanking, smooth shearing by stepped profile tool, opposed shearing process and reciprocating blanking which are vital when considering parameters under which fine blanking operates, the alternative methods of shearing should be studied in depth. Therefore a resume of previous work in this field follows.

1.2 Conventional blanking

1.2.1 Slow speed blanking

In all cases, high rates of production are demanded consistent with a high degree of accuracy and good edge finish. Extremely slow or quasi-static blanking has therefore no direct industrial application but is of considerable importance in helping to assess the effect of speed on the operation. The slow speed blanking process occupies a period of 15-20 minutes.

It appears that the earliest attempt to obtain records of punch load vs. displacement is due to Anthony (4) reported in 1911. The aims of the investigations were to determine such values as the maximum blanking force, for which punching machines should be designed, the punch penetration at which the maximum blanking load occurs and the effect of clearance between the punch and die on the maximum shear stress (maximum load divided by original area to be sheared).

It is an advantage to obtain an accurate calculation of blanking force in order that a press of suitable capacity may be used; inaccurate calculation of blanking force will result either in the use of a press of excess capacity, which is uneconomic, or else in the use of an under powered press with the consequent risk of serious damage to the machine.

A formula commonly used for the calculation of blanking force is as follows :-

Blanking force = Area in shear x *Ultimate tensile strength of material*

The ultimate tensile strength of a material does not, however, give an accurate indication of the resistance to shear, and thus the method cannot be relied upon to give an accurate determination of the blanking force.

In a P.E.R.A. report (5) recommendations are given for the accurate determination of blanking force, but since the research was mainly concerned with the investigation of a number of different factors and the scope of the tests was somewhat restricted, the recommendations for blanking force therefore applied only to a limited range of conditions. Consequently, P.E.R.A. carried out an extensive investigation (6) to determine the relationship between blanking force and area of shear (π x die diameter x material thickness) for a wide range of materials including mild steel, brass, aluminium alloy, soft and hard temper copper, spring steel, stainless steel, Nimonic '75' alloy and electrical lamination steel when blanking holes of 1 in. (2.54 cm) diameter.

A limited number of tests were also carried out using punches of 1 in. (2.54 cm) square in order to determine whether the shape of hole had any influence on the blanking force.

Tests were carried out on two single-action crank presses, one of 10 tonf (99.64 kN) capacity and the other of 30 tonf (298.9 kN) capacity. Punches of various sizes were used with one size of die to provide clearances of approximately 5% and 10% of the material thickness per side.

Based on the large number of tests carried out, recommendations are given for accurate determination of the blanking force. To calculate the blanking force for circular holes the following formula has been recommended :-

Blanking force = Diameter of hole x π x *Thickness of material* x *Ultimate tensile strength* x *Shear factor*

Graphs for shear factor for different materials are given in the report.

The required force to blank holes of 1 in. (2.54 cm) square in different thicknesses of material has also been reported. Although the tests included the blanking of 1 in. (2.54 cm) square holes as well as 1 in. (2.54 cm) diameter circular holes in all thicknesses of brass, it was not possible to deduce any relationship between blanking force and shape of the hole, since the blanking force was found to be similar for both round and square holes.

The results showed that the stripping force increases with material thickness, the rate of increase, however, decreases with increasing material thickness.

A typical punch load/displacement diagram for slow speed blanking is shown in Fig. 1-2.

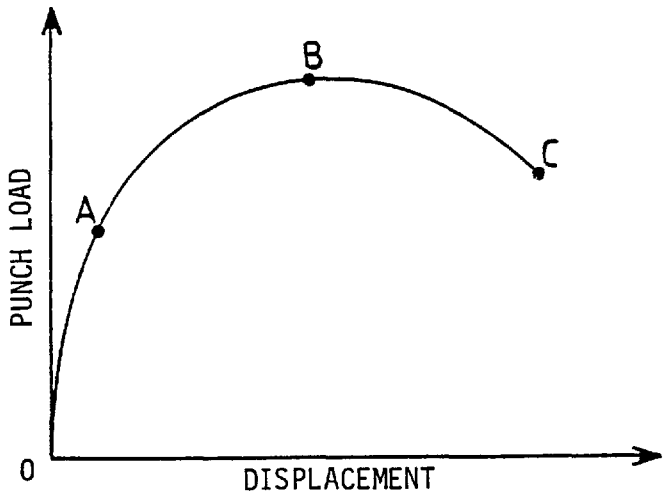

Fig. 1-2.

The substantial proportional increase in punch load with punch displacement from 0 to A represents the predominantly elastic phase of

the process. From A to B, plastic shear deformation occurs and the manner in which the magnitude of the punch force changes with the punch displacement reflects the strain-hardening characteristic of the material. The maximum blanking force is obtained at B and from B to C, although further strain-hardening of the material may occur, the punch force decreases in proportion to the decrease in the vertical area of shear. The shear stress thus increases from A to B while the shear area decreases.

It has been observed by Crasemann (7) that cracks are formed after the blanking force reaches its maximum value at B. According to Timmerbeil (8) these cracks are initiated at the die edge and propagate towards the punch edge. Noble and Oxley (9), by considering a plane strain deformation model for blanking, Fig. 1-3, used a simple stress analysis to show that the die edge is the most susceptible region to crack formation, and radiusing the die edge would eliminate the possibility of this occuring.

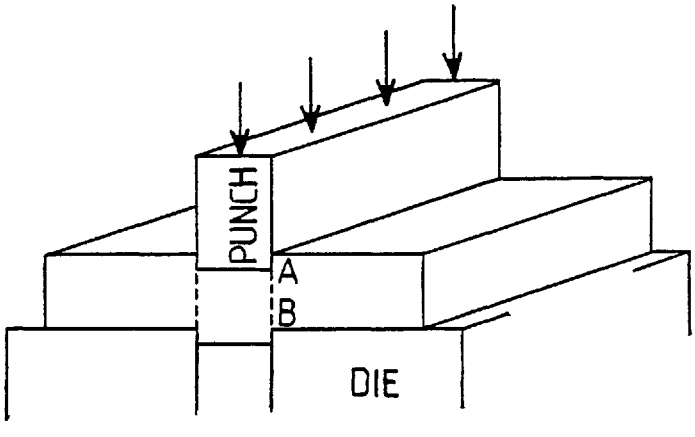

Fig. 1-3.

Noble and Oxley assume that the severely deforming zone during blanking is confined to a narrow region around the shear line 'AB' and the shear flow stress 'k' of the material in the direction x changes in a similar way as hardness values, Figs. 1-4 and 1-5.

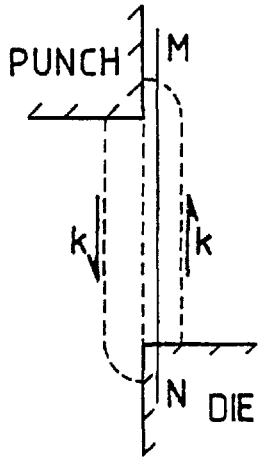

Fig. 1-4.

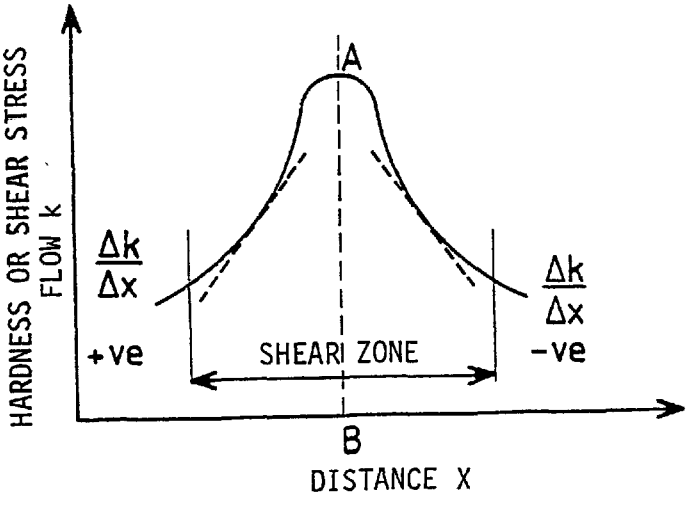

Fig. 1-5

A simple stress analysis showed that the hydrostatic component of stress in the shearing zone along any arbitrary line MN, Fig. 1-4, depends on the rate of change of shear flow stress 'k' normal to the line considered, Fig. 1-5, denoted by $\Delta k/\Delta x$. It was then shown that the hydrostatic component of stress in the shearing zone could be tensile and the maximum value was most likely to occur at the die edge.

By assuming broadening of the severely deformed region during blanking by radiusing the die edge, also observed experimentally, they showed that the maximum value of the hydrostatic component of stress in this region increases, thus crack propagation could be suppressed.

Chang (10) has investigated the effect of punch/die radial clearance and punch diameter on the blank's surface finish and on the nominal maximum shear stress of the material (maximum blanking load divided by original area to be sheared). The material tested included cast iron, mild steel, brass, copper, zinc, aluminium and lead ranging in thickness from 0.036 to 0.50 in. (0.914 to 12.7 mm). The tools employed had diameters of 1 to 6 in. (2.54 to 15.2 cm), and clearances up to 58% of the material thickness.

In blanking a tool provided with a die hole of desired profile and dimensions is usually employed. However, in practice, the resulting blanked products are not always exactly the same size as the die hole, possibly being smaller and commonly affected by dishing and doming effects. This might be caused by the severe deformation of material itself as well as that of the die. The dimensions of blanked products and the dishing effect differ according to the quality, dimensions and profile of the tools and the blanked material .

The dimensional accuracy of the blanks during the blanking of

sheet metals has been specifically studied by Maeda and Tamura (11) using circular punches. The authors performed blanking tests on cold rolled mild steel, soft copper and soft aluminium plate with percentage punch/die radial clearance up to 30 and d/t ratios (punch diameter/ material thickness) in the range 2 to 300.

1.2.2 High speed blanking

The earliest report in which a comparison is made between the energy required to perform nominally identical blanking operations at slow speed and at relatively high speed, appears to be the one by Johnson and Slater (12) in 1964. However, in a National Engineering Laboratory report, Crockcroft (13) reported a discussion which took place at a metal forming symposium in Czechoslovakia in 1960 in which Novotny discribes experiments carried out on punching holes using projectiles moving at high speeds of 100-700 ft/s (30.4-213.3 m/s). It was claimed that 15-30% less energy was required for the high speed punching than for slow speed punching. This was attributed to the fact that in the high speed punching the extent of the severely distorted zone near the shear line reduced by about 50%. This reduction in the distorted zone near the shear line was described some seventeen years later by Zener and Holloman (14) and further discussed by Zener (15).

Johnson and Slater (12) used a small linear induction motor to form circular blanks of aluminium (B.S. 1470S1C and 1470HS30WP), brass (B.S. 265CZ108 and STA7CZ 11B), copper (B.S. 1432) and mild steel (EN2) in various thicknesses of strip. The tests were carried out at punch impact speeds of up to 36 ft/s (10.97 m/s). Punches and dies were available to enable both 1 in. (2.54 cm) and 2 in. (5.08 cm) nominal diameter discs to be blanked from sheet or strip of different materials

with various thicknesses.

The area of each load-penetration diagram was found by using a planimeter, thus the energy was calculated. The results showed that in all but two cases excess energy was required for dynamic blanking. The two exceptions being mild steel (EN2), 3/32 in. (2.38 mm) thick and brass (B.S. STA7CZ 11B), 3/16 in. (4.76 mm) thick.

A visual examination of the blanks showed that, in the dynamic process, aluminium (B.S. 1470S1C) gave a smoother fracture and an increase in plastic deformation, around the shear line, and aluminium (B.S. 1470-HS30WP) gave a smoother fracture and a decrease in plastic deformation. For brass of both types a smoother fracture and a decrease in plastic deformation was observed, with copper there was no obvious difference whilst with mild steel of thickness 0.048 in. (1.21 mm) there was less burring and mild steel 3/32 in. (2.38 mm) thick gave a smoother fracture.

In 1965 Davies and Dhawan (16) reported the effect of speed and a wide range of clearances on the surface finish of the blanks. In this report the results of experiments on high speed punching of 1 in. (2.54 cm) diameter blanks and holes in aluminium, brass, mild steel, and cast iron are given and compared with the results of similar experiments carried out at slow speed.

High speed tests were carried out on an air-driven metal forming machine of an impact speed of 31 ft/s (9.44 m/s). The high speed machine was operated by the sudden release of compressed air and is shown in Fig. 1-6. The dimensional accuracy and amount of distortion of the blanks and holes were assessed and detailed comparisons made between the high and slow speed cases.

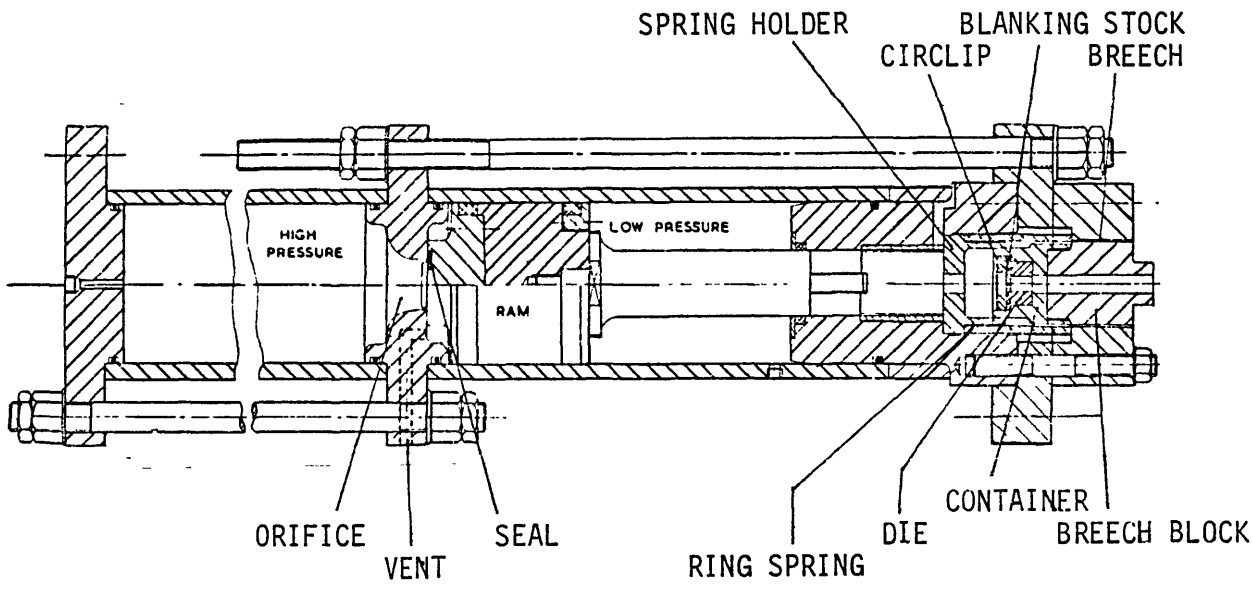

Fig. 1-6. Cross-section of air-driven machine.

A selection of punches were available which provided radial punch/die clearances of 0.0025, 0.005, 0.01, 0.015 and 0.02 in. (0.063, 0.127, 0.25, 0.38 and 0.50 mm). Both die and punch were sharp edged and no lubricant was used.

A visual examination of the mild steel blanks clearly showed the improvement in blank edge finish to be obtained by blanking at an impact speed of 31 ft/s (9.44 m/s). 'Blueing' of the fractured surface of all the blanks produced at high speed indicated that the temperature reached along the shear plane was considerable. Blanks produced at slow speed had a larger sheared band and the fractured surface was characterized by severe cracking. There was no evidence of 'blueing' on the slow speed specimens.

A rough comparison of burr height showed that the amount present on the high speed blanks was between 25 and 50% of that produced at slow speed. Edge taper was less in the high speed cases, see Fig. 1-1 for definition. For thicker material at slow speed multiple cracks were present,

and at high speed 'blueing' of the fractured surface was more severe. An interesting result obtained showed that while at slow speed the die side diameter was greater than the punch side diameter at all clearances, the reverse was true for low clearances at high speed. Considerable reduction in dishing at high speed was observed.

Higher hardness values obtained by microhardness measurements along the radial direction on the surface of diametrically sectioned specimens of $\frac{1}{4}$ in. (6.35 mm) thick mild steel showed a greater extent of work hardening around the shear line in the slow speed blanked specimens, which confirmed the greater amount of plastic deformation.

For brass, the blanks produced at high speed had smoother edges than those produced at slow speed and even at high clearances the general quality of the blank edge finish was acceptable for the majority of industrial applications. A reduction in edge taper was observed in the case of high speed. It was found that, above a clearance of about 0.01 in. (0.254 mm), the amount of doming was less for high speed, although the reverse was true below this clearance. The amount of dishing was not significantly different for blanks produced at either speed. The amount of burr produced during the high speed process was found to be negligible when compared with that produced conventionally.

For aluminium the blanks produced at both speeds were very similar. For thicker material, however, the slow speed process was associated with more severe cracking on the fractured portion and a greater amount of burr. Edge taper of the blanks produced at high speed was again less than that at slow speed. For dishing and doming the slow speed process showed a marginal improvement.

In order to assess whether the use of high speeds could be applied with advantage to the blanking of a brittle material, a limited number of tests were carried out on cast iron. Stocks of $\frac{1}{4}$ in. (6.35 mm) thickness were used with a punch/die clearance of 0.01 in. (0.254 mm). The severely cracked stock that was produced at slow speed was in direct contrast to the high speed results, in which there were no signs of distortion or cracking in either blank or stock.

The results clearly showed that the main improvement on the blank edge finish to be gained by use of high speeds was for the blanking of mild steel.

The existence of very high temperatures along the shearing zone, which arise because of the very short time available for heat conduction, must have a significant effect on the change of surface finish owing to material softening. This was reflected in the decrease in depth of work hardening and improvement in distortion. The existence of very high temperatures has been detected by Zener and Holloman (14).

One of the most interesting results obtained which applied to mild steel, brass and aluminium was that, at high speed, parallel sided blanks could be obtained with satisfactory surface finish using comparatively large punch/die clearances of between 0.005 and 0.01 in. (0.127 and 0.254 mm).

The effect of the radial punch/die clearance on the maximum quasi-static blanking force and on the energy required to effect the quasi-static and dynamic blanking of various materials together with the edge finish has been studied by Johnson and Slater (17).

Circular discs of 1 in. (2.54 cm) nominal diameter were blanked from various materials including bright and black mild steel, aluminium alloy, brass, copper and cupro-nickel.

The same linear induction motor which was used in their previous work (12) was employed, and impact velocities approaching 50 ft/s (15.2 m/s) were attained.

Die and punches were sharp edged and a suspension of molybdenum disulphide in S.A.E. 30 oil was used as a lubricant.

Blanking force results for different punch and die clearances showed that, for all materials, the magnitude of the maximum quasi-static blanking force was nearly independent of the percentage radial clearance and increased only slightly as the radial clearance approached zero. This is in agreement with the results obtained by P.E.R.A. (5).

It may be stated that greater energy is generally required to effect dynamic blanking than for the quasi-static process. This can partly be attributed to strain rate and inertia effects. In some cases, particularly bright mild steel and cupro-nickel in 'cold rolled' and 'soft' conditions, when using different clearances, obvious minima of energy required were exhibited for both the quasi-static and dynamic processes. The minimum energy values were exhibited at percentage radial clearances higher than those likely to be of paramount industrial interest. It can be stated that the desired edge finish can be achieved for some materials by the use of very small percentage radial clearances, whilst there are certain exceptions. Some of the materials investigated gave a smoother fracture and a greater degree of plastic deformation in the shearing zone by the dynamic blanking process. The most notable change in the blank edge finish, from fractured to smooth finish, was that of black mild steel.

In the same year (1965) Johnson and Travis (18) reported the results of similar work to that of Johnson and Slater (17), but at velocities an order of magnitude greater. The specimens used throughout the tests were

1½ in. (3.81 cm) diameter discs of ¼ in. (0.635 cm) thick copper (B.S. 1432). The range of die diameters employed were 0.375 + 0.01 to 0.375 + 0.07 in. (9.525 + 0.254 to 9.525 + 1.778 mm) at intervals of 0.01 in. (0.254 mm), the diameter of the punches being held constant at 0.375 in. (9.52 mm). Punch and dies were sharp edged. A schematic view of the apparatus used for the high speed test is shown in Fig. 1-7. A standard 'rapid hammer' breech loading industrial stud driver was used to fire the punch.

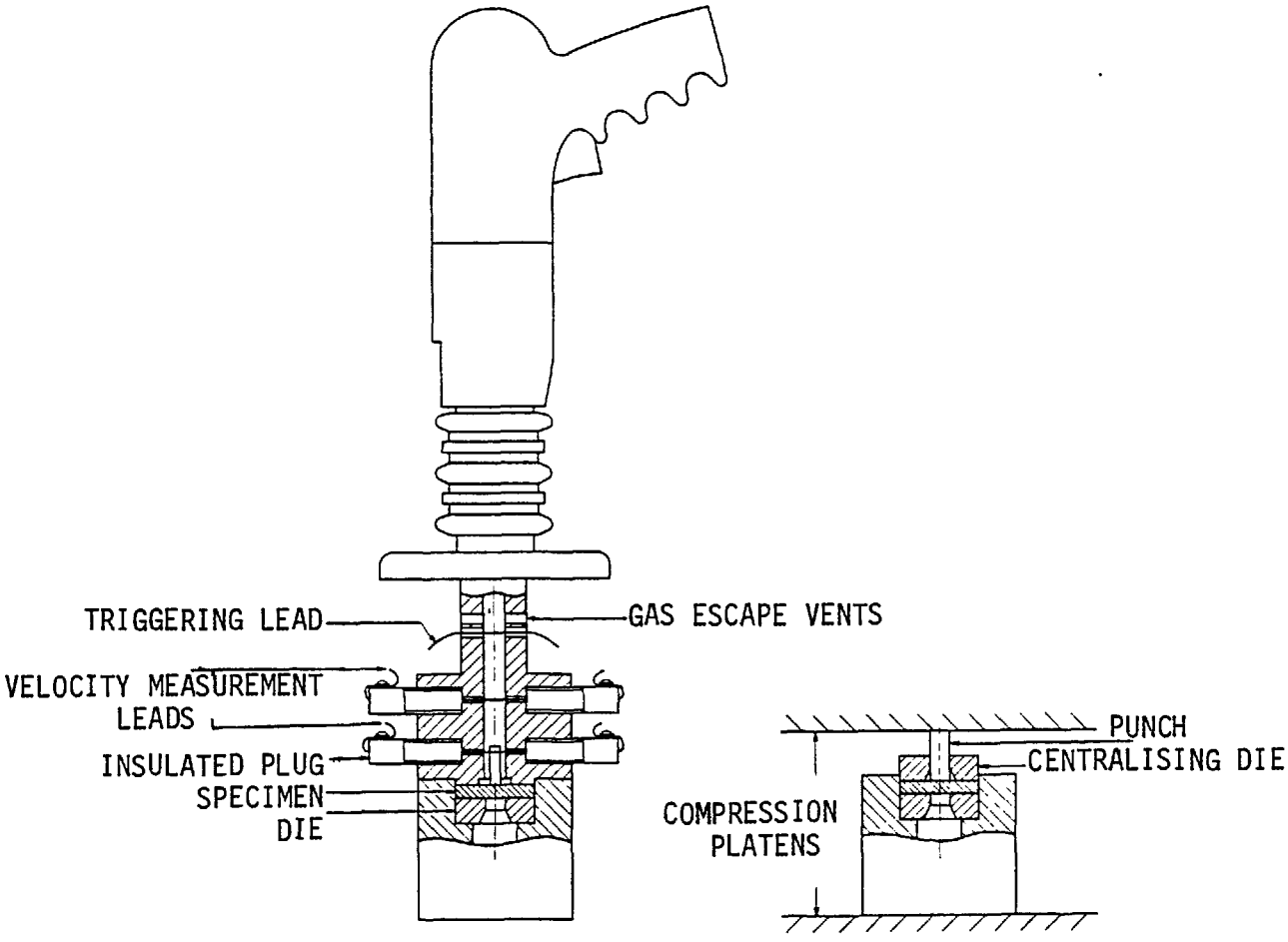

Fig. 1-7. Schematic view of blanking tool.

An optimum percentage radial clearance for the least amount of energy required to achieve blanking for both the dynamic and quasi-static operation was found. The energy required for the dynamic process for all radial clearances was considerably in excess of that for the quasi-static process. Examination of the results revealed that, by increasing the punch velocity, the kinetic energy to achieve blanking showed a continuous increase, such that at impact velocities of about 800 ft/s (243.8 m/s) the energy required for blanking was approximately 2.5 times that for the quasi-static operation. Impact velocities above about 600 ft/s (182.8 m/s) started to produce cratering which rapidly increased in severity, a well known phenomenan in high speed impact (Goldsmith, 19).

In September 1966 a detailed examination of the effects of high punch speed on the quality of the blank edge and remaining stock, including a metallurgical examination of the sheared specimens, was reported by Davies and Dhawan (20) which is an extension of their previous work (16).

The same high speed impact machine was used with an impact speed of 31 ft/s (9.44 m/s) throughout the work. A selection of punches provided radial punch/die clearances of 0.0025, 0.005, 0.01, 0.015 and 0.02 in. (0.063, 0.127, 0.254, 0.381 and 0.508 mm). The tests were carried out on three different materials, namely, mild steel, brass and aluminium.

Load penetration curves were obtained during high and slow speed tests. A typical curve for mild steel, $\frac{1}{8}$ in. (3.17 mm) thick is shown in Fig. 1-8 for radial punch/die clearance of 0.005 in. (0.127 mm).

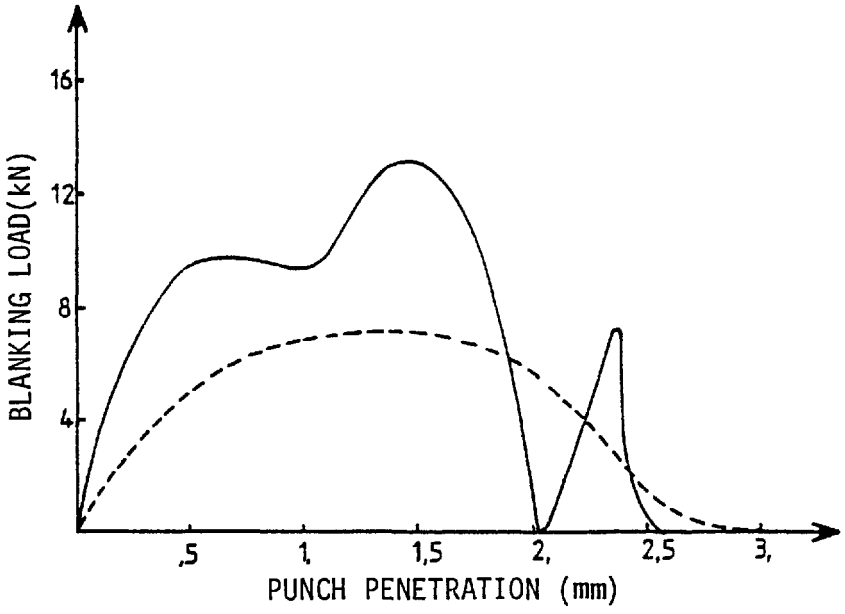

Fig. 1-8.

The obvious difference between the high and slow speed results was that the higher peak load was reached at high speed. A further effect, noticeable in the case of ¼ in. (0.635 cm) thick mild steel was that in high speed blanking the load dropped to zero approximately half way through the process. This was in complete contrast to the equivalent slow speed result where a continuous load was registered throughout the operation. A similar tendency was shown for ½ in. (1.27 cm) thick mild steel. The results can be summarized as follows :-

i) High speed blanking produced blank edge finishes with sufficiently good quality for the majority of industrial applications, and was generally superior to those produced at slow speed. The improvement in quality was particularly marked for mild steel.

ii) The difference in the amount of energy required for high and slow speed blanking depended on the material being blanked.

iii) The amount of plastic deformation in the shearing zone considerably reduced at high speeds.

iv) Both the hardness and depth of work hardening were less at high speed.

The hardness measurements showed that the hardness of the material was less at the die edge than at the punch edge at both speeds.

Considering the results of energy measurements it was concluded that it was not possible to generalize on whether the energy required for high speed blanking was greater or less than that required at slow speed.

The difference in the amount of energy and required load for blanking depends on a number of factors. Strain rate and inertia effects invariably tend to increase the energy and load requirements at high speeds, while thermal softening and a smaller amount of plastic deformation in the shearing zone tend to produce the opposite effect. The degree to which a blank edge finish is affected by these variables is in turn governed by the properties of the material, the more important of which are the density, the susceptibility to strain rate effects and the thermal conductivity. For $\frac{1}{4}$ in. (0.635 cm) and $\frac{1}{2}$ in. (1.27 cm) thick mild steel, a further factor which contributed to a decreased energy requirement at high speed was a very rapid fall of load when the punch had penetrated approximately half way through the material. This could be due to crack propagation in the shearing zone causing complete fracture at this point.

The effect of speed and temperature on the force and energy required in blanking has been investigated by Slater and Johnson (21). Nominal 1 in. (2.54 cm) diameter circular discs made from commercially

pure aluminium, copper and black mild steel were blanked quasi-statically at a typical shear strain rate of about 10^{-3} Sec^{-1} and dynamically (shear strain rate range 10^{3} to 4 x 10^{3} Sec^{-1}), at temperatures of up to 773 K (500°C), 1073 K (800°C) and 1373 K (1100°C) respectively. The dynamic blanking experiments were performed at impact speeds of up to 50 ft/s (15.24 m/s) using a linear induction motor. The tool assembly is shown in Fig. 1-9. Punches and dies were sharp edged.

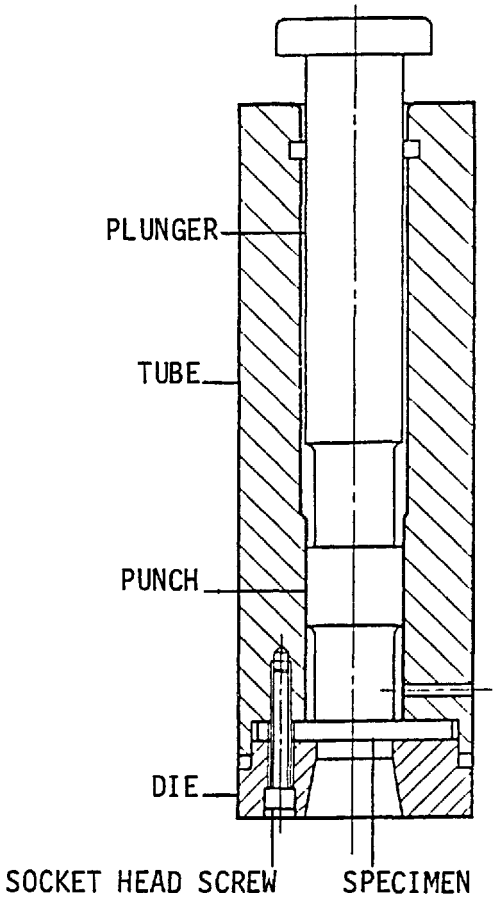

Fig. 1-9. Sectional elevation of blanking tool assembly for quasi-static operations at elevated temperatures.

A study of the results revealed that, in general, the maximum force for quasi-static blanking at elevated temperatures was substantially independent of the percentage punch/die radial clearance and exhibited only slightly rising characteristics for each of the three materials as the radial clearance approached zero. The maximum blanking force for the three materials were highly dependent on temperature and decreased as the temperature increased. The results clearly showed that, at a given temperature, much more energy was required for the dynamic than for the quasi-static process.

It was concluded that no obvious advantage was to be gained from performing the dynamic blanking operation at elevated temperatures where the quality of the edge finish of the blanked parts was of industrial importance. The increase in energy at high speed for aluminium, copper and mild steel was attributed to the effect of strain rate.

An extension of the work by Davies and Dhawan was reported two years later in 1968 (22) in which a wide range of speeds and materials were investigated. The blanking of metals using punch speeds of the order of 30 ft/s (9.14 m/s) and above was developed with the objective of punching components of better quality than could be obtained by slow speed conventional blanking.

The experiments were carried out on two experimental high speed forming devices. One machine was compressed air driven and provided a punch impact speed of 31 ft/s (9.44 m/s) and the other machine, which was explosively driven, was used for high impact speeds ranging up to 125 ft/s (38.1 m/s). Punches and dies were available for the blanking of nominal 1 in. (2.54 cm) diameter discs. A range of punches provided radial punch/die clearances of 0.0025, 0.005, 0.01, 0.015 and 0.02 in.

(0.0635, 0.127, 0.254, 0.381 and 0.508 mm). Punches and dies were sharp edged. The materials used were mild steel, high carbon steel, brass, copper and aluminium. The range of thicknesses employed was $\frac{1}{4}$ to $\frac{1}{2}$ in. (0.635 to 1.27 cm).

The blanks produced at high speed and slow speed were compared. It was observed that the surface cracking, which was always present in blanks of this order of thickness produced at slow speed with relatively large punch/die clearance , was entirely eliminated at an impact speed of 31 ft/s (9.44 m/s). Above this speed there were only very small differences in the edge surface quality of the blanks, and in some cases a slight deterioration occured as the impact speed was increased beyond about 40 ft/s (12.1 m/s). The same effect was noted during measurements of blank distortion and dimensional accuracy. Here again there was a considerable advantage to be gained by increasing speeds from slow to the range of 30 to 40 ft/s (9.14 to 12.1 m/s), and no advantage to be gained by increasing the speed beyond this range. The surface produced in ferrous metals by the high speed technique was not completely polished or sheared as could be produced by such processes as fine blanking, but was sufficiently good for the majority of applications.

For non-ferrous metals generally a small improvement occured as the punch impact speed was increased to 31 ft/s (9.44 m/s), but again there was no advantage in increasing speeds beyond this range.

A comparison of the pattern of crack propagation for blanking at slow speed and at an impact speed of 31 ft/s (9.44 m/s) was made. In the slow speed case the initial crack developed at the die edge and propagated into the bulk of the material. At a later stage in the process, a crack was initiated at the punch edge and propagated in the opposite

direction. At an impact speed of 31 ft/s (9.44 m/s) a different pattern of crack propagation was observed and the problem of uncontrolled crack propagation was largely eliminated. It was again observed that a crack was initiated at the die edge, but in this case it propagated directly between the corners of the punch and die resulting in an improved quality of the blank edge finish.

The patterns of deformation and crack propagation at various stages of punch penetration were examined for a punch impact speed of 125 ft/s (38.1 m/s). This speed is of course well above the recommended range of 30 to 40 ft/s (9.14 to 12.1 m/s). A crack was observed to have been initiated at the die edge at a punch penetration of 18% of the material thickness and did not increase significantly in length even up to a penetration of 62%. The narrow band of severe deformation, around the shear line, was established within the range of 18 to 45% punch penetration of material thickness.

An assessment of the extent of the deformation zone at various impact speeds was obtained for mild steel and high carbon steel by micro-hardness traverses. The results showed that, by increasing the speed, there was a tendency for the width of the work hardened zone and the general level of work hardening to decrease. The examination of a range of partly blanked components in copper revealed that there was no tendency for a very narrow band of deformation to be formed as was noted for mild steel.

1.3 Finish blanking

The rough sheared edge obtained on blanked components is often satisfactory for many purposes. When, however, the component is

required to have a smooth edge, subsequent shaving or machining operations frequently become necessary. These extra finishing operations are sometimes slower than the initial blanking operation itself and may consequently control the rate at which a component is produced. It is evident, therefore, that an improvement in the sheared edge condition of a blanked component, resulting in the elimination of subsequent finishing operations, will be reflected in both the cost and speed of production.

According to Tilsley and Howard (23), using thin material, up to 0.125 in. (0.317 cm) in thickness, it is usually possible, by decreasing the clearance between the punch and die to about 2% of the material thickness per side, to obtain a sheared surface which is reasonably square and free from cracks. As the stock thickness increases, however, the edge surface finish of the components deteriorates, an acceptable finish being obtained only over a small portion of the surface.

Crack formation on the edge of blanked components may be suppressed by providing the shear edges of the die with a small polished radius.

Up to 1956 no information was availableconcerning the combination of die radius with punch and die clearance to give a smooth finish for any given material or material thickness. It was, therefore, with the aim of providing further information on the use of radiused edged dies that this technique was studied at P.E.R.A.

The results of a number of tests on aluminium alloy and copper are given in a P.E.R.A. report (1). Both materials were used in their hard and soft states. In the report the limiting values of die radius and clearance between the punch and die for the production of a smooth crack-free surface when punching 1 in. (2.54 cm) diameter blanks in

aluminium alloy and copper ranging in thickness from 0.161 to 0.375 in. (0.406 to 0.952 cm) are given. .

The effect of die radius on blanking force, dishing and taper produced on the side of blanks has also been studied. Interchangeable punches of various sizes were used with dies of 1 in. (2.54 cm) bore to provide punch/die clearances ranging from 0.00025 to 0.01 in. (0.0635 to 0.254 mm) per side. The punches were ground sharp at the edges.

Results on aluminium alloy and copper showed that blanks in both hard and soft states can be produced with smooth crack-free sheared edges by using a small die radius in combination with a small clearance between the punch and die.

The results suggest that a critical value of radius exists for hard and soft aluminium and soft copper, below which the cracking of the sheared edge persists, and above which evidence of cracking is entirely eliminated. Hard copper blanks may also be produced with smooth sheared edges by using a conventional square edged die in conjunction with a small clearance between the punch and die. The maximum blanking force recorded using radiused dies was about 10% greater than that using an orthodox square edged die. Blanking forces for both materials in the soft state were all slightly higher using a square edged die than for a die with a radius of 0.006 in. (0.152 mm).

Dishing of the soft copper blanks increased with die radius. With hard copper, however, dishing was negligible for die radii up to 0.025 in. (0.635mm) but thereafter increased with die radius.

The edge taper on the side of the blanks was found to decrease with increasing die radius in the case of the hard materials, whereas for the soft material little variation was detected. No consistent

variation of edge taper with clearance was observed for either the hard or soft material.

As there are many applications where blanked steel components with good edge surface finish are required, an investigation was carried out by P.E.R.A. to determine whether or not the finish blanking technique could successfully be applied to steel components (2). A series of tests was performed on three different thicknesses of hot and cold rolled low carbon steel.

P.E.R.A. concluded that both hot and cold rolled low carbon steel blanks can be produced with smooth crack-free sheared surfaces by using a radius edged die in conjunction with a small clearance between the punch and die.

There appeared to be a critical value of die radius for both the hot and cold rolled material, below which the cracking of the sheared surface persisted, and above which cracking was eliminated. The critical value of die radius for hot and cold rolled material varied with the thickness of material. Clearance between the punch and die varied slightly with thickness for hot rolled material, but appeared to be independent of thickness for the cold rolled material. The minimum die radii and maximum clearance between the punch and die for the production of smooth crack-free surfaces are given in the report.

The variation in blanking force with radiused edge dies was about 10% greater than that when using an orthodox square edged die. The variation in stripping force with die radius showed that the stripping force decreased steadily with increasing die radius. When using the values of die radius recommended by P.E.R.A. the stripping force was not greater than 10% of the blanking force for a given thickness of material.

Dishing was measured on blanks 0.160 in. (0.406 cm) thick in the hot and cold rolled material for each die radius. The results showed that up to 0.020 in (0.508 mm) die radius, dishing of both the hot and cold rolled materials was small , but thereafter increased steadily with increasing die radius. The taper on the side of the 0.375 in. (9.52 mm) thick blanks was of the order of 0.002 in. (0.0508 mm) and appeared to be relatively unaffected by changes in die radius. The height of the burr remaining on the top edge of the slugs generally increased with increasing die radius.

Work at P.E.R.A. (1,2) showed that smooth, crack-free sheared surfaces would be produced on blanked components in one operation by the application of suitable tooling conditions. However, the application of the process to medium and high carbon steels showed that for these materials, the required quality of sheared surface could not be obtained in every case with dies having radiused edges.

In 1963 preliminary tests carried out by P.E.R.A. showed that better results would be possible if the radius was replaced by a chamfer, and a program of research was therefore undertaken to determine the most satisfactory design of die profile for the finish blanking of a number of medium and high carbon steels. The effect of varying the die profile chamfer angle and chamfer width on blank edge finish, blanking and stripping force, burr height, dishing and doming of the blanks has been investigated (24).

Square edged punches of nominal diameter 5/8 in. (1.58 cm), giving a range of punch/die clearances, was employed together with a square edged die and dies with different chamfered and radiused profiles each having a nominal diameter of 5/8 in. (1.58 cm).

The materials used were '40' carbon steel (EN8), 2½% nickel-chromium molybdenum steel (EN25), carbon spring steel (EN42), '20' carbon steel (EN3B) and low carbon steel (EN2). The tooling nomenclature is shown in Fig. 1-10. The recommended tooling conditions for the production of smooth blank edge finish of the test materials when using chamfered dies are given in the report. Also given are the values of dishing, doming and burr height obtained from the 5/8 in. (1.58 cm) diameter blanks.

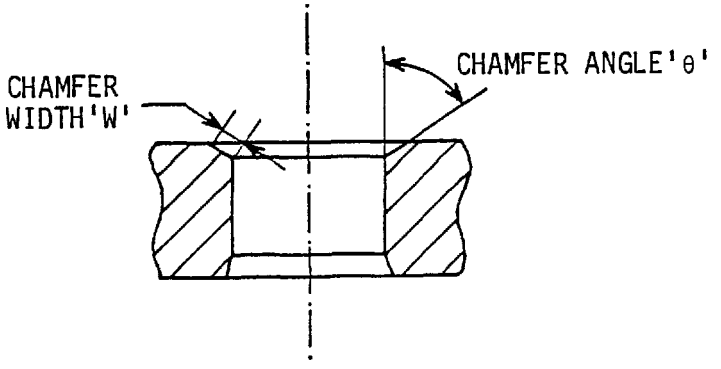

Fig. 1-10

It was noted that in three cases, i.e. 7/16 in. (1.11 cm) thick normalized EN8, 5/16 in. (0.793 cm) thick hardened and tempered EN25, and 7/16 in. (1.11 cm) thick EN42, a satisfactory blank could not be produced with a radiused die, but they were blanked successfully using chamfered dies.

Another P.E.R.A. report (3) has collected together some information on components that have been successfully finished blanked in industry. Also in the report some important information concerning the design, manufacture and use of finish blanking tools has been given which are based on accumulated experience at P.E.R.A. and many of the firms who

have applied the technique successfully.

Different materials apparently fail in different ways, for it is possible to finish blank hard copper using conventional techniques with sharp punches and dies but with small clearances, but such techniques fail when applied to a material such as mild steel, or, for that matter, soft copper. Knowledge of the nature of crack propagation and the degree and type of work hardening associated with blanking, therefore, is of prime importance in understanding the process and in assessing the tool geometry required to produce components with clean sheared surfaces.

In another P.E.R.A. report (25) the determination of the precise region of crack initiation during blanking is examined. The method adopted was to examine microscopically the severely deformed zones on part-penetrated specimens and to carry out a hardness survey over this area. Annealed 0.1% carbon steel was selected as the work material. The edges of the punches and dies were varied in shape to enable the effect of tool geometry to be assessed. A nominal total clearance of 0.002 in. (0.0508 mm) was maintained between the punch and die.

Considering the photomicrographs it was observed that the width of the severely deformed zone was markedly affected by the shape of tools used. A broadening of this region was always associated with a radius on the punch or die edges, the broadening being most pronounced in the region adjacent to the tool with the radius.

Cracks, when present, were seen to be confined to the edge of the severely deformed region and the effect of modifying the punch or die shape was to suppress cracking in the work material adjacent to the modified tool.

The graphs representing lines of equal hardness over the severely

deformed region confirmed the broadening of the work-hardened zone adjacent to the radiused edge tool. When crack propagation took place it was confined to the region where the lines of equal hardness were closest together, i.e. where the hardness gradient was greatest. No cracks were formed even when the hardness gradient was large if this region was immediately under the punch. This is, presumably, because this region is subjected to high compressive stresses due to the constraints imposed by the punch and surrounding material.

The role of clearance on the formation of smooth sheared edges was examined by Fukui, Kondo and Maeda (26) in 1971. An explanation for the requirement of very small punch/die clearance in the case of fine blanking is given and the idea is then developed into a new simple shearing method.

When a positive clearance is provided between the punch and die, during the process the material thickness in the shearing zone increases and a deficiency of material defined by the points C, C', D' and D, Fig. 1-11(a), occurs. This deficiency increases in proportion to the tool clearance and with progress of the process and also with increase in the thickness of the material. If such a deficiency of material should occur, even a high hydrostatic pressure field produced by the penetration of a blank-holder into the material would be relieved and, in the presence of tensile stresses, fracture would result. In reality it is considered likely that this deficiency of material is compensated for by the roll-over of the sheared edges at A and C but if this is not sufficient to fill the void, fracture will take place.

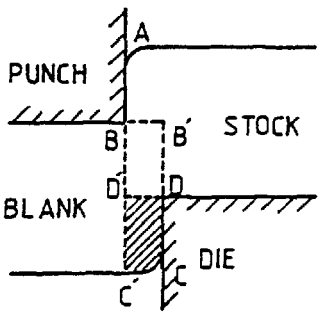

(a) POSITIVE CLEARANCE

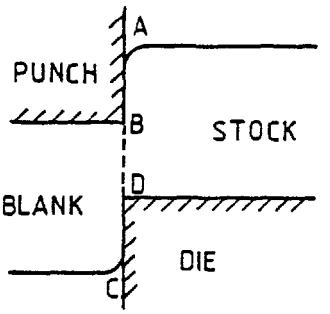

(b) ZERO CLEARANCE

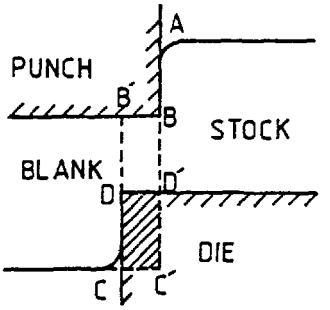

(c) NEGATIVE CLEARANCE

Fig. 1-11.

Fig. 1.11(b) shows an arrangement in which the tool clearance is zero. In this case no deficiency in the volume of the material is observed, which explains the reason why a small clearance is required in fine blanking.

In the case of negative clearance, Fig. 1.11(c), the material portion defined by C, C', D'and D becomes excessive as the process progresses. In order to proceed with the operation, the excess material must be forced outward into the stock side. This does not provide any relaxation of the pressure field in the shear region, as the stock portion on the outside restrains the flow of the material that is to be forced out and this advantageously raises the hydrostatic pressure in the shear region.

1.4 Smooth shearing by stepped profile tool

The feature of negative clearance was utilized by Kondo and Maeda (26) in 'Smooth shearing by stepped profile tool'.

In order to apply the present method to the blanking of a disc, the arrangement shown in Fig. 1-12, comprised of a stepped profile punch and a conventional die, is used to blank the specimen. In this case, after a certain amount of punch penetration, the stepped portion of the punch comes into contact with the material and hereafter not only will the deficiency of material not occur, as was defined in Fig. 1-11(a), but also due to the prevalence of a negative clearance between the punch and die additional compressive stresses develop which will help to avoid fracture. This build up in pressure is due to the fact that the stock portion on the outerside restrains the flow of the excess material that is to be forced out, thus effectively raising the hydrostatic pressure in the shear region throughout the operation.

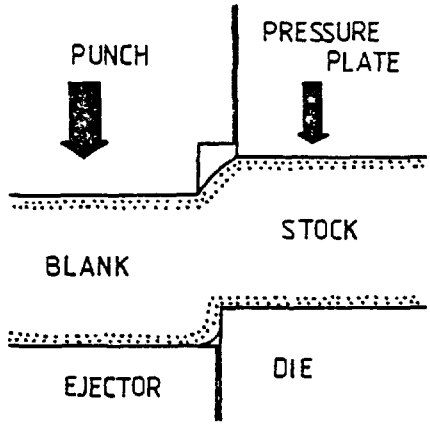

(a) EARLIER STAGE

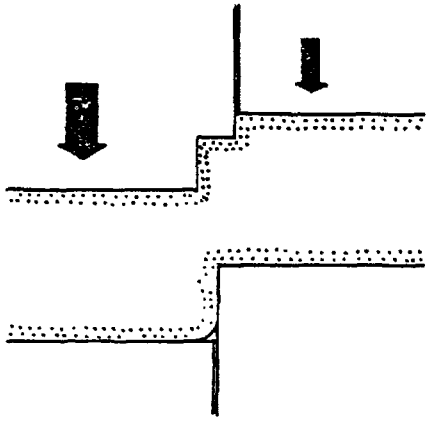

(b) MIDDLE STAGE

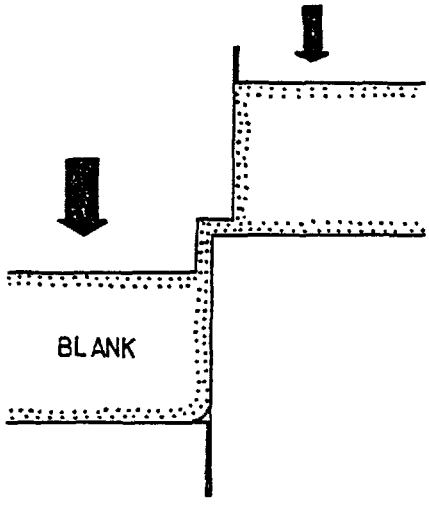

(c) FINAL STAGE

Fig. 1-12. Smooth shearing by stepped profile tool

In the smooth shearing method, unlike fine blanking in which a small clearance in the range of about 0.01 to 0.02 mm is required, a relatively large clearance of 0.07 mm is permissible. This is its most important feature because tool life is prolonged, the tool manufacture is simplified and the central alignment of tools may become much easier.

In this case, however, a correspondingly tough burr results. This is a necessary evil in gaining the above mentioned advantages.

1.5 Opposed shearing process

In the method of smooth shearing the problem of completion of separation of the blank from the stock material is not solved. Kondo and Maeda (27) proposed a new method in which this separation is completed and simultaneously the tough burr which is present in the smooth shearing method is eliminated. Tools used in blanking by this process are a conventional die, a protruding die which opposes the former, a knockout and an ejector. The process is characterized by the use of such an opposing tool with a protrusion. Arrangement of the tools and the sequence of the operation are schematically shown in Fig. 1-13.

1.6 Reciprocating blanking

A burr free blanking method was suggested by Maeda in 1958 (28). This burr free blanking method was patented and named 'Reciprocating blanking'. The principle of this process is the formation of shear droops, see Fig. 1-15 for definition, on both edges of the sheared surface so that no burr will occur. Fig. 1-14 shows an embodiment of this reciprocating blanking which comprises two steps.

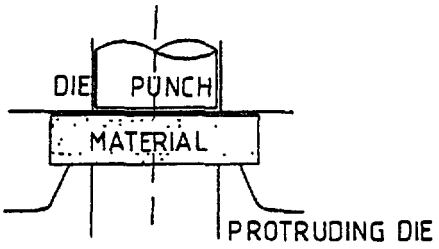

(a) CHARGING OF THE SPECIMEN

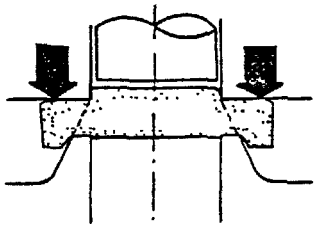

(b) CUTTING STAGE BY THE DIE

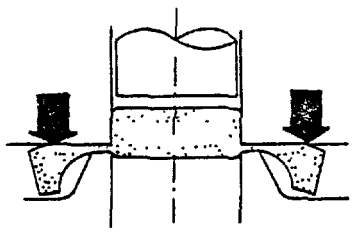

(c) CUTTING STAGE BY THE DIE IS OVER

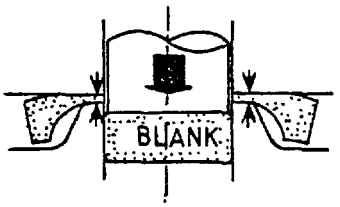

(d) SEPARATION OF THE BLANK

Fig. 1-13.

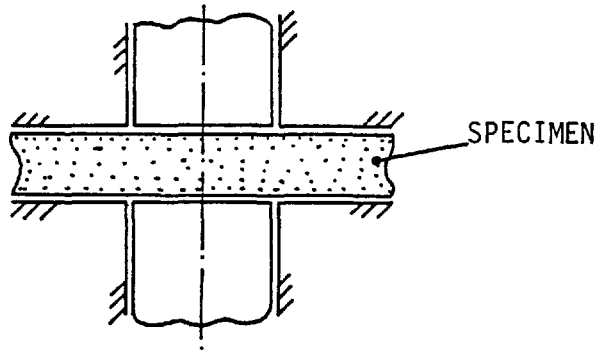

(a) TOOL SET

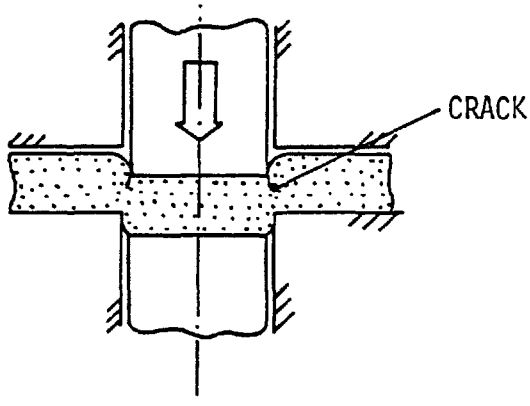

(b) HALF-SHEARED

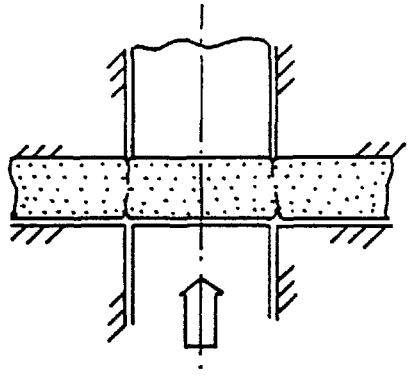

(c) REVERSE SHEARING

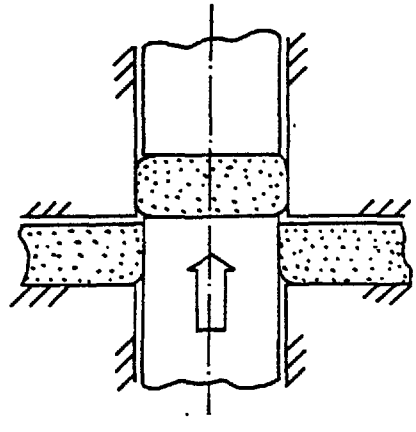

(d) END OF BLANKING

Fig. 1-14. Process of reciprocating blanking.

In the first step the material is partially penetrated by the upper punch to a predetermined depth. The second step is obtained by arranging the die and punch in the opposite direction to the first step, and then causing the half sheared portion to be completely sheared. Fig. 1-15 shows the sheared surface and the cross section obtained by this method. The droops on the blank edges are caused by the first and second steps of the process and the burr development is completely eliminated.

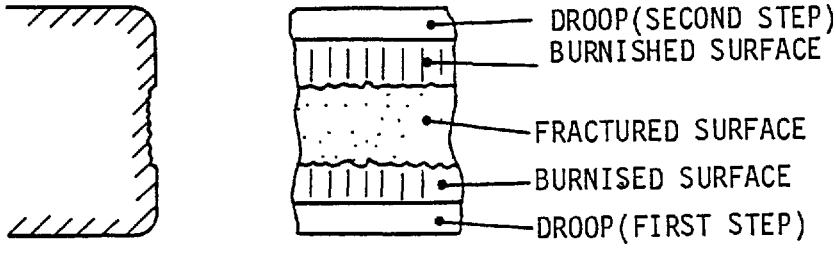

Fig. 1-15.

Jimma (29) performed an analytical solution for blanking by limit analysis. In part 1 of the report, the statically admissible stress field in a sheet material was analysed on the following assumptions :-

1) The sheet material is rigid-plastic.
2) The material near the tool edges is approximately in a state of plane strain.
3) The stress field consists of several regions of constant stress separated by straight lines of discontinuity.

In part II, the deformation process was divided into four stages, and admissible velocity fields were analyzed.

1.7 Fine blanking

Fine blanking is a technique by which blanks can be produced with the sheared surface perfectly normal to the plane of the sheet metal, and with a surface finish on the edges comparable to a machined finish.

Many reports on the fine blanking method have been published (30, 31, 32, 33, 34) but reports on the mechanism of the technique are few (35, 36, 37) .

A blank-holder, usually with a vee-shape projection on the surface, is used (Fig. 1-16) to clamp the specimen against the die-face and thus prevent the outward flow of material during blanking. This causes higher compressive stresses around the severely deforming region, where the material is being cut, thus reducing the tensile stresses prevailing in that region and can prevent fibrous fracture due to tensile stresses.

A counter-punch is used to apply a constant load to the specimen during blanking and prevent the dishing of the blank which is observed in the case of conventional and finish blanking. The application of a counter-punch not only reduces the dishing effect, but depending on the magnitude of back-load, also produces higher compressive stresses around the line of cut of the blank, through the compression of the specimen between the punch and counter-punch.

The order in which a fine blanking operation is performed is shown in Fig. 1-16 and the sequence can be summarised as follows:-

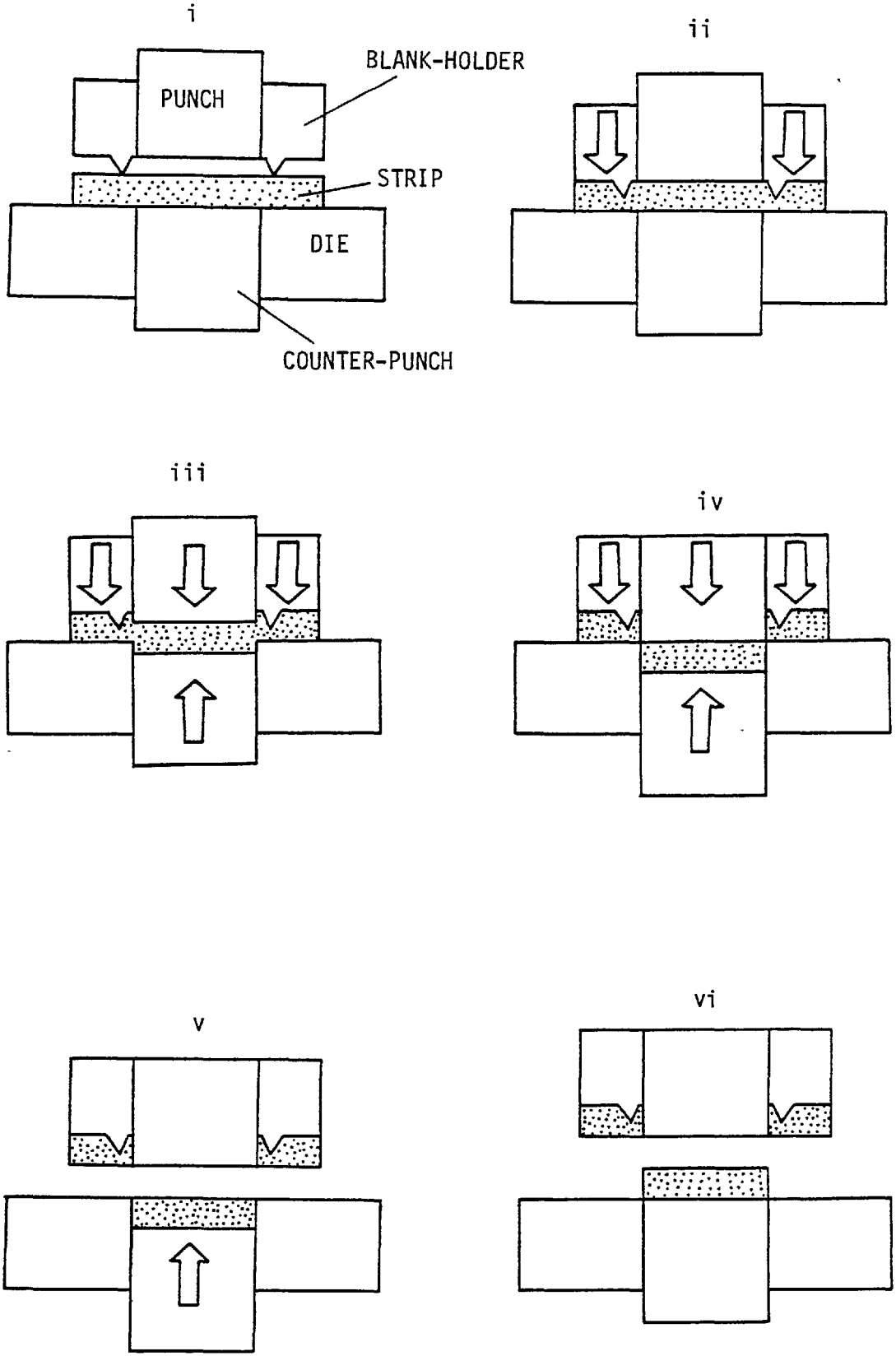

Fig. 1-16. Operation sequence in fine blanking.

i) The specimen is positioned on the die-face and the blank-holder is moved downwards until it comes in contact with the specimen.

ii) The specimen is pressed against the die using the blank-holder. Depending on the type and thickness of the material, for a certain value of clamp diameter different values of clamping force are required to perform a successful fine blanking operation. In practice it is desirable to choose a blank-holder with the smallest possible clamp diameter to keep the waste material to a minimum.

iii) The specimen remains clamped using a constant value of clamping force, and is squeezed by the punch and the counter-punch so that a predetermined value of back-load is built up. While the clamping force and the back-load are kept constant the punch begins to indent the specimen.

iv) The punch cuts through the whole thickness of the specimen and the blanked part is pressed into the die-hole.

v) The punch and the blank-holder are withdrawn to their original position and the counter-punch begins to press the blank out.

vi) The blank is forced out and a new blanking operation can be started as soon as the specimen is stripped off the punch.

The terms associated with the fine blanking operation are defined in Fig. 1-17.

Guidi (31), and Bosch and Stager (32) deal with what is termed the 'SWISS' type of blank-holder plate design. This plate incorporates an indenting ridge which coins a groove in the stock material when a load is applied to the blank-holder plate and the die. Meyer and Kienzle (35) have investigated the triple action blanking process, using a type of blank-holder plate which is conical in shape but

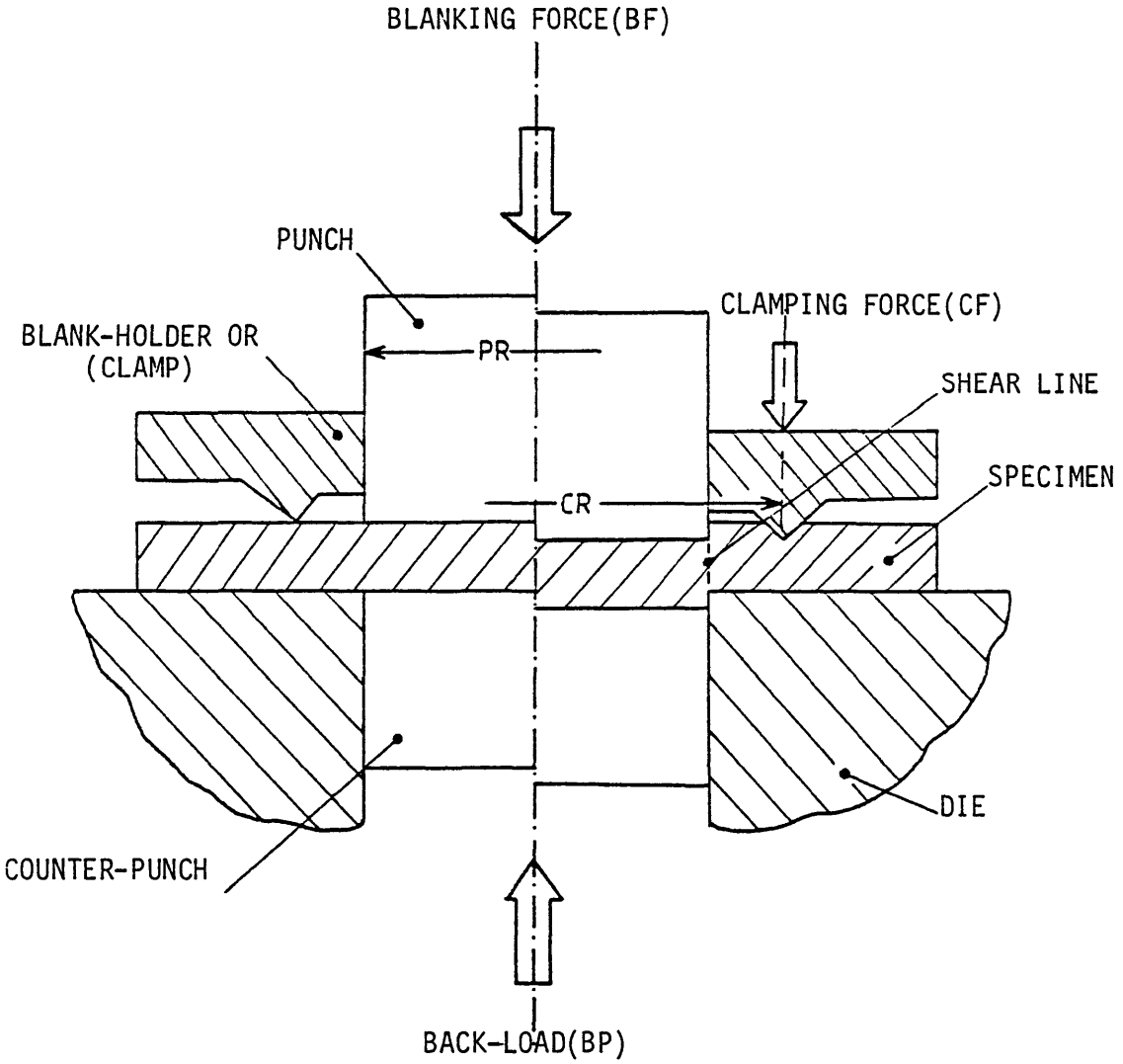

PR = Punch diameter
CR = Clamp diameter

Fig. 1-17.

with a cone angle of almost 180^{o}. Different types of blank-holder are shown in Fig. 1.18.

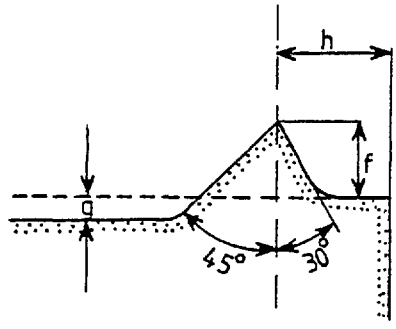

MATERIAL THICKNESS t(in)	g(in)	f(in)	h(in)
,004 to ,160	,002	,2 t	,66 to ,75t
> ,160	,003 to ,004	,17t	. ,6t

TYPE OF BLANK-HOLDER PLATE INVESTIGATED BY MEYER AND KIENZLE.

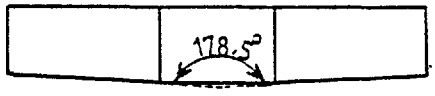

Fig. 1-18. Blank-holder indenting ridge dimensions suggested by Bosch and Stager.

When the process is operated with a blank-holder incorporating an indenting ridge, sufficient material is required between successive blanks to accommodate the coined grooves,and this results in an increase in the proportion of strip material which is scrapped. However,

with the Meyer type of blank-holder it is claimed that there is no increase in the proportion of scrap above that for conventional blanking.

Bosch and Stager (32) have made recommendations relating to the preferred geometry of the indenting ridge in relation to the thickness of strip material, Fig. 1-18 . These recommendations appear to be based on experience of operating the process commercially. However, no explanation is put forward for these preferred geometrical proportions.

The constraints provided to the additional tooling elements in the fine blanking process cause a change of fracture from fibrous to pure shear on the blank edge. An explanation for this change of fracture is sought in the work by Johnston, Fogg and Chisholm (36). The possible mechanisms are discussed relating to the part played by the tooling elements in suppressing the occurrence of a rough fractured surface at the edge of the blanked component. They have also carried out some experiments with the object of investigating how the blank-holder load, back-load, radial punch/die clearance and the distance of the indenting ridge from the line of cut affected the tendency for cracking on the blank edge.

The tools were designed to produce circular blanks nominally 1 in. (2.54 cm) diameter in 1/8 in. (0.317cm) thick commercially hot rolled mild steel. The arrangement of the tooling is shown in Fig. 1-19. The radial punch/die clearance was $\sim$ 0.15% of the material thickness. The indenter positions covered in this work range from $h/t = 0.24$ to 1.2 in six intervals, Fig. 1-20. The range of back-load investigated was from 10 to 160% of the load required to conventionally shear the blank and this was a range far wider than that recommended by previous writers (31) and (32).

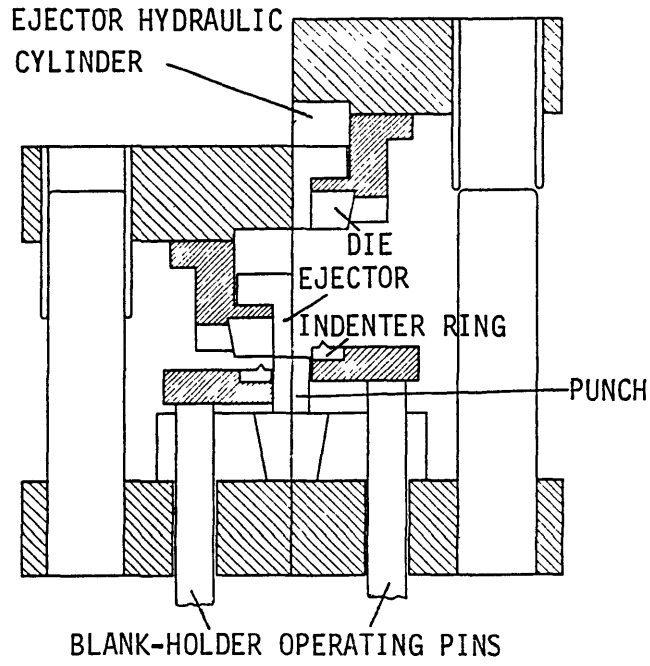

Fig. 1-19. Experimental triple action tool.

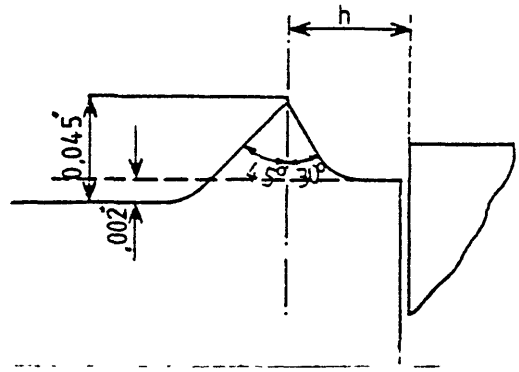

Range of inserts where h and h/t values as shown below where t = material thickness = 1/8 in. (3.1 mm).

h in.	h/t
0.03	0.24
0.05	0.40
0.07	0.56
0.09	0.72
0.11	0.88
0.13	1.04
0.15	1.20

Fig. 1-20.

The results showed that for h/t > 0.24, as the clamping force increased the minimum crack free surface portion of the blank also increased, in the case of h/t = 0.24 a maximum followed by a minimum was exhibited.

The position of the indenting ridge relative to the punch edge did not appear to be critical provided that h/t > 0.5. In the case of h/t < 0.5 the blank-holder force necessary to prevent cracking on the blank edge rose sharply.

The magnitude of the back-load did not appear to influence the edge surface of the blanks within a fairly wide range. At high values of back-load there appeared, however, to be a distinct disadvantage in the requirement of higher values of clamping force. The magnitude of back-load is more likely to be determined by considerations affecting the extent to which dishing of the blank occurs, rather than in contributing substantially to the prevention of cracking on the blank edge.

Maeda (37) has reported similar experimental work as Johnston, Fogg and Chisholm (36) . The influence of conditions on the surface quality of the blank edge and the mechanism of fine blanking have been discussed. The effect of clamping force, back-load, distance between the line of action of the blank-holder and the edge of the punch and shape of projection have been studied. The subpress used during the experiments is shown in Fig. 1-21 . The diameter of the die was 16.13 mm, and the amount of clearance between the punch and die varied from 0.0015 mm to 0.04 mm by exchanging punches of different diameters. Various forms of projections used in this experiment are shown in Fig. 1-22. Among them, the blank-holder with a vee-shape projection had seven different distances between the shearing line and the peak of the projection. The heights of the projections 'h' were each equal to 1.5 mm (0.059 in.).

1 Punch
2 Die
3 Blank-holder
4 Counter-punch
5 Punch holder
6 Die block

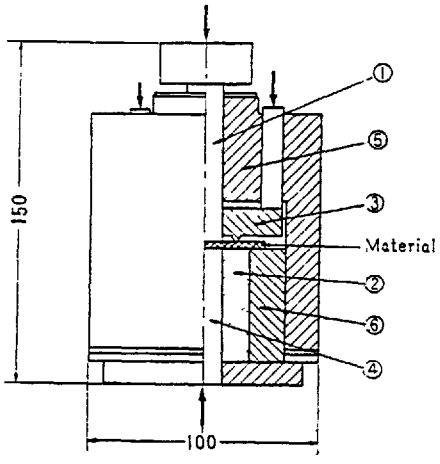

Fig. 1-21. Fine blanking tool.

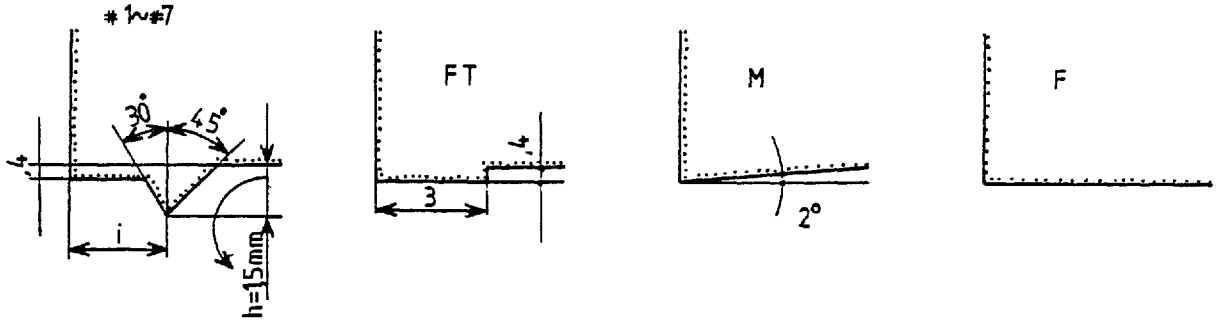

#1~#7 Knife edge type projection
FT Flat topped type projection
M Conical blank holder
F Flat blank holder

Fig. 1-22.

Six carbon steel sheets containing 0.02 to 0.48% carbon were used in the experiments. Among these six steel sheets, the investigation was mainly concentrated on the two materials with higher carbon contents of 0.23% and 0.48%, which showed the worst edge finish during conventional blanking, as this was hoped to reveal the effect of different blanking conditions on the blank edge finish much more easily.

The results showed that the increase in clamping force decreases the fractured portion of the blank edge. The clamping force was more effective when a smaller punch/die clearance was employed together with higher values of back-load. It was found that an optimum value of blank-holder diameter exists for which at any given value of clamping force the bright burnished portion of the blank edge is at a maximum. Maeda concluded that the general effect of additional toolings on the stress state in the shearing zone which causes a change of fracture from fibrous to pure shear, is due to the increase of hydrostatic pressure in the shearing region.

In Guidi's report (31) it has been suggested that materials having a high capacity for deformation are suitable for fine blanking and the reduction of the cross sectional area at fracture would be a better criterion than elongation. Particularly applicable to this process are case hardened steel, copper, brass with a copper content of 70% and above, aluminium and aluminium alloy.

1.8 Lubrication

When punching a thick ferrous material, effective lubrication is essential for preventing 'pick up' . Pick up increases the stripping force and often causes punches to fail in tension. The problem is greater in finish and fine blanking because of the considerable increase

in radial pressure applied to the punch surface, owing to a smaller punch/die clearance.

Effective lubrication prevents the axial scoring which occurs on the sheared surfaces of the blank. Apart from marring what would otherwise be a good surface finish, scoring drags up metal from the sheared surfaces and results in excessive burr on the upper edge of the blank.

A P.E.R.A. investigation (3) on finish blanking showed that scoring could be reduced by wiping the work material prior to blanking with an oil which contained an E.P. (extreme pressure) additive. The use of oil containing an E.P. additive has also been recommended by Metal Working Production (38) for the fine blanking process.

Appendix 1 of the P.E.R.A. report describes tests to determine whether the viscosity of a lubricant affects its efficiency in finish blanking; while Appendix 2 deals with the influence of the tool surface finish on the effectiveness of lubricants. Appendix 3 of the report describes the procedure adopted for removing the lubricant films from the tool surfaces between each series of tests.

By using the proper lubricant some manufacturers have been able to punch 3000 holes in medium carbon steel while without lubricant they could do only 50 before the punch failed due to pick-up.

CHAPTER 2

A FINITE ELEMENT FORMULATION FOR THE ELASTIC-PLASTIC ANALYSIS OF SMALL STRAINS AND SMALL DISPLACEMENTS

2.1 Introduction

The method of finite element is now well accepted as a powerful method of stress analysis and widely used for the solution of structural problems. The search for and development of the many consistent elements has given the method a wide area of application. Since the initial paper of Turner et al (39) on the direct stiffness method, various types of elements have been developed and different kinds of non-linearities have been dealt with. The problems of material non-linearity and geometric non-linearity due to their applicability to practical problems have received considerable attention. General purpose computer programs now exist which can be used with different types of element for the solution of large scale problems.

Since the establishment of the method, there has been much interest in extensions for non-linear analysis. There are, in general, two basic forms of non-linearities, one arising from the non-linear material behaviour and the other due to the non-linear geometric behaviour. The most common type of material non-linearity occurs in the elastic-plastic material where the stress-strain relations are usually expressed in an incremental form. For this material the linearity of the incremental stress-strain law forms the basis of the equations, its most direct application being in the incremental type solution, where the solution is built up as a series of linear increments.

There are several methods to solve the problems relating to the use of elastic-plastic material. These methods can be divided into two main categories: the variable stiffness and initial strain (or stress) method. In the first method the incremental linear constitutive relation, based on plasticity theory, is introduced directly into the governing equations. This would, modify the element stiffness matrices at each step of load increment, thereby changing the overall stiffness matrix.

In the latter method the plasticity effects are treated as initial stress or initial strains and the problem is solved as an elastic one, using the elastic stiffness matrix throughout. The main advantage of this method is the ease with which it can be implemented in a general finite element program, and that the stiffness matrix once developed for the elastic case remains unchanged throughout the whole problem. Whereas in the variable stiffness method at each step the stiffness matrix has to be reformulated and a new solution of equations obtained. When the combined (geometric and material) non-linearity is considered, the method of variable stiffness approach becomes quite attractive. Here the non-linearity arising from a change of geometry can easily be incorporated at each incremental step together with the effects due to plasticity.

2.2 Literature survey of finite element method

2.2.1 Material non-linearity(plasticity)

Progress in the inelastic analysis owes much to the simultaneous development of the direct stiffness method by Turner et al (39) and the method of initial strains by Mendelson and Manson (40). The method was originally formulated in finite difference form, but soon

Gallagher and his co-workers (41) adapted the method of initial strain to the finite element method.

In the earliest applications of the finite element method to plasticity the initial strain method was favoured. Here the works of Gallagher et al (41) and Argyris (42) are significant. Argyris proposed a matrix displacement method for the analysis of elastic-plastic three dimensional continua. He suggested a direct incremental approach and an iterative incremental approach for the solution of the problem by treating plastic strains as initial strains.

The initial strain method fails entirely, however, if non-work hardening material is considered as the strains cannot then be uniquely determined for prescribed stress levels. The initial stress process that was first applied to plasticity by Zienkiewicz et al (43) appears ideally suited here. This method has shown to yield more rapid convergence than the alternative approach and appears at the time of writing to be widely accepted.

At the same time as the method of initial strain was being developed a different method known as the tangent modulus method was introduced for elastic-plastic analysis. The non-linear problem is solved as a series of piece-wise linear problems. This makes use of the linearity of the incremental stress-strain laws to assemble a new element stiffness matrix at each stage. The equations for the tangent modulus method were developed by Pope (44), Swedlow and Yang (45), and Marcal and King (46). Marcal et al resorted to the inversion of a matrix because of the need to avoid division by zero in the case of an elastic perfectly plastic material.

Recent formulations by Yamada (47) have circumvented this

problem and allow the linear incremental relations to be obtained in closed form for all cases of elastic-plastic behaviour. The method is based on a plastic stress-strain matrix which is derivable by inverting the Prandtl-Reuss equations in plasticity theory. The matrix is of quite simple form and facilitates the incremental treatment of elastic- plastic problems. In Yamada's approach small and varying increments of load just sufficient to cause yield in the successive elements are used. As an example the method was employed to study notched tension specimens under conditions of plane-stress using triangular elements.

Among the problems solved during the study of the finite element method are those of Marcal and King (46) who solved several elastic-plastic two dimensional problems using the finite element method. A partial stiffness concept was suggested and it was used to study plane stress, plane strain and axi-symmetric cases, using Von-Mises material obeying the Prandtl-Reuss relations. Comparisons with known results have been made for the case of a long cylinder with internal pressure, a tensile specimen with a central hole in plane stress and a notched tensile specimen. Later, Marcal (48) used this method for the elastic-plastic analysis of pressure vessel components. Akyuz and Merwin (49) treated plane-strain indentation for cylindrical indenters. These examples, however, were given only to demonstrate the problem solving capability of the method with reference to constant-strain triangular elements.

Various methods have been proposed for the inclusion of surface friction in the finite element solution. Nagamatsu et al (50, 51, 52) modified the surface node displacements by a "slip-factor",

but this required a prior experiment under the appropriate conditions. Gordon and Weinstein (53), Iwata et al (54) and Odell (55) introduced forces to the surface nodes, opposing the direction of motion. Shah and Kobayashi (56), Price (57) and Matsumoto (58) allowed for friction by the introduction of a surface shear stress 'τ' evaluated from an empirical formula $\tau = mk$, where $k = \sigma_y / \sqrt{3}$, and σ_y is the yield stress of the adjacent surface element directed against motion. However, both the force method and the surface shear stress approach require prior knowledge of the flow direction. Where the direction of flow is known these methods appear to be quite effective, in processes such as forging where the direction of flow is not known the method cannot be predictive.

Several attempts were made by Hartley (59) to develop a formulation that did not require prior knowledge of the flow direction, but all the solutions obtained, displayed incorrect modes of flow and were not pursued. Later in a paper, Hartley (60) describes a method for introducing friction into the finite element analysis. This is achieved by the inclusion of a layer of elements whose stiffness is modified by a function of the interfacial shear factor. To investigate the proposed approach it was applied to the friction sensitive process of ring compression. An experiment was performed where the properties of an aluminium ring and of an applied surface layer of lead were known prior to the test. Excellent agreement between the theoretical predictions and experiments have been claimed.

2.2.2 Geometric non-linearity

Geometric non-linearity results in two classes of problems that are well known to structural engineers: the large deflection problem

and the problem of structural instability. The term large deflection is misleading since problems falling within this category need not have actual deflection which are in any sense large, in fact, they can be, and often are, as small as those arising for the linear case. However the deformed configuration of the structure must be used when writing the equilibrium equations for the large deflection problem. In addition, the strain-displacement equations must now include the appropriate higher order, non-linear terms.

Introducing the higher order terms into the strain displacement equations leads to a new class of stiffness matrices, absolutely essential for investigating large deflection and instability problems. The additional stiffness matrices required for analyzing the geometrically non-linear problem are variously termed the initial stress stiffness matrix, the geometric matrix, and the initial displacement stiffness matrix. Turner et al (61) extended the method of direct formulation of the stiffness matrix to include the effects of non-uniform heating and large deflections. The usual stiffness matrix formulation is limited to small temperature changes and small deflections. For large temperature changes additional terms are required. Such matrices are suggested in (61-64).

The derivation of the initial stress stiffness matrix was finally placed on a firm basis by the use of the Lagrangian or Green's strain by Martin (65). More recent analysis has established the importance of additional terms (66-68) which take the form of an initial displacement matrix in the incremental solution. The large displacement analysis has often been approached through an updated local coordinate system, which is usually defined for each element in the structure (69, 70). Such coordinate systems are of use only when the assumption of small strains is made. In (71) the authors solved an elastic-plastic membrane

problem with an incremental approach which accounts for small strains and large displacements. Kapur and Hartz (64) developed a finite element approach for the plate buckling problem. Analysis without the use of initial displacement matrix resulted in over estimated results and it was concluded that the initial displacement matrix should be included in the finite element analysis of large deformation and instability problems. A practical method of solution of the geometrically non-linear problem of plates is proposed in a paper by Kawai (72).

2.2.3 Combined non-linearity

The solutions of problems with combined non-linearity, material and geometric, has been attempted but are relatively few in the literature. Marcal (73) developed incremental stiffness matrices for the small strain large displacement analysis of combined non-linear problems. The element stiffness matrices were obtained from the principle of virtual work. A general purpose finite element program for combined non-linearity analysis is also described. Case studies, using the developed finite element program, the behaviour of axisymmetric shells, flat plates, and structures in plane stress were examined.

Hofmeister, Greenbaum and Evensen (74) developed a method for the large strain, elasto-plastic analysis of two dimensional structures by the finite element method. An incremental variational principle was used to develop the finite element equilibrium equations for use in a piece-wise linear solution procedure.

Hibbitt, Marcal and Rice (75) developed an incremental and piece-wise linear finite element theory for the large displacement, large strain regime with particular reference to the elastic-plastic behaviour in metals. The resulting equations, though more complex, are in a similar

form to those previously developed for large displacement, small strain problems, the only additional term being an initial load stiffness matrix which is dependent on current loads. This similarity in form indicates that existing non-linear general purpose programs may be extended to include finite strains.

McMeeking and Rice (76) presented an Eulerian finite element formulation for problems of large elastic-plastic flow. The method is based on Hill's variational principle for incremental deformations, and is ideally suited to isotropically hardening Prandtl-Reuss materials. The method was applied to the analysis of necking of a bar in tension.

In elastic-plastic analysis the additional terms must be calculated for each increment of deformation, for which the last three have a complicated form. Needleman (77) has a similar Lagrangian scheme, but he derives his equations from a variational principle due to Hill (78). A third Lagrangian formulation was presented by Felippa and Sharifi (79) who intended to place no limitation on the size of an increment of deformation.

Gunasekera (80) used the finite element displacement method to solve elastic-plastic problems with small and large deformations. Large deformations are taken into account by a Lagrangian derivation based on Green's strain tensor, and examples are given to illustrate this. An alternative method is also discussed based on the Eulerian derivation. The elastic-plastic material is represented by the Prandtl-Reuss relations together with the yield criterion of Von-Mises. The analysis is carried out step by step using small linearised increments. Application of the method to transient stages of a metal processing problem is demonstrated.

An elasto-plastic analysis of plane strain and axisymmetric flat

punch indentation was made by Lee and Kobayashi (81). Studies were made on the development of the plastic zone, the load displacement relationships and the stress and strain distributions during continued loading, with variations in the punch friction and specimen dimensions. The elements used for plane-strain deformation were quadrilateral, each consisting of four triangular elements. Quadrilateral rings were used for the axisymmetric case. They also studied (82) axisymmetric upsetting and plane-strain side pressing of solid cylinders using a step by step incremental method. Solutions were obtained up to a 33% reduction in height in axisymmetric upsetting and up to 19% reduction in diameter in side pressing. They found that by increasing the number of elements and decreasing the increment of displacement the results approached a better solution.

Blass (83) considering both material and geometrical non-linearities, presented a finite element formulation. Blass assumed isotropic material behaviour, isothermal deformation, absence of the Bauschinger effect and infinitesimal elastic deformation. The analysis was performed on a Lagrangian frame of reference. A computer program was implemented and applied to the analysis of radial upsetting. A related indentation problem was also considered. Comparing the results obtained from finite element, upper bound and experiment showed that the finite element results represented a slight improvement over the upper bound solution. The results were satisfactory at the early stages of deformation but the program failed at larger deformations.

2.3 Present work

This thesis deals with the application of the finite element method to large elastic-plastic deformation incurred during the fine blanking

operation. An incremental tangential method is used and the formulation obtained is valid only for infinitesimal strains as the extra terms in the element stiffness matrix, which will be introduced in the case of large plastic deformation, are not considered. According to Martin (65) for some large deformation problems it may be possible to omit the extra terms entirely. He claims that the results obtained for a large number of problems show that it can lead to excellent results. At the same time, he has pointed out that in solving critical loading as an eigen value problem, the presence of the geometric stiffness matrix is absolutely essential. McMeeking and Rice (76) pointed out that these extra terms are not significant in a tangent modulus approach to elastic-plastic or non-linear elastic analysis, since the increment of deformation must be small in any case.

Considering the works by Martin (65) and McMeeking and Rice (76) it was decided to exclude the extra terms which have to be introduced in the element stiffness matrix for large plastic deformation. The finite element result for a simple blanking operation was compared with the experimental result. This comparison can determine the amount of deformation that can be introduced in the finite element program without producing significant errors.

The Prandtl-Reuss equations are used for the elastic-plastic material together with the yield criterion of Von-Mises. The strain hardening of the material is approximated by two straight lines although any other form could have been incorporated. Anisotropy and the Bauschinger effect are neglected. Non-linearity due to large deformation is taken into account by a proper updating of the co-ordinates of the continuum.

2.4 General theory of the finite element method

2.4.1 Concept of the finite element method

The theory of elasticity can be utilized to analyse the stresses and the displacements in a continuum. The method serves to formulate the problem in terms of partial differential equations. The solutions of the equations would provide an exact solution of the stress analysis problem, but the configuration, loading, and boundary conditions are usually so complicated that such a solution would be very difficult indeed.

The finite element method seeks to satisfy the necessary conditions in an approximate way. The continuum is separated by imaginary lines or surfaces into a number of 'finite elements'. The elements are assumed to be interconnected at a discrete number of nodal points situated on their boundaries. The displacements of these nodal points will be the basic unknown parameters of the problem. A set of functions is chosen to define uniquely the state of displacement within each 'finite element' in terms of nodal displacements. The displacement fields must be chosen in such a way as to satisfy the compatability condition within each element and between different elements. An unsuitably chosen displacement field can cause gaps or overlaps within the elements or at inter-element boundaries.

In the finite element method the equilibrium equations and boundary conditions on stresses are satisfied only approximately. The approximation improves as more elements are used, and in the limit of an infinitely fine mesh, the stresses calculated by the finite element method would be equal to the exact values within the continuum.

2.4.2 Basic finite element formulations

2.4.2.1 Introduction

The characteristics of a 'finite element' are derived and represented in mathematical form. The virtual work principle is applied to a single element and no assumption of linearity or non-linearity of the material is made. The derived equation is in a general form and applicable to any situation. The special case for elastic continua is presented and some basic definitions which will be used during the formulation will first be given.

2.4.2.2 Displacement function

A typical finite element 'e', in a two dimensional case, defined by nodes i, j and m with straight line boundaries is shown in Fig. 2-1.

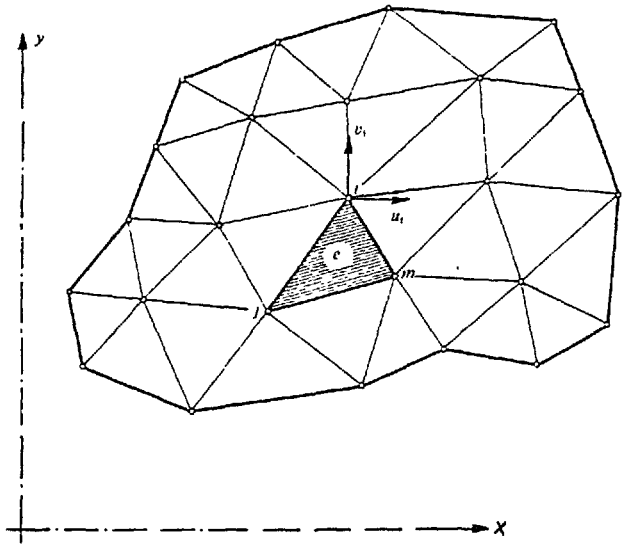

Fig. 2-1.

The displacements at any point within the elements can be interpolated in terms of nodal point displacements by column vector

$f(x,y)$.

$$\{f\} = [N]\ \{\delta\}^e = [N_i\ ,\ N_j\ ,\ N_k\ ,\ \ldots\ ] \begin{Bmatrix} \delta_i \\ \delta_j \\ \delta_k \\ \cdot \\ \cdot \\ \cdot \end{Bmatrix} \tag{2.1}$$

in which the components of $[N]$ are in general functions of position and $\{\delta\}^e$ represents nodal point displacements for a particular element. The function $[N]$ is called the shape function.

2.4.2.3 Strains

Strain-displacement relationship within an element can always be written in matrix notation as

$$\{\varepsilon\} = [B]\ \{\delta\}^e \tag{2.2}$$

The matrix $[B]$ is commonly called the strain-displacement matrix.

With displacements known at all points within the element the strains at any point can be calculated.

2.4.2.4 Stresses

In general, the material within the boundaries may be subjected to initial strains due to e.g. temperature changes, shrinkage and so on. If initial strains are denoted by $\{\varepsilon_o\}$, then stresses within the elements will be caused by the difference between the total and initial strains. In addition, it can also be assumed that, at the outset

of analysis, the material is stressed by some known initial stresses $\{\sigma_o\}$.

Assuming general elastic behaviour, the relationship between stresses and strains will be linear and of the form

$$\{\sigma\} = [D^e]\left(\{\varepsilon\} - \{\varepsilon_o\}\right) + \{\sigma_o\} \tag{2.3}$$

where $[D^e]$ is the elasticity matrix

2.4.2.5 General formulation

Equivalent nodal forces for an element are shown by $\{F^e\}$. The distributed loads $\{P\}$ are defined as those acting on a unit volume of material within the element. To derive a mathematical formulation for the finite element 'e' the method of virtual work is used.

The procedure is to impose an arbitrary (virtual) nodal displacement and to equate the external and internal work done by the various forces and stresses during that displacement. The virtual displacement at the nodes is denoted by $d\{\delta\}^e$. This results, by Eqs. (2.1) and (2.2) in displacement and strains within the element equal to:

$$d\{f\} = [N]\ d\{\delta\}^e \qquad \text{and} \qquad d\{\varepsilon\} = [B]\ d\{\delta\}^e \tag{2.4}$$

The work done by the nodal forces is equal to the sum of the products of the individual force components and corresponding displacements, i.e. in matrix notation.

$$\left(d\{\delta\}^e\right)^T \cdot \{F\}^e \tag{2.5}$$

The internal work done by the stresses and distributed forces per unit volume is :

$$d\{\varepsilon\}^T \{\sigma\} - d\{f\}^T \{P\} \tag{2.6}$$

or

$$(d\{\delta\}^e)^T \left([B]^T\{\sigma\} - [N]^T\{P\}\right) \tag{2.7}$$

The external work is equated to the total internal work obtained by integrating over the volume of the element.

$$(d\{\delta\}^e)^T \{F\}^e = (d\{\delta\}^e)^T \left(\int [B]^T [\sigma]\, d(vol) - \int [N]^T \{P\}\, d(vol)\right) \tag{2.8}$$

As this relation is valid for any value of virtual displacement, equality of the multipliers must exist and so

$$\{F\}^e = \int [B]^T \{\sigma\}\, d(vol) - \int [N]^T \{P\}\, d(vol) \tag{2.9}$$

By a proper modification of the nodal point loads the effect of distributed loads can be taken into account and Eq. (2.9) reduces to:

$$\{F\}^e = \int_{\textit{Element volume}} [B]^T [\sigma]\, d(vol) \tag{2.10}$$

Eq. (2.10) is written for a single element and a similar relationship is obtained for the entire continuum by writing Eq. (2.10) for different elements and assembling the equations together.

$$\{F\} = \int_{\textit{Entire continuum}} [B]^T [\sigma]\, d(vol) \tag{2.11}$$

where $\{F\}$ denotes the nodal forces at all the nodal points of the continuum.

Eq. (2.11) is in a general form and applicable to a linear or non-linear continuum.

2.4.3 Elastic formulation

In elastic cases the relation between stresses and strains are linear and Eq. (2.9) can be presented in a more interpretive form. On substitution of Eqs. (2.2) and (2.3) into Eq. (2.9), Eq. (2.12) will be obtained.

$$\{F\}^e = \left(\int [B]^T [D^e] [B] d(vol)\right)\{\delta\}^e - \int [B]^T [D^e]\{\varepsilon_o\}\, d(vol) + \int [B]^T \{\sigma_o\}\, d(vol) - \int [N]^T \{P\}\, d(vol) \qquad (2.12)$$

The term $[k]^e = \int [B]^T [D^e] [B]\, d(vol)$ is called the elastic element stiffness matrix.

Nodal forces due to distributed loads are:

$$\{F\}^e_P = -\int [N]^T \{P\}\, d(vol)$$

and those due to initial strains are:

$$\{F\}^e_{\varepsilon_o} = -\int [B]^T [D^e]\{\varepsilon_o\}\, d(vol)$$

Due to initial stresses present at the outset of the analysis, contributions to nodal forces are

$$\{F\}^e_{\sigma_o} = \int [B]^T \{\sigma_o\}\, d(vol)$$

In a special case where the initial stresses '$\{\sigma_o\}$' and the initial strains '$\{\varepsilon_o\}$' are zero and the distributed loads are taken into account by appropriate modification of $\{F\}^e$, Eq. (2.12) reduces to

$$\{F\}^e = [\int [B]^T [D^e] [B] \; d(vol)]\{\delta\}^e \tag{2.13}$$

2.4.4 Infinitesimal elastic-plastic formulation

As the plastic deformation is a path dependent phenomenon the equilibrium equations are given in an incremental form.

For small increments of load Eq. (2.10) can be written as

$$\{F\}^e + d\{F\}^e = \int([B] + d[B])^T(\{\sigma\} + d\{\sigma\}) \; d(vol)$$

$$\{F\} + d\{F\}^e = \int [B]^T[\sigma] \; d(vol) + \int [B]^T d\{\sigma\} \; d(vol) + \int d[B]^T[\sigma] \; d(vol) + \int d[B]^T d\{\sigma\} \; d(vol) \tag{2.14}$$

The term $\int d[B]^T d\{\sigma\} \; d(vol)$ can be ignored in comparison with the other terms. For infinitesimal strains the change in the matrix $[B]^T$ can also be ignored. Eq. (2.14) thus reduces to:

$$\{F\}^e + d\{F\}^e = \int [B]^T \{\sigma\} \; d(vol) + \int [B]^T d\{\sigma\} \; d(vol) \tag{2.15}$$

subtracting Eq. (2.10) from Eq.(2.15) yields:

$$d\{F\}^e = \int [B]^T d\{\sigma\} \; d(vol) \tag{2.16}$$

It can be shown that a similar relationship to Eq. (2.13) can be obtained for elastic-plastic continuum but in an incremental form. To do this the value of $d\{\sigma\}$ has to be expressed in terms of corresponding

strain increments. An incremental relationship between stresses and strains will be given in section 2.4.4.1.

Equation (2.16) is written for a single element, a similar equation can be obtained for the entire continuum by writing Eq. (2.16) for each element and assembling them together.

$$d\{F\} = \int [B]^T d\{\sigma\}\, d(vol) \tag{2.17}$$

Where $d\{F\}$ denotes the increment of loads at all the nodal points of the structure and the integral has to be taken over the entire continuum.

2.4.4.1 Incremental stress-strain relationship(plasticity)

According to the Von Mises criterion, yielding begins under any state of stress when the equivalent stress $\bar{\sigma}$ exceeds a certain limit, where

$$\bar{\sigma} = 1/\sqrt{2}\ \left((\sigma_x - \sigma_y)^2 + (\sigma_y - \sigma_z)^2 + (\sigma_z - \sigma_x)^2 + 6(\tau_{xy}^2 + \tau_{yz}^2 + \tau_{zx}^2)\right)^{\frac{1}{2}} \tag{2.18}$$

An equivalent plastic strain increment $d\bar{\varepsilon}^p$ is defined as a combination of the separate plastic strain increments:

$$d\bar{\varepsilon}^p = \sqrt{2}/3\left((d\varepsilon_x^p - d\varepsilon_y^p)^2 + (d\varepsilon_y^p - d\varepsilon_z^p)^2 + (d\varepsilon_z^p - d\varepsilon_x^p)^2 + 3/2(d\gamma_{xy}^p)^2 + 3/2(d\gamma_{yz}^p)^2 + 3/2(d\gamma_{xz}^p)^2\right)^{\frac{1}{2}} \tag{2.19}$$

Here the engineering definition of shear strain is used.

The relation between effective stress and effective strain may be established by a uniaxial tension test and is shown in Fig. 2-2.

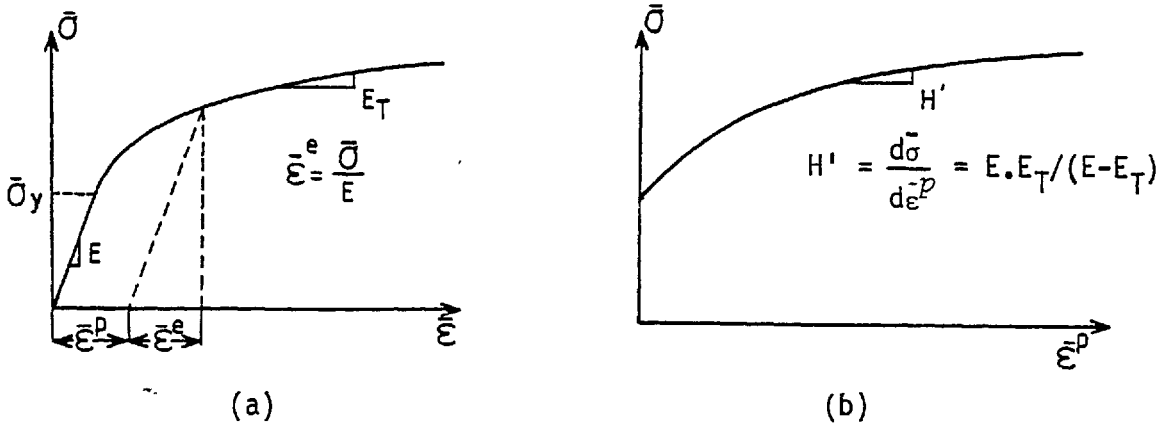

Fig. 2-2.

Notation in the figure defines the elastic component of effective strain, $\bar{\varepsilon}^e$, and the relation between slope H' and elastic modulus E and tangent modulus E_T.

Yielding first begins when $\bar{\sigma}$ exceeds $\bar{\sigma}_y$ in Fig. 2-2(a). As $\bar{\varepsilon}^p$ grows, the value of $\bar{\sigma}$ which must be exceeded to produce further yield also grows, this being due to the strain hardening characteristic of the material. If unloading occurs it is assumed that yielding resumes only when $\bar{\sigma}$ exceeds its previous maximum value. This is the assumption of isotropic hardening and ignores the Bauschinger effect.

Both sides of Eq. (2.18) are differentiated and the deviatoric stresses;

$$\sigma'_x = \sigma_x - \frac{(\sigma_x + \sigma_y + \sigma_z)}{3} = 1/3(2\sigma_x - \sigma_y - \sigma_z), \text{ etc.} \tag{2.20}$$

are substituted, Eq. (2.21) is obtained

$$d\bar{\sigma} = \{\frac{\partial\bar{\sigma}}{\partial\sigma}\}^T\{d\sigma_x\ d\sigma_y\ d\sigma_z\ d\tau_{xy}\ d\tau_{yz}\ d\tau_{zx}\} = \{\frac{\partial\bar{\sigma}}{\partial\sigma}\}^T d\{\sigma\} \tag{2.21}$$

where

$$\{\frac{\partial\bar{\sigma}}{\partial\sigma}\} = \{\frac{3\sigma'_x}{2\bar{\sigma}}\ \frac{3\sigma'_y}{2\bar{\sigma}}\ \frac{3\sigma'_z}{2\bar{\sigma}}\ \frac{3\tau_{xy}}{\bar{\sigma}}\ \frac{3\tau_{yz}}{\bar{\sigma}}\ \frac{3\tau_{zx}}{\bar{\sigma}}\} \tag{2.22}$$

The Prandtl-Reuss relations state that

$$d\{\varepsilon^p\} = \{d\varepsilon_x^p \; d\varepsilon_y^p \; d\varepsilon_z^p \; d\gamma_{xy}^p \; d\gamma_{yz}^p \; d\gamma_{zx}^p\} = \{\frac{\partial\bar{\sigma}}{\partial\sigma}\} \; d\bar{\varepsilon}^p \tag{2.23}$$

The latter equation defines the six plastic strain increments that result when the effective plastic strain increment $d\bar{\varepsilon}^p$ occurs under a known state of stress. A strain increment $d\{\varepsilon\}$ is the sum of its elastic component $d\{\varepsilon^e\}$ and its plastic component $d\{\varepsilon^p\}$. Hence from Hook's law,

$$d\{\sigma\} = [D^e] \; d\{\varepsilon^e\} = [D^e](d\{\varepsilon\} - d\{\varepsilon^p\}) \tag{2.24}$$

where $[D^e]$ is the conventional matrix of elastic constants. A relationship that yields $d\bar{\varepsilon}^p$ from the total strain increment $d\{\varepsilon\}$ is obtained as follows. Substitute Eq. (2.23) into Eq. (2.24) then premultiply both sides by $\{\partial\bar{\sigma}/\partial\sigma\}^T$. Using figure 2-2 and Eq. (2.21) the following can be written $\{\partial\bar{\sigma}/\partial\sigma\}^T d\{\sigma\} = H' \; d\bar{\varepsilon}^p$, which upon substitution into the results obtained in the previous step, Eq. (2.25) is obtained.

$$d\bar{\varepsilon}^p = \frac{\{\partial\bar{\sigma}/\partial\sigma\}^T \; [D^e]}{H' + \{\partial\bar{\sigma}/\partial\sigma\}^T \; [D^e] \; \{\partial\bar{\sigma}/\partial\sigma\}} \; d\{\varepsilon\} = [W] \; d\{\varepsilon\} \tag{2.25}$$

An incremental stress-strain relationship analogous to Hook's law but valid beyond the proportional limit, is obtained by substitution of Eq. (2.25) into Eq. (2.23) and the result into Eq. (2.24)

$$d\{\sigma\} = ([D^e] - [D^e] \; \{\partial\bar{\sigma}/\partial\sigma\} \; [W])d\{\varepsilon\} = ([D^e] - [D^p]) \; d\{\varepsilon\} = [D^{ep}] \; d\{\varepsilon\} \tag{2.26}$$

where $[D^p] = [D^e]\{\partial\bar{\sigma}/\partial\sigma\}[W]$ is called plastic stress-strain matrix. $[D^{ep}] = [D^e] - [D^p]$ is called the elastic-plastic stress-strain matrix and examination of the matrices involved has shown that $[D^{ep}]$ is symmetric. Eqs. (2.25) and (2.26) are both valid for elastic-perfectly plastic materials, as nothing in the derivation becomes indefinite if H' = 0. Matrix $[D^{ep}]$ is a 6 by 6 matrix and Yamada (47) expressed it in a very simple and closed form ready to be implemented in computer programs.

$$[D^{ep}] = \frac{E}{1+\nu}\begin{bmatrix}
\frac{1-\nu}{1-2\nu} - \frac{\sigma'^2_x}{s} & & & & & \text{symmetric} \\
\frac{\nu}{1-2\nu} - \frac{\sigma'_x\sigma'_y}{s} & \cdot & \frac{1-\nu}{1-2\nu} - \frac{\sigma'^2_y}{s} & & & \\
\frac{\nu}{1-2\nu} - \frac{\sigma'_x\sigma'_z}{s} & \cdot & \frac{\nu}{1-2\nu} - \frac{\sigma'_y\sigma'_z}{s} & \cdot & \frac{1-\nu}{1-2\nu} - \frac{\sigma'^2_z}{s} & \\
-\frac{\sigma'_x\tau_{xy}}{s} & \cdot & -\frac{\sigma'_y\tau_{xy}}{s} & \cdot & -\frac{\sigma'_z\tau_{xy}}{s} & \cdot \frac{1}{2} - \frac{\tau^2_{xy}}{s} \\
-\frac{\sigma'_x\tau_{yz}}{s} & \cdot & -\frac{\sigma'_y\tau_{yz}}{s} & \cdot & -\frac{\sigma'_z\tau_{yz}}{s} & \cdot -\frac{\tau_{xy}\tau_{yz}}{s} \cdot \frac{1}{2} - \frac{\tau^2_{yz}}{s} \\
-\frac{\sigma'_x\tau_{zx}}{s} & \cdot & -\frac{\sigma'_y\tau_{zx}}{s} & \cdot & -\frac{\sigma'_z\tau_{zx}}{s} & \cdot -\frac{\tau_{xy}\tau_{zx}}{s} \cdot -\frac{\tau_{xy}\tau_{zx}}{s} \cdot \frac{1}{2} - \frac{\tau^2_{zx}}{s}
\end{bmatrix} \qquad (2.27)$$

where $s = \frac{2}{3}\bar{\sigma}^2(1+\frac{H'}{3G})$ and G is the shear modulus. A form of $[D^{ep}]$ applicable to the axi-symmetric problem is obtained by deleting the two rows and two columns corresponding to ;

$$d\tau_{z\theta} = d\tau_{\theta r} = d\gamma_{z\theta} = d\gamma_{\theta r} = 0$$

2.4.4.2 Elastic-Plastic element stiffness matrix

On substituting Eqs. (2.26) and (2.4) into Eq. (2.16), Eq. (2.28) results.

$$d\{F\}^e = \left(\int [B]^T [D^{ep}][B]\, d(vol)\right) d\{\delta\}^e \qquad (2.28)$$

Eq. (2.28) is similar to Eq. (2.13) except for the use of $[D^{ep}]$ instead of $[D^e]$.

The $[k^{ep}] = \int [B]^T [D^{ep}][B]\, d(vol)$ is called the elastic-plastic element stiffness matrix, the value of $[D^{ep}]$ is calculated from Eq. (2.27). By writing Eq. (2.28) for every single element and assembling them together Eq. (2.29) applicable to the entire continuum will be obtained.

$$d\{F\} = \left(\int [B]^T [D^{ep}][B]\, d(vol)\right) d\{\delta\} = [K^{ep}]\, d\{\delta\} \qquad (2.29)$$

The term $[K^{ep}]$ is called the overall stiffness matrix or tangent stiffness matrix of the structure, the integral is taken over the entire continuum.

2.4.5 Elastic-plastic method of solution

The final solution to an elastic-plastic problem is obtained by solving Eq. (2.17). The equation is in an incremental form and

is valid only for infinitesimal strains. The complete solution to an elastic-plastic problem has to be carried out in a step by step method.

Depending on how the value of $d\{\sigma\}$ is substituted in Eq. (2.17) different approaches of solution will be obtained.

2.4.5.1 Incremental tangential method

By applying load in increments and following the plastic action as it develops, one may properly account for the path-dependent nature of plasticity. In section 2.4.4.2 it was shown that the equilibrium equation of the system can be written in the form $d\{F\} = [K^{ep}]\, d\{\delta\}$, where $[K^{ep}]$ depends on the current state of stresses within the elements.

In each load increment the value of $[K^{ep}]$ can be assumed constant and is built according to the state of stresses within the elements prior to load increments. By knowing the value of $[K^{ep}]$ and load increments the nodal point displacements can be determined.

A typical step of the solution is described with the aid of Fig. 2.3 which is a single degree of freedom problem.

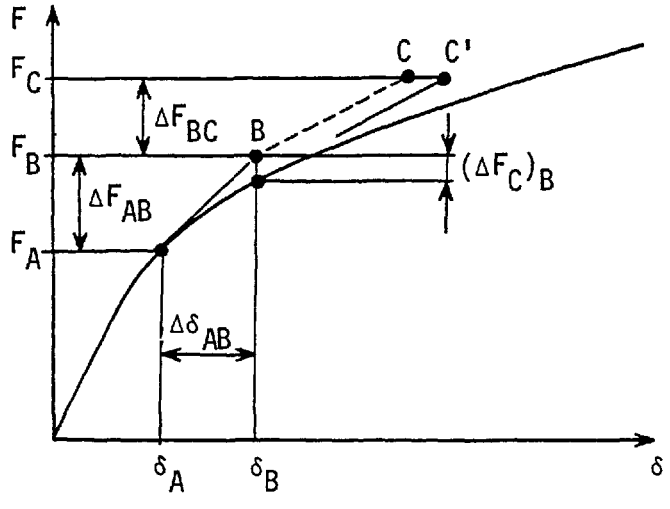

Fig. 2-3.

If under loads $\{F\}_A$, the correct displacement $\{\delta\}_A$ and structure tangent stiffness matrix $[K^{ep}]_A$ are known, the displacements produced by the next load increment are computed as:

$$[K^{ep}]_A \, \Delta\{\delta\}_{AB} = \Delta\{F\}_{AB} = \{F\}_B - \{F\}_A \tag{2.30}$$
$$\{\delta\}_B = \{\delta\}_A + \Delta\{\delta\}_{AB}$$

stresses, strains and tangent stiffness matrix must now be updated. Displacements of each element are extracted from $\Delta\{\delta\}_{AB}$. Using the updated values the appropriate $[D^{ep}]_B$ for each sampling point (for the centroid in the case of triangular elements) is found. The elastic-plastic tangent stiffness matrix of an element is evaluated in the usual way:

$$[k^{ep}] = \int_{Element\ volume} [B]^T \, [D^{ep}] \, [B] \; d(vol)$$

Upon reaching F_B in Fig. 2-3, the computed displacement $\{\delta\}_B$ is smaller than the actual amount of displacement, hence the resulting stresses will be smaller than the amount required to resist the applied load F_B. If a 'corrective' load ΔF_c were added to ΔF, the computed $\{\delta\}_B$ would be larger and closer to the correct value. Load ΔF_c plays the role of an unbalanced force which is the difference between applied loads and resistance produced by distorted elements. This resistance is evaluated from the term $\{\sigma_o\}$ of Eq. (2.12) with $\{\sigma_o\}$ now regarded as the total accumulated stress $\{\sigma\}$ in the element. Therefore, in general

$$\{\Delta F_c\} = \{F\} - \Sigma \int [B]^T \, \{\sigma\} \; d(vol)$$

where the summation extends over all elements of the structure. Force $\{F\}$ and stresses $\{\sigma\}$ are those at the end of a step. Correction force $\{\Delta F_c\}$ is applied in the subsequent step. For example, equations for the step from point B in Fig. 2-3 are,

$$[K^{ep}]_B \Delta\{\delta\}_{BC} = \Delta\{F\}_{BC} + \{\Delta F_c\}_B \tag{2.31}$$

In this way the point C' will be obtained instead of point C which is closer to the real solution. If the correction load is not considered, the final answer drifts from the actual curve as the load increment increases. The drift can be minimized by making the load increments as small as possible.

2.4.5.2 Initial stress method

As correction load $\{\Delta F_C\}$ serves to return drifting values to the proper path, it is not essential that the tangent stiffness matrix be used within a step of load $\Delta\{F\}$, Fig. 2-4.

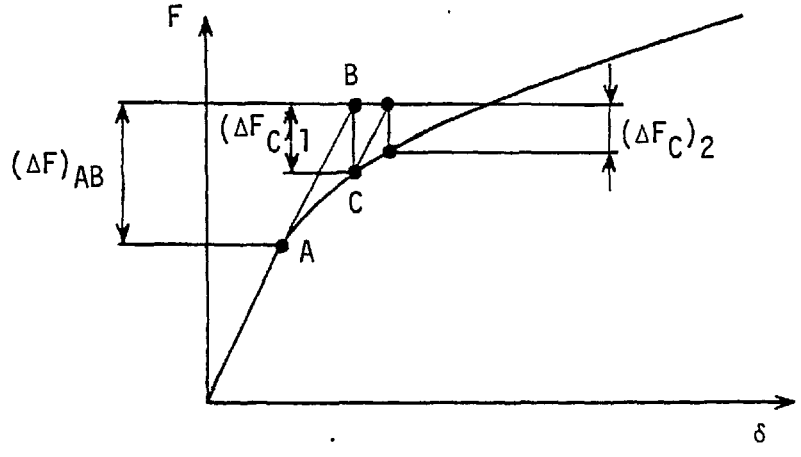

Fig. 2-4.

Indeed, the original, elastic structure stiffness matrix may be used in all loading steps. This approach of solution is called initial

stress method. Iteration within each step is mandatory, as computed points such as B in Fig. 2-4 are far from the correct path. The 'initial stress' method converges rapidly only when non-linearity is mild thus making a tangent modulus method preferable when large areas have yielded. The sequence and the formulation for the initial stress method is given in the following.

Eq. 2-26 can be written as:

$$d\{\sigma\} = [D^{ep}]\ d\{\varepsilon\} = ([D^{e}] - [D^{p}])\ d\{\varepsilon\}$$

The term $[D^{e}]\ d\{\varepsilon\}$ is denoted by $d\{\sigma\}^{e}$ and $[D^{p}]\ d\{\varepsilon\}$ by $d\{\sigma^{p}\}$ so

$$d\{\sigma\} = d\{\sigma^{e}\} - d\{\sigma^{p}\} \tag{2.32}$$

The value of $d\{\sigma\}$ is substituted into Eq. (2.17) and using Eq. (2.4)

$$d\{F\} = \int [B]^{T}\ (d\{\sigma^{e}\} - d\{\sigma^{p}\})\ d(vol)$$

$$d\{F\} = \left(\int [B]^{T}\ [D^{e}][B]\ d(vol)\right)\ d\{\delta\} - \int [B]^{T}\ d\{\sigma^{p}\}\ d(vol)$$

so

$$d\{F\} = [K^{e}]\ d\{\delta\} - \int [B]^{T}\ d\{\sigma^{p}\}\ d(vol) \tag{2.33}$$

The term $\int [B]^{T}\ d\{\sigma^{p}\}\ d(vol)$ is denoted by $\{\Delta p\}$

$$\{\Delta p\} = \int [B]^{T}\ d\{\sigma^{p}\}\ d(vol) \tag{2.34}$$

Eq. (2.33)can be written:

$$d\{F\} = [K^{e}]\ d\{\delta\} - \{\Delta p\}$$

or:

$$[K^e]^{-1} \cdot (d\{F\} + \{\Delta p\}) = d\{\delta\} \tag{2.35}$$

To solve Eq. (2.35) an iterative method is required. The following sequence is followed:

1) Assume $\{\Delta p\}_1 = 0$ and from Eq. (2.35) calculate $d\{\delta\}_o$

$d\{\delta\}_o \quad [K^e]^{-1} \, d\{F\}$

2) Using Eq. (2.4) calculate $d\{\varepsilon\}_o$

3) Calculate $d\{\sigma^e\}_o = [D^e] \, d\{\varepsilon\}_o$ and $d\{\sigma^p\}_o = [D^p]_1 \, d\{\varepsilon\}_o$ and so $d\{\sigma\}_o = d\{\sigma^e\}_o - d\{\sigma^p\}_o$

The total stress is $\{\sigma\}_2 = \{\sigma\}_1 + d\{\sigma\}_o$

4) Knowing the $d\{\sigma^p\}_o$ calculate $\{\Delta p\}_2$ from Eq. (2.34)

5) From Eq. (2.35), using the new value of $\{\Delta p\}_2$ calculate the new value for $d\{\delta\}$

6) Steps 2 to 5 are repeated until the required accuracy is obtained.

2.4.5.3 Initial strain method

The initial strain method is very similar to the initial stress method. The difference between the initial stress and initial strain approaches is perhaps best illustrated diagramatically. In Fig. 2-5 the stress-strain level reached by the first solution is shown as point 1. In the initial stress process the stresses are brought down to the correct level by introducing an initial stress $\{d\sigma\}_o$ while with the initial strain process the strains are adjusted by a correction $\{d\varepsilon\}_o$.

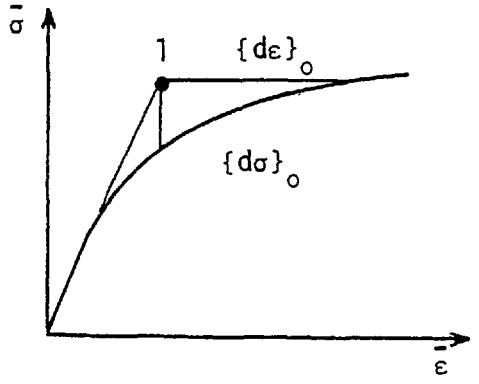

Fig. 2-5.

The formulation and sequence of the procedure which can be implemented in the computer program is given below.

The value of $d\bar{\varepsilon}^p$ in section 2.4.4 was found to be equal to:

$$d\bar{\varepsilon}^p = \frac{1}{\bar{H}'} \{\frac{\partial\bar{\sigma}}{\partial\sigma}\}^T d\{\sigma\}$$

From Eq. (2.23) the value of $d\bar{\varepsilon}^p$ is substituted into the above equation:

$$d\{\varepsilon^p\} = \frac{1}{H'} \{\frac{\partial\bar{\sigma}}{\partial\sigma}\} \{\frac{\partial\bar{\sigma}}{\partial\sigma}\}^T d\{\sigma\} \qquad (2.36)$$

using Eq. (2.36) the following equation can be written, see also Fig. 2-4.

$$d\{\sigma\} = [D^e]\, d\{\varepsilon^e\} = [D^e](d\{\varepsilon\} - d\{\varepsilon^p\}) \qquad (2.37)$$

substituting Eq. (2.37) into Eq. (2.17)

$$d\{F\} = [K^e]\, d\{\delta\} - \int [B]^T\, [D^e]\, d\{\varepsilon^p\}\, d(vol) \qquad (2.38)$$

$$\{dp\} = \int [B]^T \, [D^e] \, d\{\varepsilon^p\} \, d(vol) \tag{2.39}$$

$$d\{F\} = [K^e] \, d\{\delta\} - \{dp\} \qquad or:$$

$$[K^e]^{-1} \, (d\{F\} + \{dp\}) = d\{\delta\} \tag{2.40}$$

As the value of $\{dp\}$ and $d\{\delta\}$ are unknown to solve Eq. (2.40) an iterative method is needed, the following sequence can be employed.

1) Assume the stress increments $d\{\sigma\}$
2) Calculate $d\{\varepsilon^p\}$ from Eq. (2.36)
3) Compute $\{dp\}$ from Eq. (2.39)
4) Compute $d\{\delta\}$ from Eq. (2.40)
5) Calculate total strain increment $d\{\varepsilon\}$ from Eq. (2.4)
6) Calculate stress increment using Eq. (2.26) $d\{\sigma\} = [D^{ep}] \, d\{\varepsilon\}$
7) Repeat steps 2 to 6 until required accuracy is obtained.

2.4.6 Elements used in computer programs

Two types of ring elements were employed in the computer programs, simple triangular elements and quadrilateral isoparametric elements. In section 2.4.7 the required definitions and calculations for triangular ring elements will be given. Most of the definitions and calculations for triangular elements and quadrilateral isoparametric elements are the same. The main differences between the two elements will be given separately in section 2.4.8.

2.4.7 Axi-symmetric stress analysis

The strains, stresses, elasticity matrix, plasticity matrix and

element stiffness matrix in the axi-symmetric case are given.

2.4.7.1 Displacement function(triangular elements)

Fig. 2-6 shows the typical triangular element considered, with nodes i, j and m numbered in an anti-clockwise order. The displacements of a node have two components.

$$\{\delta i\} = \begin{Bmatrix} ui \\ vi \end{Bmatrix} \tag{2.41}$$

The six components of element displacement are listed as a vector

$$\{\delta\}^e = \begin{Bmatrix} \delta i \\ \delta j \\ \delta m \end{Bmatrix} \tag{2.42}$$

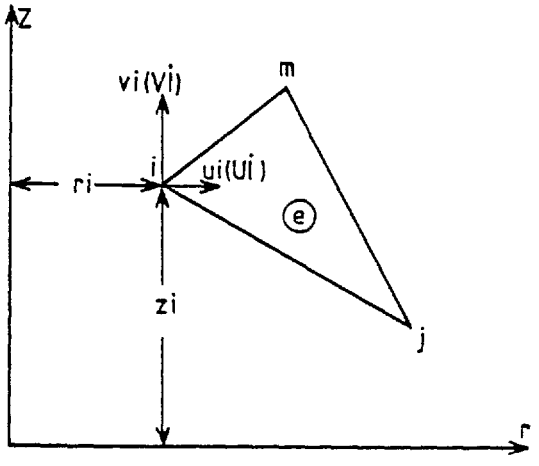

Fig. 2-6.

The displacement within an element has to be uniquely defined by these six values. The simplest representation is clearly given by two linear polynomials

$$\begin{aligned} u &= \alpha 1 + \alpha 2 r + \alpha 3 z \\ v &= \alpha 4 + \alpha 5 r + \alpha 6 z \end{aligned} \tag{2.43}$$

the six constants α can be evaluated easily by solving the two sets of three simultaneous equations which will arise if the nodal co-ordinates are inserted and the displacements equated to the appropriate nodal displacements. Writing, for example

$$\begin{aligned} u_i &= \alpha 1 + \alpha 2 r_i + \alpha 3 z_i \\ u_j &= \alpha 1 + \alpha 2 r_j + \alpha 3 z_j \\ u_m &= \alpha 1 + \alpha 2 r_m + \alpha 3 z_m \end{aligned} \tag{2.44}$$

If Eqs. (2.44) are solved for $\alpha 1$, $\alpha 2$ and $\alpha 3$ in terms of nodal displacement u_i, u_j, u_m and then substituted into Eqs. (2.43) the following is obtained.

$$u = \frac{1}{2\Delta}\{(a_i + b_i r + c_i z)\, u_i + (a_j + b_j r + c_j z)\, u_j + (a_m + b_m r + c_m z)\, u_m\} \tag{2.45}$$

in which

$$\begin{aligned} a_i &= r_j z_m - r_m z_j \\ b_i &= z_j - z_m = z_{jm} \\ c_i &= r_m - r_j = r_{mj} \end{aligned} \tag{2.46}$$

a similar expression is obtained for v.

$$v = \frac{1}{2\Delta}\{(a_i + b_i r + c_i z)\, v_i + (a_j + b_j r + c_j z)\, v_j + (a_m + b_m r + c_m z)\, v_m\} \tag{2.47}$$

Eqs. (2.45) and (2.47) can be represented in the form of

$$\{f\} = \begin{Bmatrix} u \\ v \end{Bmatrix} = [N]\{\delta\} = [IN'_i,\ IN'_j, IN'_m]\ \{\delta\}^e \tag{2.48}$$

with I a two by two identity matrix, and

$$N_i' = (ai + bir + ciz)/2\Delta \qquad \text{etc.} \tag{2.49}$$

2.4.7.2 Strains

In the case of an axi-symmetric problem four components of strain must be considered. Fig. 2-7 illustrates these strains and the associated stresses.

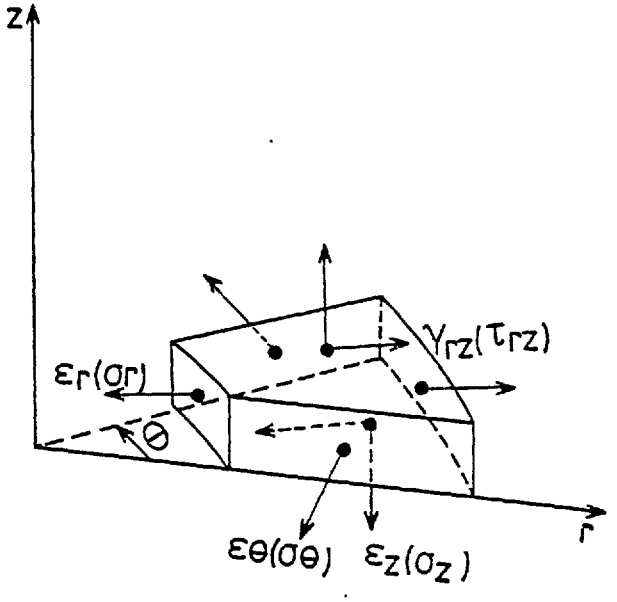

Fig. 2-7.

The strain components involved are listed below in terms of the displacement of a point.

$$\{\varepsilon\} = \begin{Bmatrix} \varepsilon_z \\ \varepsilon_r \\ \varepsilon_\theta \\ \gamma_{rz} \end{Bmatrix} = \begin{Bmatrix} \dfrac{\partial v}{\partial z} \\ \dfrac{\partial u}{\partial r} \\ \dfrac{u}{r} \\ \dfrac{\partial u}{\partial z} + \dfrac{\partial v}{\partial r} \end{Bmatrix} \tag{2.50}$$

using the displacement functions defined by Eqs. (2.43) and (2.44)

$$\{\varepsilon\} = [B]\ \{\delta\}^e = [Bi,\ Bj,\ Bm]\ \{\delta\}^e$$

in which

$$[Bi] = \begin{bmatrix} 0 & \dfrac{\partial N_i'}{\partial z} \\ \dfrac{\partial N_i'}{\partial r} & 0 \\ \dfrac{1}{r} N_i' & 0 \\ \dfrac{\partial N_i'}{\partial z} & \dfrac{\partial N_i'}{\partial r} \end{bmatrix} = \frac{1}{2\Delta} \begin{bmatrix} 0 & ci \\ bi & 0 \\ \dfrac{ai}{r} + bi + \dfrac{ciz}{r} & 0 \\ ci & bi \end{bmatrix} \quad \text{etc.} \qquad (2.51)$$

As the B matrix involves the co-ordinate r and z, the strains are not constant within an element which is in contrast to the plane stress and plane strain cases.

2.4.7.3 Elasticity matrix

The elasticity matrix $[D^e]$ links the strains $\{\varepsilon\}$ and the stresses $\{\sigma\}$ in the standard form

$$\{\sigma\} = \begin{Bmatrix} \sigma_z \\ \sigma_r \\ \sigma_\theta \\ \tau_{rz} \end{Bmatrix} = [D^e]\ (\{\varepsilon\} - \{\varepsilon_0\})$$

The stress-strain relationships for the axi-symmetric case are

$$\varepsilon_z = \frac{\sigma_z}{E} - \frac{\nu\sigma_r}{E} - \frac{\nu\sigma_\theta}{E}$$

$$\varepsilon_r = -\frac{\nu\sigma_z}{E} + \frac{\sigma_r}{E} - \frac{\nu\sigma_\theta}{E}$$

$$\varepsilon_\theta = -\frac{\nu\sigma_z}{E} - \frac{\nu\sigma_r}{E} + \frac{\sigma_\theta}{E}$$

$$\gamma_{rz} = \frac{\tau_{rz}}{G}$$

on solving for the stresses

$$\begin{Bmatrix} \sigma_z \\ \sigma_r \\ \sigma_\theta \\ \tau_{rz} \end{Bmatrix} = \frac{E(1-\nu)}{(1+\nu)(1-2\nu)} \begin{bmatrix} 1 & \frac{\nu}{1-\nu} & \frac{\nu}{1-\nu} & 0 \\ & 1 & \frac{\nu}{1-\nu} & 0 \\ & & 1 & 0 \\ \text{Symmetric} & & & \frac{1-2\nu}{2(1-\nu)} \end{bmatrix} \begin{Bmatrix} \varepsilon_z \\ \varepsilon_r \\ \varepsilon_\theta \\ \gamma_{rz} \end{Bmatrix} \quad (2.52)$$

so

$$[D^e] = \frac{E(1-\nu)}{(1+\nu)(1-2\nu)} \begin{bmatrix} 1 & \frac{\nu}{1-\nu} & \frac{\nu}{1-\nu} & 0 \\ & 1 & \frac{\nu}{1-\nu} & 0 \\ & & 1 & 0 \\ \text{Symmetric} & & & \frac{1-2\nu}{2(1-\nu)} \end{bmatrix} \quad (2.53)$$

2.4.7.4 Plasticity matrix

As was mentioned previously in section 2.4.4.1 the plasticity matrix can be obtained for an axi-symmetric case by deleting the two rows and two columns corresponding to:

$$d\tau_{z\theta} = d\tau_{\theta r} = d\gamma_{z\theta} = d\gamma_{\theta r} = 0$$

in Eq. (2.27), so

$$[D^{ep}] = \frac{E}{1-\nu}\begin{bmatrix} \frac{1-\nu}{1-2\nu} - \frac{\sigma_r'^2}{s} & & & \textit{Symmetric} \\ \frac{\nu}{1-2\nu} - \frac{\sigma_r'\sigma_z'}{s} & \frac{1-\nu}{1-2\nu} - \frac{\sigma_z'^2}{s} & & \\ \frac{\nu}{1-2\nu} - \frac{\sigma_r'\sigma_\theta'}{s} & \frac{\nu}{1-2\nu} - \frac{\sigma_z'\sigma_\theta'}{s} & \frac{1-\nu}{1-2\nu} - \frac{\sigma_\theta'^2}{s} & \\ -\frac{\sigma_r'\tau_{rz}}{s} & -\frac{\sigma_z'\tau_{rz}}{s} & -\frac{\sigma_\theta'\tau_{rz}}{s} & \frac{1}{2} - \frac{\tau_{rz}^2}{s} \end{bmatrix} \tag{2.54}$$

2.4.7.5 Element stiffness matrix

The element stiffness matrix can now be computed according to the following equations.

$$[k]^e = 2\pi \int [B]^T [D^e] [B]\, r\, dr\, dz \qquad \textit{For elastic elements} \qquad (2.55a)$$

$$[k^{ep}] = 2\pi \int [B]^T [D^{ep}] [B]\, r\, dr\, dz \qquad \textit{For plastic elements} \qquad (2.55b)$$

The volume integral has to be taken over the whole ring of material, with $[B]$ given by Eq. (2.51) and $[D^e]$ and $[D^{ep}]$ by Eqs. (2.53) and (2.54) respectively. As the matrix $[B]$ depends on the co-ordinates the integral has to be evaluated either by numerical integration or by an explicit multiplication and term by term integration.

The simplest approximate procedure, in the case of triangular elements, is to evaluate $[B]$ for a centroidal point.

$$\bar{r} = (r_i + r_j + r_m)/3$$

$$\bar{z} = (z_i + z_j + z_m)/3$$

Then the element stiffness matrix can be approximated by

$$[k]^e = 2\pi [\bar{B}]^T [D^e] [\bar{B}]\, r\, AREA \qquad \textit{For elastic elements}$$

$$[k^{ep}] = 2\pi [\bar{B}]^T [D^{ep}] [\bar{B}]\, r\, AREA \qquad \textit{For plastic elements}$$

$[\bar{B}]$ indicates the value of $[B]$ at $r = \bar{r}$ and $z = \bar{z}$

with '*AREA*' being the area of a triangular element.

2.4.7.6 External nodal forces

In the case of an axi-symmetric problem the nodal forces represent the forces acting along the whole circumference of the circle forming the element 'node'. If $\bar{R}$ represents the radial component of force per unit length of the circumference of a node at a radius r, the external 'force' which will have to be introduced in the compuation is $2\pi r\bar{R}$. In the axial direction similarly the nodal force is represented by $2\pi r\bar{Z}$.

2.4.8 Isoparametric elements

2.4.8.1 Introduction

The displacement models must be continuous within the elements, and the displacements must be compatible between adjacent elements. The first part of this requirement is readily met by choosing polynomial models, which are inherently continuous. The second part implies that adjacent elements must deform without causing openings, overlaps or discontinuities between the elements. Inter-element compatibility cannot be satisfied unless the displacements along the side of an element depend only upon the displacement of the nodes occuring on that side.

Isoparametric elements are the kind of elements in which the displacements along any side of the element depends only upon nodal displacements occurring on that side when interpolation in natural co-ordinates is employed. The term isoparametric derives from use of the same interpolation functions to define the element shape as are used to define displacements within the element. Isoparametric elements have been used with great success in various problem areas. Linear elements have straight sides, but quadratic and higher order isoparametric

elements may have either straight or curved sides, which makes them very useful for modelling curved structures.

2.4.8.2 Formulation

Isoparametric elements are formulated using a natural co-ordinate system ξ-η, which is defined by element geometry and not by the element orientation in the global co-ordinate system. There is a relation between the two systems for each element of a specific structure, and this relation must be used in element formulation. Co-ordinates ξ-η are attached to the element and are scaled so that sides of a quadrilateral are defined by $\xi = -1$, $\xi = 1$, $\eta = -1$ and $\eta = 1$. A quadrilateral having eight degrees of freedom, namely u_i and v_i at each of four corner nodes i is shown in Fig. 2-8

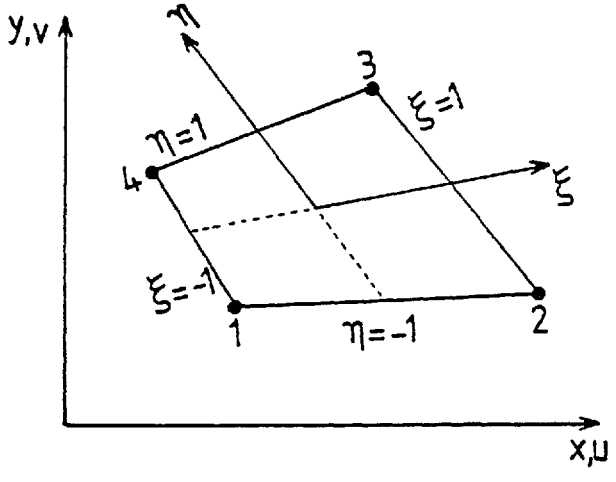

Fig. 2-8.

The mapping function is

$$\begin{Bmatrix} x \\ y \end{Bmatrix} = \begin{bmatrix} N_1 & 0 & N_2 & 0 & N_3 & 0 & N_4 & 0 \\ 0 & N_1 & 0 & N_2 & 0 & N_3 & 0 & N_4 \end{bmatrix} \begin{Bmatrix} x_1 \\ y_1 \\ x_2 \\ y_2 \\ x_3 \\ y_3 \\ x_4 \\ y_4 \end{Bmatrix} \qquad (2.56)$$

This mapping relates a unit square in isoparametric co-ordinates ξ-η to the quadrilateral in x-y co-ordinates whose size and shape are determined by the eight nodal co-ordinates x1, y1, x2, ..., y4. The mapping is also an interpolation scheme that yields the x-y co-ordinates of any point in the element when the corresponding ξ-η co-ordinates are given. Displacements within the element are defined by the same interpolation functions as used to define the element shape.

$$\{f\} = \begin{Bmatrix} u \\ v \end{Bmatrix} = [N] \begin{Bmatrix} u_1 \\ v_1 \\ \vdots \\ v_4 \end{Bmatrix} \tag{2.57}$$

where $[N]$ is the rectangular matrix of Eq. (2.56).

Eqs. (2.57) and (2.56) can be re-written in the forms

$$\begin{aligned} r &= \sum_1^4 N_i(\xi, \eta)\, r_i & z &= \sum_1^4 N_i(\xi, \eta)\, z_i \\ u &= \sum_1^4 N_i(\xi, \eta)\, u_i & v &= \sum_1^4 N_i(\xi, \eta)\, v_i \end{aligned} \tag{2.58}$$

The relation between derivatives in the two co-ordinate systems are established by the chain rule of differentiation.

$$\begin{Bmatrix} \frac{\partial(\ )}{\partial \xi} \\ \frac{\partial(\ )}{\partial \eta} \end{Bmatrix} = \begin{bmatrix} \frac{\partial r}{\partial \xi} & \frac{\partial z}{\partial \xi} \\ \frac{\partial r}{\partial \eta} & \frac{\partial z}{\partial \eta} \end{bmatrix} \begin{Bmatrix} \frac{\partial(\ )}{\partial r} \\ \frac{\partial(\ )}{\partial z} \end{Bmatrix} = [J] \begin{Bmatrix} \frac{\partial(\ )}{\partial r} \\ \frac{\partial(\ )}{\partial z} \end{Bmatrix}$$

In the standard formulation of an axi-symmetric case the element stiffness matrix is given by

$$[k^e] = 2\pi \int [B]^T [D^e] [B]\ r\ dr\ dz \qquad \textit{For elastic elements}$$

$$[k^{ep}] = 2\pi \int [B]^T [D^{ep}] [B]\ r\ dr\ dz \qquad \textit{For plastic elements}$$

In which $[B]$ is the matrix defining the strains in terms of the nodal displacements and $[D^e]$ and $[D^{ep}]$ are the elasticity and plasticity matrices respectively which relate the stresses to strains. The strain matrix is given by

$$\{\varepsilon\} = [B]\{\delta\}^e = [B_i, B_j, B_m]\{\delta\}^e$$

in which

$$[B_i] = \begin{bmatrix} 0 & \dfrac{\partial N_i}{\partial z} \\ \dfrac{\partial N_i}{\partial r} & 0 \\ \dfrac{N_i}{r} & 0 \\ \dfrac{\partial N_i}{\partial z} & \dfrac{\partial N_i}{\partial r} \end{bmatrix}$$

As N_i is defined in terms of ξ and η it is necessary to change the derivatives to $\frac{\partial}{\partial r}$ and $\frac{\partial}{\partial z}$ noting that.

$$\begin{Bmatrix} \dfrac{\partial N_i}{\partial \xi} \\ \dfrac{\partial N_i}{\partial \eta} \end{Bmatrix} = \begin{bmatrix} \dfrac{\partial r}{\partial \xi} & \dfrac{\partial z}{\partial \xi} \\ \dfrac{\partial r}{\partial \eta} & \dfrac{\partial z}{\partial \eta} \end{bmatrix} \begin{Bmatrix} \dfrac{\partial N_i}{\partial r} \\ \dfrac{\partial N_i}{\partial z} \end{Bmatrix} = [J] \begin{Bmatrix} \dfrac{\partial N_i}{\partial r} \\ \dfrac{\partial N_i}{\partial z} \end{Bmatrix}$$

in which $[J]$ is the Jacobian matrix which can easily be evaluated by a numerical process, noting that

$$[J] = \begin{bmatrix} \frac{\partial N_1}{\partial \xi}, & \frac{\partial N_2}{\partial \xi}, \cdots\cdots \\ \frac{\partial N_1}{\partial \eta}, & \frac{\partial N_2}{\partial \eta}, \cdots\cdots \end{bmatrix} \begin{bmatrix} r_1 & z_1 \\ r_2 & z_2 \\ \vdots & \vdots \end{bmatrix}$$

and so shape function derivatives in respect of r and z will be

$$\frac{\partial N_i}{\partial r} = [1, \ 0][J]^{-1} \begin{bmatrix} \frac{\partial N_i}{\partial \xi} \\ \frac{\partial N_i}{\partial \eta} \end{bmatrix}$$

$$\frac{\partial N_i}{\partial z} = [0, \ 1][J]^{-1} \begin{bmatrix} \frac{\partial N_i}{\partial \xi} \\ \frac{\partial N_i}{\partial \eta} \end{bmatrix}$$

and thus the expression for $[B_i]$ can be calculated. The only further change required is to replace the element of area ($r \, dr \, dz$) using the relationship

$$r \, dr \, dz = r \, det[J] \, d\xi \, d\eta$$

and to change the limits of integration to - 1 and + 1

Actual integration will in general have to be performed numerically using, e.g, Gauss quadrature method.

CHAPTER 3

ELASTO-PLASTIC FINITE ELEMENT COMPUTER PROGRAMS

3.1 Introduction

Two computer programs have been developed in Fortran IV for the formulation presented in Chapter 2, Eq.(2.29), with the restrictions introduced in section 2.3.

A step by step incremental tangential method was employed for the solution of the non-linear equation(2.17)

$$d\{F\} = \int [B]^T \, d\{\sigma\} \, d(vol)$$

It was shown in Chapter 2 that for small increments of load the equilibrium equation of the system can be written as Eq.(2.29) in

$$d\{f\} = [K^{ep}] \, d\{\delta\}$$

which $[K^{ep}]$ depends on the current state of stress in the continuum. For small load increments $[K^{ep}]$ can be assumed constant during each loading step and so a set of N linear simultaneous equations is obtained.

In the first program triangular ring elements were used and in the second, quadrilateral isoparametric elements were used. The programs are basically the same but extra computations are necessary in the case of isoparametric elements.

A flow chart which applies to both programs is presented, following which the important points related to the programs will be given.

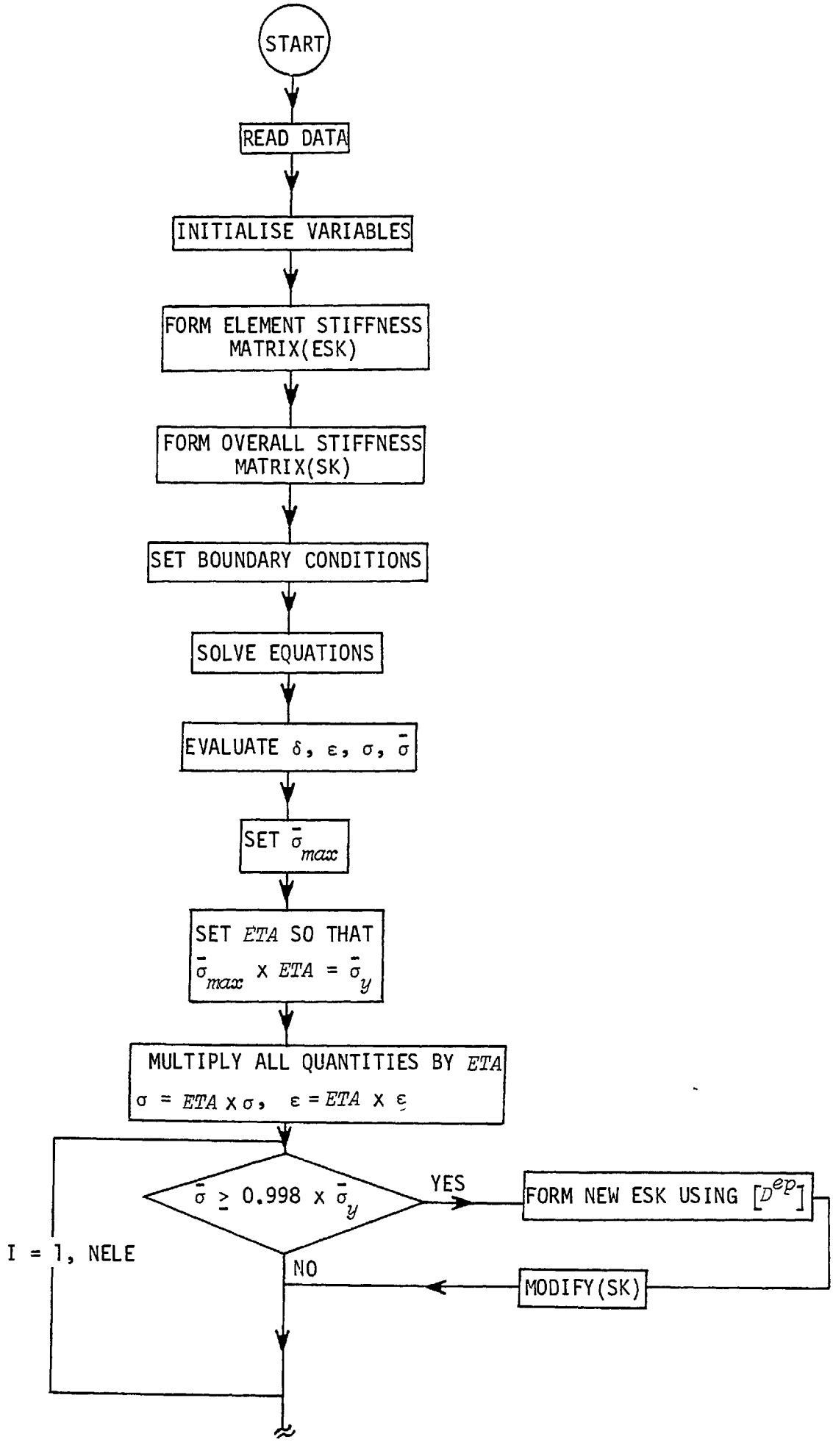
START
READ DATA
INITIALISE VARIABLES
FORM ELEMENT STIFFNESS MATRIX(ESK)
FORM OVERALL STIFFNESS MATRIX(SK)
SET BOUNDARY CONDITIONS
SOLVE EQUATIONS
EVALUATE δ, ε, σ, σ̄
SET σ̄max
SET ETA SO THAT σ̄max X ETA = σ̄y
MULTIPLY ALL QUANTITIES BY ETA
σ = ETA X σ, ε = ETA X ε
σ̄ ≥ 0.998 x σ̄y
YES
FORM NEW ESK USING [D^ep]
MODIFY(SK)
NO
I = 1, NELE

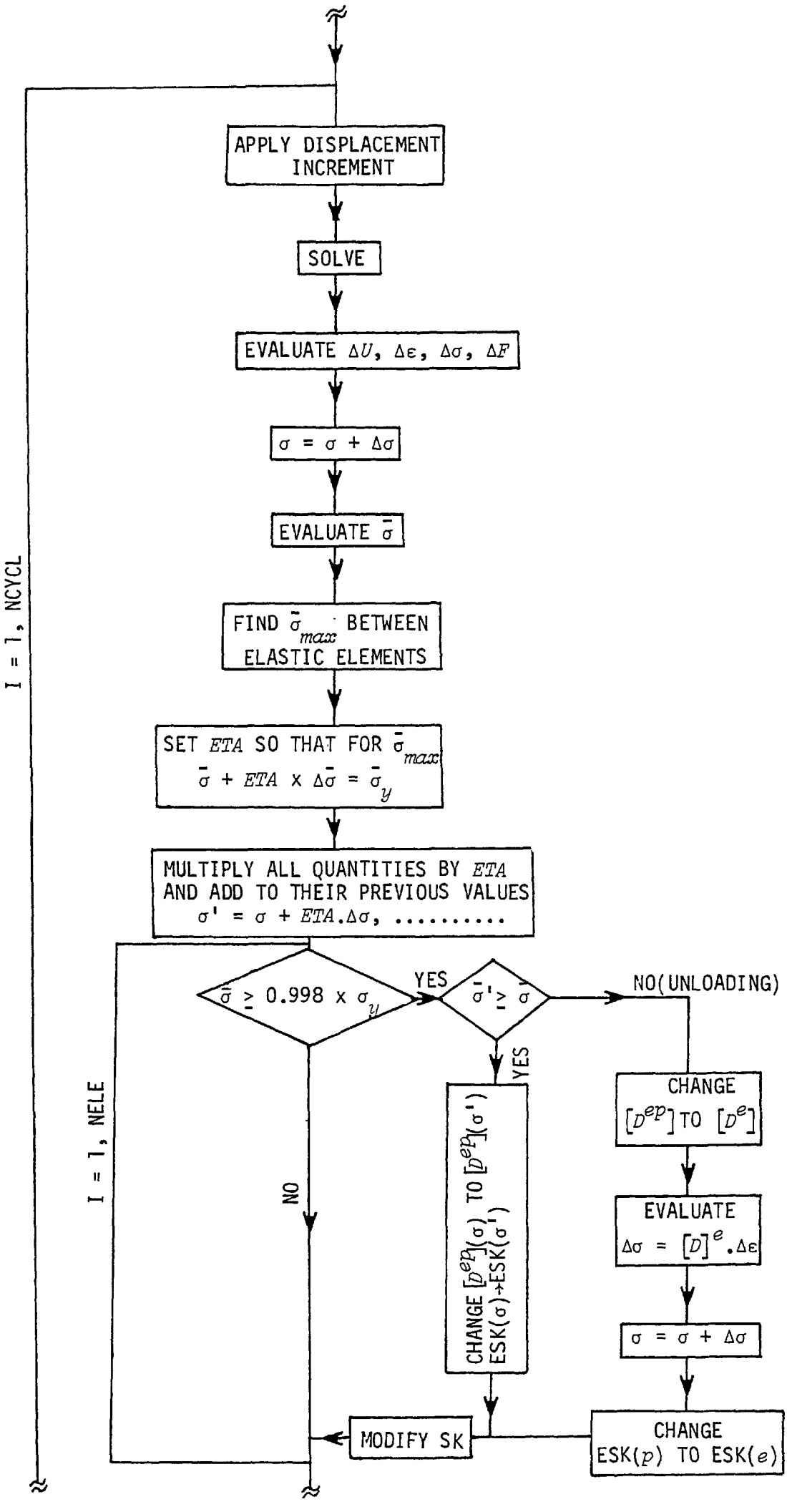
I = 1, NCYCL
APPLY DISPLACEMENT INCREMENT
SOLVE
EVALUATE ΔU, Δε, Δσ, ΔF
σ = σ + Δσ
EVALUATE σ̄
FIND σ̄max BETWEEN ELASTIC ELEMENTS
SET ETA SO THAT FOR σ̄max
σ̄ + ETA x Δσ̄ = σ̄y
MULTIPLY ALL QUANTITIES BY ETA AND ADD TO THEIR PREVIOUS VALUES
σ' = σ + ETA.Δσ, ...
I = 1, NELE
σ̄ ≥ 0.998 x σy
YES
σ'ij ≥ σij
NO(UNLOADING)
NO
YES
CHANGE [Dep](σ) TO [Dep](σ')
ESK(σ)→ESK(σ')
CHANGE [Dep] TO [De]
EVALUATE Δσ = [D]e.Δε
σ = σ + Δσ
MODIFY SK
CHANGE ESK(p) TO ESK(e)

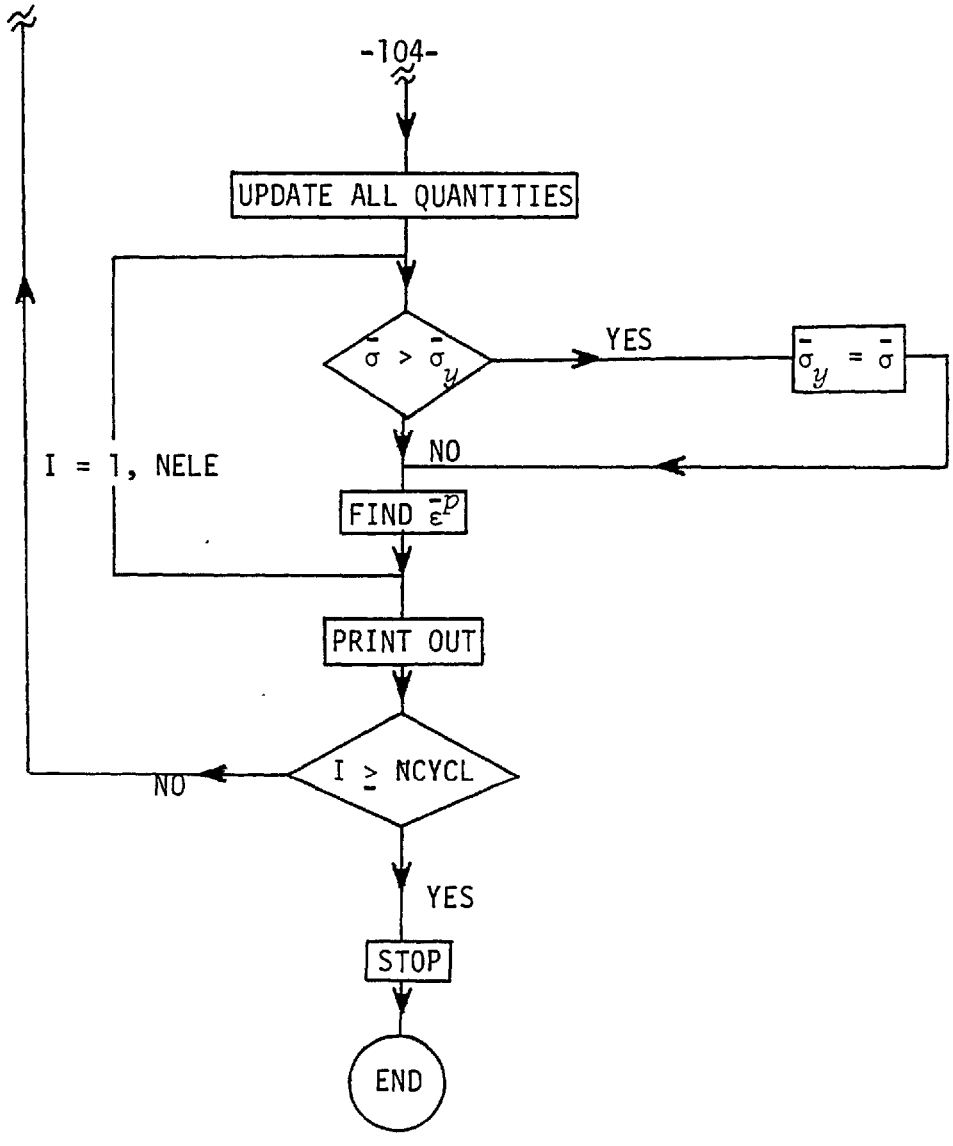
UPDATE ALL QUANTITIES
$\bar{\sigma} > \bar{\sigma}_y$
YES
$\bar{\sigma}_y = \bar{\sigma}$
NO
I = 1, NELE
FIND $\bar{\epsilon}^p$
PRINT OUT
I ≥ NCYCL
NO
YES
STOP
END

3.2 Finite element modelling of the fine blanking process

3.2.1 Introduction

In the theoretical analysis of fine blanking a constant input test displacement is chosen and introduced into the computer program at every new loading step until the desired punch penetration is obtained. At the end of each loading step some required conditions, which will be given later in this section, must be satisfied. In the case of failure to satisfy any of those conditions, the input displacement must accordingly be reduced, and the calculation for that cycle repeated, until all the conditions are satisfied at the end of the cycle. At this stage a new boundary condition must be defined so as the introduction of a fraction of input displacement does not contradict any of the conditions.

At the beginning of the analysis a boundary condition must be defined in such a way that none of the required conditions are denied at the end of the loading step. At further stages of the process the boundary condition will automatically be set by the computer program itself.

3.2.2 Punch and die

One alternative to simulation of the punch penetration at the start of the blanking process is to introduce an input displacement at the nodal points under the punch. In the actual process, due to the bending effect, higher displacements are observed at the nodal points nearer to the axis of symmetry than those further away from it, Fig. 3-1. Thus the introduction of equal displacements at these nodal points, as mentioned above, cannot realistically represent the actual process.

This simple boundary condition, however, can be used to arrive at a better assumption as will be explained in the following.

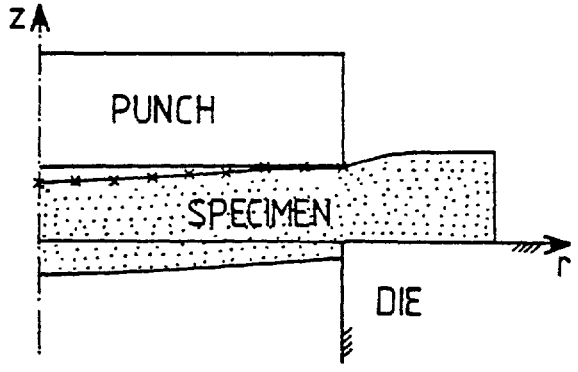

Fig. 3-1.

To distinguish between the nodal points that remain in contact with the punch and the ones that separate from it, an equal test displacement was applied at the nodal points under the punch and their corresponding nodal forces were calculated. The nodal points that remained in contact with the punch showed negative force, i.e. for these nodal points to undergo the same displacement as the punch they have to be forced downwards in the punch movement direction. The nodal points that tended to separate from the punch indicated a positive force, i.e. their extra displacement had to be suppressed by this positive force to keep them in touch with the punch surface.

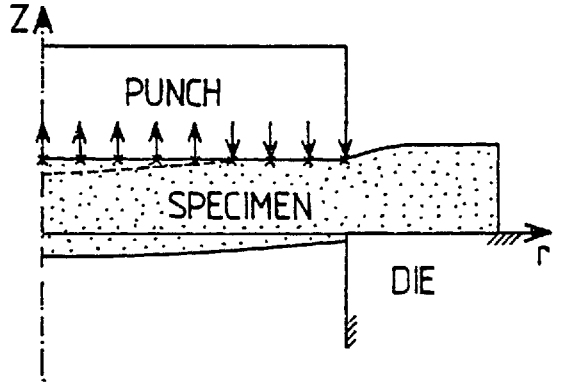

Fig. 3-2.

The positive forces indicate that if the correct boundary conditions had been chosen, the actual displacement of these nodal points would have a similar trend to that shown by the dotted line in Fig. 3-2.

It seemed that the correct boundary condition could be defined in the following manner. The nodal points showing negative force remain in contact with the punch whilst the ones displaying positive forces separate from it and can be assumed as free surfaces. However, the application of this boundary condition with triangular elements was found to be unsuccessful, as some of the nodal points which were considered as free surfaces underwent a displacement smaller than the punch penetration, which was contrary to the physical aspect of the problem, Fig. 3-3.

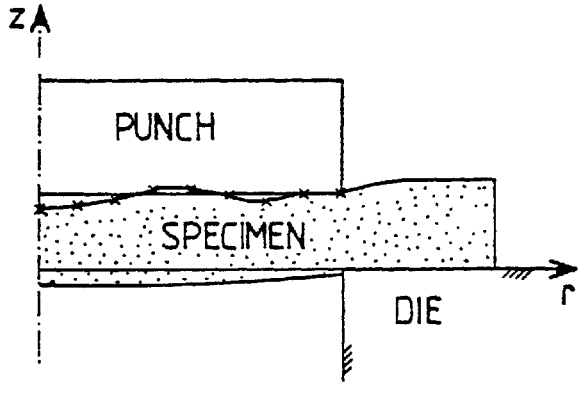

Fig. 3-3.

This difficulty was not observed when using isoparametric quadrilateral elements. In the case of triangular elements different boundary conditions were tried and the boundary condition in which the punch assumed to have only one contact point with the specimen, this being the nodal point under the punch edge, was found acceptable. All the nodal points under the punch showed displacements greater than the penetration of the punch and thus the boundary condition was not contradicted, Fig. 3-4.

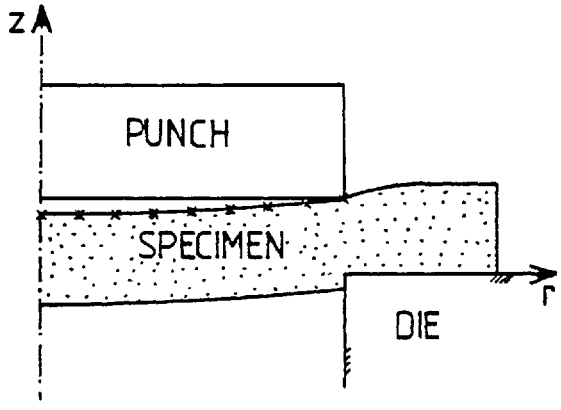

Fig. 3-4.

In the case of triangular elements it was found rather difficult to find a systematic way of defining the boundary condition, as some of the nodal points came into repeated contact with the punch and separated again from it. The use of a systematic approach in the case of the finite element mesh comprised of isoparametric quadrilateral elements was found to be successful.

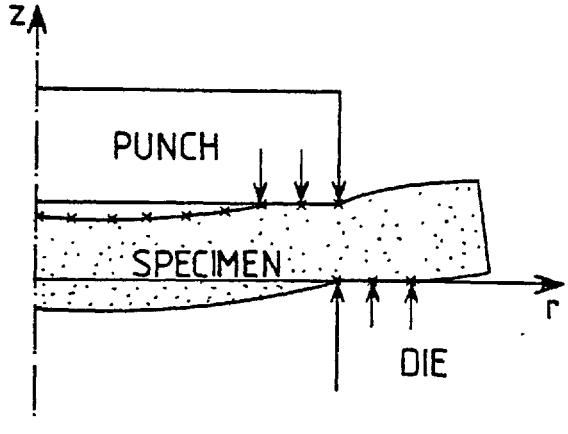

Fig. 3-5.

The nodal points under the punch and above the die are the only nodal points on the boundary surface of the material whose status of being either a 'free surface' or 'suppressed' must be continuously checked. This being due to the likelihood of these nodal points coming into contact with a surface or separating from a surface.

During the blanking process the following conditions must be checked so that none of them are contradicted, see also Fig. 3-5.

i) The axial load applied at the suppressed nodal points under the punch must be zero or negative.

ii) The absolute value of the displacement of the nodal points under the punch must be equal or greater than the punch penetration.

iii) The axial load applied at the suppressed nodal points above the die must be zero or positive.

iv) The displacement of the nodal points above the die must be zero or positive.

In assuming a boundary condition a test displacement is applied and the nodal points under the punch and above the die are checked for the conditions mentioned above and the proper boundary condition for the next loading step is set up. If, after applying an input test displacement, the above conditions at one or more nodal points are violated the value of input displacement must accordingly be reduced so that, at the end of the loading step, none of the required conditions are violated. It is obvious that to maximize the efficiency of the program, maximum permissible input displacement must be introduced into the program at each loading step.

After introducing the maximum allowable input displacement the boundary condition at the nodal point with the most critical condition

must be changed in such a way that under the application of a fraction of the input test displacement none of the aforementioned conditions at that point are violated. This point will be made more clear by considering an example given below.

The two nodal points i and $i+1$ of which the former is assumed to move with the punch and the latter being a free surface are considered, Fig. 3-6.

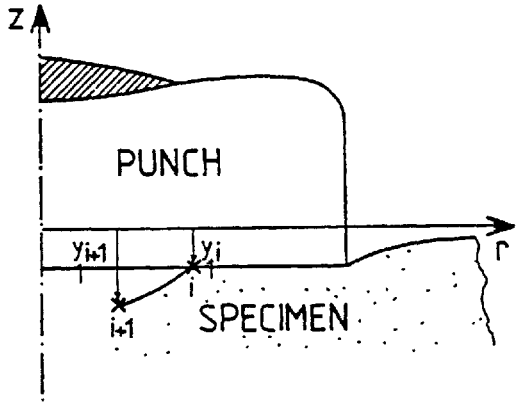

Fig. 3-6.

It is assumed that at this stage of the process a further introduction of an input test displacement will violate one of the above conditions, e.g. indicating a smaller displacement at the nodal point $i+1$ that the punch penetration, Fig. 3-7.

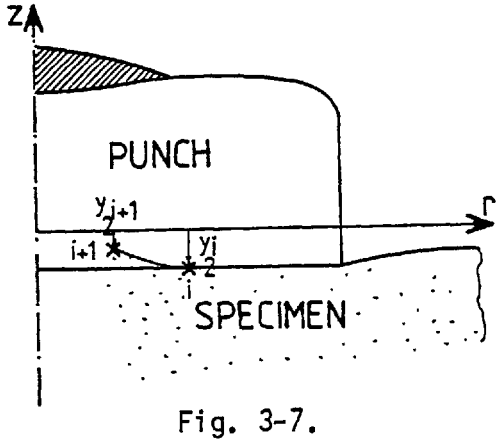

Fig. 3-7.

To overcome this problem instead of the application of the whole input test displacement, only a fraction of it, just sufficient to bring nodal points i and $i+1$ to the same level, is applied. At the end of this stage the state of the nodal point with critical condition is accordingly changed so that a further introduction of input displacement does not contradict any of the above mentioned conditions at this point.

For a small increment of displacement, as the calculation was assumed linear, it can be written :-

$$y_1 i + \lambda \, \Delta yi = y_1 i+1 + \lambda \, \Delta yi+1$$

$$\lambda \, (\Delta yi - \Delta yi+1) = y_1 i+1 - y_1 i$$

$$\text{thus } \lambda = \frac{y_1 i+1 - y_1 i}{\Delta yi - \Delta yi+1} \qquad (a)$$

where $y_1 i$ = *total displacement at node* i

" $y_1 i+1$ = " " " " $i+1$

" Δyi = *displacement increment at node* i *when applying input test displacement*

where $\Delta yi+1$ = *displacement increment at node* $i+1$ *when applying input test displacement*

λ = *rating factor*

The rating factor λ can be calculated from equation (a), and a new input test displacement equal to $\frac{1}{\lambda}$ x *input test displacement* instead of the previous one must be applied at this loading step. At the end of this stage the nodal points i and $i+1$ will be brought to the same

level. The boundary condition at node $i+1$ must now be changed from a free surface to a suppressed nodal point which will travel with the punch in further stages of the process. As was mentioned earlier all the nodal points under the punch and above the die must be checked for the violation of the conditions and upon this violation occuring the boundary condition at that point must be changed in a similar manner as mentioned above. It must be noted that the input test displacement must also be checked so that no element can pass its yield point without being first considered as a yielded element in that loading step.

To simulate the actual fine blanking process in a model applicable to the finite element program, the positions of punch and die with respect to one another, should be chosen in such a way as not only to maintain the required clearance between the punch and die but also uphold to some extent the actual nature of the shearing mode which occurs in the shearing zone.

To introduce a required clearance between the punch and the die, e.g. in Fig 3-8(a), the co-ordinates of the nodal points on the line AB are changed so that the difference in co-ordinates of points A and B becomes equal to the required clearance, Fig. 3-8(b).

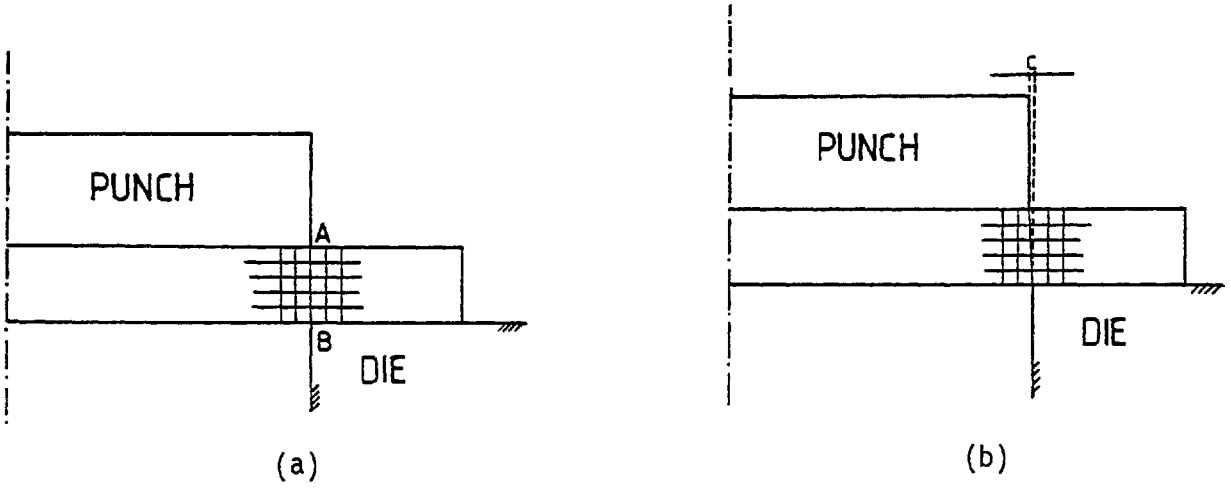

Fig. 3-8.

In the actual blanking operation the material on the left hand side proximity of the line AB actually moves (or shears) against the material on the line AB, Fig. 3-9.

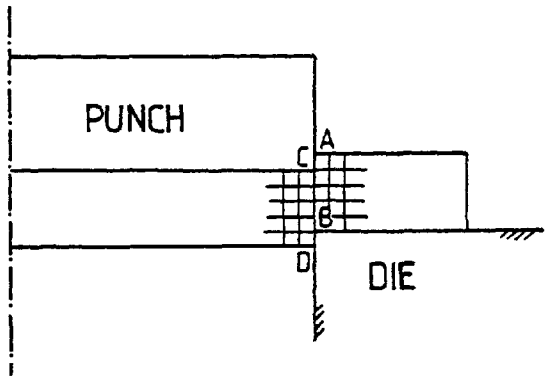

Fig. 3-9.

Since in the finite element method this discontinuity is not accounted for, it was decided to allow for the equal displacements of the corresponding nodal points on the line AB as on the line CD so that a configuration as shown in Fig. 3-10 would be obtained.

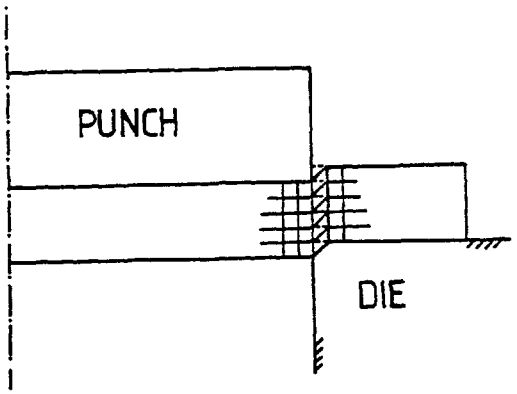

Fig. 3-10.

3.2.3 Blank-holder

The clamping of the material in the fine blanking operation must be modelled for the computer program in such a way as to meet the characteristics of the blank holder which is used in the actual process, these being compression of the material towards the centre and blocking the outward flow of material, Fig. 3-11.

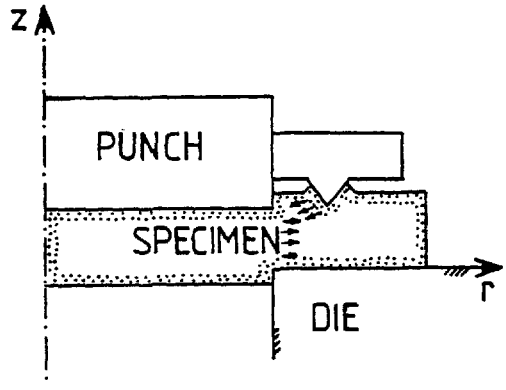

Fig. 3-11

One alternative to this simulation is the application of a concentrated load at the distance where the actual blank-holder acts in the real process, Fig. 3-12.

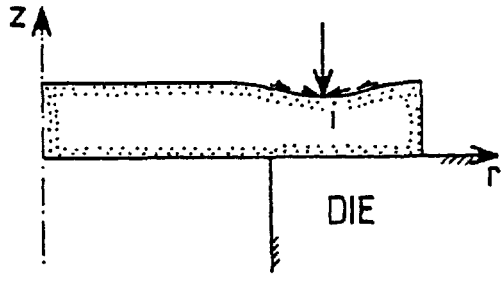

Fig. 3-12

The application of a concentrated load causes the nodal points on both sides of the line of action of the clamping force, near the material surface, to be drawn towards this line, thus producing a tensile state of stress near the surface of the material on each side. This model obviously cannot meet the requirements of compressive state of stress on both sides of the clamp and the blocking of the material flow during blanking.

A more realistic model which seemed to meet most of the features of the actual clamping operation is explained in the following. A mesh pattern was chosen to include a V-groove at the position where the clamping force was going to be applied. The projection of the blank-holder is assumed to be placed in the groove and is squeezed into the material, Fig. 3-13.

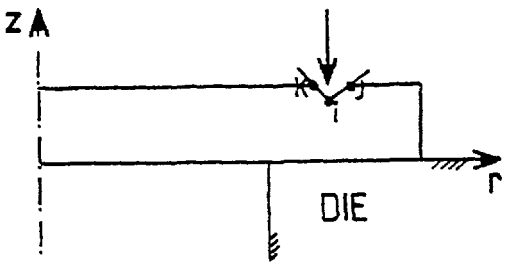

Fig. 3-13

It is assumed that the nodes k and j, Fig.3-13 can move only in the radial direction r and node i in the axial direction z.

To apply the boundary condition the blank-holder is assumed to move downwards as much as $\delta 1$, Fig. 3-14, then $\delta 2$ and $\delta 3$ are given by Eq. (3.1).

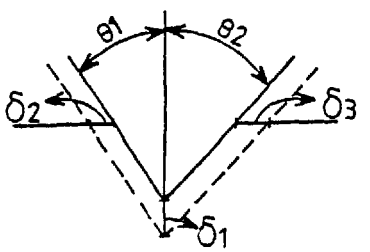

Fig. 3-14

$$\delta_2 = \delta_1 \tan\theta_1$$
$$\delta_3 = \delta_1 \tan\theta_2 \qquad (3.1)$$

By knowing the angles θ_1 and θ_2 (the angles between the edges of the blank-holder projection and the vertical line) the displacement δ_2 and δ_3 can be calculated in terms of δ_1.

3.2.4 Counter-punch

To introduce the back-load applied by the counter-punch to the specimen the following procedure was followed.

1) The specimen was assumed to be placed on a flat surface and the displacement of all nodal points of the specimen on this surface were suppressed in the r and z directions, Fig. 3-15(a).

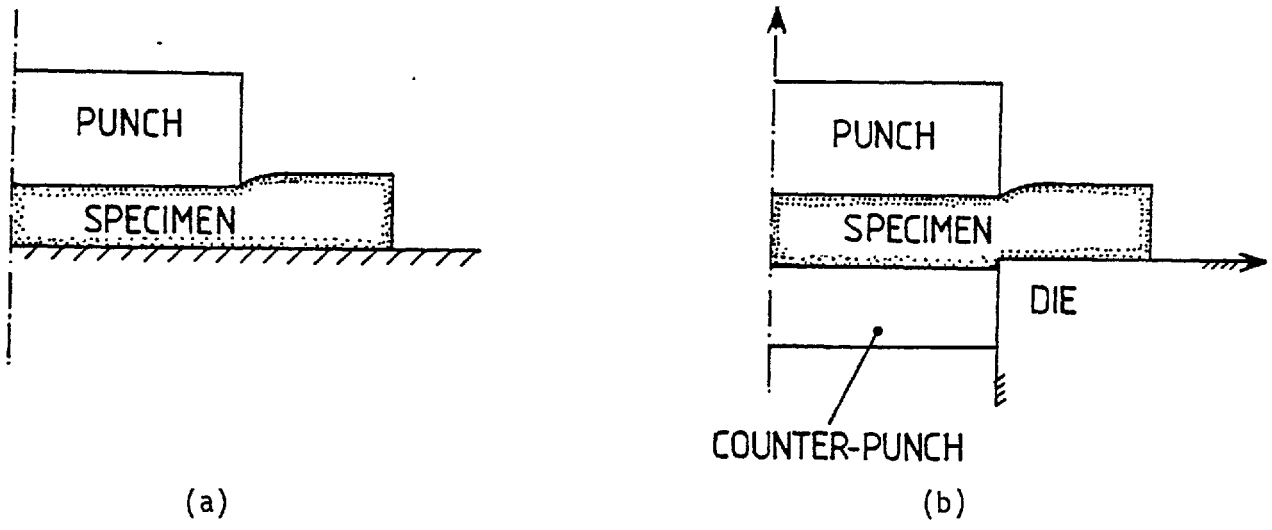

Fig. 3-15.

2) It was assumed that all the nodal points in contact with the punch at the beginning of the process would remain so until the end of the blanking operation. No contradiction to this assumption, in the results obtained from the computer program was observed during the blanking process.

3) The specimen was indented by the punch until the total load

applied to the nodal points on the counter-punch surface, Fig. 3-15(a), reached the prescribed back-load.

4) Hereafter the suppression on the displacement of the nodal points on the counter-punch surface was lifted and it was assumed that in further steps of the program these nodal points would carry the same constant load, Fig. 3-15(b).

3.3 Computer program sequences

The sequence of the computations made in the computer program can be summerized as follows:

1) Apply a unit punch displacement, assuming elastic behaviour, compute ΔU, ΔF, ε, σ and $\bar{\sigma}$

2) Find the element with maximum equivalent stress ($\bar{\sigma}_{max}$).

3) Calculate the rating factor according to $ETA = \bar{\sigma}_{max} / \bar{\sigma}_y$ where $\bar{\sigma}_y$ is the initial yield stress of the material.

4) Multiply all quantities by ETA to obtain the values corresponding to those at the elastic limit. The elements with $\bar{\sigma} \geq 0.998 \times \bar{\sigma}_y$ will be treated as yielded elements for the subsequent computations.

5) Appropriately modify $[D^e]$ and $[k^e]$ for post yielded elements to $[D^{ep}]$ and $[k^{ep}]$

6) Evaluate the current overall stiffness matrix of the structure (the post yielded elements depending on their level of stresses will have different stiffness matrices).

7) Apply an increment of punch displacement and compute the corresponding values of $\Delta\delta$, $\Delta\varepsilon$ and $\Delta\sigma$.

8) Add $\Delta\sigma$ to the previous σ and compute $\bar{\sigma}$ from the resulting σ .

9) Find the element with maximum $\bar{\sigma}$ among the remaining elastic

elements and calculate the rating factor *ETA* so that $ETA = \frac{\bar{\sigma}_y - \bar{\sigma}}{\Delta\bar{\sigma}}$

10) If *ETA* is larger than some prescribed value which limits the amount of input punch displacement, set *ETA* equal to the prescribed value.

11) Multiply $\Delta\delta$, ΔF, $\Delta\varepsilon$ and $\Delta\sigma$ by *ETA* and add to their previous values and calculate $\bar{\sigma}$ from the resulting σ. Also calculate $\Delta\bar{\varepsilon}$ from the resulting $\Delta\varepsilon$ and add to their previous values of $\bar{\varepsilon}$.

12) Check plastic elements for unloading, for unloading elements recalculate the element stress increments, using $[D^e]$ instead of $[D^{ep}]$ and add to the values from previous step.

13) For unloading elements change $[D^{ep}]$ to $[D^e]$ and $[k^{ep}]$ to $[k^e]$.

14) For plastic unloading elements change their yield point from $\bar{\sigma}_y$ to their current equivalent stress $\bar{\sigma}$.

15) Check if $\bar{\sigma}$ of any element remaining in the elastic state has reached 0.998 x $\bar{\sigma}_y$. The elements having $\bar{\sigma}$ equal to or larger than 0.998 x $\bar{\sigma}_y$ will be treated as yielded elements in the next step.

16) Repeat (7) through (15) until the desired level of punch penetration is obtained.

3.4 Introduction of the boundary conditions into the equilibrium equations

To introduce the boundary conditions into the set of N equations (equilibrium equations of the system) depending on whether load or displacement is known different procedures have to be used. The force boundary conditions are automatically taken care of by the load vector of Eq. (2.29)

$$d\{F\} = [K^{ep}]\, d\{\delta\}$$

thus for a free surface, the loading terms corresponding to the nodes on the boundary are zero.

The displacement boundary conditions are more difficult to handle. For a specified displacement the stiffness matrix together with the load vector have to be modified. In general, for ease of indexing, the size of the matrix should remain unchanged, i.e. no rows or columns of the matrix should be deleted. There are two approaches which may be applied at solution time in the application of boundary conditions. The two approaches are demonstrated in the following example. In a set of N equations, the value of δ_1 is prescribed and is equal to α.

$$\begin{bmatrix} K_{11} & K_{12} & \cdots & K_{1n} \\ K_{21} & K_{22} & \cdots & K_{2n} \\ \vdots & \vdots & & \vdots \\ K_{n1} & K_{n2} & \cdots & K_{nn} \end{bmatrix} \begin{Bmatrix} \delta_1 \\ \delta_2 \\ \vdots \\ \delta_n \end{Bmatrix} = \begin{Bmatrix} F_1 \\ F_2 \\ \vdots \\ F_n \end{Bmatrix}$$

In the first method, to apply the boundary condition the load column is modified as follows.

$$F_1' = \alpha, \text{ and } F_i' = F_i - K_{i1}\alpha (i = 2,N)$$

then the corresponding row and column of the matrix is designated zero and the diagonal term is made unity. In the special but common case of $\alpha = 0$ (i.e. fixed support), it is only necessary to modify the matrix as described above, leaving the load matrix unchanged except for $F_1' = 0$.

In the second method the appropriate diagonal term is multiplied by a large number, say, 10^8, and in the load column only the corresponding load coefficient is suitably modified. The modifications are shown below.

$$K'_{11} = K_{11} \times 10^8 \quad \text{and} \quad F'_1 = K_{11} \times 10^8 \times \alpha$$

These are the only modifications that have to be carried out when the displacement at a certain direction is known. This will yield a solution in which δ_1 is very nearly equal to α. The above procedure is suitable for all types of solution methods. The latter method is much easier to implement in computer programs than the former, and thus this method was used in both computer programs developed in this work to introduce the required boundary conditions into the equilibrium equations of the system.

3.5 Solution of the simultaneous equations

3.5.1 Introduction

All finite element analyses finally reduce to the solution of a large number of simultaneous equations. In the present analysis stepwise linearity is assumed for every load increment, giving rise to a set of linear equations. The methods commonly used to solve the simultaneous linear equations are given below.

3.5.2 Gauss elimination method

In this method the coefficient matrix is reduced to upper triangular form by successive elimination of the variables. Consider the set of N linear simultaneous equations.

$$\begin{bmatrix} K_{11} & K_{12} & \cdot & \cdot & \cdot & K_{1n} \\ \cdot & \cdot & & & & \cdot \\ \cdot & \cdot & & & & \cdot \\ K_{n1} & K_{n2} & \cdot & \cdot & \cdot & K_{nn} \end{bmatrix} \begin{Bmatrix} \delta_1 \\ \cdot \\ \cdot \\ \delta_n \end{Bmatrix} = \begin{Bmatrix} F_1 \\ \cdot \\ \cdot \\ F_n \end{Bmatrix}$$

The variable δ_1 is eliminated from the last (N - 1) equations by suitable operations with the first equation. The variable δ_2 is then eliminated from the last (N - 2) equations by suitable operations with the second equation, in its modified form with the coefficient of δ_1 equal to zero. The process is continued until the last equation is reached when the matrix has been reduced to upper triangular form. The right hand side of the equations are successively modified as the process continues and the unknowns are finally evaluated by a 'back substitution'.

3.5.3 Choleski method

In this method, the coefficient matrix is factorized in such a way that one of the factor matrices is upper triangular and the other lower triangular. Consider the system of equations

$$[K]\{\delta\} = \{F\} \tag{3.2}$$

considering only the case where $[K]$ is a symmetric matrix, it is possible to put

$$[K] = [U]^T[U] \tag{3.3}$$

in which $[U]$ is an upper triangular matrix. Substituting Eq. (3.3) in Eq. (3.2) will result in

$$[U]^T[U]\{\delta\} = \{F\}$$

assume

$$[U]\{\delta\} = \{Y\} \tag{3.4}$$

then

$$[U]^T\{Y\} = \{F\} \tag{3.5}$$

having found the upper triangular factor matrix $[U]$, the process consists of solving Eq. (3.5) for $\{Y\}$ and then solving Eq. (3.4) for $\{\delta\}$.

3.5.4 Gauss-seidel iterative method

In this method an initial guess of the nodal points displacements is made and an iterative approach is employed until the required degree of accuracy is obtained. To solve a set of N equations

$$\begin{bmatrix} K_{11} & K_{12} & \cdot & \cdot & \cdot & K_{1n} \\ K_{21} & K_{22} & \cdot & \cdot & \cdot & K_{2n} \\ \cdot & \cdot & \cdot & \cdot & \cdot & \cdot \\ \cdot & \cdot & \cdot & \cdot & \cdot & \cdot \\ K_{n1} & K_{n2} & & & & K_{nn} \end{bmatrix} \begin{Bmatrix} \delta_1 \\ \delta_2 \\ \cdot \\ \cdot \\ \delta_n \end{Bmatrix} = \begin{Bmatrix} F_1 \\ F_2 \\ \cdot \\ \cdot \\ F_n \end{Bmatrix}$$

the following procedure is followed.

1) Assume a set of initial values for displacements δ

2) Using the values $\delta_2, \ldots\ldots, \delta_n$ solve the first equaton for δ_1

3) Using the recent value of δ_1 and the values of $\delta_3, \ldots\ldots, \delta_n$ solve the second equation for δ_2 and so on.

4) After the completion of each cycle check for convergence

5) If the required degree of convergence is obtained stop the iteration, otherwise go back to 2 and continue.

The iteration can usually be accelerated for rapid convergence by the use of an over-relaxation factor. If the recent value for δ_i is denoted by U' and the old value by U'' , by using the over-relaxation factor the U_i value for next iteration cycle would be

$$U = U'' + F \times (U' - U'')$$

where F is the over-relaxation factor and it has been found that a value between 1.8 - 2.0 would be most suitable for most finite element problems. In practice the method seems to converge for most cases.

3.6 Remarks

The important factor for selecting a method is the computing time and the storage requirements. The two most commonly used methods are the Gauss-Seidel iterative method and the Gauss elimination method. In the early stages of non-linearity the former method converges rapidly and is faster than the latter method. However, as the non-linearity develops the coefficient matrix of the equations becomes more and more ill conditioned and more cycles of iteration are required for a prescribed accuracy. The number of cycles of iteration can be reduced if the right relaxation factor can be somehow determined. The use of the Gauss-Seidel iterative method for progressive non-linearities necessitates the development of a procedure for determining

the spontaneous relaxation factors. There is no assurance that the Gauss-Seidel iterative method will always converge. In addition an extra computing procedure to find the proper values of the relaxation factors makes the program more complicated.

With regard to the above considerations it was thus decided to use the Gauss elimination method with the cost of more computing time but with the assurance of obtaining results, with reasonably good accuracy and saving the development of methods for determinig relaxation factors.

3.7 Computer programs (elastic-plastic)

3.7.1 Using triangular elements

The input data are read in. The data consists of co-ordinates of nodal points, elements with their defining nodal numbers, material properties, number of elements, number of nodal points and nodal points on the boundary. A status vector POINTR was employed to specify the state of force and displacement in directions r and z at any nodal point.

POINTR(r, z)

0	displacement known
1	force known

The vector is used later in the program to introduce the boundary conditions into the set of N equations of the system. A status vector PL is also used to identify the state of stresses within the elements.

PL

0	elastic state of stress
1	plastic state of stress

This status vector will specify the use of $[D^e]$ or $[D^{ep}]$ at the time of forming the element stiffness matrices and calculating the stresses within the elements.

All the variables and variable increments are initialized and the boundary condition is set and a test displacement input is introduced at the appropriate boundary nodal points.

The elements are scanned and a call is made to subroutine BMATX, DMATX, DBE and ESTIF to calculate the element stiffness matrices. The calculated matrices are stored in array TSK for further calculations. The BMATX routine constructs the strain displacement matrix B and DMATX forms the stress strain relationship $[D^e]$ or $[D^{ep}]$. Routine DBE carries out the matrix multiplication $B^T DB$ which is used in routine ESTIF to calculate the element stiffness matrix. In the routine ESTIF the element area 'AREA' and the value of $\bar{r}$ (centroid co-ordinate) are evaluated and the multiplication $2\pi\ \bar{r}\ B^T D\ B\ AREA$ is carried out which yields the element stiffness matrix.

To form the overall stiffness matrix of the system elements are scanned and the stiffness matrices are added in turn to the appropriate locations of the overall stiffness matrix in accordance with the nodal numbers of the element in question. The overall stiffness matrix is a banded matrix. The set of N equations of the system are solved simultaneously for unknown values of displacement and loads, using Gauss elimination method in routine SOLVE.

Having found the nodal displacement from routine SOLVE, the element stresses can be calculated. Elements are scanned and a call is made to routine DMATX and BMATX, and matrix multiplication $[D][B]\{\delta\}$ is carried out to calculate the stresses within the elements. The

equivalent stresses within the elements are evaluated and the maximum value is determined.

In this method of solution the problem is assumed linear at each increment of displacement, so the increment of every variable at every step would be proportional to the input displacement. A rating factor ETA is defined to specify the required amount of input displacement to cause yield in the element with maximum $\bar{\sigma}$, $ETA = \bar{\sigma}_{max} / \bar{\sigma}_{y}$. All the variables are multiplied by rating factor ETA to give the value of different variables at the elastic limit (or first yield), the required variables are printed out.

The elements with $\bar{\sigma} \geq 0.998 \times \sigma_{y}$ will be considered plastic and will be treated as yielded elements hereafter. An increment of displacements are introduced at the appropriate boundary nodal points. As some of the elements have passed their elastic limits and are considered as post yielded elements, new element stiffness matrices must be defined for these elements. The overall stiffness matrix must be appropriately modified to take into account the change of element stiffness matrix from elastic to plastic for post yielded elements. A call is made to routine SKINCR. In this routine the difference between the new and old stiffness matrices of an element are determined and appropriately added to the proper rows and columns of the overall stiffness matrix. The procedure leads to the replacement of the old element stiffness matrix by the new one in the overall stiffness matrix.

Using the new overall stiffness matrix and having set the boundary conditions, the set of N equations are solved for the prescribed displacement increment input. The stress increments are calculated, added to their previous values and equivalent stresses for the elements are evaluated. The maximum value of $\bar{\sigma}$ among the elastic elements is

specified. A rating factor ETA1 is defined to specify the amount of input displacement required to cause yield in the element with maximum value of $\bar{\sigma}$.

$$(\bar{\sigma} + ETA_1.\Delta\bar{\sigma})^2 = Y^2 = \frac{1}{2}\{(\sigma_x + \Delta\sigma_x - \sigma_y - \Delta\sigma_y)^2 + ...\} \qquad (3.6)$$

The value of ETA1 is calculated from Eq. (3.6). The rating factor 'ETA1' is compared with a prescribed value ETA. The rating factor is

$$\text{rating factor} = \begin{cases} \text{ETA} & \text{for ETA1} > \text{ETA} \\ \text{ETA1} & \text{for ETA1} \leq \text{ETA} \end{cases}$$

The rating factor must be compared with a prescribed value, as in some cases values greater than unity may be found. A rating factor with a value greater than unity means that the input displacement will be multiplied by a factor greater than unity and thus the input displacement may become too big for one step of loading and can cause serious errors.

The stress increments are multiplied by the rating factor and added to their previous values. The element equivalent stresses are calculated and the elements are checked for unloading. The post yielded elements with current equivalent stresses less than their previous values will be considered to be unloading. The stress increments for unloading elements are recalculated using $[D^e]$ instead of $[D^{ep}]$ in the stress calculation.

The equivalent stresses within the elements are calculated. The variable increments are multiplied by the rating factor and added to their previous values to obtain the current values of different

variables. For post yielded elements the status vector 'PL' is changed from 0 to 1 and for unloading post yielded elements from 1 to 0. For yielded elements the value of yield stress is replaced by the current value of equivalent stress. The new overall stiffness matrix is formed for the next increment of displacement and the required variables are printed out.

A new increment of displacement is introduced at the boundary nodal points until the desired punch penetration is obtained.

3.7.2 Using isoparametric quadrilateral elements

The elastic-plastic program using isoparametric elements is in many ways similar to the program described previously. The main difference is that for isoparametric elements a natural system of co-ordinates has to be defined. The elemental calculations are carried out in this system of co-ordinates and then transferred to the global co-ordinates. The $[K^e]$ matrix which is the element stiffness matrix has to be numerically integrated. In the computer program developed, the integration is carried out using the Gauss quadrature integration method by employing 2 x 2 Gauss points.

An integer number KKK is defined to identify the boundary conditions during the blanking operation.

$$KKK = \begin{cases} 1 & CF = BP = 0 \\ 2 & CF \neq 0 \quad BP = 0 \\ 3 & CF \neq 0 \quad BP \neq 0 \end{cases}$$

The maximum value of clamping force (CF) and back-load (BP) are defined by CLFORCE and BPFORCE respectively.

The elements are scanned and a call is made to subroutine FORMK.

By calling this routine for every element, the elements of the matrix of the element stiffness matrix are appropriately placed in the proper rows and columns of the overall stiffness matrix. By scanning the elements and calling this routine, the overall stiffness matrix of the structure is assembled. The boundary condition for the elastic part is set by making a call to subroutine BOUND1. In this routine the displacement of the nodal points on the die surface in the r and z directions are suppressed. As the nodal points on the axis of symmetry should have no displacement in the r direction, the nodal points displacements in this direction are prohibited. Depending on the value of KKK different boundary conditions will be introduced.

For KKK = 1 (CF = 0, BP = 0) a negative unit displacement is introduced at the nodal point under the punch edge.

For KKK = 2 a negative unit displacement is applied in the z direction at a distance where the blank-holder must act, and the corresponding displacements calculated from Eq. (3.1) are introduced at the adjacent nodal points to this point.

For KKK = 3 the nodes on the counter-punch are suppressed in the r and z directions and a negative unit displacement is applied at the nodal points under the punch.

The set of N equations are solved and the elements are scanned to calculate the stresses at the Gauss points. A call is made to subroutine SDBE for every Gauss point. In this routine the natural co-ordinates of the Gauss points are determined and a call is made to internal subroutine SHAPFU, JACOB2, DMATX, BMATX and DBE.

In the routine 'SHAPFU' the shape functions and their derivatives are calculated at the specified Gauss point. In routine JACOB2, the co-ordinates of Gauss points, the Jacobian matrix and its inverse

at the sampling Gauss point are calculated. The determinant of the Jacobian matrix and cartesian shape function derivaties are also calculated. In BMATX routine the strain matrix for the isoparametric quadrilateral element is built (at every Gauss point). DMATX simply evaluates the elasticity matrix $[D^e]$ or the plasticity matrix $[D^{ep}]$ depending on the state of stress (elastic or plastic). The matrix multiplication DB is carried out in routine DBE. The stresses at each Gauss point within each element are calculated by multiplication of matrix DB and the corresponding nodal displacement of the element. The equivalent stresses at the Gauss points within the elements are calculated. The rating factor is defined and the same procedure as for triangular elements is followed. The load increment is introduced and a call is made to BOUND2 to set the boundary conditions. In BOUND2 depending on the value of KKK different routines are followed.

For KKK = 1 the force at the nodal points on the die surface are checked, the forces should have positive values. A negative force means that the node tends to separate from the die, at the next loading step the node is assumed separated and the nodal forces at this point are set to zero. The nodes on the die are also checked for the displacement, any point with negative displacement will be suppressed and assumed to be fixed onto the die surface for the next step.

A displacement increment is introduced at the nodal points adhered to the punch surface. The separated points are checked for displacement, if their absolute value of displacement is less than the punch displacement they will be suppressed and assumed to travel with the punch in further steps. The points travelling with the punch are checked for force, any point with positive force will be

assumed separated and the nodal forces acting in that node will be set to zero. If KKK = 2 the nodal force in the z direction at 'ICLAMP' node, where the blank-holder acts, is checked and if it is less than a prescribed value the blank-holder indentation is stopped and the boundary condition is changed so that the punch starts blanking the specimen. The boundary condition at the nodes i, j and k, Fig. 3-13, is changed so that the vertical load in point i and the radial forces at nodes j and k remain constant during the further steps. At this stage a similar procedure to part 1 is followed to blank the specimen.

If the nodal force in the z direction at the ICLAMP node is not less than a prescribed value an increment of displacement as explained in BOUND1 is applied so that the required clamping force is obtained (note that the value of clamping force is compared with a negative prescribed value, because it applies in the negative z direction). For kkk = 3 the value of back-load is compared with the prescribed value. If BP is smaller than the prescribed value the loading continues as explained in BOUND1. If the back-load has reached the required value the boundary condition of the nodal points on the counter-punch is changed so that the nodal loads remain constant for the rest of the process. The clamping force is applied and checked as case KKK = 2 until the clamping load reaches the prescribed value, then the clamping force is kept at a constant value and the blanking operation as explained in KKK = 1 starts. The sequence of the rest of the program is similar to that for triangular elements.

CHAPTER 4

EXPERIMENTAL WORK

4.1 Aim of the present work

A smaller punch/die clearance and additional tooling, are the main features which differentiate between fine blanking and conventional blanking. The load-displacement characteristics in the case of conventional blanking has been described by Johnson (84). The effect of punch/die clearance on the blanking load has been previously studied by P.E.R.A. (5) and it has been shown that a decrease in the radial punch/die clearance causes an increase in the blanking load. P.E.R.A. (6) has also shown that a decrease in the radial punch/die clearance in the case of thin materials can cause an increase in the smooth portion of the blank edge. As the material thickness increases, however, the edge condition of the component deteriorates and an acceptable finish is obtained only over a small portion.

The unknown facts which remain about the fine blanking process are the effect of the blank-holder, blank-holder diameter and clamping force, and the back-load on the load/displacement characteristics and the quality of the blank edge when blanking specimen materials with different thicknesses.

In industry the exact position of the blank-holder and the amount of clamping force for the production of blanks with smooth edge finish is determined by trial and error. The back-load is usually used to prevent the dishing of the blanks and the magnitude of it depends on the amount of dishing.

In the present work strips of mild steel were blanked at a punch speed of 1 in/min. (2.54 cm/min) under different conditions of blank-holder

diameter, clamping force and back-load. Three different thicknesses of 0.076, 0.101 and 0.120 in. (1.93, 2.56 and 3.04 mm) were used together with three different values of clamp diameter, clamping force and back-load during the experiments.

Load vs. displacement curves under different blanking conditions of clamping force, back-load and clamp-diameter are plotted and the effect of different variables on the load-displacement characteristics is studied.

To examine the rate of work hardening in different regions a hardness survey across the partially blanked parts was performed.

A visual examination of the quality of the blank edge surface finishes was made and the effect of blank-holder on the mode of deformation was sought by etching partially blanked sections.

The experiments were carried out only to examine the general effect of different variables on the quality of the blank edge surfaces, the exact values of different parameters for the production of blanks with crack-free surfaces were not tackled.

To perform an accurate determination of the clamping force and clamp diameter for a certain material and thickness a highly accurate test rig is required which must be designed, manufactured and set up by experts in this field. The experiments performed in this work proved the fact that to tackle the exact values of the clamping force, clamp diameter and back-load the recommended presses and tooling for fine blanking are imperative.

4.2 Design considerations

To simplify the manufacture of the tools, an experimental sub-press was designed to produce circular blanks of 28 mm (1.102 in.) in diameter,

using strips of mild steel of up to 0.120 in. (3.04 mm) thick.

The main design requirements for the sub-press were as follows :

1) The clearance between the punch and die must be kept to a minimum (around 0.0005 in. (0.0127 mm)).

2) The diameter of the blank should be around 1 in. (25.4 mm) which is the diameter commonly used previously in the analysis of the conventional blanking process.

3) It should be possible to clamp the specimen against the die-face using different clamping forces and clamp diameters.

4) The sub-press should provide a constant back-load (applied to the specimen) during the blanking operation.

5) A stripping system must be provided to strip the specimen off the punch after the blanking operation is complete.

6) A cut out should be provided to ease removal of the blank.

7) The design should utilize the feature of an existing 'Denison' compression testing machine in the experiments.

8) Instrumentation should be provided for the simultaneous recording of blanking-load and punch-displacement. The direct reading of clamping force and back-load must also be provided for.

4.3 Experimental set-up

A 50 tonf (498.2 kN) 'Denison' compression testing machine with the capability of providing ram speeds of between 0-9 in./min. (0-22.8 cm/min) was used to house the specially designed fine blanking test rig, Fig. 4-1.

The test rig comprises a die set to accommodate the tooling and can provide similar conditions as the actual fine blanking process by the use of a very small punch/die clearance together with a specially designed

blank-holder and counter punch. The die-set ensures accurate alignment of the tooling during the operation, a schematic view of the test rig is shown in Fig. 4-2.

To perform a fine blanking operation the specimen material was clamped against the die face by the blank-holder and the blank was supported from underneath by the counter punch. The operation was effected by the penetration of the punch into the material.

The punch-displacement, blanking load, clamping force and back-load could be measured by the instrumentation provided.

A circular collar was used to bolt the punch to the top platten of the die-set. To ensure that the punch remained concentric with the die, a guide pin was fixed between the punch and the top platen. Strain gauge load cell 'A' was placed on top of the die-set to measure the blanking load, Fig. 4-1.

A blank-holder plate was used to accommodate different blank-holders which were secured to it by four screws. The die was lodged in a die-holder made of mild steel and fixed to it by four screws, the die-holder itself being bolted to the bottom platen of the die-set. To ensure the alignment of blank-holder, die and punch two guide pins were used. The bottom part of the guide pins were driven into the drilled and reamed holes in the bottom platen of the die-set, Fig. 4-2.

A strain gauge load cell 'B' was mounted in the bolster to measure the back-load applied to the specimens, Fig. 4-2. The strain gauge load cell 'B' was screwed onto the plunger of a hydraulic jack used to apply the back-load, to prevent any undesirable movement and thus possible damage to the strain gauges.

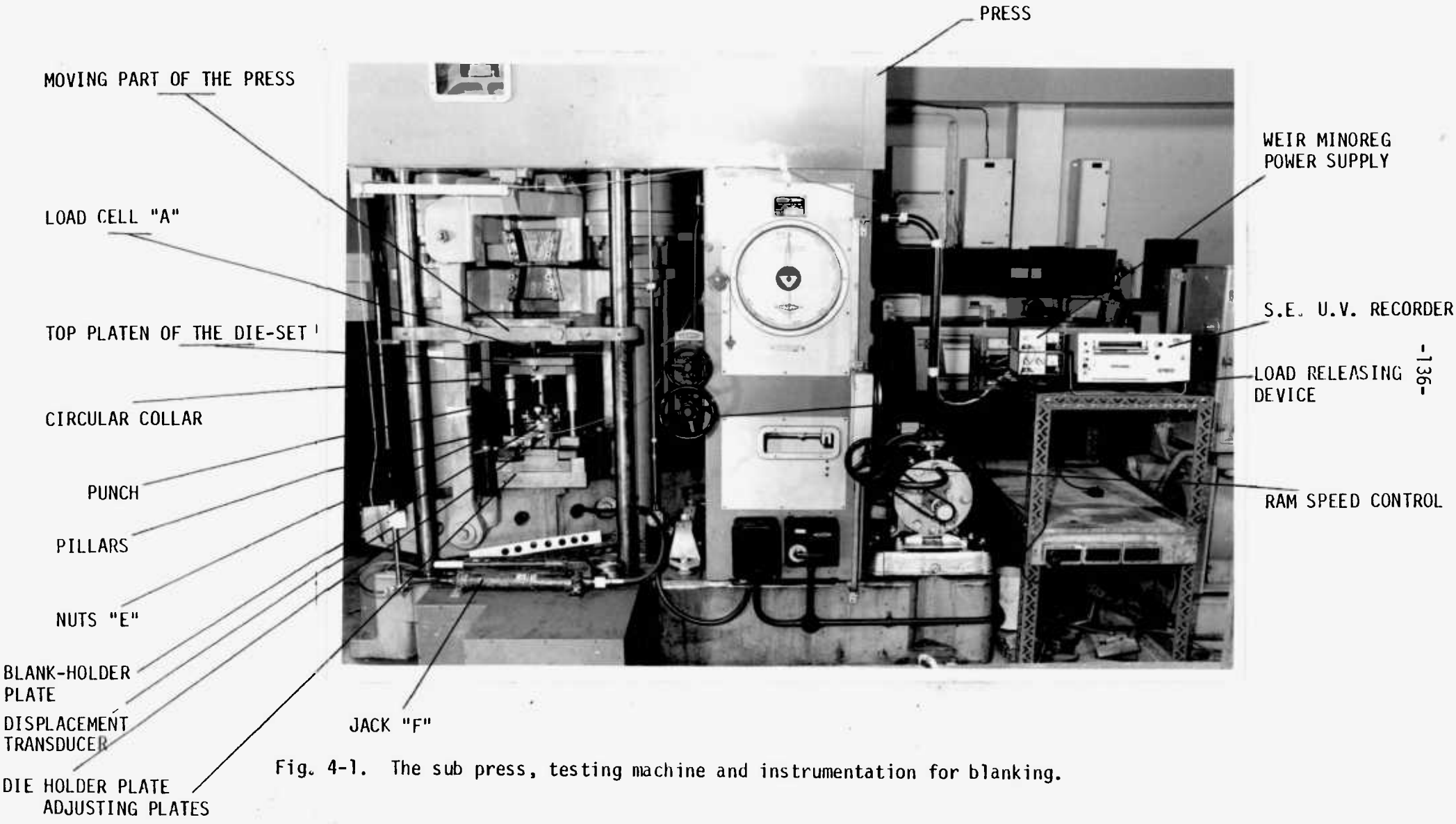

Fig. 4-1. The sub press, testing machine and instrumentation for blanking.

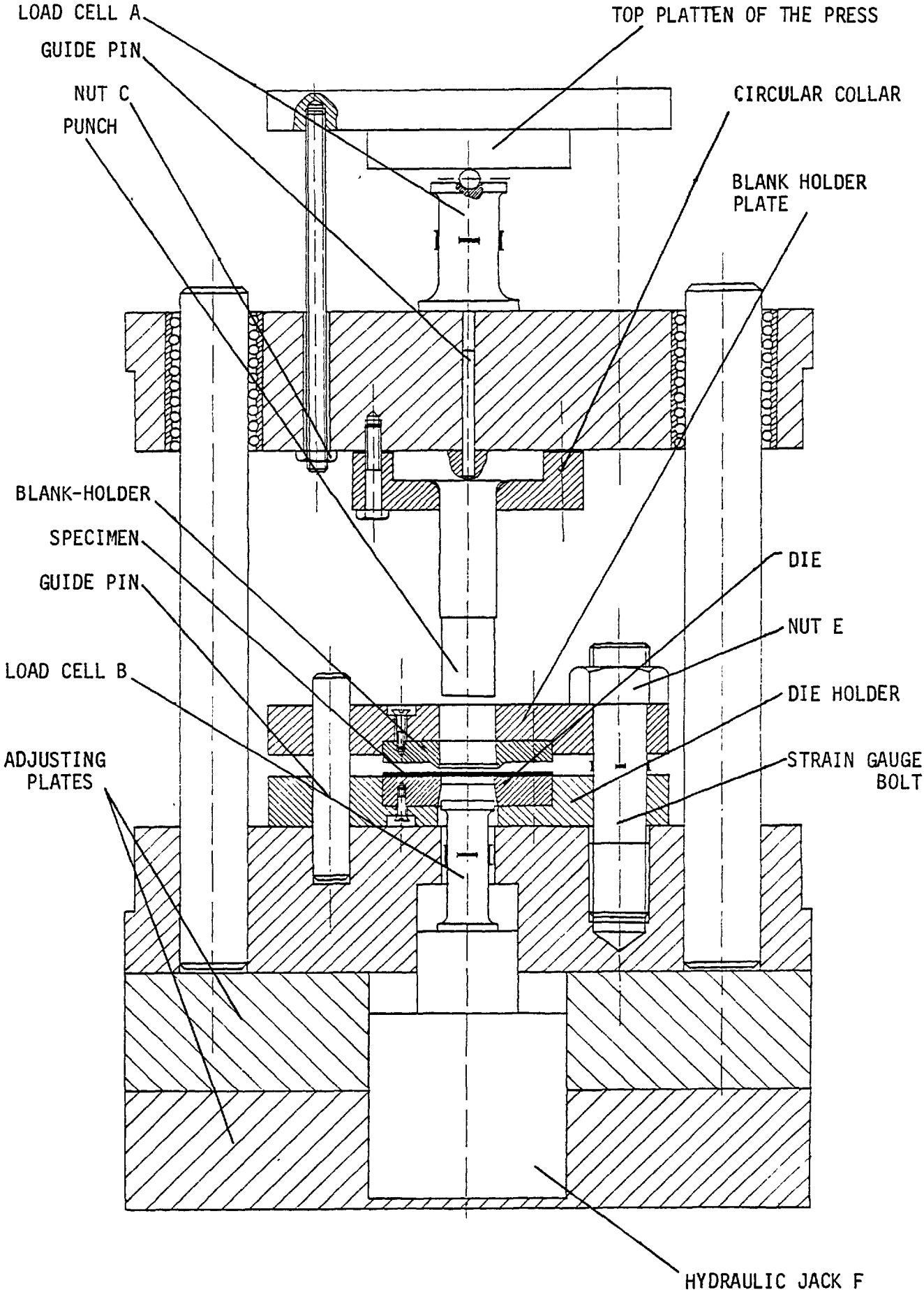

Fig. 4-2. Sub-press experimental set up.

The back-load was provided by a 10 tonf (99.64 kN) hydraulic jack. To maintain a constant pre-determined back-load, the oil pressure fed into the hydraulic jack had to be kept at a certain constant value and so an 'Electraulic' pressure relief valve was used in line with the pump and jack. The pressure relief valve could operate at pressures ranging from 0 up to 500 kgf/cm^2 (0-49 MN/m^2). A manually operated hydraulic pump, 10,000 lbf/in.^{2} (68.94 MN/m^2) maximum capacity, was used to pump the oil from a tank to the pressure relief valve and in turn to the hydraulic jack, Fig. 4-3.

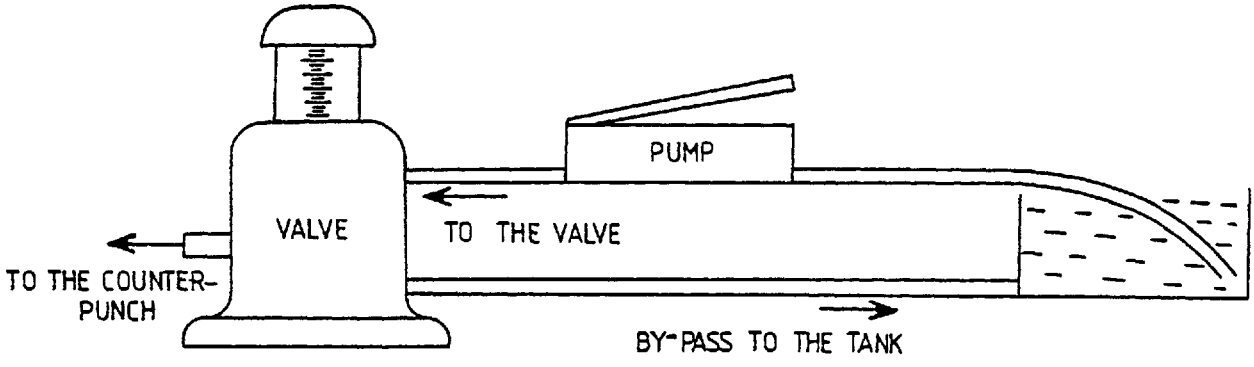

Fig. 4-3.

The predetermined pressure is set by turning the adjuster on top of the valve which in turn changes the amount of compression of an internal spring. When the pressure in the system becomes higher than a certain prescribed value the by-pass opening, which is closed by the spring pressure, is forced open and the oil in the system is by-passed to the tank until the pressure drops to the pre-determined value.

Four 1 in. (2.54 cm) diameter bolts were used to press the blank-holder against the specimen. The bolts were all made of commercial mild steel. By tightening up the nuts 'E', Fig. 4-1, the blank-holder plate, and in turn the blank-holder itself moves downwards and the required force is applied to the specimen.

The punch, die and blank-holders were all manufactured from K.E.A. 180 (oil hardening tool steel). The tools were heat treated by first being pre-heated in a furnace to 750^{o}-780^{o}C for 30 minutes and then removed and immediately placed into another furnace for heating to 980^{o}-1000^{o}C. The tools were left for 15 minutes to allow the temperature to equalise and then removed and quenched in oil. Tempering was performed at 250^{o}C to obtain a hardness of 59-60 Rockwell-C.

The die opening was ground parallel for 3 mm (0.118 in.) which is approximately equal to the thickness of the thickest specimen to be blanked, and then backed off at $\frac{1}{2}^{o}$ per side. Three blank-holders with three different diameters 1.272, 1.352 and 1.43 in. (32.3, 34.3 and 36.3 mm) were manufactured by profile grinding so that the distance of the apex of the blank-holder projection from the edge of the punch could be varied.

The punch and die were ground to a clearance of 0.0005 in. (0.0127 mm) which is the value recommended by Guidi (31) and is the clearance commonly used for this range of thickness by most manufacturers. To ease manufacture, the punch was ground only at the nose over a length of 40 mm (1.574 in.) allowing the punch to blank the specimen and pass freely through the blank-holder plate and the blank-holder itself.

The top platen of the die-set is connected to the moving part of the press by means of two studs and its position with respect to this part of the press can be adjusted by means of the two nuts 'C'. The position of the top platen of the die-set is adjusted in such a way that the load cell 'A' lightly touches the moving part of the press and remains in position. The bottom platen and the adjusting plates are clamped down to the stationary part of the press, the adjusting plates being used to lodge the hydraulic jack, Fig. 4-2.

As was explained earlier, the clamping force is applied to the specimen by tightening up the nuts 'E', Fig. 4-1. As the clamping force increases, the frictional forces between the nuts and the blank-holder plate increase. Under the high compressive stresses developed during tightening, the sharp edges of ordinary nuts dig into the blank-holder plate, Fig. 4-4(a), causing pitting of the plate and thus intensifying the frictional forces. To overcome this difficulty a type of nut with semi-spherical bottoms was used, Fig. 4-4(b). The nuts were found much easier to tighten and thus higher clamping forces were obtained. A common solution to this problem is the use of pilgrim nuts, Fig. 4-4(c). Pilgrim nuts are tightened by pumping oil into compartment A of the nut. The pressurized oil in compartment A forces apart the parts B and C and so the blank-holder plate is forced into the specimen. Shims are placed in the gaps to ensure a constant tension in the bolt.

In this experimental work, as the blank-holder plate was removed repeatedly, the use of pilgrim nuts was avoided. The industrial solution to this problem is the use of specially designed fine blanking presses, where the blank-holder plate can be pressed into the material by a separate ram and hydraulic system provided by the press.

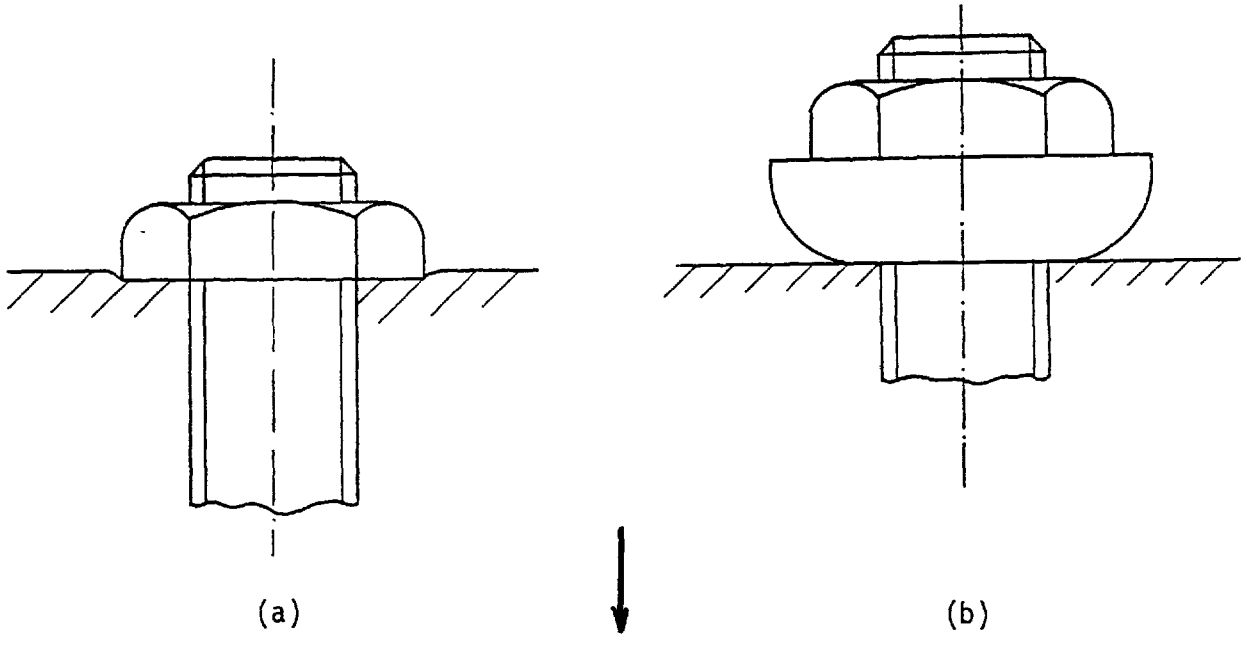

(a) (b)

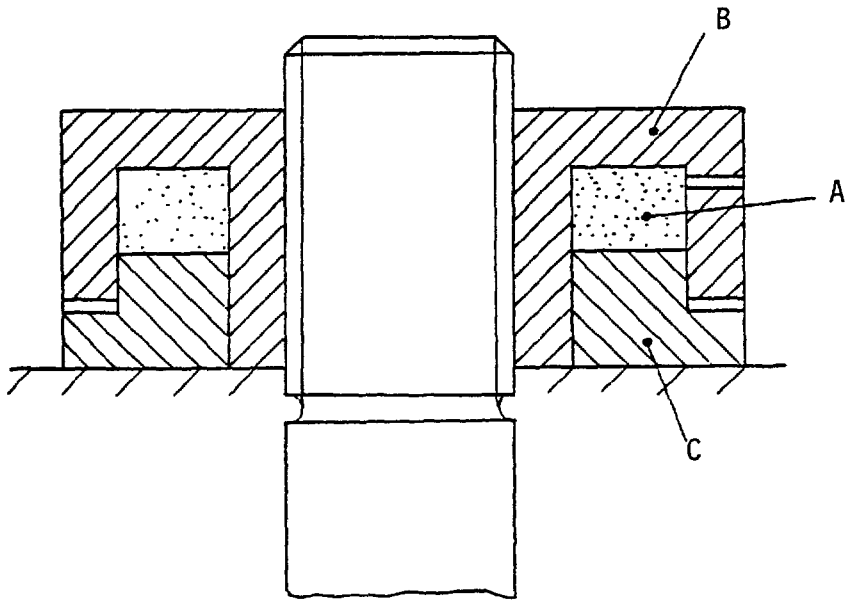

(c)

Fig. 4-4.

4.4 Tool manufacture

The quality of the blank edge surface finish is totally dependent on the degree of precision with which the tools have been manufactured and the material used for the production of the tools.

A small and critical clearance between the punch and die is one of the main characteristics of fine blanking which differentiates the process from conventional blanking. An improper choice of materials will result in premature wear of the tools and consequently change of clearance between the punch and die.

The alignment of the tools is one of the main difficulties encountered in the production of fine blanking tools. Any misalignment will impair the critical clearance between the punch and die, and consequently blanks with non-uniform edge surface finishes will result.

A longer punch not only magnifies any misalignment in the system but also gives way to more distortion during blanking. The length of the punch must be kept to a minimum or it will be extremely difficult to align the punch and die. The difficulty lies in the fact that even an accurately centred punch and die may distort under the blanking load and although the system is accurately centred before blanking, there is no assurance that it will remain so during the operation.

Removing the blank after blanking can be effected by forcing it back through the die-hole, however, it was found that some degree of ironing took place during this operation. Although ironing can have the desirable effect of increasing the smooth surface finish of the blank edge, it can conceal the effect of different parameters on the true blank finish. Therefore, to minimize this ironing effect a secondary system was devised in which a groove was diametrically cut across the bottom part of the die-holder, thus allowing manual removal without having to force the blank back through the die.

To manufacture the fine blanking tools two basic methods of die and blank-holder production can be used. These are profile grinding and spark eroding and neither method influences tool life.

The choice of manufacturing method to be applied is mainly dependent upon the geometric form of the part, and of course the types of machine tools available.

A proper sequence of tool manufacture is an important factor in producing an accurate and reliable fine blanking rig. The die-set pillars are usually employed to guide the different parts of the test rig such as blank-holder and die-holder. To simplify tool manufacture and ease tool handling it was decided not to use the pillars as guides for the blank-holder plate and die-holder plate, but to introduce two

extra guide pins to fulfil this function.

In industry the die and the blank-holder are lodged in the conical shoulders turned in the top and bottom bolsters of the die-set. This provides a better means of positioning the parts. To manufacture and set up the tools the following procedure was used :

1) A piece of alloy steel 'A' is turned to a diameter equal to the die-holder or blank-holder diameter (die-holder diameter is assumed to be the same as that of the blank-holder), Fig. 4-5(a).

2) Two shoulders are turned on both ends of the alloy steel piece 'A' to lodge the die and blank-holder, Fig. 4-5(b).

3) The bottom platen of the die-set and alloy steel piece 'A' are centred and clamped on the face of the lathe, Fig. 4-6(a)

4) A hole of a diameter equal to the die opening is drilled and bored through the piece 'A' and the die-set bolster, Fig. 4-6(b).

5) While piece 'A' and bottom platen of the die-set are still clamped together, two holes diametrically opposite each other are drilled and reamed to place guide pins, Fig. 4-7.

6) The piece 'A' is sawn into two pieces 'B' and 'C', Fig. 4-8.

7) Pieces 'B' and 'C' corresponding to their turned shoulder are faced to the exact thickness of the die-holder and the blank-holder plate.

8) The die is heat treated and ground to its final shape and size and secured to the die-holder plate by four screws, Fig. 4-9.

9) The die-holder plate is placed on the bottom bolster of the die-set, the guide pins are driven in and the die-holder plate is bolted down to the bolster, Fig. 4-10.

10) A punch is made with exactly the same diameter as the die-opening.

11) The punch is placed in the die-hole and the top platen of the die-set is brought down, Fig. 4-11.

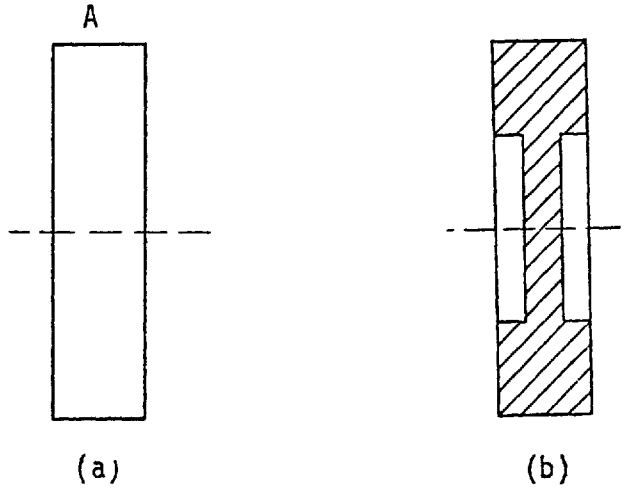

Fig. 4-5.

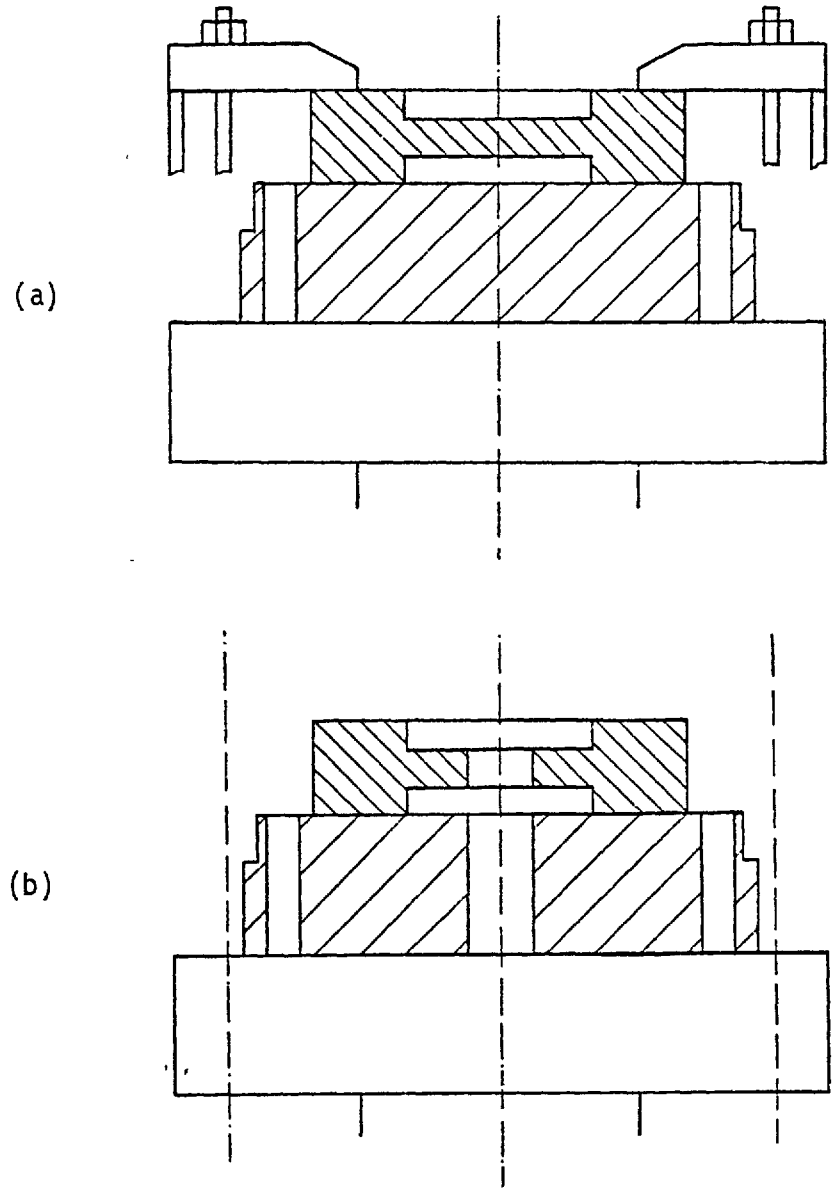

Fig. 4-6.

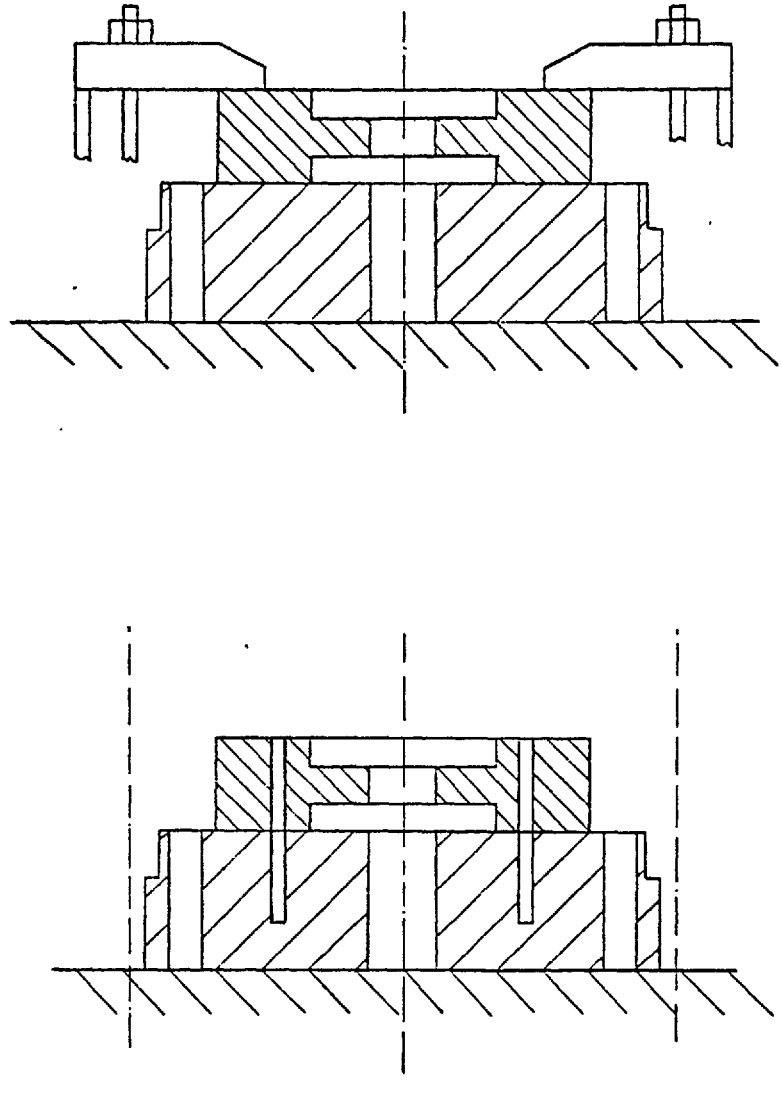

Fig. 4-7.

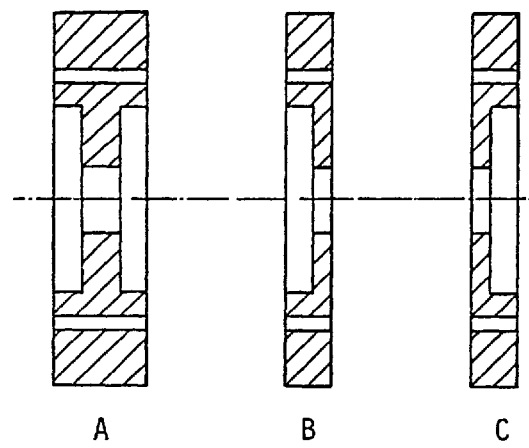

Fig. 4-8.

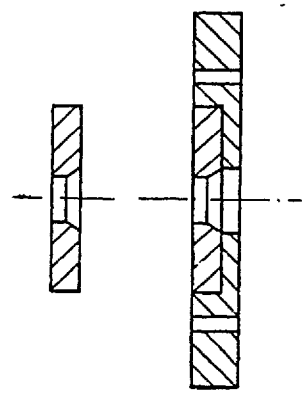

Fig. 4-9.

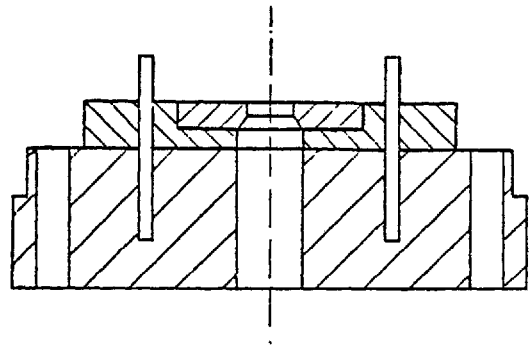

Fig. 4-10.

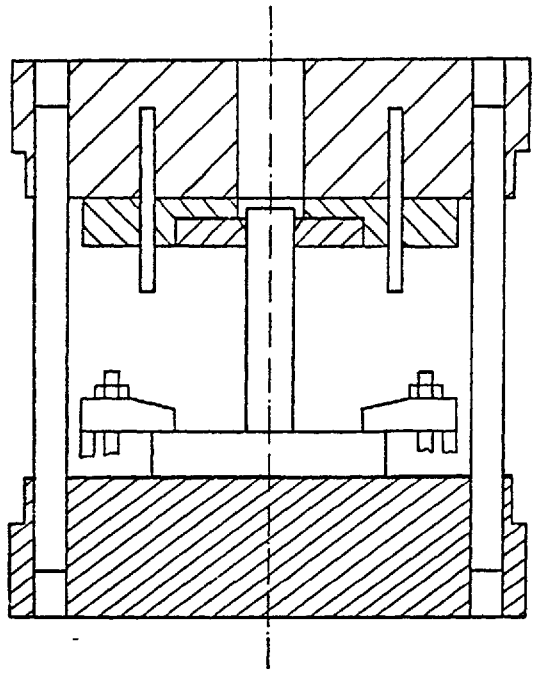

Fig. 4-11.

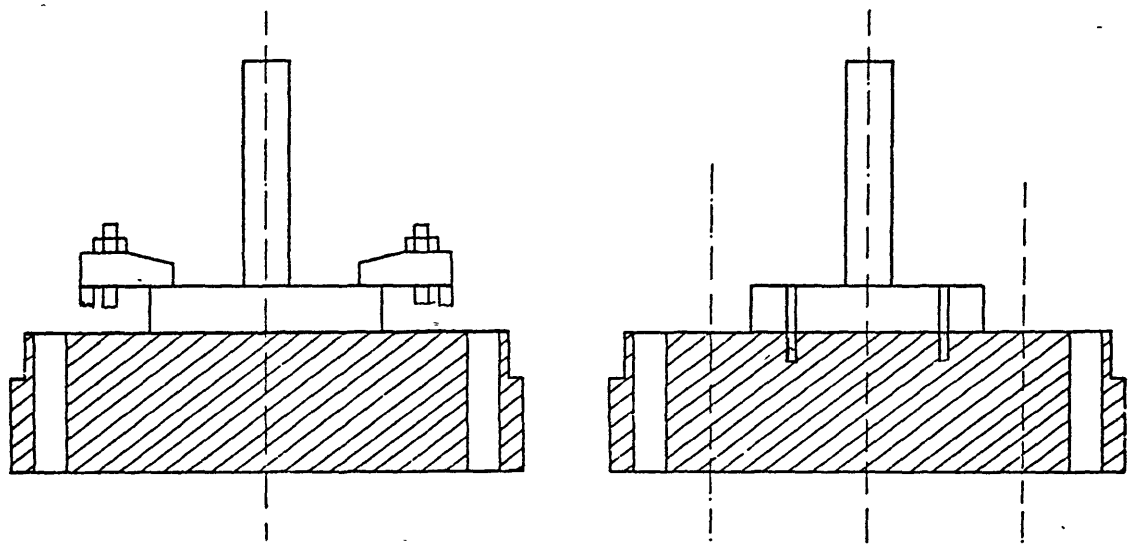

Fig. 4-12.

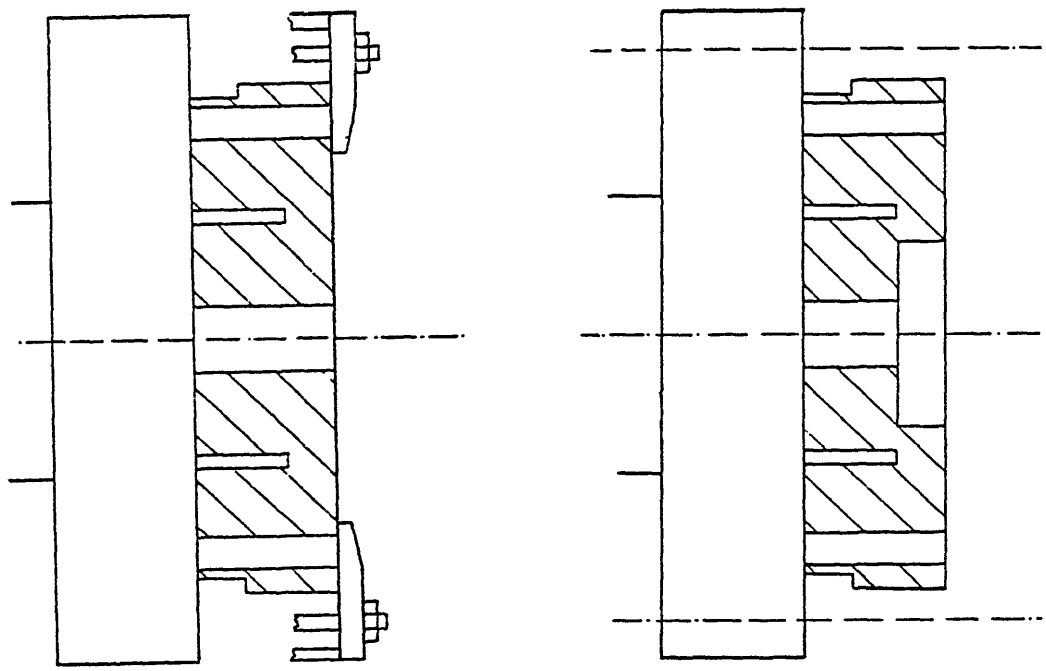

Fig. 4-13.

12) The punch is clamped to the top bolster and the whole assembly is removed. Two holes through the punch and bolster diametrically opposite each other are drilled and reamed and two guide pins are driven through them, Fig. 4-12.

13) The punch is removed and ground to the required punch/die clearance.

The pillars from the bottom platen of the die-set are removed. The bottom bolster is centred and clamped onto the face of a lathe and a shoulder is turned to accommodate the plunger of the hydraulic jack, Fig. 4-13.

4.5 Instrumentation

Two strain gauge load cells were used to measure the blanking -load and back-load during blanking. To measure the clamping force two strain gauge bolts were employed. On each load cell and strain gauge bolt four strain gauges were fixed and connected to form a full bridge and energized by a 6 volt 'Weir Minoreg' power supply. Two of the strain gauges were fixed in the circumferential direction opposite each other to compensate for temperature changes and the other two in the axial direction to eliminate bending effects.

A variable resistance displacement transducer was used to measure the punch displacement. The transducer was energized by a 24 volt 'Weir Minoreg' power supply.

A 120,000 lbf (533.7 kN) 'Tininus-Olsen' testing machine was used to calibrate the load cells and the bolts in compression and tension respectively. The load was applied in increments and the output signals were amplified and transferred to a S.E. U.V. recorder type 3006 and

recorded. The corresponding results were plotted to obtain the constant of calibration.

A 'Hilger' TT 500 projector was used to measure the crack-free length of the blanked specimens.

4.5.1 S.E. U.V. recorder

The U.V. recorder incorporates an ultra-violet lamp which emits beams of light onto moving mirror galvanometers. The deflected beams from these galvanometers are in turn directed onto a photosensitive paper chart. This paper is driven by a synchronous motor via a gearbox and clutch with provision for several chart speeds from 0.2(5) to 5 in./sec (125 mm/sec). An electronic timing device is incorporated in the U.V. recorder, based on the frequency of the mains supply. Lines are printed across the full width of the chart at intervals of several preselected periods, varying from 1 to 25 seconds, for which provision is made in the recorder. Reference lines are printed along the length of the paper, simultaneously with recordings and timing lines. This facilitates the evaluation of recordings. Once the record is obtained, it may be stabilised by spraying it with a stabilising lacquer.

A typical load/displacement graph recorded by the S.E. U.V. recorder on the photosensitive paper is shown in Fig. 4-14, also given in this Figure is the "Grid" definition which will be used below for the calibration curves.

4.5.2 Load cell 'A'

The load cell 'A' was made of K.E.A. 180 (oil hardening tool steel) and designed to carry up to 50 tonf (498.2 kN). During the calibration of the load cell it was found that, by rotating the load cell, under a

constant load, output signals would change. To minimize the effect of directional loading the load cell was centre drilled at the top end and a steel ball placed in the centre and partly pressed into the load cell to produce a single contact area during loading. The load is transferred to the load cell through the steel ball and so the effect of directional loading was eliminated. Both ends of the load cell were flanged to provide a more uniform load distribution along the load cell and better means of gripping. The load cell 'A' was repeatedly loaded and unloaded up to 50 tonf (498.2 kN) to eliminate any hysteresis or residual strains. To calibrate the load cell, the load was then applied in increments of 20 kN (4,500 lbf) and corresponding results recorded. The calibration curve is shown in Fig. 4-15.

4.5.3 Load cell 'B'

Load cell 'B' was designed to carry up to 30 tonf (298.9 kN). The top diameter of the load cell is the same as the die opening diameter. The bottom part was flanged for the same reason as mentioned for load cell 'A'. The middle part of the load cell was turned to a smaller diameter to ensure that the strain gauges and their protective coating of 'Araldite' would not touch the body of the die-set. Before calibrating the load cell a maximum load of 30 tonf (298.9 kN) was applied on the load cell several times as in section 4.5.2. To calibrate the load cell, load was applied in increments of 20 kN (4,500 lbf). The calibration curve is shown in Fig. 4-16.

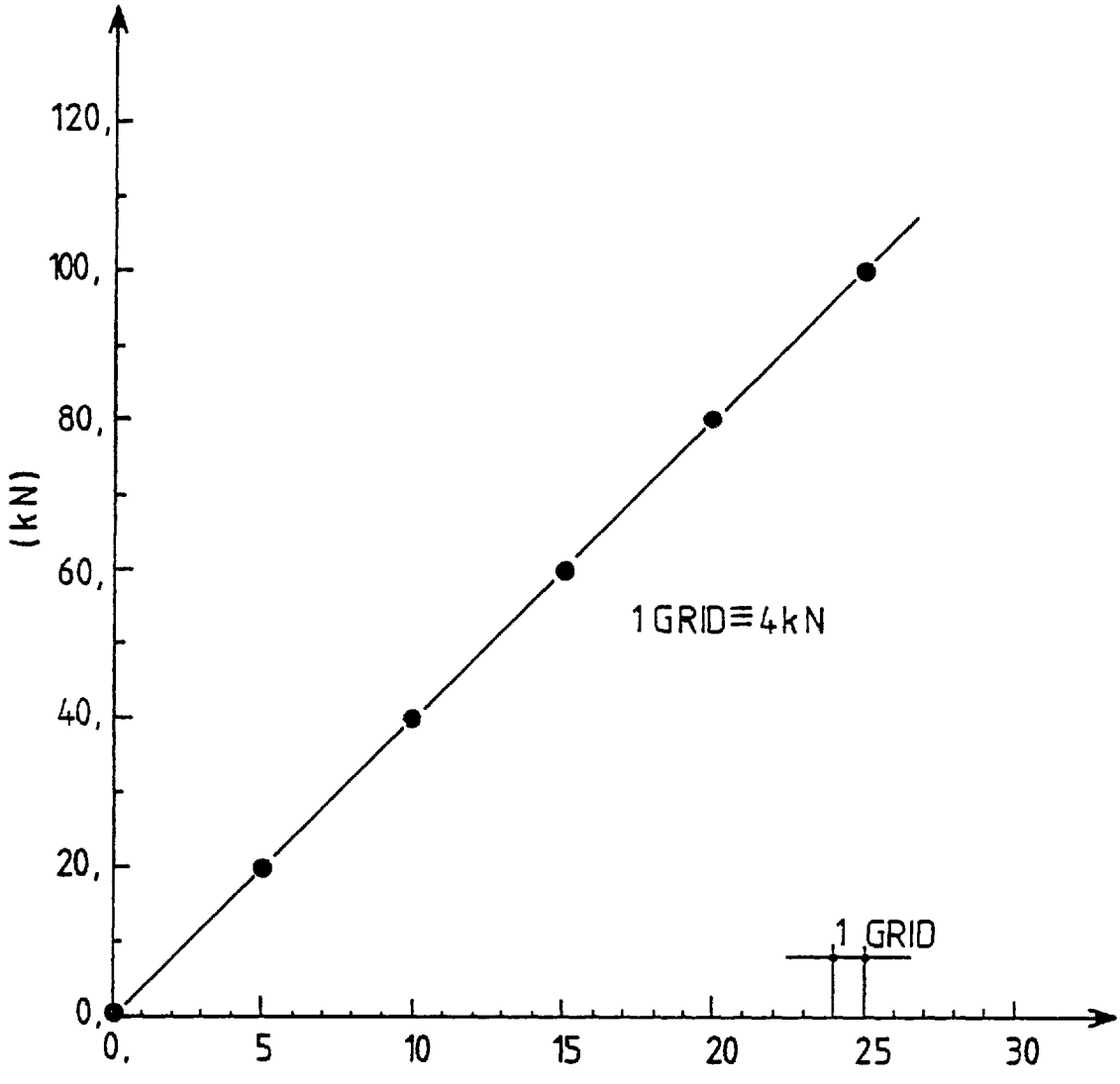

Fig. 4-15. Calibration curve for load cell 'A'

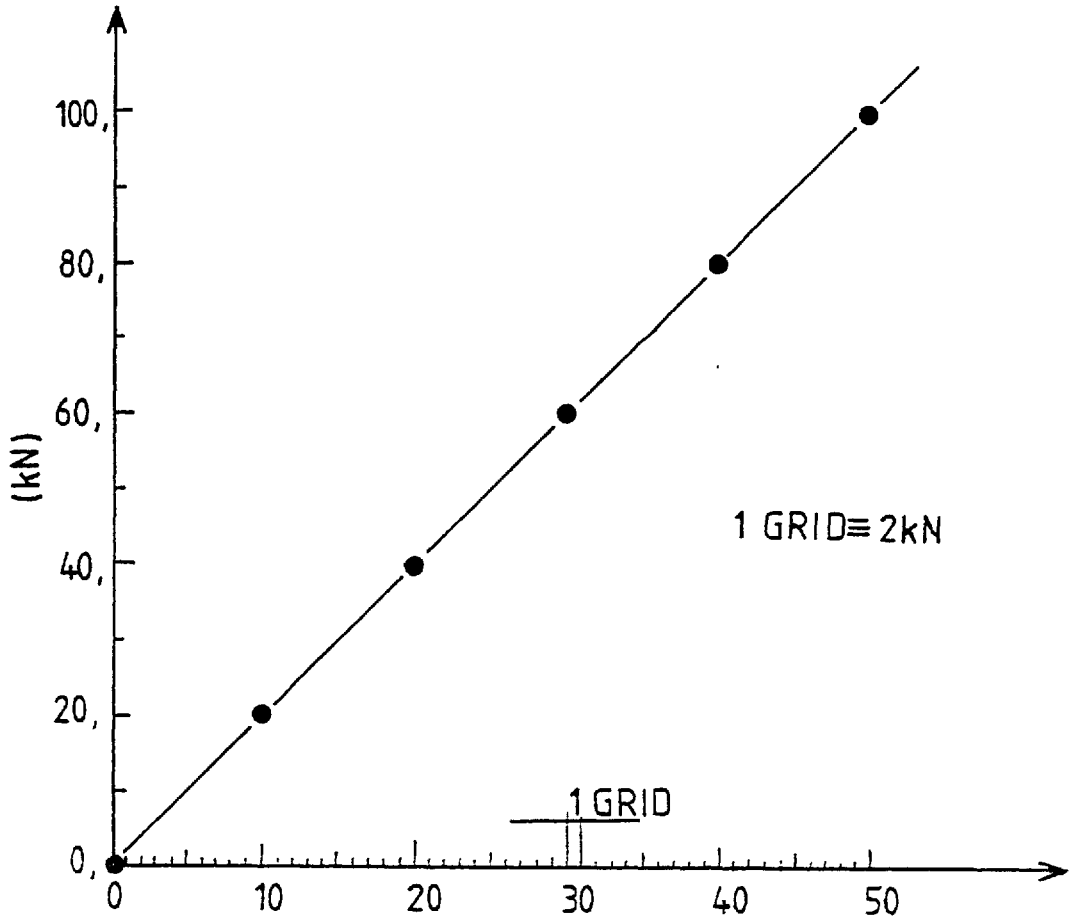

Fig. 4-16. Calibration curve for load cell 'B'.

4.5.4 Strain gauge bolts

The bolts were designed to carry up to 10 tonf (99.6 kN) and were threaded at both ends and machined to a smaller diameter in between to provide a more uniform distribution of load. Prior to calibration, the bolts were loaded several times up to 10 tonf (99.6 kN). To calibrate the bolts, load increments of 4 kN (900 lbf) were applied and the corresponding results recorded. As the bolts were made from the same material and turned to the same size their calibration curves were found to be the same. The calibration curve which applies to both bolts is shown in Fig. 4-17.

4.5.5 Displacement transducer

A variable resistance displacement transducer was used to measure punch displacement. The output signal from the transducer was transferred to the U.V. recorder and printed out on the photosensitive paper. To calibrate the transducer the punch displacement was measured by a high accuracy dial gauge and plotted against the corresponding values printed by the U.V. recorder. The calibration curve is shown in Fig. 4-18.

4.5.6 'Hilger' TT 500 projector

Measurements of crack-free length were made by means of a 'Hilger' TT 500 projector in which the sheared surface of the blank was projected with X50 magnification on to a glass screen. The screen is finely greyed to give the best luminosity and definition of the image projected through it and has broken lines marked permanently upon it along two diameters at right angles to each other, forming reference lines for point-to-point measurements by the stage micrometers. The work stage, which is designed

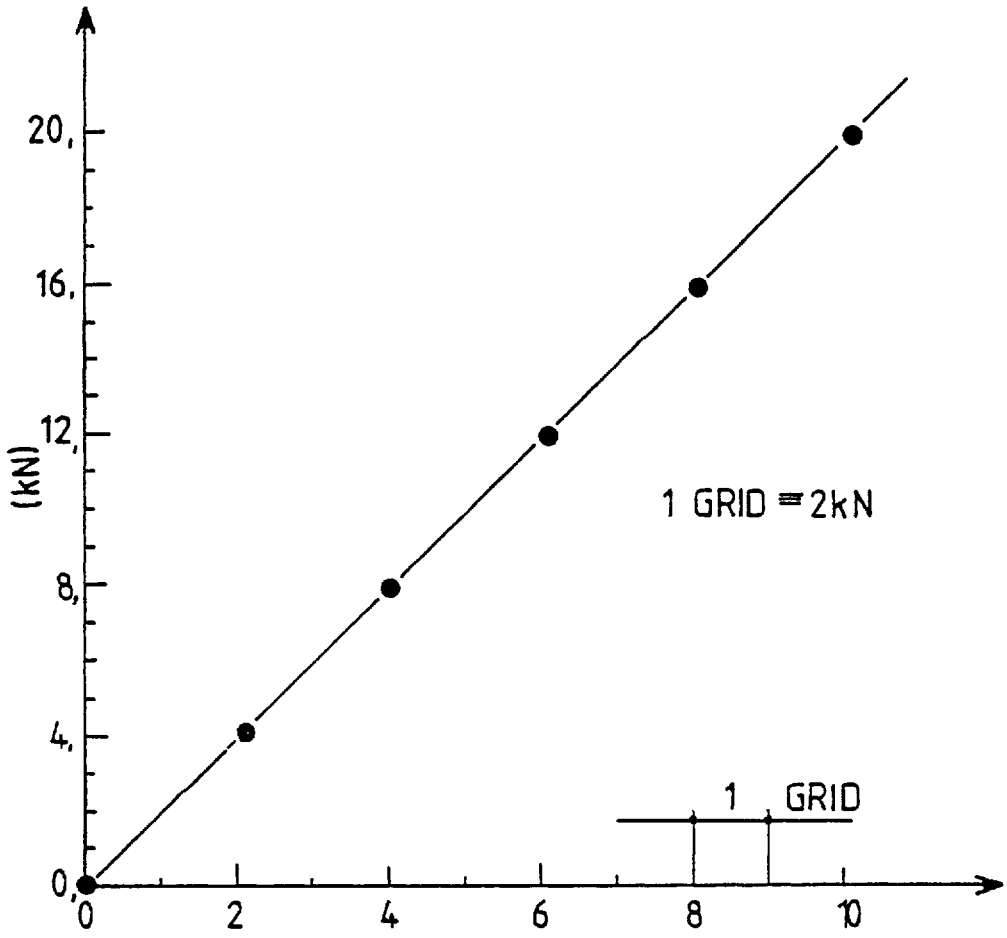

Fig. 4-17. Calibration curve for strain gauge bolts.

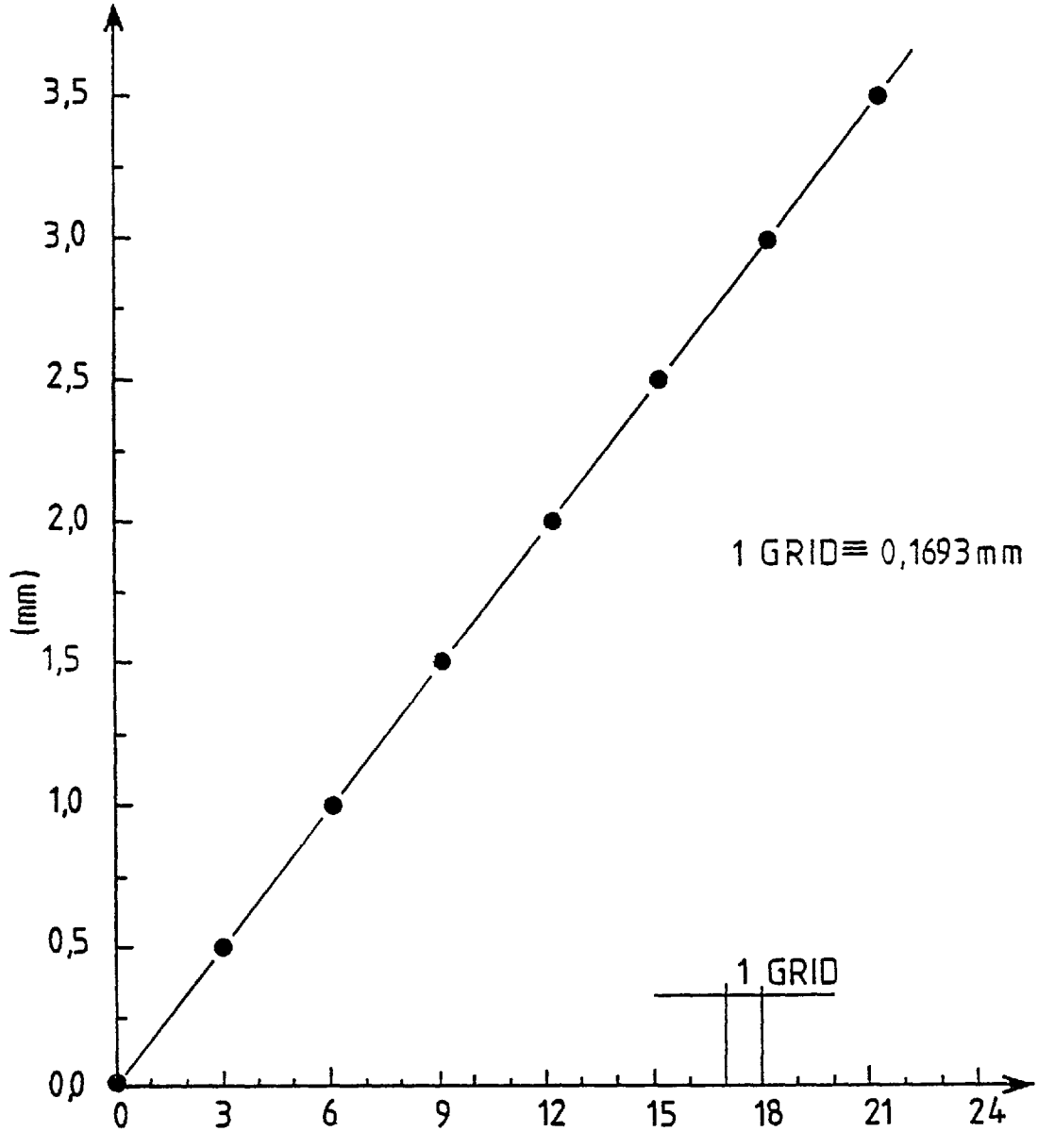

Fig. 4-18. Calibration curve for displacement transducer.

to accommodate objects weighing up to 60 lbf (0.26 kN) and up to 8 inches (20.3 cm) in diameter by 14 inches (35.5 cm) in length, is provided with a micrometer reading to 0.0001 in. (0.002 mm), permitting accurate measurement.

4.6 Specimen material

Commercially mild steel sheets of three different thicknesses of 0.076, 0.101 and 0.120 in. (1.93, 2.56 and 3.04 mm) were guillotined into strips 2 in. (5.08 cm) wide by 3 ft (91.44 cm) long and used as specimen materials during the experimental work. A chemical analysis of the material was made in the Metallurgy Department at Imperial College of Science and Technology (C = 0.07%, Si = 0.02%, S = 0.019%, P = 0.009%, Mn = 0.27%). The specimen materials were subjected to the Vicker's hardness test and the results obtained showed a hardness value of 120. A compression test was made to obtain the stress/strain relationship of the material and the corresponding results are shown in the illustration below.

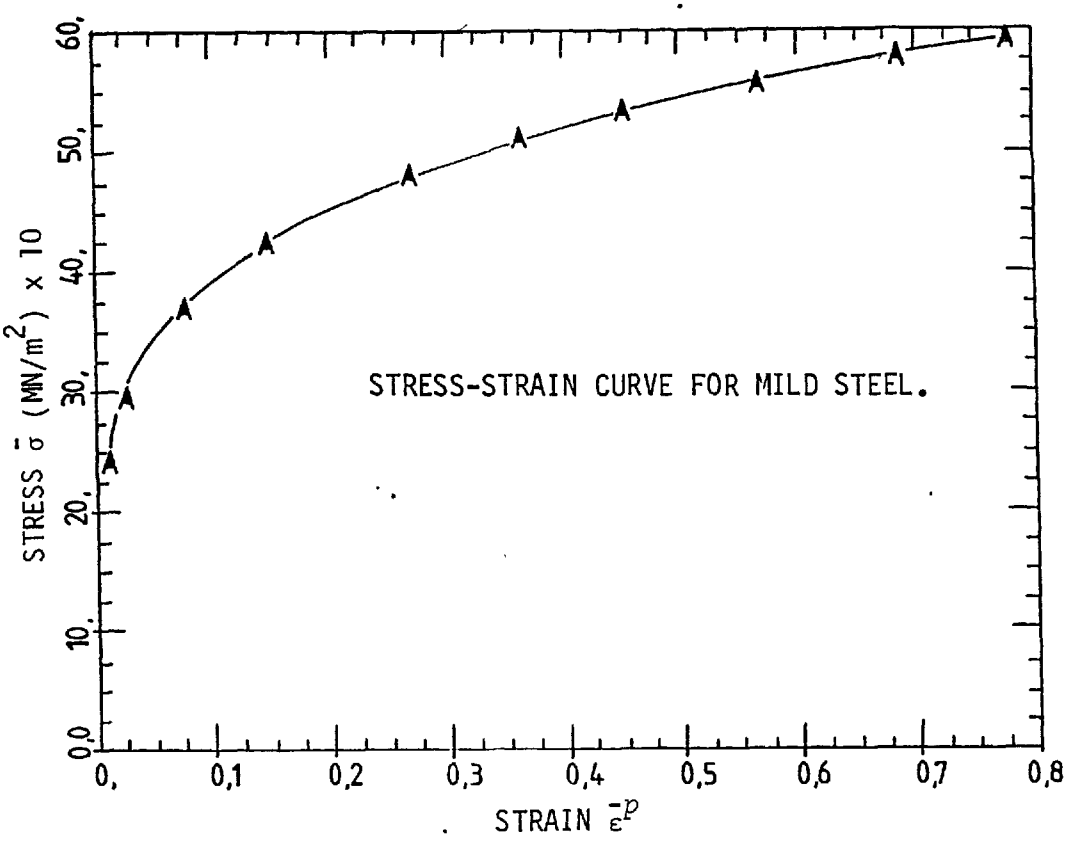

4.7 Experimental procedure

To expedite the operation the specimen material was chosen as strips. Before performing any new blanking the punch and die were carefully cleaned to remove any pick-up from the previous operation.

After each blanking the strip of material was repositioned under the punch. Between each blank a space of at least 1 cm (0.393 in.) was allowed to eliminate any possible edge effects of the blanked part. Molybdenum disulphide was applied on both sides of the specimen to act as a lubricant prior to blanking.

To investigate the effect of different variables on the surface finish of the blank edge and on the blanking force, three different groups of experiments were carried out.

i) Without clamping force (CF) and back-load (BP).

ii) Three different values of the clamping force (CF), no back-load (BP)

iii) Three different values of both clamping force (CF) and back-load (BP)

Depending on which set of experiments was going to be performed different approaches had to be taken.

Case (i) CF = 0, BP = 0

The specimen was positioned accurately under the punch, the latter was moved downwards until it nearly touched the specimen. The drive button on the U.V. recorder was switched on. The speed of ram travel was adjusted to a constant speed of 1 in./min.(25.4 mm/min.). The process continued until the punch cut through the specimen.

At this stage blanking was completed and the loading device on the press was brought back to zero to stop further movement of the punch. The drive button on the U.V. recorder was switched off.

Because of the relatively high friction between the punch and the strip of material caused by elastic recovery, the strip adhered to the punch and had to be forced out. The 'Denison' machine which was used in the experiments was a single action press. Blanking different thicknesses of mild steel 0.078, 0.101 and 0.120 in. (1.93, 2.56 and 3.04 mm) showed that the spring return force was only adequate to strip off the punch when 0.076 in. (1.93 mm) thick mild steel was blanked. For higher thicknesses additional tooling was necessary. To strip off the punch the nuts 'E', Fig. 4-1, were tightened to suppress upward movement of the blank-holder and thus the strip. The load was released through the load releasing device provided on the press. If the draw-back force was larger than the frictional forces then the punch would strip off the specimen. In cases when the draw-back force was not large enough a small hydraulic jack 4 tonf (39.85 kN) was placed between the circular collar and the blank-holder plate. Oil was pumped into the jack and the punch was forced out of the strip.

Case (ii) $CF \neq 0$, $BP = 0$

The specimen was positioned accurately under the punch, the latter was moved downwards until it nearly touched the specimen. The nuts 'E', Fig. 4-1, were tightened, the clamping force induced in the bolts was measured through the output signals from strain gauge bolts, until the clamping force reached the prescribed value. The blanking and stripping operation was then performed as explained in case (i).

Case (iii) $CF \neq 0$, $BP \neq 0$

The punch was moved downwards until it touched the specimen. A fraction of the maximum blanking load was applied to the specimen. Oil was slowly pumped into the jack 'F' until the load shown by the strain gauge load cell 'A' , Fig. 4-1, started to change. This showed that the load applied by the counter punch was approximately equal to the punch load. Another increment of load was applied by the punch and the same procedure was followed. This procedure would cause the specimen to remain in contact with the die-holder while applying the back pressure thus eliminating lift. Another increment of the load was applied by the punch and the same procedure was followed. This operation was continued until the load shown by the load cell 'B', Fig. 4-2, reached the prescribed value. The load increment was stopped and the clamping force was applied as explained previously. After the specimen was cut through, the back load was released to prevent the blank being forced back into the strip. The stripping operation was followed as in case (i).

After each blanking operation some pick-up on the die and punch surfaces were observed, being more pronounced for thicker materials, which can scratch the ground surface of the die and thus the blank surface. Consequently the punch and die surfaces were lightly polished with fine grade emery paper between each experiment

4.8 Experimental results and discussion

Load displacement characteristics when blanking three different thicknesses of mild steel using different values of clamping force, clamp diameter and back-load are now presented and a general description regarding the shape of the load/displacement curve, when using additional

tooling , is given.

A hardness survey in the radial direction, for different values of punch penetration, and across the shear line was made and the corresponding results are presented. The hardness measurements in the radial direction when the specimen was clamped at three different positions are also presented and the effect of clamp diameter on the hardness values around the shearing zone is studied.

Partly blanked specimens were cut into halves and etched and the effect of clamp diameter on the severely deformed region, during conventional blanking studied.

Finally, the effect of different parameters, clamping force, clamp diameter and back-load on the surface finish of the blank edges is investigated.

4.8.1 Load/displacement characteristics

The effect of clamping force, clamp diameter and back-load, using constant value of punch and die diameter, on the load/displacement characteristics when blanking three different thicknesses of mild steel 0.076, 0.101 and 0.120 in. (1.93, 2.56 and 3.04 mm), were studied and the corresponding results are presented in this section. The sequence in which the results are presented can be placed into three categories :

i) Three different values of clamping force (30, 50, 70 kN) were used together with three different clamp diameters with clamp/punch diameter ratios of $\frac{CR}{PR}$ = 1.14, 1.21 and 1.28, Fig. 4-19. For every clamp diameter the results for different values of clamping force are compared.

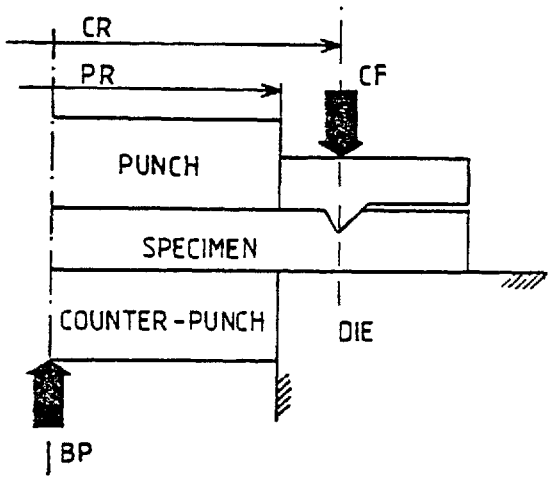

$\frac{CR}{PR} = \begin{Bmatrix} 1.14 \\ 1.21 \\ 1.28 \end{Bmatrix} \rightarrow$ CF = 30, 50 and 70 kN

BP = 0.

Fig. 4-19.

Fig. 4-20(a) shows load vs. displacement in blanking 0.076 in. (1.93 mm) thick strips of mild steel when the blank-holder with minimum diameter ($\frac{CR}{PR}$ = 1.14) was used together with three different values of clamping force (30, 50, 70 kN).

The results for similar experiments when blank-holders with medium and maximum diameters were used ($\frac{CR}{PR}$ = 1.21 and 1.28) are presented in Figs. 4-20(b) and 4-20(c) respectively. The experimental results in all cases are compared with the case when the clamping force is zero. This can easily indicate any change in the load/displacement curve due to the effect of the clamping force. Studying Figs. 4-20(a), 4-20(b) and 4-20(c) shows that there is no obvious increase or decrease in the blanking-load by using the blank-holder even when a large clamping force was applied, i.e. 70 kN. All the curves follow the same trend and the results are scattered around a common curve.

Irrespective of the value of clamping force and clamp diameter, the maximum blanking load occurs at a certain value of punch penetration.

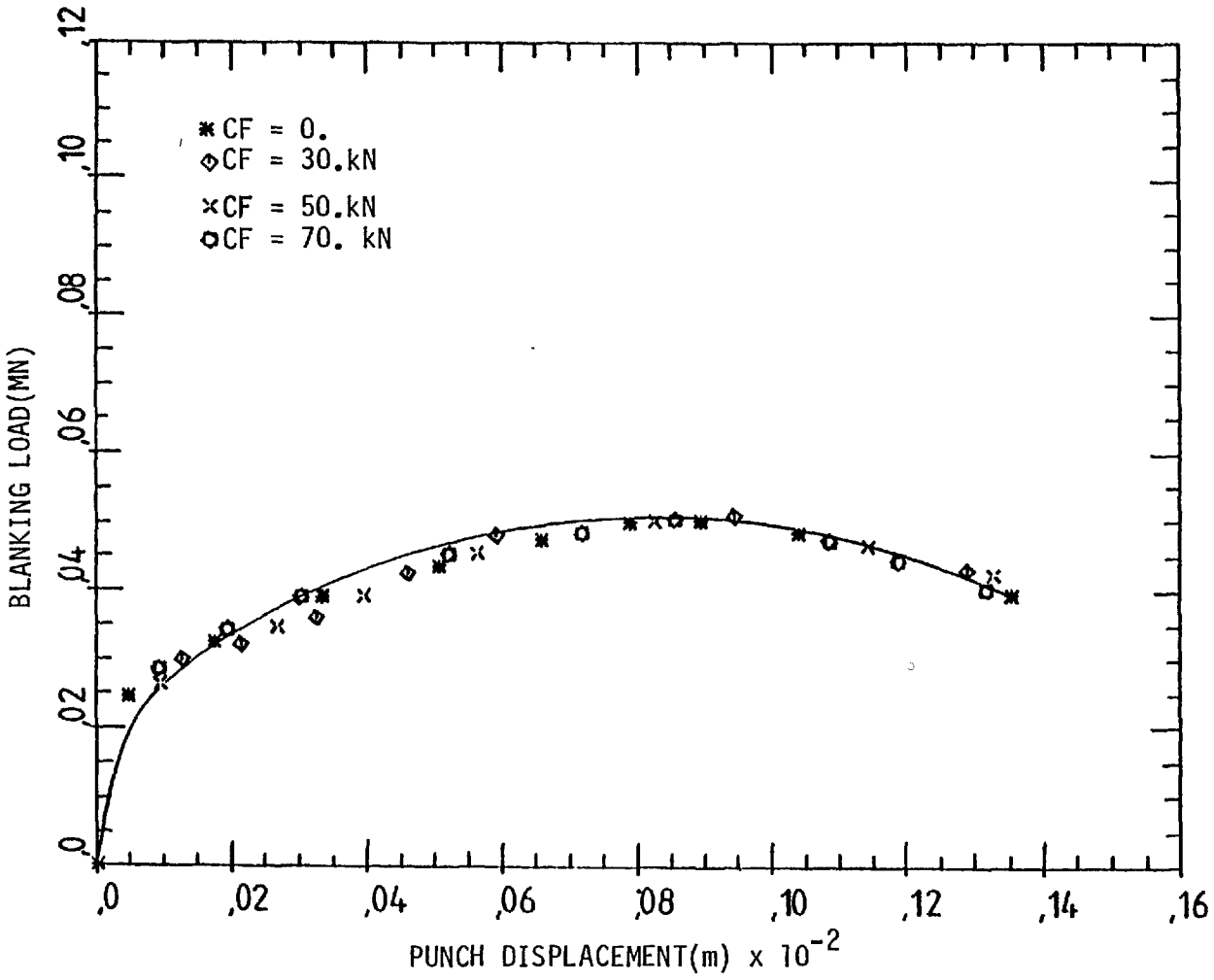

Fig. 5-20(a). Effect of clamping force(CF) on the load/displacement characteristics during blanking strips of mild steel of thickness t = 0.078in.(1.93mm) using a blank-holder with clamp/punch diameter ratio of (CR/PR = 1.14) in the absence of back-load(BP = 0.).

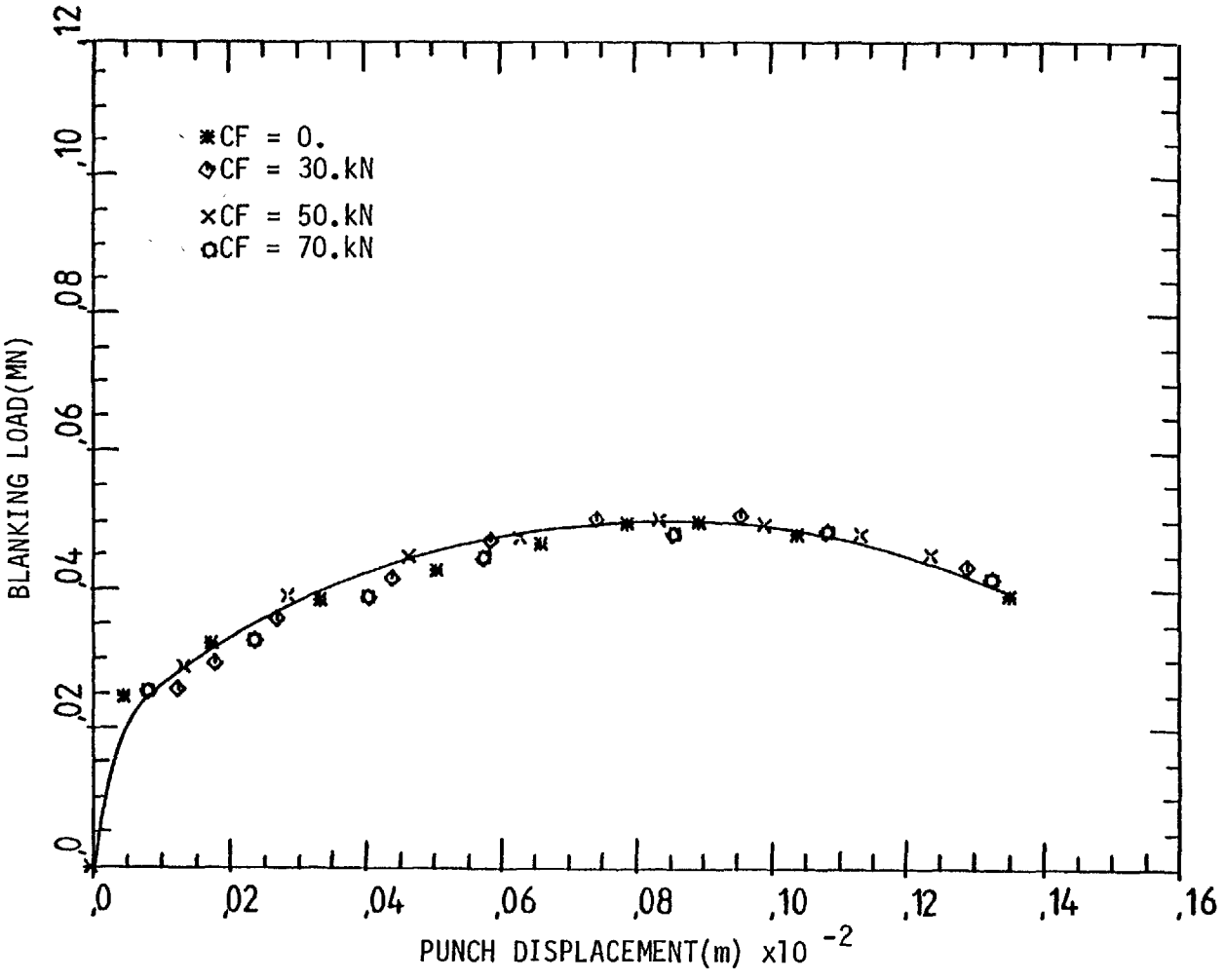

Fig. 5-20(b). Effect of clamping force(CF) on the load/displacement characteristics during blanking strips of mild steel of thickness t = 0.078 in.(1.93mm) using a blank-holder with clamp/punch diameter ratio of (CR/PR = 1.21) in the absence of back-load(BP = 0.).

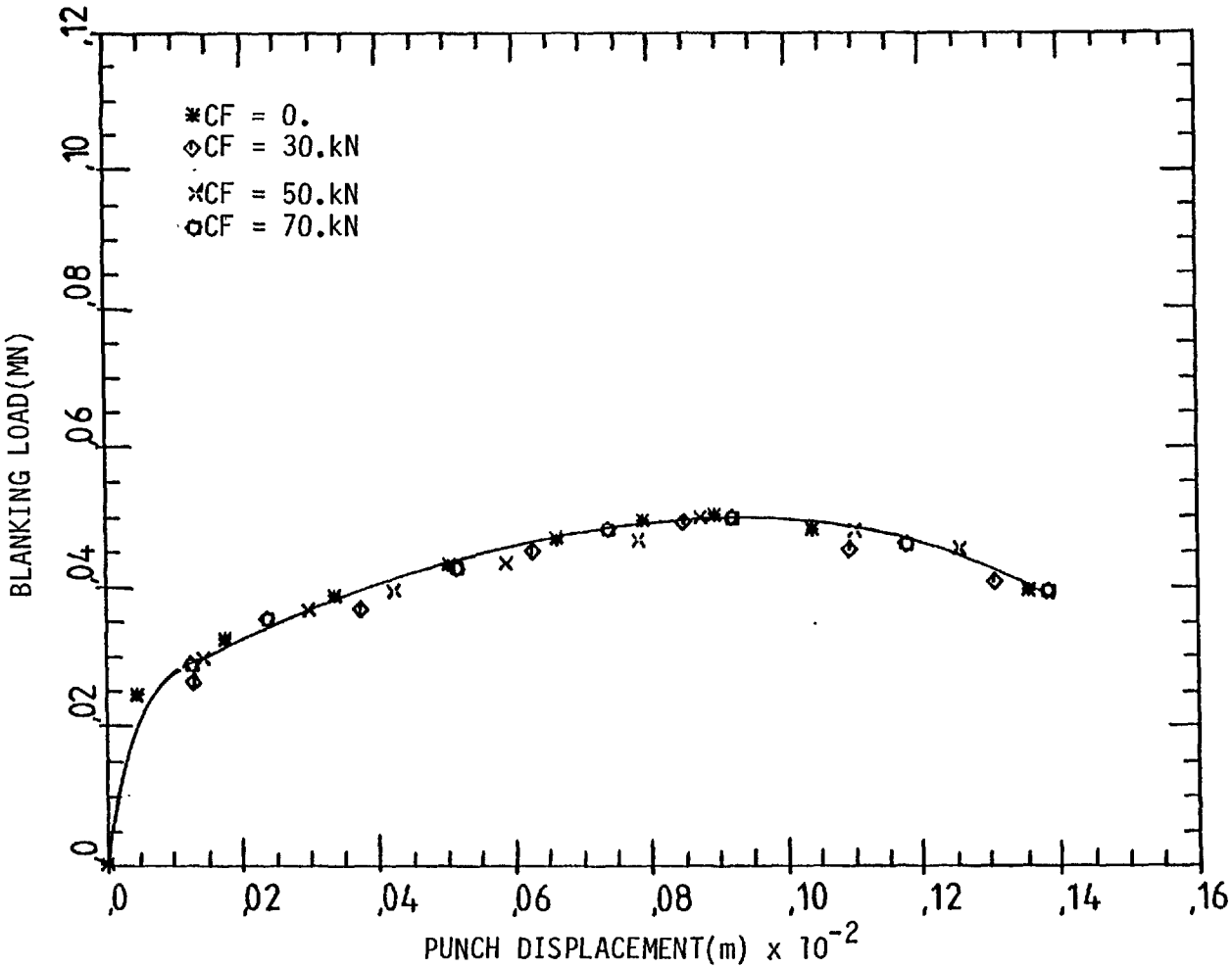

Fig. 5-20(c). Effect of clamping force(CF) on the load/displacement characteristics during blanking strips of mild steel of thickness t = 0.078 in.(1.93mm) using a blank-holder with clamp/punch diameter ratio of (CR/PR = 1.28) in the absence of back-load(BP = 0.).

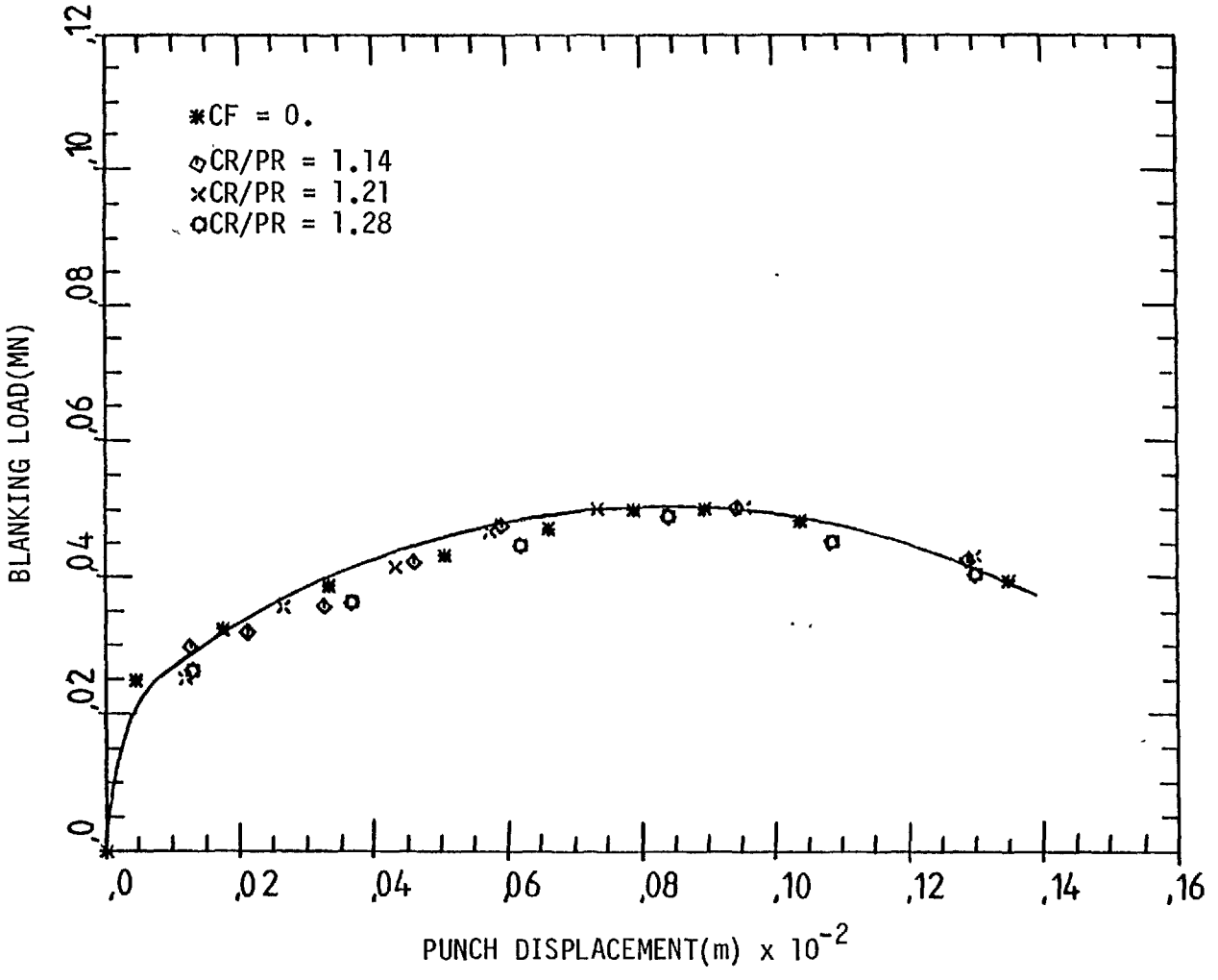

Fig. 5-20(d). Effect of clamp diameter(CR/PR = 1.14, 1.21 and 1.28) on the load/displacement characteristics when blanking mild steel strips of thickness t = 0.078 in.(1.93mm) in the presence of 30 kN clamping force(CF = 30 kN) and no back-load(BP = 0.).

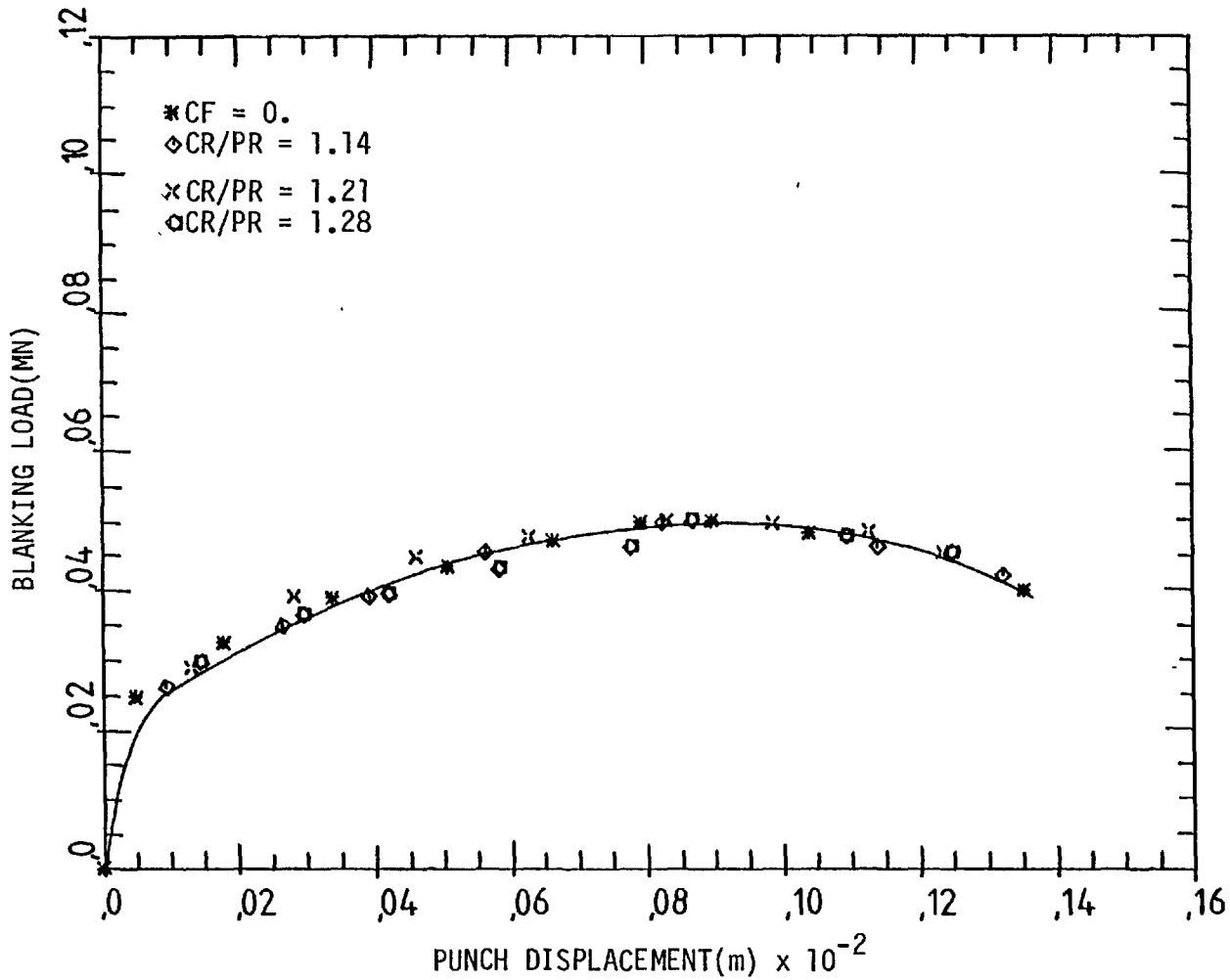

Fig. 5-20(e). Effect of clamp diameter(CR/PR = 1.14, 1.21 and 1.28) on the load/displacement characteristics when blanking mild steel strips of thickness t = 0.078 in.(1.93mm) in the presence of 50 kN clamping force(CF = 50 kN) and no back-load(BP = 0.).

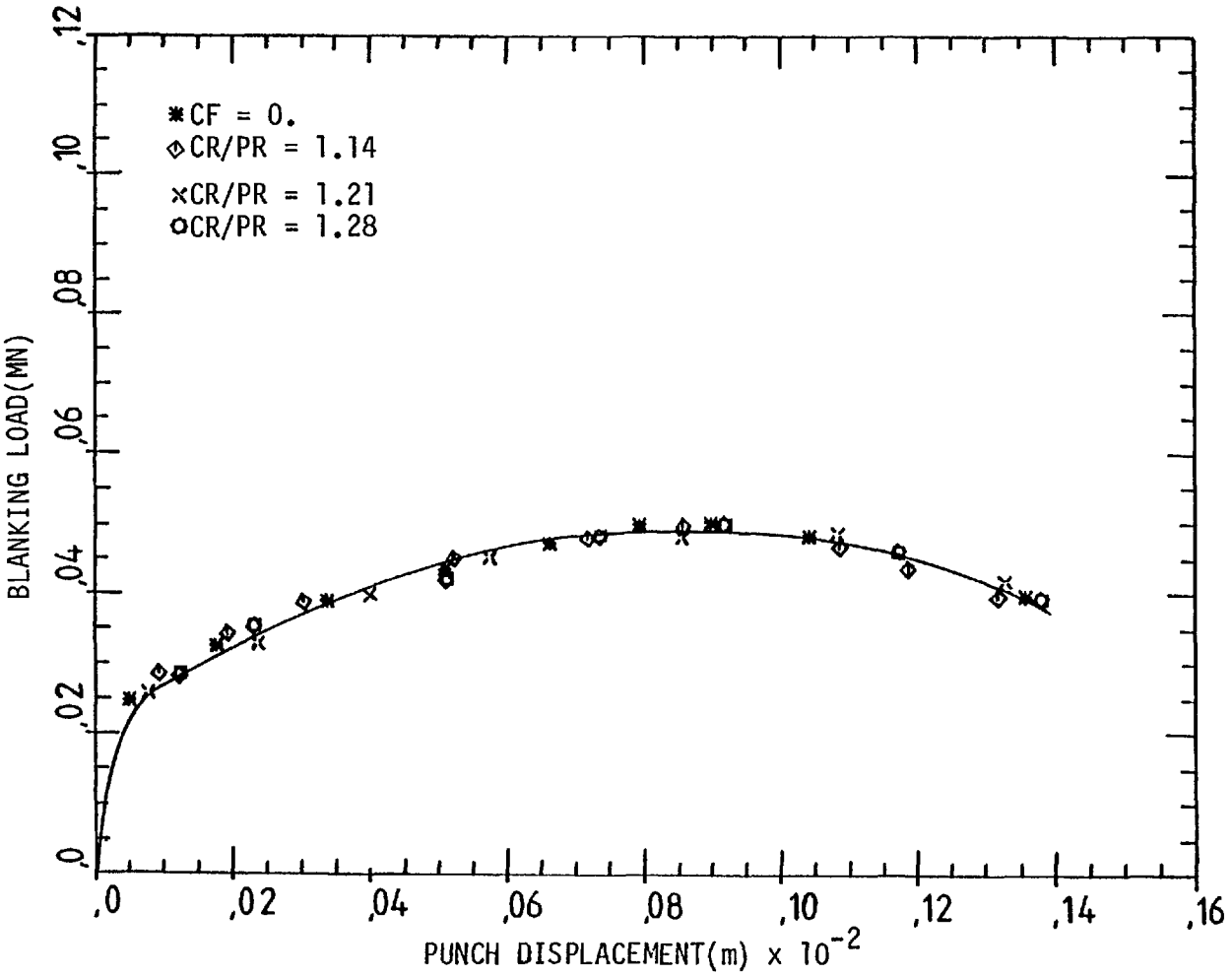

Fig. 5-20(f). Effect of clamp diameter(CR/PR = 1.14, 1.21 and 1.28) on the load/displacement characteristics when blanking mild steel strips of thickness t = 0.078 in.(1.93mm) in the presence of 50 kN clamping force(CF = 50 kN) and no back-load(BP = 0.).

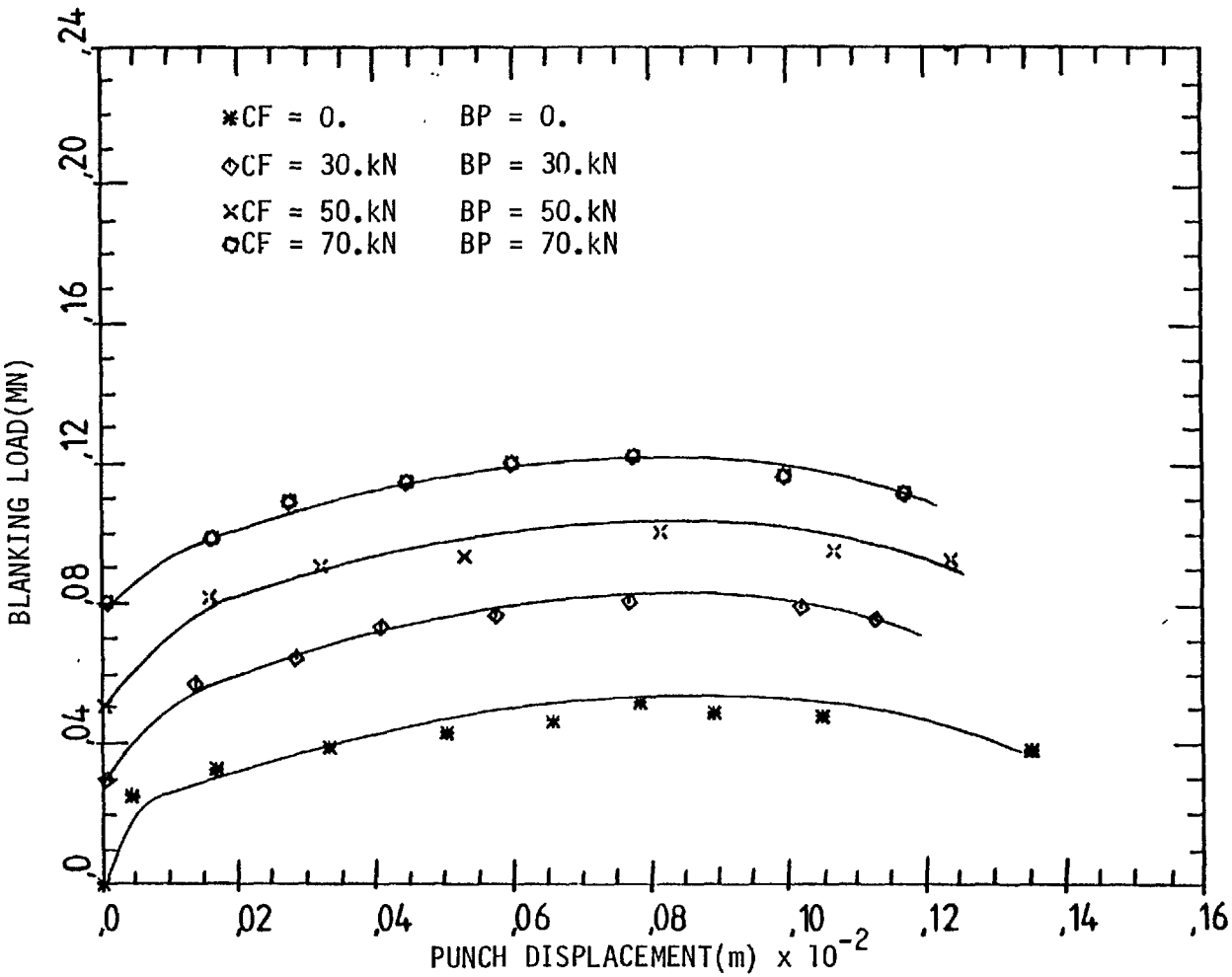

Fig. 5-20(g). Combined effect of clamping force and back-load(CF and BP) on the load/displacement characteristics when blanking strips of mild steel of thickness t = 0.078 in. (1.93 mm) using a blank-holder with clamp/punch diameter ratio of CR/PR = 1.14.

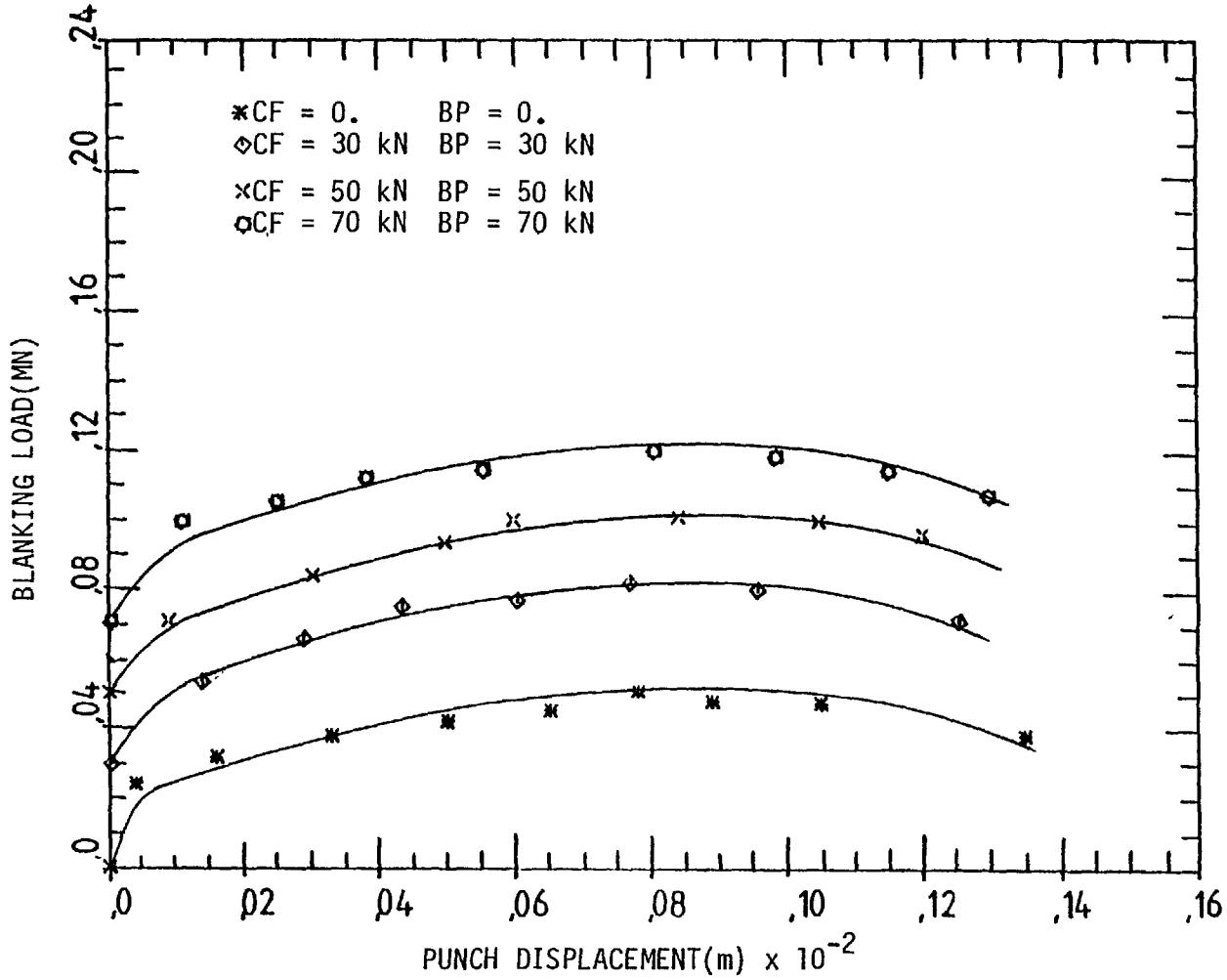

Fig. 5-20(h). Combined effect of clamping force and back-load(CF and BP) on the load/displacement characteristics when blanking strips of mild steel of thickness t = 0.078 in. (1.93 mm) using a blank-holder with clamp/punch diameter ratio of CR/PR = 1.21.

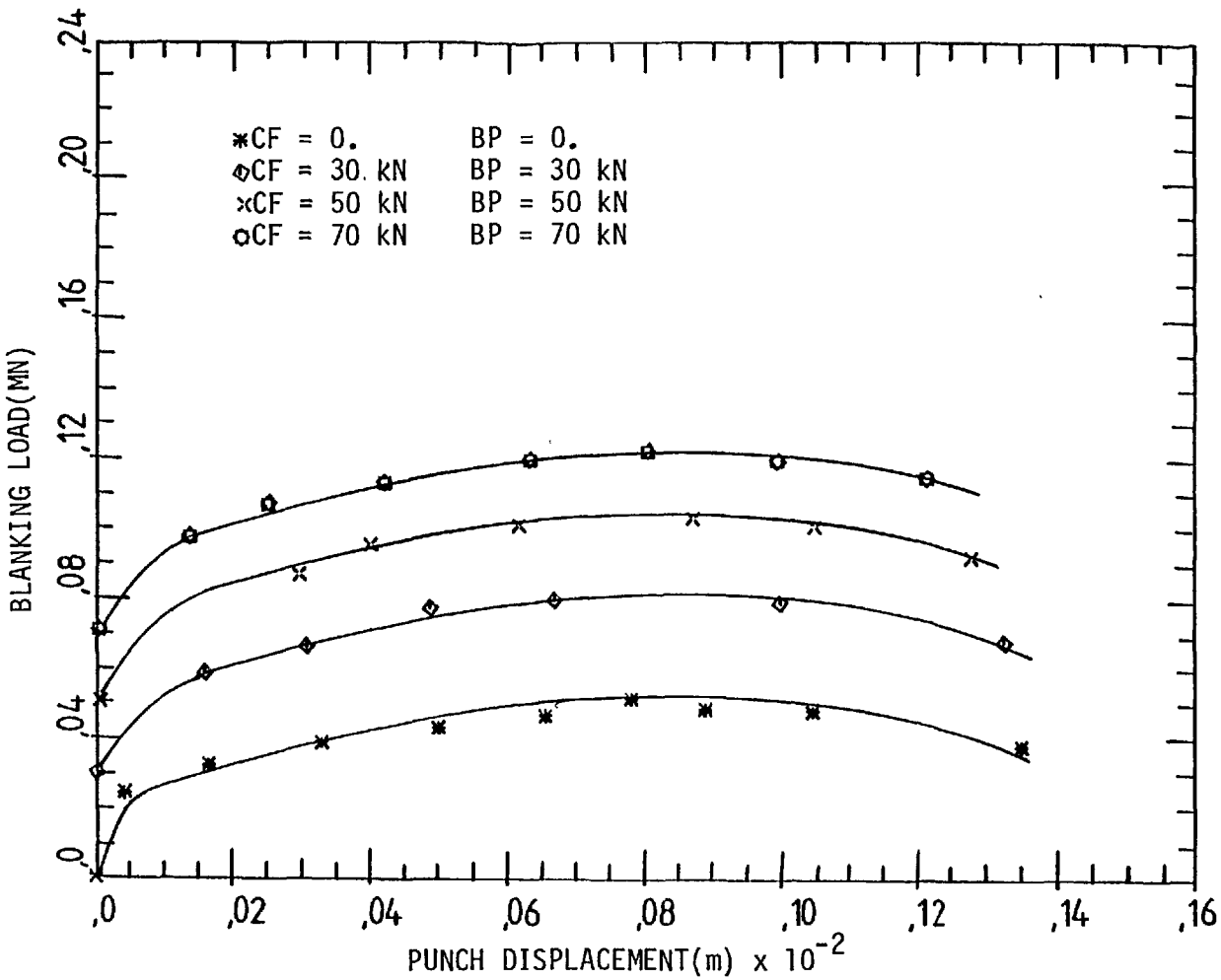

Fig. 5-20(i). Combined effect of clamping force and back-load(CF and BP) on the load/displacement characteristics when blanking strips of mild steel of thickness t = 0.078 in.(1.93 mm) using a blank-holder with clamp/punch diameter ratio of CR/PR = 1.28.

It can be concluded that the application of a clamping force in blanking does not change the load/displacement curve.

ii) For every value of clamping force, three different clamp diameters were used, Fig. 4-21, and the corresponding results compared.

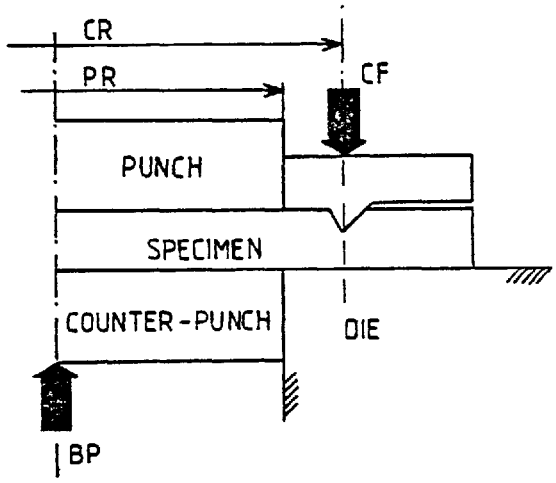

$CF = \begin{Bmatrix} 30 \\ 50 \\ 70 \end{Bmatrix}$ kN, $\frac{CR}{PR} = 1.28,\ 1.21$ and 1.14

$BP = 0$

Fig. 4-21.

Fig. 4-20(d) shows the results obtained in blanking when using 30 kN clamping force and three different blank-holder diameters. Similar results when using clamping forces equal to 50 and 70 kN are presented in Fig. 4-20(e) and 4-20(f).

Figs. 4-20(d), 4-20(e) and 4-20(f) indicate that all curves follow the same trend and, for different values of clamping force and different blank-holder diameters, the difference in the load/displacement curves is negligible. It can be concluded that, by changing the blank-holder diameter under a certain amount of clamping force, the maximum value of blanking force does not change and the maximum load occurs at the same magnitude of punch penetration irrespective of the blank-holder diameter.

iii) Three equal values of clamping force and back-load were used while the clamp diameter took three different values, Fig. 4-22.

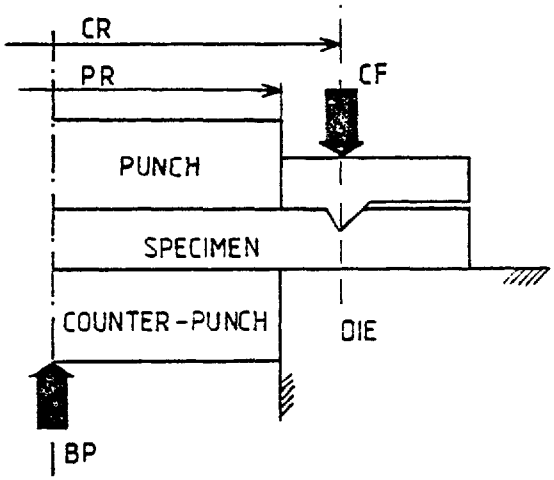

$$CF = BP = \begin{Bmatrix} 30 \\ 50 \\ 70 \end{Bmatrix} \text{ kN}, \quad \frac{CR}{PR} = 1.28,\ 1.21,\ 1.14$$

Fig. 4-22.

Fig. 4-20(g) shows the results obtained from blanking specimens when using three equal values of clamping force and back-load. The clamping force acted at a clamp/punch diameter ratio of $\frac{CR}{PR} = 1.21$ and 1.28 are shown in Figs. 4-20(h) and 4-20(i) respectively. The results show that, by employing a back-load, the blanking force increases by the amount of the back-load. The curves follow the same trend and each curve differs from the others by an amount equal to the difference in the back-load. The maximum blanking force occurs at the same punch penetration irrespective of the value of the back-load, clamping force and blank-holder diameter. The blanking-load at the starting point for each curve shows the amount of back-load present for that particular curve .

Figs. 4-23(a) to 4-23(i) and 4-24(a) to 4-24(i) show that the same conclusions can be drawn for material thicknesses of t = 0.101 in. (2.56 mm) and t = 0.120 in. (3.04 mm) as for t = 0.076 in. (1.93 mm).

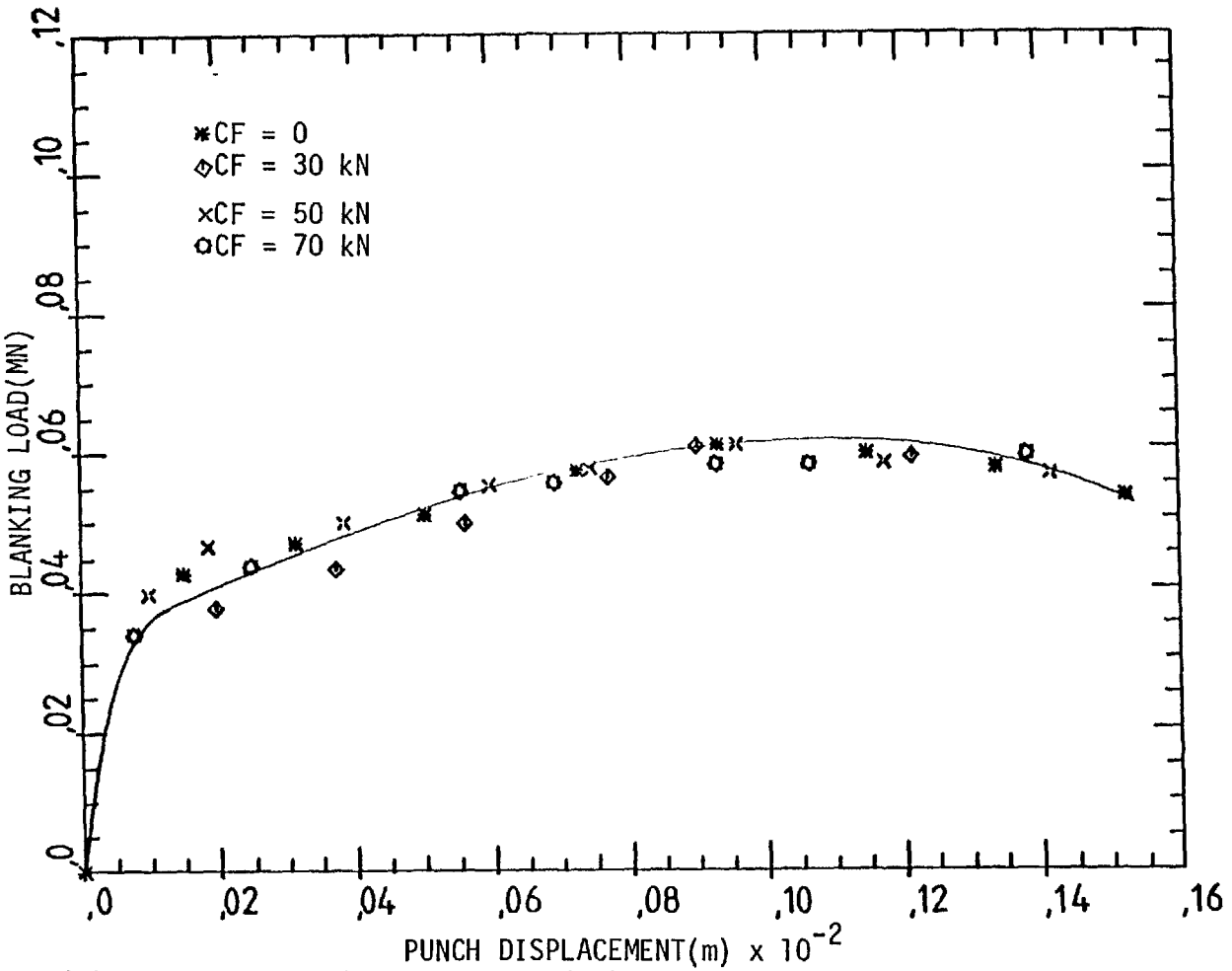

Fig. 5-23(a). Effect of clamping force (CF) on the load/displacement characteristics during blanking strips of mild steel of thickness t = 0.101 in. (2.56 mm) using a blank-holder with clamp/punch diameter ratio of (CR/PR = 1.14) in the absence of back-load (BP = 0).

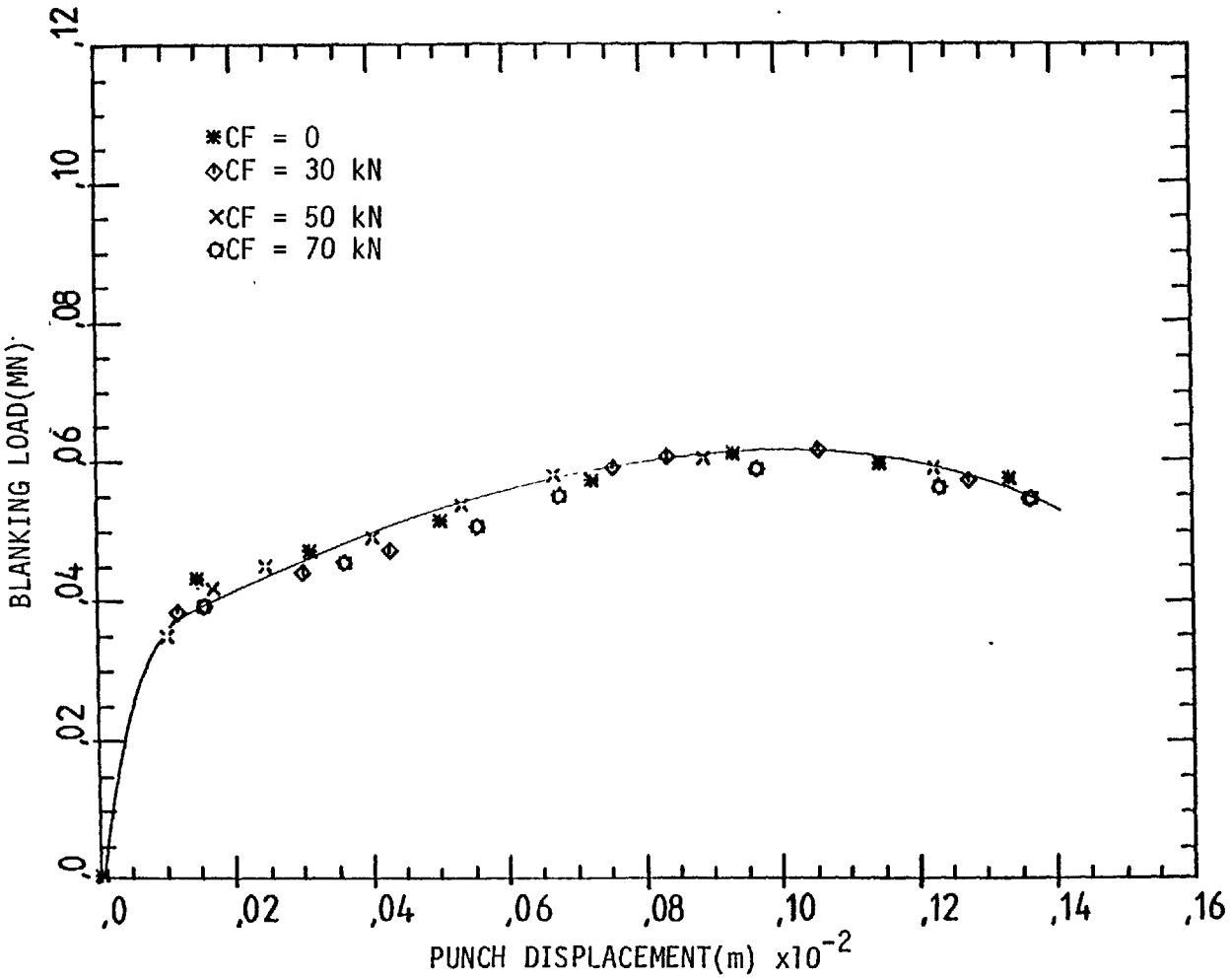

Fig. 5-23(b). Effect of clamping force (CF) on the load/displacement characteristics during blanking strips of mild steel of thickness t = 0.101 in. (2.56 mm) using a blank-holder with clamp/punch diameter ratio of (CR/PR = 1.21) in the absence of back-load (BP = 0).

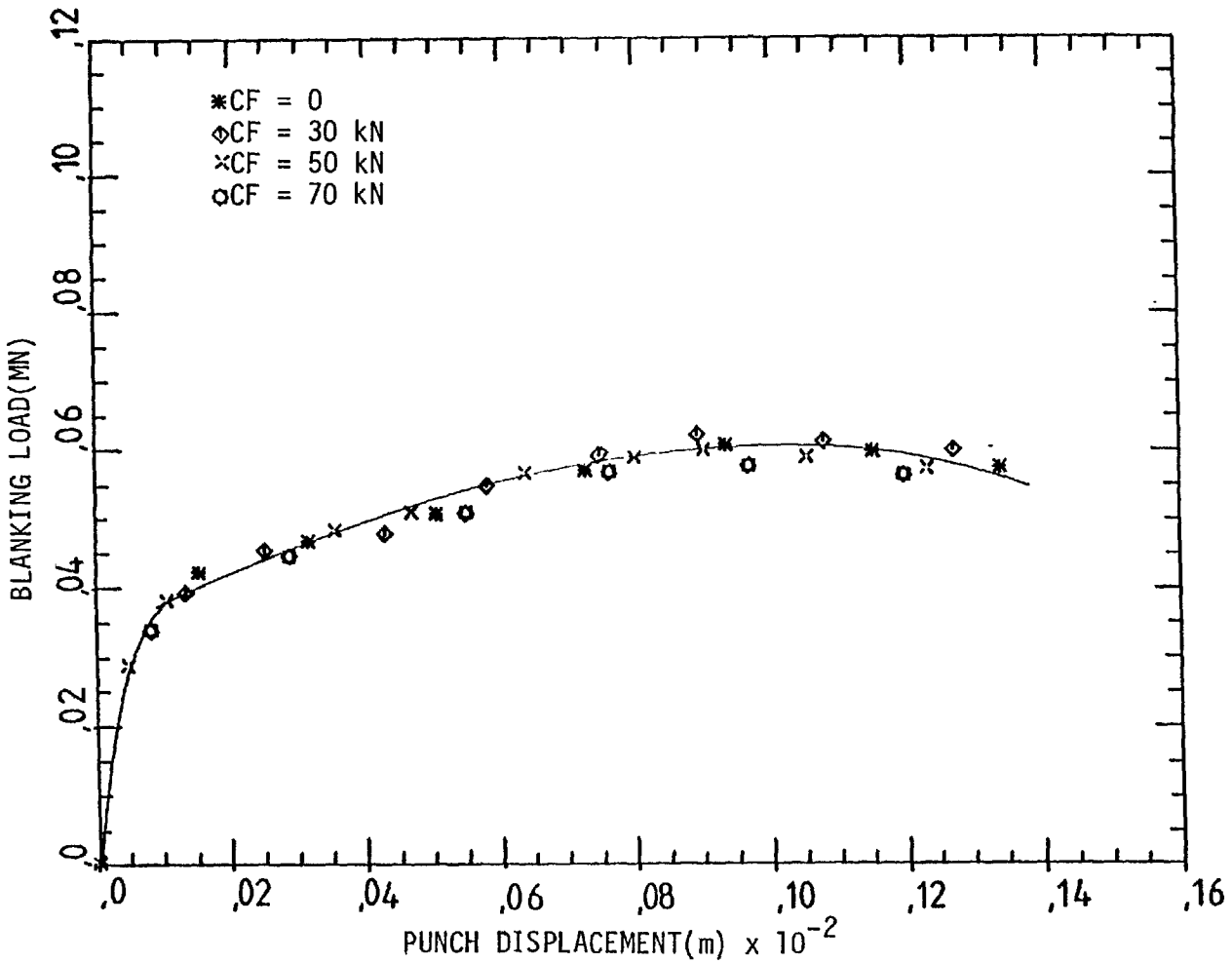

Fig. 5-23(c). Effect of clamping force (CF) on the load/displacement characteristics during blanking strips of mild steel of thickness t = 0.101 in. (2.56 mm) using a blank-holder with clamp/punch diameter ratio of (CR/PR = 1.28) in the absence of back-load (BP = 0).

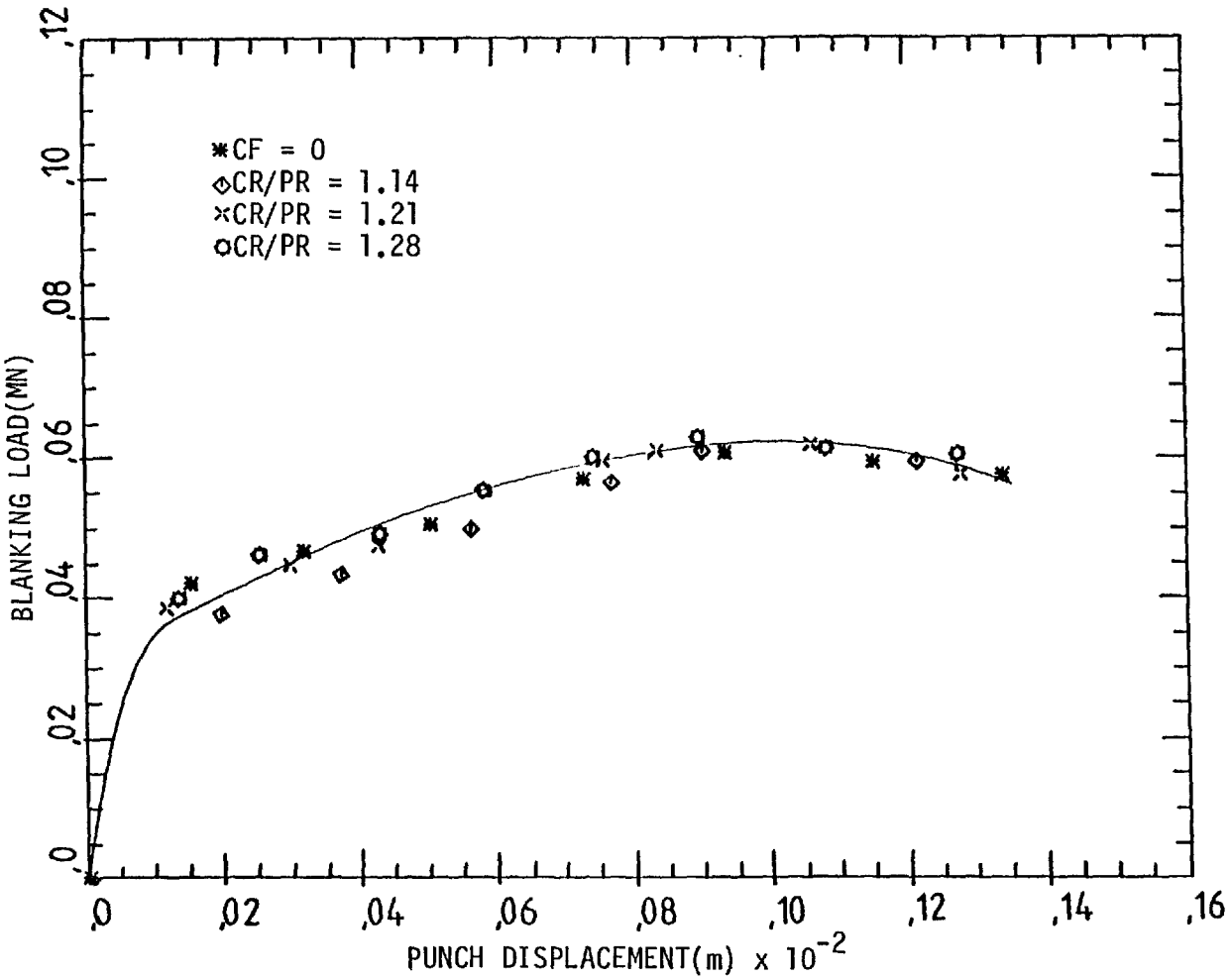

Fig. 5-23(d). Effect of clamp diameter (CR/PR = 1.14, 1.21 and 1.28) on the load/displacement characteristics when blanking strips of mild steel of thickness t = 0.101 in. (2.56 mm) in the presence of 30 kN clamping force (CF = 30 kN) and no back-load (BP = 0).

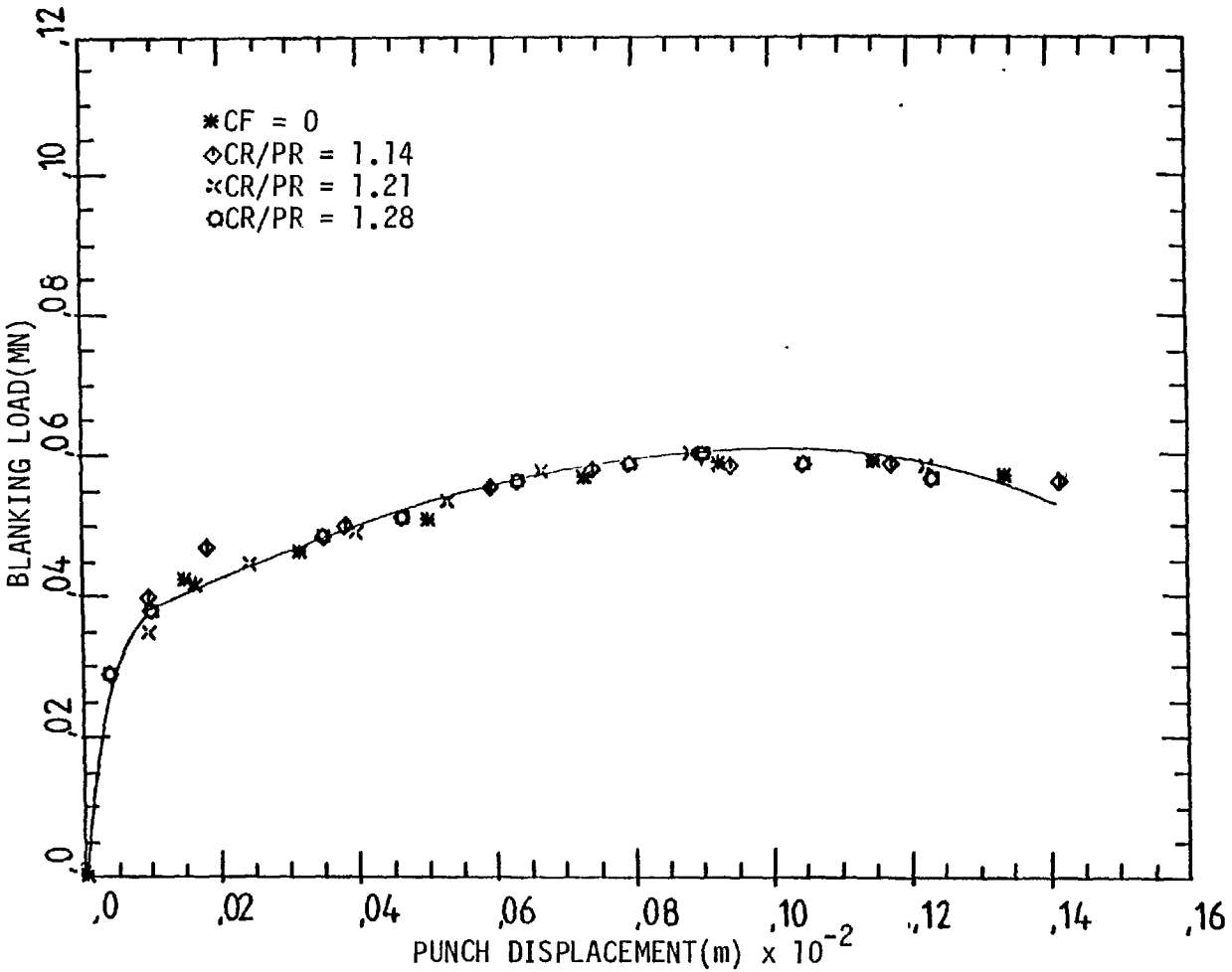

Fig. 5-23(e). Effect of clamp diameter (CR/PR = 1.14, 1.21 and 1.28) on the load/displacement characteristics when blanking mild steel strips of thickness t = 0.101 in. (2.56 mm) in the presence of 50 kN clamping force (CF = 50 kN) and no back-load (BP = 0).

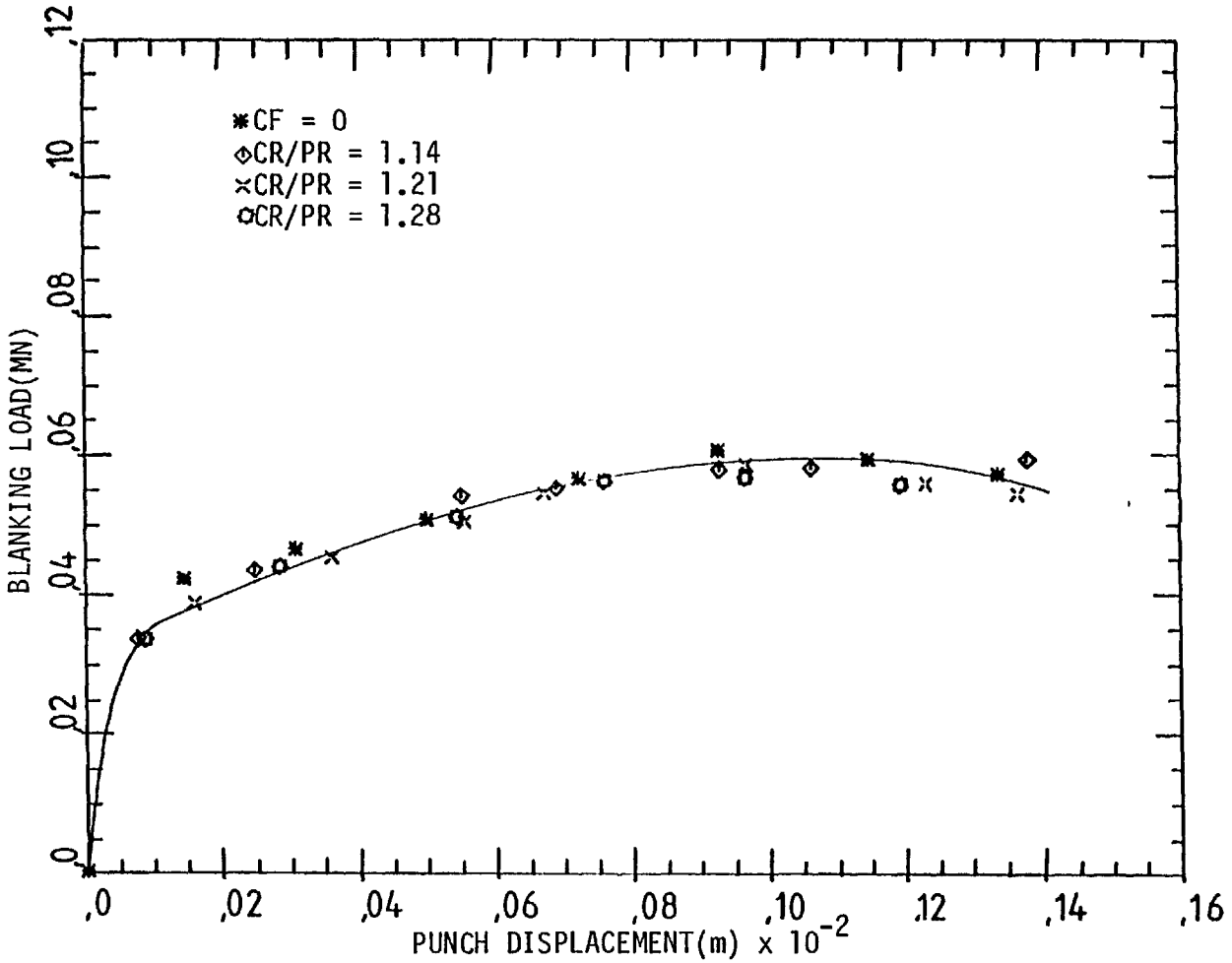

Fig. 5-23(f). Effect of clamp diameter (CR/PR = 1.14, 1.21 and 1.28) on the load/displacement characteristics when blanking mild steel strips of thickness t = 0.101 in. (2.56 mm) in the presence of 70 kN clamping force (CF = 70 kN) and no back-load (BP = 0).

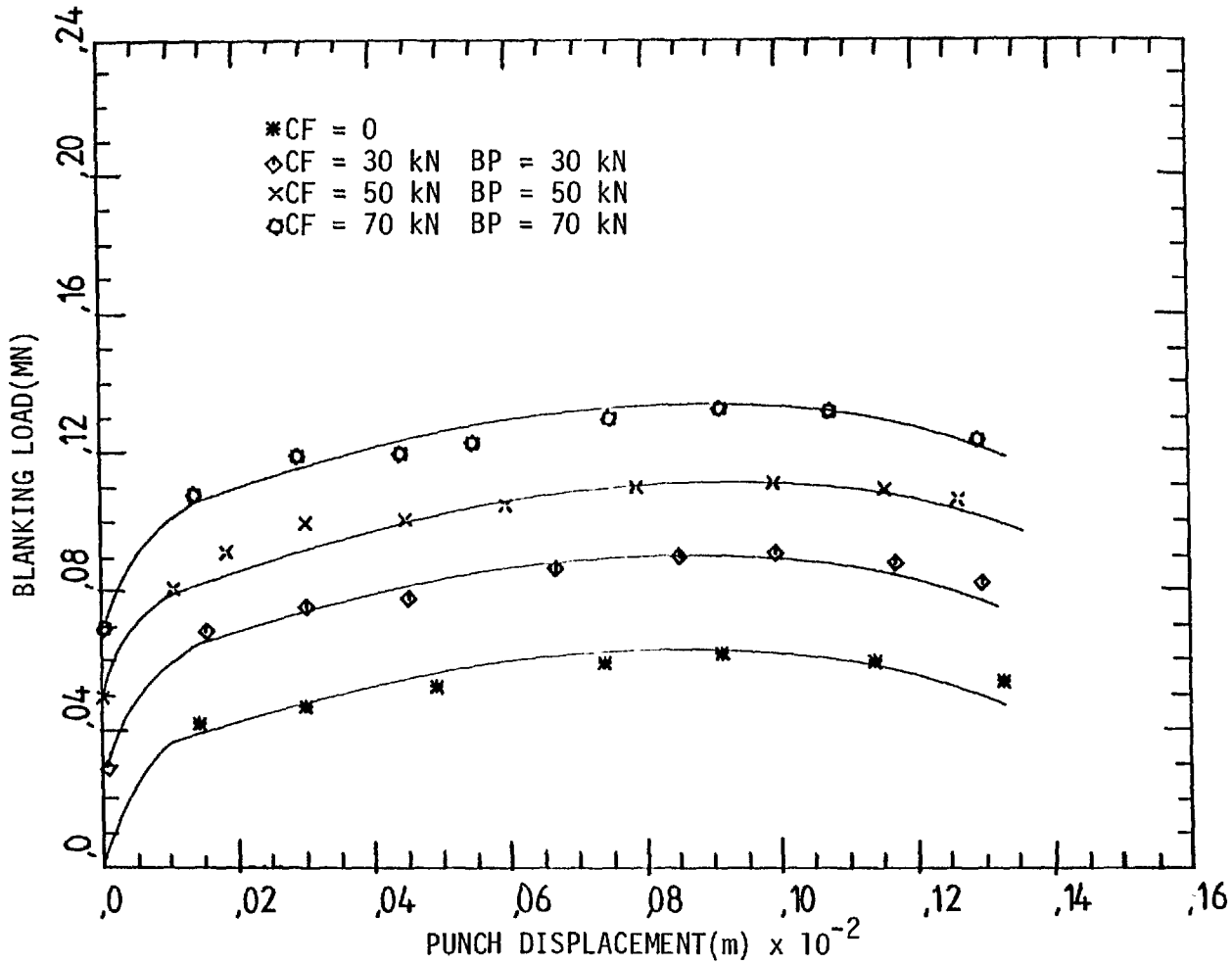

Fig. 5-23(g). Combined effect of clamping force and back-load (CF and BP) on the load/displacement characteristics when blanking strips of mild steel of thickness t = 0.101 in. (2.56 mm) using a blank-holder with clamp/punch diameter ratio of CR/PR = 1.14.

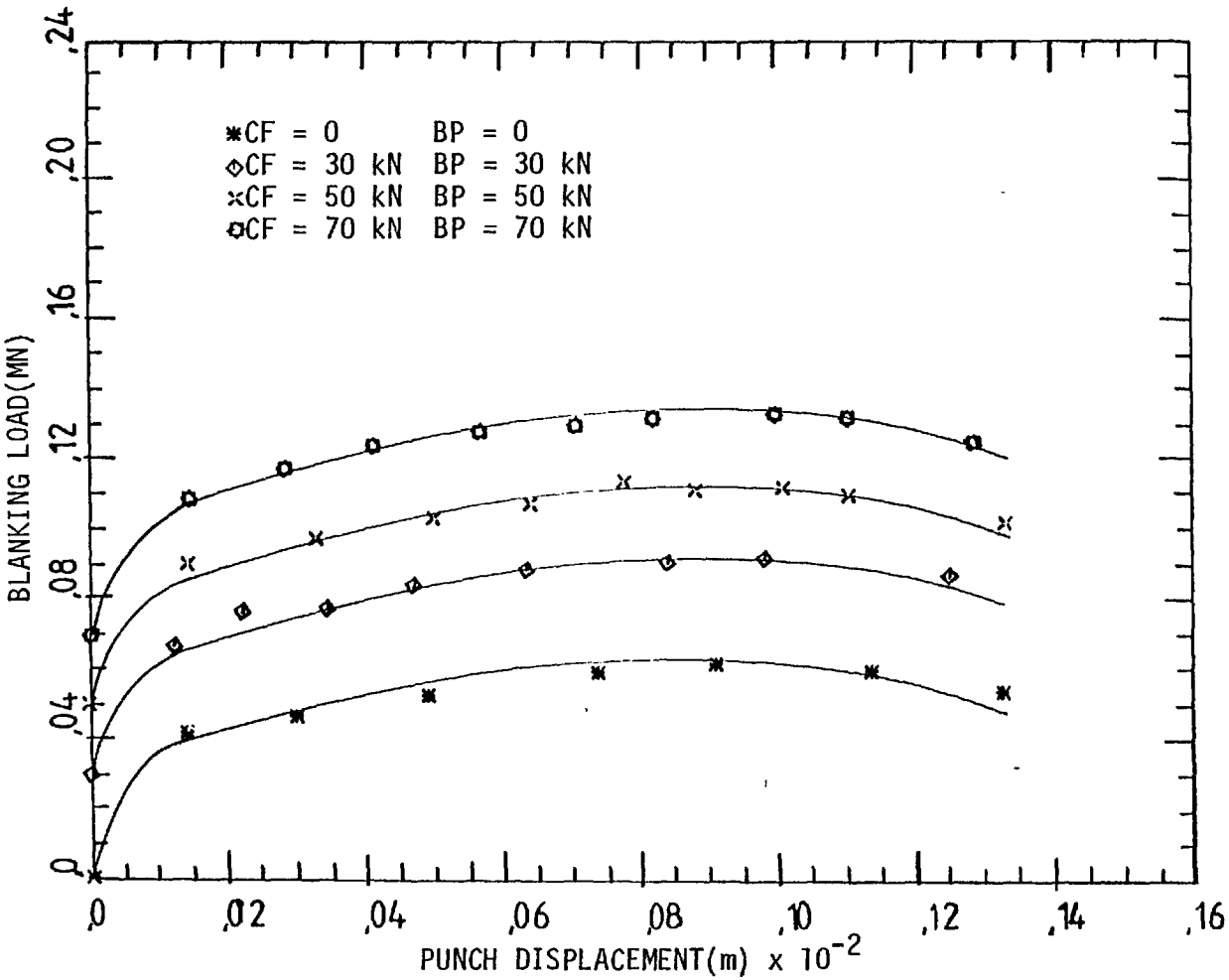

Fig. 5-23(h). Combined effect of clamping force and back-load (CF and BP) on the load/displacement characteristics when blanking strips of mild steel of thickness t = 0.101 in. (2.56 mm) using a blank-holder with clamp/punch diameter ratio of CR/PR = 1.21.

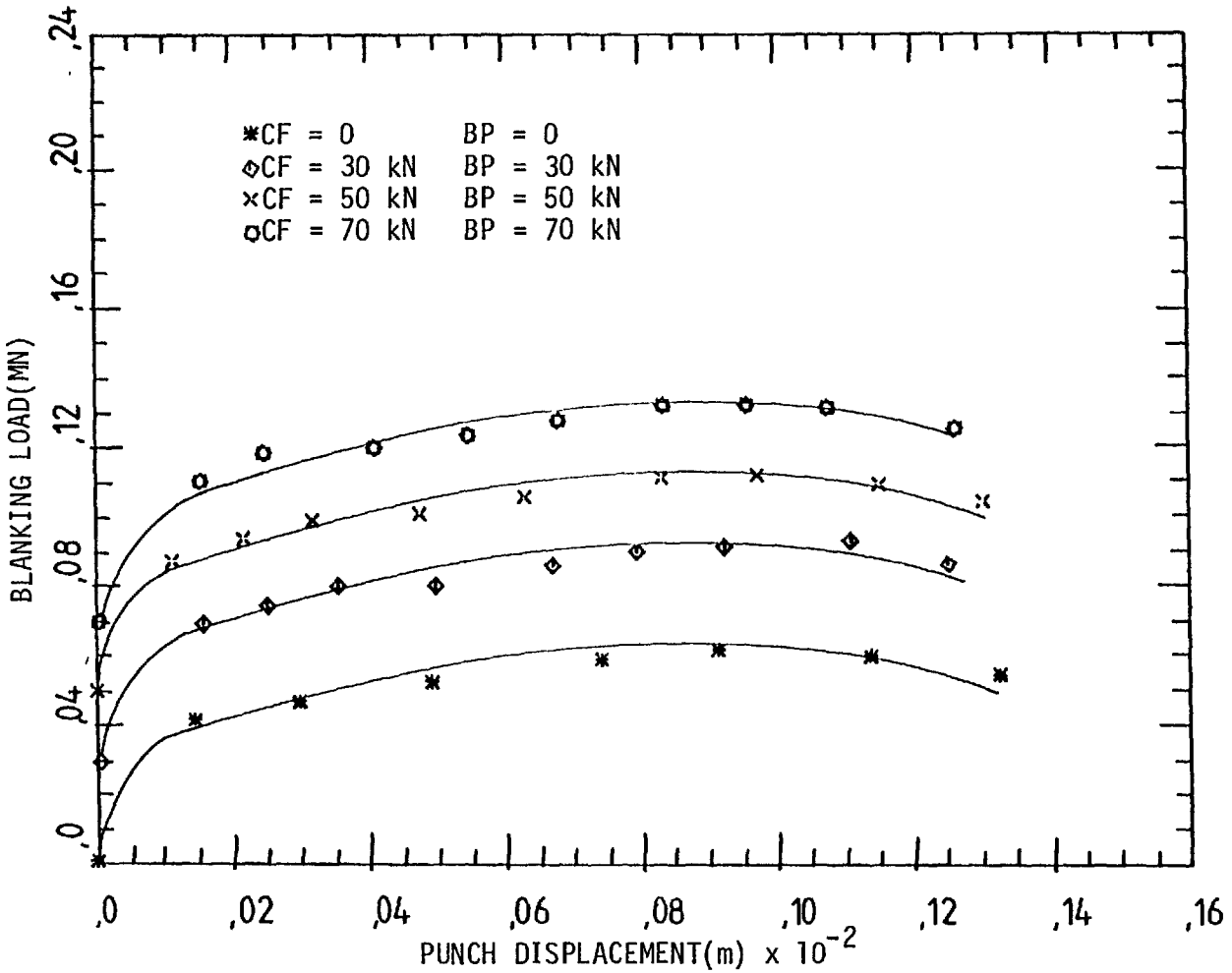

Fig. 5-23(i). Combined effect of clamping force and back-load (CF and BP) on the load/displacement characteristics when blanking strips of mild steel of thickness t = 0.101 in. (2.56 mm) using a blank-holder with clamp/punch diameter ratio of CR/PR = 1.28.

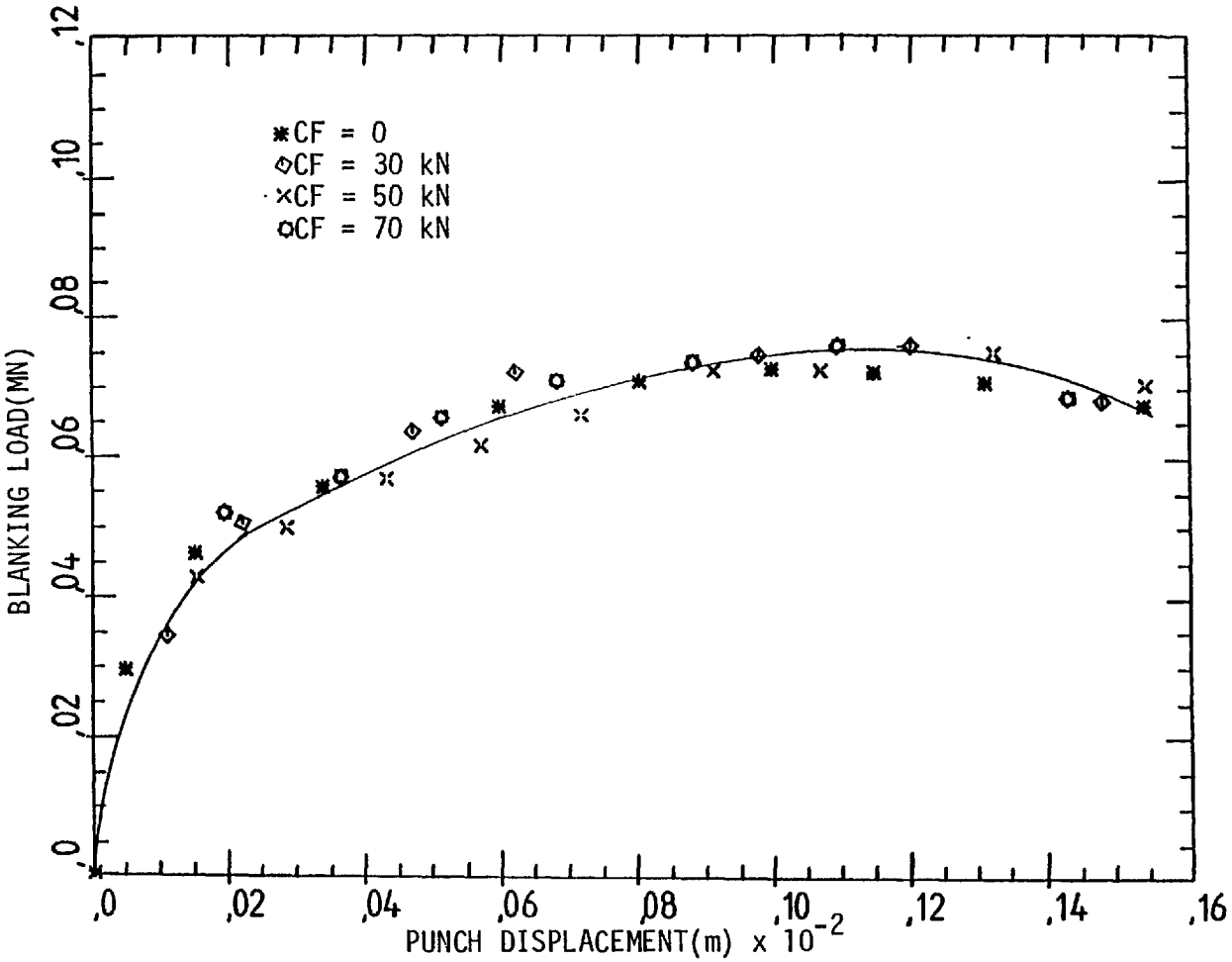

Fig.5-24(a). Effect of clamping force (CF) on the load/displacement characteristics during blanking strips of mild steel of thickness t = 0.120 in. (3.04 mm) using a blank-holder with clamp/punch diameter ratio of (CR/PR = 1.14) in the absence of back-load (BP = 0).

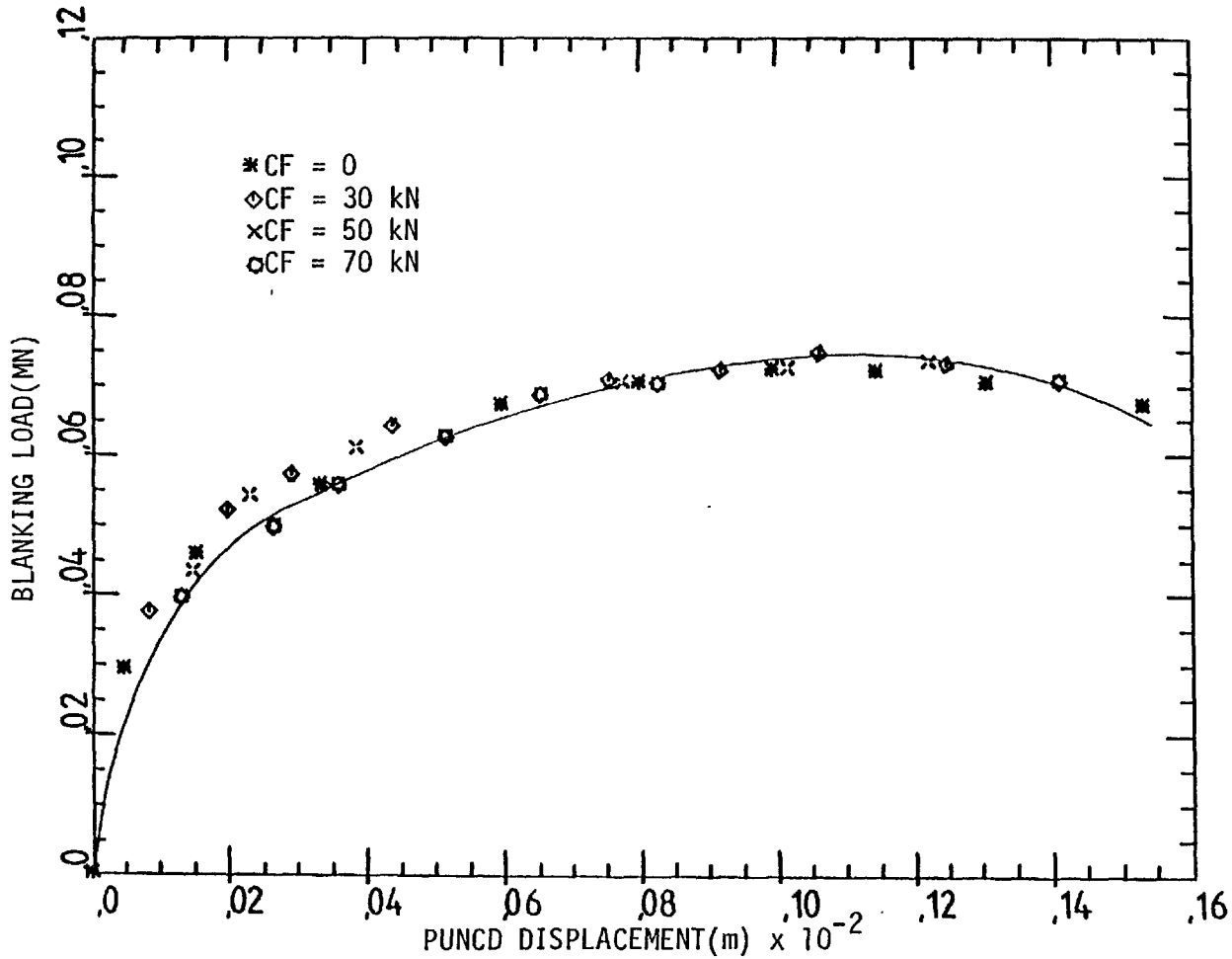

Fig. 5-24(b). Effect of clamping force (CF) on the load/displacement characteristics during blanking strips of mild steel of thickness t = 0.120 in. (3.04 mm) using a blank-holder with clamp/punch diameter ratio of (CR/PR = 1.21) in the absence of back-load (BP = 0).

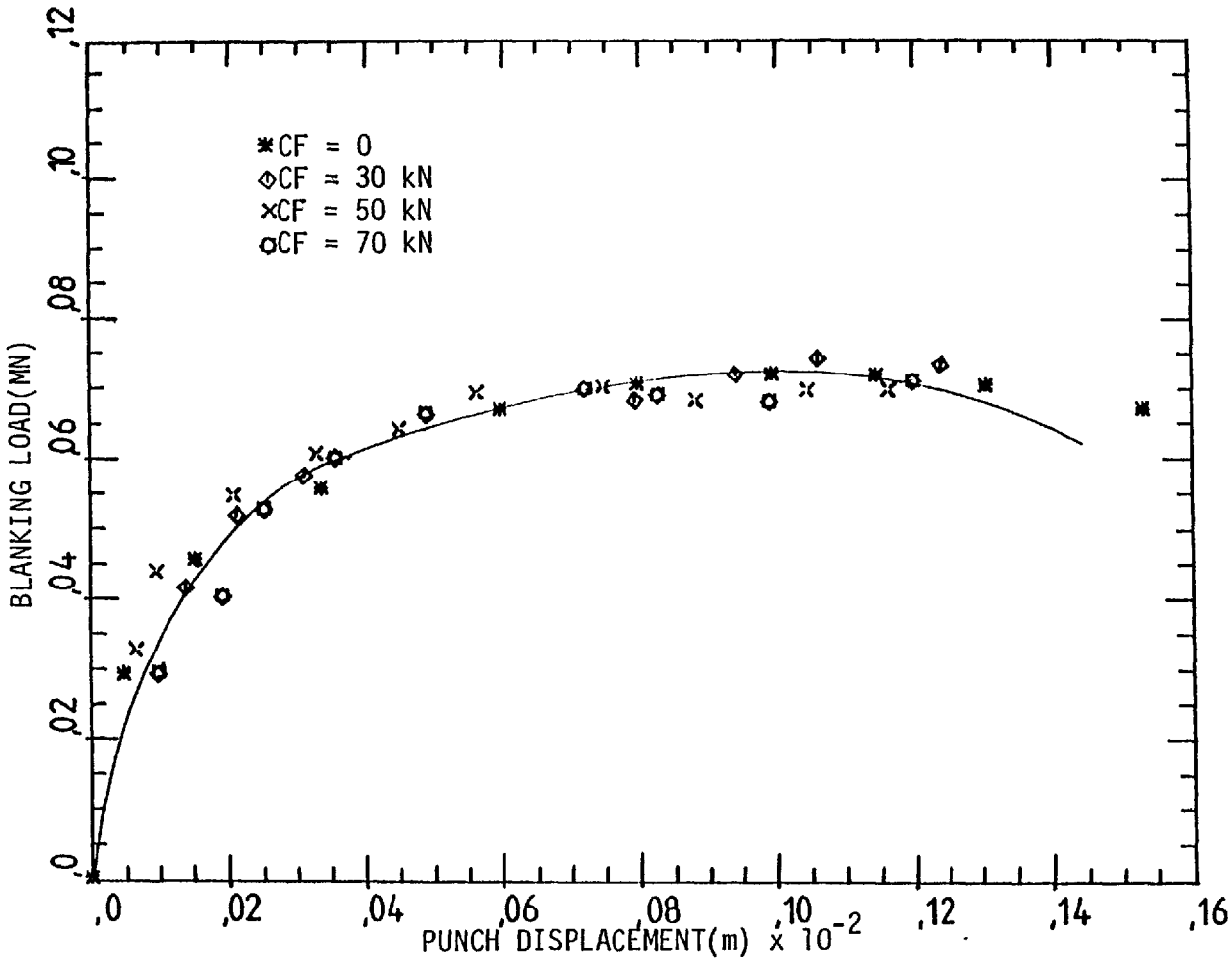

Fig. 5-24(c). Effect of clamping force(CF) on the load/displacement characteristics during blanking strips of mild steel of thickness t = 0.120 in. (3.04 mm) using a blank-holder with clamp/punch diameter ratio of (CR/PR = 1.28) in the absence of back-load (BP = 0).

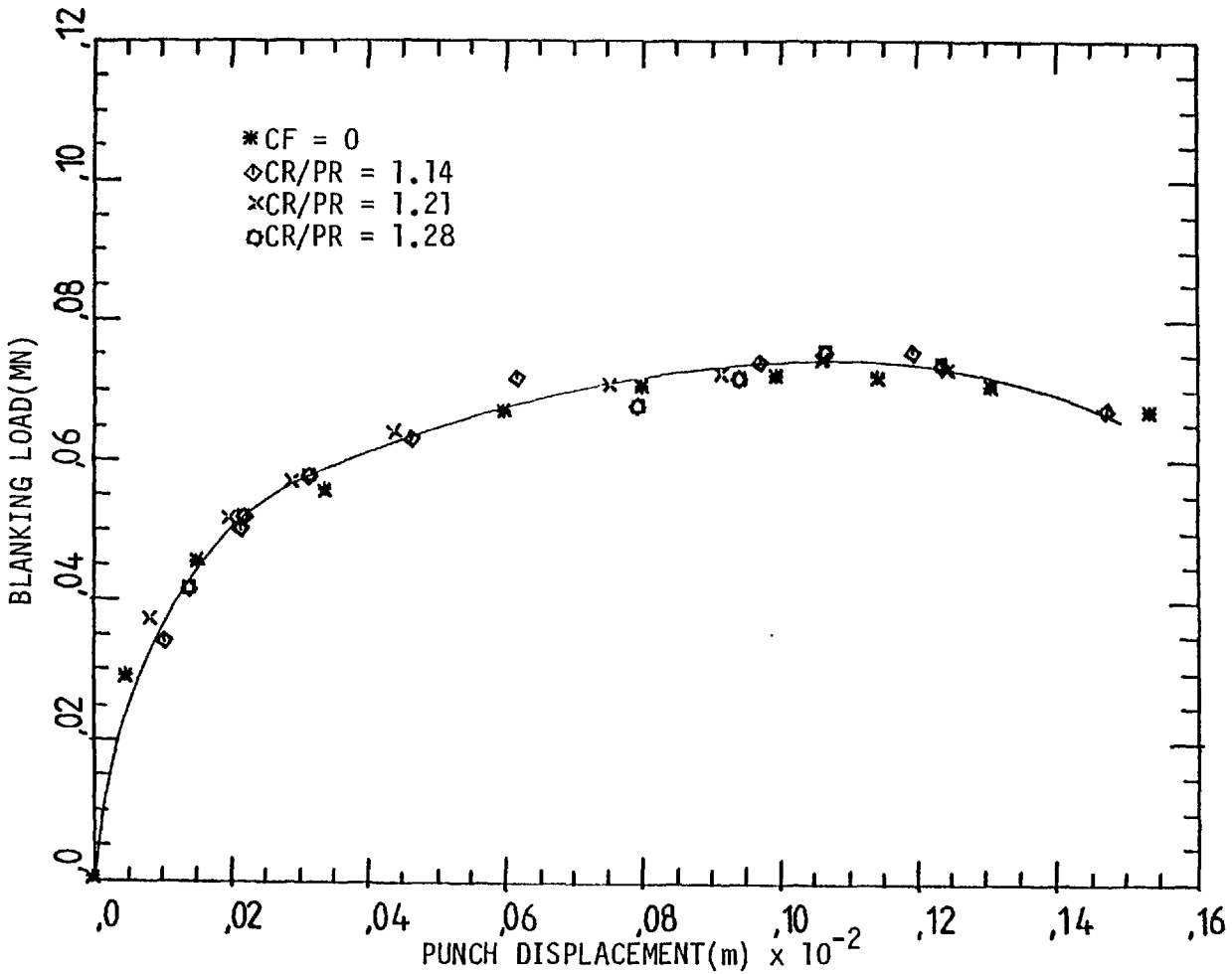

Fig. 5-24(d). Effect of clamp diameter (CR/PR = 1.14, 1.21 and 1.28) on the load/displacement characteristics when blanking strips of mild steel of thickness t = 0.120 in. (3.04 mm) in the presence of 30 kN clamping force (CF = 30 kN) and no back-load (BP = 0).

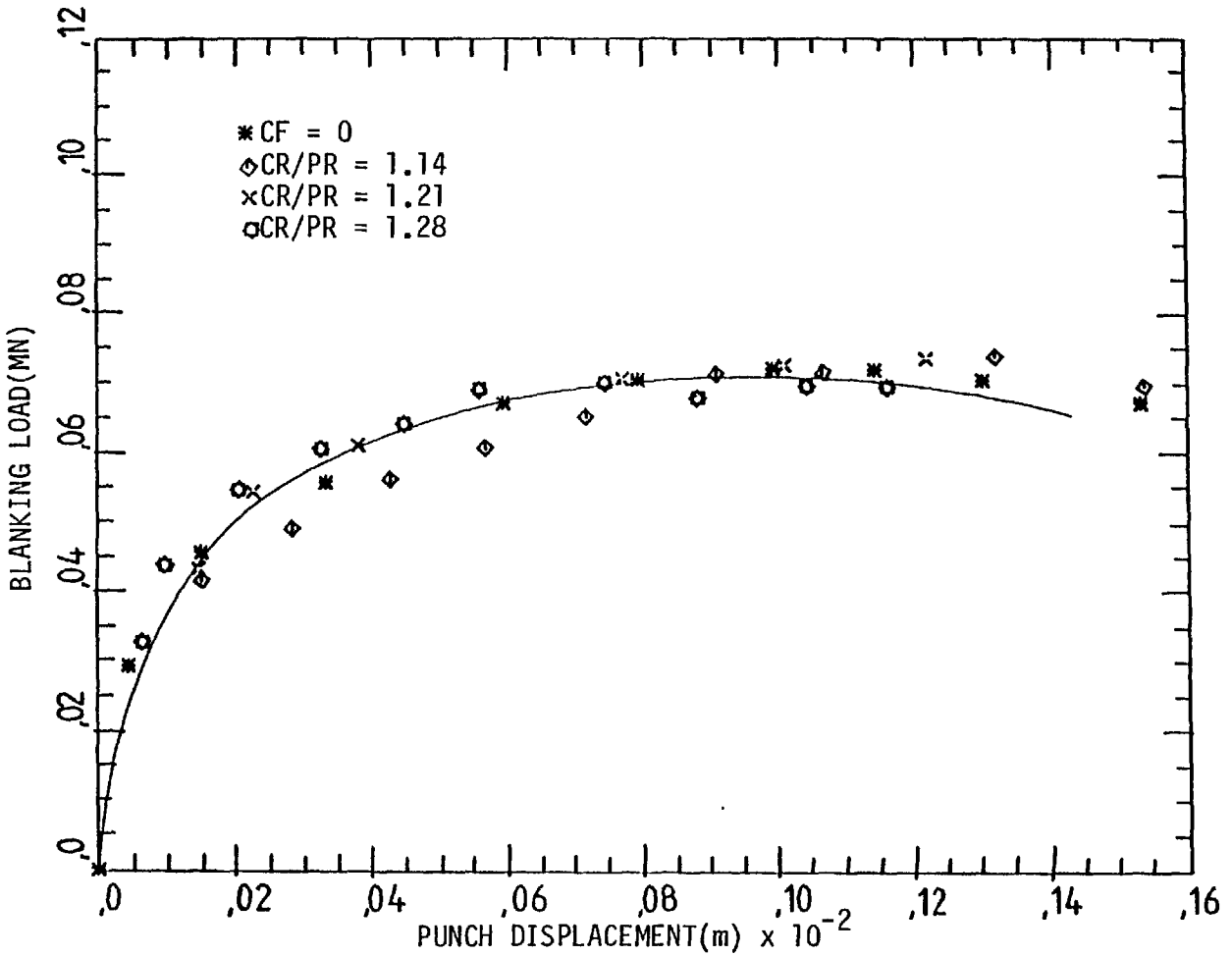

Fig. 5-24(e). Effect of clamp diameter (CR/PR = 1.14, 1.21 and 1.28) on the load/displacement characteristics when blanking mild steel strips of thickness t = 0.120 in. (3.04 mm) in the presence of 50 kN clamping force (CF = 50 kN) and no back-load (BP = 0).

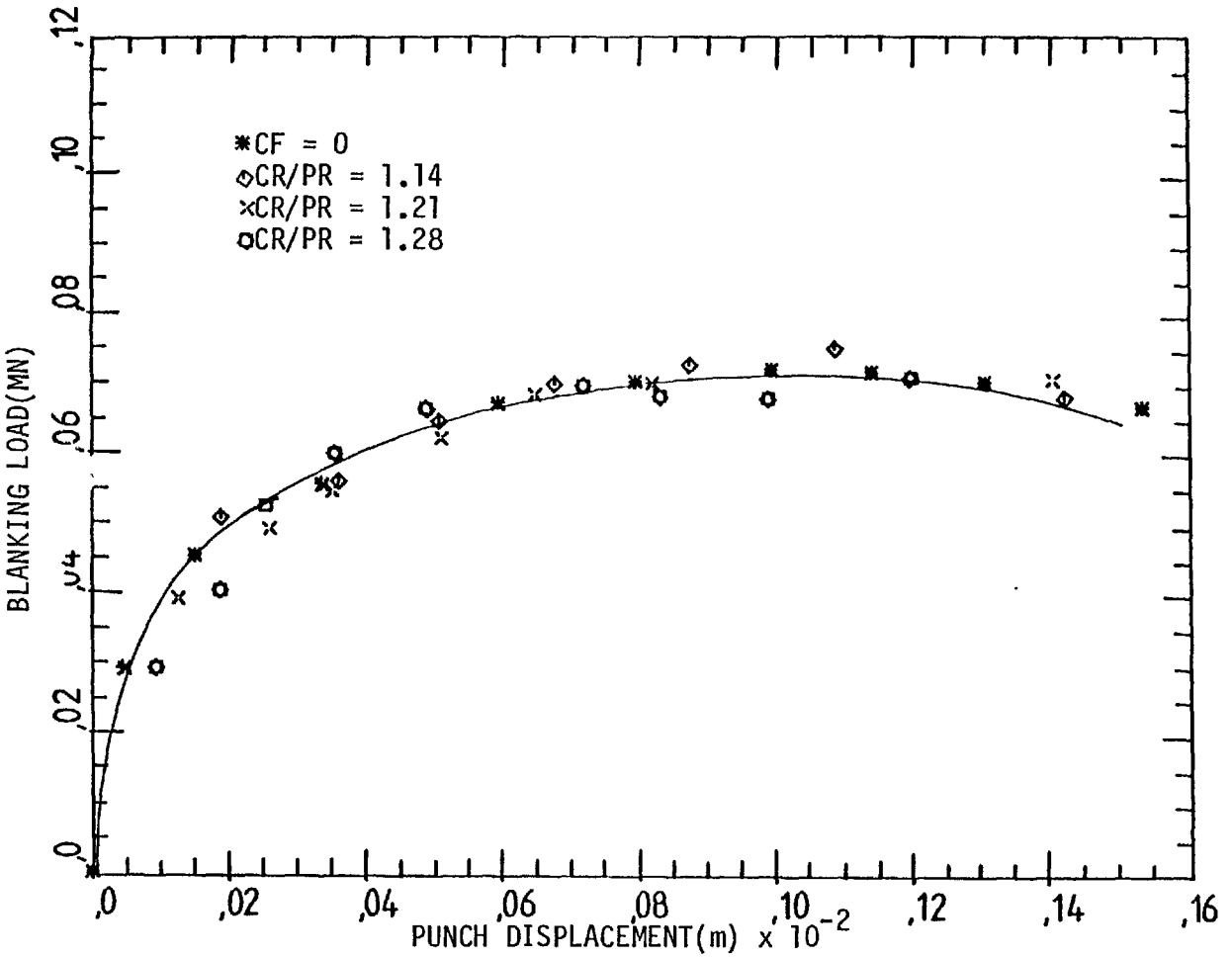

Fig. 5-24(f). Effect of clamp diameter(CR/PR = 1.14, 1.21 and 1.28) on the load/displacement characteristics when blanking mild steel strips of thickness t = 0.120 in. (3.04 mm) in the presence of 70 kN clamping force (CF = 70 kN) and no back-load (BP = 0).

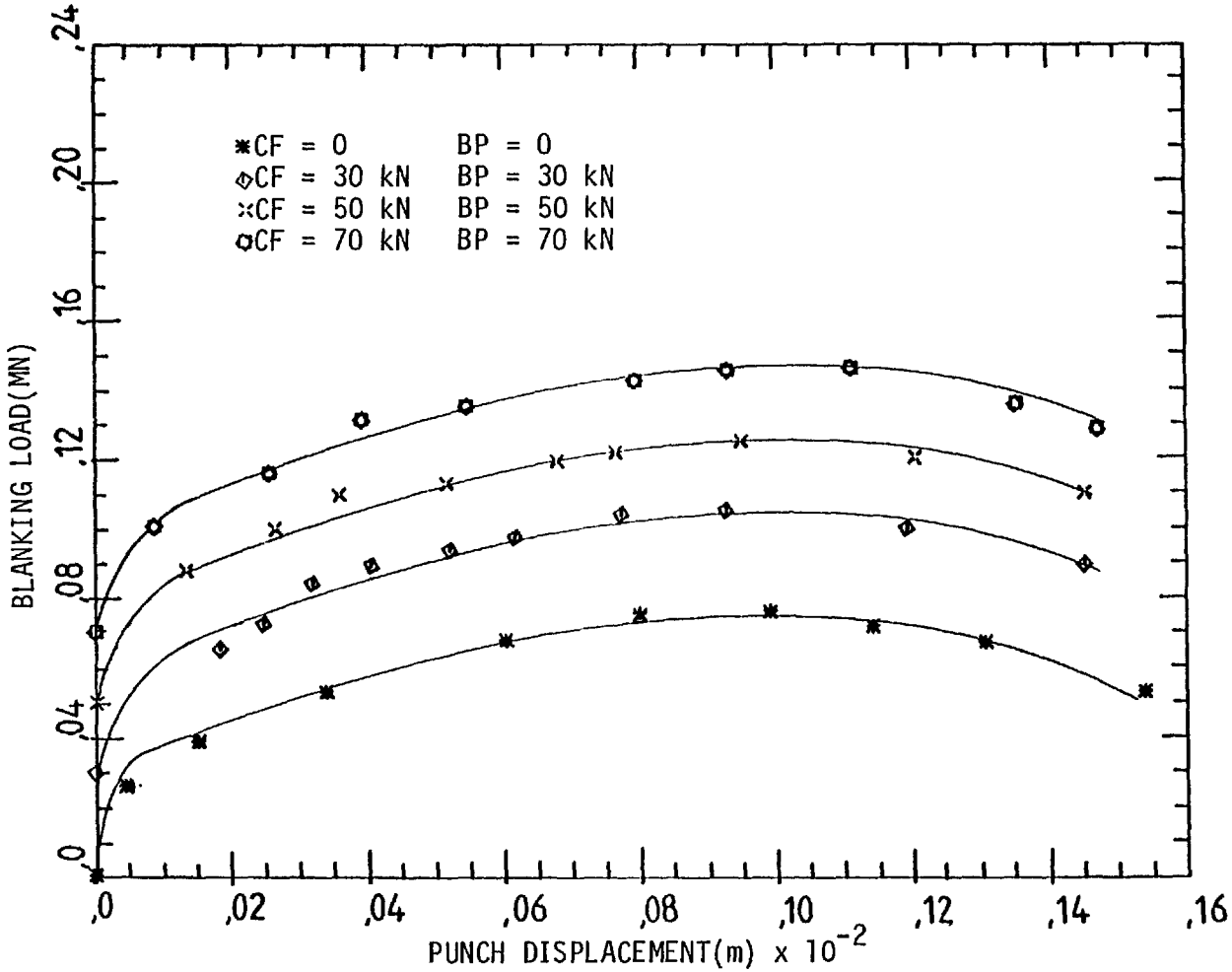

Fig. 5-24(g). Combined effect of clamping force and back-load (CF and BP) on the load/displacement characteristics when blanking strips of mild steel of thickness t = 0.120 in. (3.04 mm) using a blank-holder with clamp/punch diameter ratio of CR/PR = 1.14.

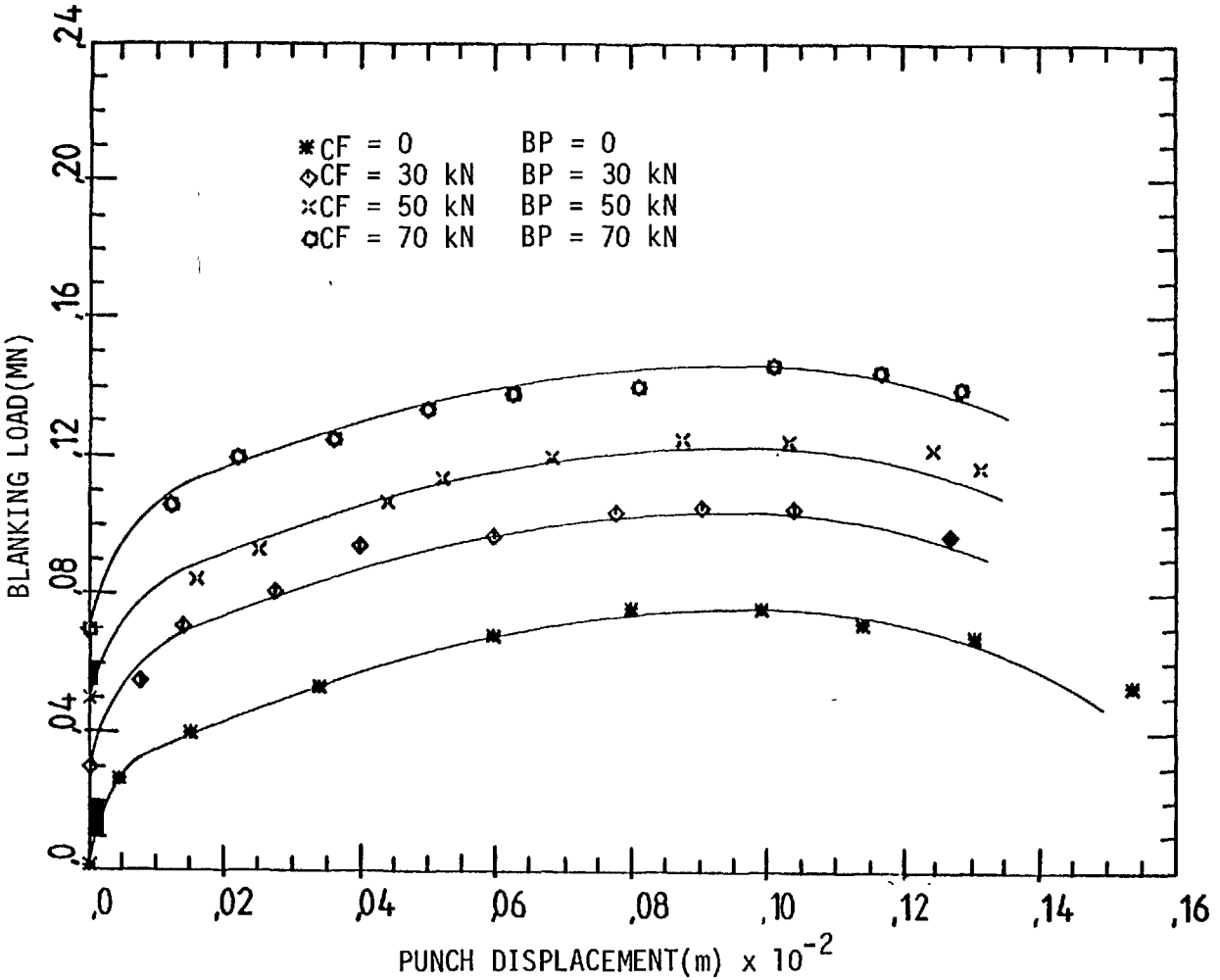

Fig. 5-24(h). Combined effect of clamping force and back-load (CF and BP) on the load/displacement characteristics when blanking strips of mild steel of thickness t = 0.120 in. (3.04 mm) using a blank-holder with clamp/punch diameter ratio of CR/PR = 1.21.

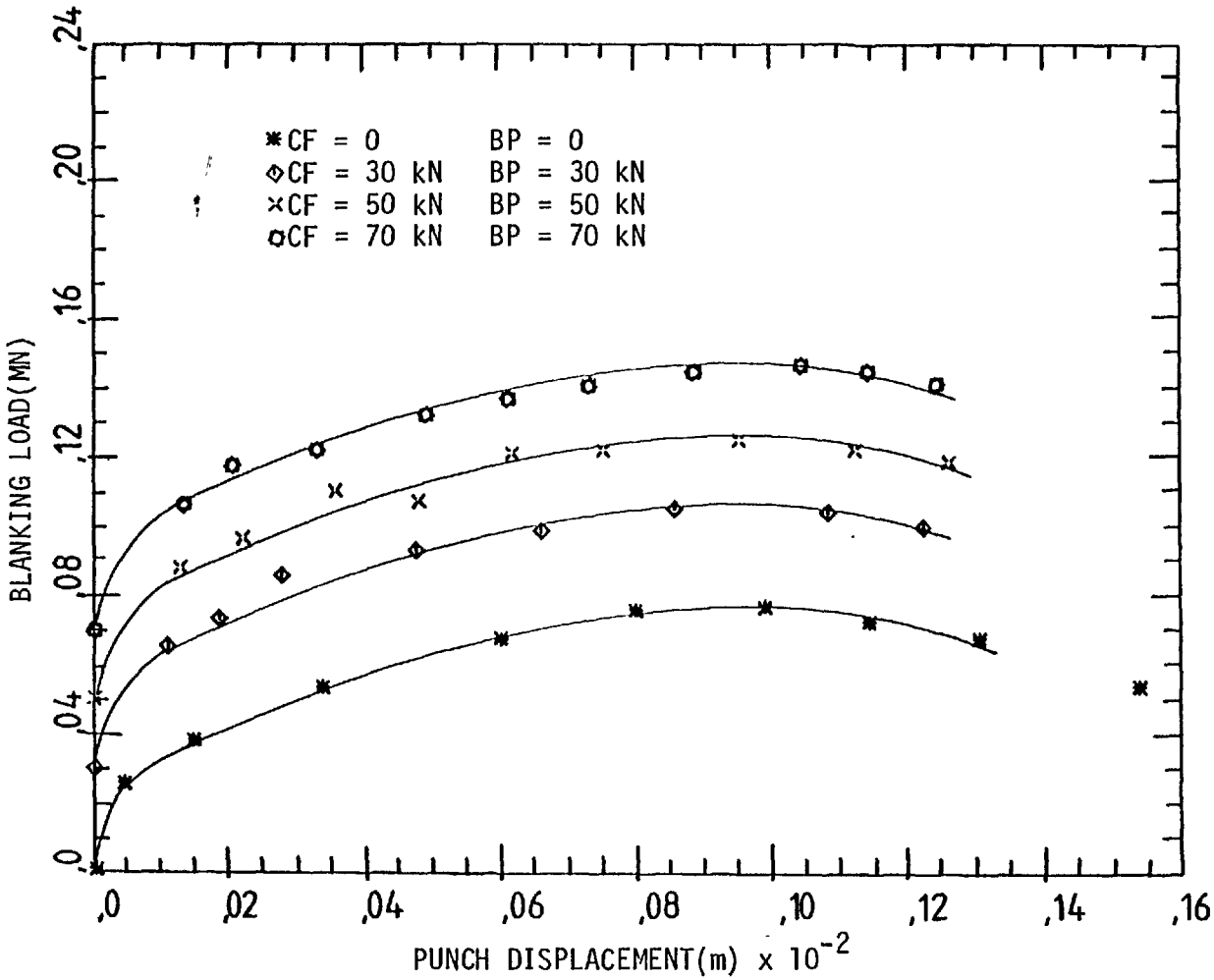

Fig. 5-24(i). Combined effect of clamping force and back-load (CF and BP) on the load/displacement characteristics when blanking strips of mild steel of thickness t = 0.120 in. (3.04 mm) using a blank-holder with clamp/punch diameter ratio of CR/PR = 1.28.

A typical load displacement diagram in slow speed blanking combined with small radial punch/die clearance and clamping force, which is similar to conventional blanking, can be described as follows :

1. Approximately proportional increase in punch force with punch displacement at the early stages which represents the predominantly elastic phase of the process. By removal of the load at this stage no detectable indentation on the material will be observed.
2. Shear deformation occurs and the change in punch load/displacement will depend on the strain hardening characteristics of the material. The blanking load increases up to a maximum at this stage and, although further work-hardening of the material may occur, the load decreases afterwards as the sheared area decreases.

In conventional blanking according to Crasemann (7) cracks are initiated when the blanking force reaches its maximum value. These cracks according to Timmerbeil (8) are initiated at the die edge and propagate towards the punch edge. It has been observed that similar cracks are developed at the punch edge which propagate towards the die edge. When the developed cracks from the die edge and the punch edge meet each other the blank separates from the stock, Fig. 4-25, which is accompanied by a sudden drop in blanking load.

In fine blanking, by changing the value of clamping force, the crack-free length of the blank changes. The higher the clamping force the larger will be the crack-free length, until the fractured area disappears completely. In cases when some clamping force is used, high enough to decrease the fractured zone, the stage at which crack initiation

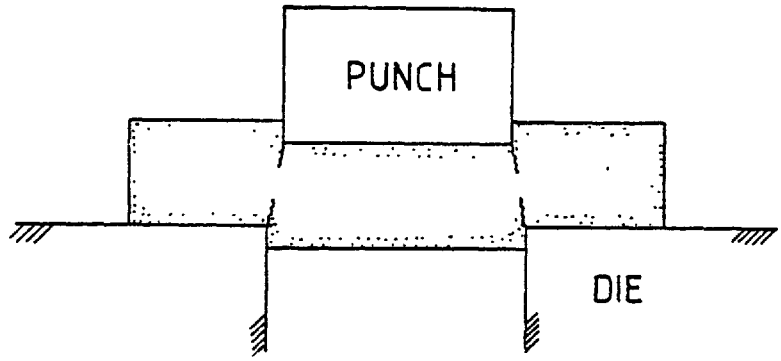

Initiation of crack propagation

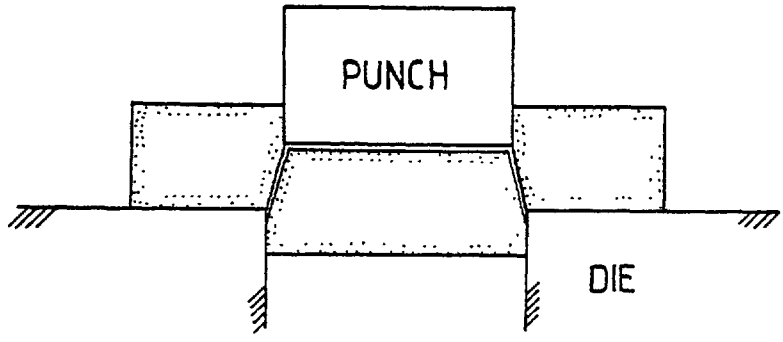

Separation of blank

Fig. 4-25.

begins and the way it propagates is not known. A possible explanation can be put forward as follows .

The cracks initiate at the die edge after the blanking load has reached its maximum value, similar to conventional blanking, but their propagation is delayed to some extent due to the compressive state of stress caused by the clamp. As the process continues the stresses in the shear line become more and more tensile. If the compressive stress superimposed by the clamp is not high enough, the state of stress in the shear line will reach such a high level of tension that the cracks will start growing and propagating, until they meet the punch edge or the tip of similar cracks propagating from the punch edge. This will result in a fracture zone which is smaller than in conventional blanking.

4.8.2 Hardness measurement

Micro-hardness measurements in a work-hardening deformed material can indicate the rate of deformation in different regions. The regions with a higher rate of deformation will indicate higher hardness values.

To specify regions of high deformation in a simple blanking operation, partly blanked specimens were cut into halves and the cut surfaces were ground and polished. A survey of micro-hardness values along the radial direction, Fig. 4-26, was made on the polished surfaces of partly blanked strips of mild steel of thickness t = 0.120 in. (3.04 mm).

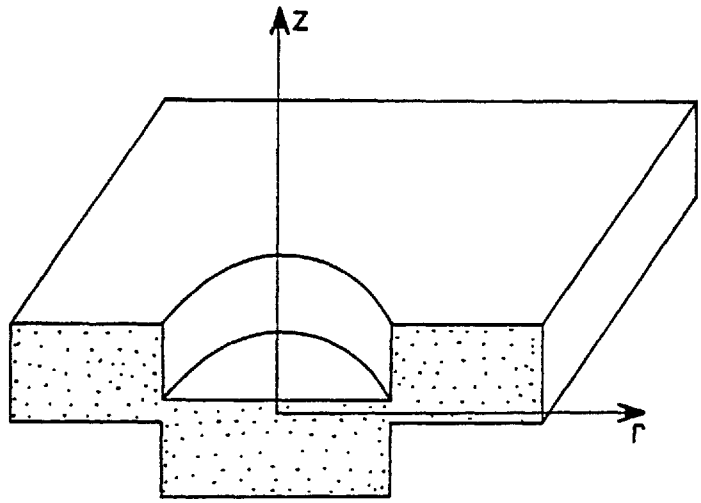

Fig. 4-26.

The hardness results in the radial direction for 0.01 in. (0.254 mm) punch penetration are shown in Fig. 4-27. The hardness has a constant value along the radius until, at the vicinity of the shear line, it begins to increase. The hardness value reaches a maximum at the shear line and then drops to a constant value. Considering the scale of Fig. 4-27 it becomes obvious that the rise and fall of the hardness value occurs in a small region. The micro-hardness survey for two other punch penetrations, 0.025 and 0.06 in. (0.635 and 1.52 mm) are shown in Figs. 4-28 and 4-29

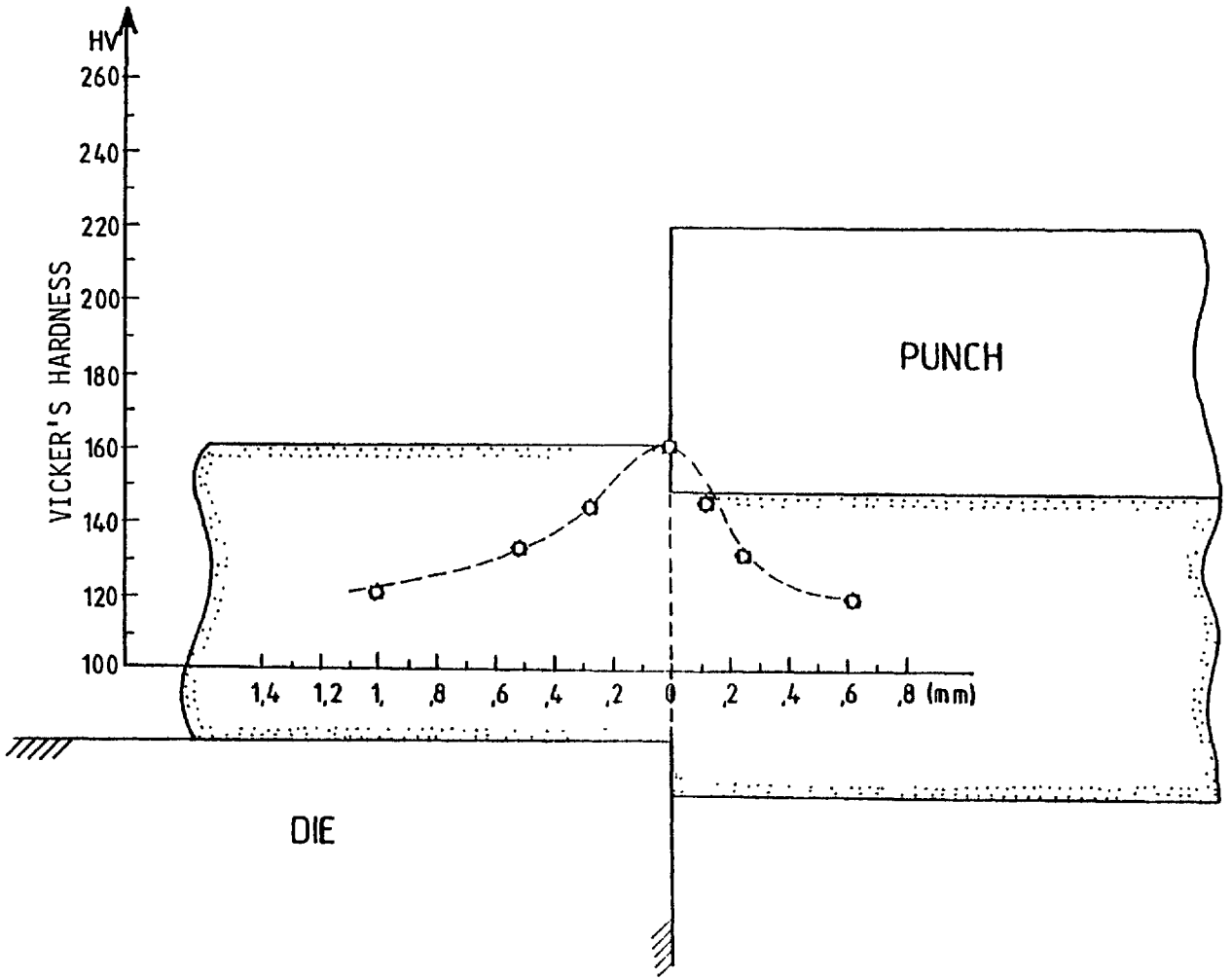

Fig. 4-27. Hardness values along the radial direction at a punch penetration of PP = 0.01 in. (0.254 mm) when blanking a strip of mild steel of thickness t = 0.120 in. (3.04 mm).

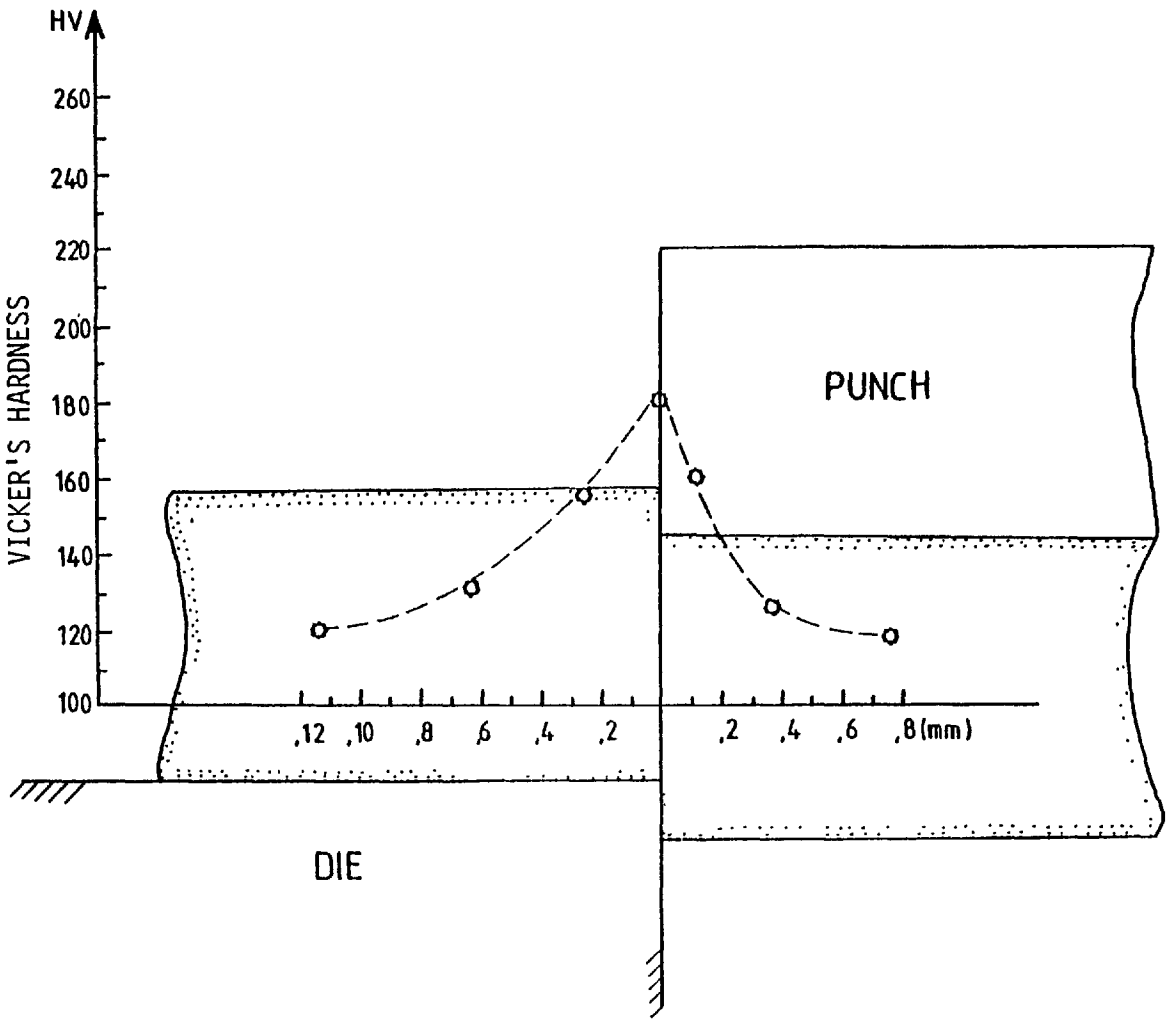

Fig. 4-28. Hardness values along the radial direction at a punch penetration of PP = 0.025 in. (0.635 mm) when blanking a strip of mild steel of thickness t = 0.120 in. (3.04 mm).

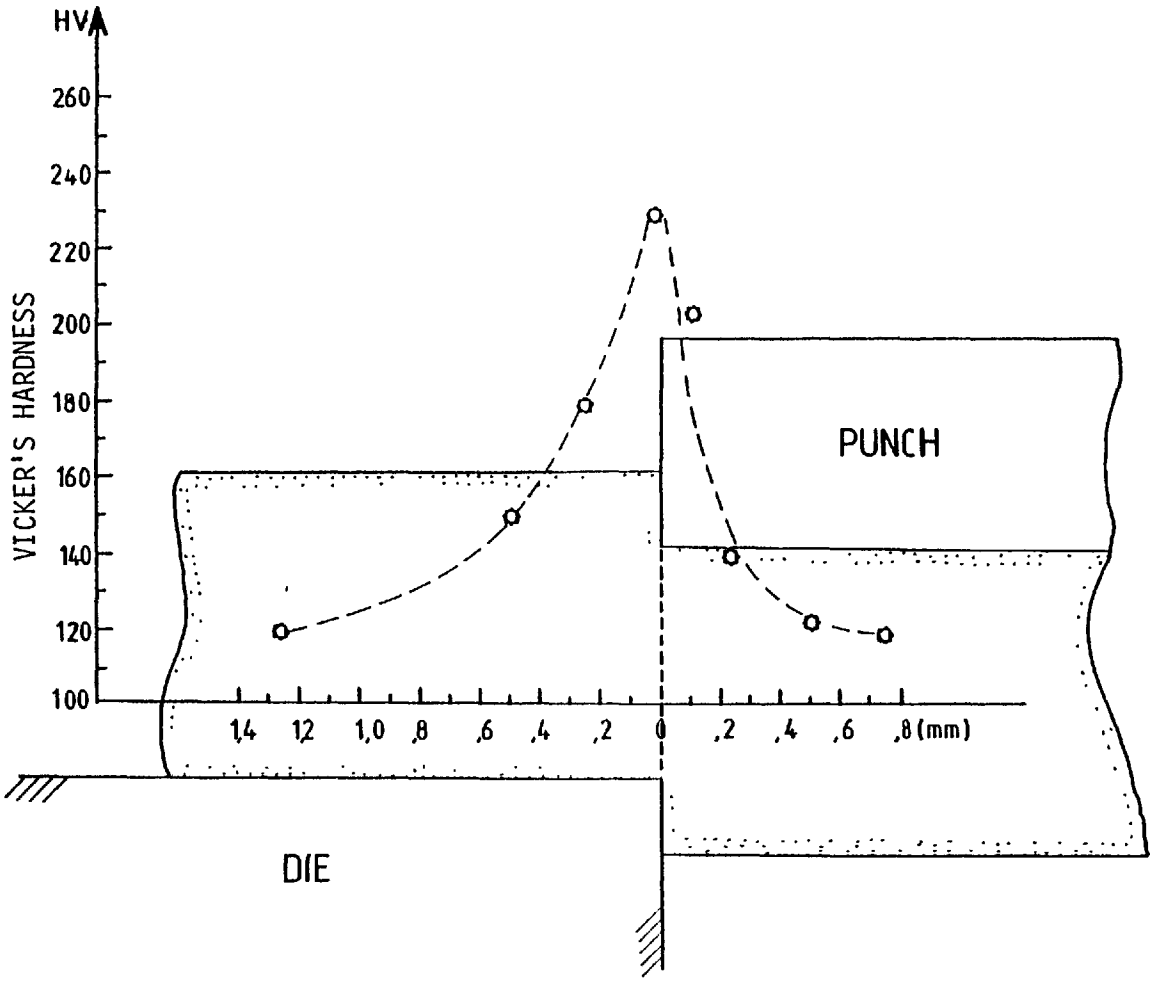

Fig. 4-29. Hardness values along the radial direction at a punch penetration of PP = 0.06 in. (1.52 mm) when blanking a strip of mild steel of thickness t = 0.120 in. (3.04 mm).

respectively. For comparison all three curves are presented in Fig. 4-30.

By increasing punch penetration the hardness in the vicinity of the shear line increases and beyond a short distance from the shear line the hardness is nearly independent of punch penetration, and the position of the maximum hardness gradient relative to the shear line is independent of punch penetration. The two former conclusions are in agreement with the results obtained by P.E.R.A. (25).

To prove the idea that the cracks are formed and propagated first from the die and then from the punch edges, a micro-hardness survey was made along the shear line and the results are shown in Fig. 4-31. Hardness is at its highest value at the die and punch edges, indicating maximum severity of deformation in these two regions, and at the die edge it is considerably higher than at the punch edge which proves a higher rate of deformation and thus more susceptibility to crack formation.

It must be noted however, that the hardness value alone cannot verify the first formation of the cracks, but the density of the lines of constant hardness, showing hardness gradient, at different regions must also be considered, the closer the lines of constant hardness, the higher the hardness gradient. Experimental results obtained by P.E.R.A. (25) showed that the crack propagation is confined to the regions of greatest hardness gradient and these regions can well be identified by a hardness survey on a single line across the centre of the disturbed zone, Fig. 4-32.

Referring to Fig. 4-30 which shows the hardness values across the centre of the disturbed zone and considering the conclusion obtained by P.E.R.A. that the crack propagation is confined to the regions of greatest hardness gradient, it could be said that, in this case, the maximum values

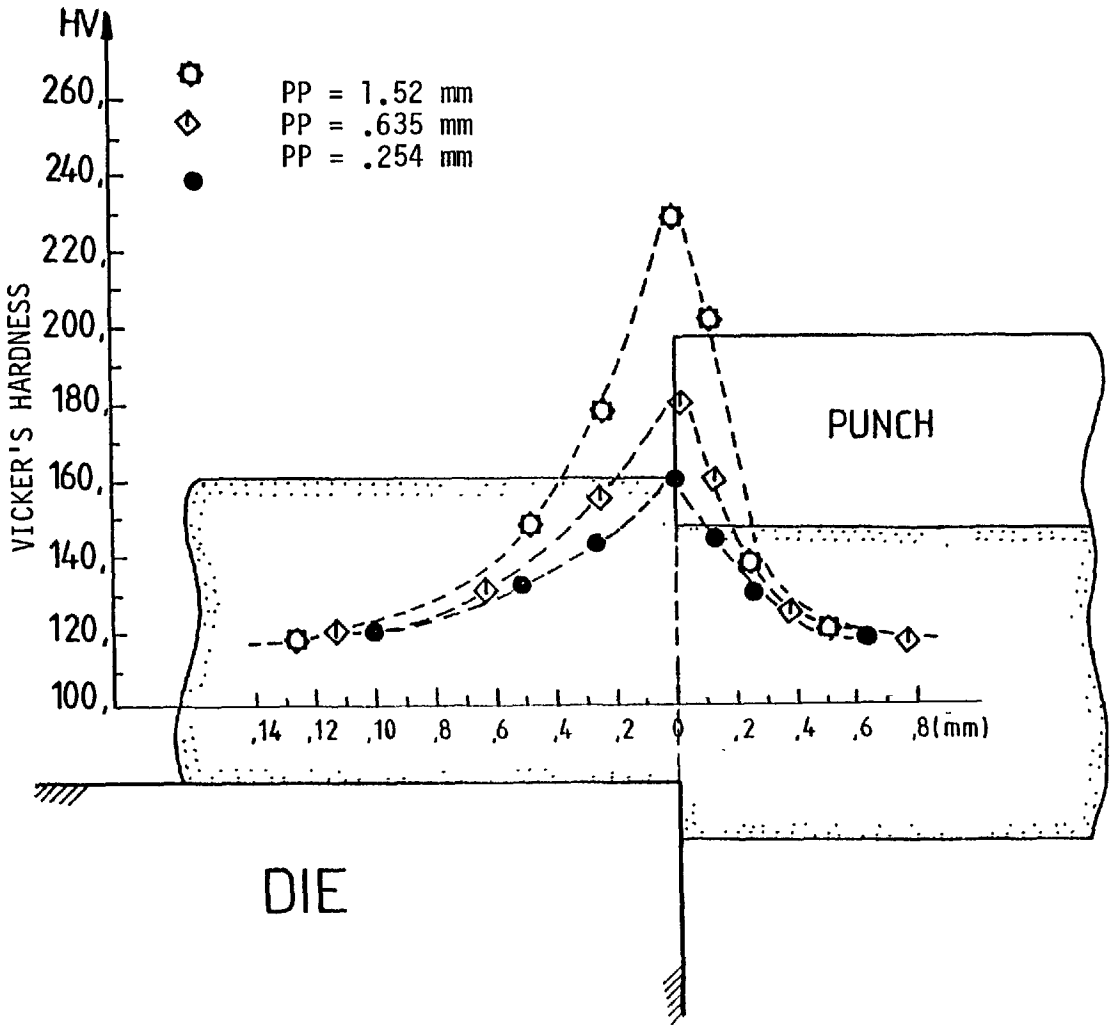

Fig. 4-30. Effect of punch penetration (PP) on the hardness values along the radial direction, when blanking a strip of mild steel of thickness t = 0.120 in. (3.04 mm).

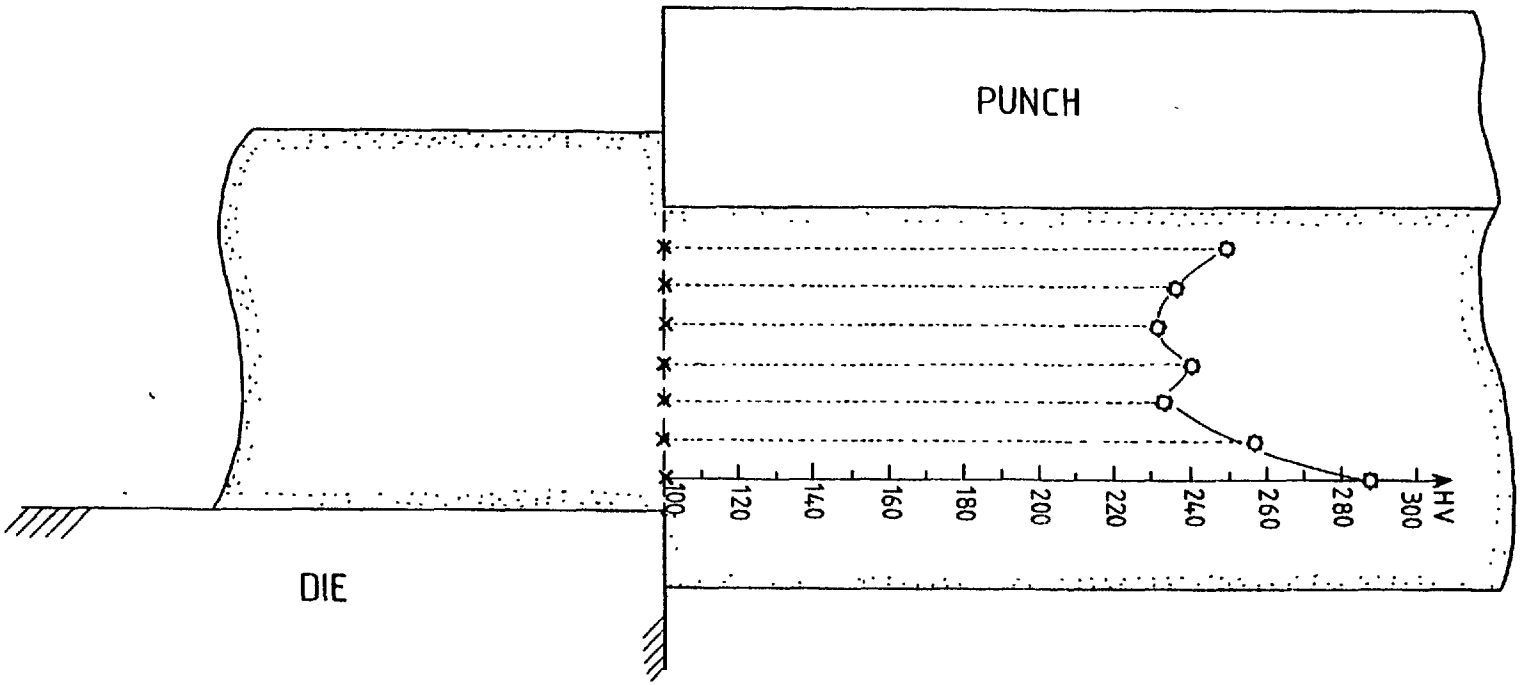

Fig. 4-31. Hardness measurement along the shear line at a punch penetration of PP = 0.045 in. (1.14 mm).

of hardness at the punch and die edges do represent the most susceptible regions to crack propagation.

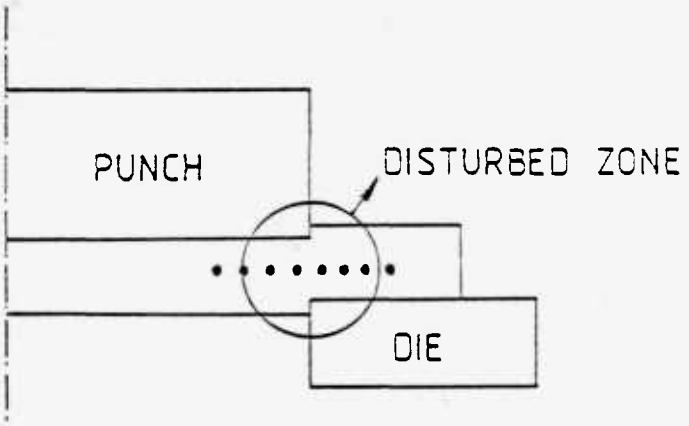

Fig. 4-32. The greatest hardness gradient can be identified by a hardness survey on a single line along the centre of the disturbed zone.

One of the specimens used for measuring the hardness in the radial direction and across the shear line with the hardness measurement impressions is shown in Fig. 4-33.

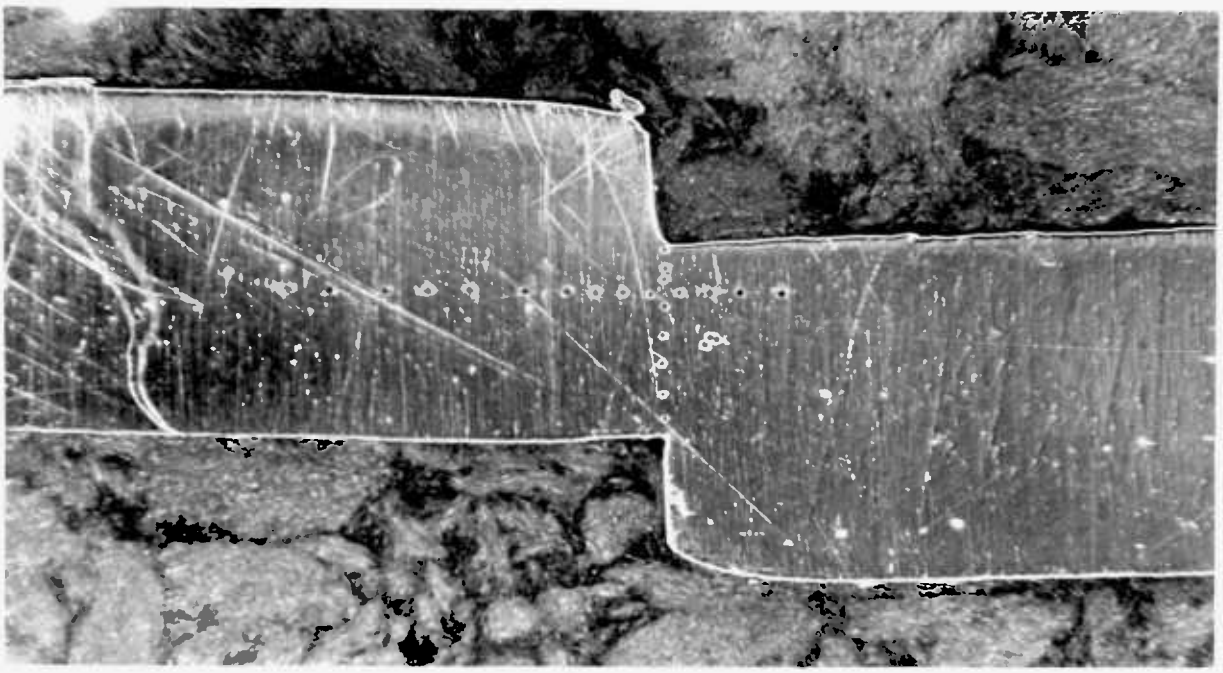

Fig. 4-33. Hardness measurement at PP = 1.14 mm punch penetration. X15

P.E.R.A. (25) has shown that in piercing (a similar process to conventional blanking) the position of the region of maximum hardness can be influenced by punch and die geometry and to this extent the direction of crack propagation can be controlled. By proper design of tool geometry the crack can be confined to the waste material. This is performed in fine piercing by chamfering the punch, and so displacing the region of maximum hardness gradient from the work material into the waste material, Fig. 4-34, which leads to a smooth pierced finish.

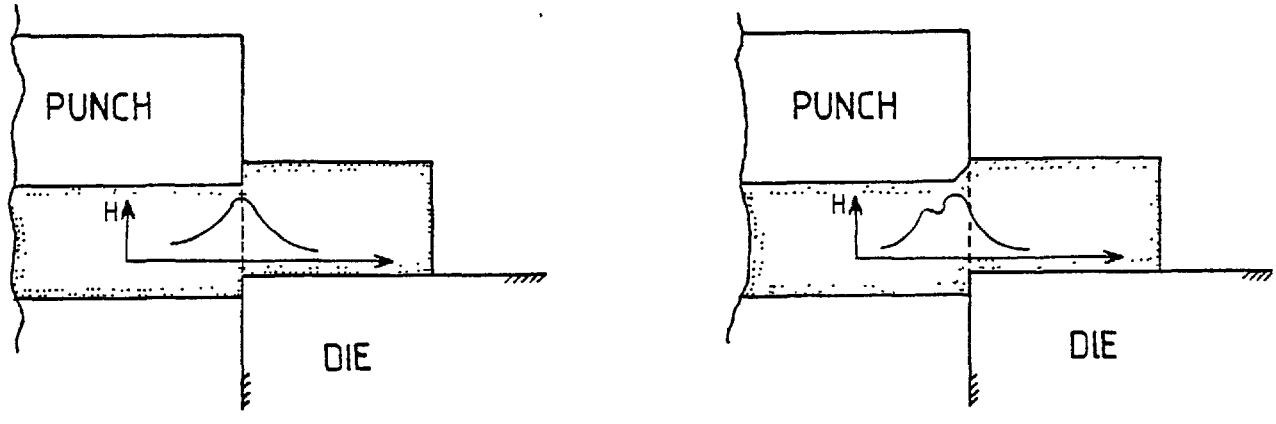

Fig. 4-34. In piercing the position of maximum hardness gradient can be displaced from the work material into the waste material by a proper tool geometry.

The transition from a blank with cracked surface to a crack-free blank can be envisaged as either prevention of crack propagation due to high compressive stresses caused by the blank-holder and counter punch, or by a similar effect as explained for fine piercing, i.e. displacement of the maximum hardness gradient from the work material to the waste material caused by the blank-holder.

To investigate the effect of blank-holders with different diameters on the deformed regions in blanking, a micro-hardness survey

along the diameter of partly blanked specimens was made. The hardness measurements at clamping force of (CF = 70 kN) for three different blank-holders with clamp/punch diameter ratios of ($\frac{CR}{PR}$ = 1.28, 1.21 and 1.14) are shown in Fig. 4-35, 4-36 and 4-37 respectively.

Fig. 4-35 shows that for $\frac{CR}{PR}$ = 1.28 the hardness increases from a constant value to a maximum, under the blank-holder, and then drops to the same value. It remains constant for some distance and then starts to rise near the shear line. Fig. 4-36 for blank-holder with $\frac{CR}{PR}$ = 1.21 shows a similar trend to Fig. 4-35, except that the constant region of hardness, between the blank-holder and punch edge, is nearly cancelled and the blank-holder affects the hardness in the proximity of the shear line. Fig. 4-37 shows the hardness results for blank-holder with minimum diameter, i.e. $\frac{CR}{PR}$ = 1.14. After a peak under the blank-holder the hardness drops slightly and then starts to rise so that the deformation due to the blank-holder is combined with the deformation due to punch penetration and so not only the constant region of hardness between the blank-holder and the punch edge is cancelled but the general level of hardness in this region is increased.

Considering the hardness results for blank-holders with different diameters, Figs. 4-35, 4-36 and 4-37, an important conclusion can be drawn that the blank-holder in the fine blanking process does not displace the region with maximum hardness gradient. In other words unlike fine piercing, the crack-free surface of the blank which is obtained in fine blanking by an introduction of a blank-holder is not due to the displacement of the maximum hardness gradient from the work piece to the waste material. The reasons for obtaining crack-free surfaces must be sought in other possible effects of the blank-holder on the deformed

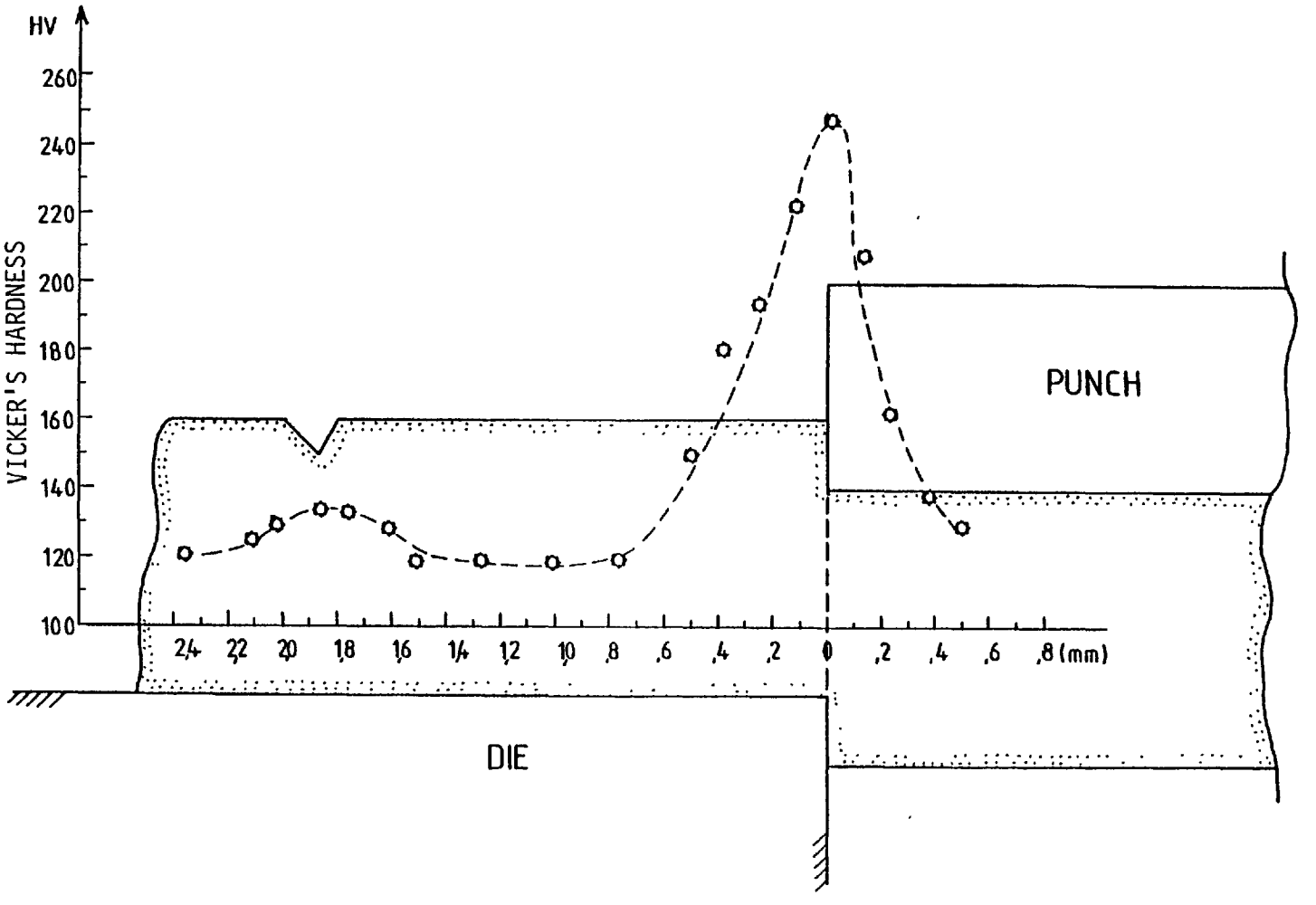

Fig. 4-35. Hardness values along the radial direction of a partly blanked strip of mild steel of thickness t = 0.120 in. (3.04 mm) at a punch penetration of PP = 0.055 in. (1.39 mm) when a clamping force of (CF = 70 kN) acted at a clamp/punch diameter ratio of CR/PR = 1.28.

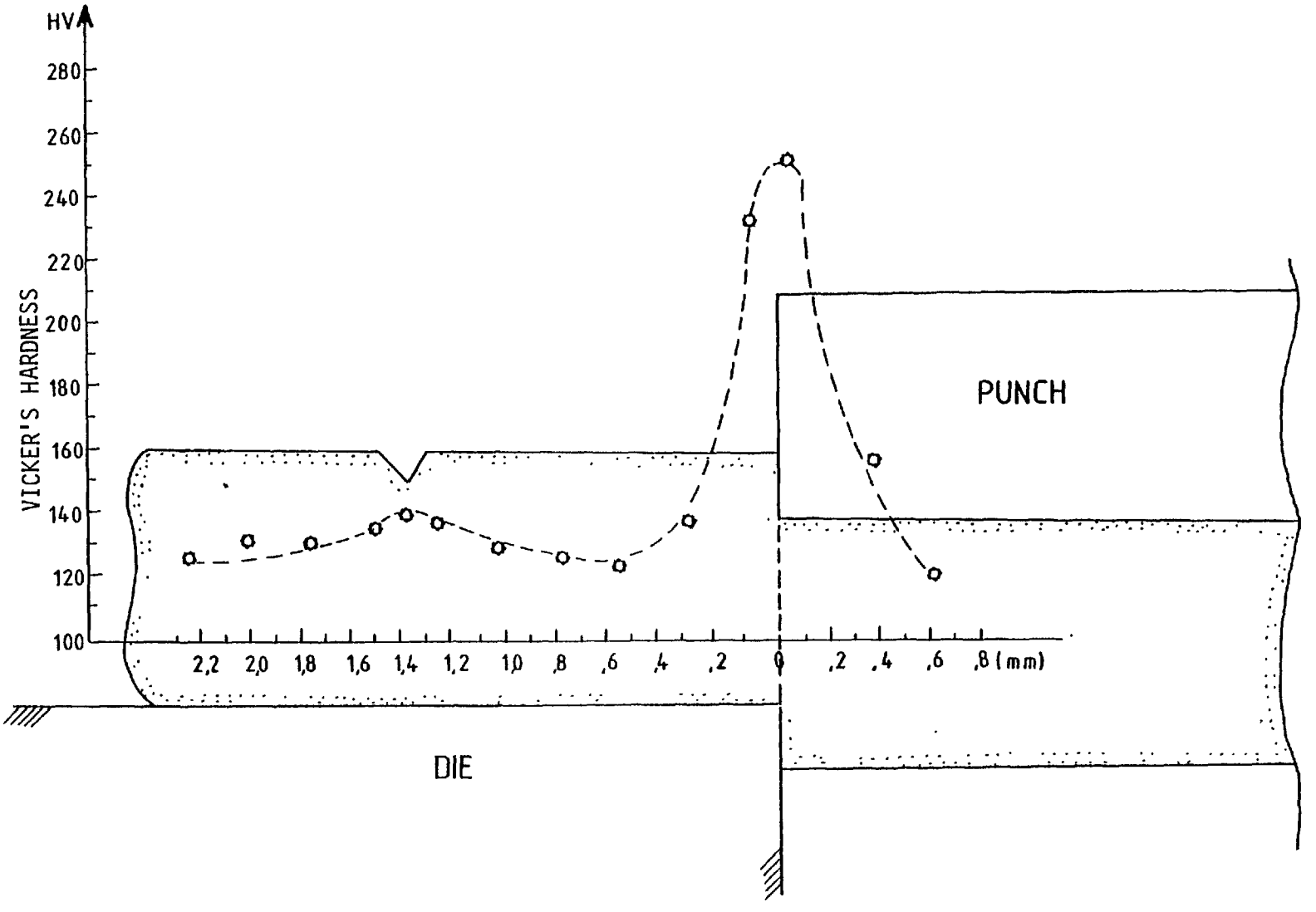

Fig. 5-36. Hardness values along the radial direction of a partly blanked strip of mild steel of thickness t = 0.120 in. (3.04 mm) at a punch penetration of PP = 0.075 in. (1.90 mm) when a clamping force of (CF = 70 kN) acted at a clamp/punch diameter ratio of CR/PR = 1.21.

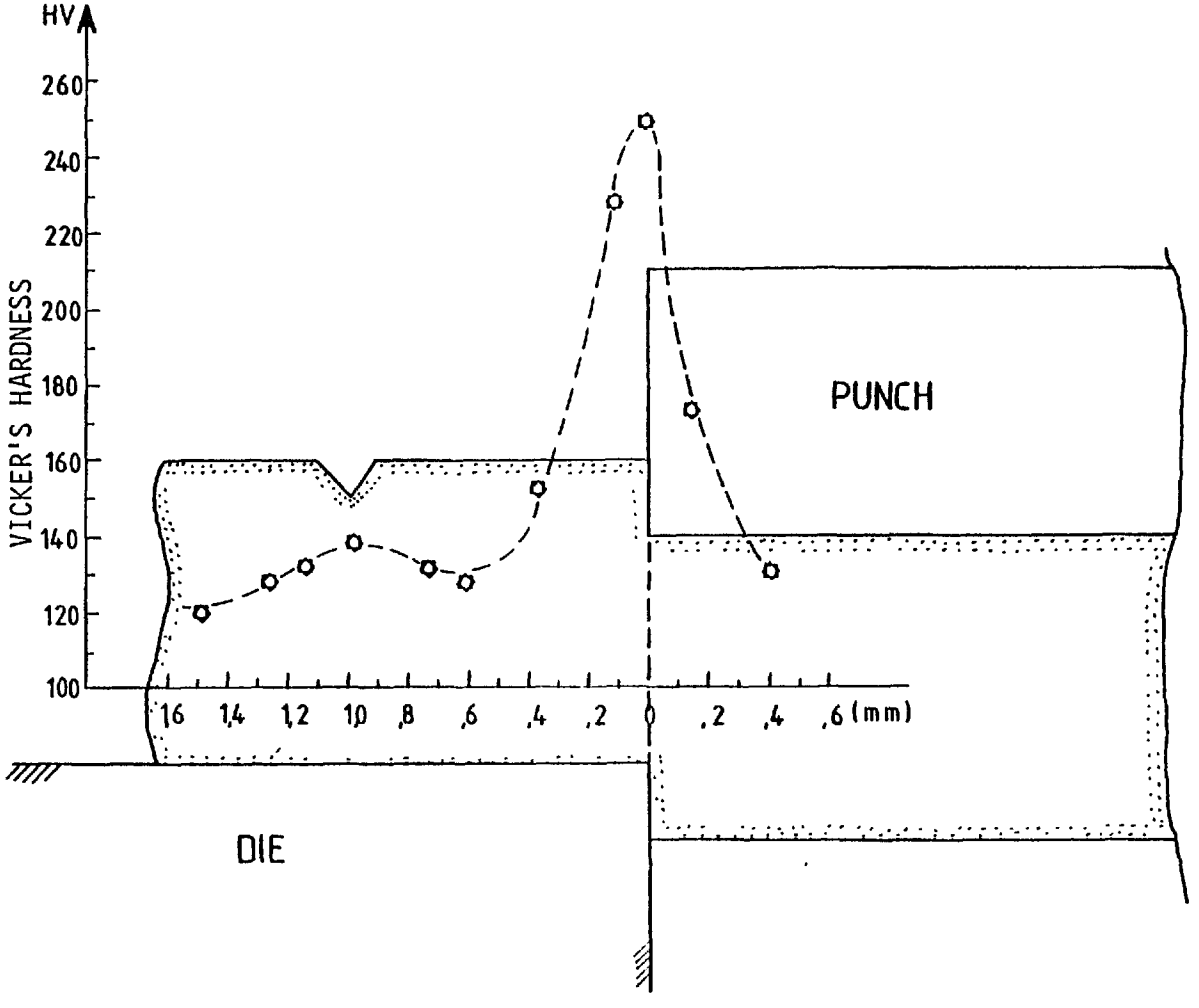

Fig. 5-37. Hardness values along the radial direction of a partly blanked strip of mild steel of thickness t = 0.120 in. (3.04 mm) at a punch penetration of PP = 0.075 in. (1.90 mm) when a clamping force of (CF = 70 kN) acted at a clamp/punch diameter ratio of CR/PR = 1.21.

region, such as an increase in the hydrostatic component of compressive stress.

The three specimens used for hardness measurements are shown in Figs. 4-38, 4-39 and 4-40.

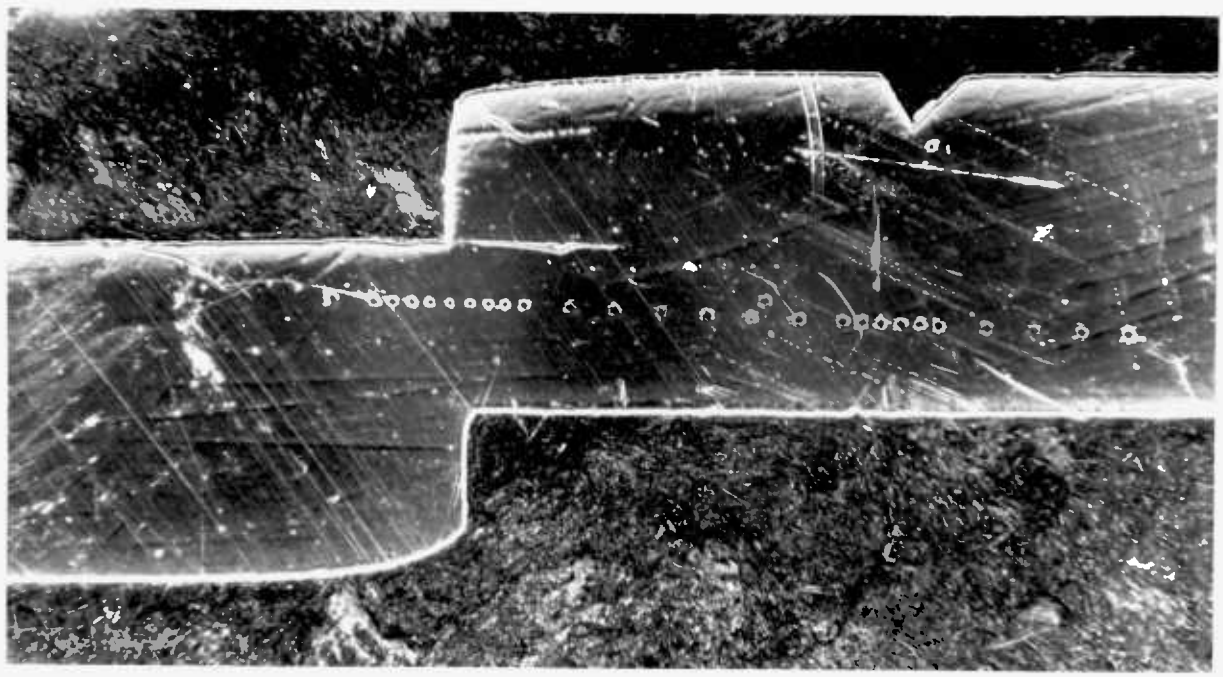

Fig. 4-38. Hardness measurement impressions when a clamp/punch diameter ratio of CR/PR = 1.28 was used, magnification x15.

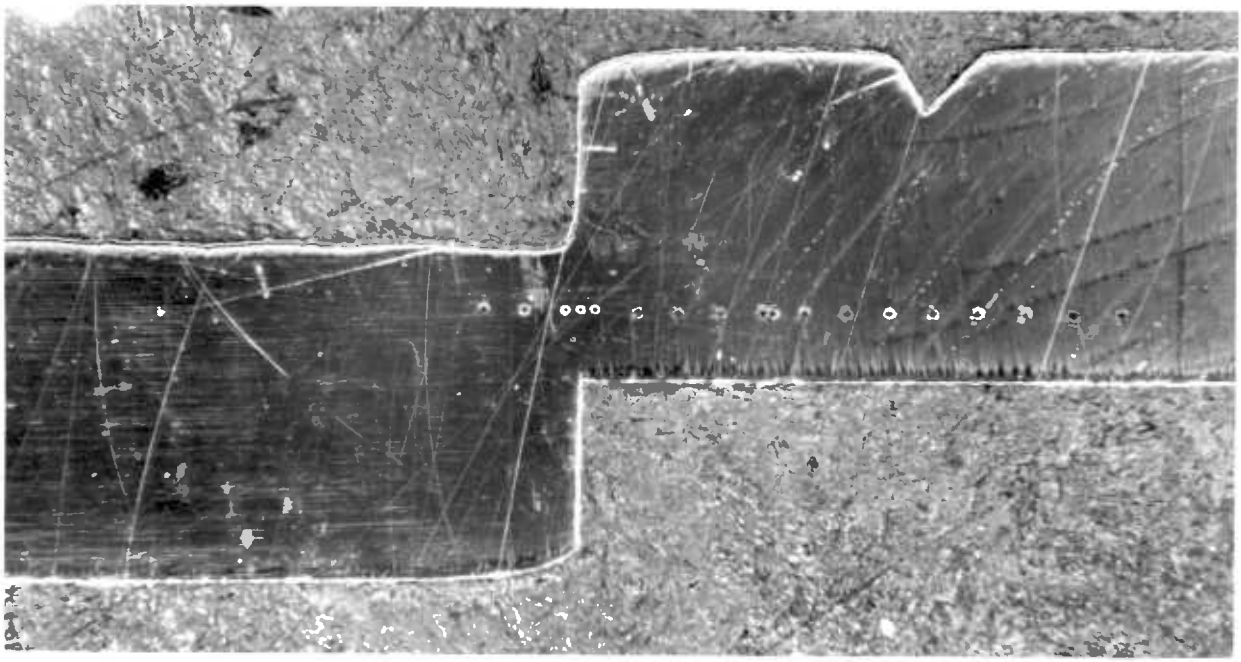

Fig. 4-39. Hardness measurement impressions when a clamp/punch diameter ratio of CR/PR = 1.21 was used, magnification x 15.

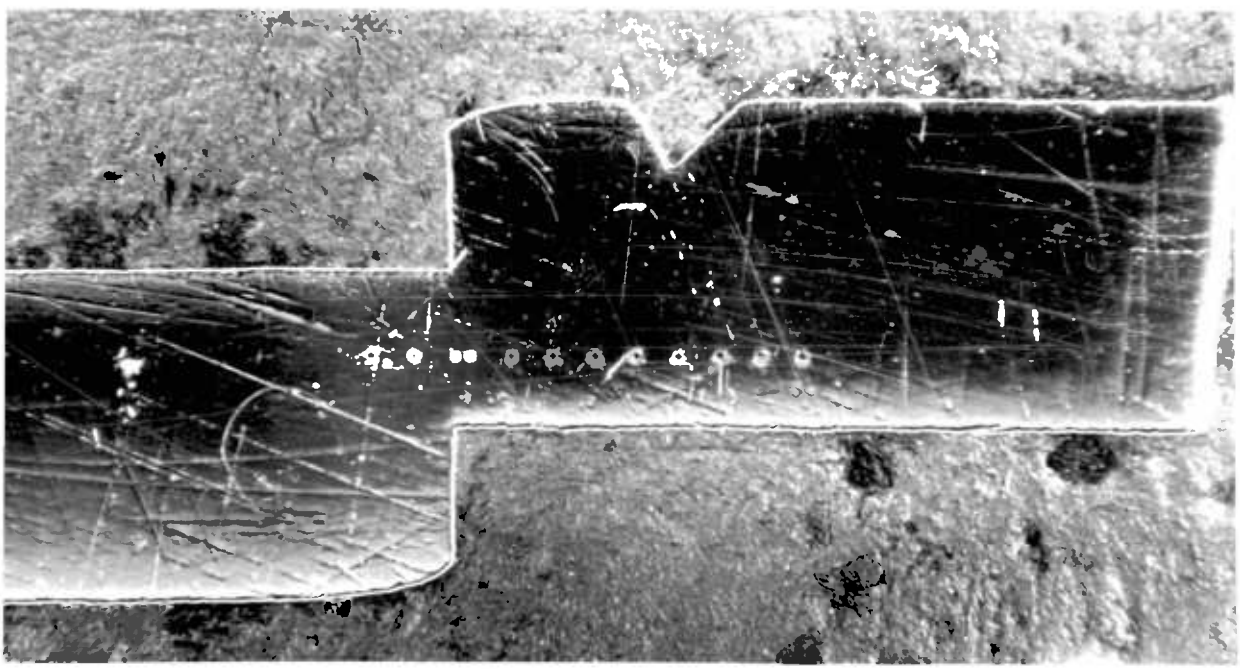

Fig. 4-40. Hardness measurement impressions when a clamp/punch diameter ratio of CR/PR = 1.14 was used, magnification x 15.

4.8.3 Etching of partly blanked specimens

Etching reagents can be used to identify the material flow pattern and specify the locally stressed regions.

A partly blanked specimen was etched using 4% Nital which is recommended for micro-etching mild steel, Fig. 4-41.

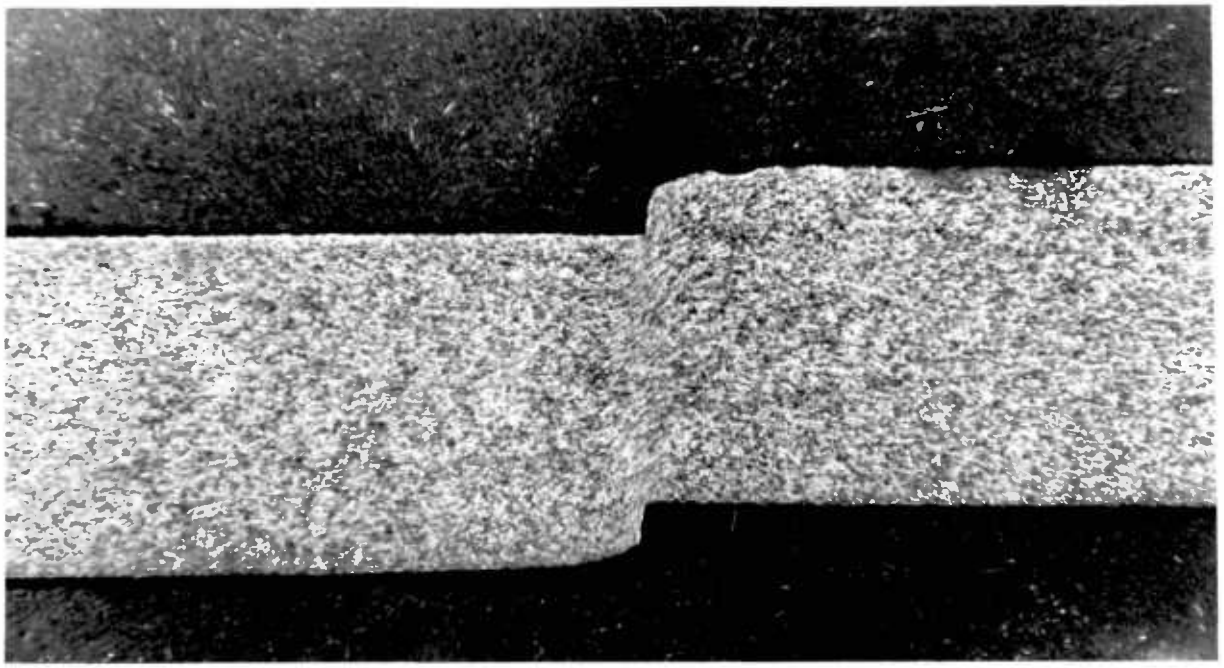

Fig. 4-41. A mild steel specimen etched in 4% Nital at a punch penetration of PP = 0.026 in. (0.66 mm), magnification x 15.

The material flow is confined to a narrow region around the shear line, indicating the deformation of material in that region.

In the case of specimens indented by a blank-holder several etching reagents including 4% Nital were used, but all failed to reveal any obvious flow of material. To examine the effect of blank-holder on the

stressed regions during blanking, three partially blanked specimens, clamped with three different blank-holder diameters, were macro-etched using 10% Nitric acid in distilled water. The etching reagent was rubbed over the surface of the specimen using a piece of cotton wool and then surface washed and lightly polished with very fine emery paper. The etching was continued until a clear etched zone, around the blank-holder and shear line was revealed, Figs. 4-42, 4-43 and 4-44.

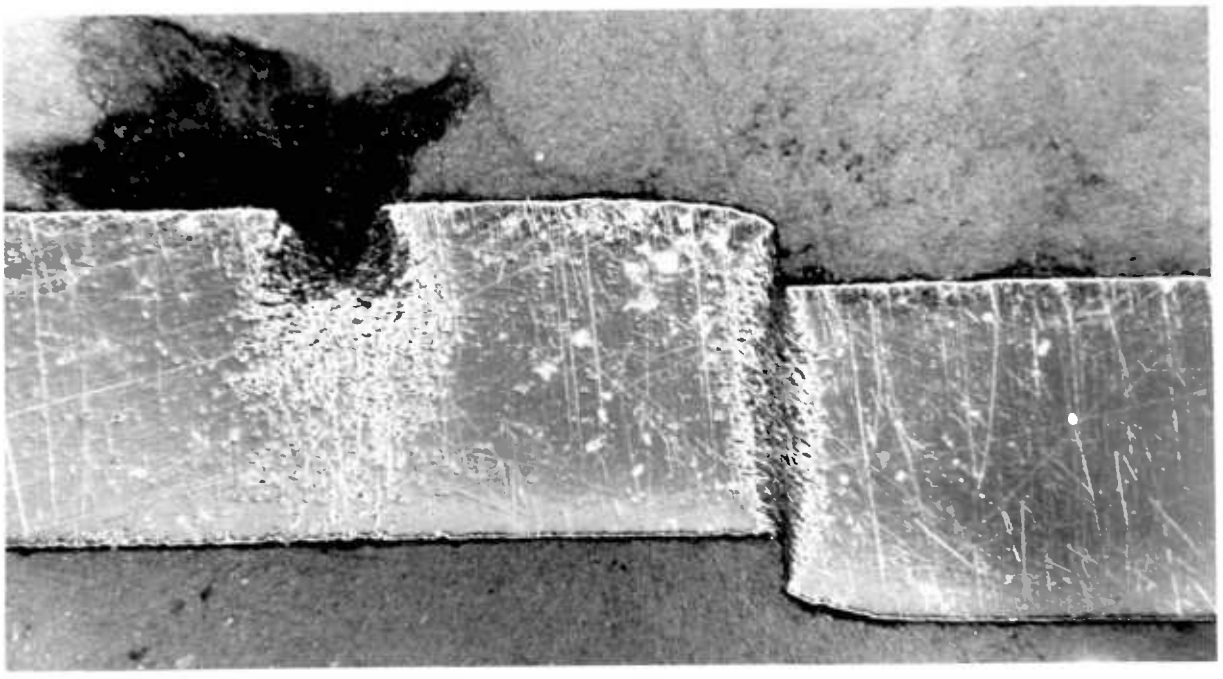

Fig. 4-42. A mild steel specimen etched in 10% Nitric acid when using a 70 kN clamping force at a clamp/punch diameter ratio of (CR/PR = 1.28) at a punch penetration of PP = 0.889 mm, magnification x 15.

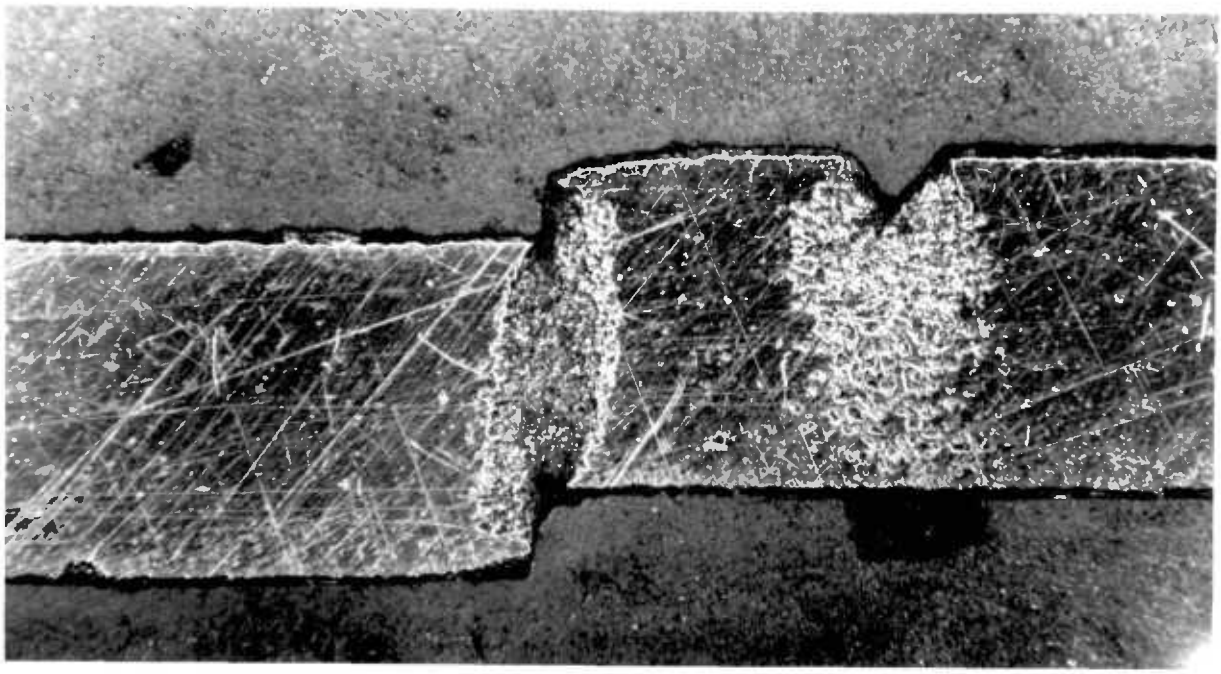

Fig. 4-43. A mild steel specimen etched in 10% Nitric acid when using a 70 kN clamping force at a clamp/punch diameter ratio of 1.21 and at a punch penetration of 0.889 mm, magnification x 15.

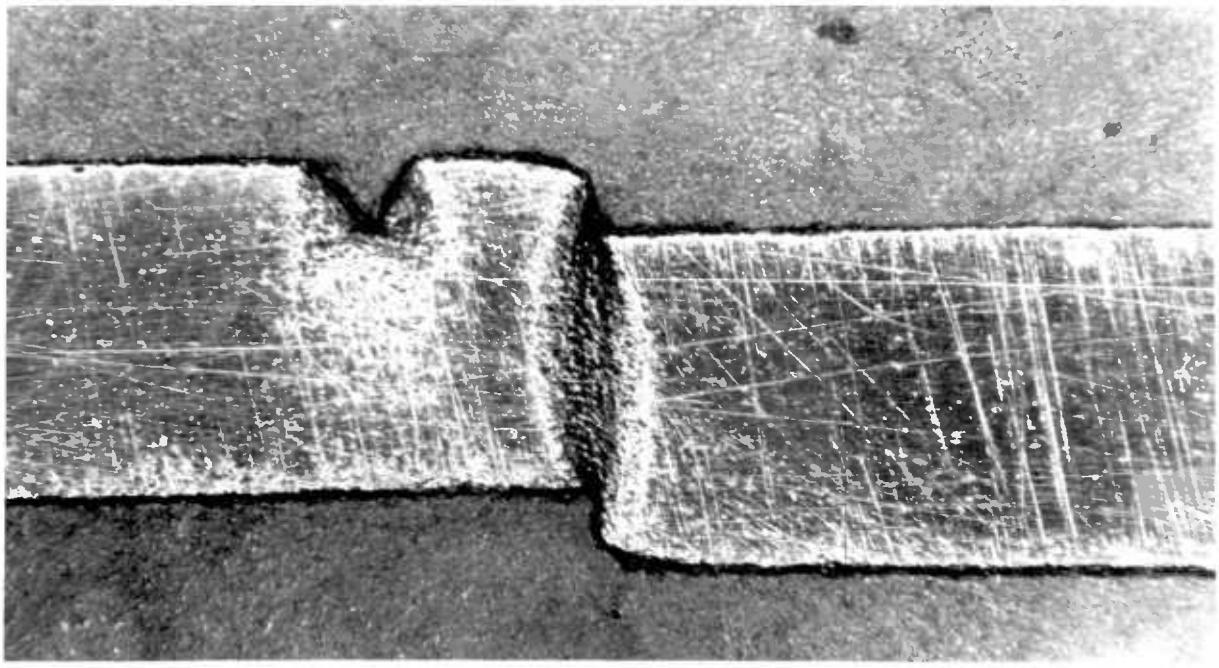

Fig. 4-44. A mild steel specimen etched in 10% Nitric acid when using a 70 kN clamping force at a clamp/punch diameter ratio of 1.14, at a punch penetration of 0.635 mm, magnification x 15.

The illustrations show that the highly stressed regions are confined to the vicinity of the blank-holder and around the shear line. When the blank-holder diameter has it's maximum value, $\frac{CR}{PR} = 1.28$, the stress zone caused by the blank-holder is completely separate from the stressed zone around the shear line. As the blank-holder diameter decreases the two stressed regions become closer and when the blank-holder diameter has its maximum diameter the two regions are very close and meet each other.

4.8.4 Blank surface finish

In conventional blanking the blank surface finish consists mainly of three different regions, (Fig. 4-45).

i) The periphery of the bottom part of the blank is usually slightly rounded.

ii) A bright burnished band which is caused by shearing effect during the blanking operation.

iii) A tapered, rough, uneven band caused by fracture of the material under high tensile stresses.

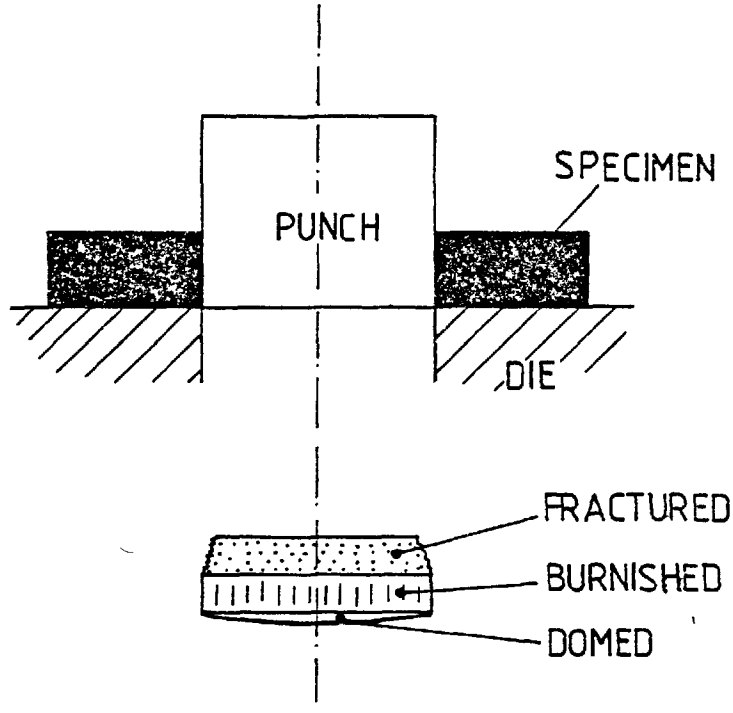

Fig. 4-45.

Fracture, which consists of crack formation and propagation, occurs at the regions of high stress concentration, i.e. die and punch edges. Two cracks are initiated and start to grow from these two regions of high stress concentration, together or separately, towards each other. The pattern of crack propagation to some extent depends on the tool geometry. A general opinion is that at optimum percentage radial clearance the cracks will propagate along a single line and, on meeting, a single fairly clean fracture occurs, Fig. 4-46.

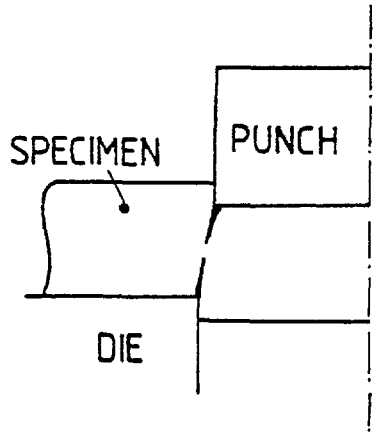

Optimum clearance

Fig. 4-46.

At small clearances, the two cracks tend to embrace a very small part of the work sheet, Fig. 4-47.

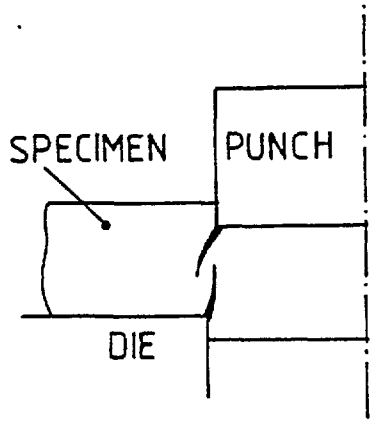

Small clearance

Fig. 4-47.

For relatively large clearances, the two cracks grow more or less parallel but out of line and when they have proceeded sufficiently far, a secondary crack transverse to the two primary crack tips develops, Fig. 4-48. This causes a jagged edge finish.

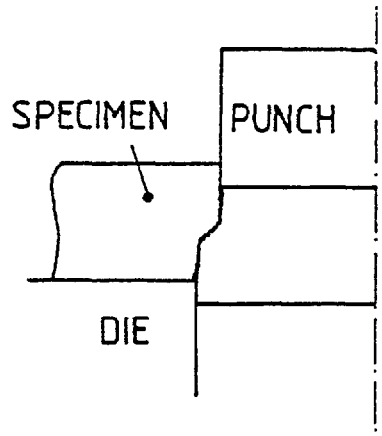

Large clearance

Fig. 4-48.

In conventional blanking, even when using an optimum clearance, the separation of the blank from the work material is effected by the meeting of cracks propagated from the die and punch edges towards one another, causing a rough fractured surface. This is in contrast to the requirement of a fine blanked specimen, where highly polished surfaces are required.

To obtain the blanks with bright surface finishes the mode of blank separation from the waste material must be changed, the blanks must separate under pure shear deformation instead of crack propagation. To fulfil this purpose it has been found that a very small punch/die clearance together with some additional toolings, blank-holder and counter-punch, are required.

In this section the effect of different parameters including blank-holder diameter, clamping force and back-load on the blank edge surface finishes are studied. The minimum crack-free lengths, Fig. 4.49, for different blanked specimens were measured and the results for three different thicknesses of t = 0.076, 0.101 and 0.120 in. (1.93, 2.56 and 3.04 mm) are shown in Figs. 4-50, 4-51 and 4-52 respectively.

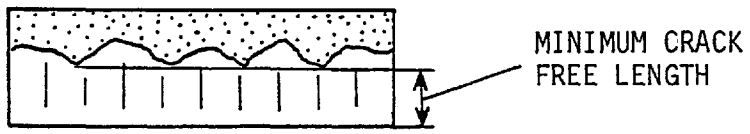

Fig. 4-49.

By increasing the clamping force the crack-free length increases almost proportionally for all thicknesses. The addition of a back-load (equal to the clamping force) increases the crack-free length further. As this increase for the applied range of back loads was not considerable, the corresponding results are not presented here.

For the thickness of t = 0.078 in. (1.93 mm) for any given value of clamping force the crack-free length increases as the clamp diameter decreases. The maximum value occurs at the minimum clamp diameter, with clamp/punch diameter ratio of $\frac{CR}{PR}$ = 1.14. For the other two thicknesses tt = 0.101 and 0.120 in. (2.56 and 3.04 mm), for any given value of the clamping force the values corresponding to the blank-holder with medium diameter, $\frac{CR}{PR}$ = 1.21, are the highest which indicates the existence of an optimum clamp diameter.

The print on the vertical axis which represents the percentage of crack-free length when blanking without any clamping force indicates that the blank with the smallest thickness yields the highest percentage of

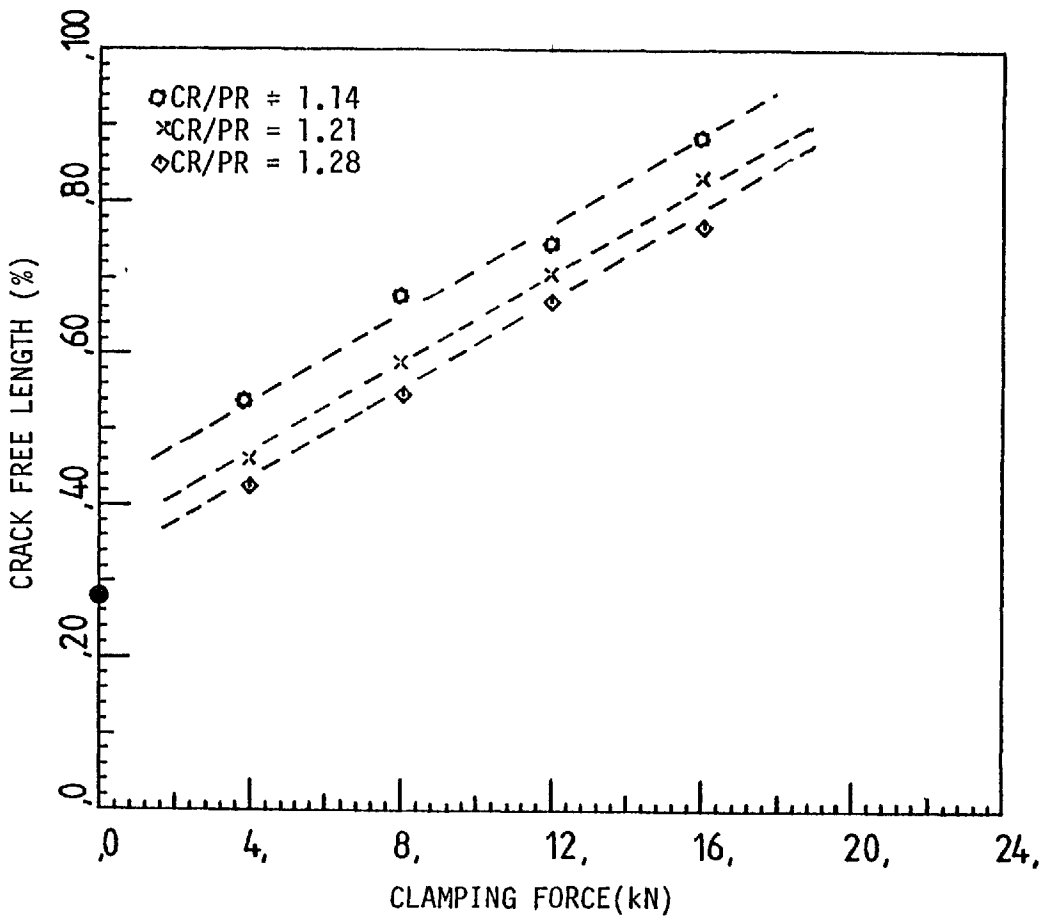

Fig. 4-50. Effect of clamping force (CF) and clamp/punch diameter ratio (CR/PR) on the crack-free-length percentage of the blank edges obtained from blanking strips of mild steel of thickness t = 0.078 in. (1.93 mm).

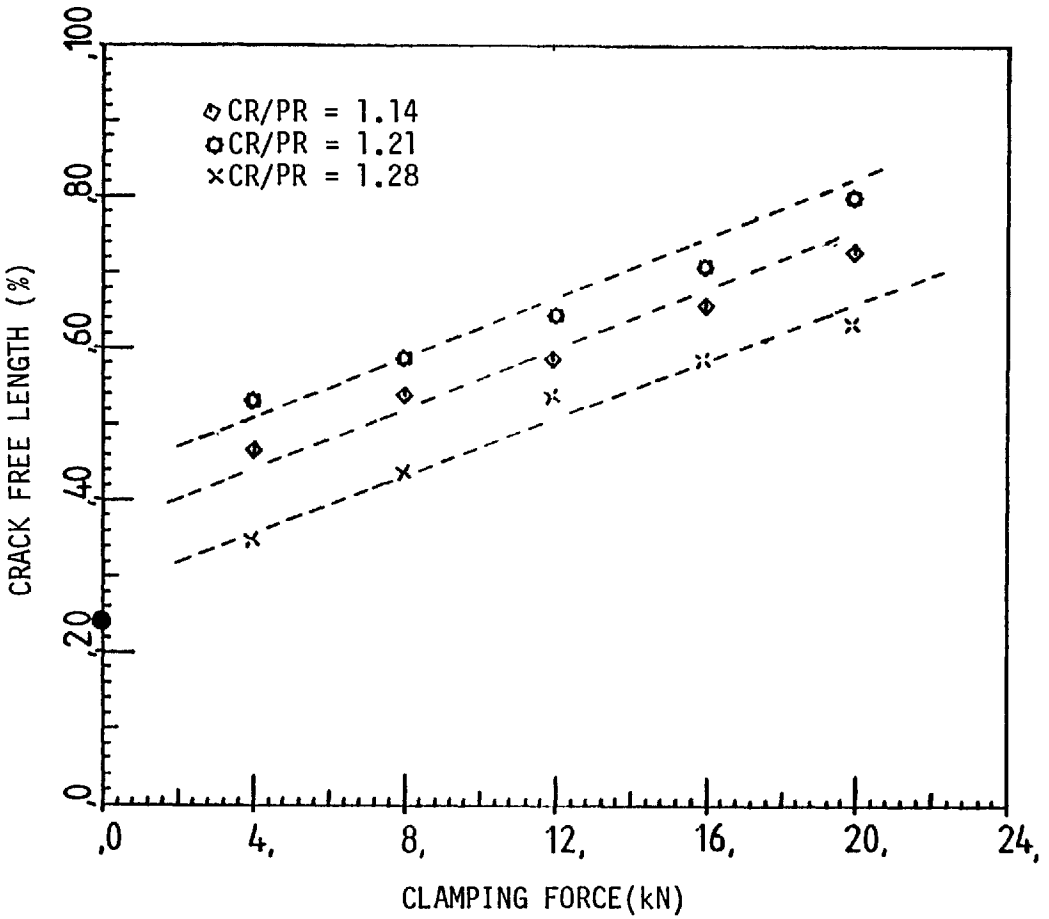

Fig. 4-51. Effect of clamping force (CF) and clamp/punch diameter ratio (CR/PR) on the crack-free-length percentage of the blank edges obtained from blanking strips of mild steel of thickness t = 0.101 in. (2.56 mm).

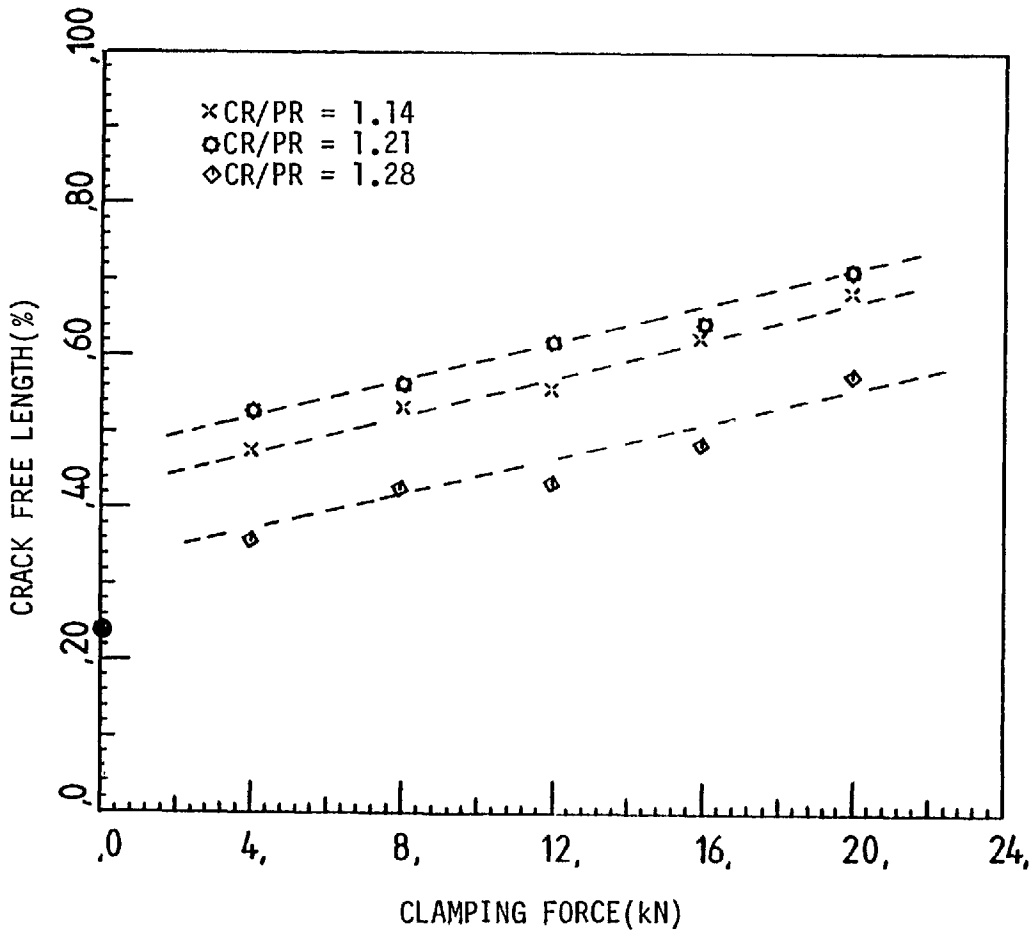

Fig. 4-52. Effect of clamping force (CF) and clamp/punch diameter ratio (CR/PR) on the crack-free-length percentage of the blank edges obtained from blanking strips of mild steel of thickness t = 0.120 in. (3.04 mm).

crack-free length. From these three figures it can also been seen that, as the material thickness increases, the slope of the curves decreases, indicating a smaller percentage of clean area for the thicker materials when using an equal value of clamping force.

In Fig. 4-53 photographs are presented which show the change of blank surface finish when using different values of clamping force and back load.

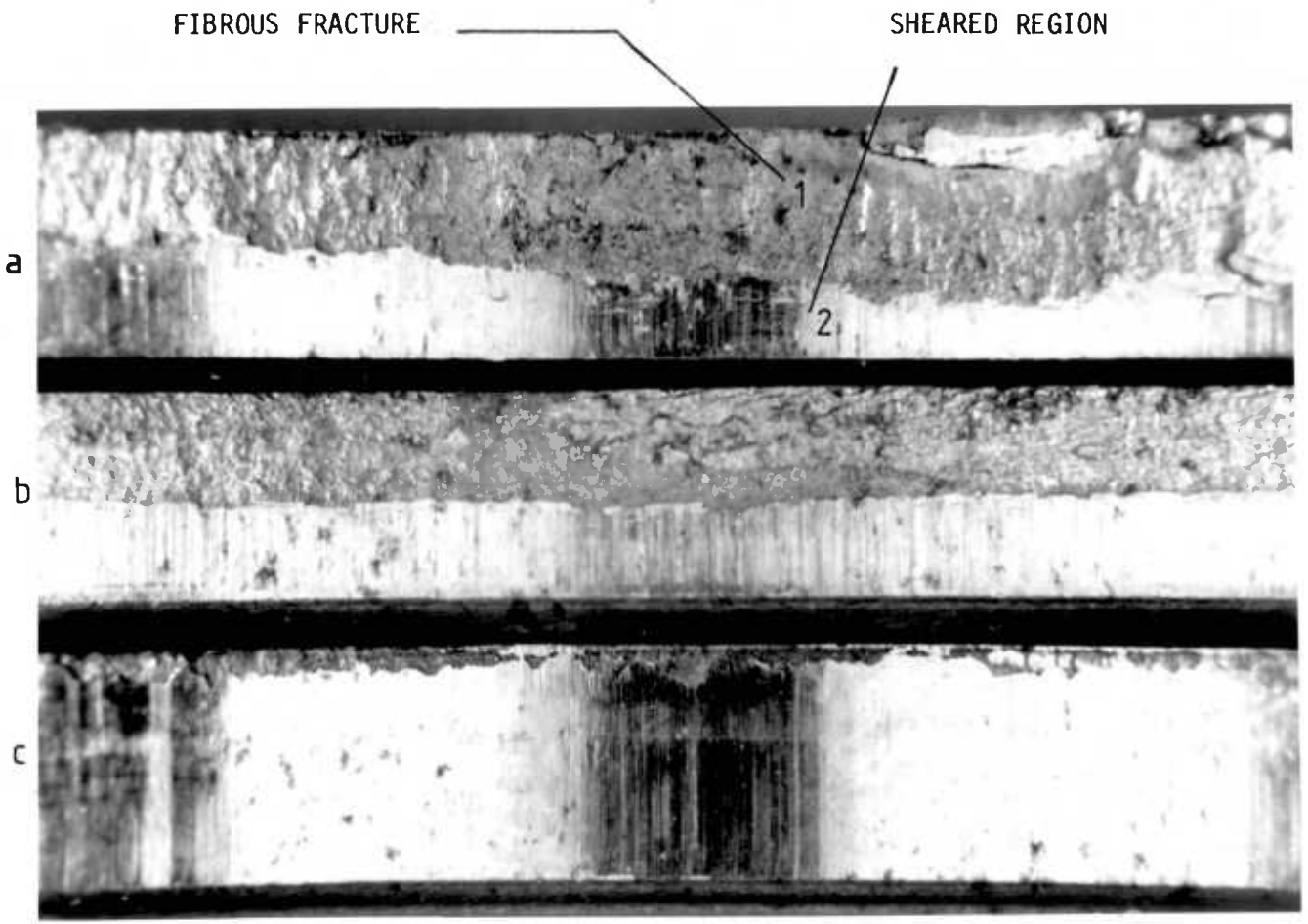

a. CF= 0 BP = 0
b. CF = 30 kN BP = 30 kN
c. CF = 70 kN BP = 70 kN

Fig. 4-53. Transition from fibrous fracture to pure shear when using clamping force and back-load for a t = 0.120 in. (3.04 mm) thick strip of mild steel.

CHAPTER 5

THEORETICAL WORK

5.1 Introduction

The elastic-plastic finite element program which was explained in section (3.7.2) was used in the finite element analysis of the fine blanking process.

A preliminary finite element analysis of the blanking operation, using quadrilateral isoparametric and triangular elements, was made in order to select the most suitable type of element. The load/displacement characteristics during blanking were obtained by using two different finite element meshes comprised of 318 triangular elements in one alternative , while 88 quadrilateral isoparametric elements were used in the other. The choice of elements was based on a compromise between economy and accuracy of the load/displacement characteristics during the blanking operation. For a similar load/displacement result with equal required computing time the choice between the two cases was made on the basis of the stress distribution within the continuum. With regard to the facts mentioned above and the study of the load/displacement characteristics obtained by using different meshes it was decided to use the mesh composed of 88 quadrilateral isoparametric elements throughout this work.

In the preliminary study for the choice of type of element, a further study concerning the effect of number of elements on the load/displacement characteristics in the case of triangular elements was also carried out.

To examine the convergence of the computed results, a comparison between theoretical and experimental punch-load/displacement for three thicknesses of mild steel was made.

The effect of friction, clamping force, clamp diameter and back load on the punch-load/displacement characteristics during the blanking operation is studied in what follows. For a certain value of clamping force and back load, the effect of clamping force, back load and clamp diameter on the developed plastic zone is studied and compared with the plastic zone developed during conventional blanking.

Normal load per unit length distribution along the punch, die and counter punch surfaces under different boundary conditions was calculated and a comparison between different cases is made.

Shear force and normal load per unit length distribution along the punch and die surfaces when punching three different thicknesses of material are presented. Conclusions are drawn concerning the contact area between the specimen, punch and die interfaces, and the direction of material flow above the die surface.

The hydrostatic component of stress and the maximum principal stress in the shearing zone are computed and the effects of different boundary conditions, i.e. clamping force, back load and clamp diameter on these two parameters are studied. The stress contours for the hydrostatic component of stress and different components of stresses are drawn and the effect of clamping force, back load and clamp diameter on the different stress contour patterns is discussed.

5.2 Choice of element

To decide on the choice between quadrilateral isoparametric and triangular elements a comparison of the load/displacement characteristics had to be made. The load/displacement characteristics using two different meshes with 88 quadrilateral isoparametric elements and the other with

318 triangular elements were obtained. It was found that for both cases the load/displacement characteristics and the required computing time were nearly the same. A comparison of the stress distribution within the continuum for both cases showed that the mesh with quadrilateral isoparametric elements yielded a smoother stress distribution than the mesh with triangular elements. This could be due to the fact that the stresses within the quadrilateral isoparametric elements can vary linearly, in contrast to the triangular elements where the stresses are calculated at a single point, usually centroid, and are assumed constant within the element. It should be noted that, as was mentioned earlier in section (3.2.2), this condition of constant stress in the triangular elements resulted in an unrealistic change of the boundary condition which was contrary to the physical characteristics of the problem.

With regard to the facts mentioned above and bearing in mind that the entire analysis of the fine blanking process studied in this thesis is based on the study of the stress distribution within the continuum, it was decided to use a mesh pattern with 88 quadrilateral isoparametric elements throughout this work.

5.3 Mesh patterns

As the fine blanking process considered is an axi-symmetric case, half of the specimen cross section was divided into three different regions of finite element mesh, shown in Figs. 5-1, 5-2 and 5-3. It should be noted that the elements used in axi-symmetric finite element problems are ring elements.

All the meshes were numbered across the thickness, Figs. 5-1, 5-2 and 5-3 since, owing to the special patterns of the meshes, the band width of the overall stiffness matrices would automatically be minimized.

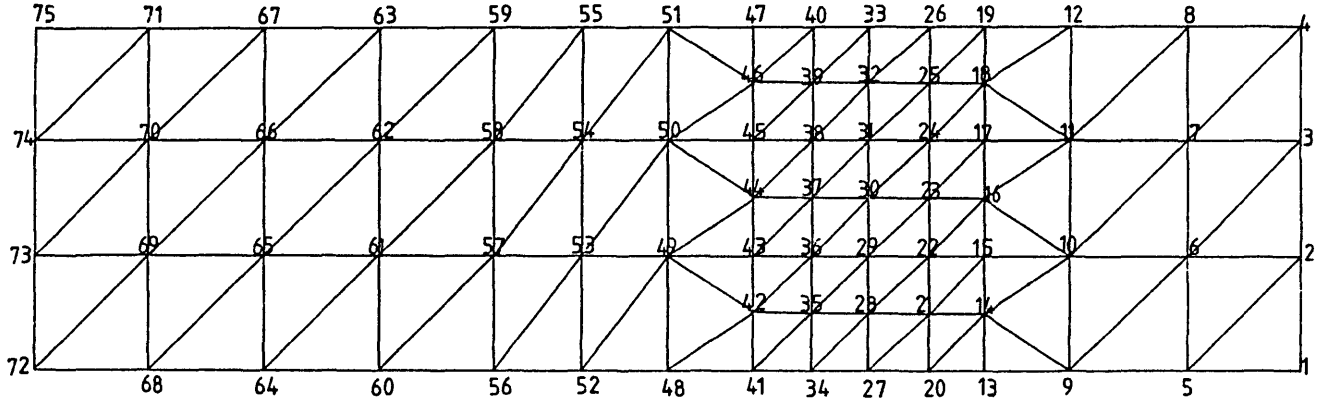

Fig. 5-1. Finite element mesh with 114 triangular elements and 75 nodes.

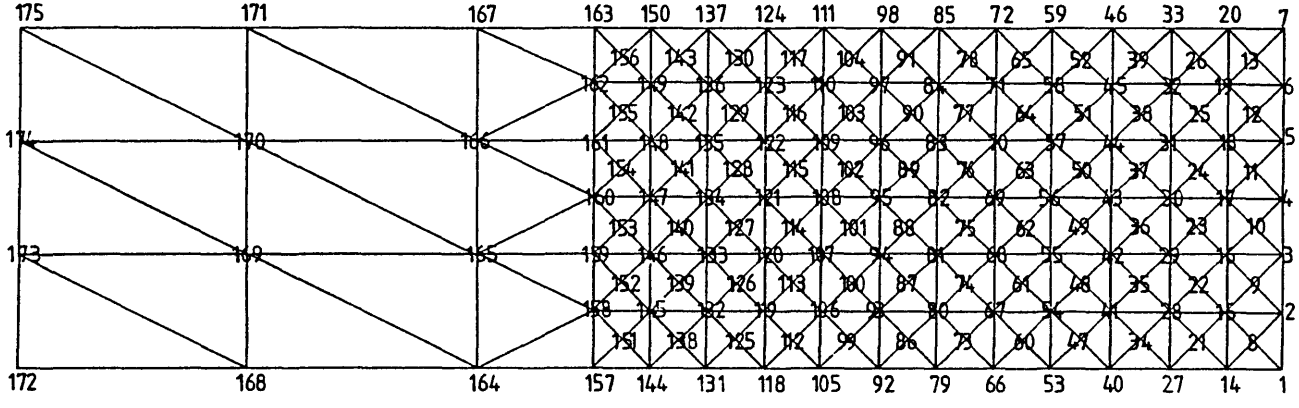

Fig. 5-2. Finite element mesh with 308 triangular elements and 175 nodes.

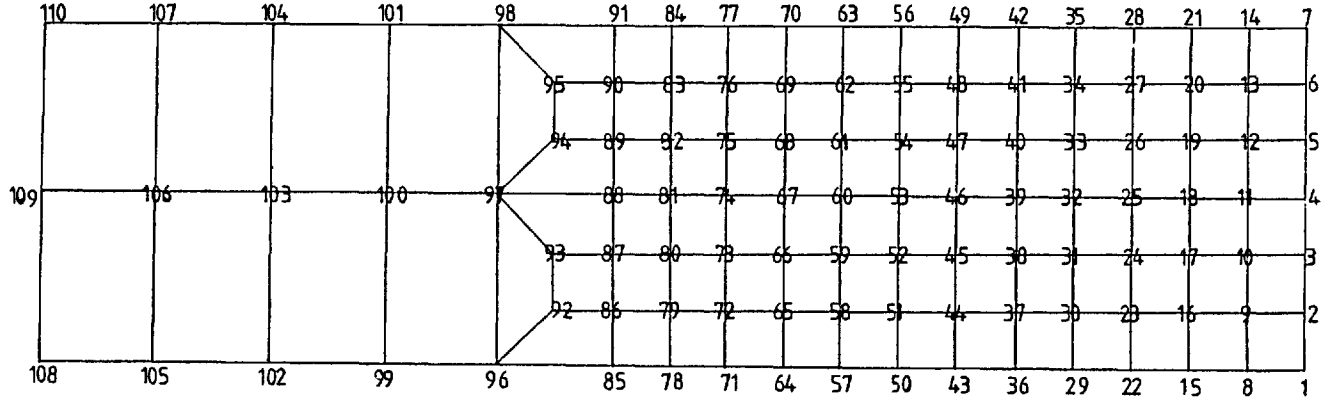

Fig. 5-3. Finite element mesh with 88 quadrilateral isoparametric elements and 110 nodes.

Fig. 5-1 shows a mesh pattern with 114 triangular elements and 75 nodes. The elements are more concentrated around the shear line in order to yield a better approximation of the state of stress in this region. It should be noted that it is important to have enough elements in this region since the stress variation is at its highest level and an appropriate mesh would yield better load/displacement and stress distribution within the continuum.

The second type of mesh which was used was a mesh with 308 triangular elements with 175 nodes, Fig. 5-2. In this pattern the elements in the region of high stress intensity are chosen in such a way that every four triangles form a quadrilateral. This type of division has proved to be nearly as efficient as quadrilateral elements. A rough mesh pattern is chosen towards the centre, as the stress level here is considerably lower than at other regions and the variation is more gradual.

Fig. 5-3 shows the division of the specimen into 88 isoparametric quadrilateral elements with 110 nodes. An increase in the number of elements especially around the shear line would yield a better solution. As the program had to be solved for different boundary conditions, it was found that any increase in the number of elements in the case of quadrilateral isoparametric elements would be too costly to run. Using this mesh pattern for a blanking load of 74 kN, which is the maximum blanking load obtained experimentally when blanking mild steel strips of thickness t = 0.120 in. (3.04 mm), the computing time on the C.D.C. 6400 computer was approximately 800 seconds.

5.4. True stress-strain curve

To introduce the true stress-strain curve of the material into the computer program a compression test was performed on a strip of mild steel measuring 2 in. (50.8 mm) wide and 0.120 in. (3.04 mm) thick and the corresponding results plotted, Fig. 5-4. For use in the computer program the actual curve was approximated by two straight lines. The section of the curve after the yield point can be approximated by either a straight line parallel to the curve or by joining the yield point to a point on the curve corresponding to the maximum presumed strain that material might reach during deformation, Fig. 5-4. The computer results obtained for both types of approximation showed that even at maximum deformation the difference between the results was very small.

The material properties used for the computation were :

$E = 2.1 \times 10^6 kg/cm^2$ ($20.6 \times 10^4 MN/m^2$), $\nu = 0.291$ and
$H' = 30000\ kg/cm^2$ ($2943\ MN/m^2$) for $\bar{\sigma} \leq 4000\ kg/cm^2$ ($392\ MN/m^2$)
and $H' = 3000\ kg/cm^2$ ($294.3\ MN/m^2$) for $\bar{\sigma} > 4000\ kg/cm^2$ ($392\ MN/m^2$)
with Y (initial yield stress) = $2000\ kg/cm^2$ ($196\ MN/m^2$)

These values approximate the static stress-strain curve for commercially available mild steel used in the experiments.

5.5 Convergence of the computed results

As errors in finite element programs of the incremental form used for non-linear problems are additive, to examine the validity and convergence of the computed results it was decided that a comparison between theoretical and experimental results must be made.

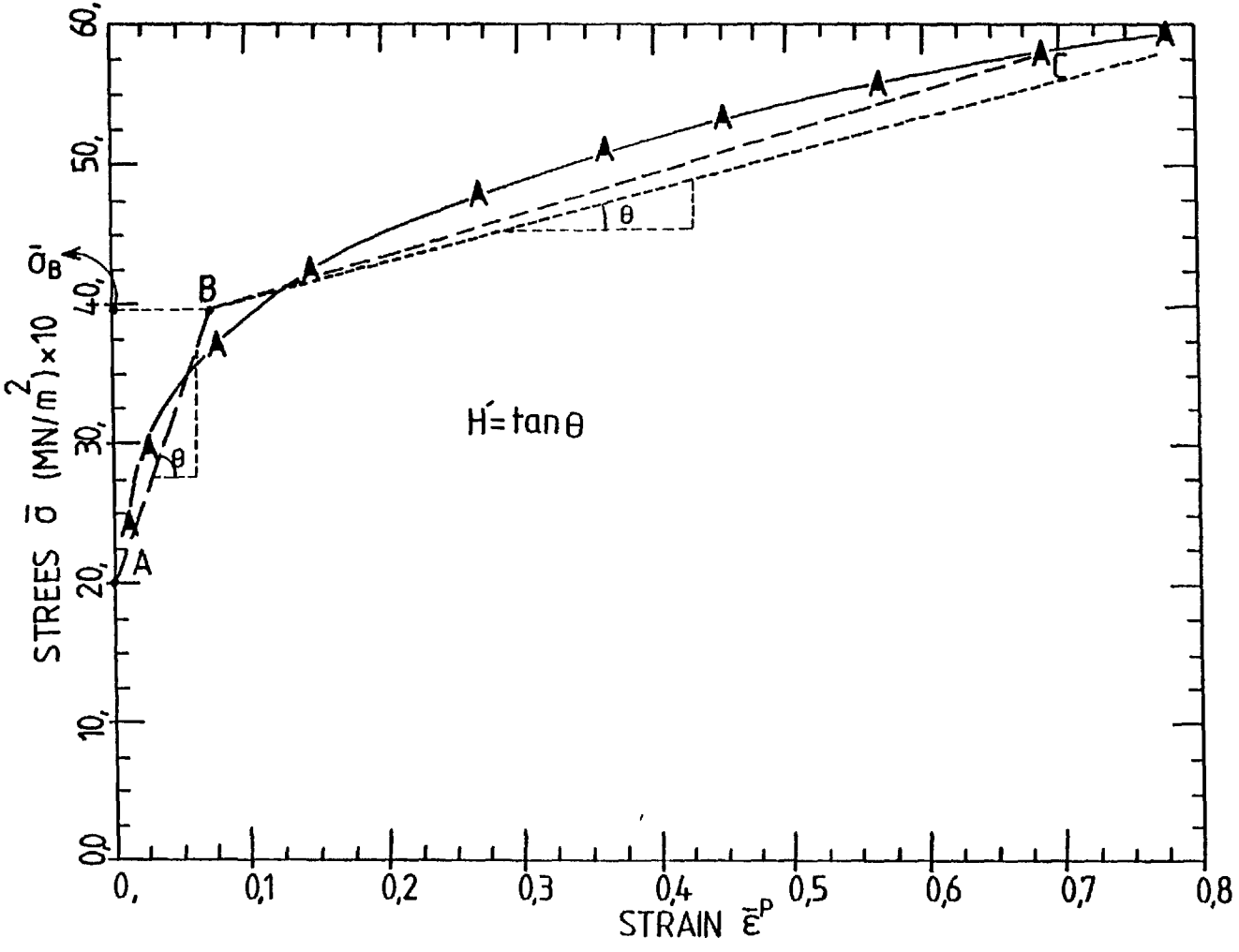

Fig. 5-4. True stress strain curve for mild steel.

The only parameter which could be measured experimentally was the punch-load/displacement characteristics. Therefore a comparison of the theoretical and experimental results of this parameter was made to show the deviation of the computed results from the experiments and to check the convergence of the computer program. This can also verify the amount of deformation that can be introduced into the computer program without unrealistic errors developing.

5.6 Effect of type and number of elements on the punch-load/displacement characteristics

To study the effect of the number of elements on the punch-load/displacement characteristics two different meshes containing 308 and 114 triangular elements, with 175 and 75 nodal points respectively, were used in the study of a punching operation of a typical thickness of t = 0.120 in. (3.04 mm) strip of mild steel and the results are shown in Fig. 5-5. Also shown in this figure is the corresponding result obtained by using a mesh containing 88 quadrilateral isoparametric elements with 110 nodal points.

The difference in the results at the early stages of the process is negligible and an increase in the number of elements in the case of triangular elements, from 114 to 308, causes a decrease in the blanking load. As the finite element method yields an upper bound solution it can be said that an increase in the number of elements will yield an answer closer to the real solution.

Fig. 5-5 shows that the load/displacement characteristics obtained using a mesh with 88 quadrilateral isoparametric elements and 318 triangular elements are almost identical. This proves the fact that for the same degree of accuracy a mesh with triangular elements can be replaced with

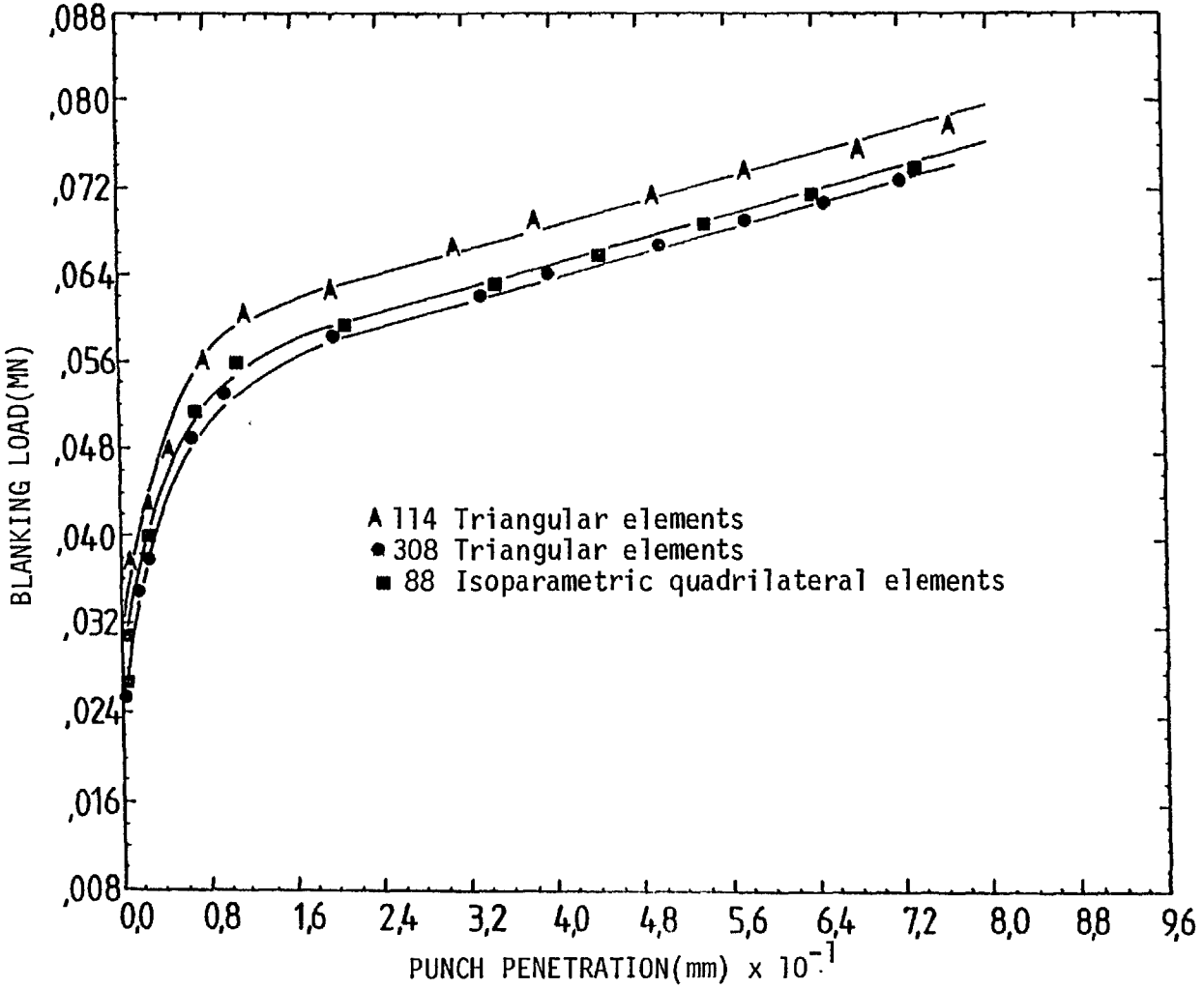

Fig. 5-5. Effect of type and number of elements on the punch load/displacement characteristics when punching t = 0.120 in. (3.04 mm) thick strips of mild steel.

a mesh with a much smaller number of quadrilateral isoparametric elements.

Hereafter throughout the thesis the required computations will be carried out using the computer program which employs quadrilateral isoparametric elements, explained in section (3.7.2), and the 88 quadrilateral isoparametric element mesh shown in Fig. 5-3 will be used as a computer program model for the specimen.

5.7 Effect of friction on the punch-load/displacement characteristics

To study the effect of frictional forces on the load/displacement characteristics two limiting conditions of friction, i.e. sticking and frictionless, were investigated.

In the frictional condition of sticking, in order to introduce the effect of frictional forces in the boundary condition it was assumed that all points on the punch/specimen or die/specimen interface can have no radial displacement.

In the frictionless condition the nodes on the contact area between the punch, die and specimen are free to move in the radial direction and can take no radial force.

The effect of friction at the punch/specimen and die/specimen interface on the punch-load/displacement characteristics is shown in Fig. 5-6.

The curves follow the same trend and the blanking load corresponding to each value of punch penetration for the frictionless case is below the sticking case values. However, the difference between the two curves is small and remains nearly constant throughout the blanking operation. The small change in the punch-load/displacement curve shows that, in blanking, the relative movement of the specimen against the punch and die

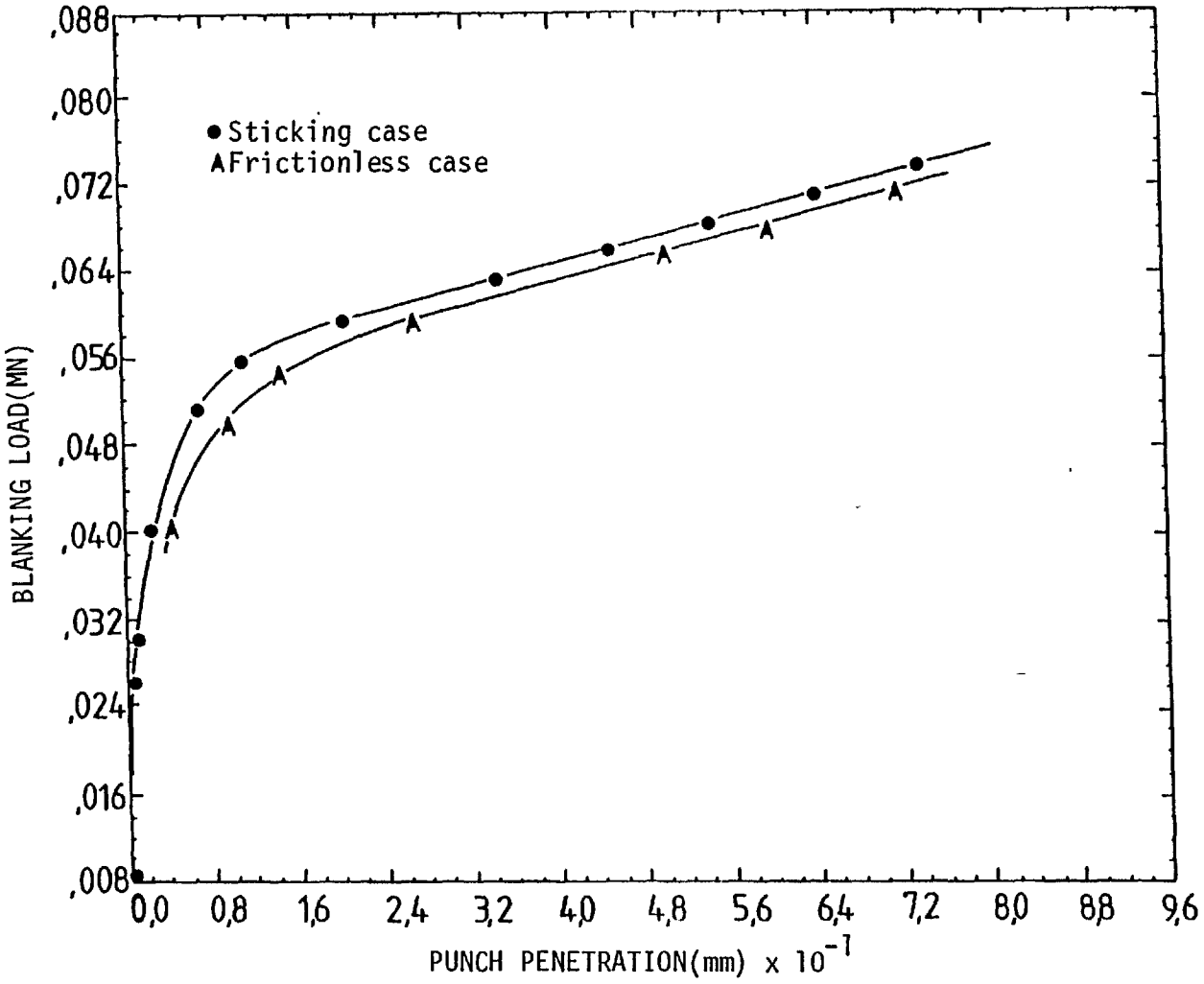

Fig. 5-6. Theoretical comparison of blanking load vs. punch penetration for two different conditions of friction when punching t = 0.120 in. (3.04 mm) thick strips of mild steel.

is small. This is in contrast to simple indentation such as that studied by Kobayashi (81), in which there is a considerable difference between the load/displacement results for sticking and frictionless cases, indicating the high tendency of the material to flow against the punch and the surface on which the specimen is supported.

Throughout the rest of this work sticking friction between the punch/specimen and die/specimen interfaces will be assumed, because the strips of material used during the experiments were commercially rolled mild steel, which had far from smooth surfaces and, although a lubricant was used, still substantial frictional forces could build up. It should be noted that as the contact areas between punch/specimen and die/specimen are small even for small values of coefficient of friction, the normal forces will be sufficiently high for a sticking condition of friction to prevail.

5.8 A comparison of the theoretical and experimental load/displacement characteristics

To check the convergence and so the validity of the computer program, using 88 quadrilateral isoparametric elements, a comparison of theoretical and experimental results was made for three different thicknesses of mild steel, 0.076, 0.101 and 0.120 in. (1.93, 2.56 and 3.04 mm) and the results are given in Figs. 5-7, 5-8 and 5-9.

The computer program can predict the blanking load with a very good degree of accuracy for all the three thicknesses during the blanking process. The experimental load/displacement curves which were used for comparison with the theoretical results were obtained by measuring the amount of indentation made by the punch under different values of punch load, using a depth gauge, Fig. 5-10.

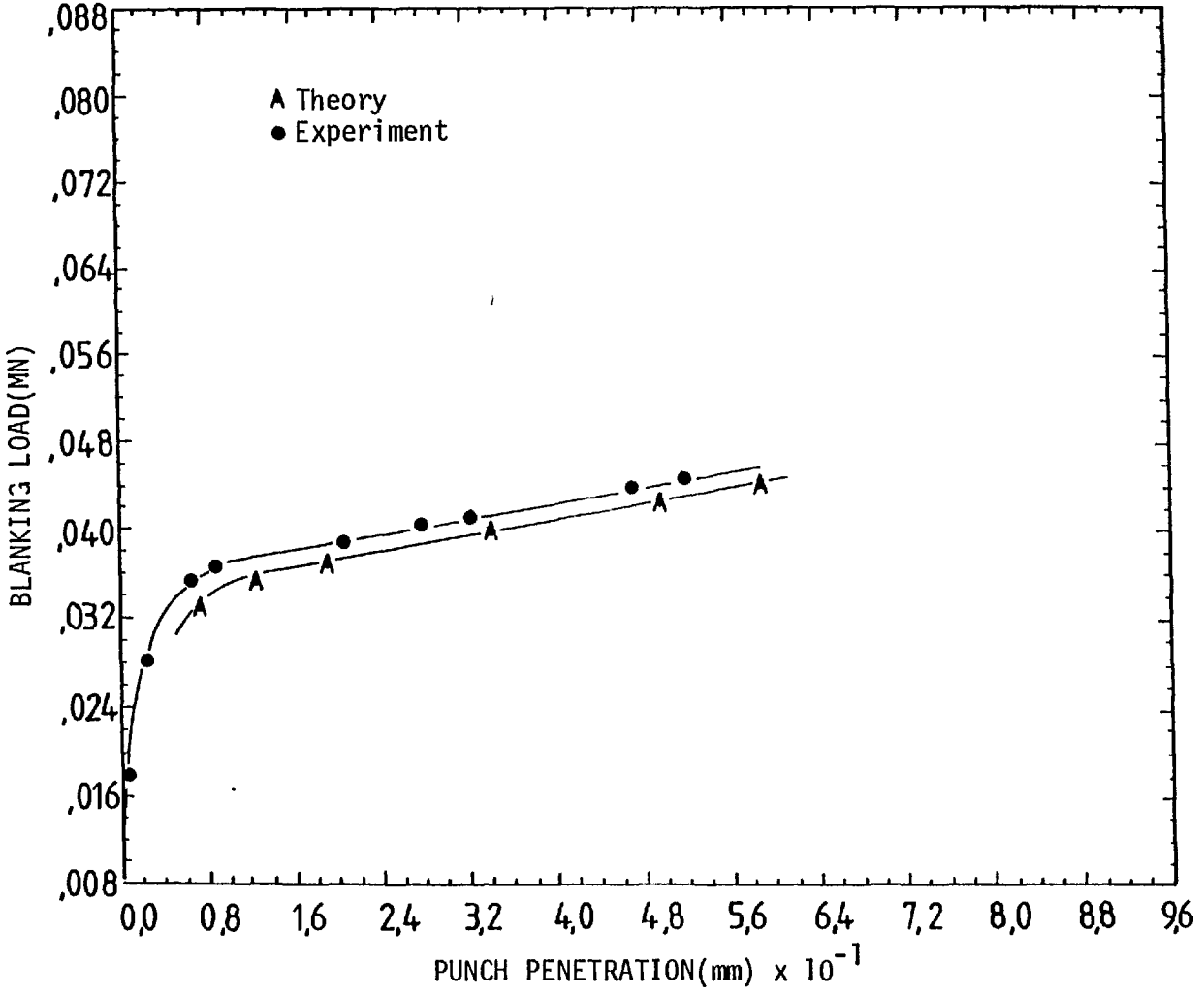

Fig. 5-7. A comparison of theoretical and experimental punch-load/displacement results when punching a strip of mild steel of thickness t = 0.078 in. (1.93 mm).

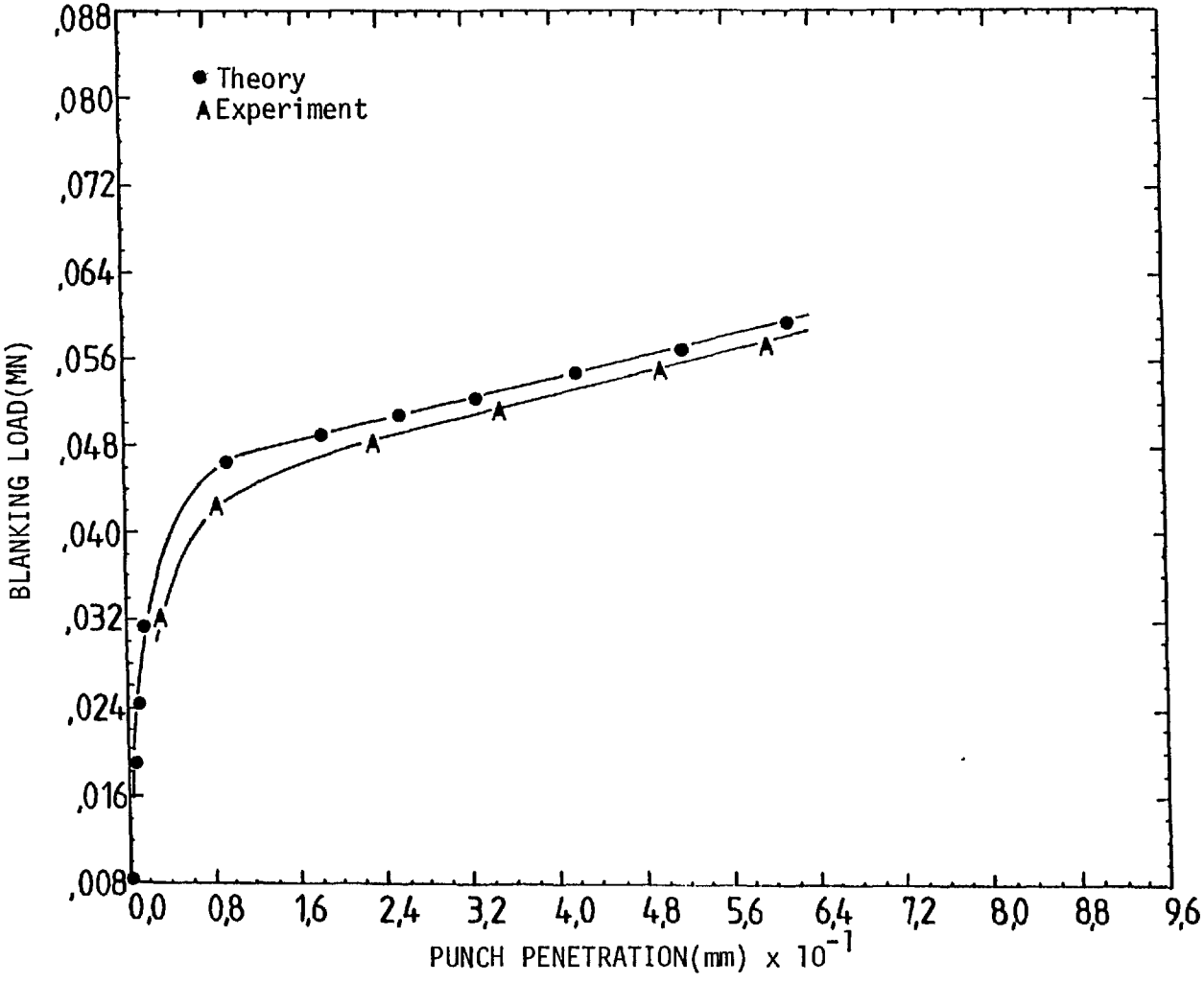

Fig. 5-8. A comparison of theoretical and experimental punch load/displacement results when punching a strip of mild steel of thickness t = 0.101 in. (2.56 mm).

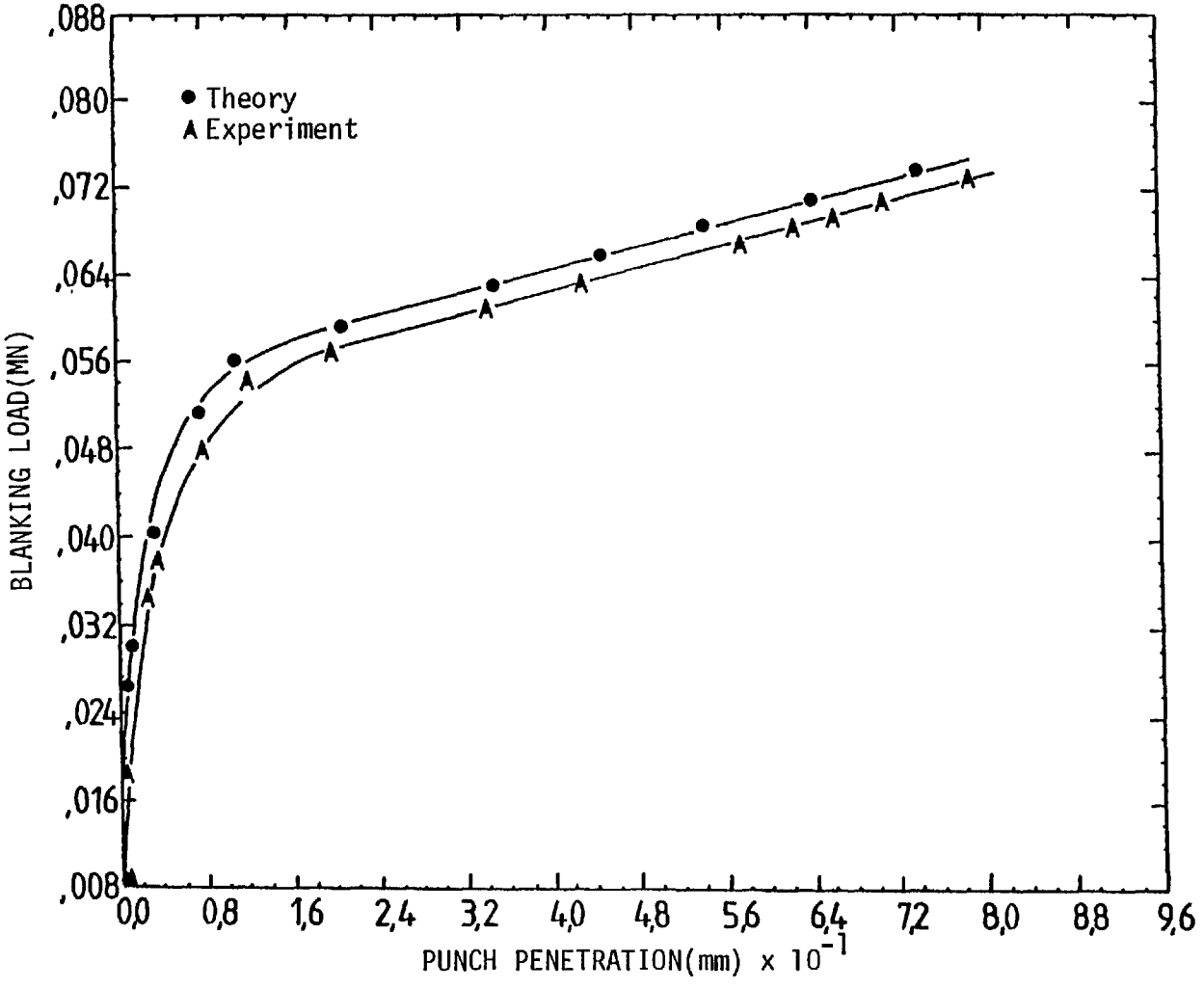

Fig. 5-9. A comparison of theoretical and experimental punch-load/displacement results when punching a strip of mild steel of thickness t = 0.120 in. (3.04 mm).

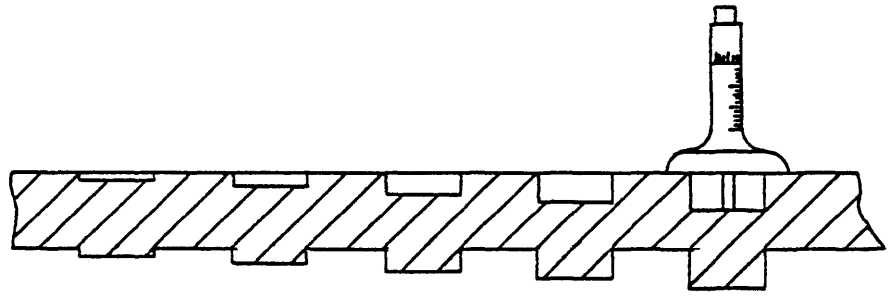

Fig. 5-10. Punch indentation measurements using a depth gauge.

By this method the true values of indentation, excluding elastic deformation of the specimen are measured whilst the values measured by the displacement transducer include the overall elastic distortions of the immediate parts between the two platens of the press, including any slackness in the system. The measurements obtained by the depth gauge were taken as the true values of punch penetration for comparison with the theoretical results.

All the curves have about the same pattern and the theoretical punch-load/displacement curves consist of three distinguishable sections. In the first part the load increases with a slight bend which corresponds to the elastic-plastic deformation of the material while the equivalent stresses of the post yielded elements are, in the main, less than $\bar{\sigma}_B$, Fig. 5-4. The blanking loads increase up to a point and then a rapid bend in the curves is observed. A change of constrained to unconstrained plastic flow, see illustration overleaf, was suspected to be the cause of the sudden bend in the load/displacement curves. The plastic zone at different punch penetrations was examined, when punching a strip of mild steel of thickness t = 0.120 in.(3.04 mm), and it was found that a change of constrained to unconstrained plastic flow occurs at a punch penetration

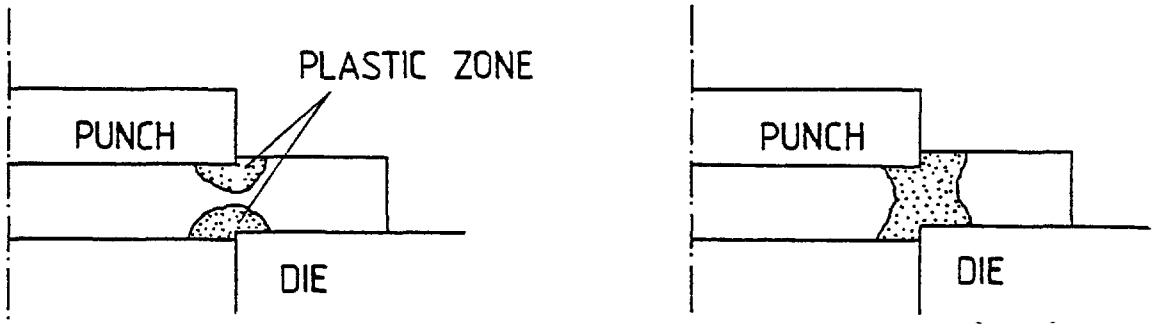

Constrained deformation

Unconstrained deformation

A change of constrained to unconstrained plastic flow could be the reason for sudden bend in the load/displacement curve.

of 0.026 mm. This is well before the punch penetrations corresponding to the sharp bend in the curve, which are in the range of 0.08 mm to 0.12 mm.

This sharp bend in the load/displacement curve can possibly be explained by considering the method of construction of the element stiffness matrices which depends on their corresponding equivalent stresses. For the post yielded elements, the stiffness matrices are first built by using the slope of the line AB, Fig. 5-4. When the equivalent stress of a post yielded element exceeds $\bar{\sigma}_B$, the element stiffness matrix is newly built using the slope of the line BC instead of AB. As the slope of the line BC is much smaller than that of the line AB (by nearly a factor of 10) this causes an abrupt drop in the element stiffness matrix and consequently a considerable drop in the element's resistance to deformation.

Considering the plastic zone and the level of equivalent stresses in the yielded elements it becomes clear that the plastic zone is confined to a small region and that the majority of the yielded elements have very

close values of equivalent stresses. These elements form a large portion of the plastic region and take most of the blanking load.

At a certain amount of punch penetration the equivalent stresses in these elements will all simultaneously reach the vicinity of the stress level at point B, Fig. 5-4. By small advancement of the punch the equivalent stresses of these elements exceed $\bar{\sigma}_B$, which is accompanied by a sudden decrease in the element stiffness matrices. A sudden drop in the stiffness matrices of these elements can be envisaged as being able to decrease the overall stiffness matrix of the structure considerably and thus cause a sharp bend in the direction of the punch-load/displacement curve.

After the rapid bend in the theoretical punch-load/displacement curve, the punch-load increases along a straight line. The finite element model used for the blanking operation can predict the increase in load which occurs due to work-hardening. However, it cannot predict the decrease in load which occurs after a maximum in the actual process, due to the decrease in the unsheared area. This decrease in the area could be achieved in the theoretical model only by changing some of the nodal point connections, Fig. 5-11.

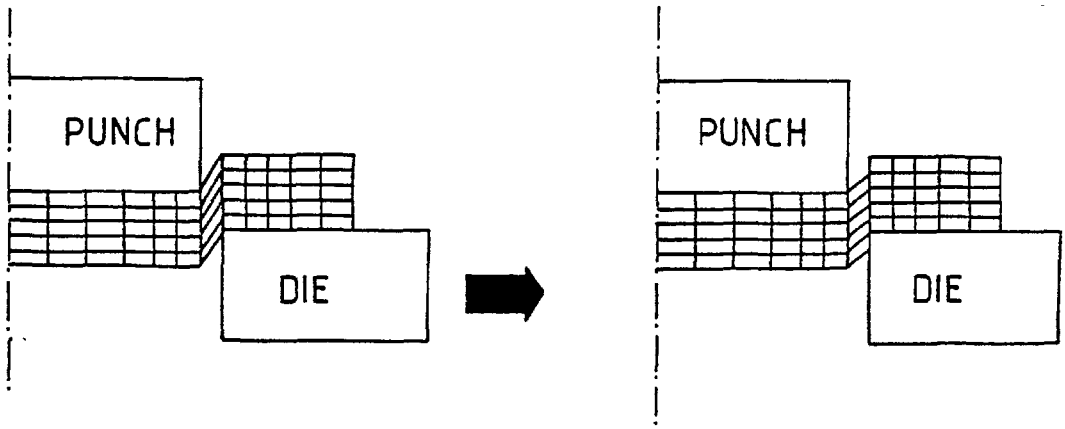

Fig. 5-11. The decrease in the unsheared area in the theoretical model can be modelled by changing of some the nodal point connections.

However, as this changing of nodal point connection is not permitted in the finite element method, it is not possible to predict a maximum in the blanking load when using finite element method. Consequently, it was decided to continue the deformation in the theoretical model until a blanking load equal to the maximum blanking load obtained in the experiments was reached. The theoretical punch-load/displacement curves for three different thicknesses of mild steel are shown in Fig. 5-12.

The load/displacement curves after the rapid bend follow nearly a parallel trend and the change of direction in the curves occurs at a smaller amount of punch penetration as the thickness of the specimen decreases. In the parallel region of the curves the value of the blanking load (at a certain punch penetration) was divided by the corresponding thickness of the material and it was found that the results for the three thicknesses of the material were nearly the same. This indicates that the blanking load predicted by the finite element method, in the parallel region of the curves, is related to the material thickness in an approximately linear manner.

It is interesting to note that, for a certain amount of punch penetration, the blanking load for thicker material is higher than for the thinner materials. This must be due to the fact that, for thinner materials, the plastic zones developed at the punch and die edges merge at a smaller amount of punch penetration (illustration overleaf) and, as was previously explained, shortly after this a decrease in the resistance to deformation occurs which results in a drop in the rate of increase in the blanking load in the further stages of the process.

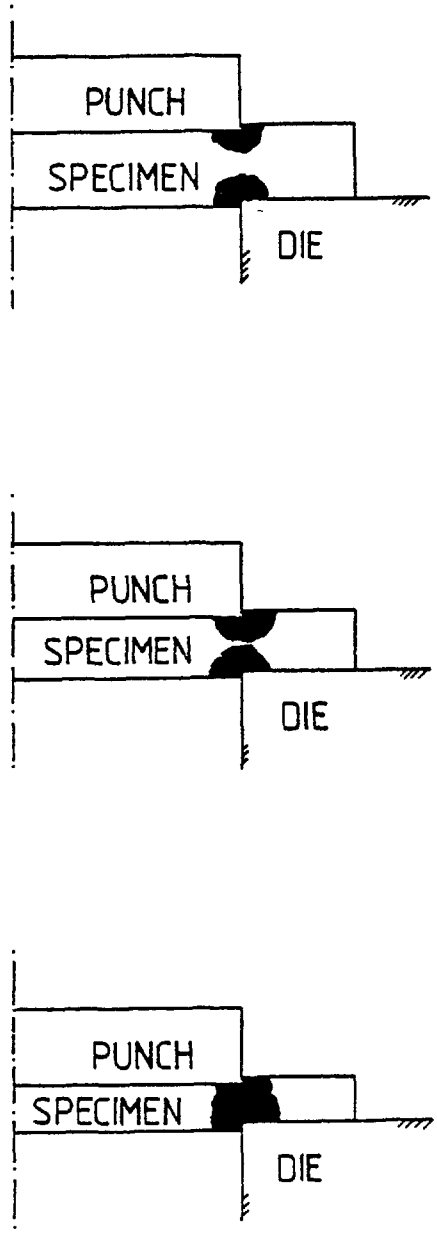

For thinner materials the plastic zones nucleated at the punch and die edges will meet at a smaller amount of punch penetration.

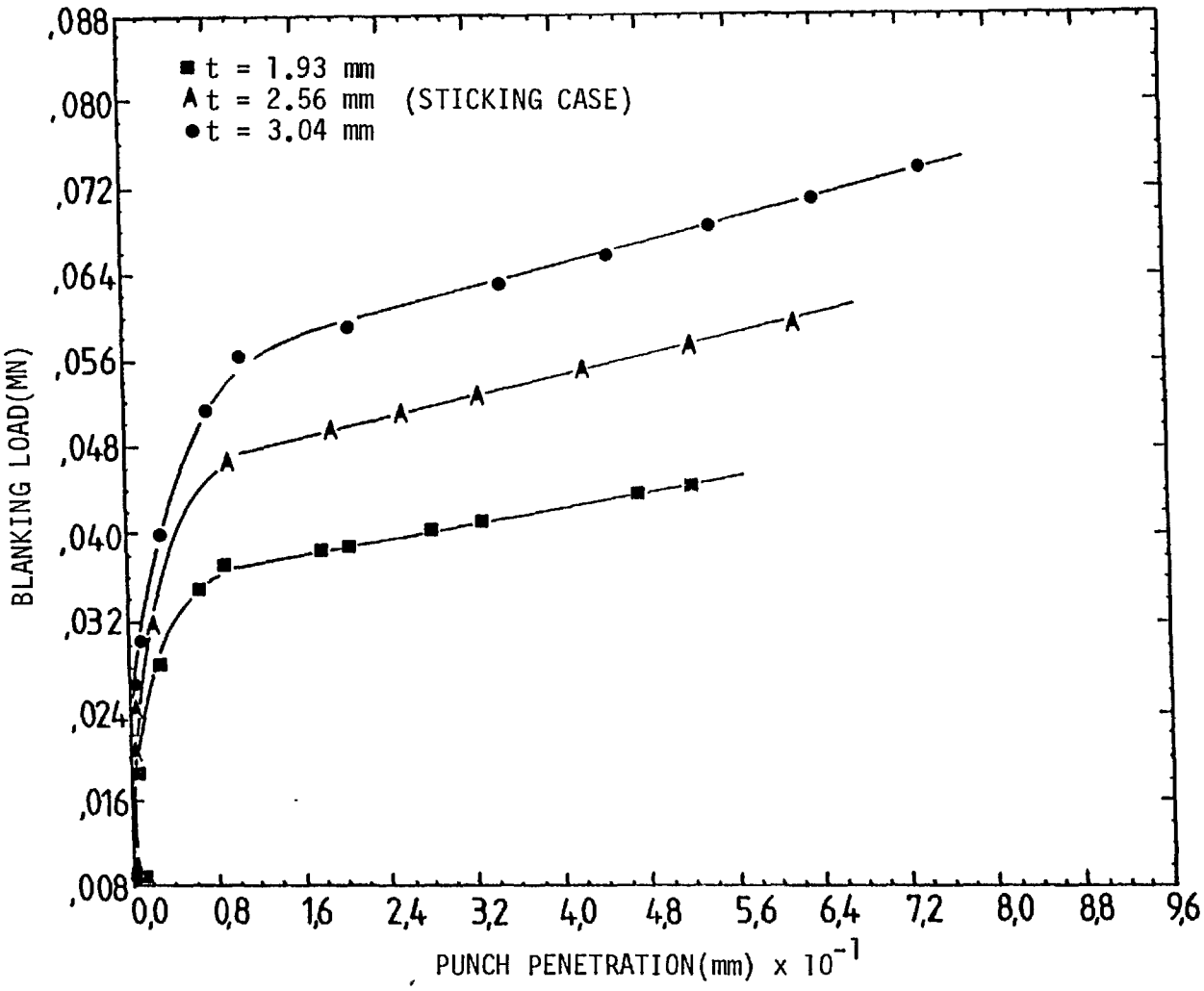

Fig. 5-12. Theoretical comparison of punch load vs. punch penetration for different thicknesses of mild steel (t = 1.93, 2.56 and 3.04 mm).

5.9 Effect of clamping force and back-load on the punch-load/displacement characteristics

The experimental results presented in Chapter 4 indicated that the magnitude of clamping force and clamp diameter does not affect the load/displacement characteristics during the blanking operation. To verify these results theoretically, three different values of clamping force together with three values of clamp diameter were considered and the corresponding results for three clamp diameters with clamp/punch diameter ratios of ($\frac{CR}{PR}$ = 1.14, 1.21 and 1.28) are shown in Figs. 5-13, 5-14 and 5-15 respectively.

The results for different values of clamping force, and a certain clamp/punch diameter ratio, all follow the same trend. Considering these figures it can be concluded that the application of clamping force does not affect the punch-load/displacement characteristics of the material. These results are in line with the experimental results presented in Chapter 4.

This analysis can be used as a good criterion to verify the validity of the computer program, as the combined effect of blank-holder and punch penetration could easily bring to light any possible error.

The effect of back-load on the blanking load for a typical thickness of t = 0.120 in. (3.04 mm) for three different values of back-load 30, 50 and 70 kN in the absence of clamping force are presented in Fig. 5-16.

The curves all follow the same trend and the difference between any two curves (after the rapid bend) is nearly constant and equal to the difference between the corresponding back-loads. These results are again in agreement with the experimental results presented in Chapter 4, which showed that the addition of the back-load does not change the trend of the curves and that the difference between the two curves is

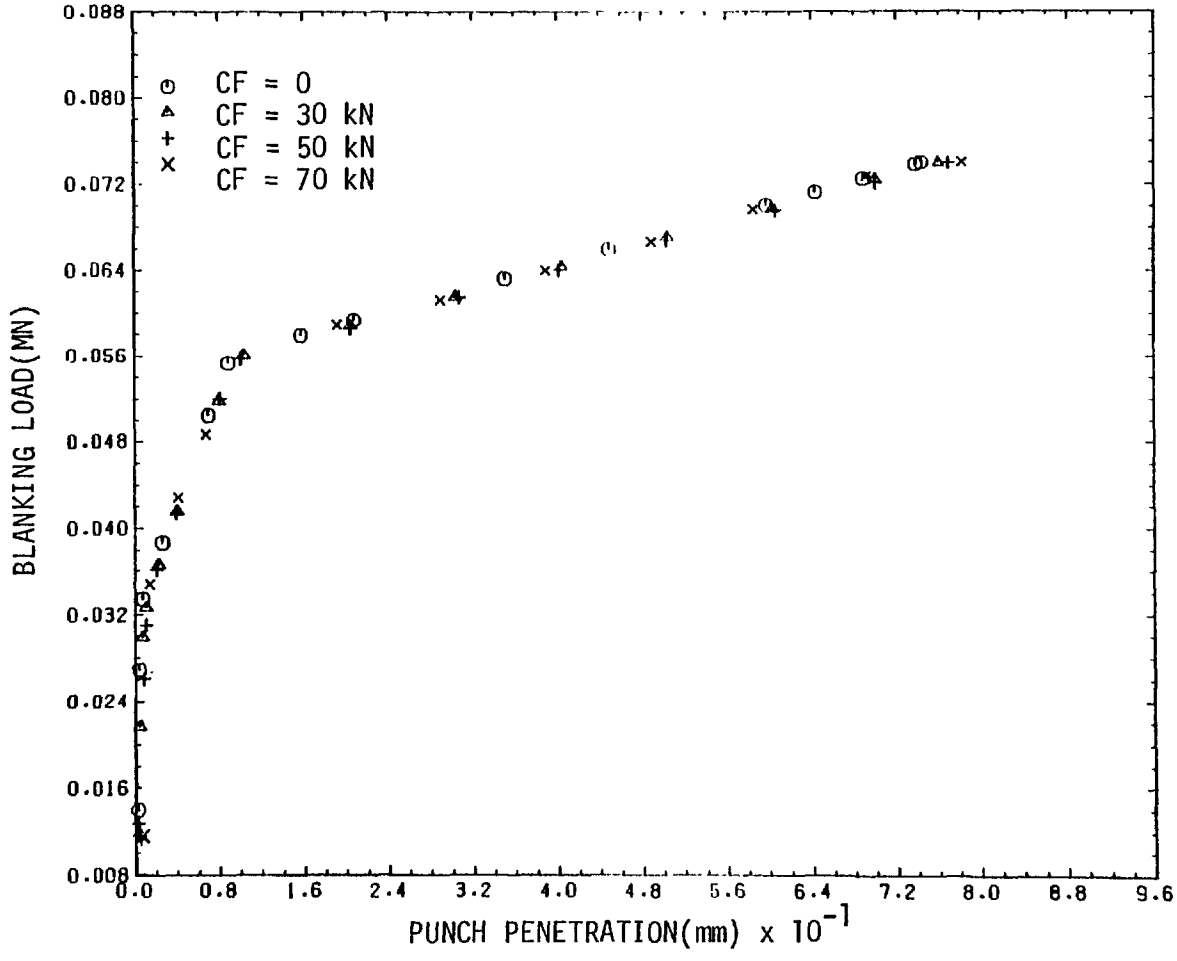

Fig. 5-13. Effect of clamping force (CF) on the punch-load/displacement characteristics of mild steel strips of thickness t = 0.120 in. (3.04 mm) in the absence of back-load (BP = 0) when a clamp/punch diameter ratio of (CR/PR = 1.14) was used.

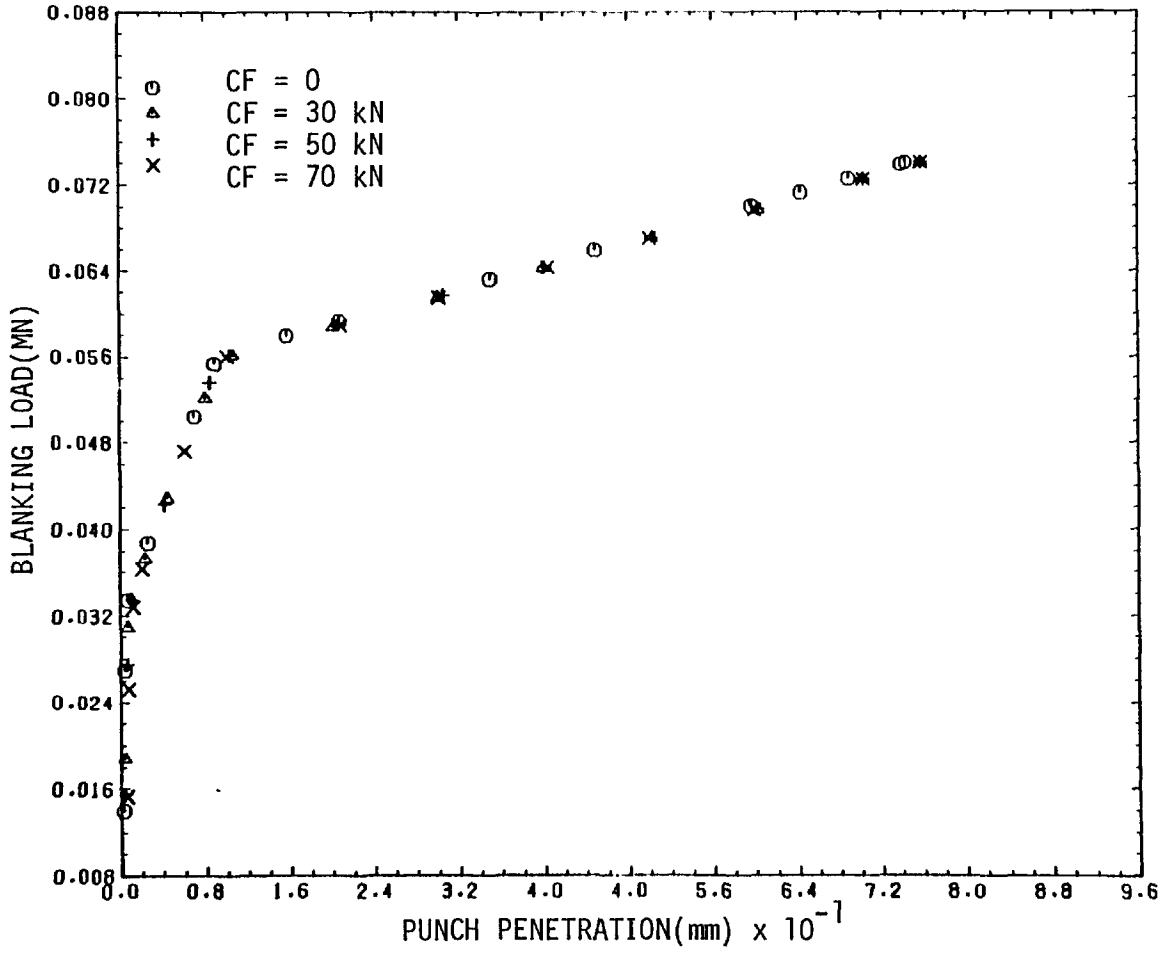

Fig. 5-14. Effect of clamping force (CF) on the punch-load/displacement characteristics of mild steel strips of thickness t = 0.120 in. (3.04 mm) in the absence of back-load (BP = 0) when a clamp/punch diameter ratio of (CR/PR = 1.21) was used.

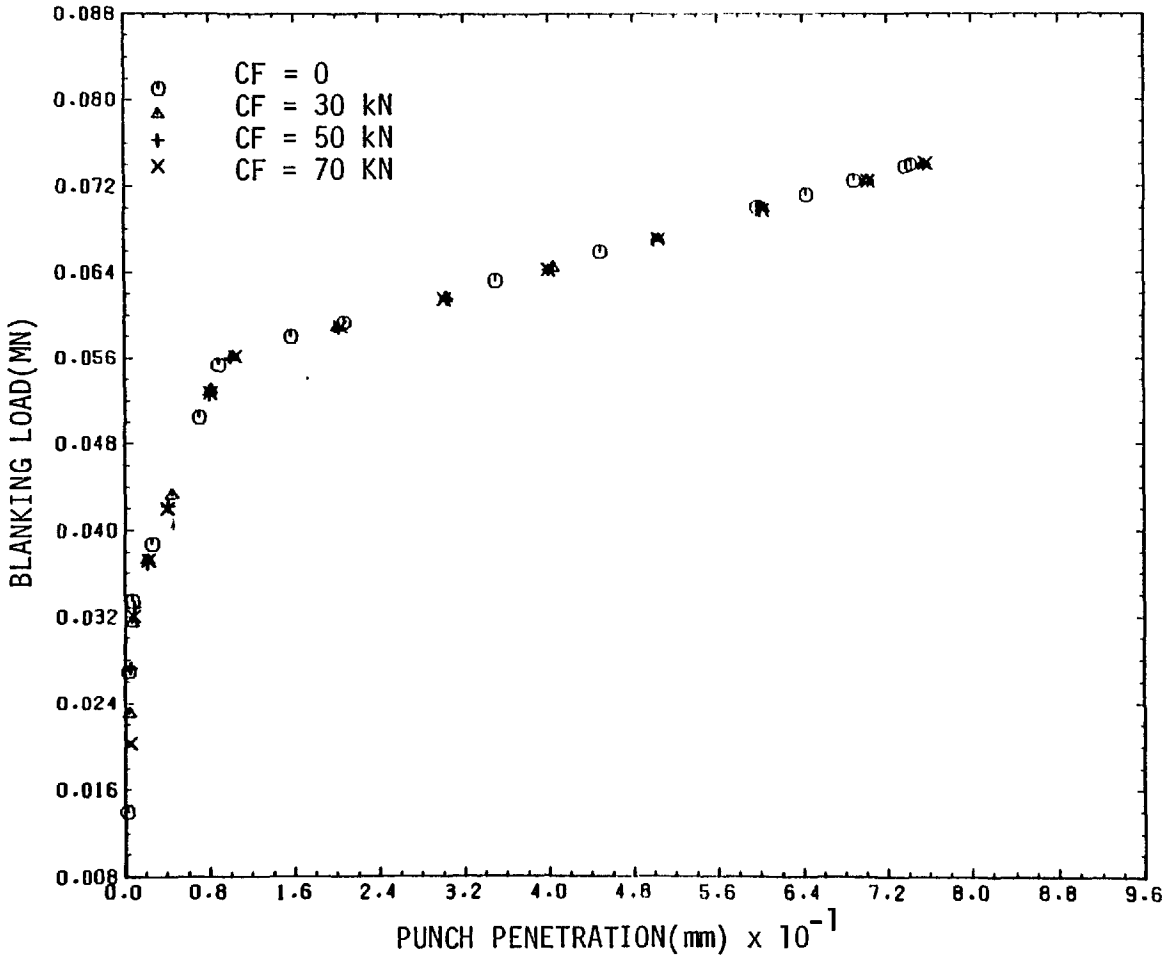

Fig. 5-15. Effect of clamping force (CF) on the punch-load/displacement characteristics of mild steel strips of thickness t = 0.120 in. (3.04 mm) in the absence of back-load (BP = 0) when a clamp/punch diameter ratio of (CR/PR = 1.28) was used.

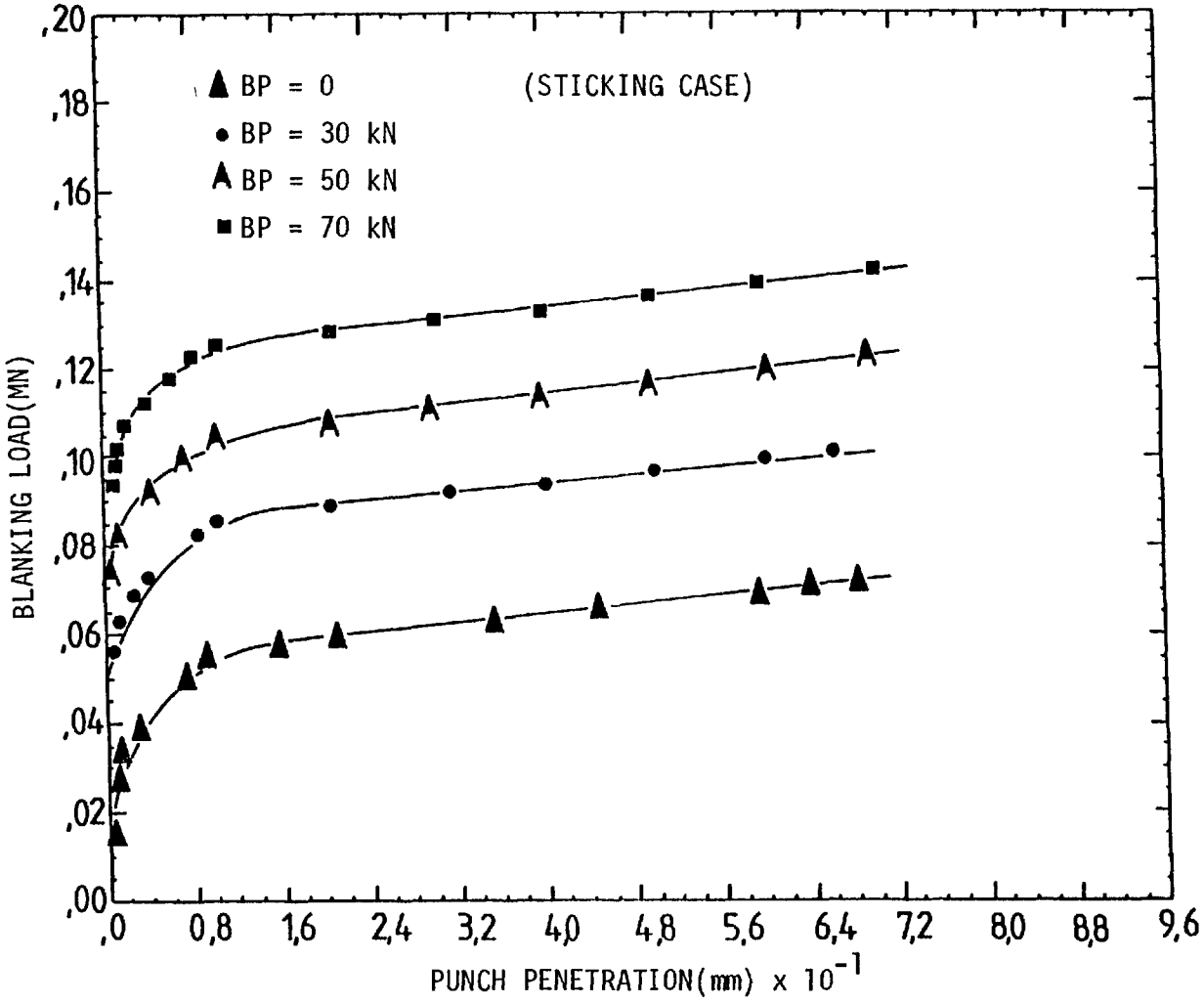

Fig. 5-16. Effect of back-load (BP) on the punch-load/displacement characteristics of mild steel strips of thickness t = 0.120 in. (3.04 mm) with no clamping force present (CF = 0).

equal to the difference between the corresponding back-loads. The computation of the load/displacement characteristics, with the back-load present, can be used as a further verification of the validity of the computer program, as the addition of back-load will change the stress zone and possible errors would be detected much more easily.

5.10 Development of the plastic zone during the blanking operation

A unique feature of the finite element method is that it permits one to follow the path of deformation from the initial stress-free state to the final stage. The development of the plastic zone and the manner in which the plastic zone spreads are important aspects of the solution.

The mesh configuration during the blanking operation at different values of punch penetration for two meshes with triangular elements and quadrilateral isoparametric elements are shown in Figs. 5-17 and 5-18 respectively. This will be of assistance when considering the pattern in which the plastic zone develops during blanking.

The development of the plastic zone with punch penetration in a simple blanking operation, in the absence of back-load and clamping force (BP = CF = 0) is shown in Fig. 5-19. The plastic zone first develops at the punch and die edges, and then spreads between the punch and die. After the region between the punch and die has become completely plastic, the plastic zone spreads under the punch and above the die. By increasing the amount of punch indentation the plastic zone spreads further away from the shear line. It is worth noting that, even at the maximum amount of punch penetration, the plastic zone is still confined to a small region around the shear line.

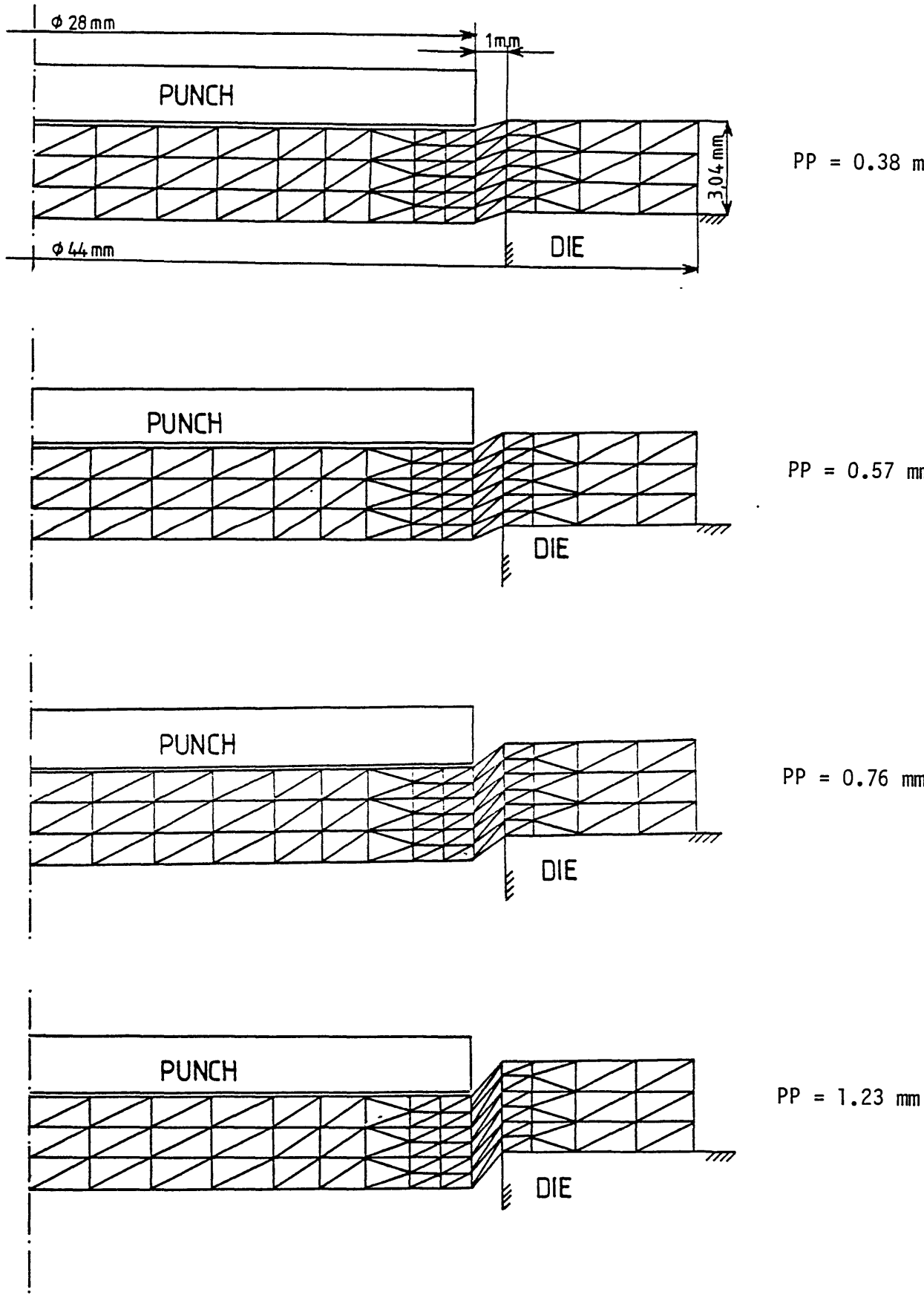

Fig. 5-17. Mesh configuration during the blanking of a t = 0.120 in. (3.04 mm) thick strip of mild steel at different punch penetrations (PP) when using a mesh with triangular elements.

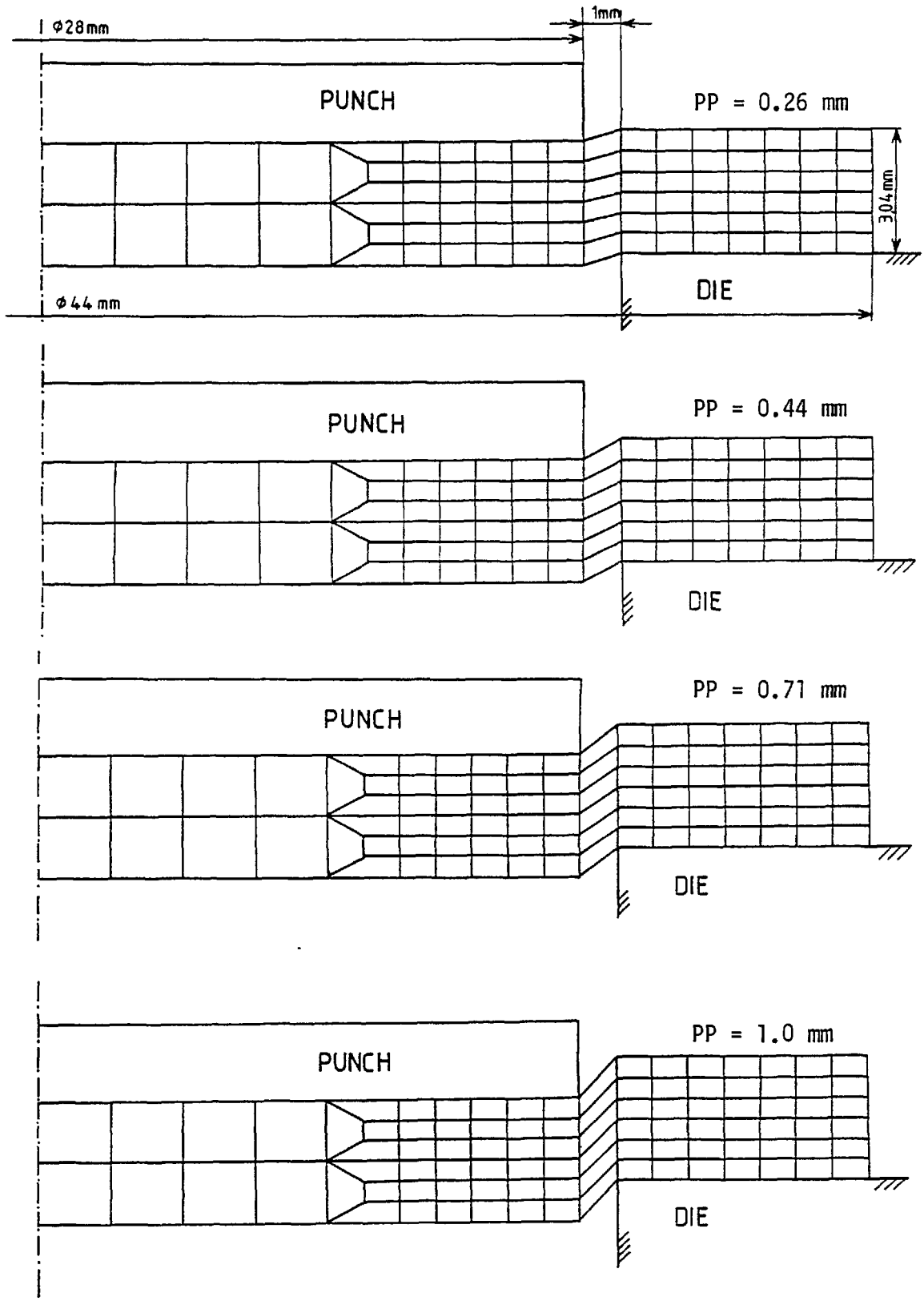

Fig. 5-18. Mesh configuration during the blanking operation of a t = 3.04 mm thick strip of mild steel at different punch penetrations (PP) when using a mesh with quadrilateral isoparametric elements.

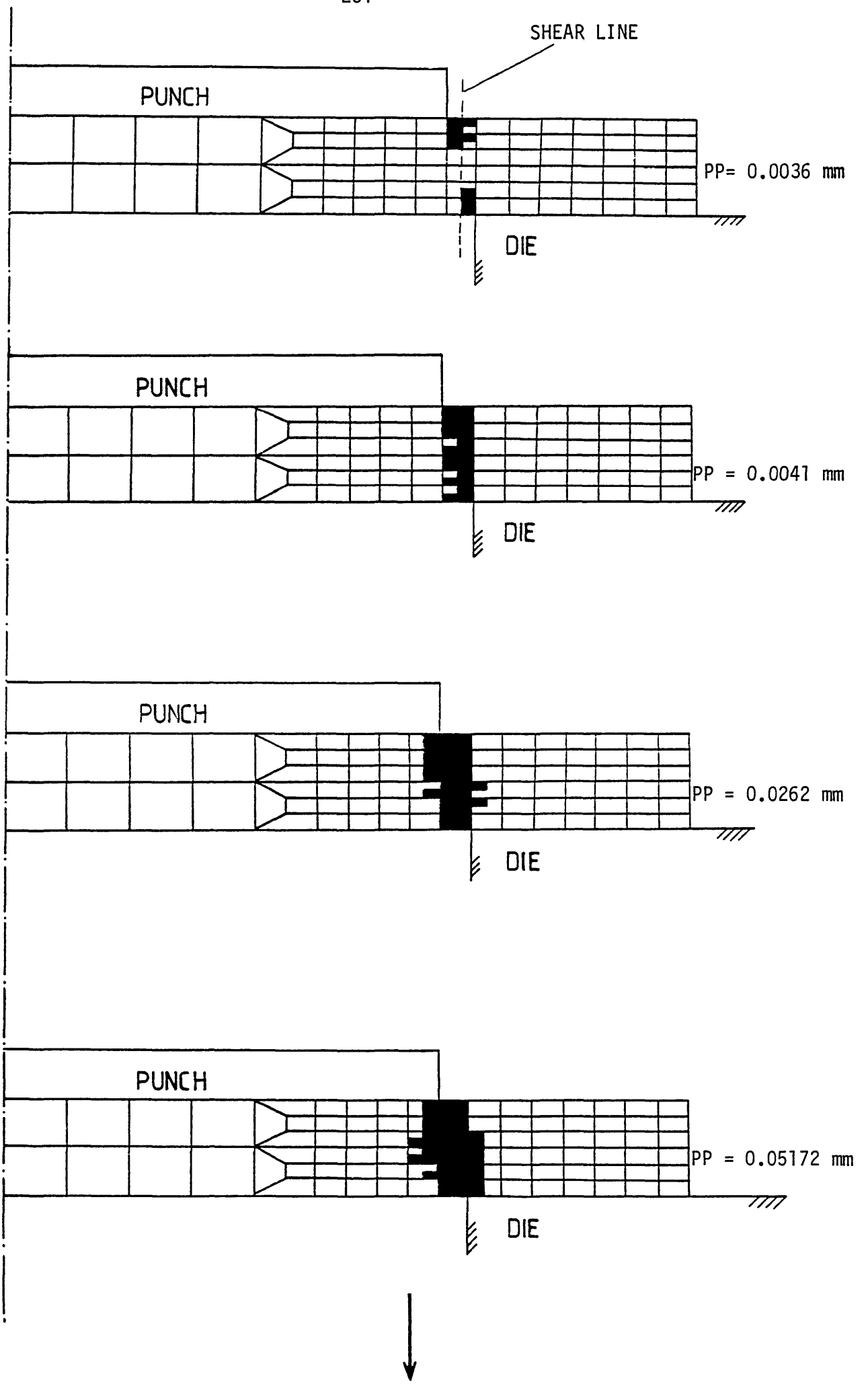
SHEAR LINE
PUNCH
PP= 0.0036 mm
DIE
PUNCH
PP = 0.0041 mm
DIE
PUNCH
PP = 0.0262 mm
DIE
PUNCH
PP = 0.05172 mm
DIE

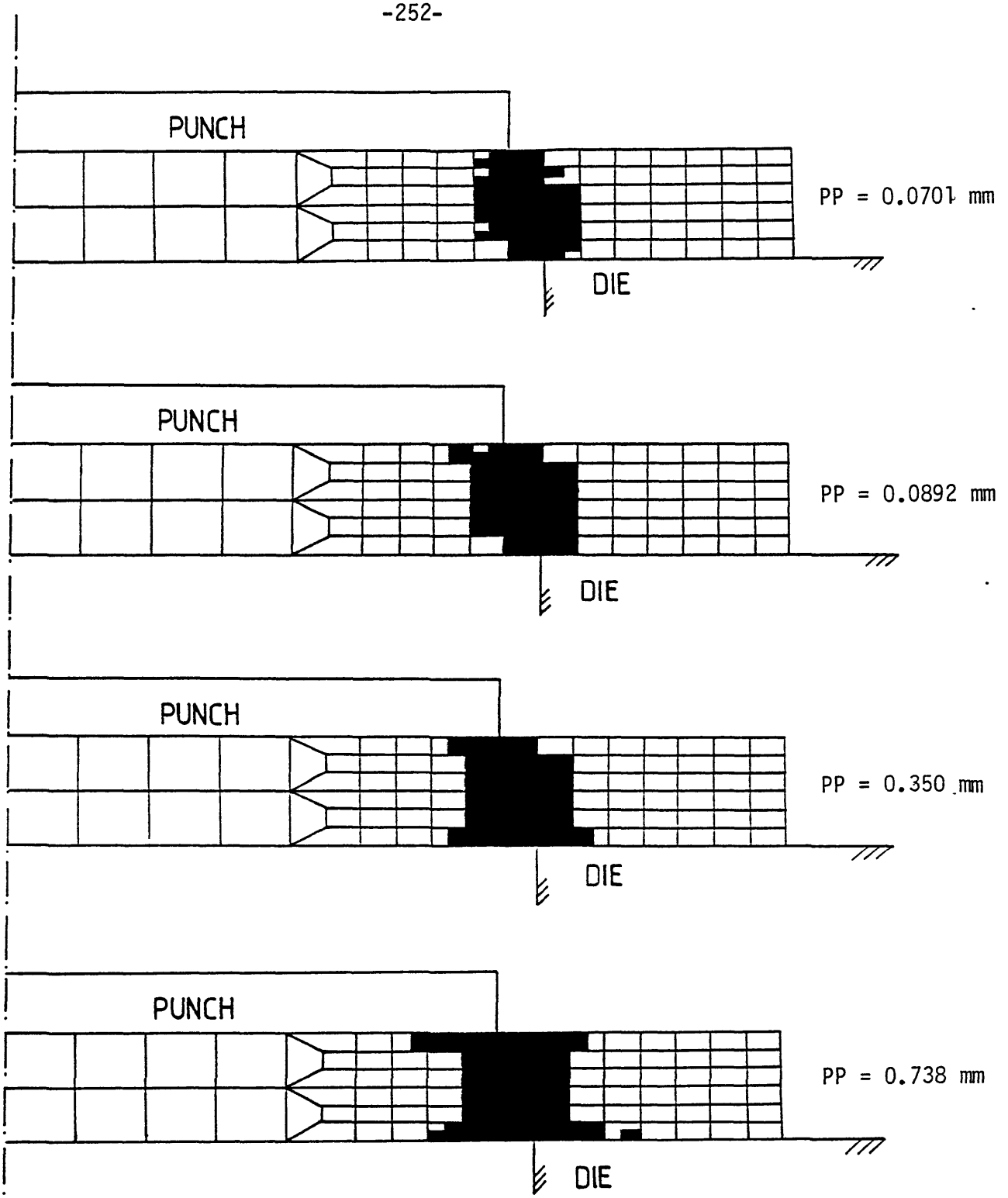

Fig. 5-19. Plastic zone development in conventional blanking at different punch penetrations when punching a strip of mild steel of thickness t = 0.120 in. (3.04 mm).

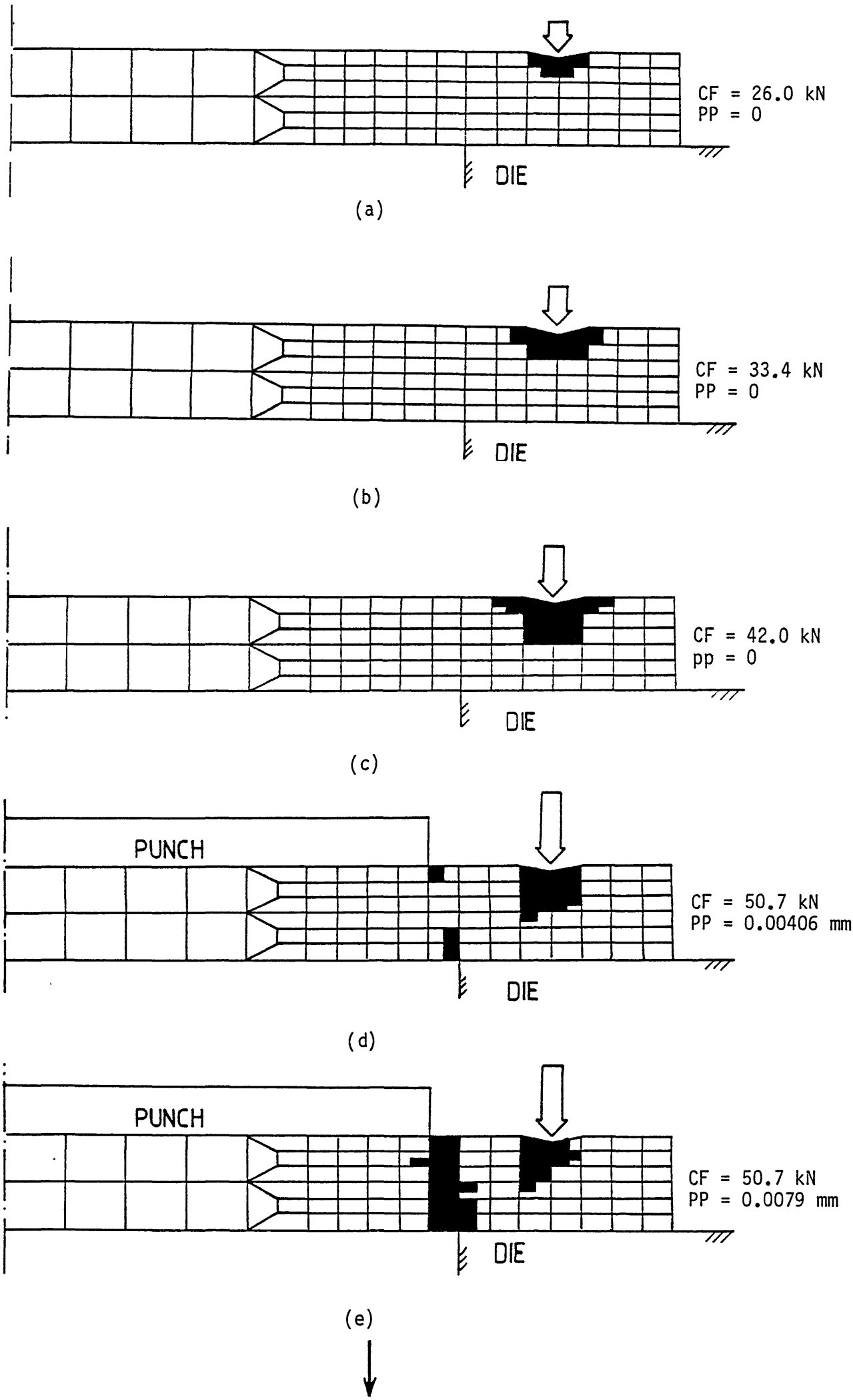
CF = 26.0 kN
PP = 0
DIE
(a)
CF = 33.4 kN
PP = 0
DIE
(b)
CF = 42.0 kN
pp = 0
DIE
(c)
PUNCH
CF = 50.7 kN
PP = 0.00406 mm
DIE
(d)
PUNCH
CF = 50.7 kN
PP = 0.0079 mm
DIE
(e)

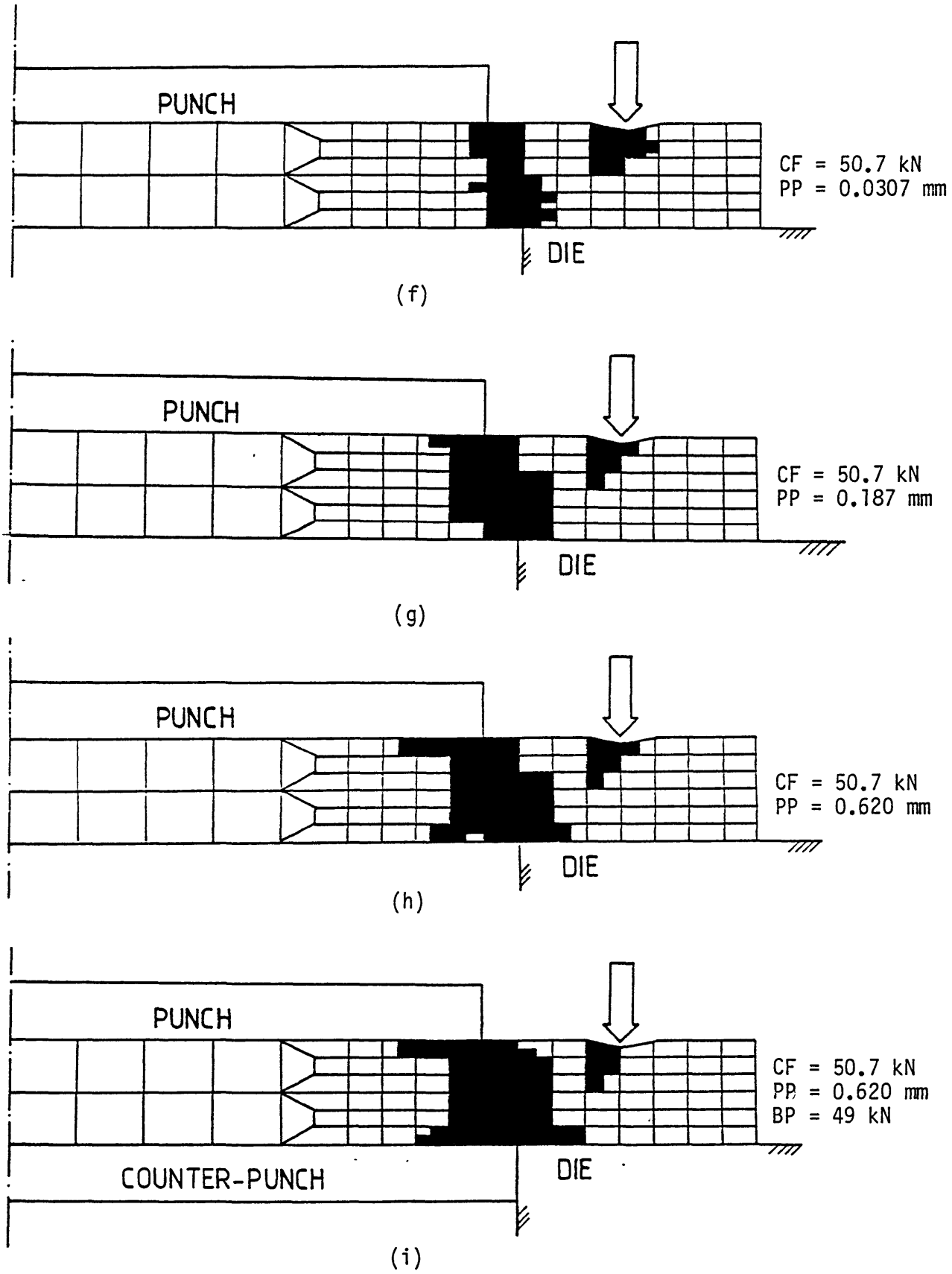

Fig. 5-20. Plastic zone development during the blanking operation of a strip of mild steel of thickness t = 0.120 in. (3.04 mm) at different values of punch penetrations (PP) when a blank-holder with a clamp/punch diameter ratio of (CR/PR = 1.28) was used.

The combined effect of clamping force and punch indentation, when the blank-holder with maximum diameter was used ($\frac{CR}{PR} = 1.28$) is shown in Fig. 5-20. The clamping force is applied first, increased to a predetermined value and then kept constant while the punch begins to penetrate the specimen. By clamping the specimen, a plastic zone is developed around the blank-holder, which spreads deeper into the material as the clamping force increases. If a sufficiently high clamping force is applied, the plastic zone will spread through the whole thickness of the specimen. After the clamping operation is completed the punch penetration begins and this is accompanied by the development of the plastic zone in the region between the punch and die, especially at the punch and die edges. Further penetration of the punch into the specimen causes a spread of the plastic zone into the material around the shear line which is similar to the plastic zone obtained in simple blanking. As the punch penetrates, the top layers of the element near the free surface seem to be pulled downwards, Fig. 5-21, and so an unloading condition in the elements on the top left hand side of the blank-holder could be expected and this is confirmed by the computer results in Fig. 5-20.

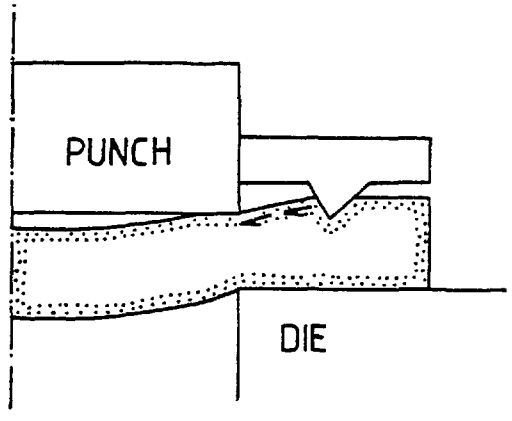

Fig. 5-21.

Fig. 5-20 shows that, in the case when the clamp is acting at its farthest distance from the punch edge ($\frac{CR}{PR} = 1.28$), the plastic zone developed around the shear line under the prescribed loading condition does not meet the plastic zone caused by the blank-holder.

The plastic zone for the general case of fine blanking, when clamping force and back-load were both present, is almost the same as the case ($CF \neq 0$, $BP = 0$), Fig. 5-20(i). Comparing Figs. 5-20(h) and 5-20(i) it becomes clear that when back-load is employed, more nodal points in the vicinity of the blank-holder are unloaded. This could be due to the additional material flow away from the axis of symmetry caused by the compression of the specimen between the punch and counter punch. When a back-load is used in addition to the clamping force, a development of the plastic zone above the die on the left hand side of the blank-holder, near the punch edge, can be observed. This could be, as was previously mentioned, due to the additional material flow caused by the compression of the specimen between the punch and counter punch.

In order to show the effect of the clamp diameter on the plastic zone, two further cases of clamp diameters with clamp/punch diameter ratios of ($\frac{CR}{PR} = 1.21$ and 1.14) are presented in Figs. 5-22 and 5-23 respectively. By decreasing the clamp diameter, the two plastic zones developed by the punch and blank-holder merge, which is in contrast to the previous case where the blank-holder with maximum diameter was used ($\frac{CR}{PR} = 1.28$), Fig. 5-20.

In the case of a blank-holder with minimum diameter ($\frac{CR}{PR} = 1.14$), the blank-holder is very close to the punch edge and the whole region between the punch and blank-holder becomes plastic very quickly and no elastic element in this region remains.

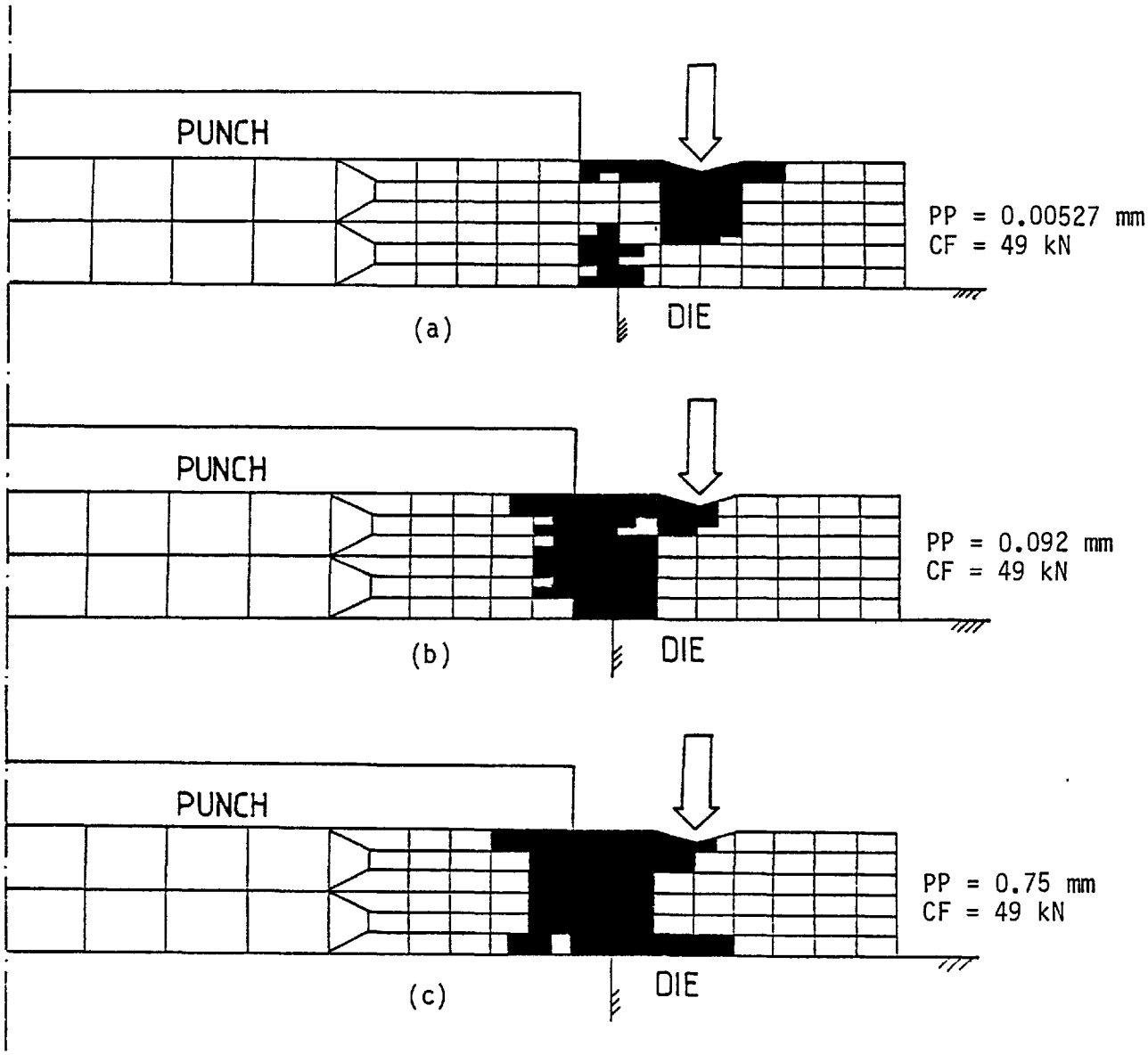

Fig. 5-22. Plastic zone development during the blanking of mild steel of thickness t = 0.120 in. (3.04 mm) at different punch penetrations (PP) when a blank-holder with a clamp/punch diameter ratio of (CR/PR = 1.21) was used.

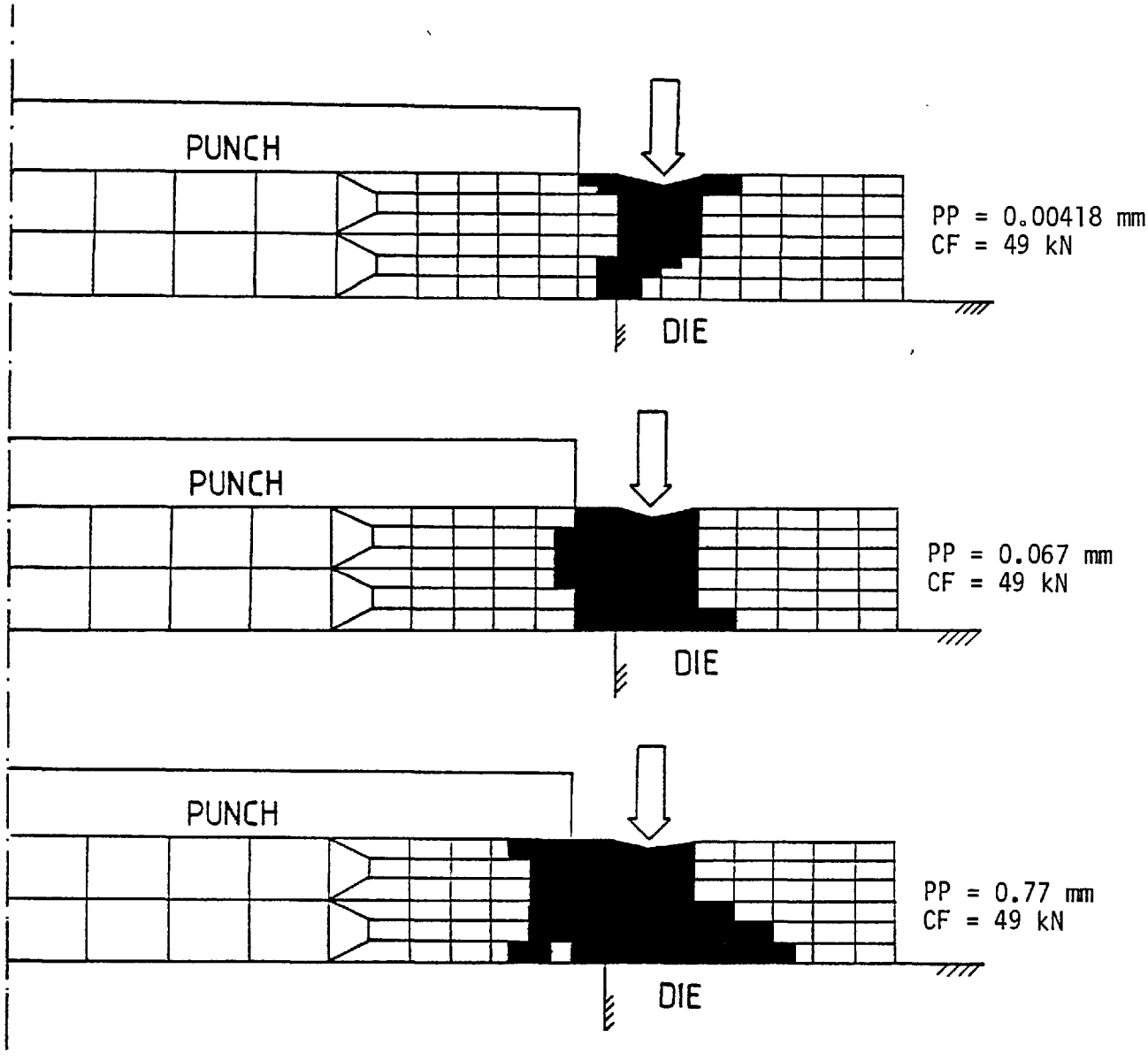

Fig. 5-23. Plastic zone development during the blanking operation of mild steel of thickness t = 0.120 in. (3.04 mm) at different punch penetrations (PP) when a blank-holder with a clamp/punch diameter ratio of (CR/PR = 1.14) was used.

By studying the graphs 5-20, 5-22 and 5-23 it becomes clear that in all cases the elements on the right hand side of the blank-holder are unloaded which could be due to the outward flow of the material during blanking, Fig. 5-24. This direction of material flow can be substantiated by reference to the direction of the shear load applied to the die face through the specimen, which will be studied later in this chapter in section 5.11.

The flow of material away from the shear line has also been predicted and explained by Maeda (37). In his report Maeda explains that the effect of the blank-holder is to stop the flow of waste material (on the die face) away from the shear line during the blanking process especially when using small clearances.

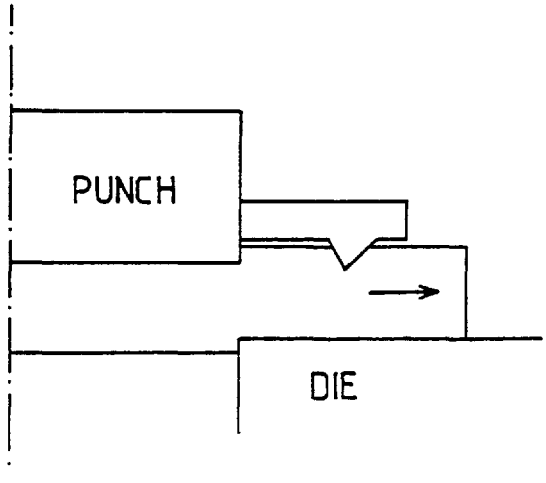

Fig. 5-24.

5.11 Distribution of load per unit length

The calculation of pressure distribution along the surface boundary of the deforming material with the finite element method is not possible as it can only predict the loads applied to the nodal points, including the nodal points on the boundary. However, as the nodal point loads calculated in axial symmetry for every nodal point represent the total load acting on a circle, the load per unit length at different radii can easily be calculated by dividing the total load by the circumference of the circle. The normal load per unit length distribution along the boundary of the deforming material can be used similarly to some extent to represent the pressure distribution applied to the boundary surface of the deforming material. This can be of great assistance when designing the punch and die plates.

The results in this section are presented in three different parts, in the first part the effect of clamping force and back-load on the load per unit length distribution normal to the punch and die surfaces, applied through the specimen, are presented, also given in this section is the distribution of normal load acting along the counter punch surface. In the second part the effect of clamping force and back-load on the tangential forces applied to the die-face through the specimen is studied, and finally in the third part the effect of material thickness both on the normal and tangential forces applied to the punch and die surfaces through the specimen are examined.

It should be noted that the value of load per unit length cannot be defined at the centre of symmetry, since the radius of the circle on which the load is acting is zero.

The results are given in this section for a punch penetration of PP = 0.74 mm, as predicted by the theoretical method for the maximum blanking load used experimentally in punching mild steel of thickness t = 0.120 in. (3.04 mm).

5.11.1 Load per unit length distribution normal to the punch and die surfaces

5.11.1.1 Normal to the punch face

The load per unit length distribution normal to the punch face during blanking for different boundary conditions of (CF = 0, BP = 0), (CF = 30 kN, BP = 0) and (CF = 30 kN, BP = 30 kN) are shown in Fig. 5-25.

In simple blanking (CF = BP = 0), the load remains zero for some distance from the centre and then increases slowly. In the vicinity of the punch edge the load per unit length increases at a much higher rate and reaches a maximum value at the punch edge. The region with zero load per unit length indicates that part of the specimen which has separated from the punch surface due to the bending effect. Also shown in this figure is the load per unit length distribution for the case of (CF = 30 kN, BP = 0). The curve follows almost the same trend as in the previous case, but it remains zero for a greater distance away from the centre, which indicates that bending of the material extends further.

An experiment was carried out to check the validity of the results obtained from the computer program concerning the contact area between the punch and the specimen under different boundary conditions, with and without a clamping device. To determine the approximate contact area between the punch and the specimen a strip of material was painted blue and then punched under different boundary conditions. It was found

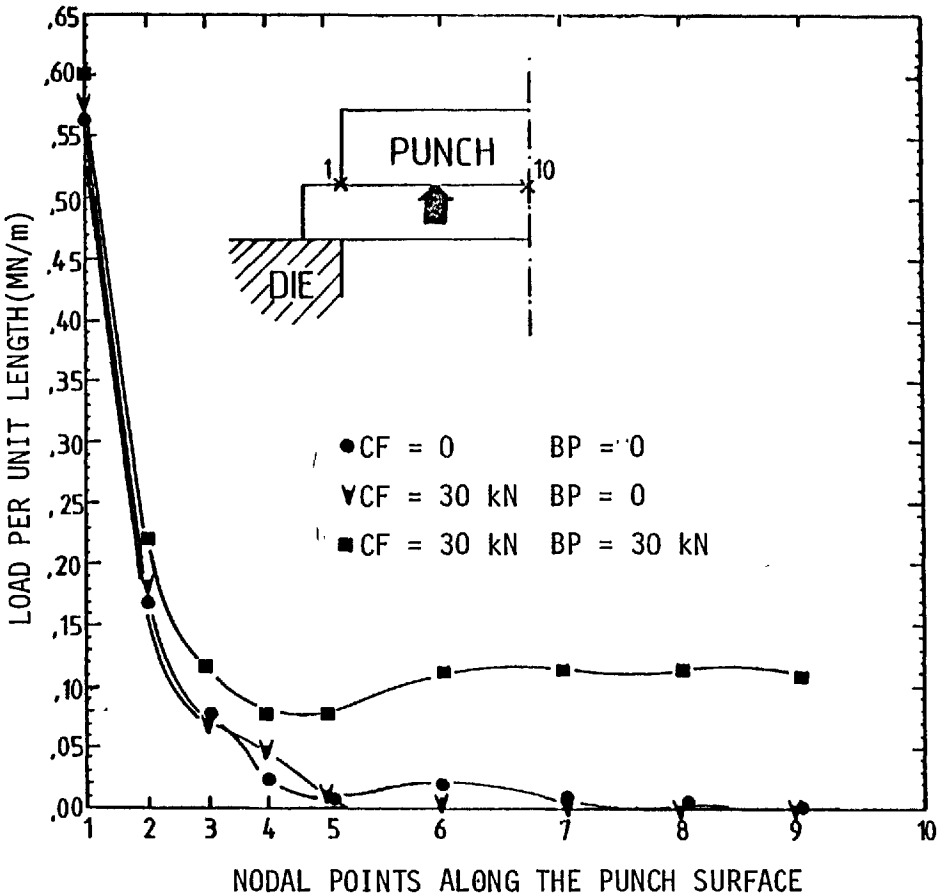

Fig. 5-25. Effect of clamping force (CF) and back-load (BP) on the load per unit length distribution normal to the punch face at a punch penetration of (PP = 0.74 mm) when punching a strip of mild steel of thickness t = 0.120 in. (3.04 mm).

that the paint on the contact area between the punch and the blank was scratched and mostly removed so forming a bright ring, Fig. 5-26.

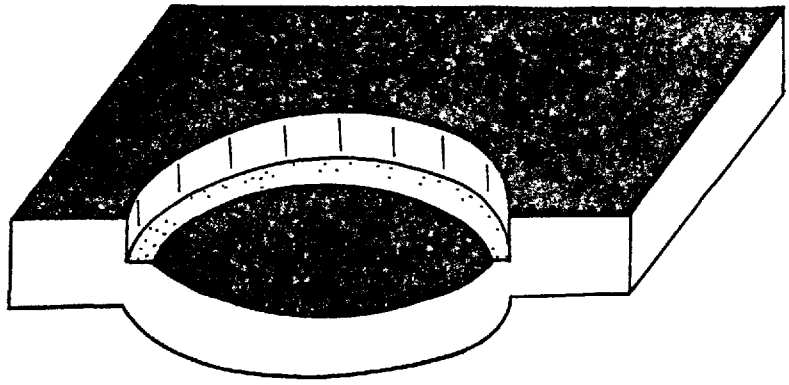

Fig. 5-26. The ring of scratched paint on a partly blanked specimen indicates the contact area between the punch and the specimen during blanking.

The paint on the blank surface which did not touch the punch surface, due to the bending effect, remained intact. By using this simple method two specimens were blanked under different clamping conditions, with and without the blank-holder. A visual examination of the scratched painted area was made and it was found that the blank without the clamping device showed a larger ring of bright area representing an increased contact area. It was thus concluded from the theoretical results and experimental findings that the blanks bend more when using the clamping device.

The load per unit length distribution normal to the punch face when back-load and clamping force were both present (CF = BP = 30 kN), using a clamp/punch diameter ratio of ($\frac{CR}{PR}$ = 1.28) are also shown in Fig. 5-25. A nearly uniform distribution of load per unit length prevails

over a large portion of the punch surface which then drops slightly and finally rises. The maximum load in this case is bigger than in the two previous cases. The specimen in this case remains in contact with the punch over the whole blank area, indicating a blank with much less distortion which is one of the main requirements of a fine blanked product. The interesting point to be noted is that the maximum value of load per unit length in all cases occurs at the punch edge and it was shown to decrease very rapidly in moving away from it. This information can be useful in considering tool life when the punch is at the design stage.

5.11.1.2 Normal load distribution along the die face

The load per unit length distribution normal to the die face for different boundary conditions of (CF = 0, BP = 0), (CF = 30 kN, BP = 0) and (CF = 30 kN, BP = 30 kN) are shown in Fig 5-27.

The load per unit length in the case of simple blanking (CF = BP = 0) is at its maximum value at the die edge and decreases rapidly away from it, becoming zero for part of the work piece/die interface. This indicates that the specimen in that region has lifted due to bending and is not touching the die surface. This bending of the waste material was also observed experimentally. The specimen/die interface clearly formed a bright narrow ring which indicated the intensity of the stresses in a narrow band, and no contact of the specimen with the die outside this ring was observed. For a blanked strip of material with a thickness of t = 0.120 in. (3.04 mm) a contact ring of maximum width 2 mm (0.078 in.) was detected. Above 2 mm (0.078 in.) there could be a small amount of load transfer between the strip and the die face over a short distance, but this should be very small since bending of the strip becomes quite apparent a short distance away from the die edge.

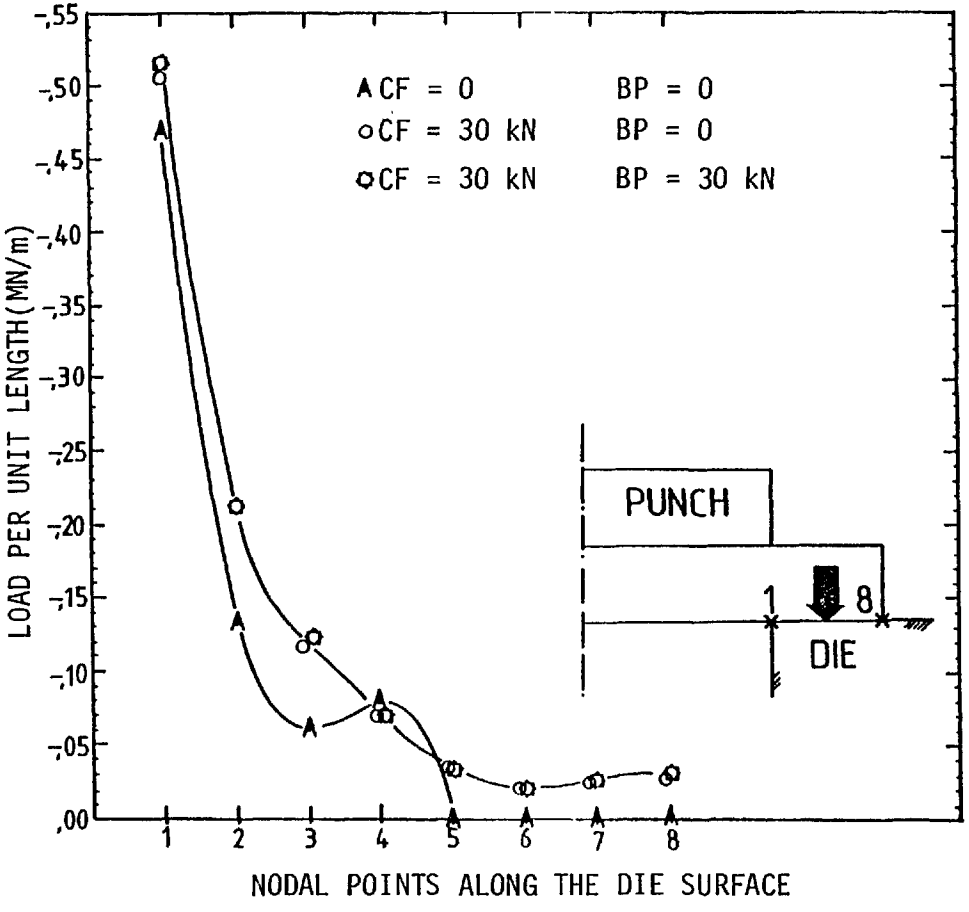

Fig. 5-27. Effect of clamping force (CF) and back-load (BP) on the load per unit length distribution normal to the die face at a punch penetration of (PP = 0.74 mm) when punching a strip of mild steel of thickness t = 0.120 in. (3.04 mm).

The load per unit length distribution for the two cases : (CF = 30 kN, BP = 0) and (CF = BP = 30 kN), when using a clamp/punch diameter ratio of ($\frac{CR}{PR}$ = 1.28), are very similar. Both curves have a maximum value at the die edge then rapidly decrease away from it and remain constant over the rest of the specimen/die interface. In this case the blank-holder not only prevents lifting but also presses the specimen against the die. It is again worth noting that in all cases the high load per unit length distribution only occurs in the vicinity of the die edge, an information useful in the design of the die.

5.11.1.3 Normal load distribution along the counter punch surface

The load per unit length distribution normal to the counter punch face in the case of (CF = 0, BP = 30 kN) is shown in Fig. 5-28. In moving away from the centre of the counter punch the load per unit length remains constant for approximately half of the counter punch radius, thereafter it gradually decreases to a point then remains almost constant over the rest of the counter punch surface.

5.11.2 Shear force per unit length distribution along the die face

The idea of using a blank-holder in blanking was mainly based on the assumption that during the process the material on the die surface moves away from the shear line. It was postulated that the use of a blank-holder would stop this material flow thus cause higher compressive stresses in the shearing zone.

The direction of the shear forces applied to the die face through the specimen can adequately identify the direction of the material flow on the die surface. The shear force per unit length distribution along

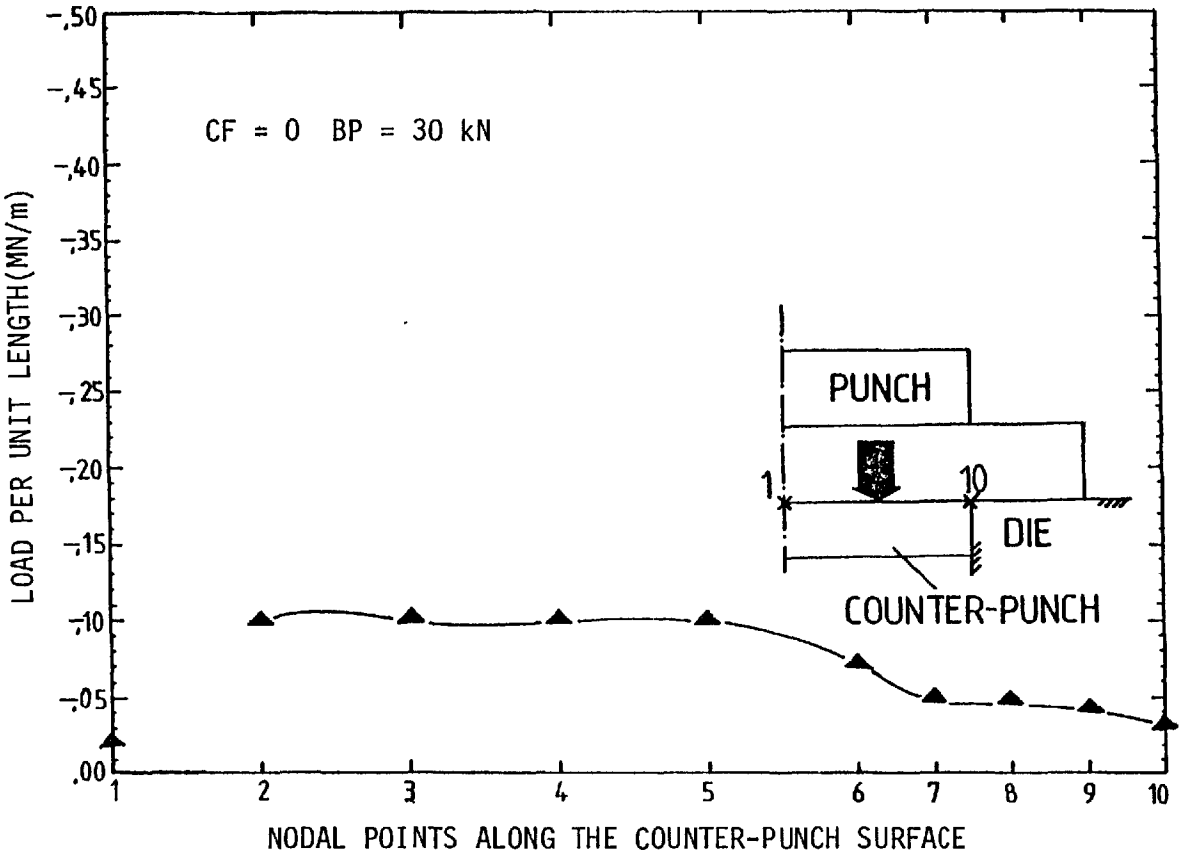

Fig. 5-28. Load per unit length distribution normal to the counter-punch face at a punch penetration of (PP = 0.74 mm) when punching a strip of mild steel of thickness t = 0.120 in. (3.04 mm).

the die face under different boundary conditions of clamping force and back-load, (CF = BP = 0), (CF = 30 kN, BP = 0) and (CF = BP = 30 kN), is given in Fig. 5-29.

In all cases the shear forces applied to the die face through the specimen have positive values, indicating that the material on the die face tends to move in the positive 'r' direction, away from the shear line. This substantiates the basic idea that the material moves away from the shear line over the die face and the provision of a blank-holder to stop this material flow would cause higher compressive stresses in the shearing zone.

An interesting point to note is that, with the application of a back-load, there is a uniform increase in the shear forces on the die face, an indication of the increased tendency of the material to flow away from the shear line, caused by the compression of the material between the punch and counter-punch.

5.11.3 Effect of material thickness on the load per unit length distribution along the punch and die surfaces

The results for the punch and die are presented in two different groups. The load per unit length distributions are all calculated at a certain value of blanking force, BF = 0.046 MN, the maximum blanking load obtained experimentally when blanking the thinnest strip of material : t = 0.078 in. (1.93 mm).

5.11.3.1 Along the punch face

The load per unit length distribution along the punch face in the tangential and normal directions, for three different thicknesses of mild steel, 0.076, 0.101 and 0.120 in. (1.93, 2.56 and 3.04 mm) are shown in Figs. 5-30 and 5-31 respectively.

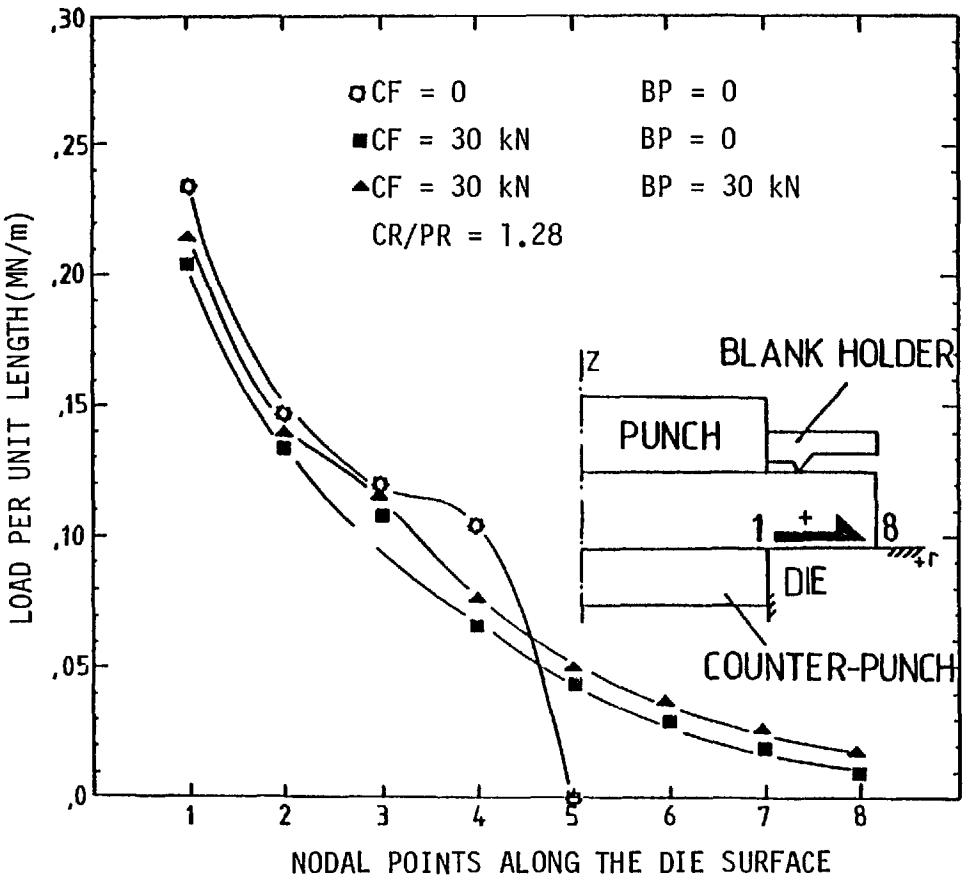

Fig. 5-29. Effect of clamping force (CF) and back-load (BP) on the tangential forces applied to the die face through the specimen at a punch penetration of PP = 0.74 mm when punching a strip of mild steel of thickness t = 0.120 in. (3.04 mm).

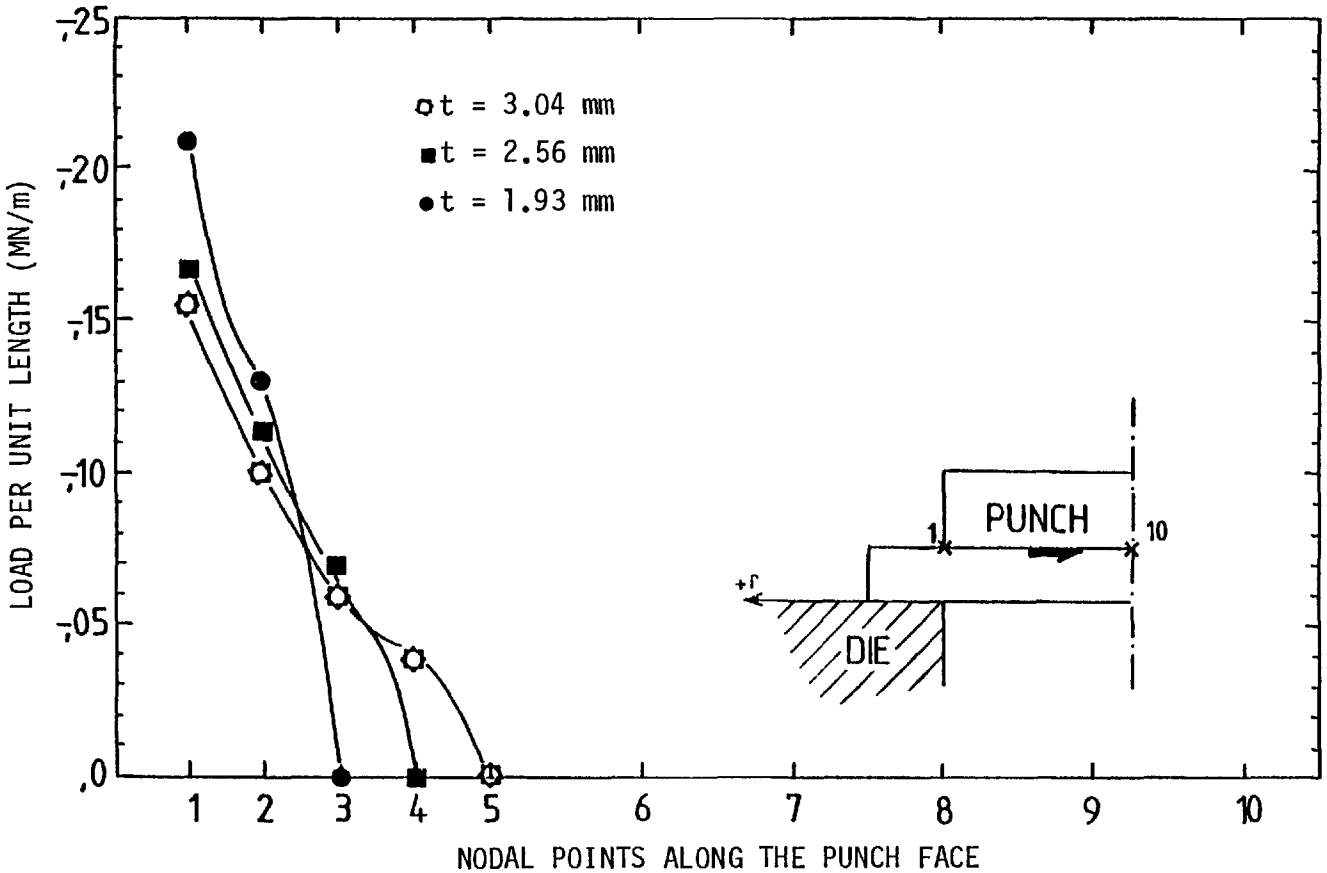

Fig. 5-30. Load per unit length distribution at a BF = 0.046 MN blanking force in the tangential direction along the punch face, for three different thicknesses of mild steel (t = 1.93, 2.56 and 3.04 mm).

For the same value of blanking force the thinner specimens indicate a higher value of load per unit length, acting over a shorter radial distance. This smaller contact area between the punch and the specimen indicates a higher bending effect for thinner materials, Fig. 5-32.

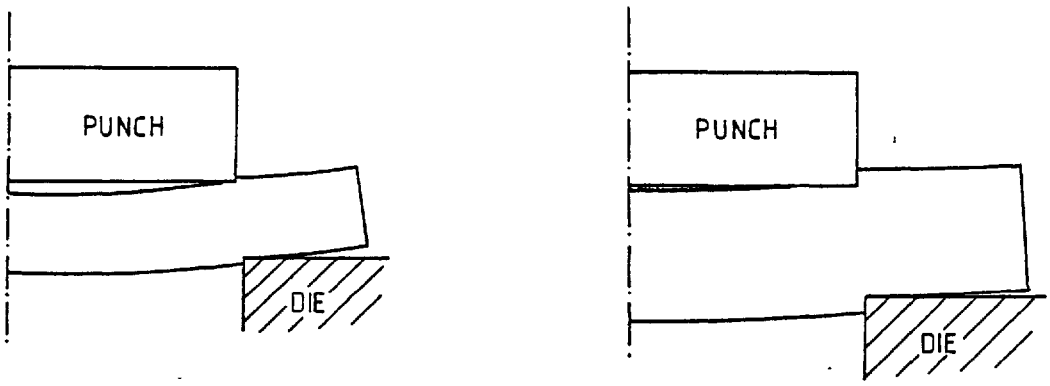

Fig. 5-32. A schematic sketch of bending of strips of material with different thicknesses.

5.11.3.2 Along the die face

The load per unit length distribution along the die face in the tangential and normal directions for three different thicknesses of material, t = 0.078, 0.101 and 0.120 in. (1.93, 2.56 and 3.04 mm), are shown in Figs. 5-33 and 5-34 respectively.

The load per unit length in the tangential direction at different nodal points has a positive value, indicating that the material on the die surface, during blanking, moves away from the shear line irrespective of the material thickness.

Here again the load per unit length, for an equal value of blanking load, for thinner materials has higher values and acts over a smaller radial distance. This indicates that the bending of the strip along the die surface is more pronounced for thinner materials, Fig. 5-32.

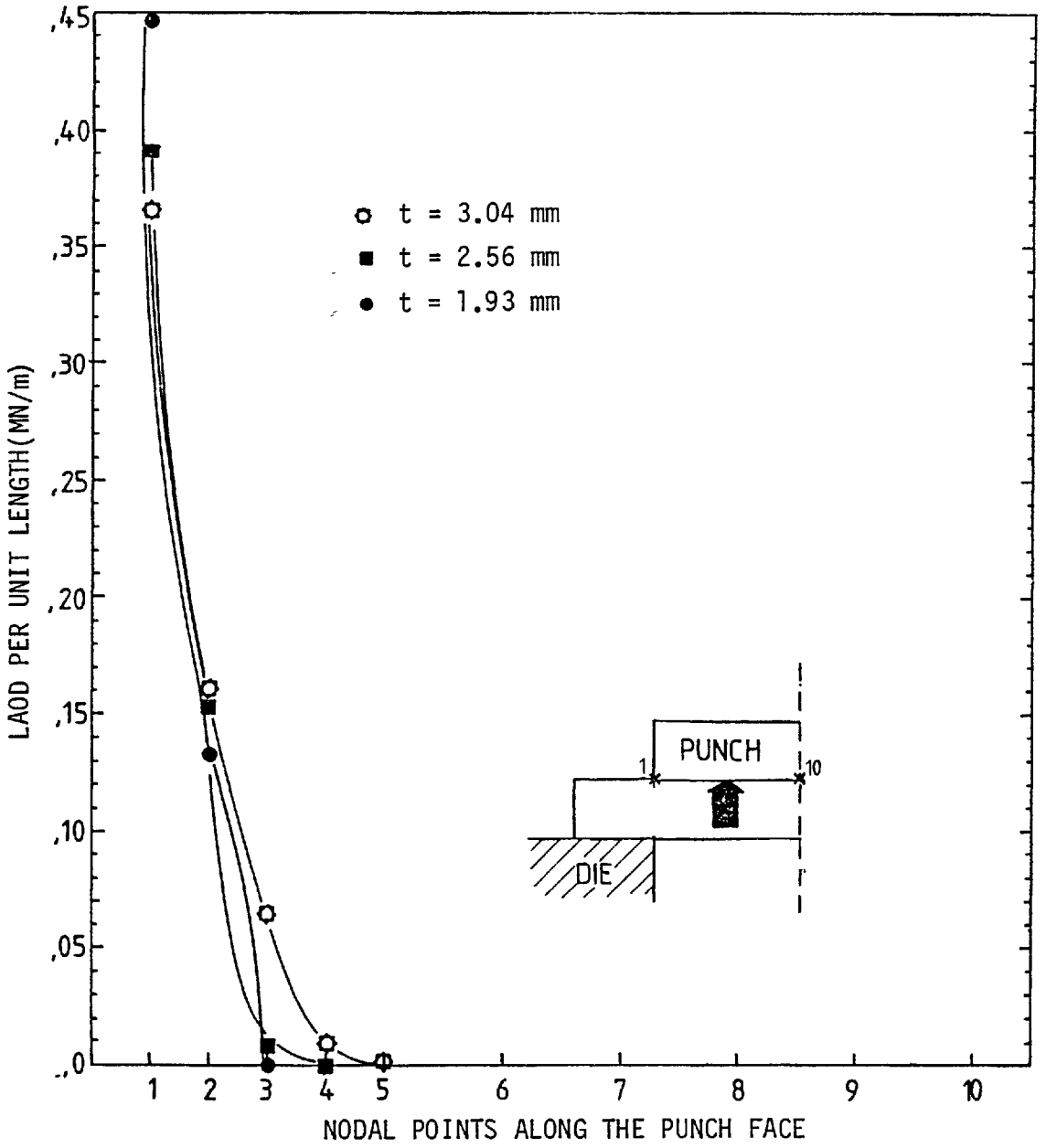

Fig. 5-31. Load per unit length distribution at a BF = 0.046 MN blanking force normal to the punch face for three different thicknesses of mild steel (t = 1.93, 2.56 and 3.04 mm).

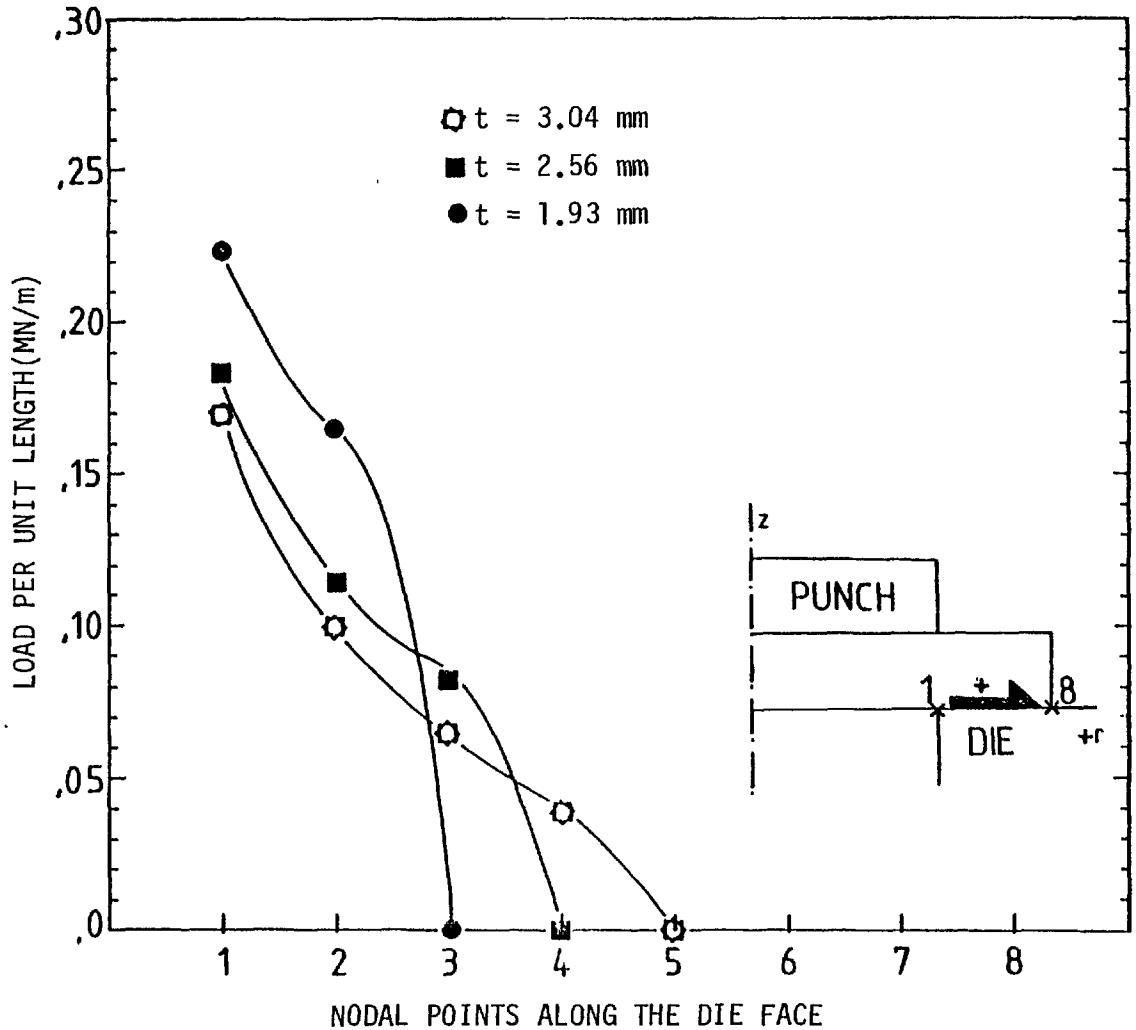

Fig. 5-33. Load per unit length distribution at a BF = 0.046 MN blanking force in the tangential direction along the die face, for three different thicknesses of mild steel (t = 1.93, 2.56 and 3.04 mm).

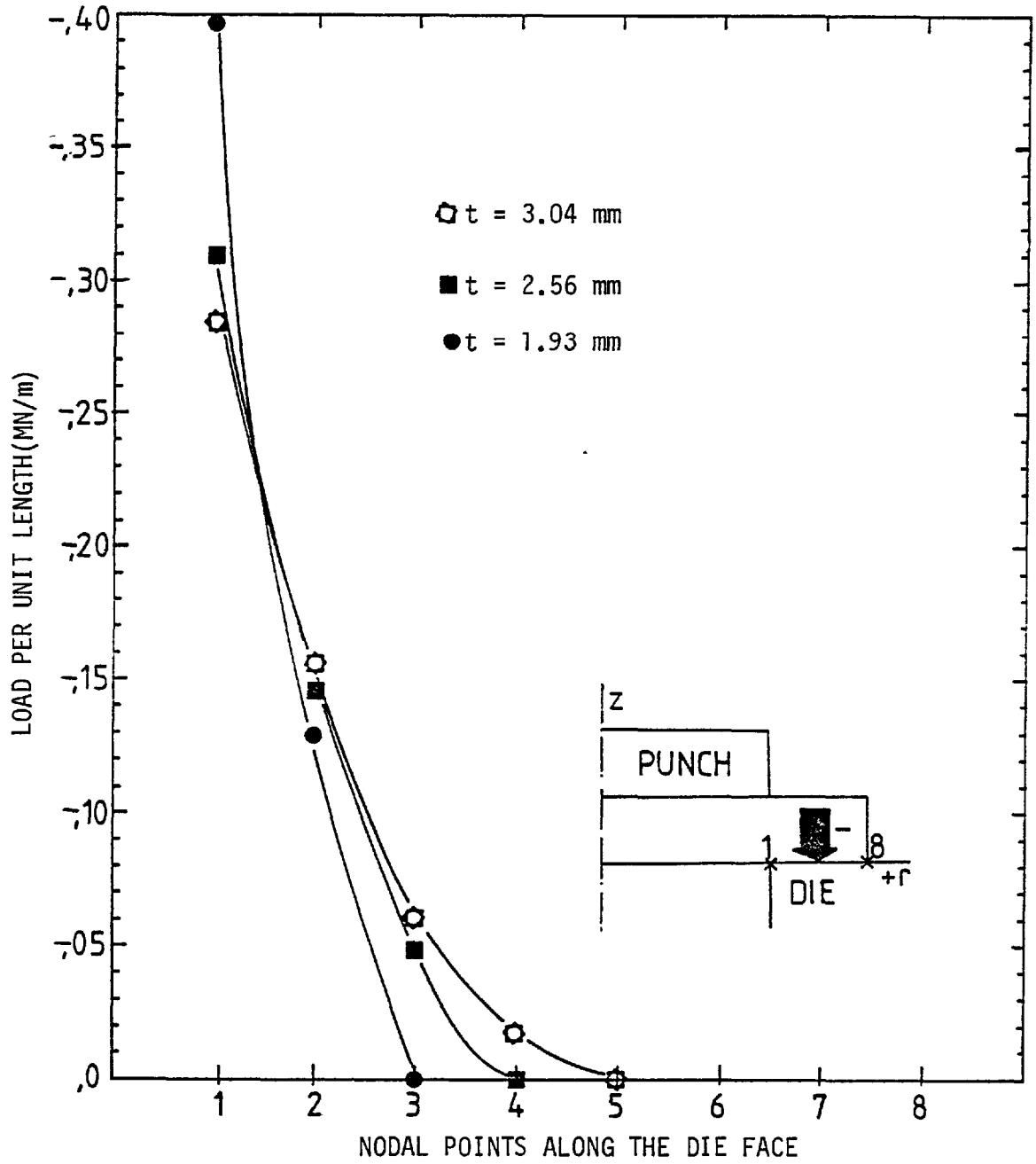

Fig. 5-34. Load per unit length distribution at a BF = 0.046 MN blanking force normal to the die face for three different thicknesses of mild steel (t = 1.93, 2.56 and 3.04 mm).

From these four figures it can be concluded that the maximum values of tangential and normal load per unit length always occur at the punch and die edges irrespective of material thickness. It is worth noting that the load per unit length has a maximum value at the punch and die edges which rapidly drops away from the edges, especially in the case of normal forces.

5.12 Effect of hydrostatic pressure on ductility

A considerable amount of work has been carried out by a number of investigators on the effect of superimposed high fluid pressure on the mechanical properties of materials. As a result of studies on a wide variety of metals it has been found that, in general, the ductility or strain to fracture increased with hydrostatic pressure. Bridgman (85, 86) found that for all but two of the steels tested, the strain to fracture for two stainless steels (15-0, 18-0) and for two high carbon steels (19-1, 19-3) was linear with pressure. Bridgman (86) also concluded that fracture of a tensile specimen will be delayed until much higher strains have been imposed if the specimen is immersed in a pressurized fluid during the test. A similar effect was also observed in extrusion by Pugh et al (87), in compression by Von Karman (88) and in torsion tests by Crossland and Dearden (89).

Metals such as cast iron, bismuth or high speed steel, which normally break up in extrusion due to surface tensile stresses imposed at the die exit, may be cold extruded satisfactorily if a sufficiently high hydrostatic pressure is superimposed. The experiments of Von Karman (88) showed that marble and sandstone become increasingly more ductile under increasing fluid pressure.

Bridgman (90) found that mild steel specimens fractured at increased strains in uniaxial tension under superimposed fluid pressure of up to 200 tonf/in.^{2} (3080 MN/m^2). The correlation between strains to fracture and pressure was linear. Cast rods of phosphor bronze of 93% copper and 7% phosphorus, which is a completely brittle material in tension under atmospheric pressure, were exposed to direct contact with the high pressure fluid under 310,000 lbf/in.^{2} (2108 MN/m^2) when the reduction in area was 12.6% and under 410,000 lbf/in.^{2} (2788 MN/m^2) 18.5%. A third specimen fractured with 80.2% reduction in area under 420,000 lbf/in.^{2} (2856 MN/m^2) pressure.

Crossland (91) carried out torsion tests on annealed mild steel, work hardened (cold rolled) high conductivity copper and a silicon-aluminium alloy containing approximately 10% Si, besides zinc and Mazak, a zinc-aluminium alloy. The strain to failure with pressure increased considerably, except for zinc and Mazak, and the correlation was linear.

The application of hydrostatic pressure to metal working can cause reduction or elimination of the damage to the product which otherwise occurs due to plastic deformation. This has been demonstrated by Pugh and Green (92) in experiments in which hydrostatic back pressure was applied to conventional cold extrusion. This led directly to new processes, such as differential pressure extrusion and to the appreciation of the importance of hydrostatic pressure in forming processes in general. It has been shown that the application of hydrostatic pressure to different metal working processes results in similar advantages. A brief review of the various techniques for the application of hydrostatic pressure in different forming processes will be given below.

Techniques for applying a restraining pressure in the forging of

beryllium have been reported by Hayes and Yoblin (93). Commercially pure beryllium is brittle at room and elevated temperatures and only a small degree of unrestrained deformation in tension can be obtained. In forging tests on small 2 in. (5.08 cm) diameter and 4 in. (10.1 cm) long unclad beryllium specimens, at forging temperatures ranging from 704°C to 1120°C, only 25 per cent reduction in height could be obtained and the product was shattered after a 50 per cent reduction. When the billet was enclosed in a ½ in. (1.27 cm) thick steel jacket, a reduction of 85 per cent in height could be obtained both by impact and press forging.

One technique for the closed die cold forging of beryllium was to use a spring loaded annular punch, illustration 'A', which applied pressure to the outer annulas of the the beryllium while it was being deformed.

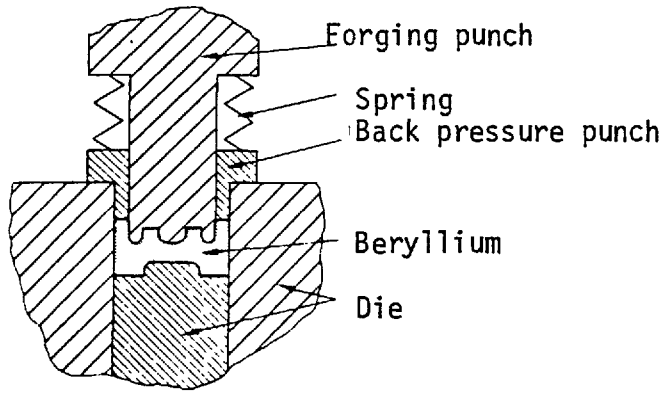

Illustration A. Spring loaded forging of beryllium (Hayes and Yoblin[93]).

The effect of restraining hydrostatic pressure on the process of upsetting has been investigated by Cogan (94, 95) who worked on both rod and tube, by Alexander and Lengyel (96) on rod and by Fuchs (97, 98) on tube. In the upsetting of rod against hydrostatic pressure, Cogan placed the billet in the bore of the upper tooling and applied a pressure p_1 at the end face of the rod, illustration 'B'.

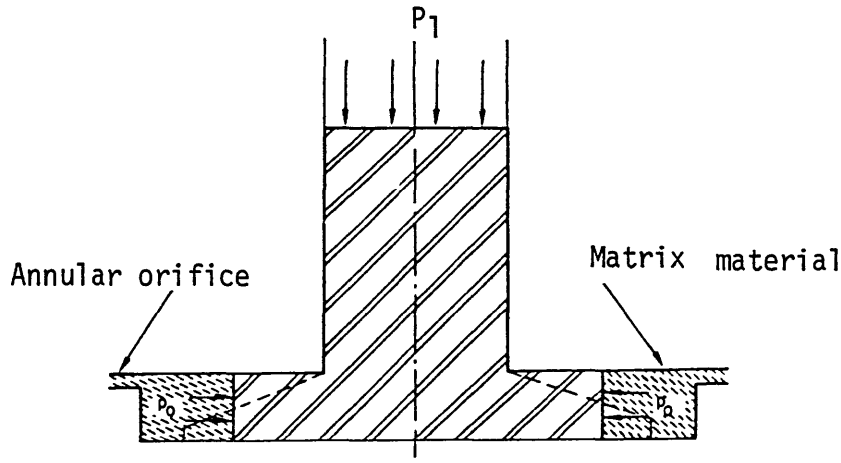

Illustration B . Upsetting of rod against a hydrostatic pressure (Cogan)

This caused the work material to extrude into the die cavity, which was of fixed height, thereby displacing and extruding a matrix material through the annular exhaust ports. These ports restricted the flow of the matrix material causing a back pressure p_o to act on the periphery of the billet. The design of the die set was such that a predetermined pressure of up to 60,000 lbf/in.^{2} (408 MN/m^2) could be generated in the matrix material in the die cavity of $1\frac{5}{8}$ in. (4.12 cm) diameter before the dies were forced apart allowing the matrix material to extrude, illustration 'B'.

Cogan used a similar method for upsetting a ring or tube with hydrostatic pressure, illustration 'C'.

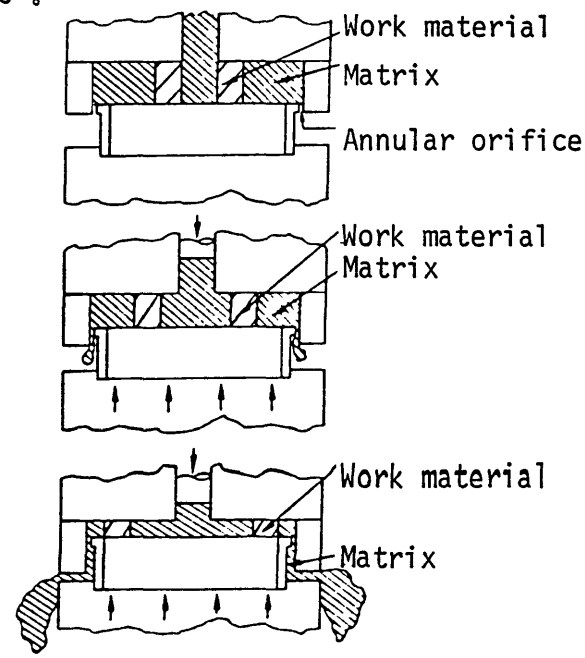

Illustration C. Upsetting of a ring or tube with hydrostatic pressure(Cogan)

A similar method to that of Cogan for the upsetting of flanges was used by Alexander and Lengyel (96) except that a mixture of castor oil and methanol was used as the pressurizing medium, the pressure being maintained constant by a relief valve. A brittle 10% silicon-aluminium alloy, which fractured in upsetting without a back pressure, successfully deformed into an uncracked flange against back pressure of 90,000 lbf/in.^{2} (612 MN/m^2).

Little work seems to have been done on the effect of hydrostatic pressure on bending. Some tests were carried out (99) to investigate the degree of bending that could be obtained in tungsten and beryllium sheet at various hydrostatic pressures. For tungsten, a significant increase in the degree of bending was obtained at a pressure of 450,000 lbf/in.^{2} (3060 MN/m^2) without any cracking. Despite its brittleness beryllium sheet was bent into a horseshoe shape without cracking in the presence of a hydrostatic pressure of 450,000 lbf/in.^{2} (3066 MN/m^2). Bending tests were also carried out by Komoly (100) at pressures of up to 56,000 lbf/in.^{2} (386 MN/m^2) by using uncoated standard charpy notched specimens of cast iron and cast 10% silicon-aluminium alloy which were deformed at speeds of 1 in./min. (2.54 cm/min) or less. The variation of load with angle of bend was determined for each specimen and the ductility defined by the angle corresponding to maximum load. A relatively small increase in ductility from ½ to 1½% was observed for cast iron which is in general agreement with the tensile results obtained by Pugh and Green (101) for the same metal. By analogy with the tension results, much larger ductilities would have been obtained with coated specimens and a pressure range that extended above 150,000 lbf/in.^{2} (1034 MN/m^2). In the case of the silicon-aluminium alloy the degree of bending obtained without fracture with a hydrostatic pressure of 41,000 lbf/in.^{2} (282 MN/m^2)

was about three times that possible at atmospheric pressure.

Bridgman (85) was the first to investigate the effect of pressure on the punching of sheet material. His tests were carried out on a 0.03 in. (0.76 mm) thick sheet of 0.4% carbon steel in both the annealed and heat treated conditions with the apparatus shown in illustration 'D'. At atmospheric pressure, the material fractured after the punch had penetrated only 1/10 th of the plate thickness and this fracture was accompanied by a sudden decrease in the shear force. As the hydrostatic pressure was increased, the depth of penetration before fracture increased, until at a sufficiently high pressure the punch completely penetrated the sheet thickness without fracture.

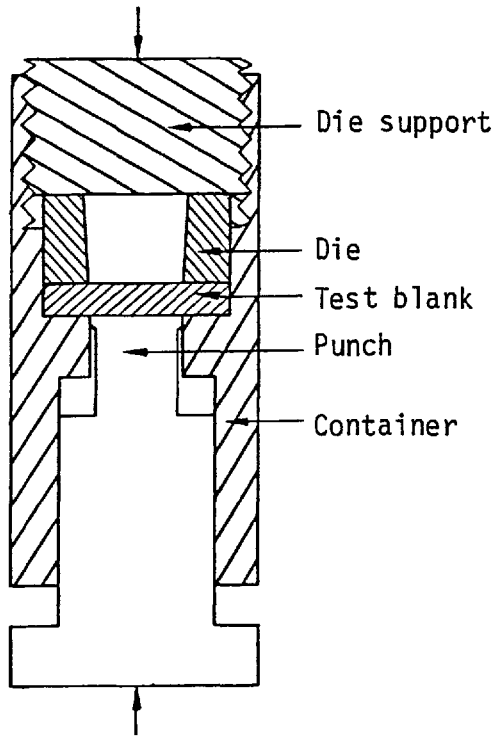

Illustration D. Punching under hydrostatic pressure (Bridgman)

An associated process in which a similar effect is obtained is the cropping of bar. Normally in this process the material partly shears to burnish part of the cropped surface, but finally fractures

through the remaining thickness giving a torn rough surface often not at right angles to the axis of the bar. However, if the cropping is carried out on a bar that is simultaneously subjected to an axial force, then accurate shearing is obtained throughout the thickness of the bar to give a smooth burnished surface which is, if the tooling is correct, perpendicular to the axis of the bar. As the axial force is increased, the relative amount of the smooth burnished surface is increased. The process of cropping under axial compression is sometimes known as the 'Planar cold flow process' or the 'Hungarian bar shearing process' (101).

Bridgman (85) was the first to carry out wire drawing in a pressurized fluid. Piano wire, 0.076 in. (1.93 mm) in diameter with a tensile strength of 330,000 lbf/in.^{2} (2244 MN/m^2) and a fracture stress of 480,000 lbf/in.^{2} (3264 MN/m^2) was drawn under a hydrostatic pressure of 168,000 lbf/in.^{2} (1142 MN/m^2) to 0.026 in. (0.066 cm) diameter in 6 passes without interstage annealing. At atmospheric pressure, 15 passes were required without interstage annealing for the same reduction. The wire at this stage lost all capacity for further extension and broke with no preliminary yield.

From the above results it can be concluded that the introduction of hydrostatic pressure on a deforming material can cause an increase in the strain to fracture of the material. The introduction of hydrostatic pressure in many metal forming processes has led to successful products which could not be made at atmospheric pressure.

The fine blanking process, although not using a liquid pressure, utilizes the advantage of an increased hydrostatic component of stress applied by the blank-holder and counter punch. In a later section (5.14) it will be shown that the introduction of a blank-holder and counter punch will cause an increase in the prevailing hydrostatic component of

stress within the deforming material in the shearing zone, which together with the consequent decrease in the maximum tensile principal stress, will be suggested as the cause of change of fracture from fibrous to pure shear in fine blanking.

In section 5.12.1 it will be discussed that a 100% crack-free blank surface finish can be obtained if such a level of hydrostatic component of stress is superimposed on the prevailing maximum principal stresses in the shearing zone, so that the maximum principal stresses are reduced to zero or become negative. This will prevent the cracks formed due to the severe plastic deformation in the shearing zone from opening up and propagating and so causing fracture.

5.12.1 Effect of the hydrostatic component of stress and maximum principal stress on the sheared surface of the blank edge

According to Zener (15), the movement of dislocations during slip is arrested at obstacles such as grain boundaries, complex carbides and precipitated particles, resulting in a pile up of dislocations and formation of micro-cracks. Both Mott (102) and Stroh (103) have suggested that the extension of a micro-crack would result in the relief of stress concentrations at the crack tip due to plastic deformation. The micro-crack is thus not propagated and fibrous fracture occurs by linking of a number of micro-cracks. Thus Mott and Stroh suggest that under the action of an external shear stress, such as occurs in the blanking process, micro-cracks can only grow to the extent of the order of the spacing between the Frank-Read sources which is a few microns. An additional applied tension is required to cause macroscopic fracture across the whole section.

Clearly it is desirable to eliminate this macroscopic fracture in blanking and it would seem that any device which prevents tensile stresses developing in the shearing zone should improve the quality of the blank edge.

For plane strain deformation of a rigid perfectly plastic material having shear yield stress k, Johnston et al (36) regard the blanking as a process of pure shear, Fig. 5-35, with principal stresses of k acting at 45^{o} to the line of cut and corresponding to a situation in which the hydrostatic component of stress is zero. Johnston et al suggest that, if the stress state on the line of cut were such that the hydrostatic component of stress was compressive, then the algebrically greatest principal stress would be reduced and become zero for a hydrostatic compression of amount k. This was shown in a slip line solution to the fine blanking problem and indicated that the addition of clamping force induced a higher hydrostatic component of stress in the shearing zone.

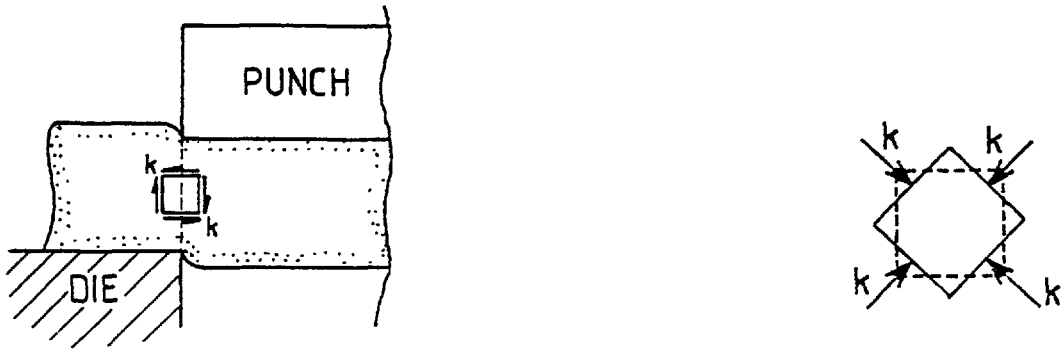

Fig. 5-35.

As it is generally recognized that the maximum tensile principal stress has a critical effect on crack propagation, it was decided to study the effect of clamping force and back pressure not only on the hydrostatic component of stress but also on the maximum principal stress along the shear line.

5.13 Maximum principal stress calculation

To calculate the maximum principal stresses at different nodal points in the shearing zone, a systematic approach was followed. The stresses which occur in an axi-symmetric problem are shown in the illustration below.

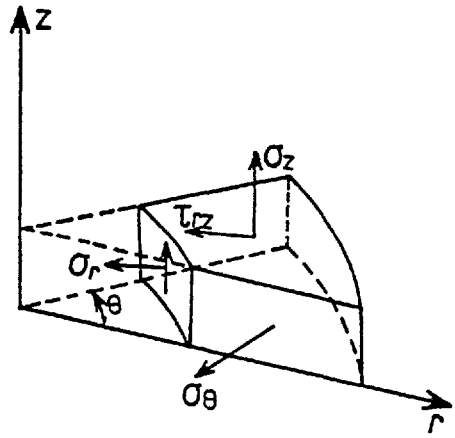

The plane on which $\sigma\theta$ acts is a principal plane as the shear on this plane must be zero due to symmetry. To calculate the maximum principal stress at a sampling point, the principal stresses on a plane passing through the sampling point and perpendicular to the direction θ are first calculated and the maximum value between these two values and hoop stress $\sigma\theta$ will determine the maximum principal stresses on a plane perpendicular to direction θ,the following formulas were used :

$$\sigma' = \frac{\sigma r + \sigma z}{2} + \sqrt{\left(\frac{\sigma r - \sigma z}{2}\right)^2 + \tau^2 rz}$$

$$\sigma'' = \frac{\sigma r + \sigma z}{2} - \sqrt{\left(\frac{\sigma r - \sigma z}{2}\right)^2 + \tau^2 rz}$$

In the calculations only σ' was calculated as, obviously, between σ' and σ'', σ' has the bigger algebraic value.

5.14 Hydrostatic component of stress and maximum principal stress results

The computed results obtained for the hydrostatic component of stress and maximum principal stress for three values of clamping force and back-load (30, 50 and 70 kN) equal to the values used in the experimental work, and three blank-holder diameters with clamp/punch diameter ratios of ($\frac{CR}{PR}$ = 1.28, 1.21 and 1.14) are given in this section. It should be noted that, in the computer model, the blank-holder diameter can only take values equal to the nodal point coordinates.

The results given below, viz. hydrostatic component of stress and maximum principal stress, are the values computed at 6 different sampling points equally distributed along the shear line, Fig. 5-36, at a punch penetration of PP = 0.74 mm, which is the corresponding punch penetration predicted by the theoretical method for a blanking load equal to the maximum blanking load obtained experimentally when punching mild steel strips of t = 0.120 in. (3.04 mm) thickness.

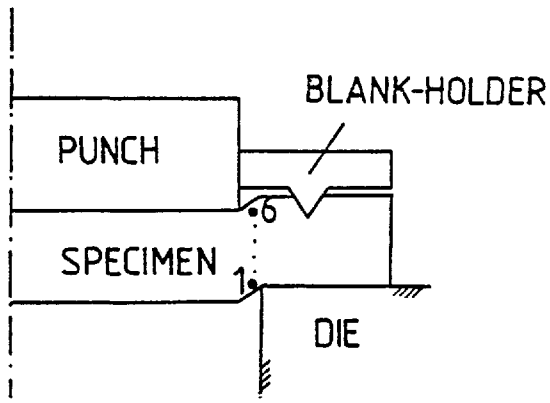

Fig. 5-36. The hydrostatic component of stress and maximum principal stress are calculated at 6 different points equally distributed along the shear line.

In the hydrostatic component of stress and maximum principal stress curves the values at the two sampling points 1 and 6, illustration below, will not be discussed. This is because at the punch penetration at which the results are plotted the two points 1 and 6 in the actual process will be part of the material which has already sheared, thus the analysis will be confined to the unsheared section of the material which is located between sampling points 1 and 6.

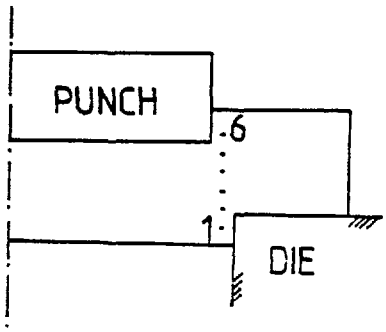

Actual blanking operation

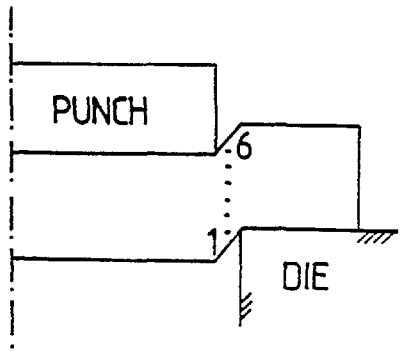

Computer model for the blanking operation

As in this section there will be much reference made to the hydrostatic component of stress which in the computational results will have a negative sign, hereafter when an increase in this component is mentioned it always means an increase in its absolute value, i.e. increasingly compressive.

The effect of different parameters on the hydrostatic component of stress and maximum principal stress are presented in 9 different parts, which can be summarized as follows :

1) Clamping force with no back-load present (BP = 0, CF = 30, 50 and 70 kN).

2) Back-load with no clamping force present (CF = 0, BP = 30, 50 and 70 kN).

3) A comparison of the effect of clamping force and combined effect of clamping force and back-load (CF = 30, 50 and 70 kN, BP = 0) and (CF = BP = 30, 50 and 70 kN).

4) A comparison of the effect of clamping force, back-load and combined effect of clamping force and back-load together, for a typical clamp/punch diameter ratio of CR/PR = 1.14 (CF = 30, 50 and 70 kN, BP = 0.), (CF = 0., BP = 30, 50 and 70.kN) and (CF = BP = 30, 50 and 70 kN).

5) The combined effect of clamping force and back-load (CF = BP =30, 50 and 70 kN).

6) The effect of the clamp diameter when using three different values of clamp diameter with clamp/punch diameter ratios of (CR/PR = 1.28, 1.21 and 1.14).

7) The effect of material thickness, when using three different thicknesses of mild steel t = 0.078, 0.101 and 0.120 in. (1.93, 2.56 and 3.04 mm), in the absence of clamping force and back-load (CF = BP = 0).

8) The effect of material thickness, when using a clamping force of 70 kN in the absence of back-load (CF = 70 kN, BP = 0).

9) The effect of clearance between the punch and die when using different values of punch-die clearance (C = 1.0, 0.7 and 0.3 mm) in the absence of clamping force and back-load.

5.14.1 Effect of clamping force on the hydrostatic component of stress and maximum principal stress prevailing in the shearing zone.

The effect of clamping force on the hydrostatic component of stress when different values of clamp diameter with clamp/punch diameter

ratios of (CR/PR = 1.28, 1.21 and 1.14) were used, which correspond to the maximum, medium and minimum clamp diameter, are shown in Figs. 5-37, 5-38 and 5-39 respectively.

From these figures it can be concluded that, for a certain value of clamp diameter, all the curves follow almost the same trend and an increase in the clamping force will cause an increase in the hydrostatic component of stress. This increase is more pronounced as the clamp diameter decreases, coming closer to the punch edge. In the case of the blank-holder with minimum diameter the state of stress near the punch edge is not affected by the clamping force as much as in the other two cases, when blank-holders with medium or maximum diameter were used. Apart from the vicinity of the punch edge the increase in the hydrostatic component of stress in this case is more marked than in the two previous cases. The corresponding results for the maximum principal stress are shown in Figs. 5-40, 5-41 and 5-42 respectively. By increasing the clamping force the maximum principal stress is reduced and this reduction is more pronounced when a smaller clamp diameter is used.

Referring to Fig. 5-42 it becomes clear that by the application of a blank-holder with the smallest diameter (CR/PR = 1.14) the maximum principal stress at the maximum value of the clamping force (70 kN) reduces considerably. This decrease in the maximum principal stress(except in the vicinity of the punch edge) for a given increase in the clamping force is more than that in the two previous cases (CR/PR = 1.21 and 1.28).

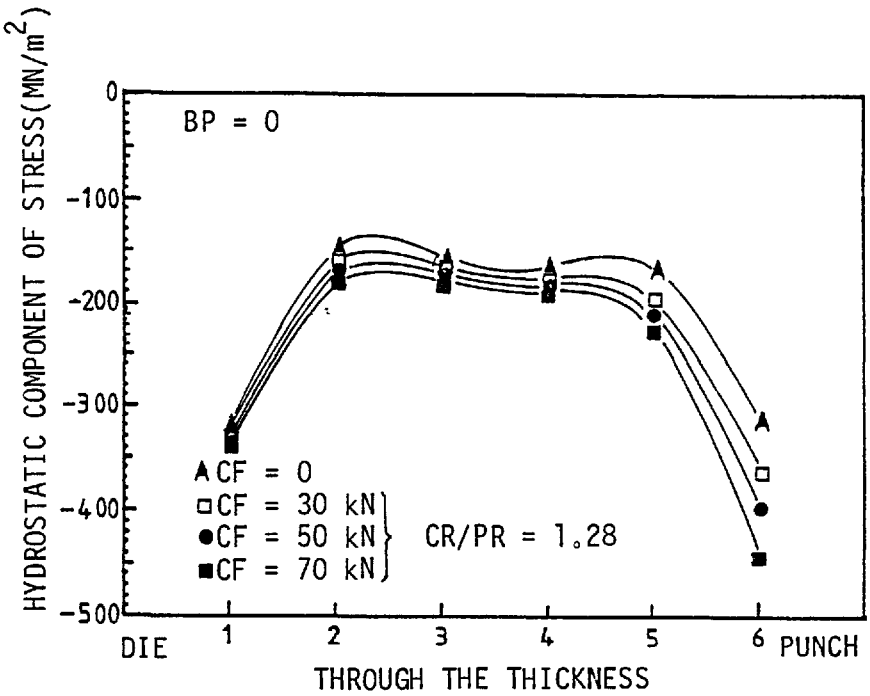

Fig. 5-37. Effect of clamping force (CF), for a clamp/punch diameter ratio of (CR/PR = 1.28), on the hydrostatic component of stress in the shearing zone during the blanking of mild steel strips of thickness t = 0.120 in. (3.04 mm) at a punch penetraion of (PP = 0.74 mm) when no back-load was used (BP = 0).

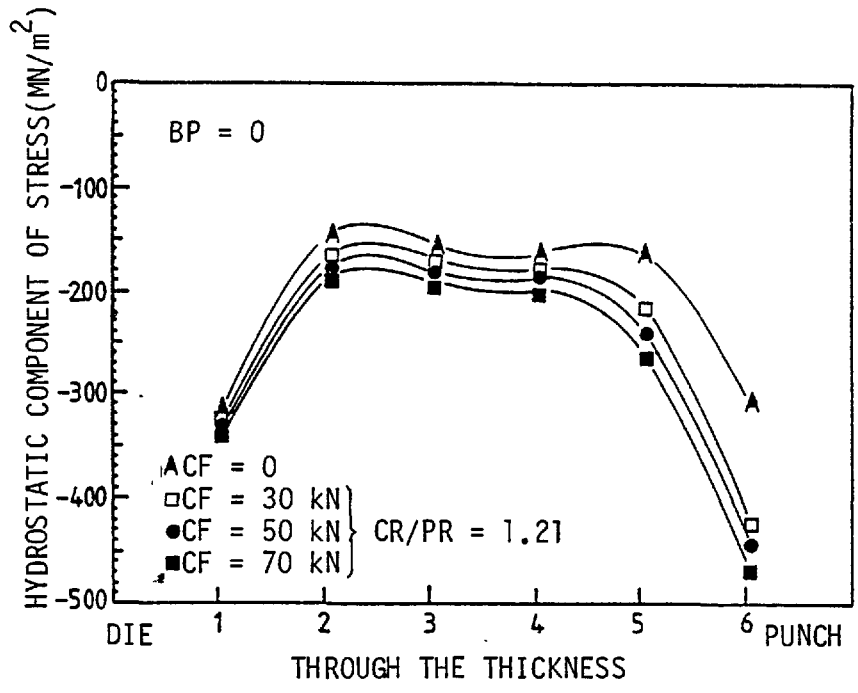

Fig. 5-38. Effect of clamping force (CF), for a clamp/punch diameter ratio of (CR/PR = 1.21), on the hydrostatic component of stress in the shearing zone during the blanking of mild steel strips of thickness t = 0.120 in. (3.04 mm) at a punch penetration of (PP = 0.74 mm) when no back-load was used (BP = 0).

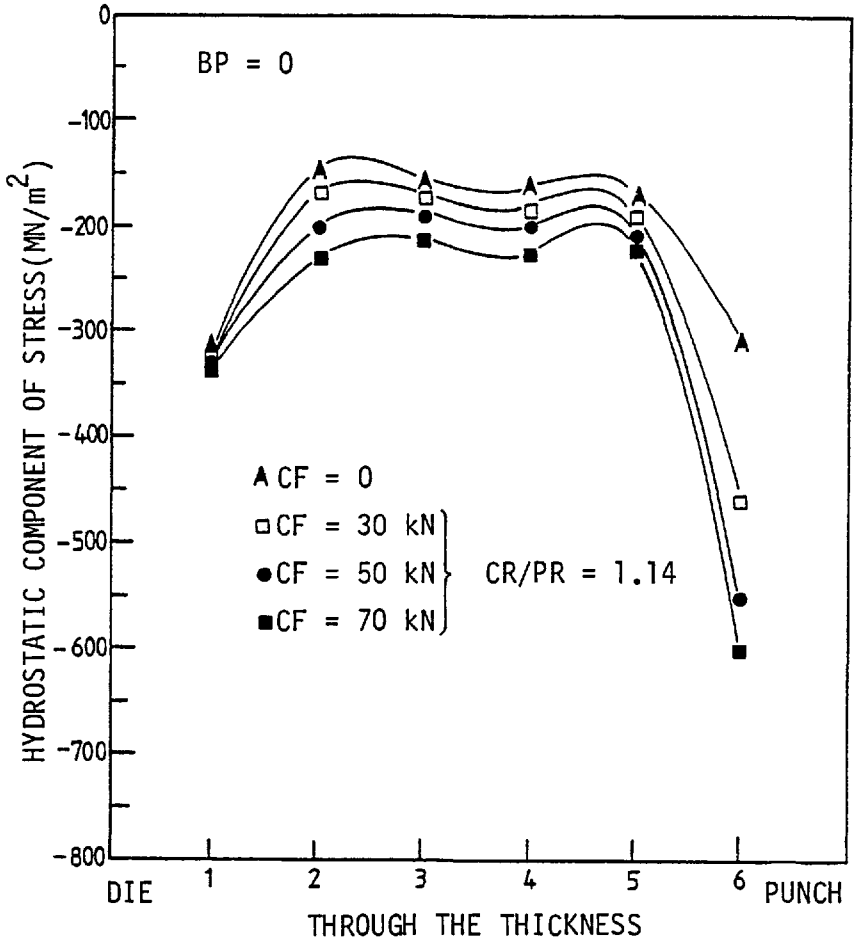

Fig. 5-39. Effect of clamping force (CF), for a clamp/punch diameter ratio of (CR/PR = 1.14), on the hydrostatic component of stress in the shearing zone during the blanking of mild steel strips of thickness t = 0.120 in. (3.04 mm) at a punch penetration of (PP = 0.74 mm) when no back-load was used (BP = 0).

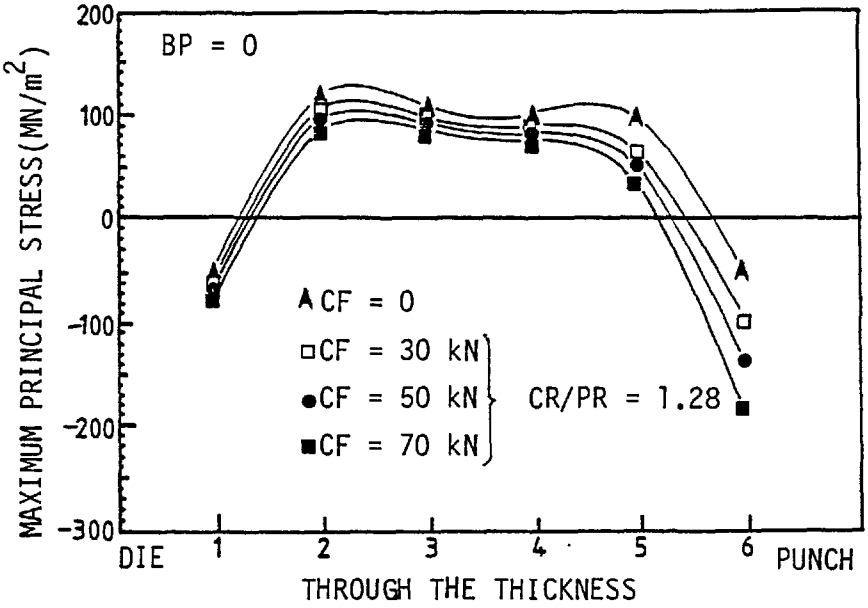

Fig. 5-40. Effect of clamping force (CF), for a clamp/punch diameter ratio of (CR/PR = 1.28) on the maximum principal stress in shearing zone during the blanking of mild steel strips of thickness t = 0.120 in. (3.04 mm) at a punch penetration of (PP = 0.74 mm) when no back-load was used (BP = 0).

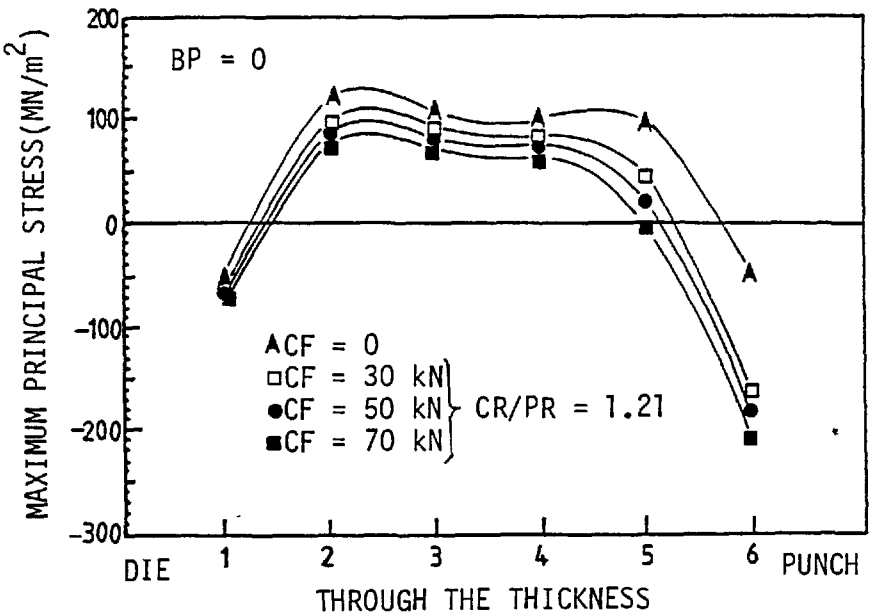

Fig. 5-41. Effect of clamping force (CF), for a clamp/punch diameter ratio of (CR/PR = 1.21), on the maximum principal stress in the shearing zone during the blanking of a t = 0.120 in. (3.04 mm) thick strip of mild steel at a punch penetration of (PP = 0.74 mm) when no back-load was used (BP = 0).

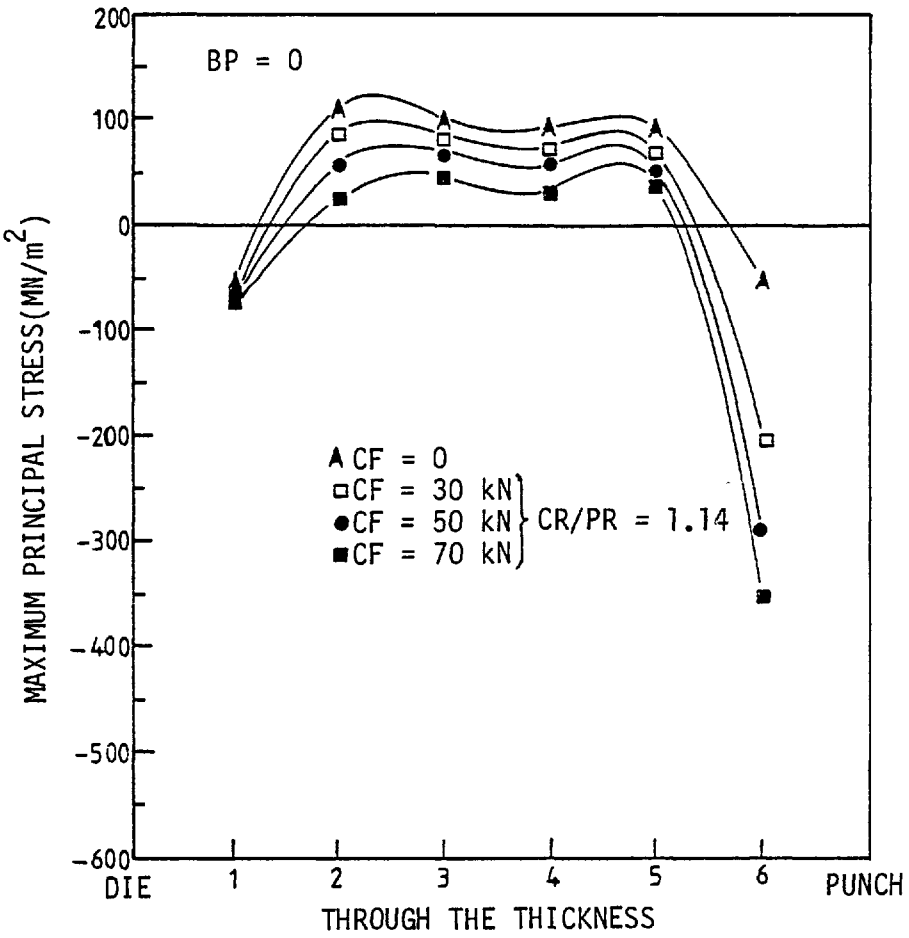

Fig. 5-42. Effect of clamping force (CF), for a clamp/punch diameter ratio of (CR/PR = 1.14), on the maximum principal stress in the shearing zone during the blanking of a t = 0.120 in. (3.04 mm) thick strip of mild steel at a punch penetration of (PP = 0.74 mm) when no back-load was used (BP = 0).

5.14.2 Effect of back-load on the hydrostatic component of stress and maximum principal stress in the absence of clamping force

The effect of back-load on the hydrostatic component of stress and maximum principal stress in the absence of clamping force is shown in Figs. 5-43 and 5-44 respectively.

By increasing the back-load the hydrostatic component of stress along the shear line increases. This increase is almost the same around the punch edge as well as the die edge.

By increasing the back-load the maximum principal stress along the shear line decreases. The application of a 70 kN back-load considerably reduces the maximum principal stress, but it still remains tensile along a large portion of the specimen thickness.

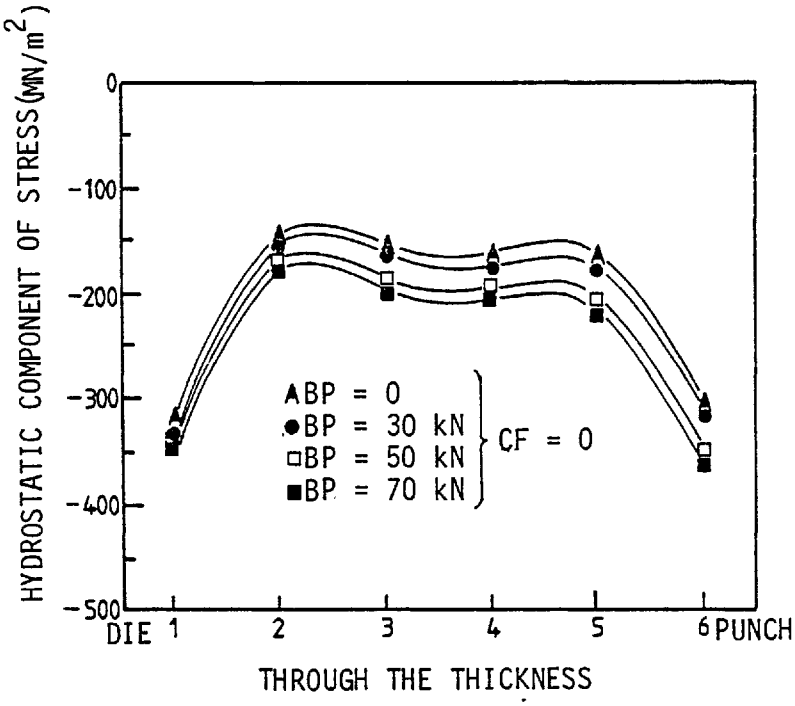

Fig. 5-43. Effect of back-load (BP) on the hydrostatic component of stress at a punch penetration of (PP = 0.74 mm) when punching a t = 0.120 in. (3.04 mm) thick strip of mild steel, with no clamping force (CF = 0).

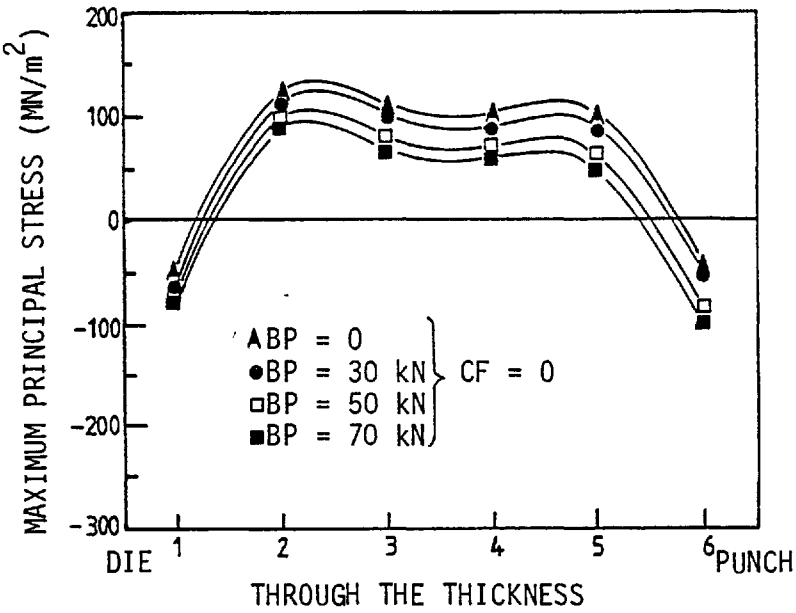

Fig. 5-44. Effect of back-load (BP) on the maximum principal stress at a punch penetration of (PP = 0.74 mm) when punching a t = 0.120 in. (3.04 mm) thick strip of mild steel with no clamping force (CF = 0).

5.14.3 A comparison of the effect of clamping force with the combined effect of clamping force and back-load

The effect of clamping force compared with the combined effect of clamping force and back-load on the hydrostatic component of stress along the shear line, when using different values of clamp diameter with clamp/punch diameter ratios of (CR/PR = 1.28, 1.21 and 1.14) which corresponds to the maximum, medium and minimum clamp diameters, are shown in Figs. 5-45 to 5-47, Figs. 5-48 to 5-50 and Figs. 5-51 to 5-53 respectively.

In all cases the hydrostatic component of stress increases by the application of a clamping force and the addition of a back-load causes a further increase. From the corresponding results it can be concluded that the application of a back-load together with a clamping force develops the highest hydrostatic component of stress in the shearing zone. This build up in the hydrostatic component of stress must be due to the blocking of the outward flow of material caused by the compression of the specimen between the punch and counter-punch.

The corresponding results, the effect of clamping force and combined effect of clamping force and back-load on the maximum principal stress along the shear line are given in Figs. 5-54 to 5-62. By the application of a clamping force the maximum principal stress in the shearing zone decreases and the addition of a back-load causes a further decrease in the maximum principal stress. An increase in both clamping force and back-load causes a decrease in the maximum principal stress. The decrease in the maximum tensile principal stress in the shearing zone reduces the possibility of occurrence of fibrous fracture during the blanking operation, which is due to the propagation and coalescence of micro-cracks under the tensile stresses.

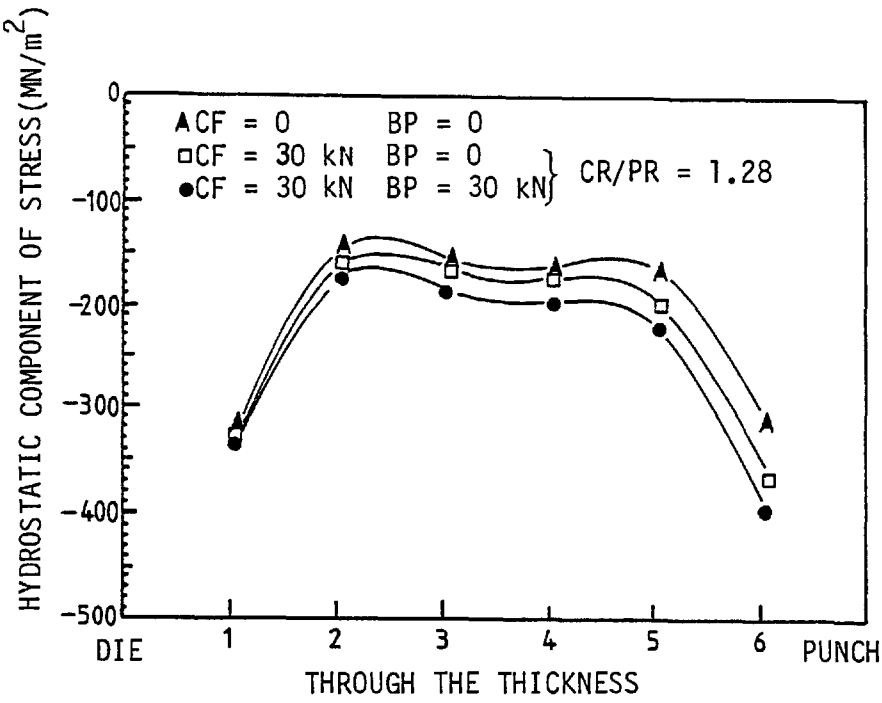

Fig. 5-45. Effect of clamping force (CF), for a clamp/punch diameter ratio of (CR/PR = 1.28), and combined effect of clamping force and back-load (BP) on the hydrostatic component of stress on the shear line at a punch penetration of (PP = 0.74 mm) when punching a t = 0.120 in. (3.04 mm) thick strip of mild steel.

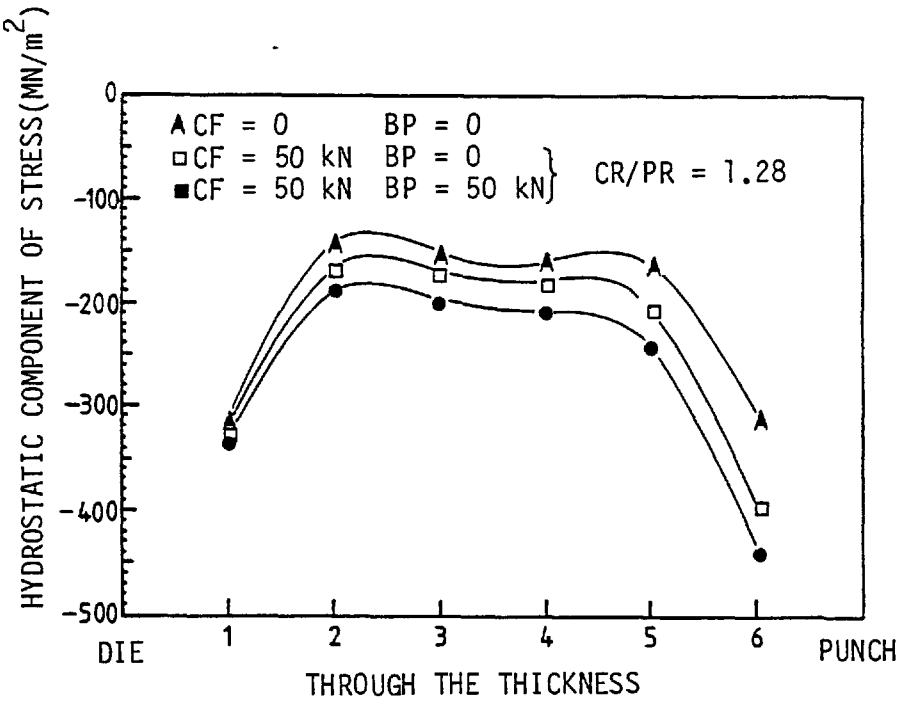

Fig. 5-46. Effect of clamping force (CF), for a clamp/punch diameter ratio of (CR/PR = 1.28), and combined effect of clamping force (CF) and back-load (BP) on the hydrostatic component of stress at a punch penetration of (PP = 0.74 mm) when punching a t = 0.120 in. (3.04 mm) thick strip of mild steel.

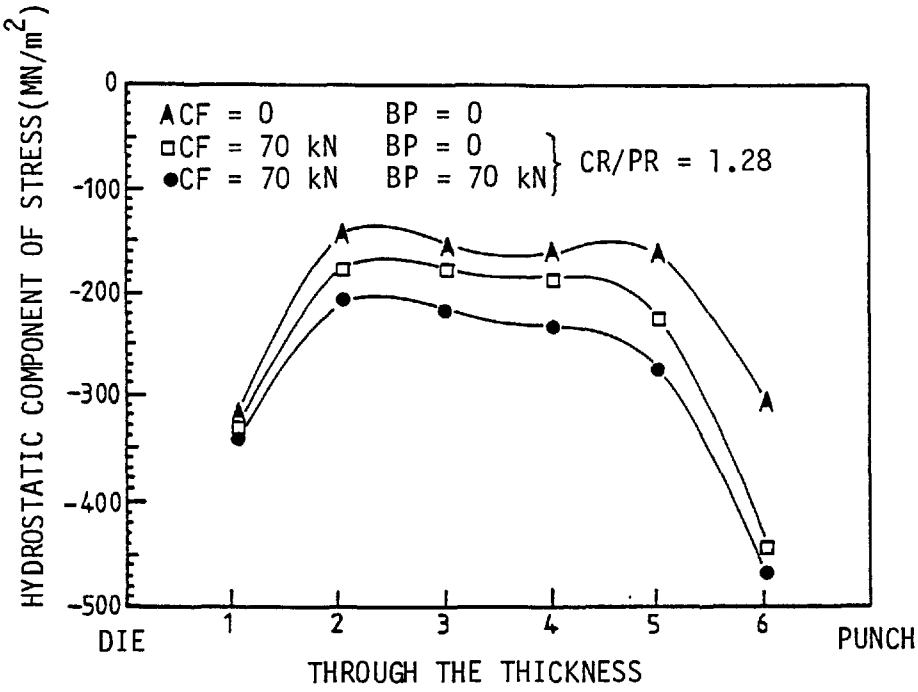

Fig. 5-47. Effect of clamping force (CF), for a clamp/punch diameter ratio of (CR/PR = 1.28), and combined effect of clamping force (CF) and back-load (BP) on the hydrostatic component of stress at a punch penetration of (PP = 0.74 mm) when punching a t = 0.120 in. (3.04 mm) thick strip of mild steel.

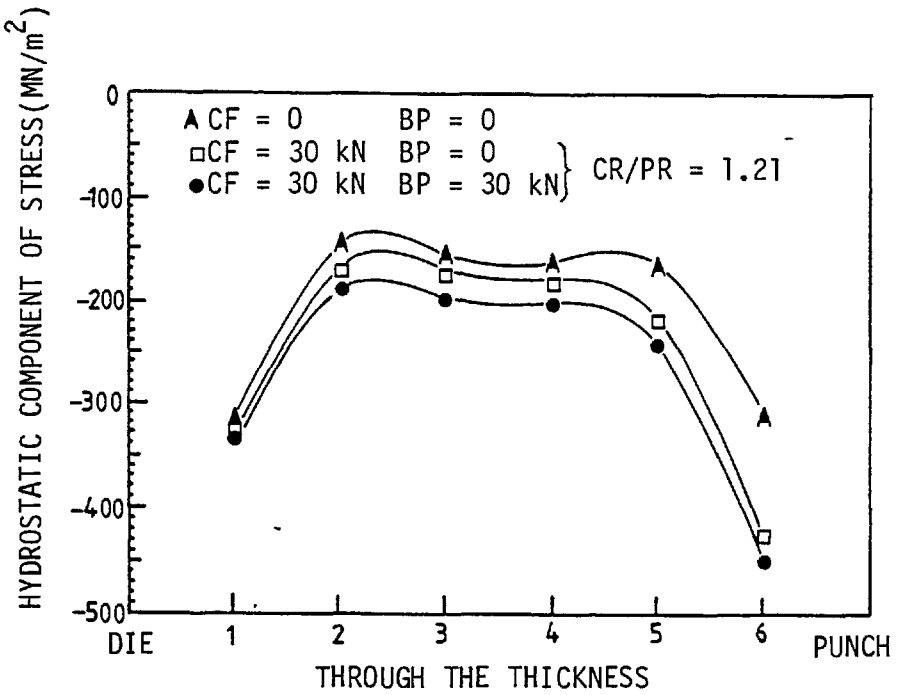

Fig. 5-48. Effect of clamping force (CF), for a clamp/punch diameter ratio of (CR/PR = 1.21), and combined effect of clamping force (CF) and back-load (BP) on the hydrostatic component of stress at a punch penetration of (PP = 0.74 mm) when punching a t = 3.04 mm thick strip of mild steel.

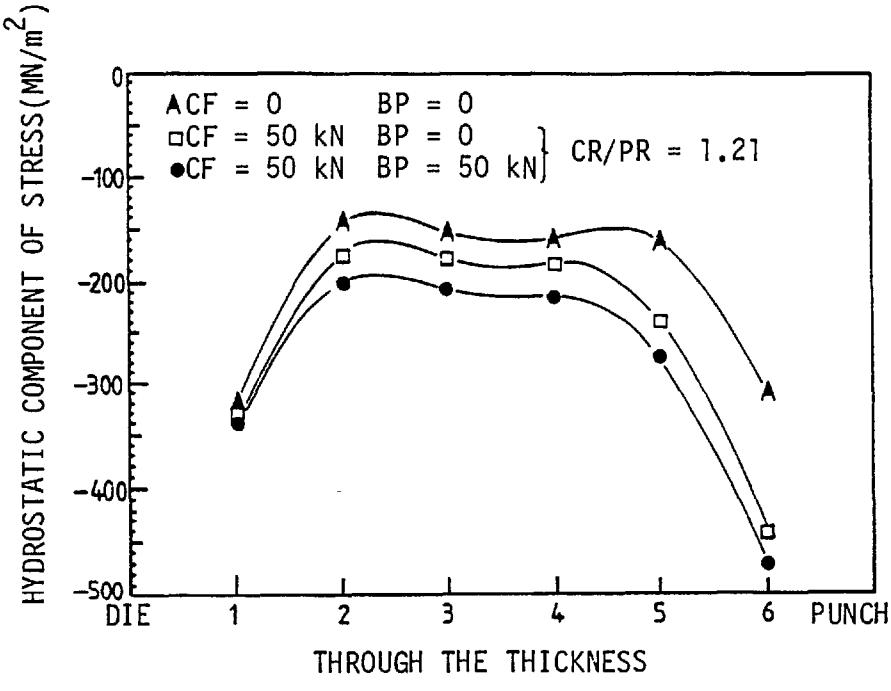

Fig. 5-49. Effect of clamping force (CF), for a clamp/punch diameter ratio of (CR/PR = 1.21), and combined effect of clamping force (CF) and back-load (BP) on the hydrostatic component of stress at a punch penetration of (PP = 0.74 mm) when punching a t = 3.04 mm thick strip of mild steel.

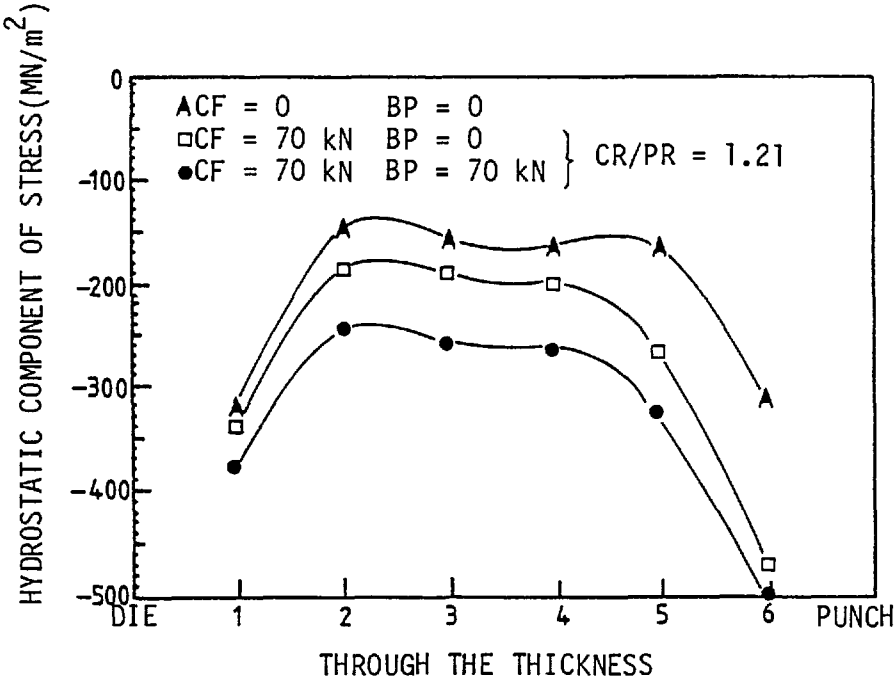

Fig. 5-50. Effect of clamping force (CF), for a clamp/punch diameter ratio of (CR/PR = 1.21), and combined effect of clamping force and back-load (CF and BP) on the hydrostatic component of stress at a punch penetration of (PP = 0.74 mm) when punching a t = 3.04 mm thick strip of mild steel.

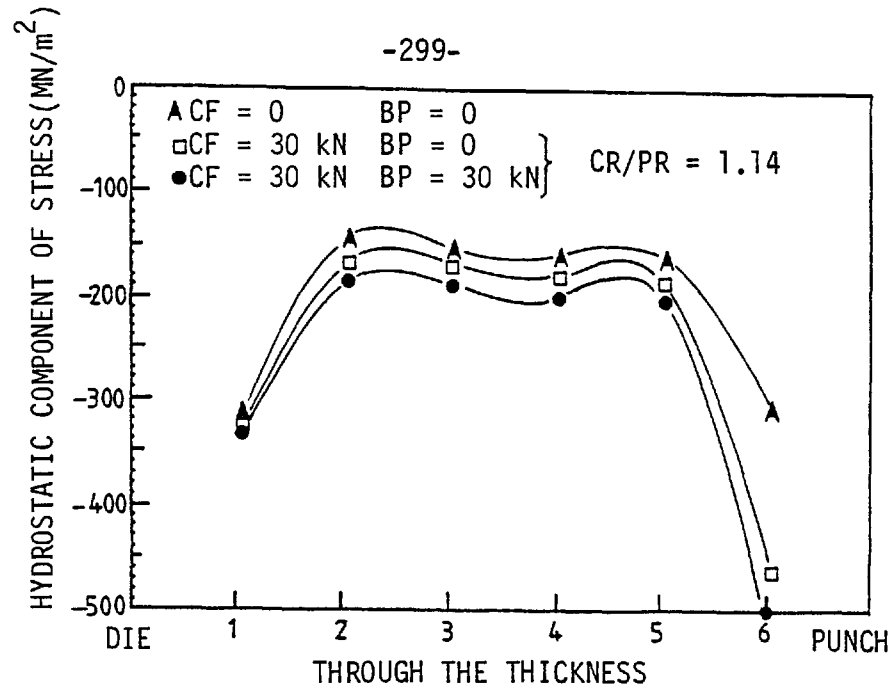

Fig. 5-51. Effect of clamping force (CF), for a clamp/punch diameter ratio of (CR/PR = 1.14), and combined effect of clamping force and back-load (CF and BP) on the hydrostatic component of stress at a punch penetration of (PP = 0.74 mm) when punching a t = 3.04 mm thick strip of mild steel.

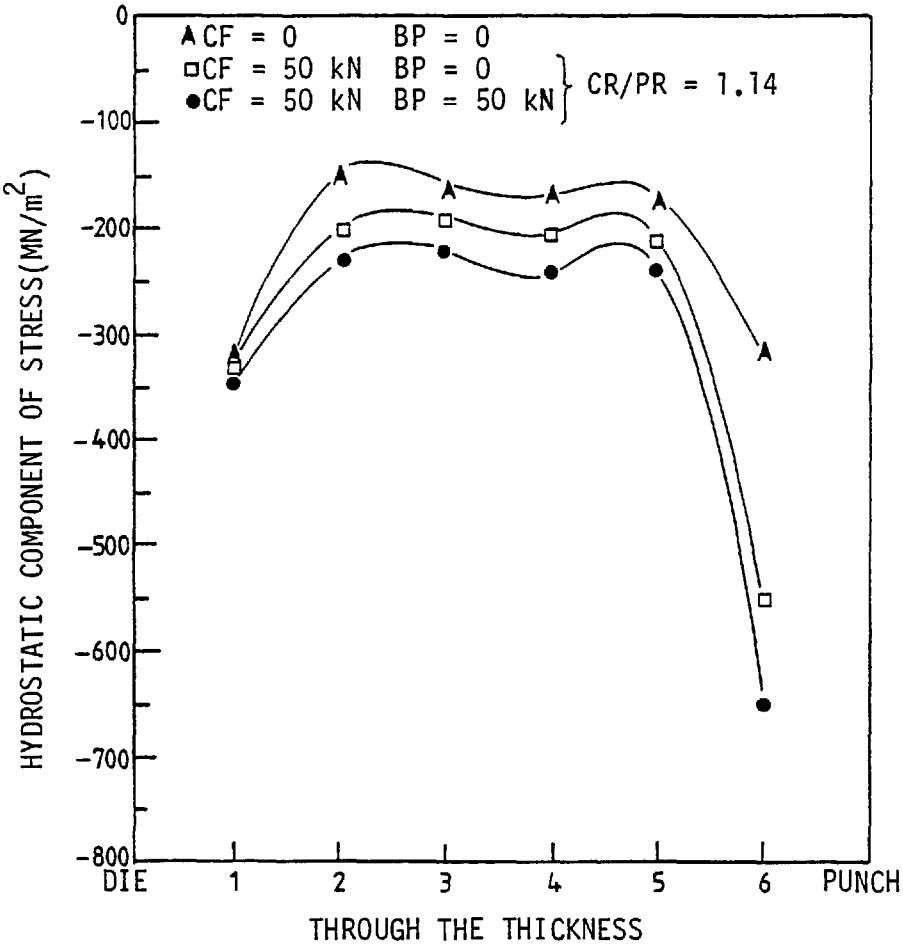

Fig. 5-52. Effect of clamping force (CF), for a clamp/punch diameter ratio of (CR/PR = 1.14), and combined effect of clamping force and back-load (CF and BP) on the hydrostatic component of stress at a punch penetration of (PP = 0.74 mm) when punching a t = 0.120 in. (3.04 mm) thick strip of mild steel.

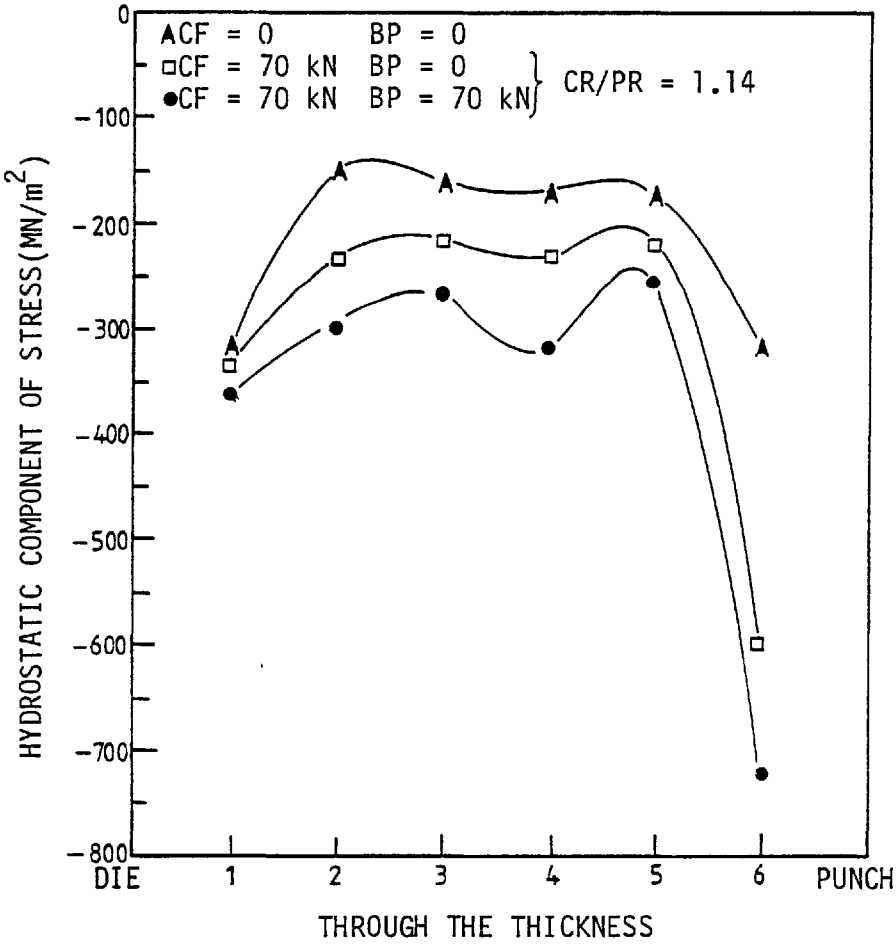

Fig. 5-53. Effect of clamping force (CF), for a clamp/punch diameter ratio of (CR/PR = 1.14), and combined effect of clamping force and back-load (CF and BP) on the hydrostatic component of stress at a punch penetration of (PP = 0.74 mm) when punching a t = 3.04 mm thick strip of mild steel.

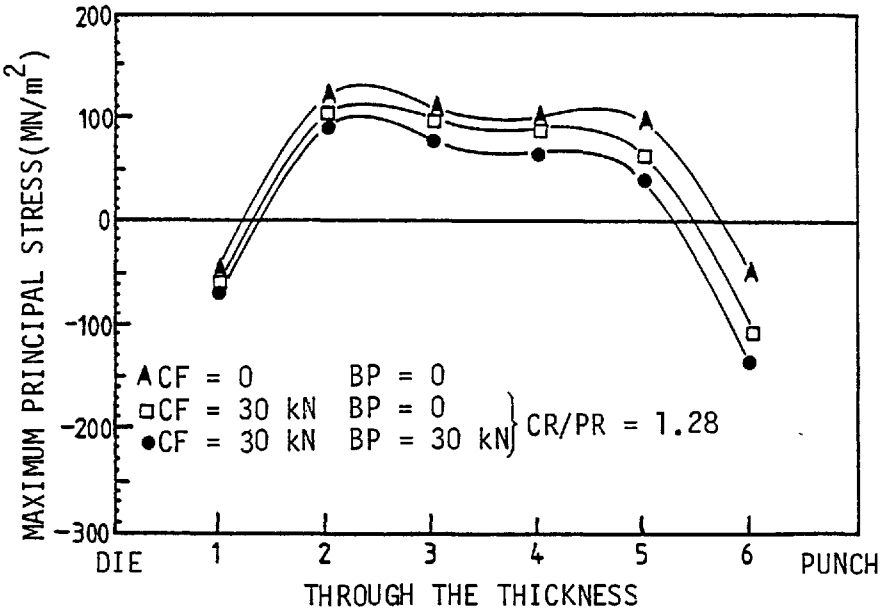

Fig. 5-54. Effect of clamping force (CF), for a clamp/punch diameter ratio of (CR/PR = 1.28), and combined effect of clamping force and back-load (CF and BP) on the maximum principal stress at a punch penetration of (PP = 0.74 mm) when punching a t = 0.120 in. (3.04 mm) thick strip of mild steel.

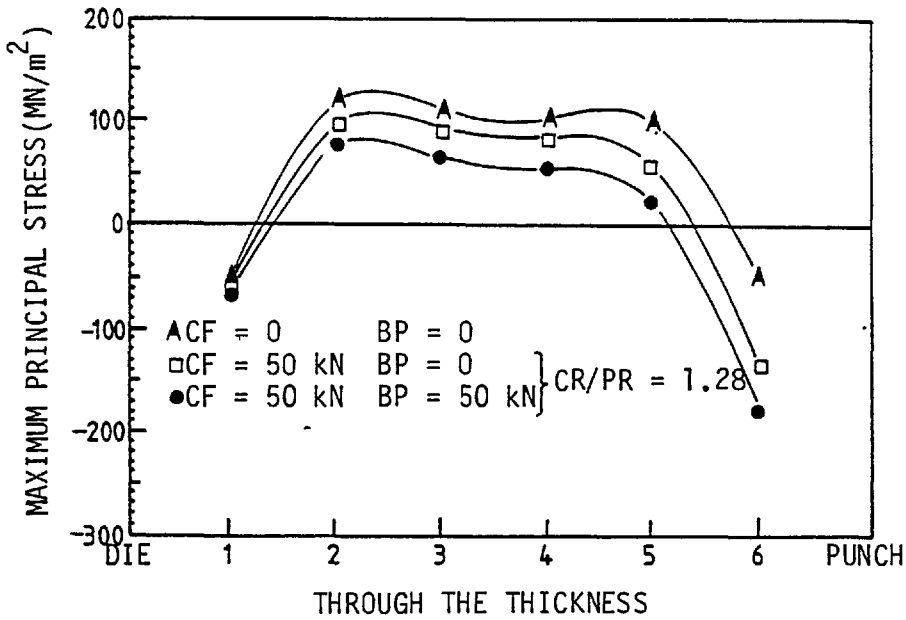

Fig. 5-55. Effect of clamping force (CF), for a clamp/punch diameter ratio of (CR/PR = 1.28), and combined effect of clamping force and back-load (CF and BP) on the maximum principal stress at a punch penetration of (PP = 0.74 mm) when punching a t = 0.120 in. (3.04 mm) thick strip of mild steel.

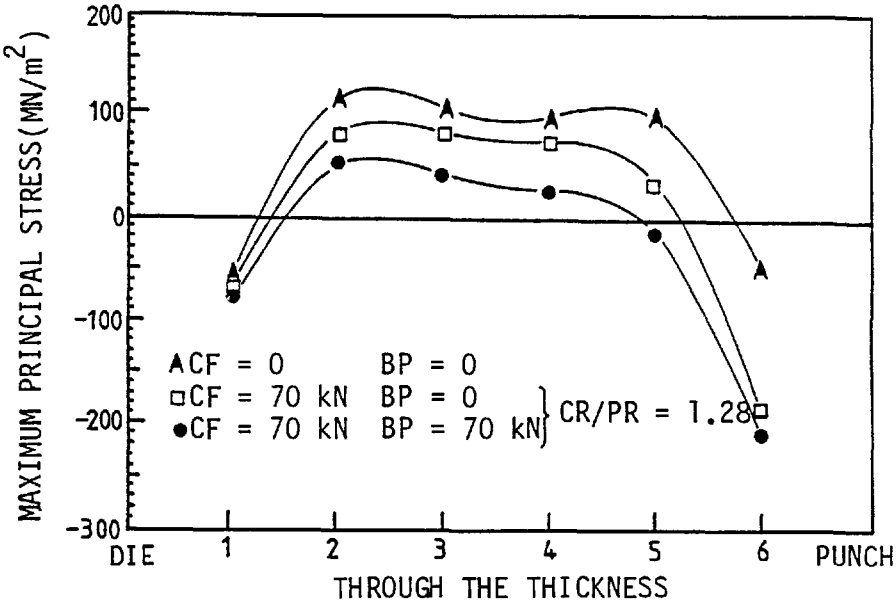

Fig. 5-56. Effect of clamping force (CF), for a clamp/punch diameter ratio of (CR/PR = 1.28), and combined effect of clamping force and back-load (CF and BP) on the maximum principal stress at a punch penetration of (PP = 0.74 mm) when punching a t = 0.120 in. (3.04 mm) thick strip of mild steel.

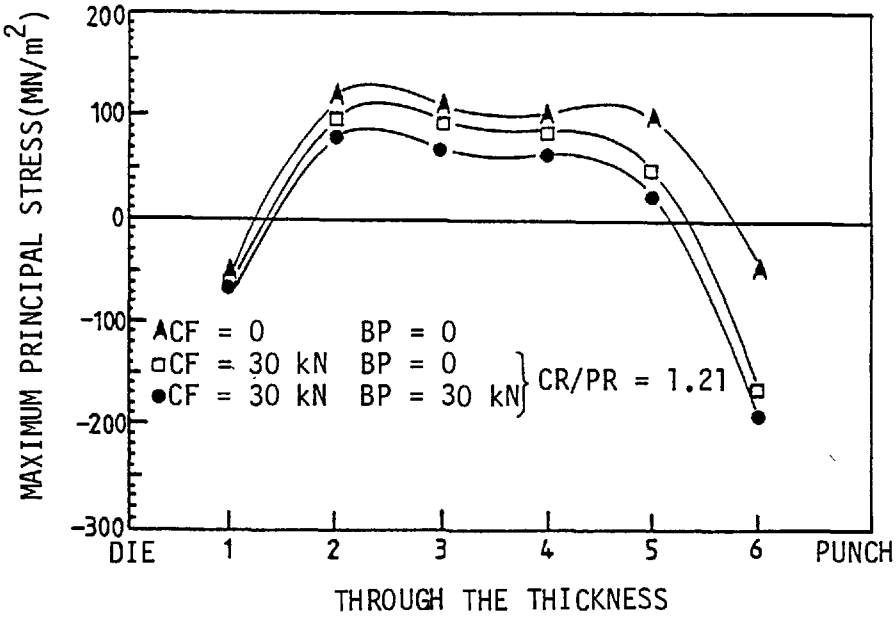

Fig. 5-57. Effect of clamping force (CF), for a clamp/punch diameter ratio of (CR/PR = 1.21), and combined effect of clamping force and back-load (CF and BP) on the maximum principal stress at a punch penetration of (PP = 0.74 mm) when punching a t = 0.120 in. (3.04 mm) thick strip of mild steel.

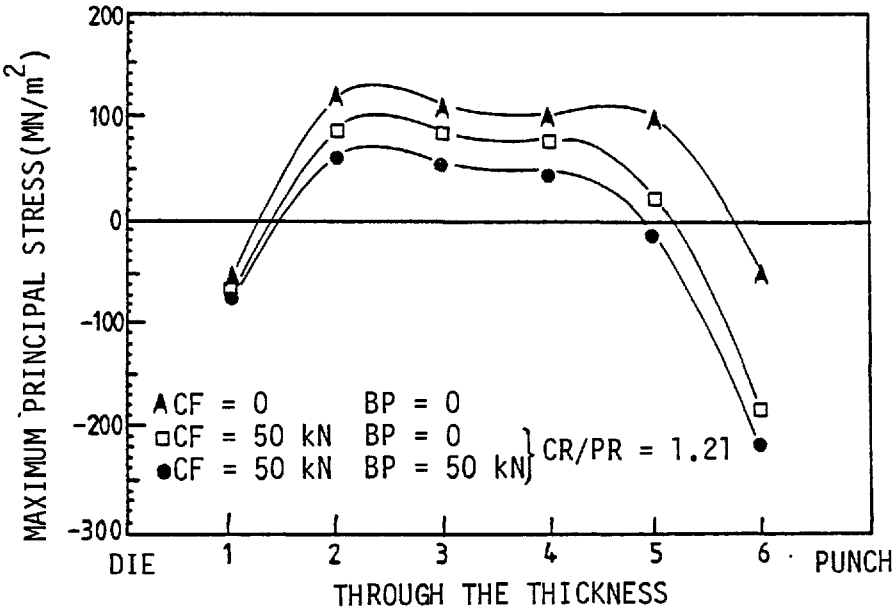

Fig. 5-58. Effect of clamping force (CF), for a clamp/punch diameter ratio of (CR/PR = 1.21), and combined effect of clamping force and back-load (CF and BP) on the maximum principal stress at a punch penetration of (PP = 0.74 mm) when punching a t = 0.120 in. (3.04 mm) thick strip of mild steel.

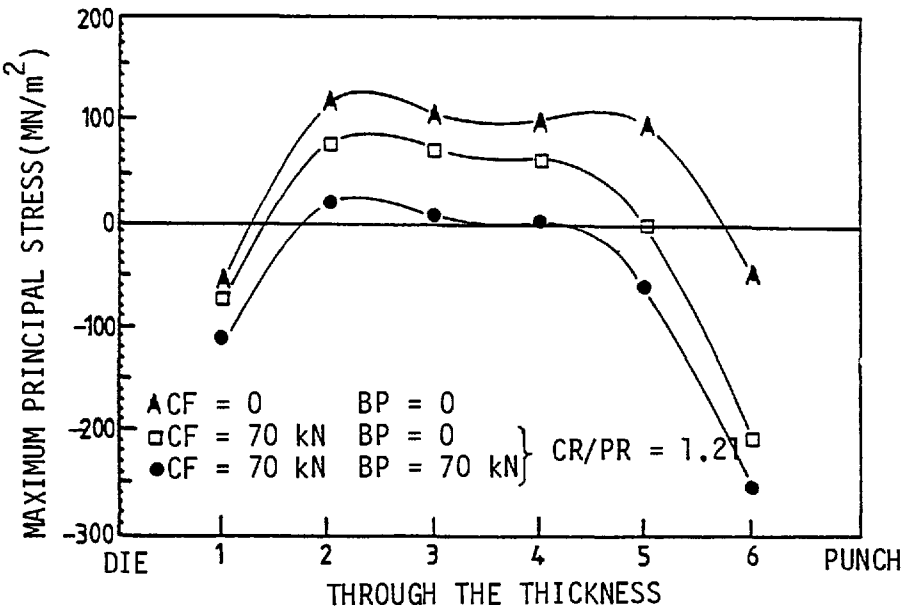

Fig. 5-59. Effect of clamping force (CF), for a clamp/punch diameter ratio of (CR/PR = 1.21), and combined effect of clamping force and back-load (CF and BP) on the maximum principal stress at a punch penetration of (PP = 0.74 mm) when punching a t = 0.120 in. (3.04 mm) thick strip of mild steel.

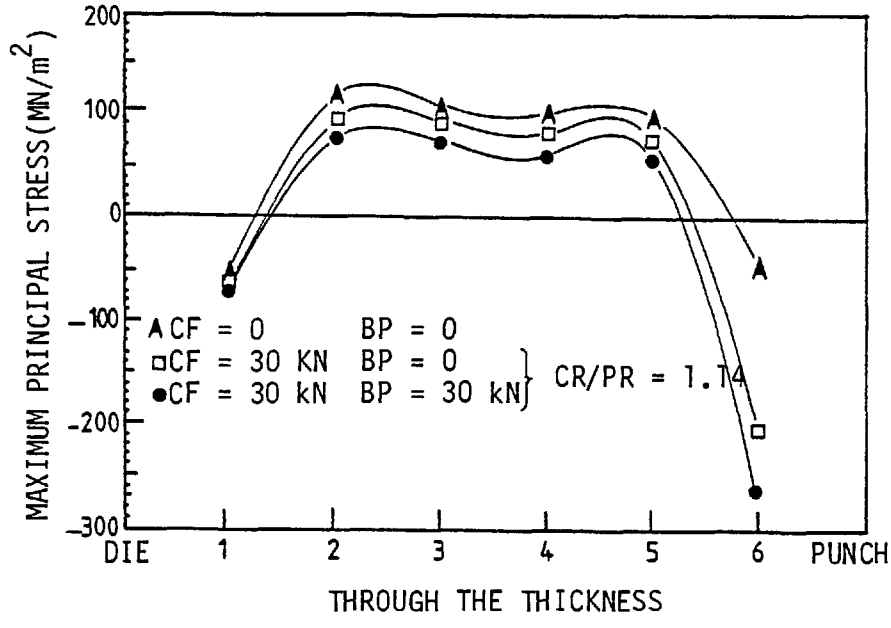

Fig. 5-60. Effect of clamping force (CF), for a clamp/punch diameter ratio of (CR/PR = 1.14), and combined effect of clamping force and back-load (CF and BP) on the maximum principal stress at a punch penetration of (PP= 0.74 mm) when punching a t = 0.120 in. (3.04 mm) thick strip of mild steel.

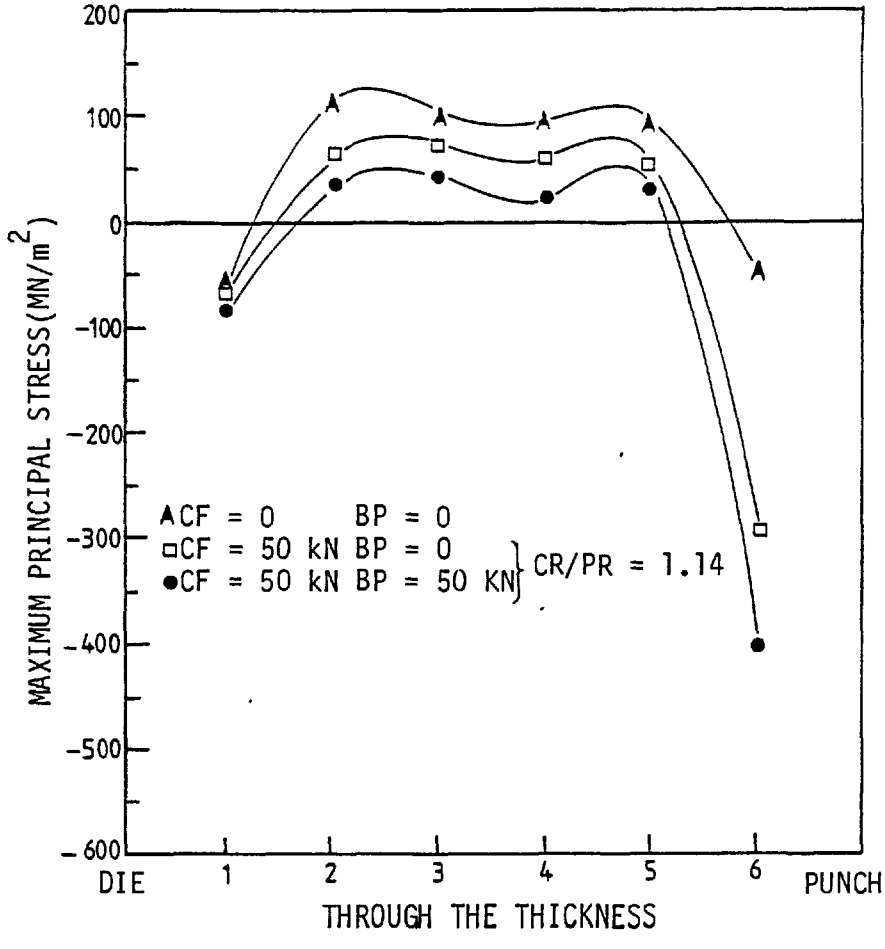

Fig. 5-61. Effect of clamping force (CF),for a clamp/punch diameter ratio of (CR/PR = 1.14), and combined effect of clamping force and back-load (CF and BP) on the maximum principal stress at a punch penetration of (PP = 0.74 mm) when punching a t =0.120 in. (3.04 mm) thick strip of mild steel.

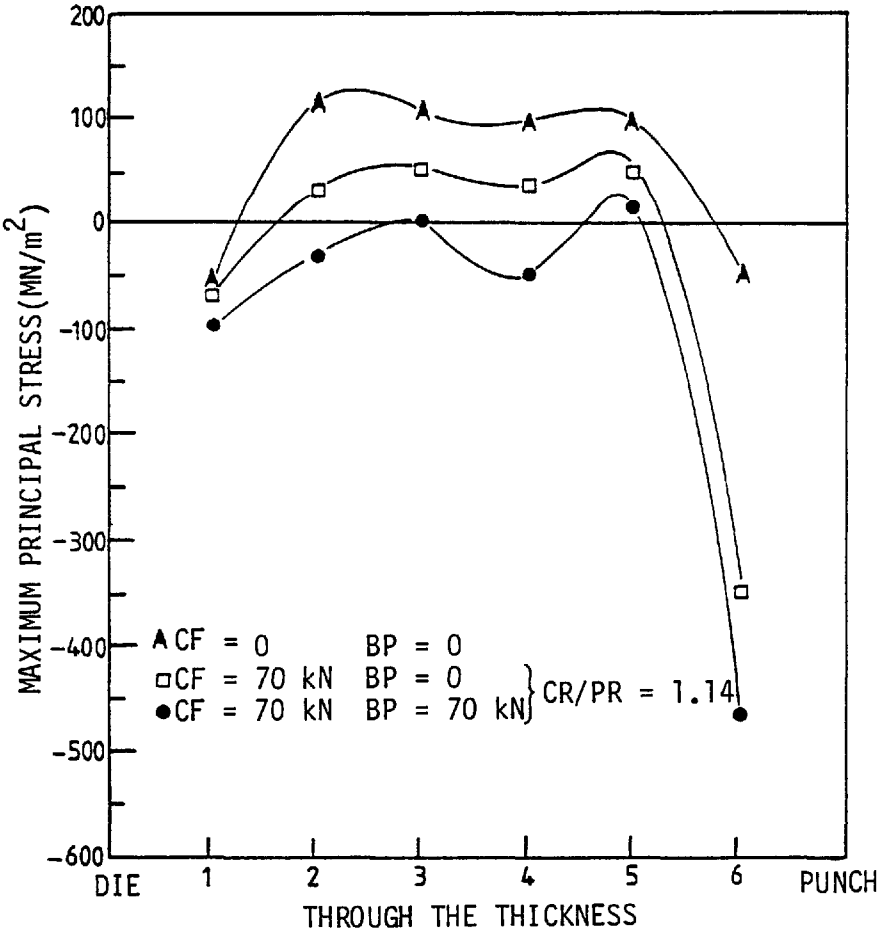

Fig. 5-62. Effect of clamping force (CF), for a clamp/punch diameter ratio of (CR/PR = 1.14), and combined effect of clamping force and back-load (CF and BP) on the maximum principal stress at a punch penetration of (PP = 0.74 mm) when punching a t = 0.120 in. (3.04 mm) thick strip of mild steel.

5.14.4 A comparison of the effect of clamping force, back-load and combined effect of clamping force and back-load for a typical clamp/punch diameter ratio of (CR/PR = 1.14)

A comparison is made of the effect of clamping force and back-load acting separately and clamping force and back-load together on the prevailing hydrostatic component of stress along the shear line for a typical clamp diameter with a clamp/punch diameter ratio of (CR/PR = 1.14).. The results for three different values of clamping force and back-load (30, 50 and 70 kN) are given in Figs. 5-63, 5-64 and 5-65 respectively.

From these three figures it can be concluded that, for an equal value of clamping force and back-load, the clamping force produces a higher hydrostatic component of stress than does the back-load. Furthermore, the back-load and clamping force together will have a higher effect on the hydrostatic component of stress than either of them acting alone.

The corresponding results for the maximum principal stress are shown in Figs. 5-66, 5-67 and 5-68. These three figures show that the effect of clamping force, when using a typical blank-holder with clamp/punch diameter ratio of CR/PR=1.14, in reducing the maximum principal stress along the shear line is more pronounced than the effect of an equal value of back-load. The combined effect of clamping force and back-load on the maximum principal stress is higher than either the clamping force or the back-load acting alone.

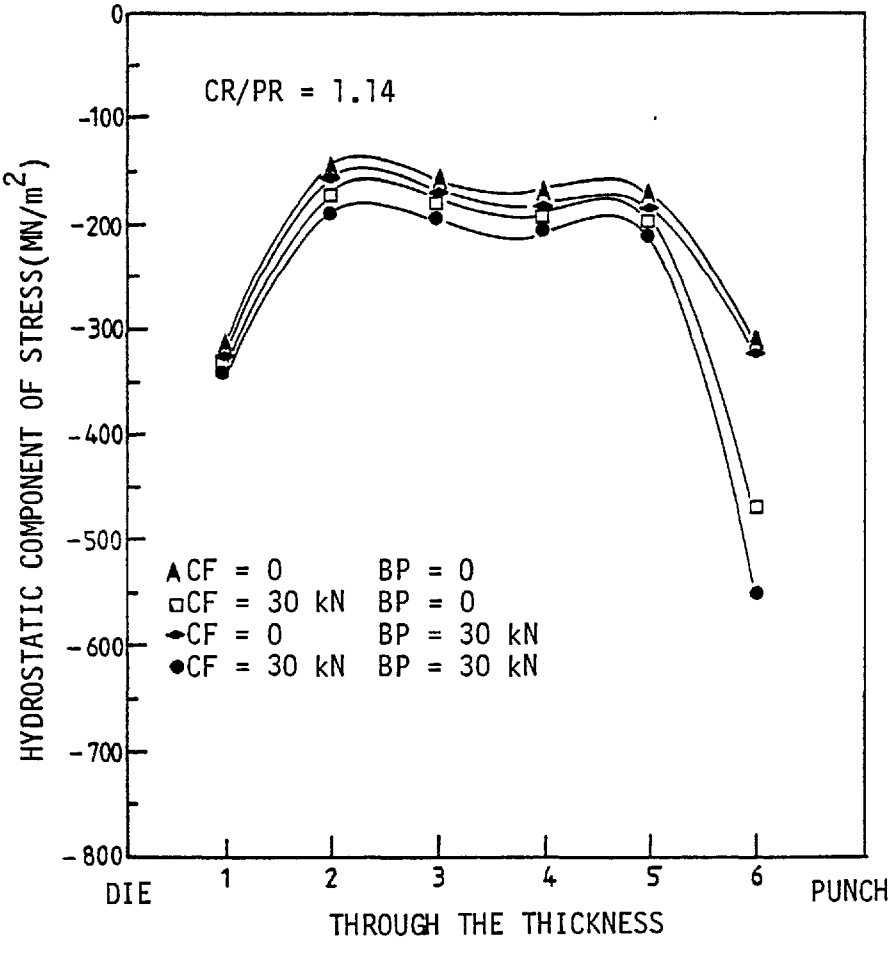

Fig. 5-63. Effect of clamping force (CF), for a clamp/punch diameter ratio of (CR/PR = 1.14), back-load (BP) and combined effect of clamping force and back-load on the hydrostatic component of stress at a punch penetration of (PP = 0.74 mm) when punching a t = 0.120 in. (3.04 mm) thick strip of mild steel.

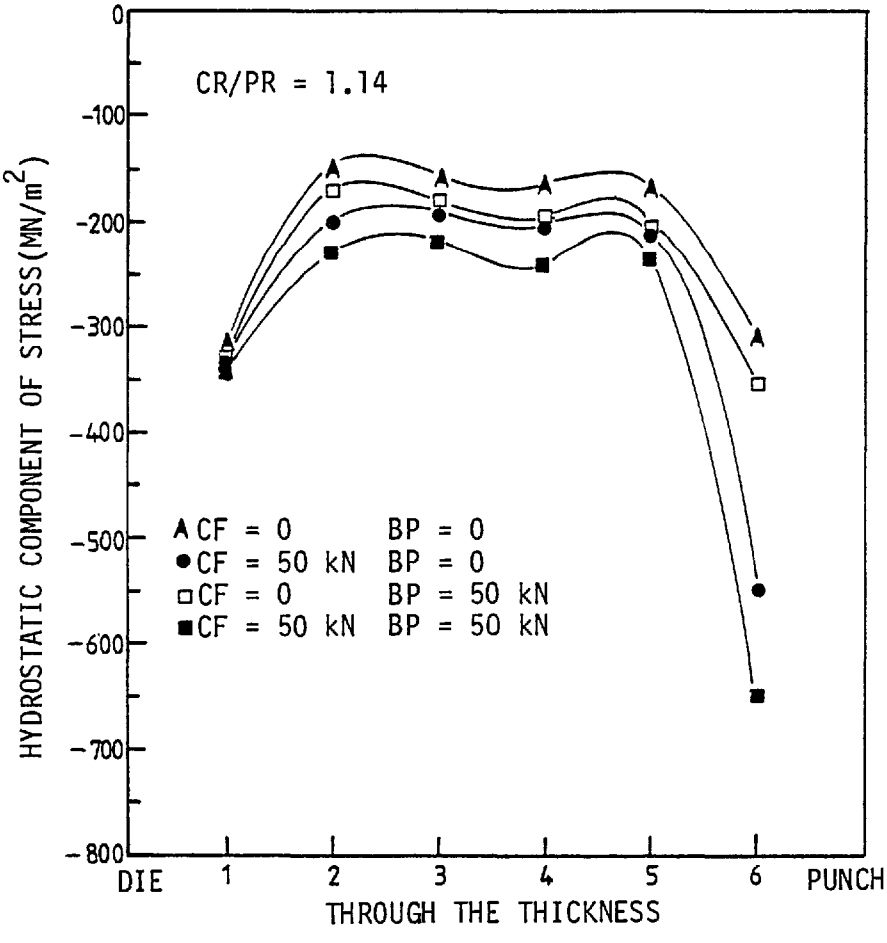

Fig. 5-64. Effect of clamping force (CF), for a clamp/punch diameter ratio of (CR/PR = 1.14), back-load (BP) and combined effect of clamping force and back-load on the hydrostatic component of stress at a punch penetration of (PP = 0.74 mm) when punching a t = 0.120 in. (3.04 mm) thick strip of mild steel.

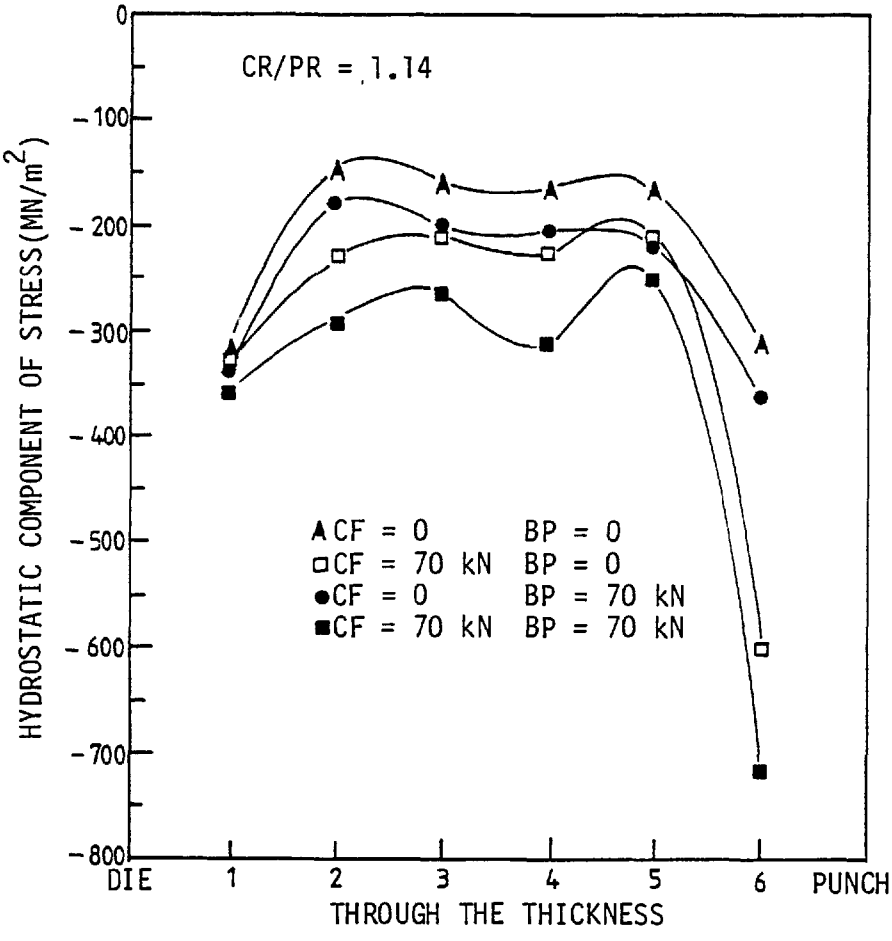

Fig. 5-65. Effect of clamping force (CF), for a clamp/punch diameter ratio of (CR/PR = 1.14), back-load (BP) and combined effect of clamping force and back-load (CF and BP) on the hydrostatic component of stress at a punch penetration of (PP = 0.74 mm) when punching a t = 0.120 in. (3.04 mm) thick strip of mild steel.

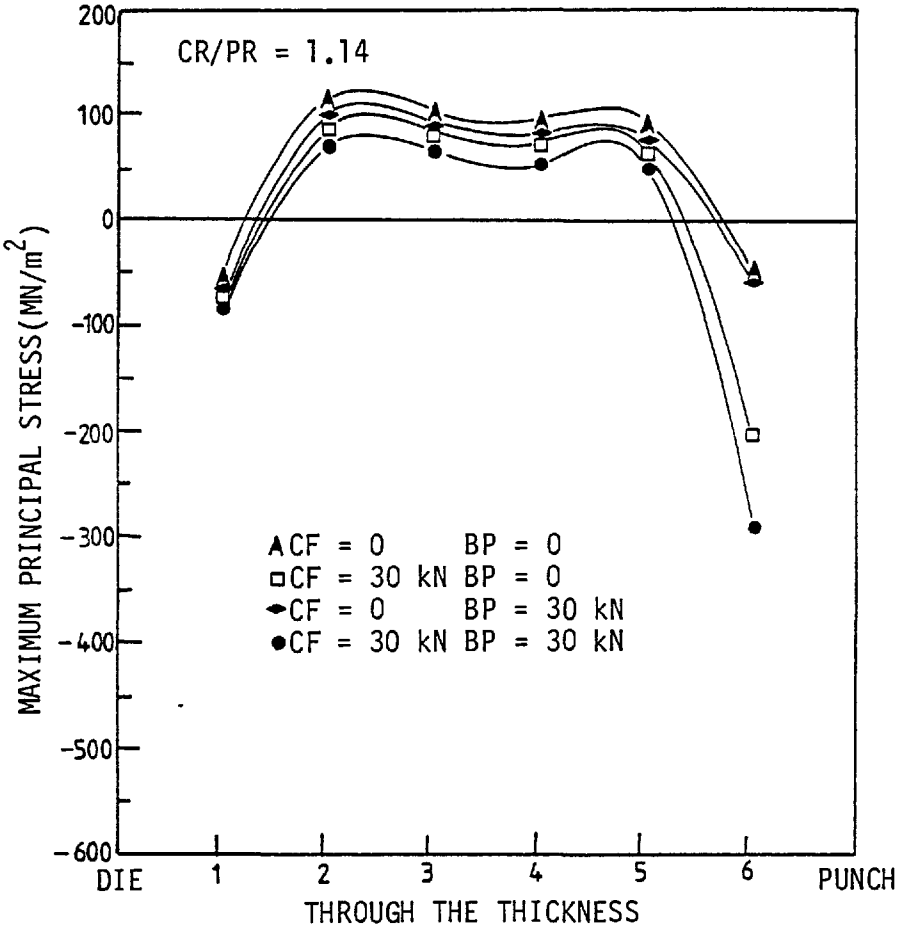

Fig. 5-66. Effect of clamping force (CF), for a clamp/punch diameter ratio of (CR/PR = 1.14), back-load (BP) and combined effect of clamping force and back-load on the maximum principal stress at a punch penetration of (PP = 0.74 mm) when punching a t = 0.120 in. (3.04 mm) thick strip of mild steel.

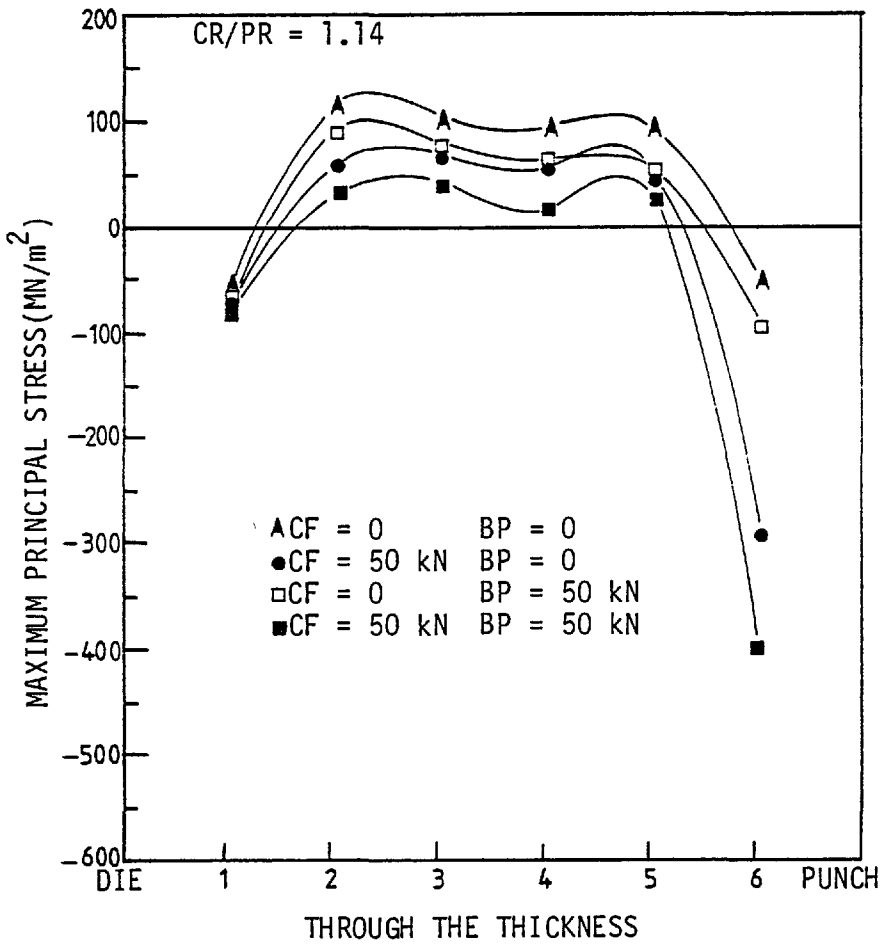

Fig. 5-67. Effect of clamping force (CF), for a clamp/punch diameter ratio of (CR/PR = 1.14), back-load (BP) and combined effect of clamping force and back-load on the maximum principal stress at a punch penetration of (PP = 0.74 mm) when punching a t = 0.120 in. (3.04 mm) thick strip of mild steel.

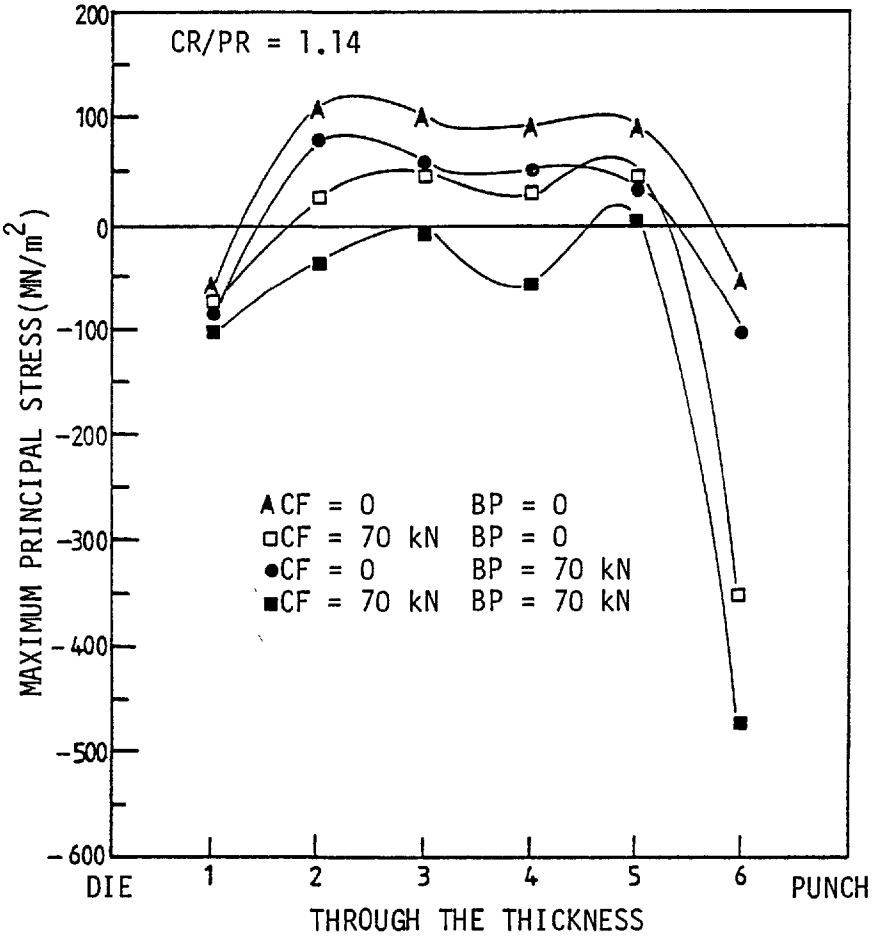

Fig. 5-68. Effect of clamping force (CF), for a clamp/punch diameter ratio of (CR/PR = 1.14), back-load (BP) and combined effect of clamping force and back-load on the maximum principal stress at a punch penetration of (PP = 0.74 mm) when punching a t = 0.120 in. (3.04 mm) thick strip of mild steel.

5.14.5 Combined effect of clamping force and back-load

As was shown previously, in section 5.14.3, the combined effect of clamping force and back-load resulted in a higher hydrostatic component of stress than in the two cases when the back-load or clamping force acted alone. A general comparison of the hydrostatic component of stress along the shear line when the clamping force and back-load attained equal values (of 30, 50 and 70 kN) for blank-holders with maximum, medium and minimum diameter are shown in Figs. 5-69, 5-70 and 5-71 respectively.

For different values of clamping force and back-load, at a certain value of clamp diameter, all the curves follow almost the same trend and an increase in the clamping force and back-load causes an increase in the hydrostatic component of stress.

The corresponding results for the maximum principal stress along the shear line are given in Figs. 5-72, 5-73 and 5-74. In all cases, for blank-holders of different diameters, increasing the clamping force and back-load causes the maximum principal stress to decrease. In the case of the blank-holder with maximum diameter (CR/PR = 1.28), the maximum principal stress remains tensile even when using the maximum values of clamping force and back-load (CF = BP = 70 kN), whilst under the same condition of clamping force and back-load in the other two cases (CR/PR = 1.21 and 1.14) the maximum principal stress along the shear line noticeably reduces and becomes zero or negative along the whole thickness of the material.

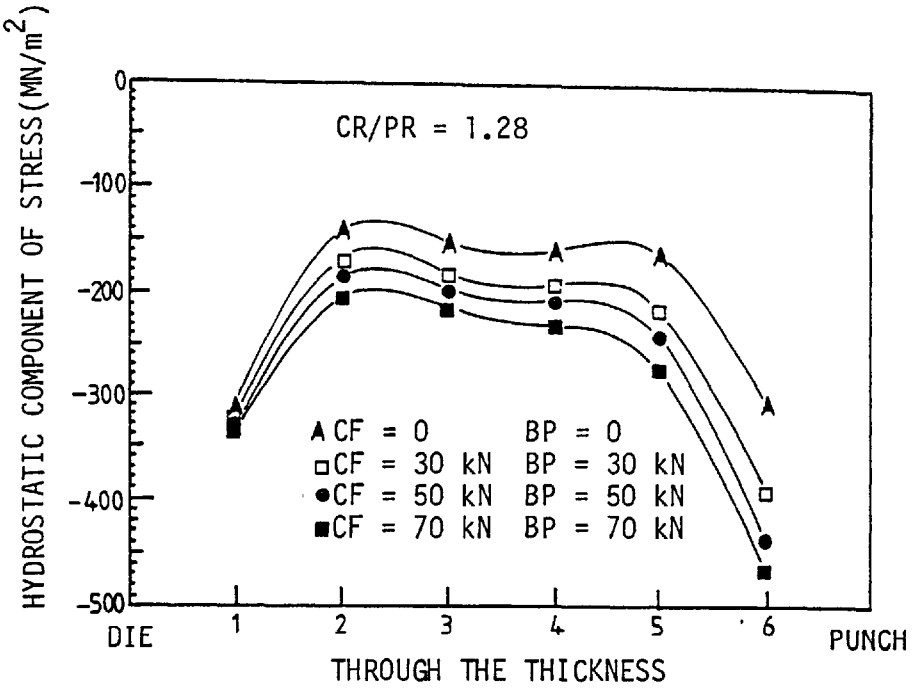

Fig. 5-69. Combined effect of clamping force (CF) and back-load (BP), when a clamp/punch diameter ratio of (CR/PR = 1.28) was used, on the hydrostatic component of stress at a punch penetration of (PP = 0.74 mm) when punching a t = 0.120 in. (3.04 mm) thick strip of mild steel.

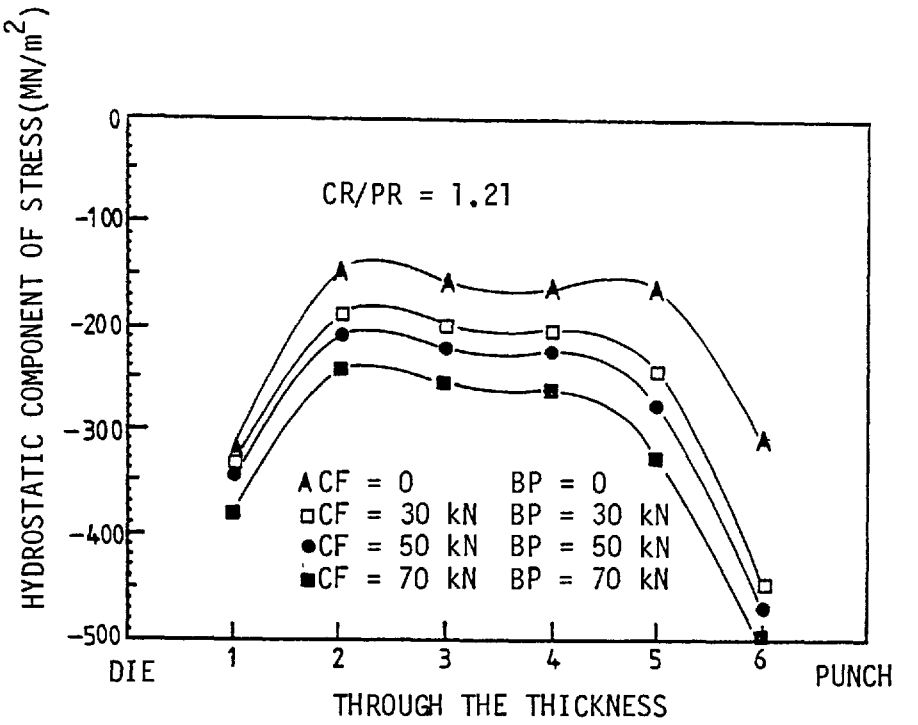

Fig. 5-70. Combined effect of clamping force (CF) and back-load(BP), when a clamp/punch diameter ratio of (CR/PR = 1.21) was used, on the hydrostatic component of stress at a punch penetration of (PP = 0.74 mm) when punching a t = 0.120 in. (3.04 mm) thick strip of mild steel.

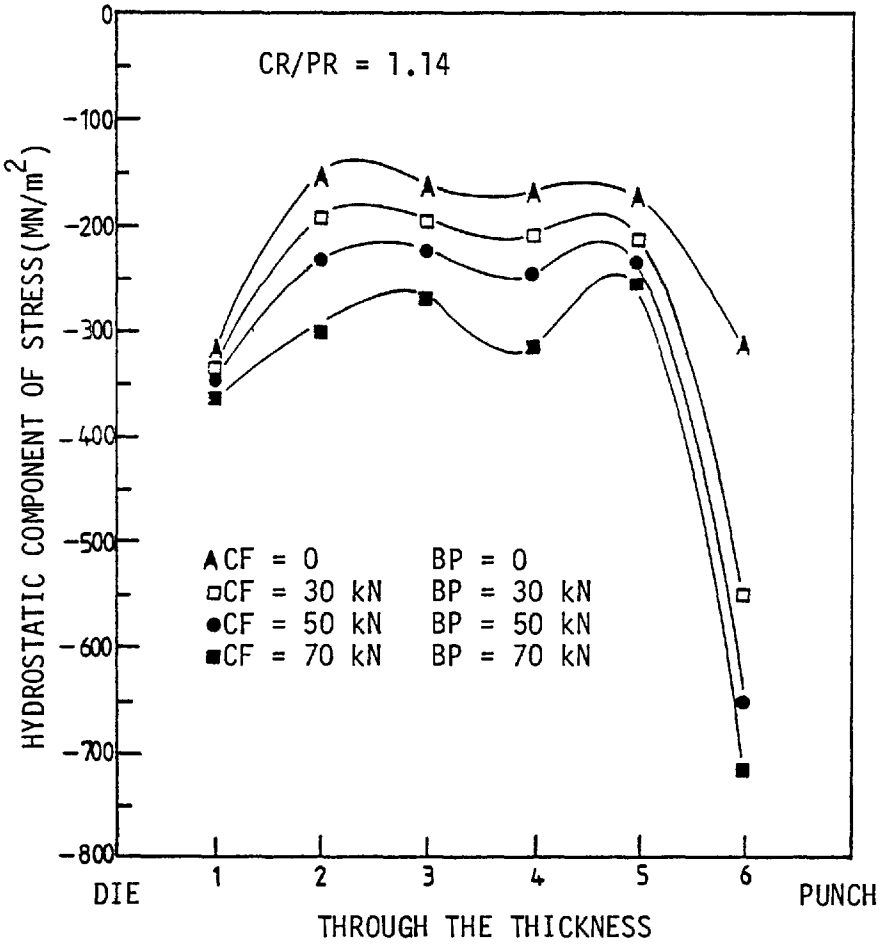

Fig. 5-71. Combined effect of clamping force (CF) and back-load(BP), when a clamp/punch diameter ratio of (CR/PR = 1.14) was used, on the hydrostatic component of stress at a punch penetration of (PP = 0.74 mm) when punching a t = 0.120 in. (3.04 mm) thick strip of mild steel.

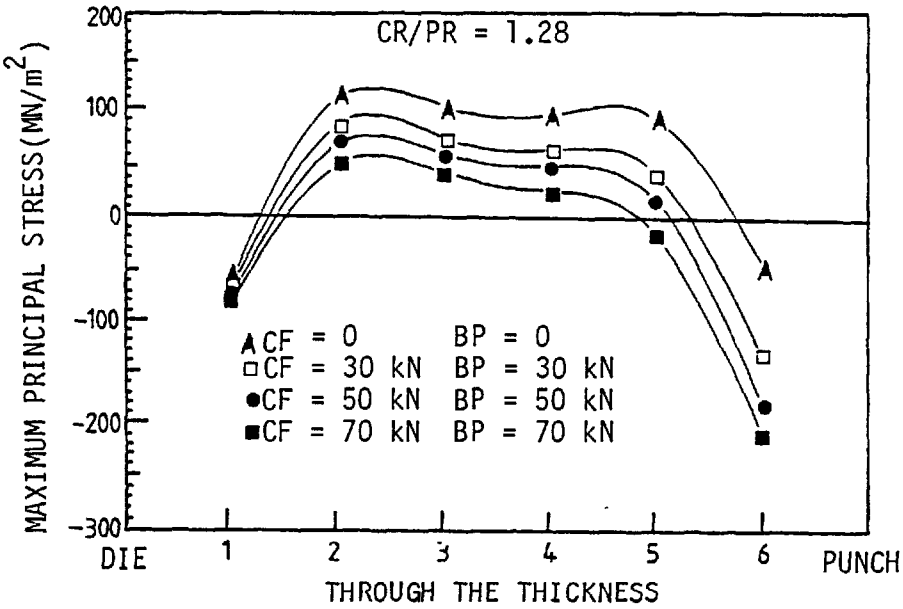

Fig. 5-72. Combined effect of clamping force (CF) and back-load (BP), when a clamp/punch diameter ratio of (CR/PR = 1.28) was used, on the maxmium principal stress at a punch penetration of (PP = 0.74 mm) when punching a t = 0.120 in. (3.04 mm) thick strip of mild steel.

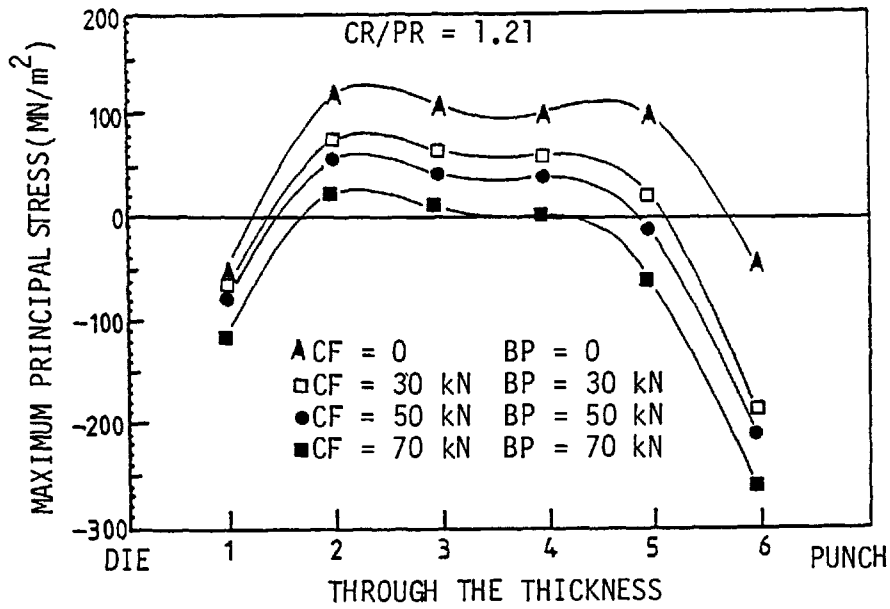

Fig. 5-73. Combined effect of clamping force (CF) and back-load (BP), when a clamp/punch diameter ratio of (CR/PR = 1.21) was used, on the maximum principal stress at a punch penetration of (PP = 0.74 mm) when punching a t = 0.120 in. (3.04 mm) thick strip of mild steel.

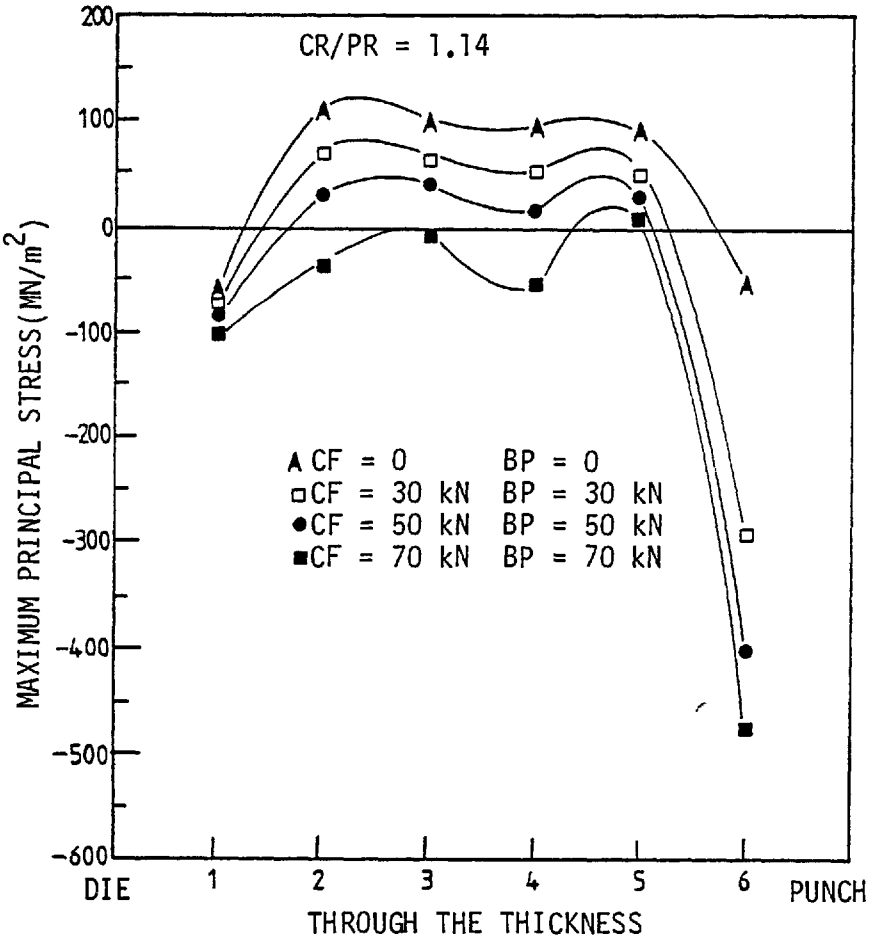

Fig. 5-74. Combined effect of clamping force (CF) and back-load (BP), when a clamp/punch diameter ratio of (CR/PR = 1.14) was used on the maximum principal stress at a punch penetration of (PP = 0.74 mm) when punching a t = 0.120 in. (3.04 mm) thick strip of mild steel.

5.14.6 Effect of clamp diameter

To study the effect of clamp diameter on the hydrostatic component of stress and maximum principal stress along the shear line, some of the results for the three clamp diameters with clamp/punch diameter ratios of CR/PR = 1.14, 1.21 and 1.28 are plotted together.

5.14.6.1 CF ≠ 0, BP = 0

The effect of clamping force on the hydrostatic component of stress along the shear line, when different values of clamp diameter were used (CR/PR = 1.28, 1.21 and 1.14) for three different values of clamping force (CF = 30, 50 and 70 kN) are shown in Figs. 5-75, 5-76 and 5-77. The corresponding results for the maximum principal stress are shown in Figs. 5-78, 5-79 and 5-80.

The blank-holder has a greater effect on the hydrostatic component of stress and maximum principal stress along the shear line as the clamp diameter decreases. The above mentioned parameters are strongly affected by the clamping force near the die-edge but the effect on the values near the punch edge is not considerable and this will be discussed in section 5.16.

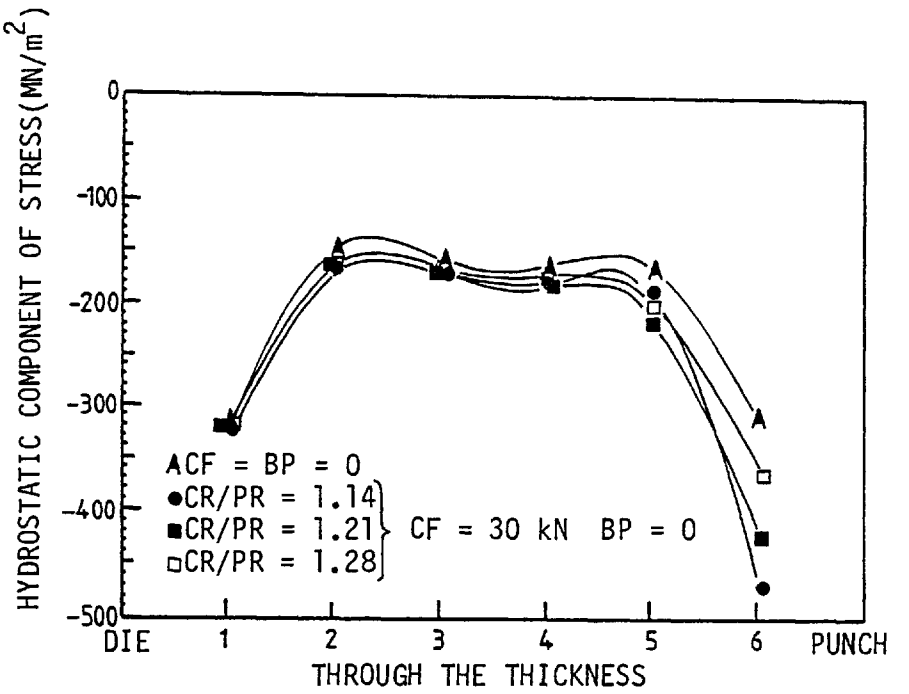

Fig. 5-75. Effect of clamp/punch diameter ratio (CR/PR) on the hydrostatic component of stress for a certain value of clamping force (CF = 30 kN) at a punch penetration of (PP = 0.74 mm) when punching mild steel strips of thickness t = 0.120 in. (3.04 mm) with no back-load present (BP = 0).

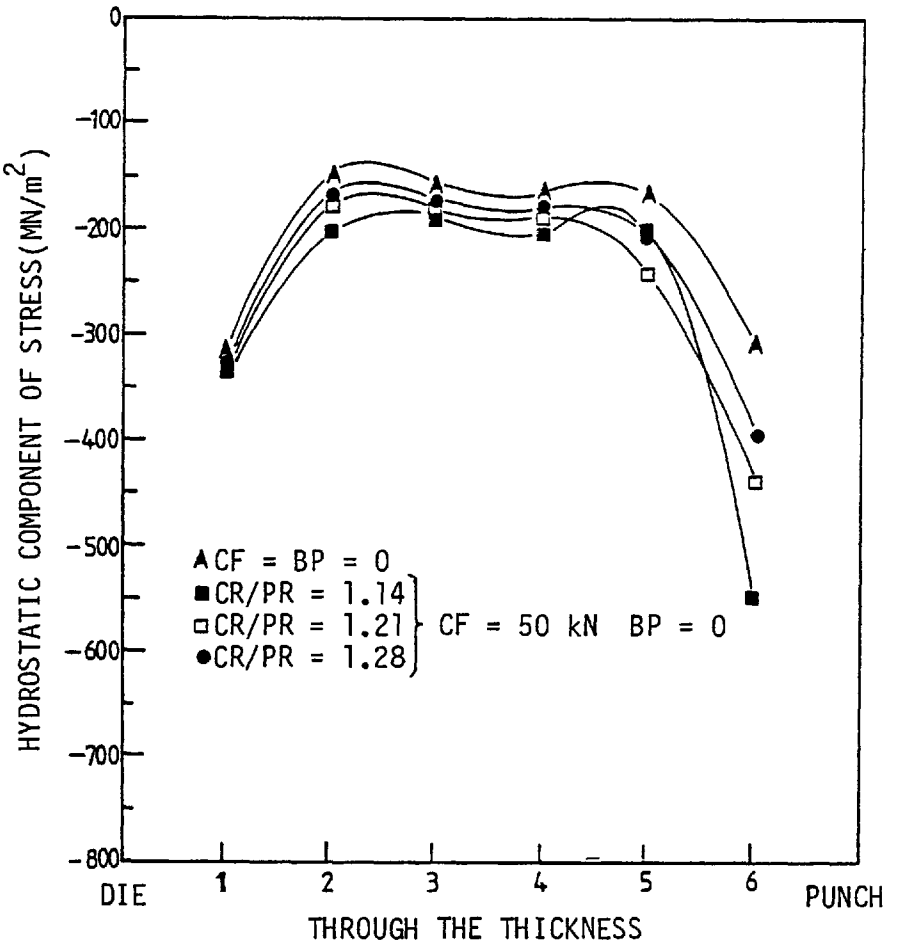

Fig. 5-76. Effect of clamp/punch diameter ratio (CR/PR) on the hydrostatic component of stress for a certain value of clamping force (CF = 50 kN) at a punch penetration of (PP = 0.74 mm) when punching mild steel strips of thickness t = 0.120 in.(3.04 mm) with no back-load present (BP= 0).

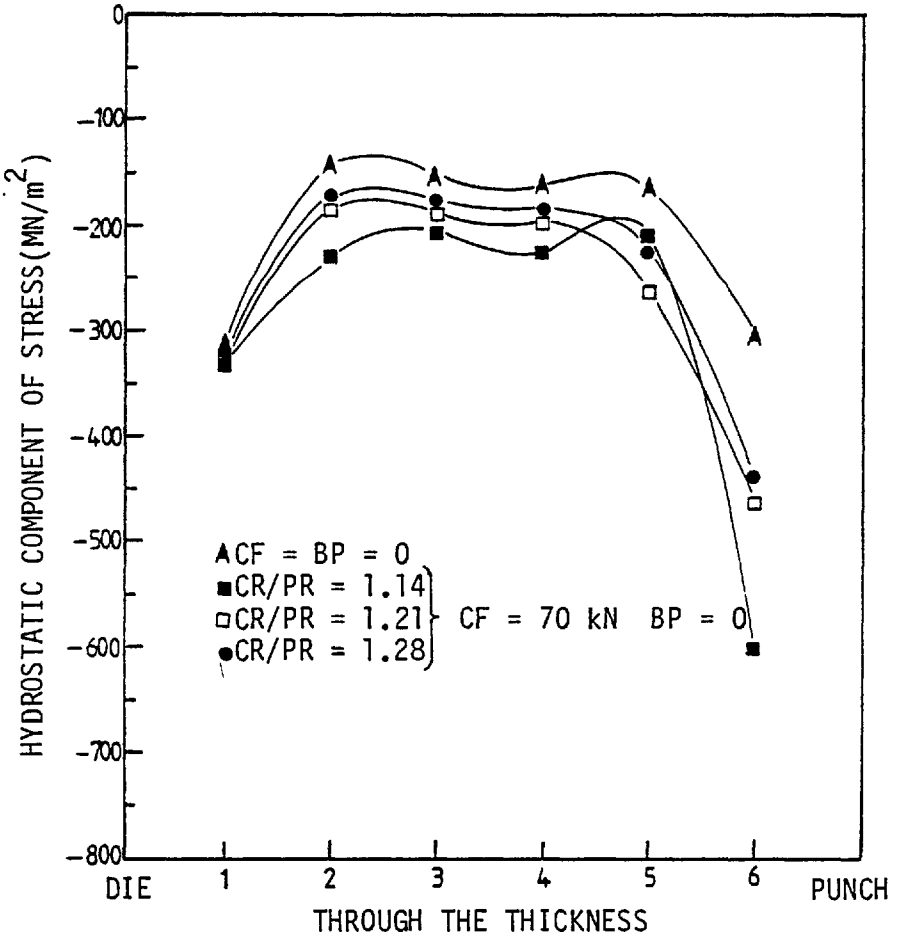

Fig. 5-77. Effect of clamp/punch diameter ratio (CR/PR) on the hydrostatic component of stress for a certain value of clamping force (CF = 70 kN) at a punch penetration of (PP = 0.74 mm) when punching mild steel strips of thickness t = 0.120 in. (3.04 mm) with no back-load present (BP = 0).

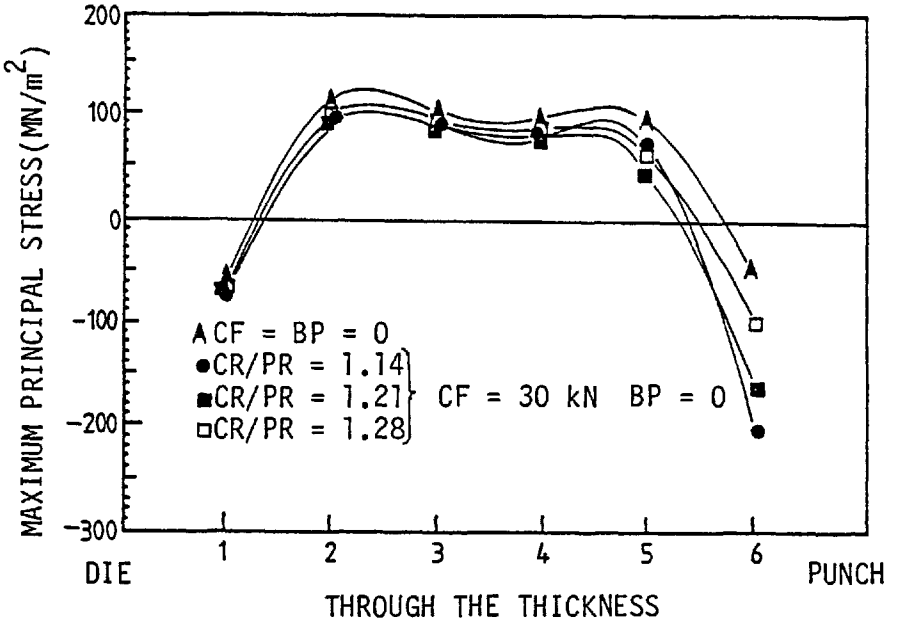

Fig. 5-78. Effect of clamp/punch diameter ratio (CR/PR) on the maximum principal stress for a certain value of clamping force (CF = 30 kN) at a punch penetration of (PP = 0.74 mm) when punching a t = 0.120 in. (3.04 mm) thick strip of mild steel with no back-load present (BP = 0).

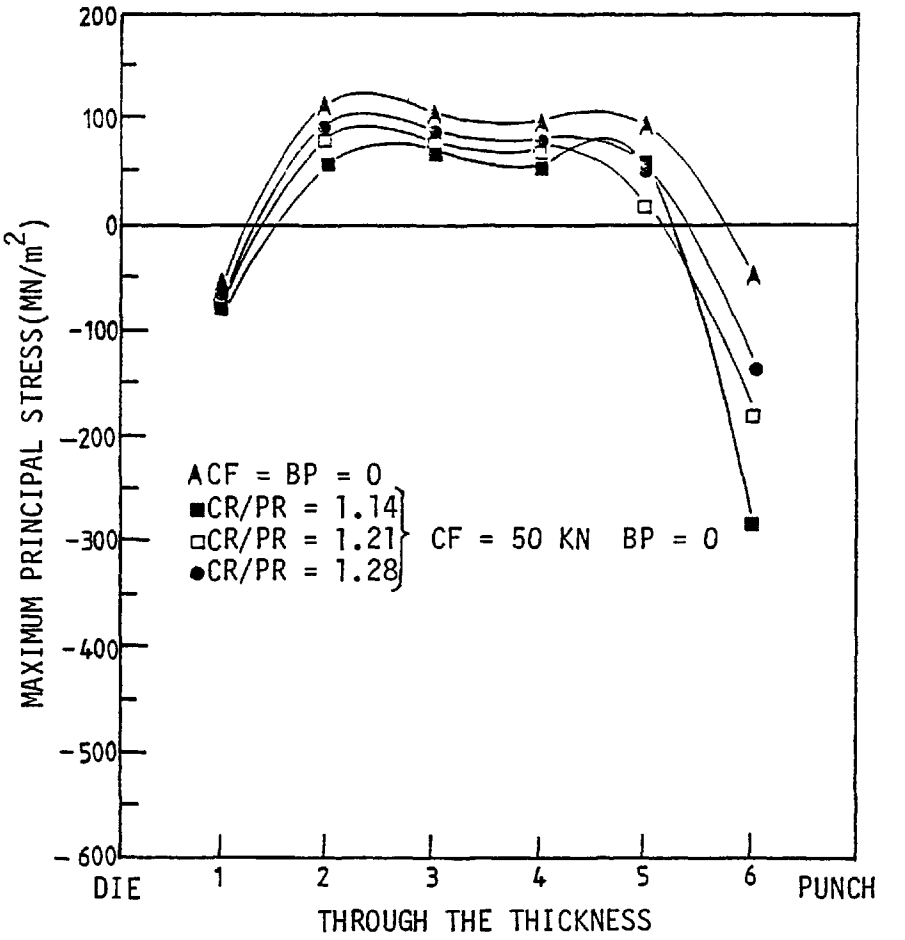

Fig. 5-79. Effect of clamp/punch diameter ratio (CR/PR) on the maximum principal stress for a certain value of clamping force (CF = 50 kN) at a punch penetration of (PP = 0.74 mm) when punching a t = 0.120 in. (3.04 mm) thick strip of mild steel with no back-load present (BP = 0).

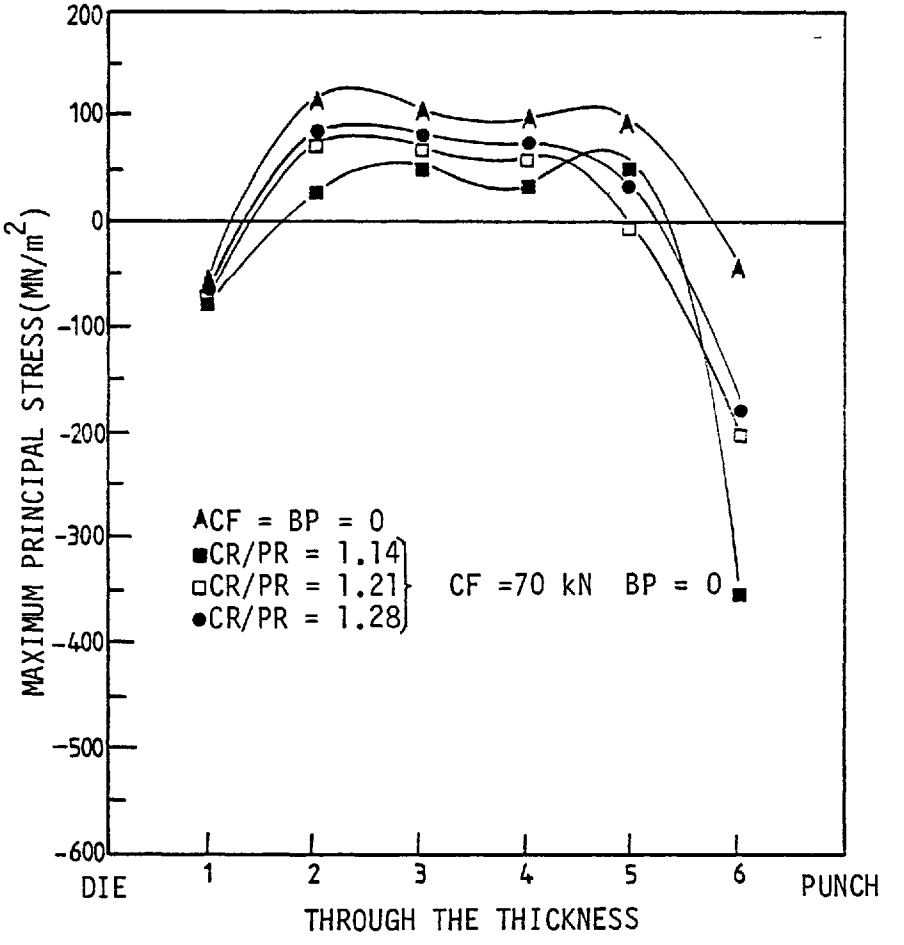

Fig. 5-80. Effect of clamp/punch diameter ratio (CR/PR) on the maximum principal stress for a certain value of clamping force (CF = 70 kN) at a punch penetration of (PP = 0.74 mm) when punching a t = 0.120 in. (3.04 mm) thick strip of mild steel with no back-load present (BP = 0).

5.14.6.2 CF ≠ 0, BP ≠ 0

The effect of clamp diameter (CR/PR = 1.28, 1.21 and 1.14) on the hydrostatic component of stress, when an equal value of back-load is used in addition to the clamping force for three different values of clamping force and back-load (CF = BP = 30, 50 and 70 kN), are shown in Figs. 5-81,5-82 and 5-83 respectively. The corresponding results for different values of clamping force and back-load are similar and therefore only a general description concerning these figures will be given.

The results in this case (CF ≠ 0, BP ≠ 0) are similar to the results previously explained in section 5.14.6.1 (CF ≠0, BP = 0) but an increase in the hydrostatic component of stress in the present case is quite noticeable especially at higher values of clamping force and back-load.

For various clamp diameters the curves follow almost the same trend except in the case of the clamp with minimum diameter (CR/PR = 1.14) in which the hydrostatic component of stress curve in the vicinity of the punch edge yields values smaller than those of the other two corresponding cases, CR/PR = 1.21 and 1.28.

The effect of different values of clamping force and back-load on the maximum principal stress for different clamp diameters was also studied and the corresponding results are given in Figs. 5-84, 5-85 and 5-86. The combined effect of clamping force and back-load on the maximum principal stress is higher when using a medium clamp diameter (CR/PR = 1.21) than when using a clamp with maximum diameter (CR/PR = 1.28), i.e., when it acts closer to the punch edge. For the medium clamp diameter, when applying the maximum values of clamping force and back-load (CF = BP = 70 kN) the maximum principal stress

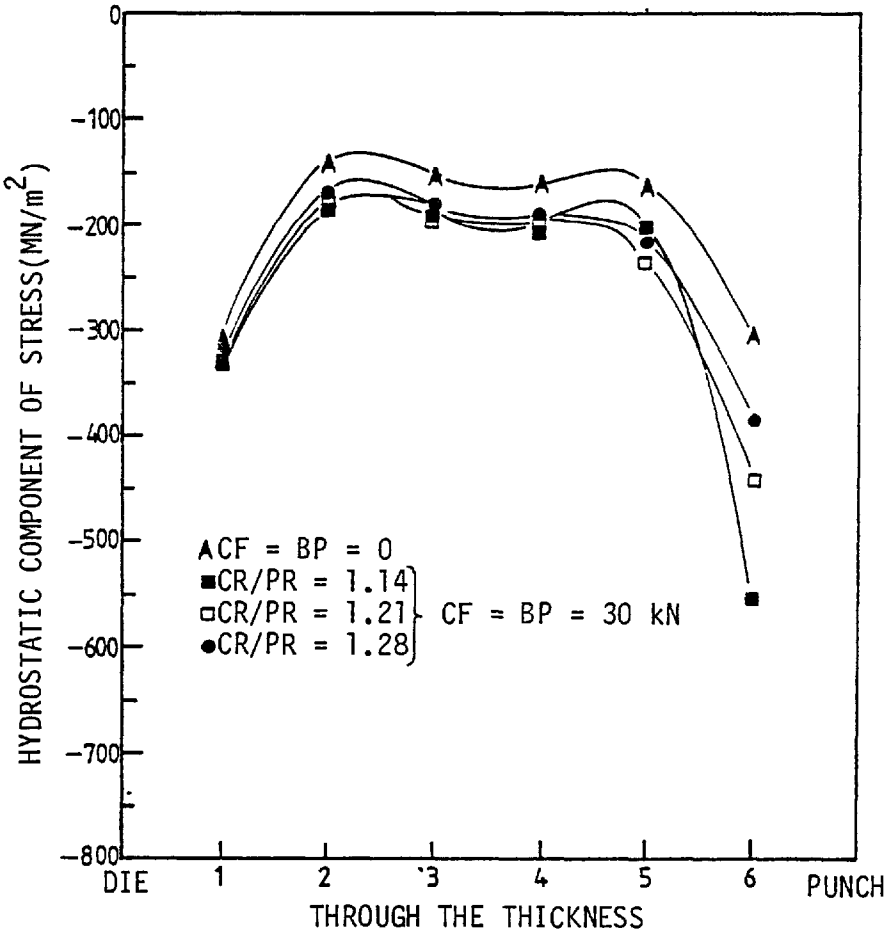

Fig. 5-81. Effect of clamp/punch diameter ratio (CR/PR) on the hydrostatic component of stress for a value of clamping force and back-load equal to 30 kN (CF = BP = 30 kN) at a punch penetration of (PP = 0.74 mm) when punching a t = 0.120 in. (3.04 mm) thick strip of mild steel.

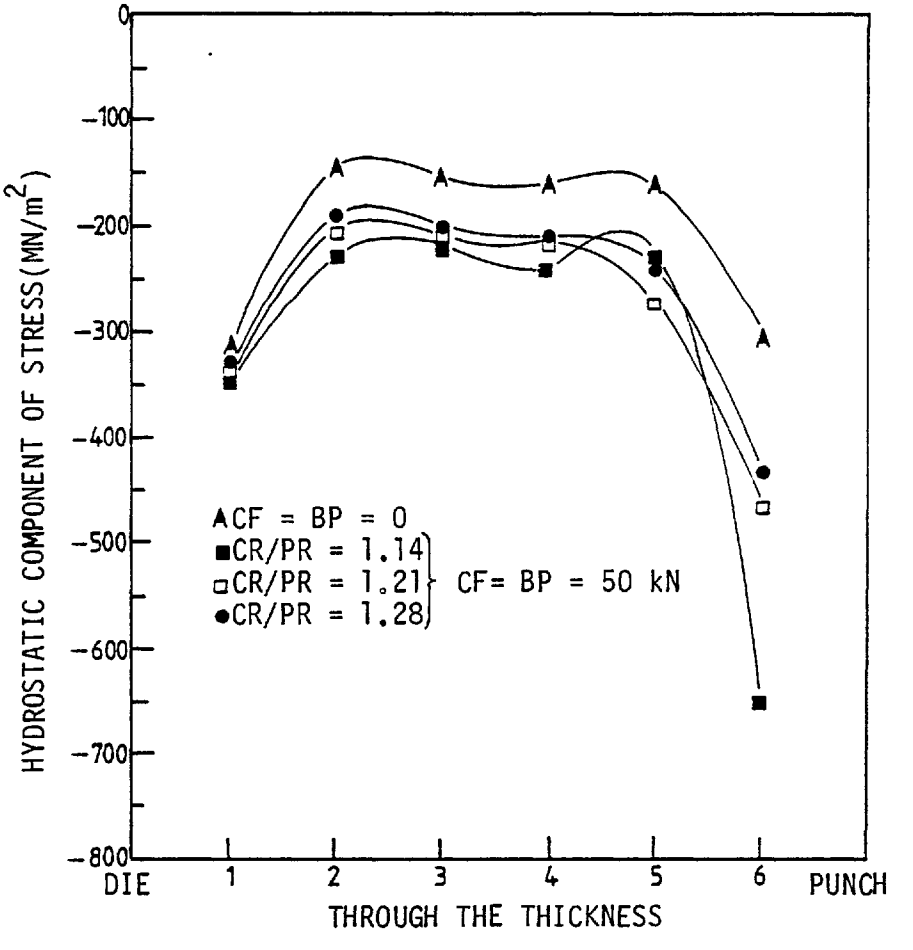

Fig. 5-82. Effect of clamp/punch diameter ratio (CR/PR) on the hydrostatic component of stress for a value of clamping force and back-load equal to (CF = BP = 50 kN) at a punch penetration of (PP = 0.74 mm) when punching a t = 0.120 in. (3.04 mm) thick strip of mild steel.

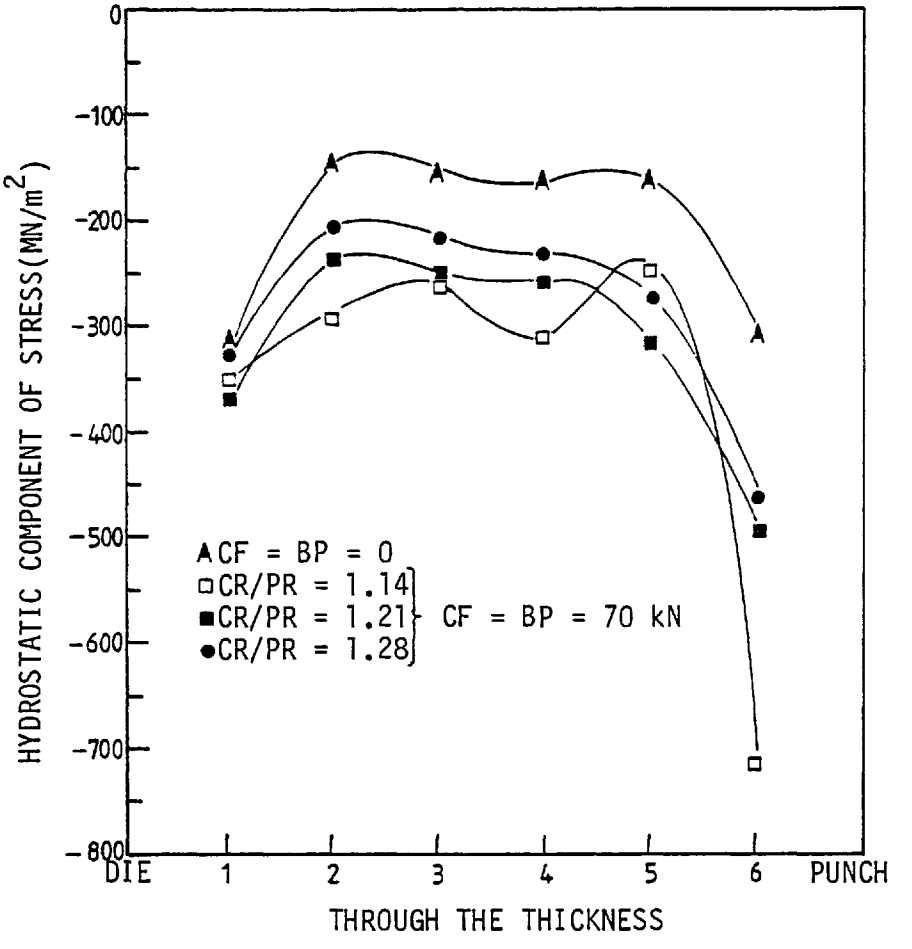

Fig. 5-83. Effect of clamp/punch diameter ratio (CR/PR) on the hydrostatic component of stress for a value of clamping force and back-load equal to (CF = BP =70 kN) at a punch penetration of PP = 0.74 mm when punching a t= 0.120 in. (3.04 mm) thick strip of mild steel.

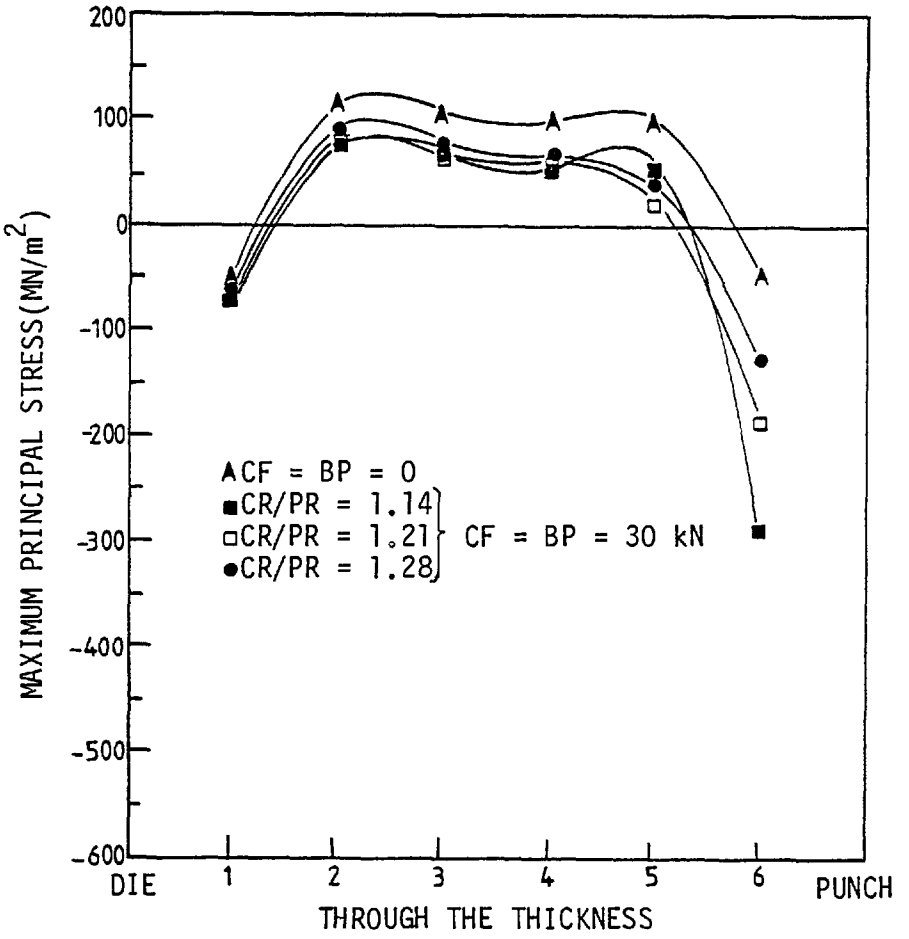

Fig. 5-84. Effect of clamp/punch diameter ratio (CR/PR) on the maximum principal stress for a value of clamping force and back-load equal to (CF = BP = 30 kN) at a punch penetration of PP = 0.74 mm when punching a t = 0.120 in. (3.04 mm) thick strip of mild steel.

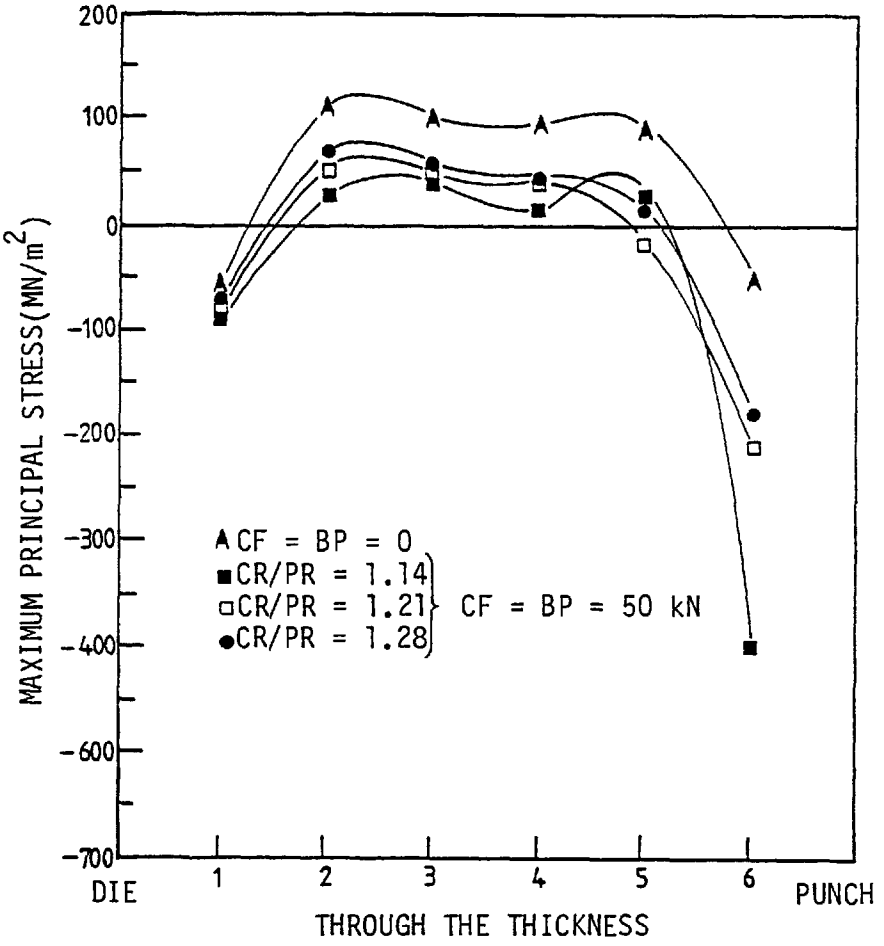

Fig. 5-85. Effect of clamp/punch diameter ratio (CR/PR) on the maximum principal stress for a value of clamping force and back-load equal to (CF = BP = 50 kN) at a punch penetration of PP = 0.74 mm when punching a t = 0.120 in. (3.04 mm) thick strip of mild steel.

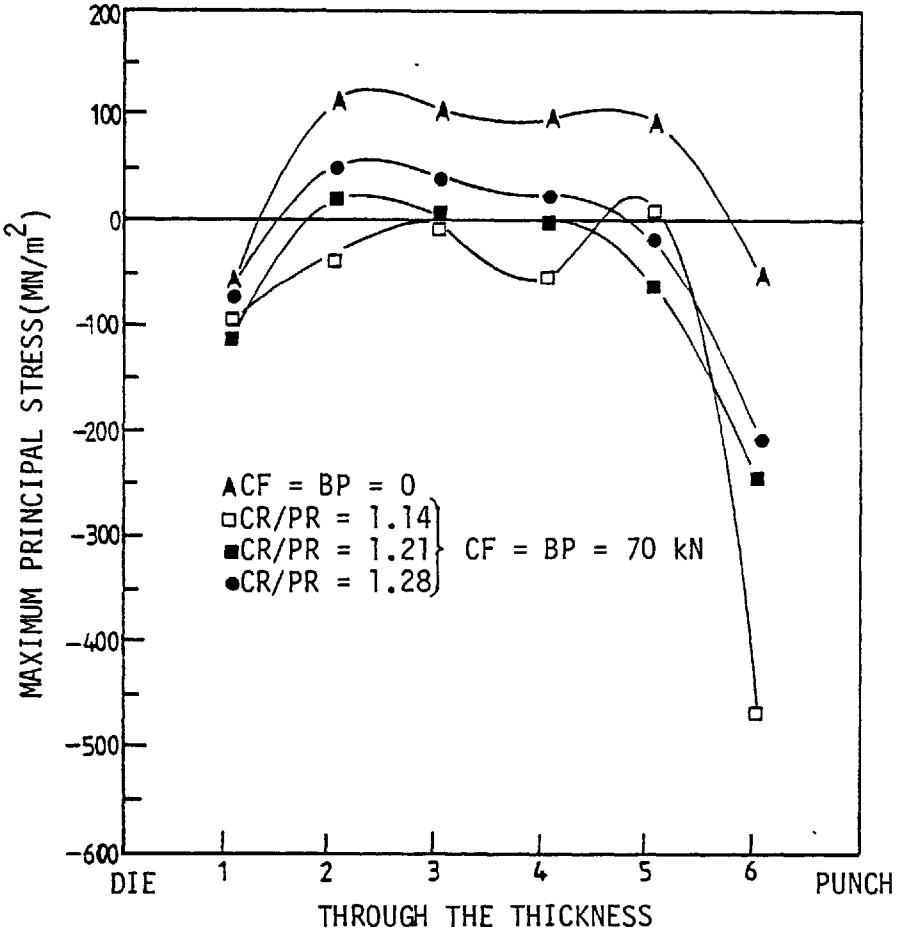

Fig. 5-86. Effect of clamp/punch diameter ratio (CR/PR) on the maximum principal stress for a value of clamping force and back-load equal to (CF = BP = 70 kN) at a punch penetration of PP = 0.74 mm when punching a t = 0.120 in. (3.04 mm) thick strip of mild steel.

at the sampling points along the shear line is mostly zero or negative.

When a minimum clamp diameter is used (CR/PR = 1.14), i.e., closest to the punch edge, the corresponding maximum principal stress curve takes a strong wavy form compared with the other two cases, when medium and maximum clamp diameters are used. In this case the maximum principal stress curve at the die edge yields values smaller than those of the other two cases, but higher values at the punch edge. This must be due to the excessive bending of the specimen which occurs when the clamp acts too close to the punch edge, this will be discussed in section 5.16.

5.14.7 Effect of material thickness on the prevailing hydrostatic component of stress and maximum principal stress in the shearing zone

To study the effect of material thickness on the prevailing hydrostatic component of stress and maximum principal stress in the shearing zone, a comparison of the corresponding results when blanking three different thicknesses of mild steel, t = 0.078, 0.101 and 0.120 in. (1.93, 2.56 and 3.04mm) is now made. As the load-displacement characteristics during the blanking operation depend on the material thickness, the comparison of the corresponding results must be made either at an equal value of punch penetration or at an equal value of blanking force. The comparison of the results obviously cannot be made at a blanking load greater than maximum blanking load obtained when punching the thinnest material, t = 0.078 in. (1.93 mm). The dependence of the blanking load on punch penetration was previously indicated in section 5.8 and it was shown that for a certain amount of punch penetration thicker materials would require higher blanking forces than thinner materials.

The comparison of the corresponding results for three different thicknesses of mild steel, t = 0.078, 0.101 and 0.120 in. (1.93, 2.56 and 3.04 mm), for the hydrostatic component of stress and maximum principal stress at a punch penetration pf 0.60 mm are shown in Figs. 5-87 and 5-88 respectively. This punch penetration corresponds to that predicted by the theoretical method at a blanking load equal to the maximum blanking load obtained experimentally, when punching mild steel strips of thickness t = 0.078 in. (1.93 mm).

In the results for the hydrostatic component of stress and maximum principal stress the trend of the curves for the two thicknesses of

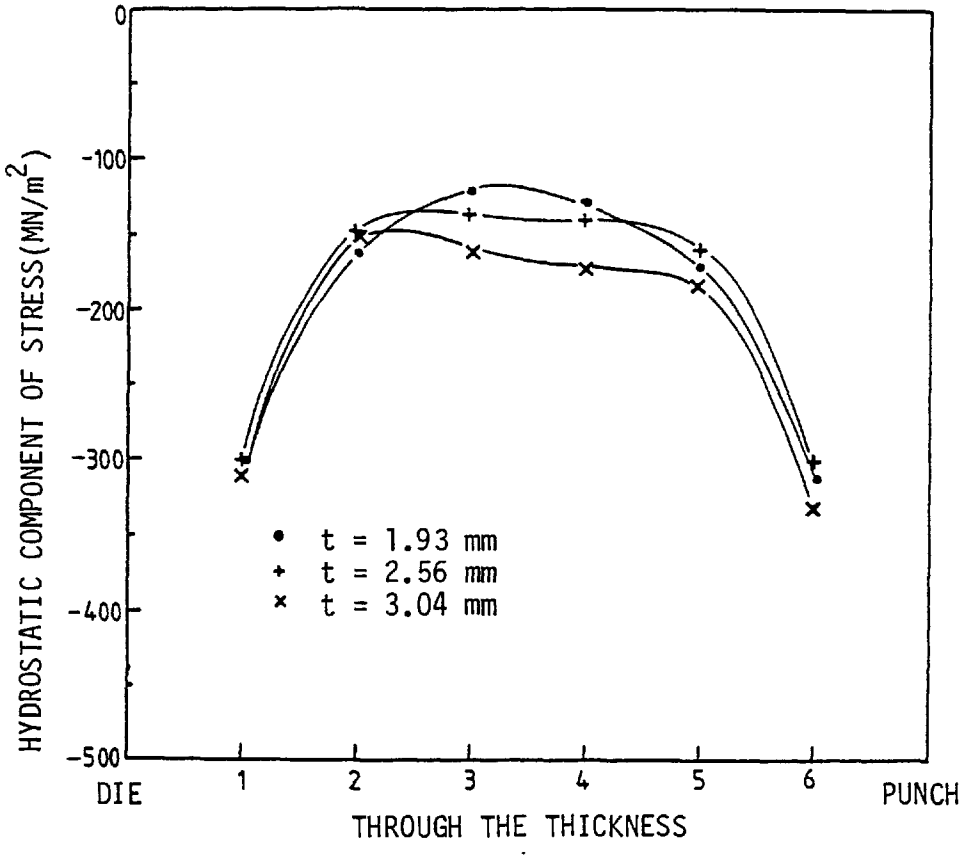

Fig. 5-87. Effect of material thickness (t) on the prevailing hydrostatic component of stress in the shearing zone, at a punch penetration of (PP = 0.60 mm) when no clamping force and back-load were used (CF = BP = 0).

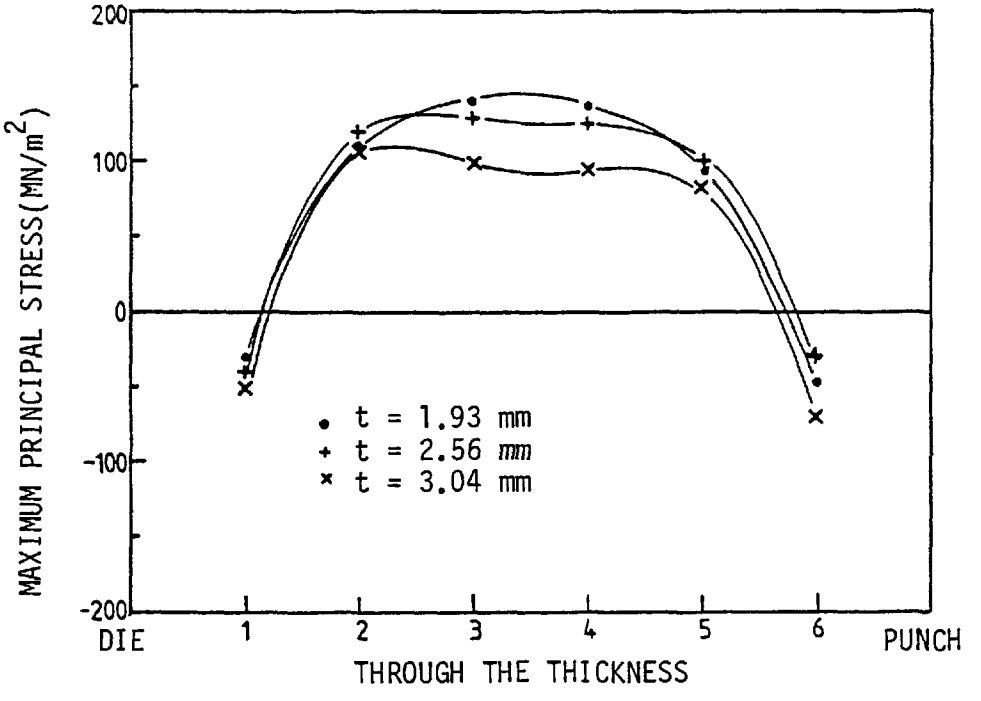

Fig. 5-88. Effect of material thickness (t) on the prevailing maximum principal stress in the shearing zone, at a punch penetration of (PP = 0.60 mm) when no clamping force and back-load were used (CF = BP = 0).

0.101 and 0.120 in. (2.56 and 3.04 mm) are similar, whereas the corresponding curves for the thinnest material (t = 0.078 in. (1.93 mm)) indicate a different pattern. From Figs. 5-87 and 5-88 it can be concluded that in general, at an equal value of punch penetration the hydrostatic component of stress in the shearing zone for thicker materials is more compressive and the corresponding maximum principal stress is less tensile than in the thinner materials. This indicates that for thinner material the tensile stresses will reach their critical level at a smaller amount of punch penetration and thus fracture will occur earlier.

The corresponding results for the hydrostatic component of stress and maximum principal stress at an equal value of blanking force (BF = 46 kN) are presented in Figs. 5-89 and 5-90 respectively. This blanking force corresponds to the maximum blanking load obtained experimentally for the thinnest material (t = 0.078 in. (1.93 mm)). The trend of the two curves corresponding to hydrostatic component of stress and maximum principal stress, are almost the same.

The results indicate that for the same value of blanking force, as the material thickness decreases, the hydrostatic component of stress prevailing in the shearing zone becomes more compressive whilst the corresponding maximum principal stress becomes more tensile. This again indicates that under equal values of blanking force the tensile maximum principal stress in the thinner material will reach its critical level earlier than in thicker materials and thus fracture will occur at a smaller amount of blanking force.

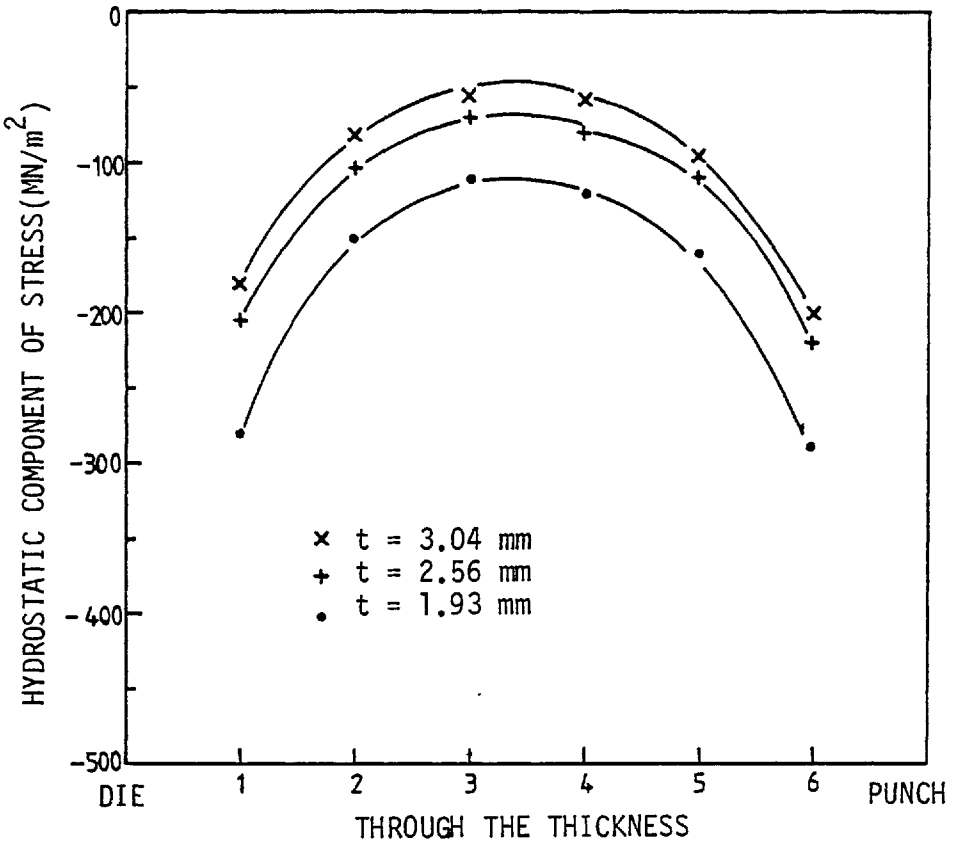

Fig. 5-89. Effect of material thickness on the hydrostatic component of stress prevailing in the shearing zone, at a blanking force of (BF = 46 kN) when no clamping force and back-load were used (CF = BP = 0).

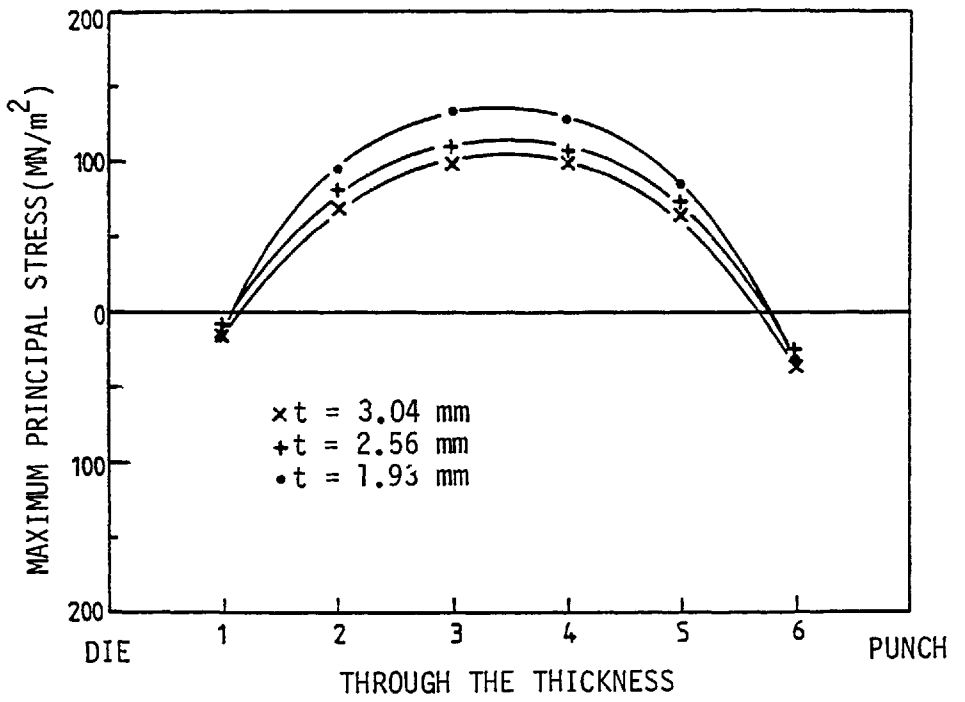

Fig. 5-90. Effect of material thickness on the maximum principal stress in the shearing zone, at a blanking force of (BF = 46 kN) when no clamping force and back-load were used (CF = BP = 0).

5.14.8 Effect of material thickness on the hyrostatic component of stress and maximum principal stress in the shearing zone

It has been previously discussed, sections 5.14.1 to 5.14.6, that clamping force, back-load and clamp diameter are the main variables which need studying in the fine blanking analysis of a material. It was shown that any increase in the clamping force and back-load improves the state of stress in the shearing zone by producing a more compressive hydrostatic component of stress and less tensile maximum principal stress. The only parameter which yielded an optimum value to obtain the most desirable state of stress in the shearing zone was the clamp diameter. It is thus considered that the clamp diameter is the only parameter which requires further study in analyzing the fine blanking of different material thicknesses. To demonstrate the effect of clamp diameter on the prevailing state of stress in the shearing zone when blanking 3.04 mm thick material has already been investigated. Now for a different thickness of mild steel (t = 0.078 in. (1.93 mm)) the corresponding results for the hydrostatic component of stress and maximum principal stress when using a 70 kN clamping force (this being the maximum clamping force used previously to clamp the specimen during blanking mild steel strips of thickness t = 0.120 in. (3.04 mm) are shown in Figs. 5-91 and 5-92 respectively. These results correspond to a punch penetration of PP = 0.60 mm, which is the punch-penetration predicted by the theoretical method at a blanking load equal to the maximum blanking load obtained experimentally when punching mild steel strips of thickness t = 0.078 in. (1.93mm).

From Figs. 5-91 and 5-92 it can be concluded that here again, similar to the previous case when blanking mild steel strips of thickness

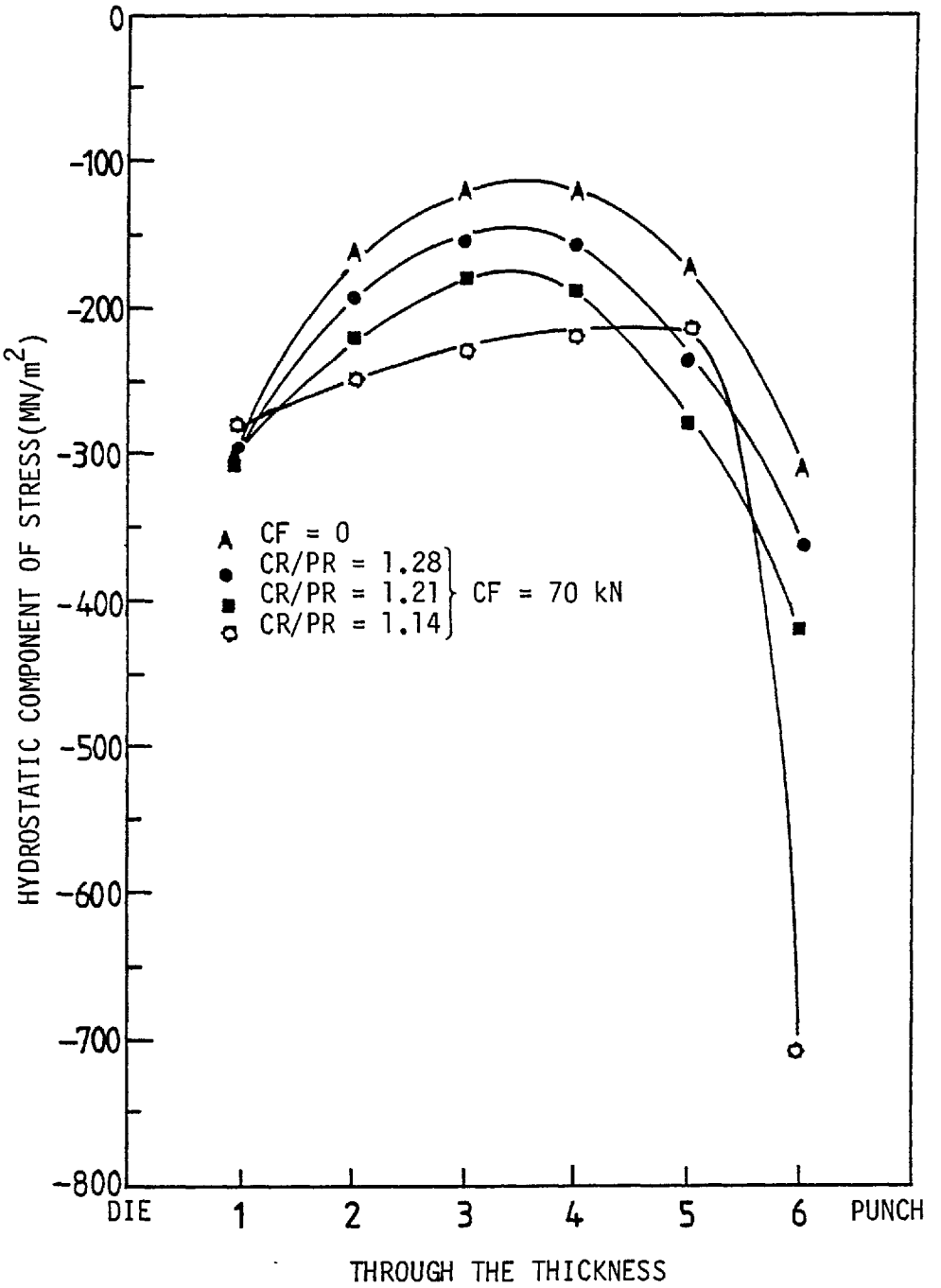

Fig. 5-91. Effect of clamp diameter on the prevailing hydrostatic component of stress in the shearing zone when blanking a t = 0.078 in. (1.93 mm) thick strip of mild steel in the presence of a 70 kN clamping force (CF = 70 kN) at a punch penetration of PP = 0.60 mm with no back-load present (BP = 0).

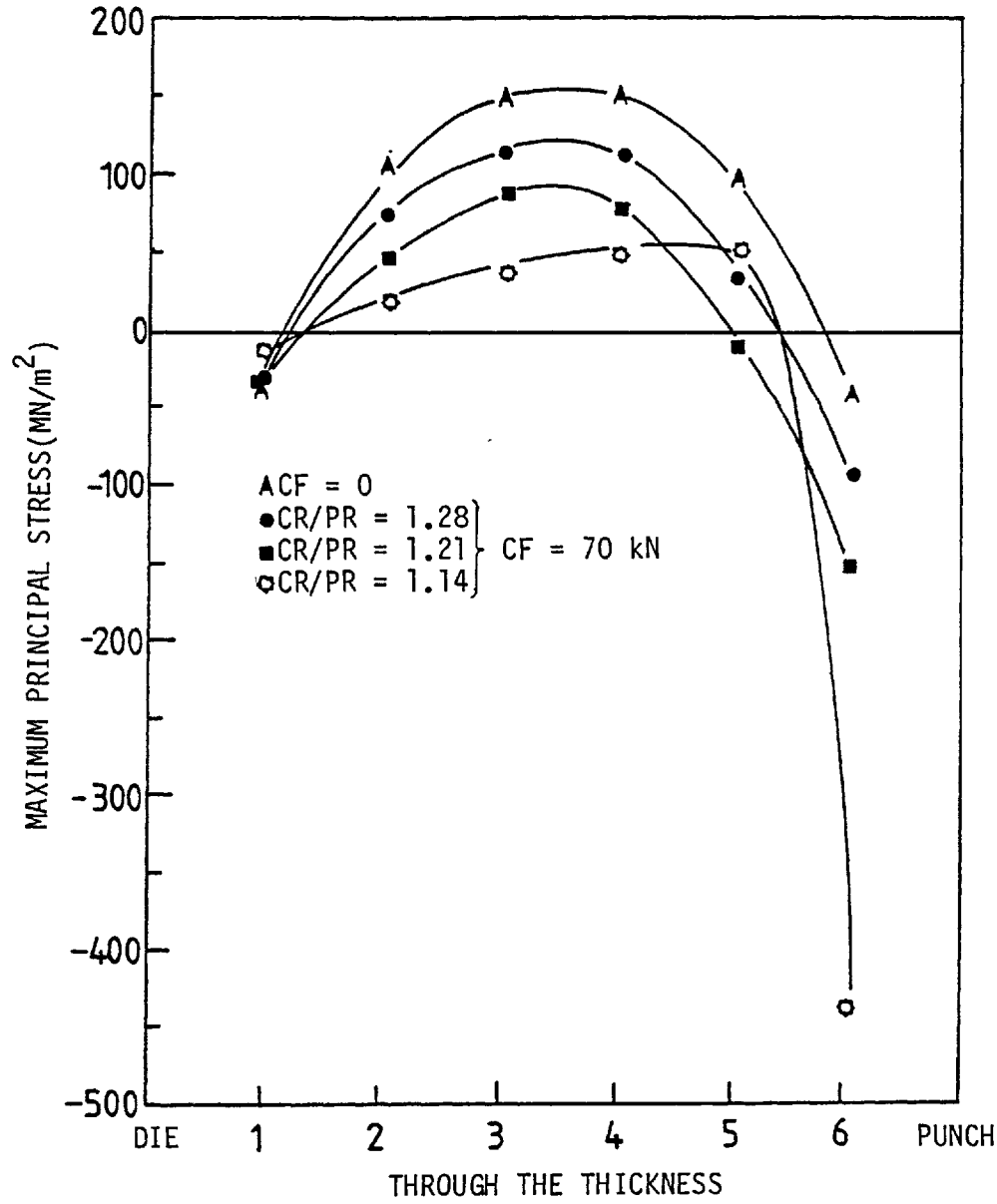

Fig. 5-92. Effect of clamp diameter on the prevailing maximum principal stress in the shearing zone when blanking a t = 0.078 in. (1.93 mm) thick strip of mild steel in the presence of a 70 kN clamping force (CF = 70 kN) at a punch penetration of PP = 0.60 mm with no back-load present (BP = 0).

t = 0.120 in. (3.04 mm), by decreasing the clamp diameter the hydrostatic component of stress becomes more compressive and the corresponding maximum principal stress becomes less tensile. This favourable change no longer continues for the smallest clamp diameter, when an opposite trend is indicated in Figs. 5-91 and 5-92 near the punch and die edges, clearly the most critical points, where fracture is initiated. This change in the trend of the hydrostatic component of stress and maximum principal stress curves indicates that for a material thickness of t = 0.078 in. (1.93 mm), as in the previous case of t = 0.120 in. (3.04 mm) an optimum clamp diameter exists when, for a particular value of the clamping force, the hydrostatic component of stress in the shearing zone is at its highest level and is accompanied by the lowest value of the maximum principal stress.

5.14.9 Effect of clearance between the punch and die on the prevailing hydrostatic component of stress and maximum principal stress in the shearing zone.

The load/displacement characteristics in blanking predicted by the theoretical method depends on the clearance between the punch and die, Fig. 5-93. To compare the state of stress in the shearing zone

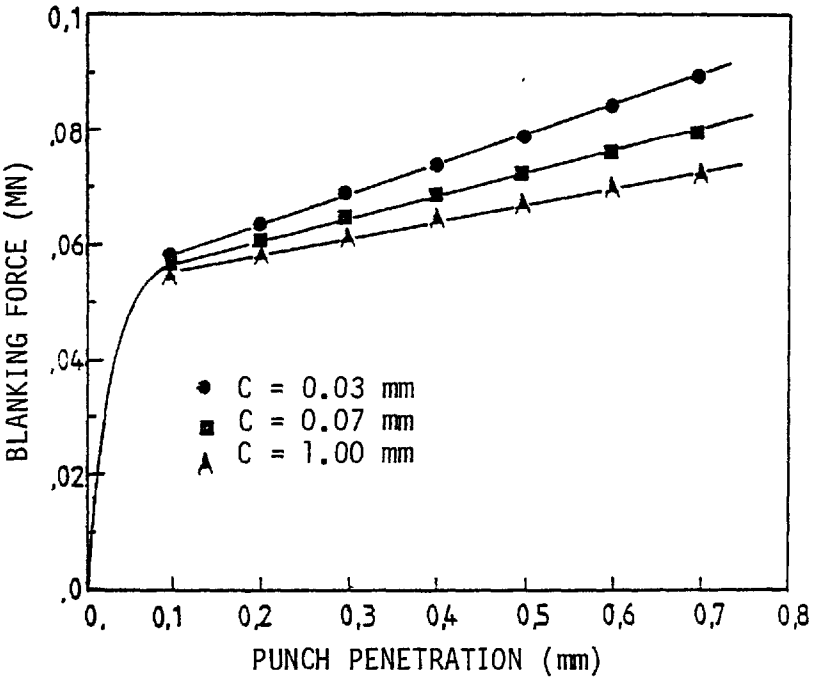

Fig. 5-93. Effect of the clearance between the punch and die(c) on the load/displacement characteristics when punching mild steel strips of thickness t = 0.120 in. (3.04 mm).

for different values of clearance, a comparison of the results could be made either at an equal value of blanking force or an equal value of punch penetration. The hydrostatic component of stress and maximum principal stress results at a blanking force of BF = 74 kN are presented in Figs. 5-94 and 5-95 respectively. This load corresponds to the maximum blanking load obtained experimentally for mild steel strips

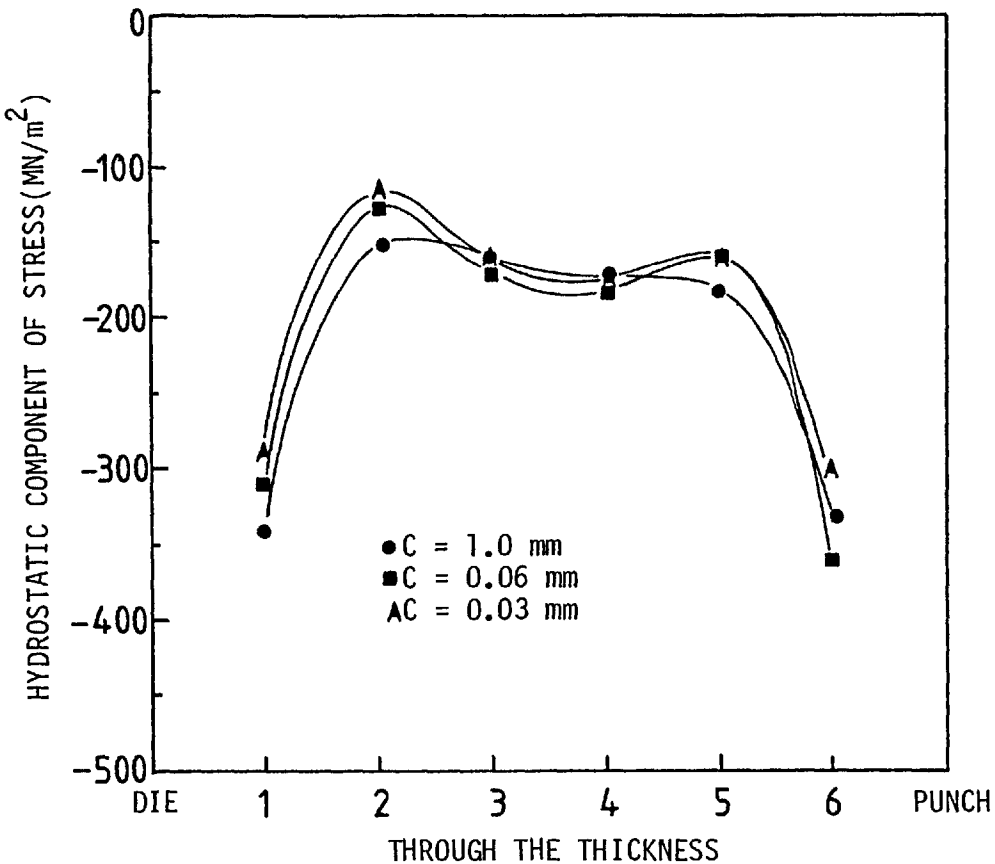

Fig. 5-94. Effect of clearance between the punch and die (C) on the prevailing hydrostatic component of stress in the shearing zone when punching a 0.120 in. (3.04 mm) thick strip of mild steel at a blanking force of BF = 74 kN

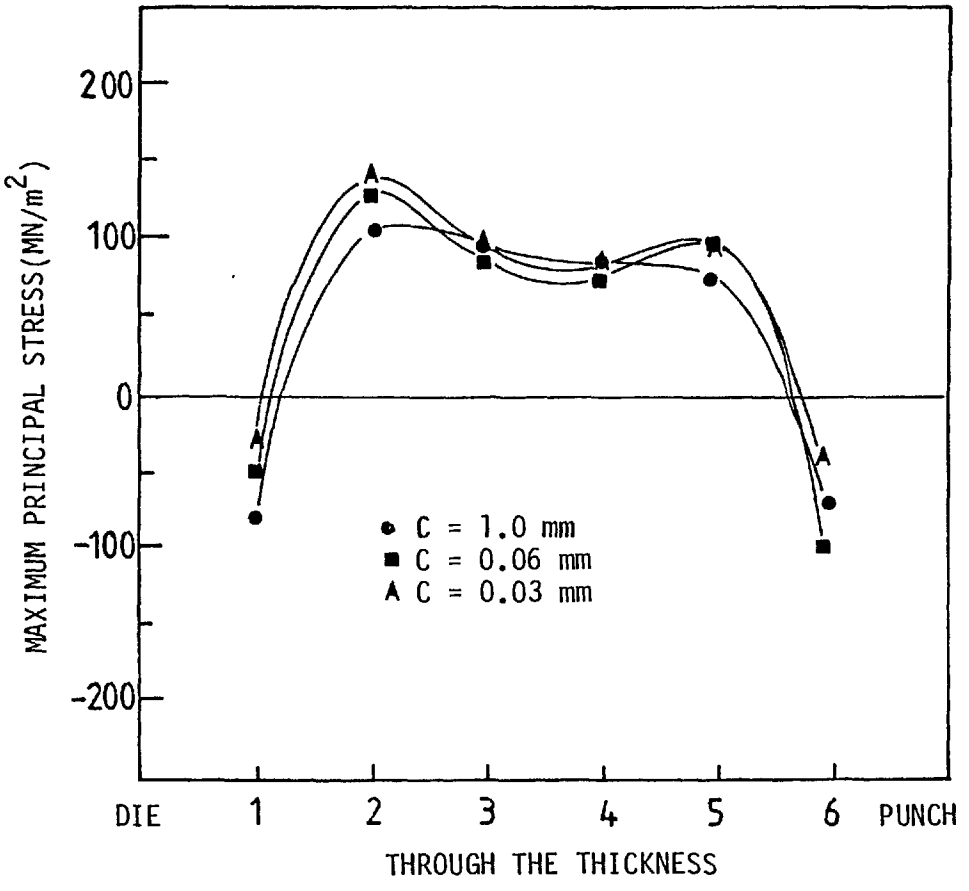

Fig. 5-95. Effect of the clearance between the punch and die (C) on the maximum principal stress in the shearing zone when punching a 0.120 in. (3.04 mm) thick strip of mild steel at a blanking force of BF = 74 kN.

of thickness t = 0.120 in. (3.04 mm) with a punch die/clearance of C = 1 mm. The curves follow almost the same trend and in both illustrations the difference between results for each of the three curves is small. This indicates that at a given value of blanking force the corresponding results for the hydrostatic component of stress and maximum principal stress in the shearing zone for different values of punch/die clearance are almost the same.

The corresponding results at an equal value of punch penetration PP = 0.74 mm are shown in Figs. 5-96 and 5-97 respectively. This punch penetration corresponds to that predicted by the theoretical method, when using a punch-die clearance of C = 1 mm, at a load equal to the maximum blanking load obtained by experiment. As the clearance between the punch and die decreases the hydrostatic component of stress in the shearing zone also decreases(becoming more compressive) and is accompanied by a decrease in the corresponding maximum principal stresses. These results are in agreement with the experimental results obtained by Tilsley and Howard (23), in which they showed that in the case of thin materials the decrease in the clearance between the punch and die causes an increase in the bright surface finish of the blank.

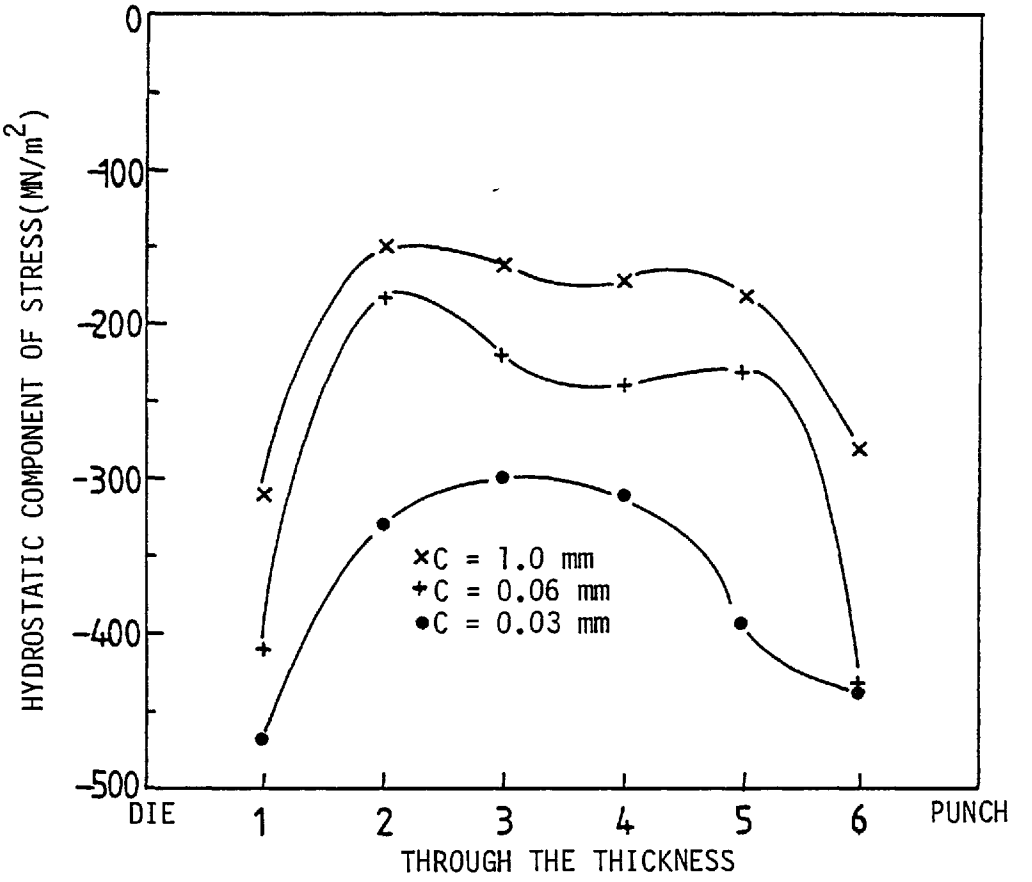

Fig. 5-96. Effect of the clearance between the punch and die on the prevailing hydrostatic component of stress in the shearing zone when punching mild steel strips of thickness t = 0.120 in. (3.04 mm) at a punch penetration of PP = 0.74 mm.

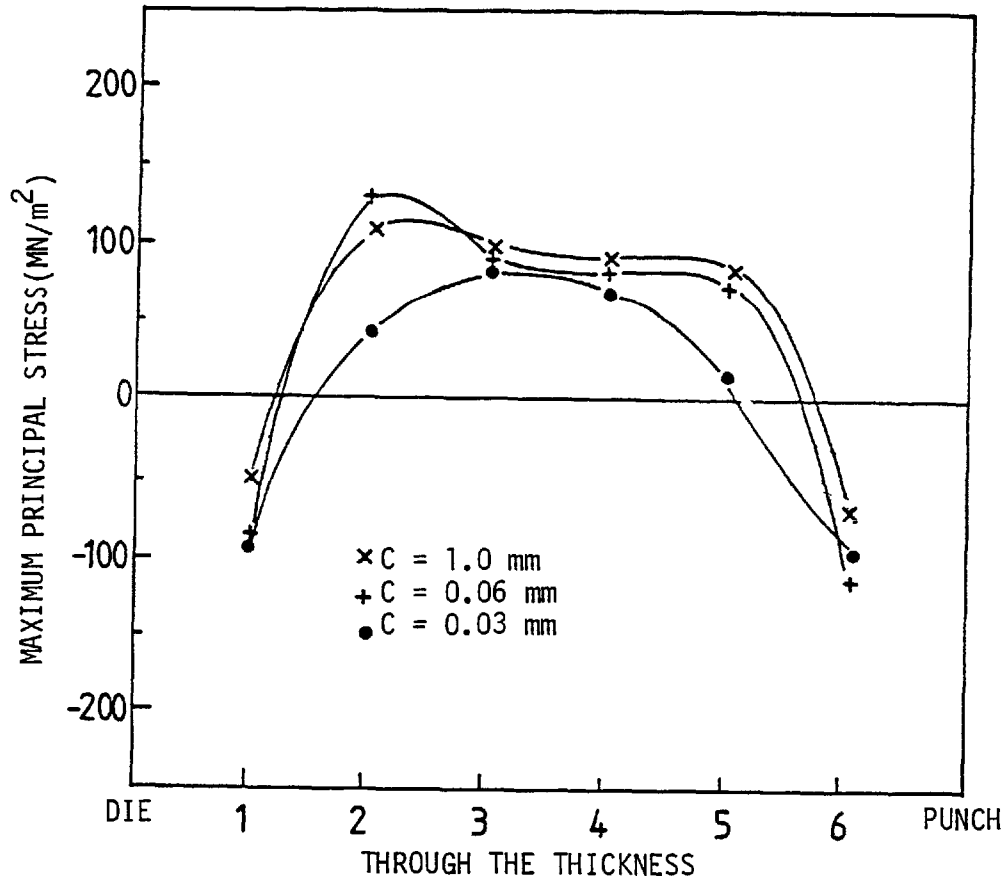

Fig. 5-97. Effect of the clearance between the punch and die on the prevailing maximum principal stress in the shearing zone when punching mild steel strips of thickness t = 0. 120 in. (3.04 mm) at a punch penetration of PP = 0.74 mm.

5.15 Stress contours in the deforming material

In this section, general information concerning the effect of clamping force, back-load and clamp diameter on the state of stress within the specimen is provided. The stress contours are considered to be the best illustrative approach in presenting a wide perspective of information within the deforming material. Here the radial, hoop and axial stress together with the equivalent stress and hydrostatic component of stress contours will be given. Although the exact values of the hydrostatic component of stress along the shear line were previously presented in section 5.14, the corresponding interpolated contours have the advantage of providing information over the whole specimen. The stress contours, together with the information discussed in the previous section, collectively provide explanation for the change of fracture from fibrous to pure shear.

The stress contours are drawn for a mild steel strip of thickness t = 0.120 in. (3.04 mm) at a punch penetration of PP = 0.74 mm which corresponds to the theoretical punch penetration at the maximum experimental blanking load. Two clamp diameters, CR/PR = 1.14 and 1.28, and a typical value of (70 kN) for clamping force and back-load will be considered.

To ease the calculation of the stress contours the two sections A and B(indicated in the illustration over-leaf) were not considered, the calculations were carried out for section C only. In describing the stress contours, reference will be made to the material inside the line of action of the blank-holder, shown by the shaded area, which will hereafter be referred to as the 'confined material'.

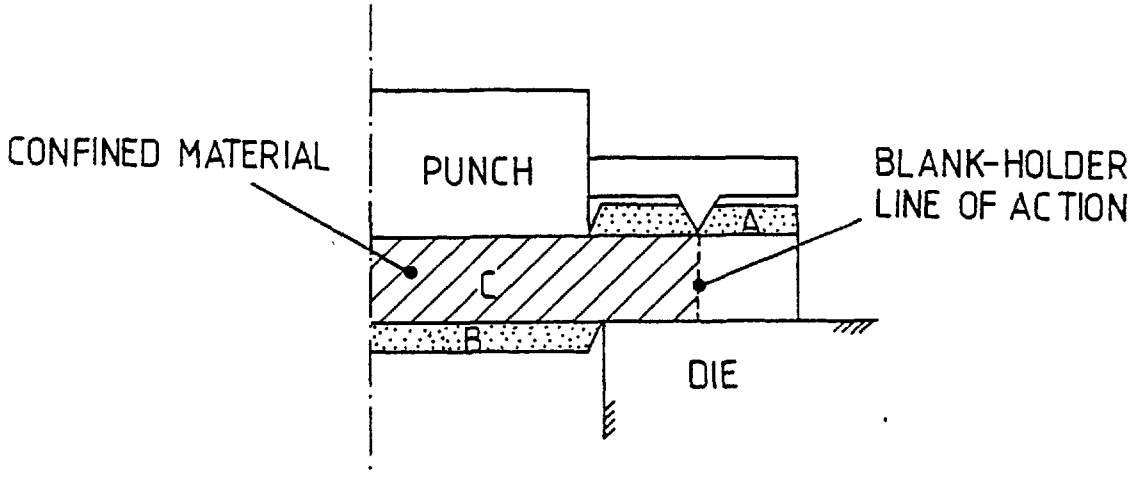

Before presenting the stress contours three dimensional views of the equivalent stress distributions for three different cases of (CF = BP = 0, PP = 0.74 mm), (CF = 70 kN, BP = 0, CR/PR = 1.28) and (CF = BP = 70 kN, PP = 0.74 mm, CR/PR = 1.14) over the specimen cross section are given,Figs. 5-98, 5-99 and 5-100 which illustrate clearly the general pattern of the stress contours presented in this section. For simplicity the results are presented over the original mesh pattern and it should be noted that the graphs have different scales.

Fig. 5-98 shows the equivalent stress at different nodal points of the mesh pattern when the specimen is being conventionally blanked (CF = BP = 0) which has the highest values near the shear line indicating the severity of the stresses in this region, while the specimen nearer the axis of symmetry is stressed very little.

The equivalent stress distribution is shown in Fig. 5-99 for the case when only a (70 kN) clamping force is applied with clamp/punch diameter ratio of (CR/PR = 1.28). It has the highest values in the vicinity of the blank-holder, while the material nearer the axis of symmetry is low stressed, which must be due to the compression of the material by the blank-holder. The stresses are relatively high at the die/specimen interface, where the blanking load is transferred

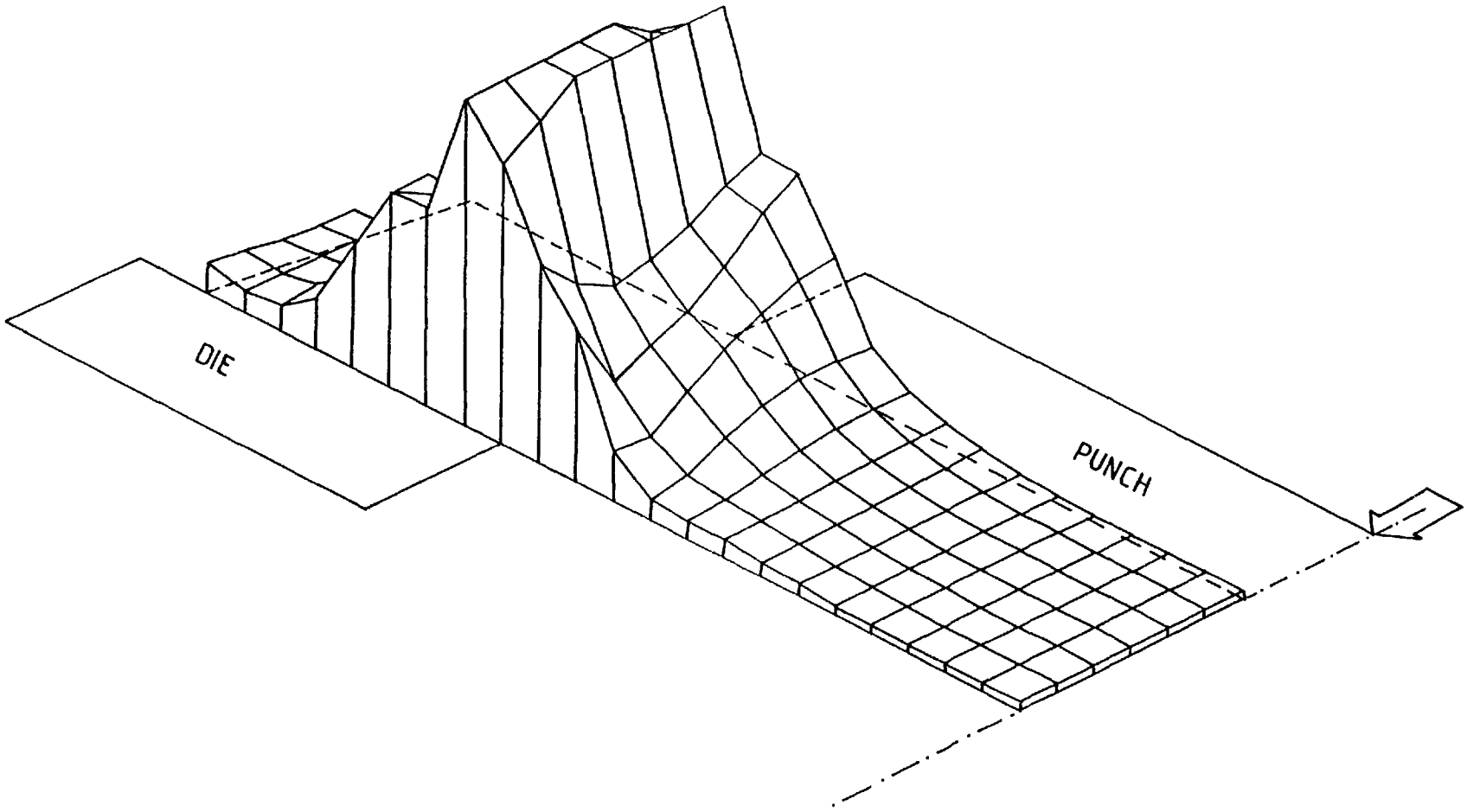

Fig. 5-98. Equivalent stress distribution over the specimen cross section when zero clamping force and back-load are used (CF = BP = 0) at a punch penetration of (PP = 0.74 mm).

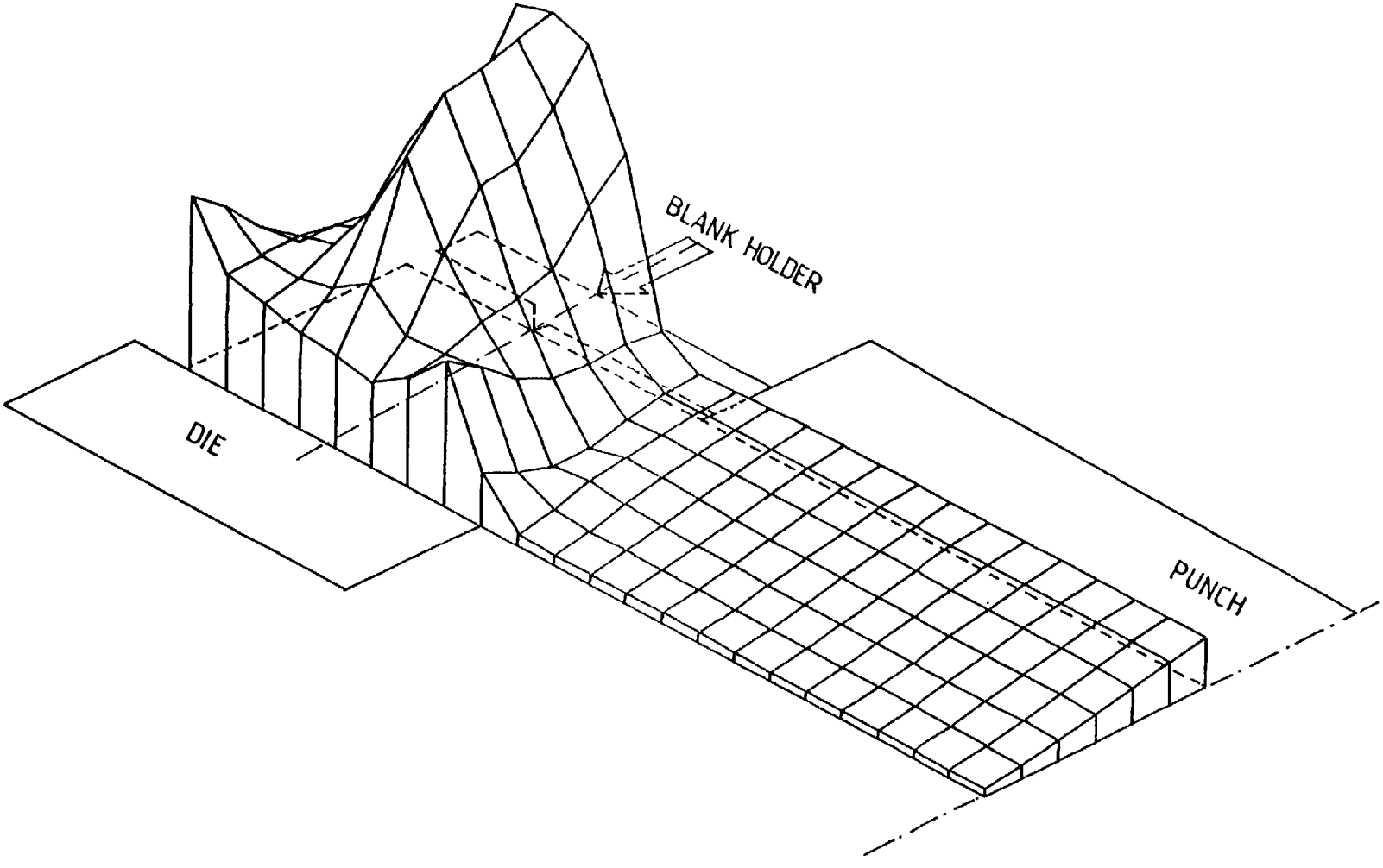

Fig. 5-99. Equivalent stress distribution over the specimen cross section when the specimen is being indented by a 70 kN clamping force (CF = 70 kN) at a clamp/punch diameter ratio of (CR/PR = 1.28) with no back-load present (BP = 0).

to the die face.

Fig.5-100 indicates the equivalent stress distribution at a punch penetration of (PP = 0.74 mm) when a clamping force together with a back-load of (CF = BP = 70 kN) are used, the clamp is acting at a clamp/punch diameter ratio of (CR/PR = 1.14). The equivalent stresses are particularly high around the shear line and along the die face. Towards the axis of symmetry higher stresses are developed in comparison with the previous case shown in Fig. 5-98, which must be due to further compression of the material between the punch and counter-punch.

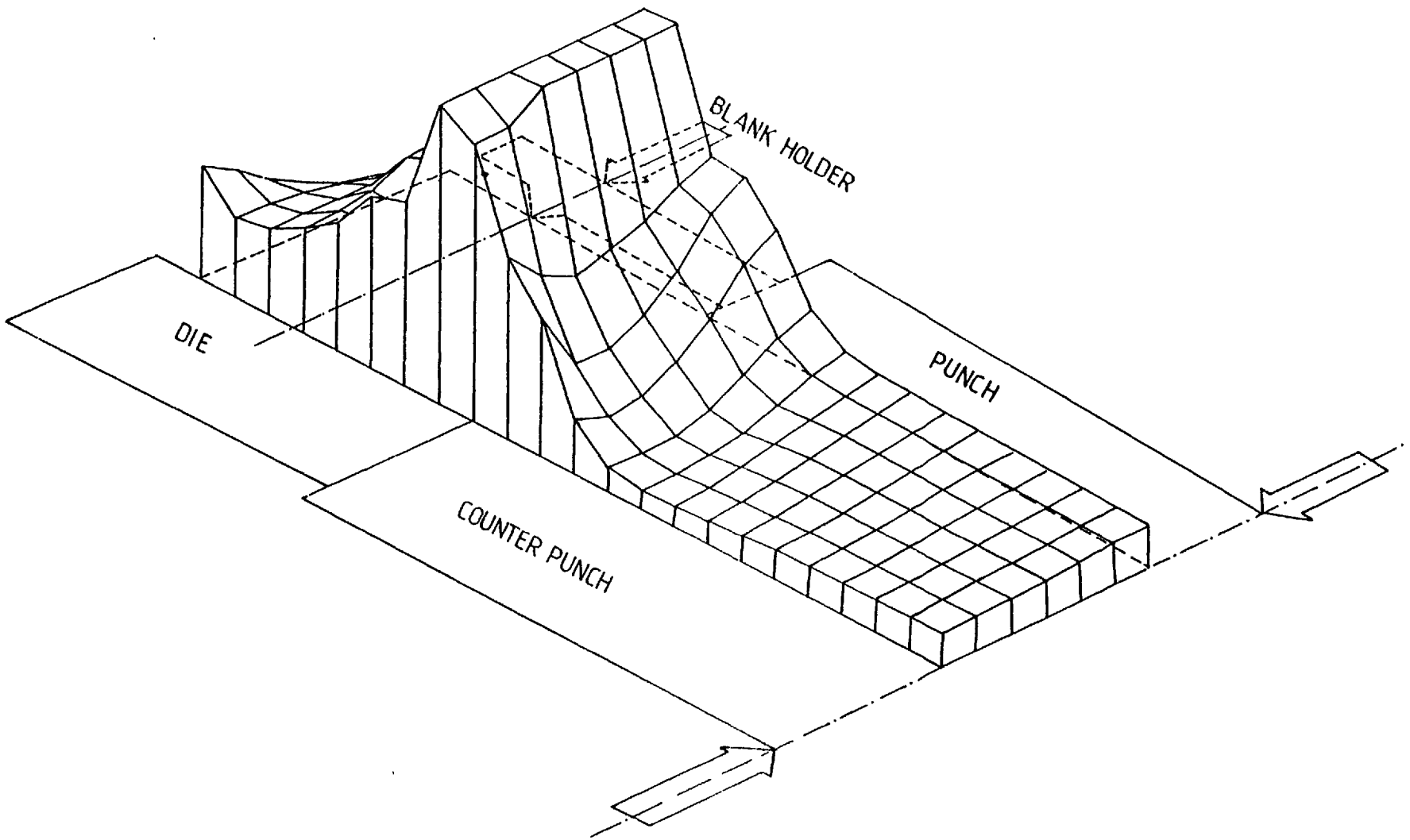

Fig. 5-100. Equivalent stress distribution over the specimen cross section when a 70 kN value of clamping force and back-load are used (CF = BP = 70 kN) at a punch penetration of (PP = 0.74 mm) with a clamp/punch diameter ratio of CR/PR = 1.28.

5.15.1 Equivalent stress contours

The equivalent stress contours for different boundary conditions are shown in Figs. 5-101 to 5-107. Fig. 5-101 shows the equivalent stress contours in blanking without clamping force and back-load. Stresses develop mostly around the shear line and their value increases towards it. The uniaxial yield stress of the material of 200 MN/m^2 is reached only in the vicinity of the shear line, indicating that the plastic zone is confined to a very narrow region. The material towards the axis of symmetry and around the specimen edge are stressed very little.

The equivalent stress contours with values of more than 200 MN/m^2 are nearly parallel with the shear line,indicating a uniform plastic deformaton of the material in that region. Fig. 5-102 shows the equivalent stress contours for a clamp indentation at a clamping force equal to 70 kN, when the blank-holder with maximum diameter was used(CR/PR = 1.28). As could be expected only the material in the vicinity of the blank-holder is stressed heavily. The stress contours with high values are mostly located around the blank-holder itslf and only a few of them, with low values, run through the whole thickness of the specimen. The stress field within the material towards the axis of symmetry is not affected by the stress zone developed by the clamp and is stressed very little. The stress contours with a value of 200 MN/m^2, which corresponds to the uniaxial yield stress of the material, only embraces a small region around the blank-holder, indicating the yielded region. It is important to note that, in this case, when the clamp is acting away from the punch edge, the effect on the stress field around the shear line is small.

The equivalent stress contours at a punch penetration of (pp = 0.74 mm),

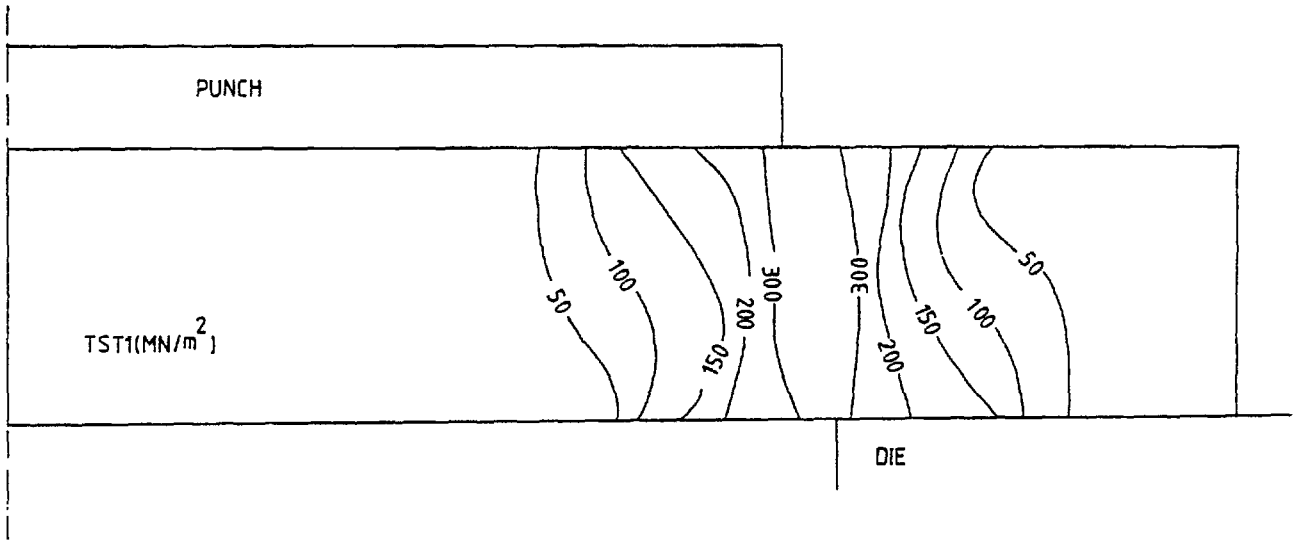

Fig. 5-101. Equivalent stress contours when blanking without clamping force and back-load (CF = BP = 0).

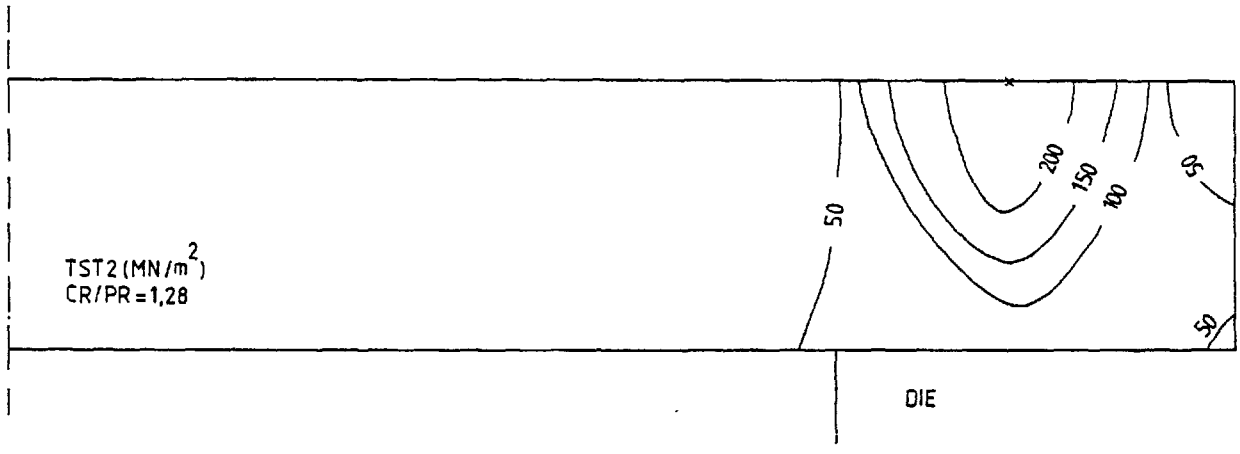

Fig. 5-102. Equivalent stress contours when indenting the specimen with a blank-holder with clamp/punch diameter ratio of CR/PR = 1.28 at a clamping force of CF = 70 kN and no back-load present BP = 0, PP = 0.

with a clamping force away from the punch edge(CR/PR = 1.28), are shown in Fig. 5-103. A stress contour with a value of 50 MN/m^2 runs from the bottom part of the specimen to the axis of symmetry, contrary to simple blanking when the material in this region is stressed very little. This must be due to the additional stresses caused by the blank-holder through blocking the outward flow of the material. Comparing Figs. 5-103 and 5-101, with the addition of a clamping force away from the punch there is no change in the stress pattern near the die edge, but an increase in the concentration of the stress contours between the clamp and punch is noticeable.

When using a back-load in addition to the clamping force during the blanking operation the stress contour pattern on the right hand side of the shear line, Fig. 5-104, is nearly the same as when blanking with only the clamping force present, Fig. 5-103. A noticeable difference between the two cases is a higher concentration of the stress contours of the left hand side of the shear line when back-load was used. This must be due to the displacement of the material away from the axis of symmetry caused by the compression of the specimen between the punch and counter-punch.

The equivalent stress contours when the specimen is being indented by a blank-holder only, at a clamping force of 70 kN, with minimum diameter (CR/PR = 1.14), is shown in Fig. 5-105. In this case the stressed region runs deeper into the material than the corresponding case shown in Fig. 5-102, where the clamp with maximum diameter was used(CR/PR = 1.28). Comparing Figs. 5-105 and 5-102, when using a blank-holder with minimum diameter, a somewhat larger plastic zone forms around the blank-holder and a higher concentration of stress develops around the die-edge. The stress contours start from the

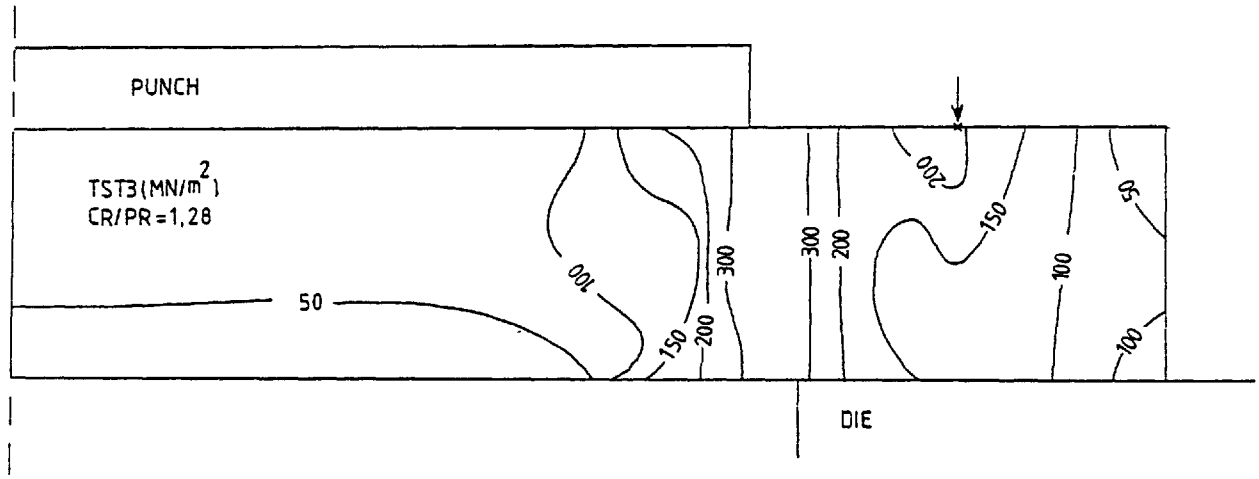

Fig.5-103. Equivalent stress contours during blanking when a 70 kN clamping force (CF = 70 kN) was used at a clamp/punch diameter ratio of (CR/PR = 1.28).

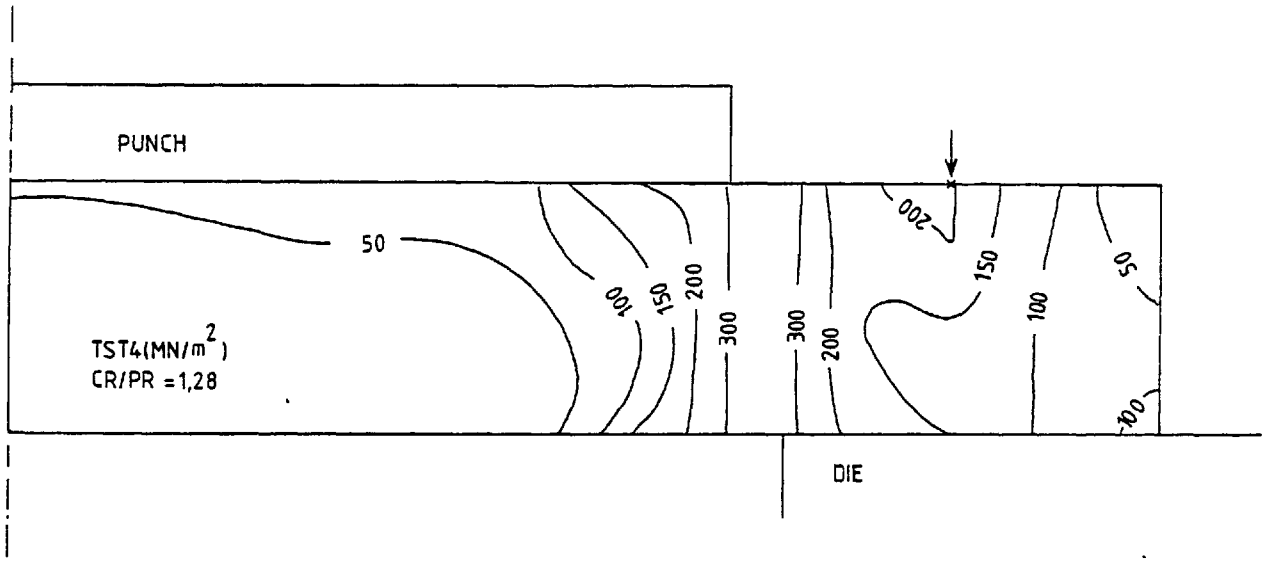

Fig. 5-104. Equivalent stress contours during blanking when a 70 kN back-load (BP = 70 kN) and a 70 kN clamping force (CF = 70 kN) at a clamp/punch diameter ratio of (CR/PR = 1.28) were used.

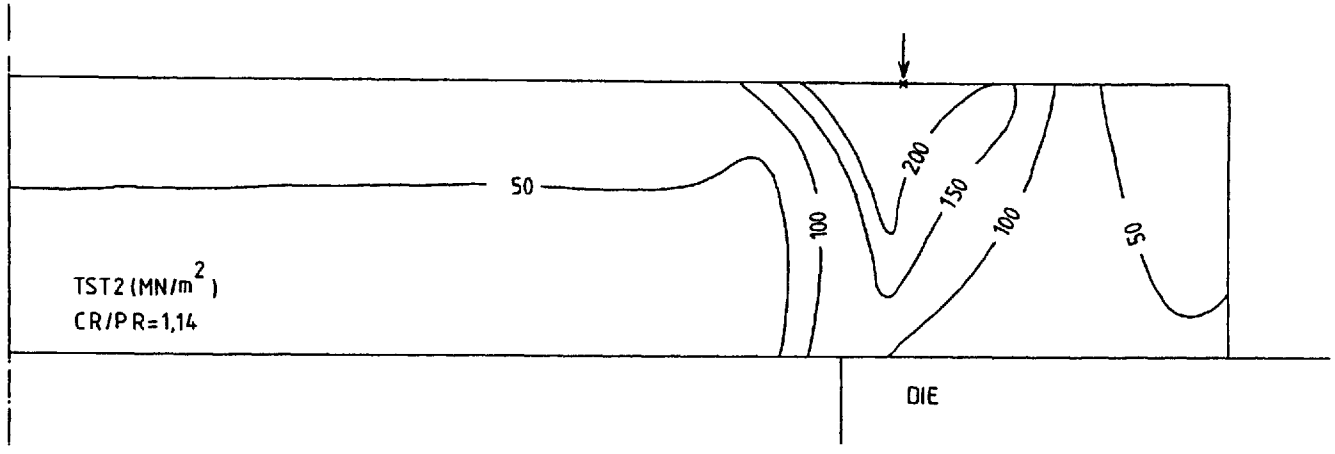

Fig. 5-105. Equivalent stress contours when indenting the specimen with a 70 kN clamping force (CF = 70 kN) at a clamp/punch diameter ratio of (CR/PR = 1.14).

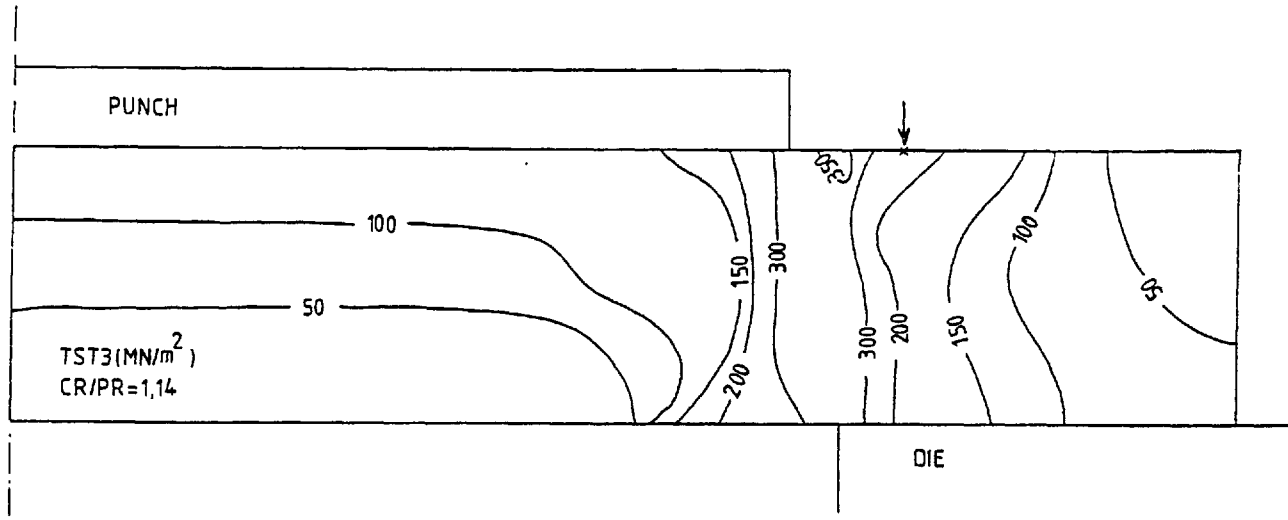

Fig. 5-106. Equivalent stress contours during blanking when a CF = 70 kN clamping force with a clamp/punch diameter ratio of (CR/PR = 1.14) were used.

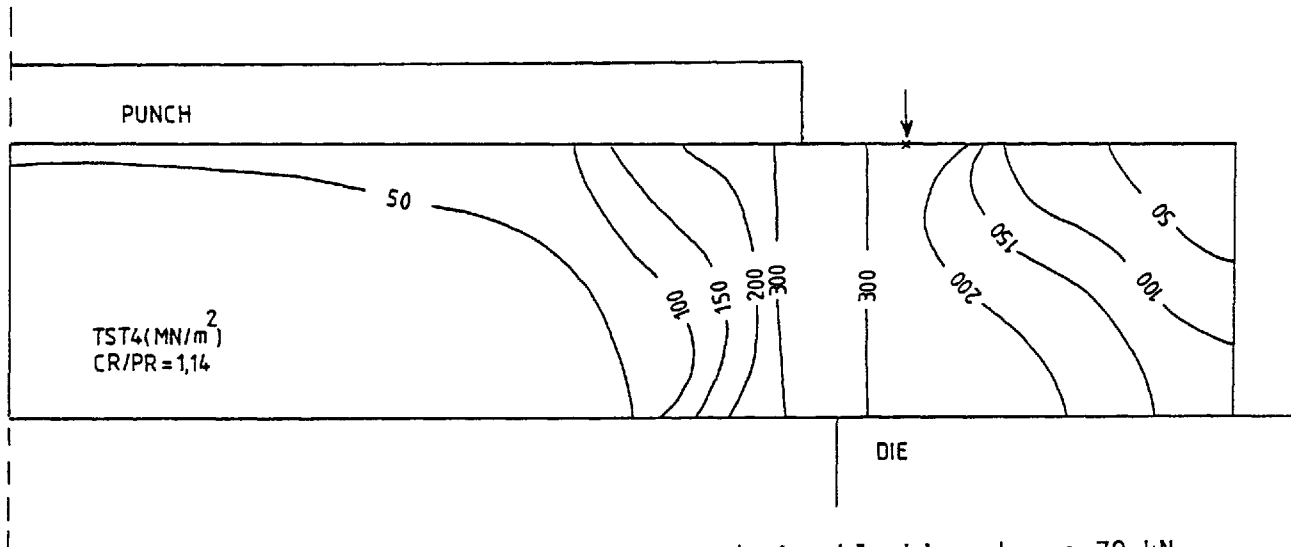

Fig. 5-107. Equivalent stress contours during blanking when a 70 kN back-load (BP = 70 kN) and a 70 kN clamping force (CF = 70 kN) with a clamp/punch diameter ratio of (CR/PR = 1.14) were used.

vicinity of the blank-holder and are directed towards the die-edge. As the clamp diameter decreases, thus producing a smaller volume of the confined material, the stress contours become more concentrated on the left hand side of the blank-holder and a stress contour of 50 MN/m^2 runs from the die side of the specimen to the axis of symmetry. This build up in the stresses in that region compared to the corresponding case shown in Fig. 5-102 must be due to the smaller volume of confined material, resulting from a decrease in blank-holder diameter, which causes higher stresses to be built up for the same value of clamping force. The stress contours during blanking for the case when the blank-holder with minimum diameter was used(CR/PR = 1.14) are shown in Fig. 5-106. The results for the case when an equal value of back-load was used in addition to the clamping force are shown in Fig. 5-107.

Comparing Figs. 5-107 and 5-104 it becomes clear that the main difference between the two cases is a change in the state of stress on the right hand side of the shear line. The 200 MN/m^2 stress contour which corresponds to the uniaxial yield stress of the material starts from the vicinity of the blank-holder and, contrary to the corresponding case shown in Fig. 5-104 embraces a larger volume of the material, particularly close to the die face, because the line of action of the clamping force is now nearer to die edge and the same clamping force now restrains a smaller volume of material than was the case for the larger clamp.

5.15.2 Axial stress contours

The axial stress contours for different boundary conditions are presented in this section. Before presenting the results it is worth noting that in spite of the argument made in section 5.11 that the finite element method cannot predict the pressure distribution on the surface boundary of the deforming material, in the special case where the material surface boundary is perpendicular to the axial direction, the axial stresses will be identical to the pressure distribution. The pressure distribution on the deforming material surface boundary cannot be calculated if none of the axial, hoop or radial stress directions coincide with the normal to that surface, in this case the pressure will not be identical to any of the stresses.

The axial stress contours during blanking, without using clamping force and back-load, are shown in Fig. 5-108. The stress contours are concentrated around the shear line and especially around the punch and die edges. The stress contours on the die and punch surfaces are confined to a small region away from the shear line which indicates the partial contact area between the punch, die and the specimen. The rest of the specimen, especially a large volume of the material towards the axis of symmetry is stressed very little.

The axial stress contours when the specimen is being indented by a blank-holder only, at a clamping force of 70 kN, with maximum diameter (CR/PR = 1.28), are shown in Fig. 5-109. The stress contours are concentrated around the blank-holder and especially under it. Some of the stress contours run through the whole thickness of the specimen, but the region with high stress intensity is confined to the proximity of the blank-holder.

The axial stress contours for the case when the blank-holder

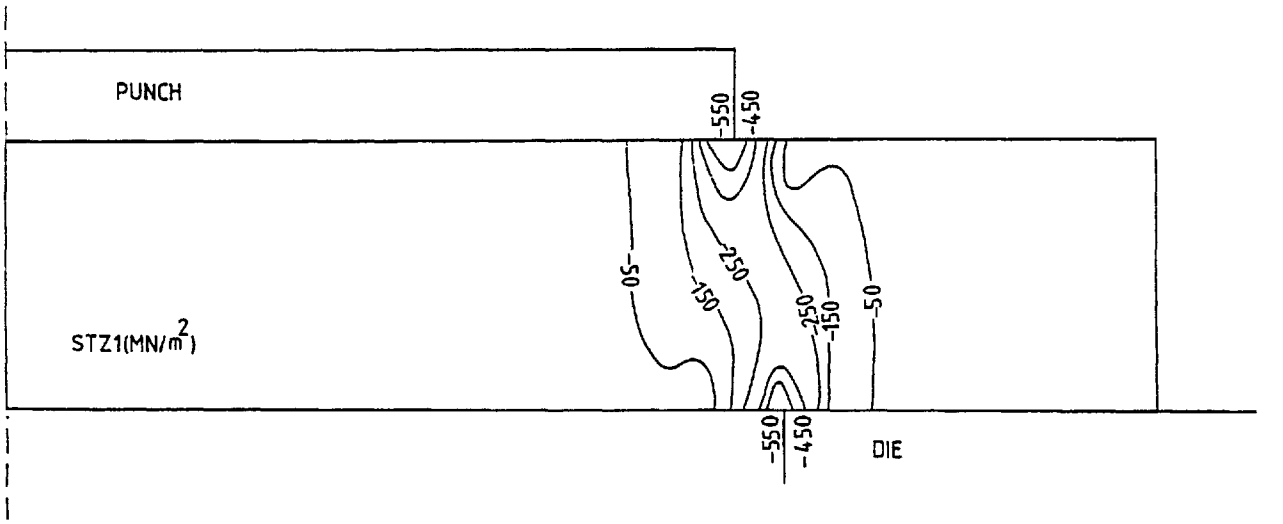

Fig. 5.108. Axial stress contours during blanking without clamping force and back-load (CF = BP = 0).

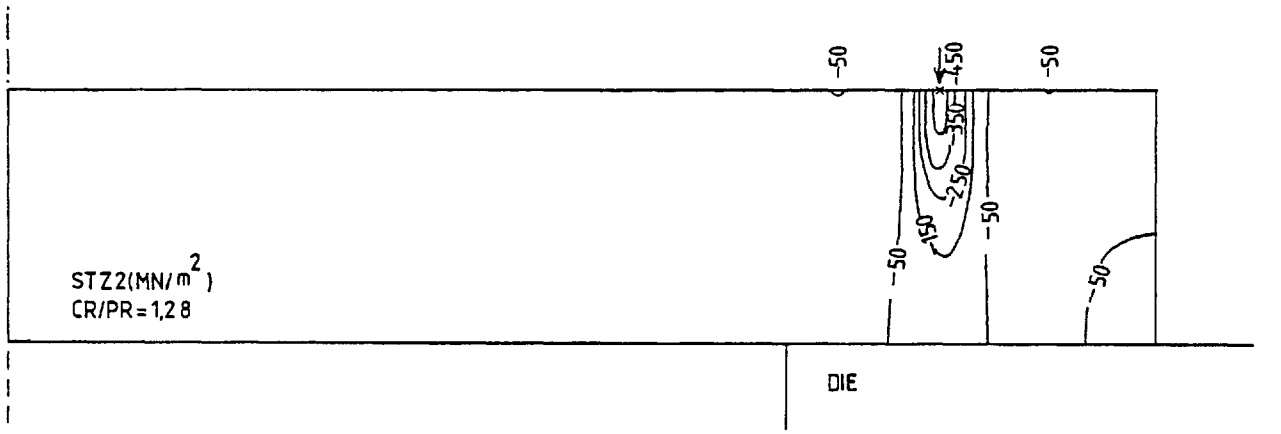

Fig. 5-109. Axial stress contours when indenting the specimen with a 70 kN clamping force at a clamp/punch diameter ratio of (CR/PR = 1.28).

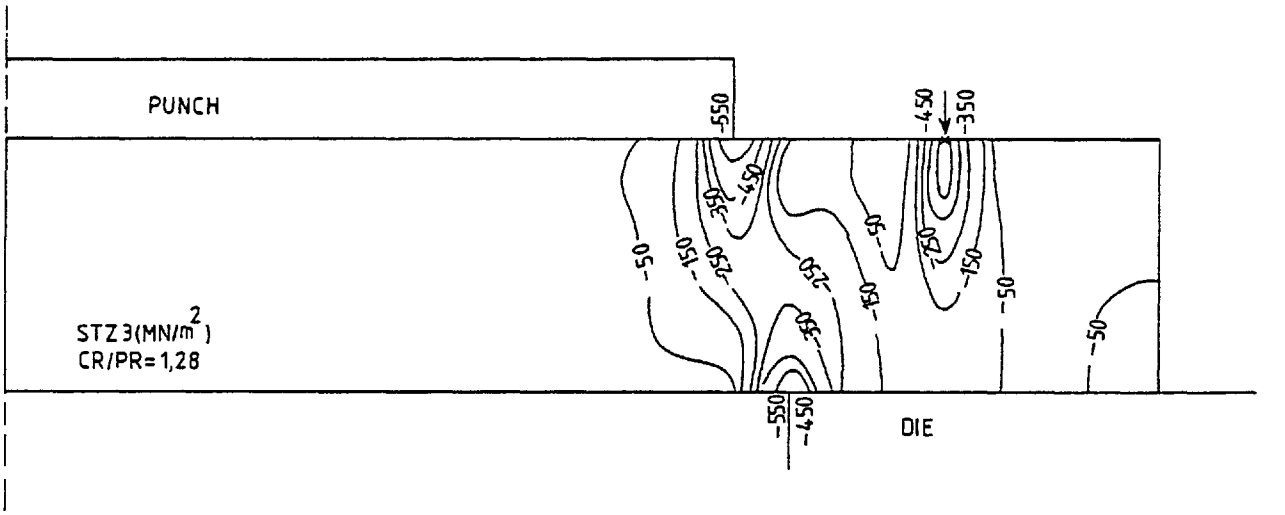

Fig. 5-110. Axial stress contours during blanking when a CF = 70 kN clamping force at a clamp/punch diameter ratio of (CR/PR = 1.28) was used.

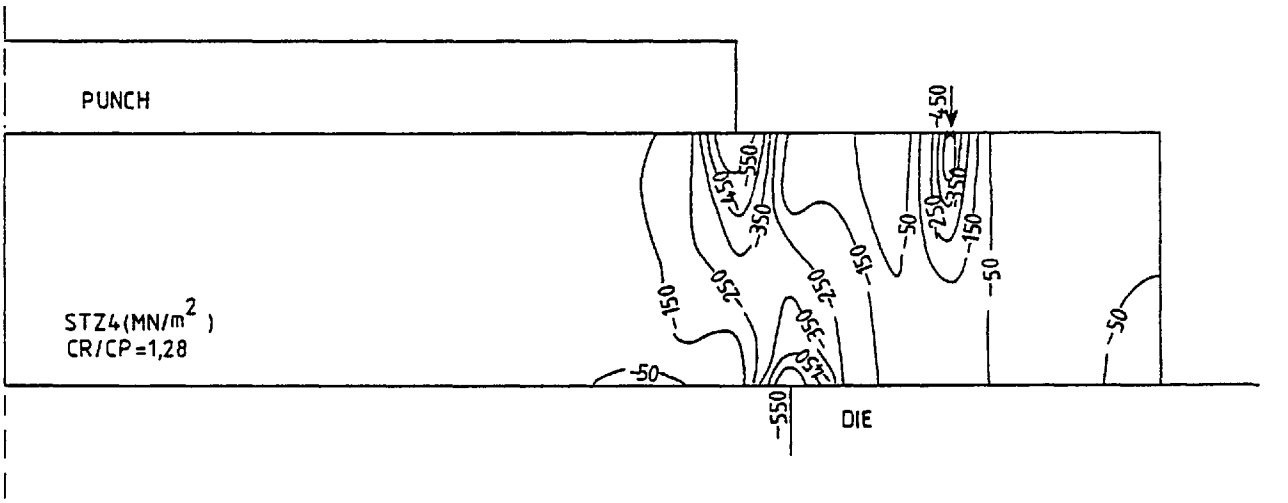

Fig. 5-111. Axial stress contours during blanking when a BP = 70 kN back-load and a CF = 70 kN clamping force, at a clamp/punch diameter ratio of (CR/PR = 1.28), were used.

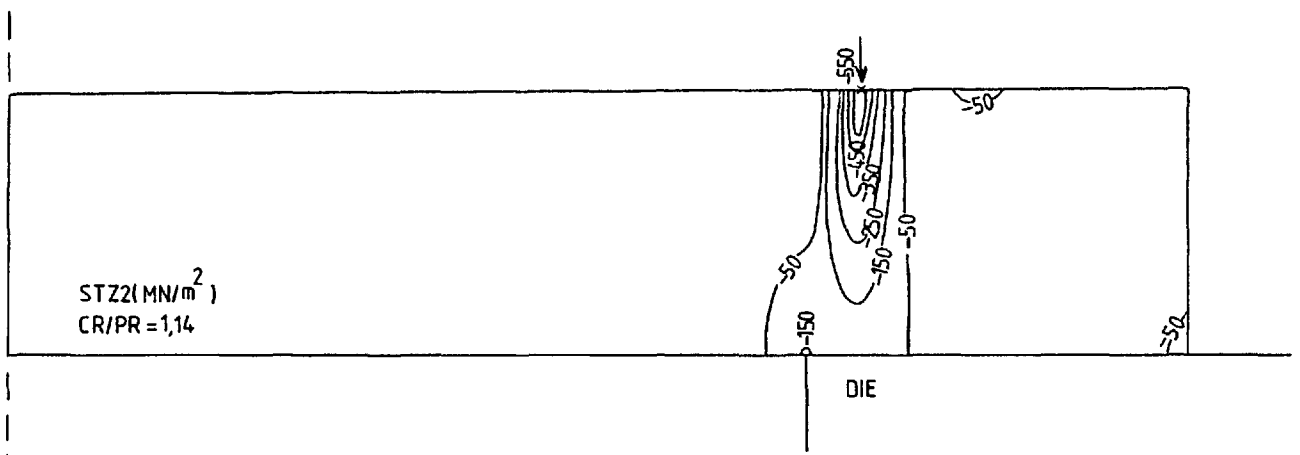

Fig. 5-112. Axial stress contours when indenting the specimen with a CF = 70 kN clamping force at a clamp/punch diameter ratio of CR/PR = 1.14.

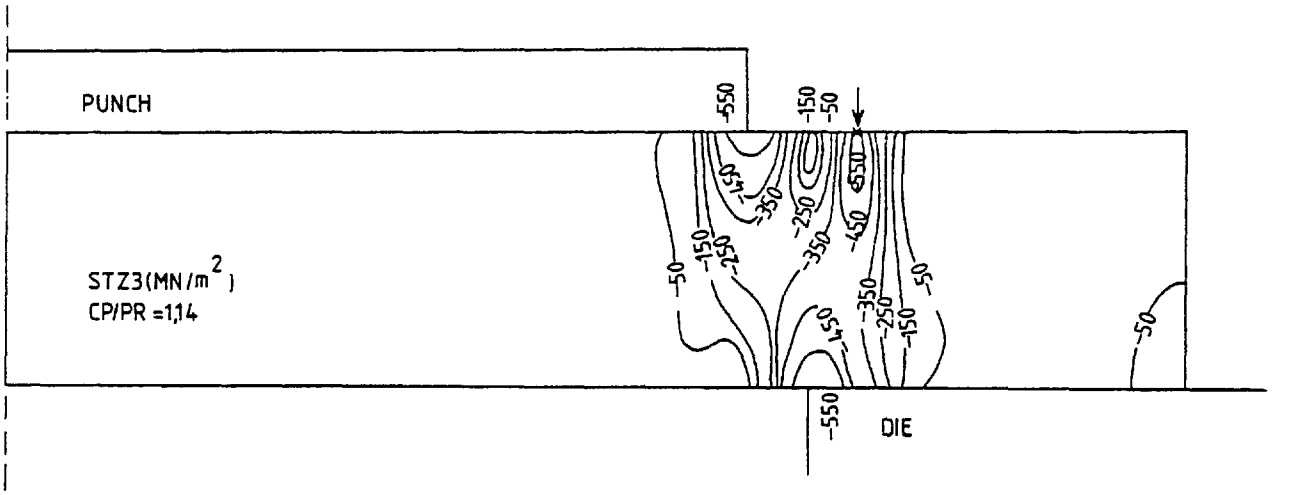

Fig. 5-113. Axial stress contours during blanking when a CF = 70 kN clamping force at a clamp/punch diameter ratio of CR/PR = 1.14 was used.

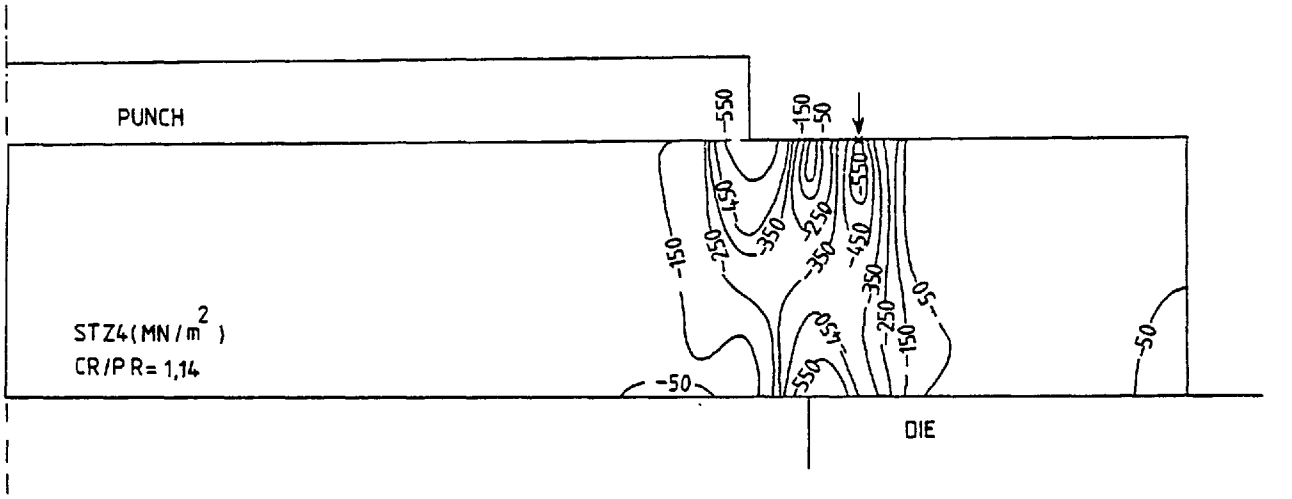

Fig. 5-114. Axial stress contours during blanking when a BP = 70 kN back-load and a CF = 70 kN clamping force, at a clamp/punch diameter ratio of (CR/PR = 1.14), were used.

with maximum diameter (CR/PR = 1.28) was used to clamp the specimen during the blanking operation, is shown in Fig. 5-110. Comparing this figure with Figs. 5-108 and 5-109 it becomes clear that the axial stress contours during blanking when a clamping force is present is almost a combination of stress contours for a simple blanking operation and a blank-holder indentation. The stress contour pattern in most regions is very similar to that of simple blanking except in the region between the punch and blank-holder where the stress contours from the two cases converge, this being a low stressed region.

The axial stress contours for the general case of the blanking operation, when clamping force and back-load are both present, using the blank-holder with maximum diameter (CR/PR 1.28), are shown in Fig. 5-111. Comparing Figs. 5-111 and 5-110, the general pattern for the two cases is very similar except that, when using a back-load in addition to the clamping force, the highly stressed regions spread further into the material on the left hand side of the shear line and particularly at the punch edge. This must be due to the compression of the specimen between the punch and counter-punch when a back-load is used. The spread of highly stressed regions around the punch edge, when back-load was used, must be simply due to the fact that a high percentage of back-load is transferred to the punch through a narrow region around the punch edge which results in the spread of high stressed regions around that area.

The axial stress contours when the specimen was indented by the blank-holder only, with minimum diameter (CR/PR = 1.14) at a clamping force of 70 kN are shown in Fig. 5-112. Similar to the corresponding case shown in Fig. 5-109, blank-holder with maximum diameter, the stress contours are mostly concentrated around the

blank-holder itself. However, in contrast to the corresponding case, some of the stress contours in this case are directed towards the die edge, causing relatively high stresses in that region.

The axial stress contours during blanking are shown in Fig. 5-113, when a blank-holder with minimum diameter (CR/PR = 1.14) was used. In this case the stress contours developed by the blank-holder and the punch combine and form a high stressed region around the punch edge, particularly in the part of the material situated on the right hand side of the shear line. As the blank-holder diameter decreases (CR/PR = 1.14), coming closer to the punch edge, stress contour concentration around the die edge compared to the corresponding case shown in Fig. 5-110 increases. This must be due to the displacement of the line of action of the clamping force, when using a smaller clamp diameter, which causes a larger portion of the clamping force to be transferred to the die face through the area close to the die edge and thus causing a higher concentration of stress contours in that region.

The combined effect of clamping force and back-load on the stress contours of the axial stress during blanking is shown in Fig. 5-114. Comparison of Figs. 5-114 and 5-113 indicates that, when using a back-load in addition to the clamping force during blanking, the concentration of stress contours at the punch edge increases considerably. This again must be due to the compression of the specimen between the punch and counter-punch when a back-load is used.

5.15.3 Hoop stress contours

Hoop stress contours for the simple blanking operation are shown in Fig. 5-115. As in the corresponding previous cases of equivalent stress and axial stress, the stress contours are concentrated around the shearing zone and mostly around the punch and die-edges.

The hoop stress contours when the specimen was indented by the blank-holder only, with maximum diameter (CR/PR = 1.28) at a clamping force of 70 kN are shown in Fig. 5-116. The stress contours similar to the corresponding cases for equivalent stress and axial stress are concentrated around the blank-holder only.

The hoop stress contours when the specimen was clamped by the blank-holder with maximum diameter (CR/PR = 1.28) throughout the blanking operation are shown in Fig. 5-117. In this case the stress contours around the shearing zone and at the punch and die edges are similar to that of simple blanking shown in Fig. 5-115.

The hoop stress contours when an equal value of back-load was also used in addition to the clamping force are shown in Fig. 5-118. In this case, an increase in the volume of the highly stressed region around the shearing zone, compared to the previous case shown in Fig. 5-117, is noticeable. This increase is particularly high around the punch edge.

The hoop stress contours when the specimen is only indented by a blank-holder with minimum diameter (CR/PR = 1.14) and a clamping force of 70 kN are shown in Fig. 5-119. The stress field pattern is similar to the corresponding case shown in Fig. 5-116 for the blank-holder with maximum diameter, except on the left hand side of the blank-holder where a stress contour of 50 MN/m^2 runs from the vicinity of the blank-holder to a point on the axis of symmetry. This must be due to a smaller volume of confined material, as the clamp diameter decreases,

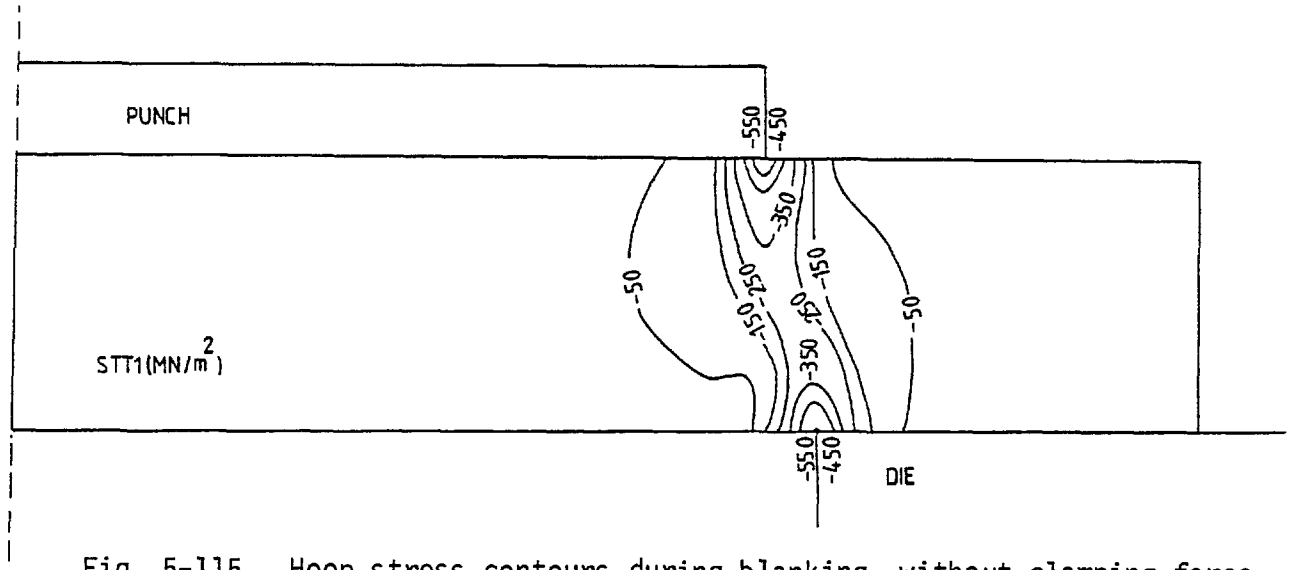

Fig. 5-115. Hoop stress contours during blanking, without clamping force and back-load (CF = BP = 0).

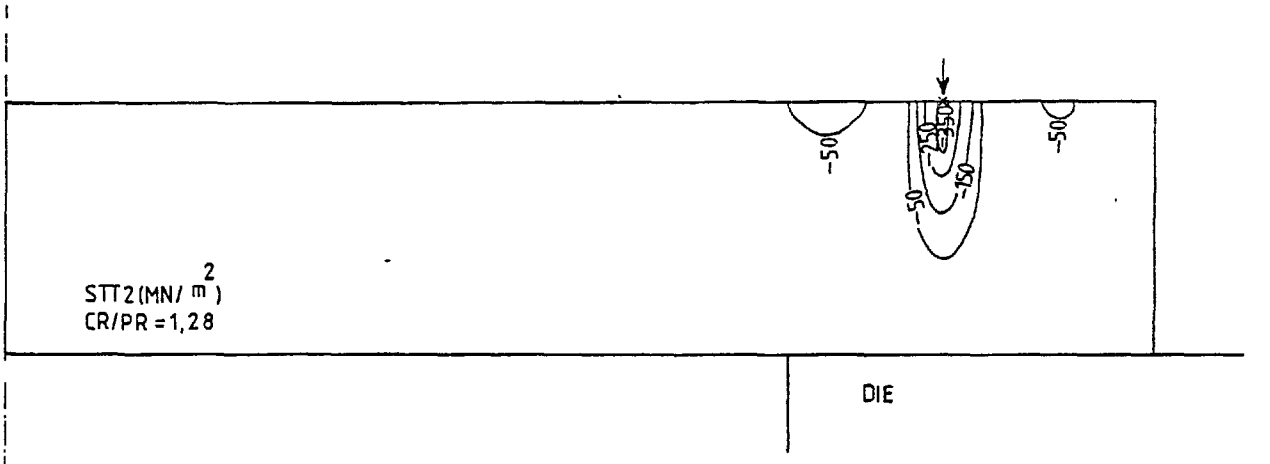

Fig. 5-116. Hoop stress contours when indenting the specimen with a CF = 70 kN clamping force at a clamp/punch diameter ratio of (CR/PR = 1.28).

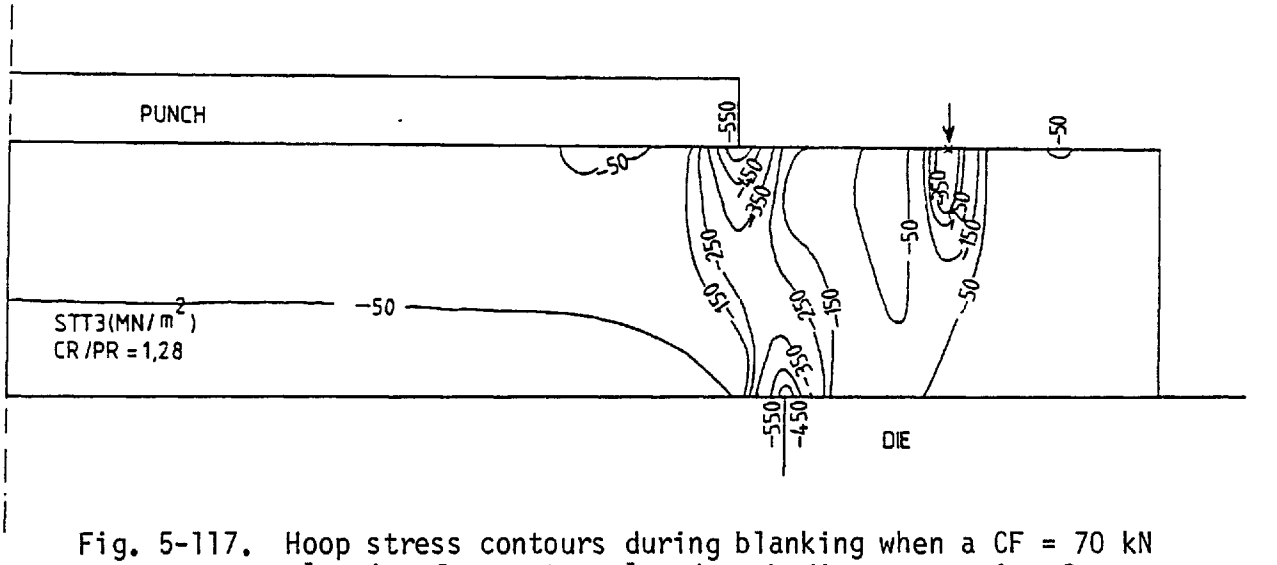

Fig. 5-117. Hoop stress contours during blanking when a CF = 70 kN clamping force at a clamp/punch diameter ratio of (CR/PR = 1.28) was used.

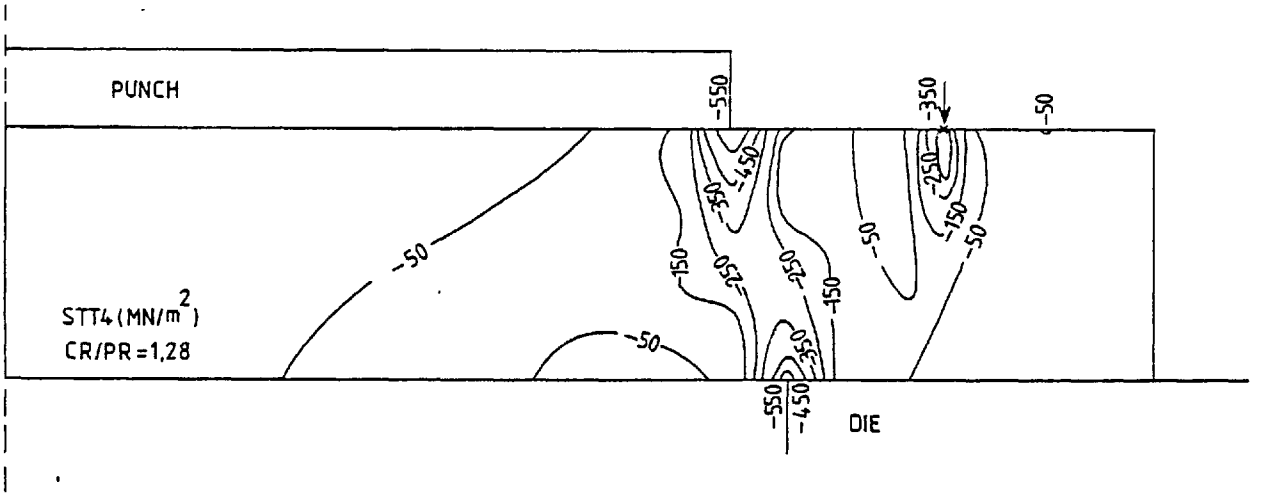

Fig. 5-118. Hoop stress contours during blanking when a BP = 70 kN back-load and a CF = 70 kN clamping force, at a clamp/punch diameter ratio of (CR/PR = 1.28), were used.

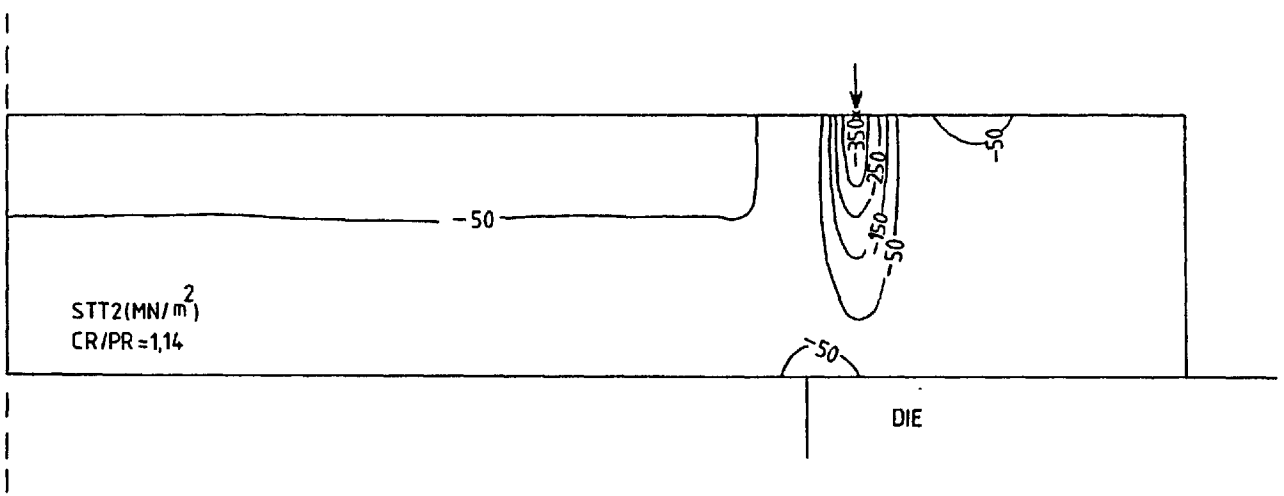

Fig. 5-119. Hoop stress contours when indenting the specimen with a CF = 70 kN clamping force at a clamp/punch diameter ratio of (CR/PR = 1.14).

which reduces the capability of this part of the material to offset the stresses caused by the blank-holder indentation.

The stress contours during blanking are shown in Fig. 5-120, when the blank-holder with minimum diameter (CR/PR 1.14) was used. A decrease in the concentration of stress contours at the die dege, compared to that of simple blanking shown in Fig. 5-115, is quite noticeable. This must be due to the excessive bending effect of the specimen as the clamp diameter decreases and will be discussed later in section 5-16.

The hoop stress contours when an equal value of back-load is used in addition to the clamping force is shown in Fig. 5-121. An increase in the concentration of the stress contours around the shearing zone, compared to the previous case shown in Fig. 5-120, particularly around the punch and die edges is quite noticeable. The sudden increase in the stress concentration around the die edge, when the back-load is used, must be due to the prevention of excessive bending of the specimen through the application of the back-load, which once again causes the blank-holder to act effectively and cause a high state of compression in that region.

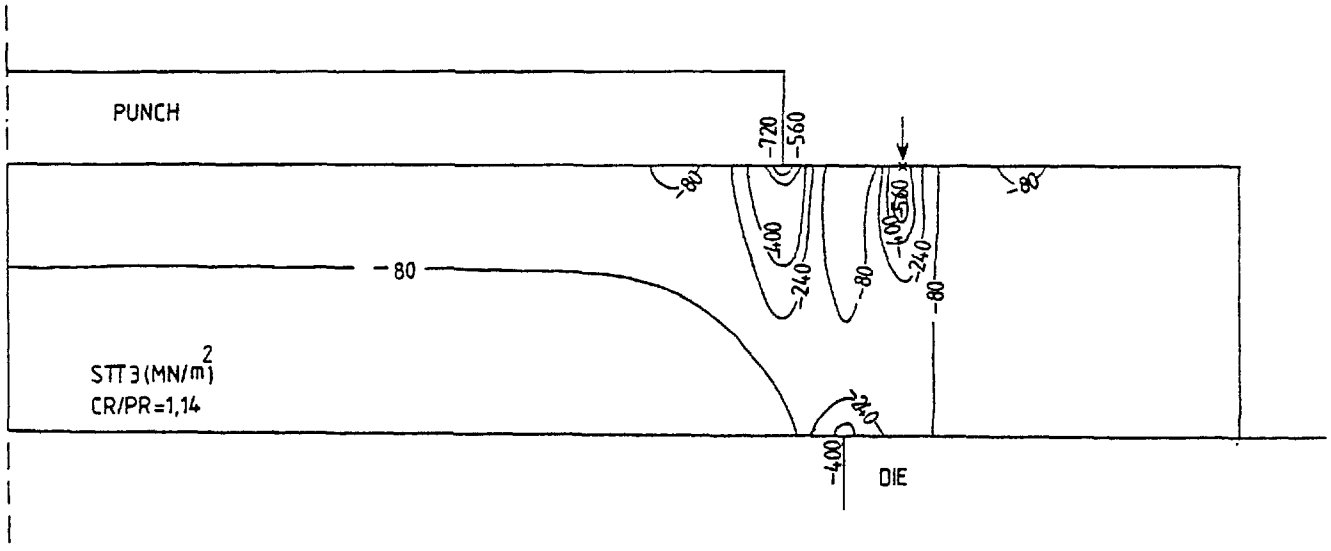

Fig. 5-120. Hoop stress contours during blanking when a CF = 70 kN clamping force at a clamp/punch diameter ratio of (CR/PR = 1.14) was used.

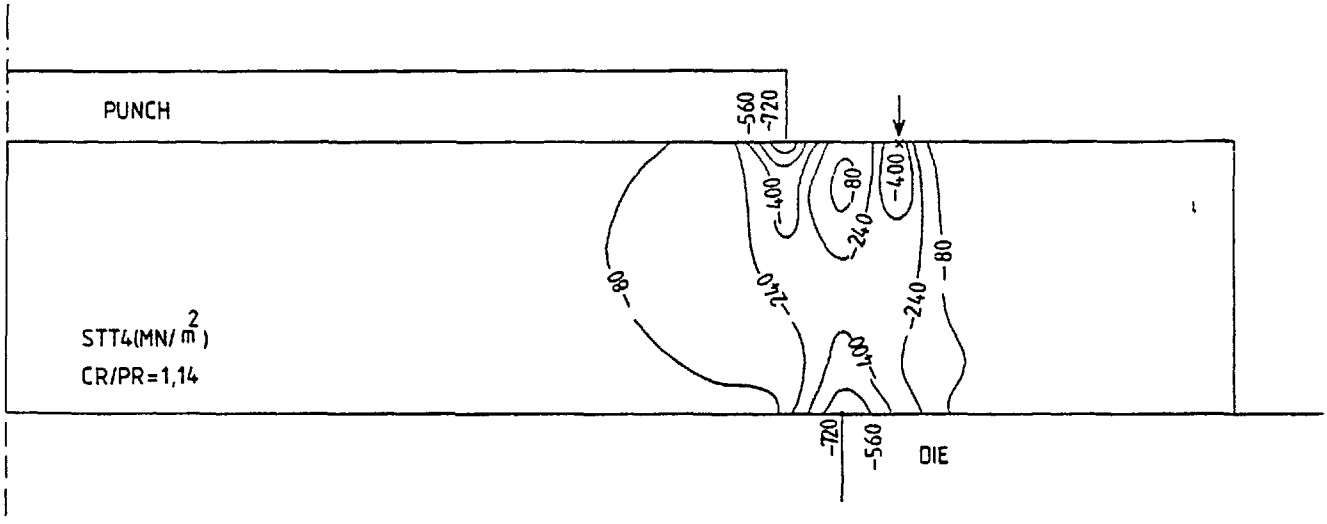

Fig. 5-121. Hoop stress contours during blanking when a BP = 70 kN back-load and a CF = 70 kN clamping force, at a clamp/punch diameter ratio of (CR/PR = 1.14), were used.

5.15.4 Radial stress contours

Radial stress contours for simple blanking are shown in Fig. 5-122. The stress contours are concentrated around the shear line, particularly around the punch and die edges. Unlike the two previous corresponding cases of axial and hoop stress contours shown in Figs. 5-108 and 5-115 respectively, the stress contours are not confined to a narrow region around the shear line but are spread more through the specimen.

The radial stress contours when the specimen was indented by the blank-holder only, with maximum diameter (CR/PR 1.28) at a clamping force of 70 kN are shown in Fig. 5-123. The concentration of stress contours is almost symmetric with respect to the line of action of the clamping force. The stress contours run through the specimen only to a limited depth. The squeezing of the material in the radial direction develops a stressed region on both sides of the blank-holder.

The radial stress contours during blanking are shown in Fig. 5-124, when the blank-holder with maximum diameter (CR/PR = 1.28) was used. The stress field around the shearing zone is almost identical to that of simple blanking shown in Fig. 5-122. Compared to Fig. 5-122, the stress contour of 50 MN/m^2 on the left hand side of the shearing zone changes direction and runs from the vicinity of the die edge to a point on the axis of symmetry, indicating a higher radial stress in that region.

The radial stress contours, when an equal value of back-load was used in addition to the clamping force, are shown in Fig. 5-125. Comparing Figs. 5-125 and 5-124, by the addition of back-load the heavily stressed region around the shearing zone spreads considerably through the specimen. The stress contour of 150 MN/m^2 on the left hand side of the shearing zone bends towards the axis of symmetry,

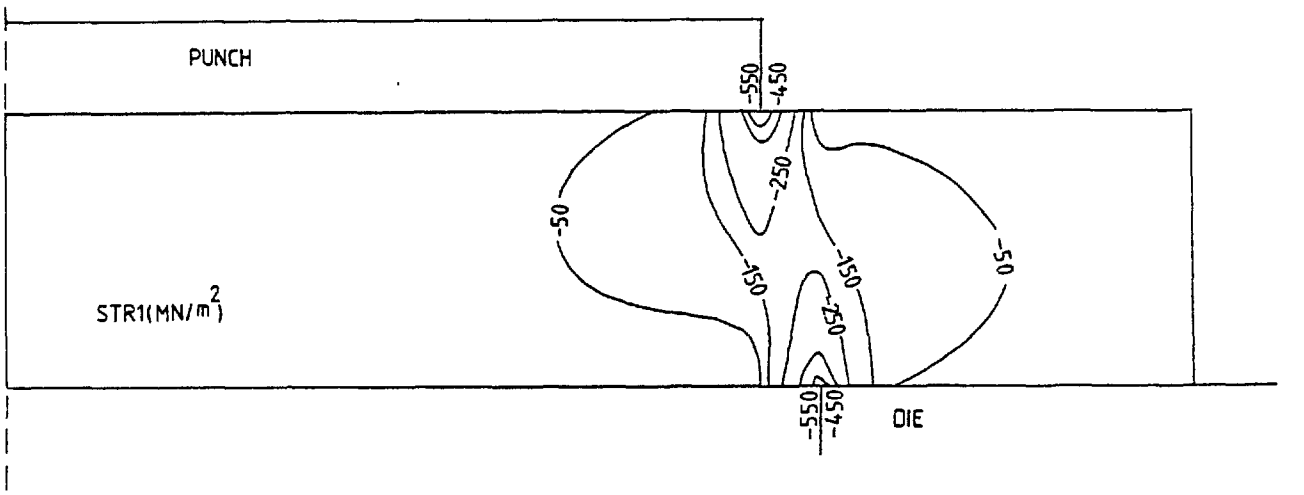

Fig. 5-122. Radial stress contours during blanking, without clamping force and back-load (CF = BP = 0).

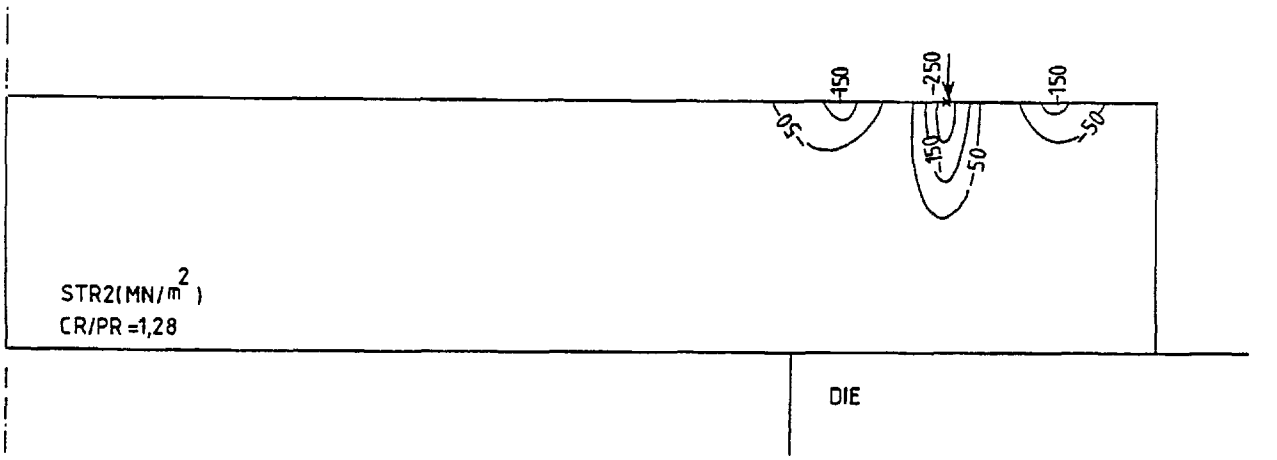

Fig. 5-123. Radial stress contours when the specimen was indented by a CF = 70 kN clamping force at a clamp/punch diameter ratio of (CR/PR = 1.28).

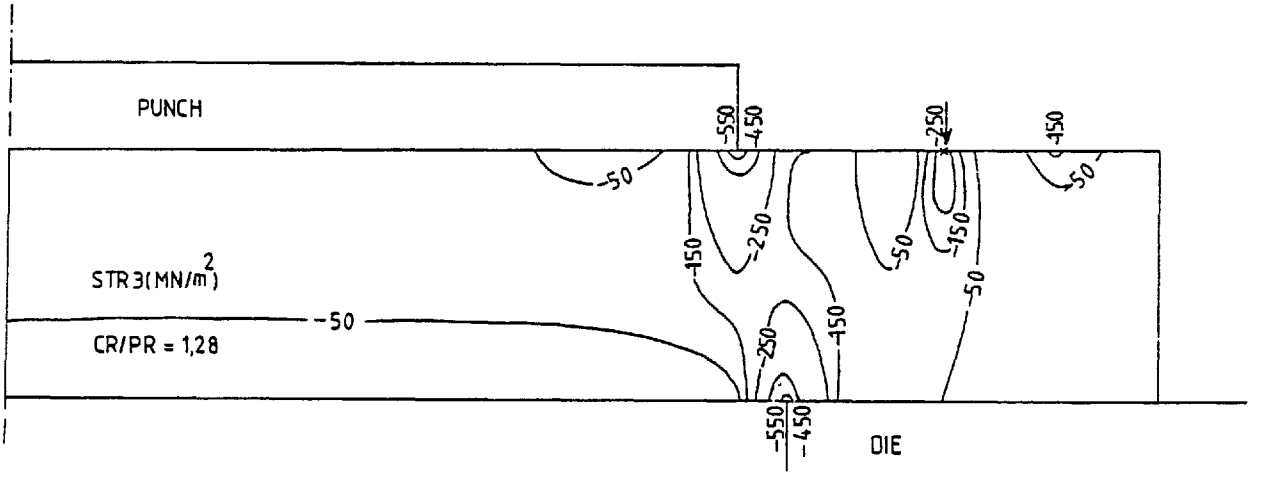

Fig. 5-124. Radial stress contours during blanking when a CF = 70 kN clamping force at a clamp/punch diameter ratio of (CR/PR = 1.28) was used.

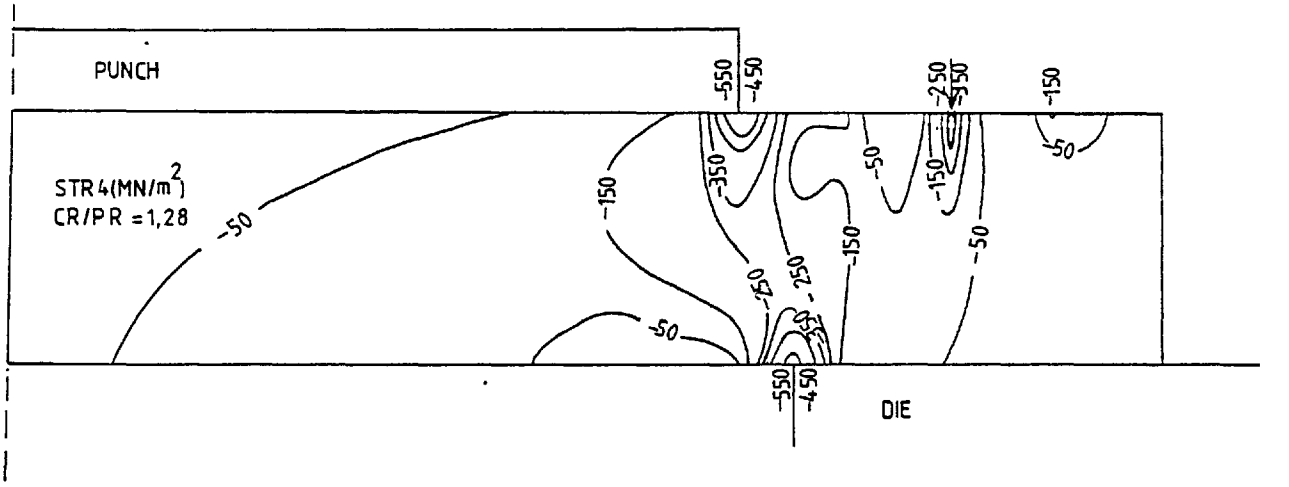

Fig. 5-125. Radial stress contours during blanking when a BP = 70 kN back-load and a CF = 70 kN clamping force, at a clamp/punch diameter ratio of (CR/PR = 1.28), were used.

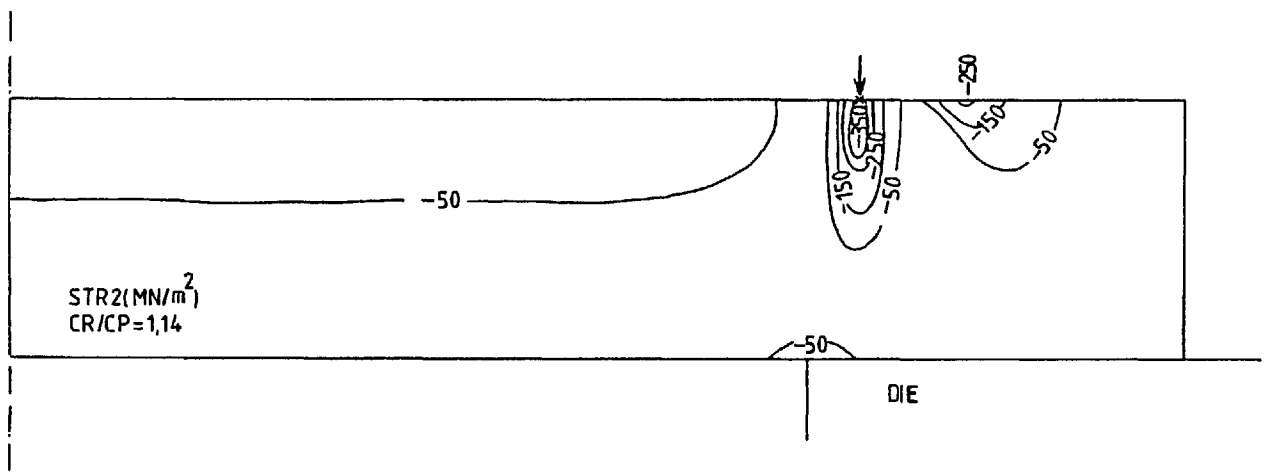

Fig. 5-126. Radial stress contours when the specimen was indented by a CF = 70 kN clamping force at a clamp/punch diameter ratio of (CR/PR = 1.14).

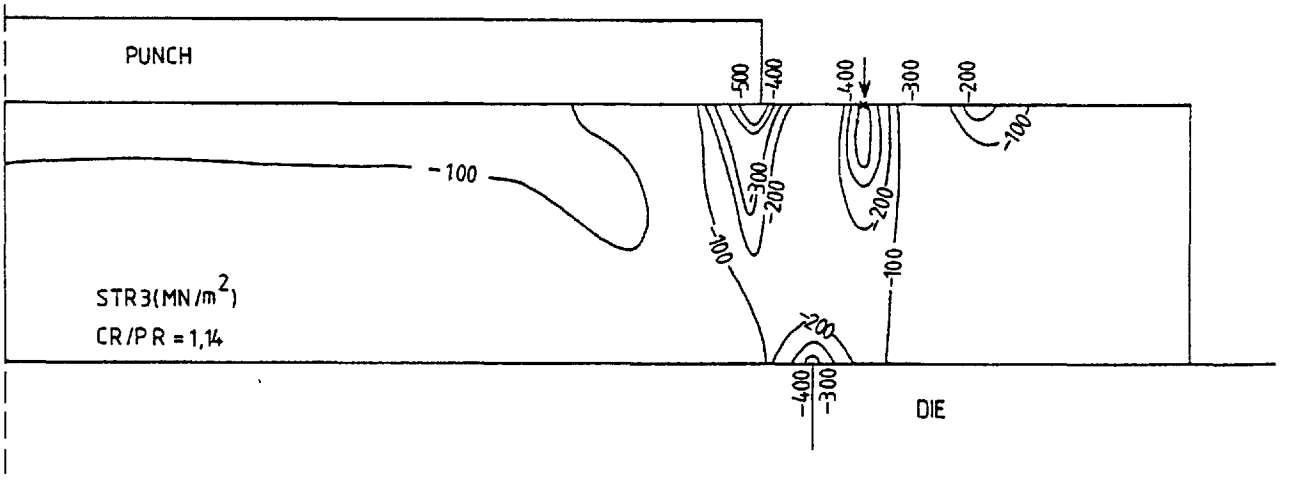

Fig. 5-127. Radial stress contours during blanking when a CF = 70 kN clamping force at a clamp/punch diameter ratio of (CR/PR = 1.14) was used.

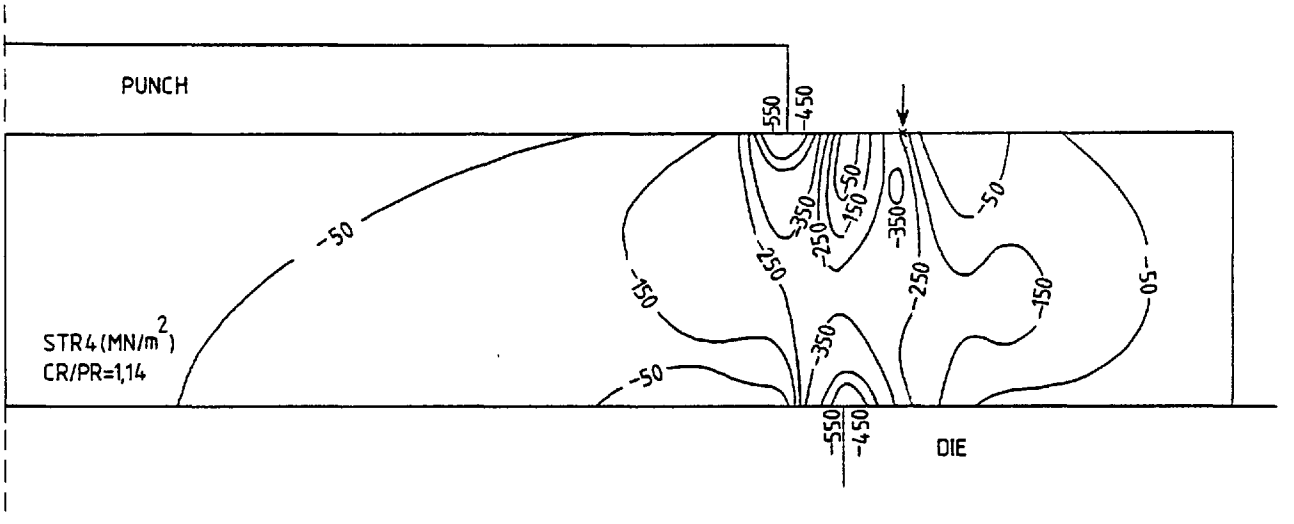

Fig. 5-128. Radial stress contours during blanking when a BP = 70 kN back-load and a CF =70 kN clamping force, at a clamp/punch diameter ratio of (CR/PR = 1.14), were used.

indicating a higher value of radial stress in that region. A new stress contour of 50 MN/m^2 now runs from the bottom surface to the top surface of the specimen in the central region. This must be due to the compression of the specimen between the punch and counter-punch when a back-load is used.

The radial stress contours when the specimen was indented by the blank-holder only, with minimum diameter (CR/PR = 1.14) at a clamping force of 70 kN is shown in Fig. 5-126. Unlike the corresponding case shown in Fig. 5-123, instead of a local stressed region a line of 50 MN/m^2 runs from the left hand side of the blank-holder to the axis of symmetry. This again must be due to the displacement of the line of action of the clamping force, nearer to the die edge, and thus the same clamping force now restrains a smaller volume of material than was the case for the larger clamp diameter.

The radial stress contours, when a blank-holder with minimum diameter (CR/PR = 1.14) was used to clamp the specimen during blanking, are shown in Fig. 5-127. Similar to the hoop stress field, shown in Fig. 5-120, the introduction of the blank-holder with minimum diameter (CR/PR = 1.14) causes a considerable decrease in the stress contour concentration at the die edge, compared to that produced by simple blanking, shown in Fig. 5-122.

The radial stress contours when an equal value of back-load was used in addition to the clamping force are shown in Fig. 5-128. Comparing this figure with the corresponding case shown in Fig. 5-125, it becomes clear that, as the clamp diameter decreases, coming closer to the punch edge, there is a considerable increase in the radial stresses in the regions around the shearing zone and particularly around the die edge. This again must be due to a smaller volume of

confined material resulting from the decrease in clamp diameter, and thus the same clamping force restrains a smaller volume of material than was the case for the larger clamp diameter.

5.15.5 Shear stress contours

The shear stress contours for simple blanking are shown in Fig. 5-129. The stress contours are concentrated around the shearing zone and mostly on the right top and left bottom part of the shear line. The spacing between the contours meeting the punch and die surfaces increases away from the shear line, indicating a more gradual variation in the shear stress in those regions. It is interesting to note that the stress contours become more concentrated and almost parallel with the shear line in the proximity of the shearing zone, indicating a prevalence of a constant shear stress in that region.

The shear stress contours when the specimen was only indented by the blank-holder with maximum diameter (CR/PR = 1.28) at a clamping force of 70 kN are shown in Fig. 5-130. The stress contours with high values are all concentrated on the right hand side of the blank-holder.

The shear stress contours, when the blank-holder with maximum diameter (CR/PR = 1.28) was used during blanking, are shown in Fig. 5-131. In this case a higher concentration of stress contours around the shearing zone compared to simple blanking shown in Fig. 5-129 is noticeable.

When an equal value of back-load is used in addition to the clamping force, a stress field similar to that of simple blanking is obtained, Fig. 5-132.

The shear stress contours when the specimen was indented by the blank-holder only, with minimum diameter (CR/PR = 1.14) at a clamping force of 70 kN is shown in Fig. 5-133. The stress field is similar to that of the corresponding case shown in Fig. 5-130, when the specimen was indented by the blank-holder with maximum diameter (CR/PR = 1.28).

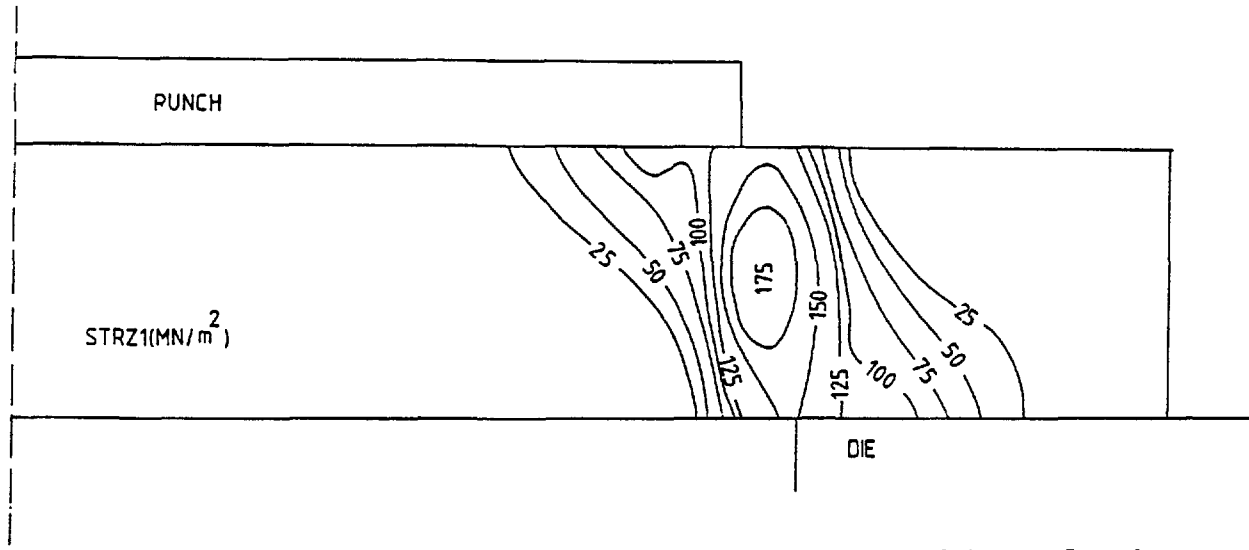

Fig. 5-129. Shear stress contours during blanking, without clamping force and back-load.

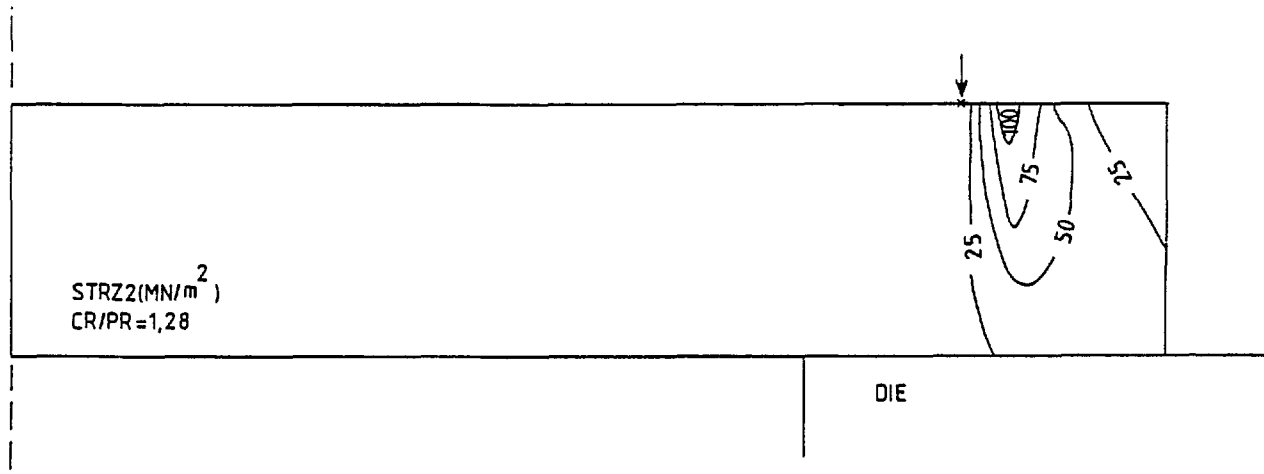

Fig. 5-130. Shear stress contours when the specimen was indented by a CF = 70 kN clamping force at a clamp/punch diameter ratio of (CR/PR = 1.28).

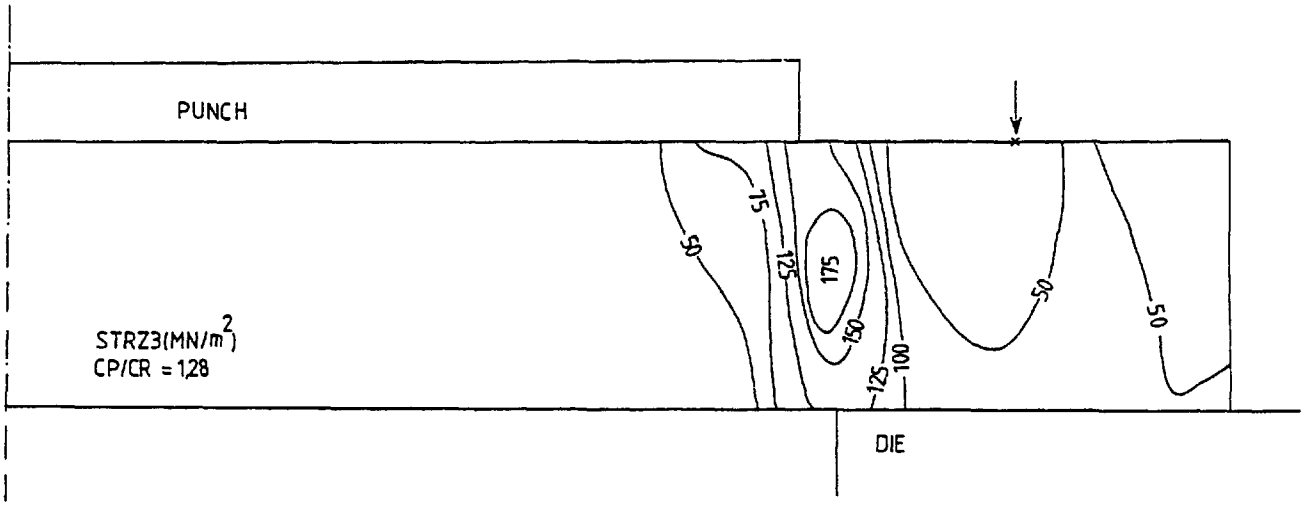

Fig. 5-131. Shear stress contours during blanking when a CF = 70 kN clamping force at a clamp/punch diameter ratio of (CR/PR = 1.28) was used.

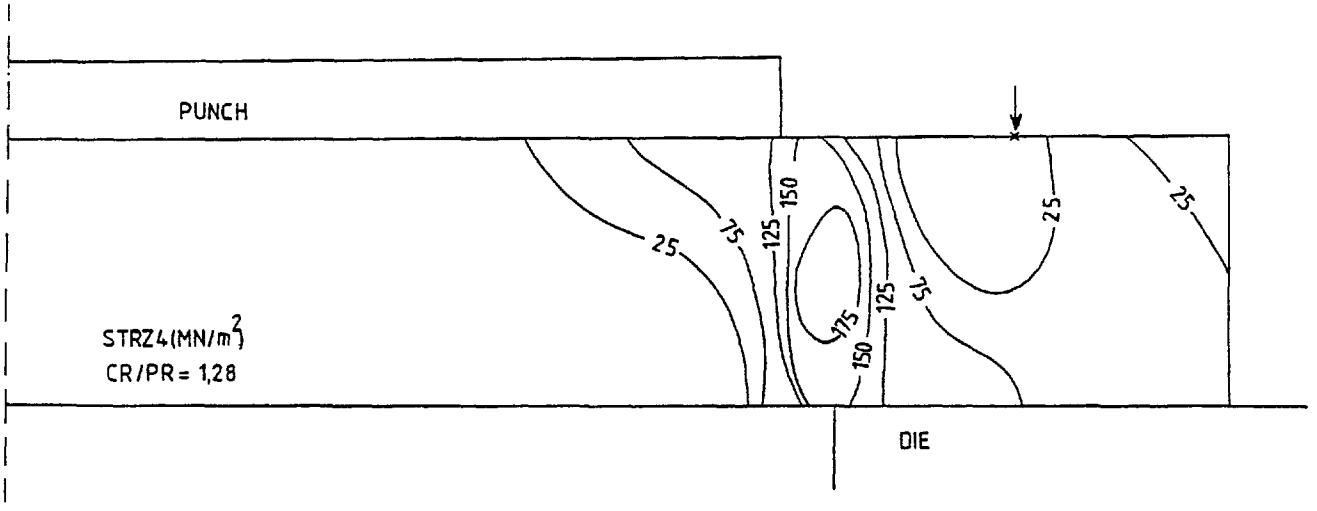

Fig. 5-132. Shear stress contours during blanking when a BP = 70 kN back-load and a CF = 70 kN clamping force, at a clamp/punch diameter ratio of (CR/PR = 1.28), were used.

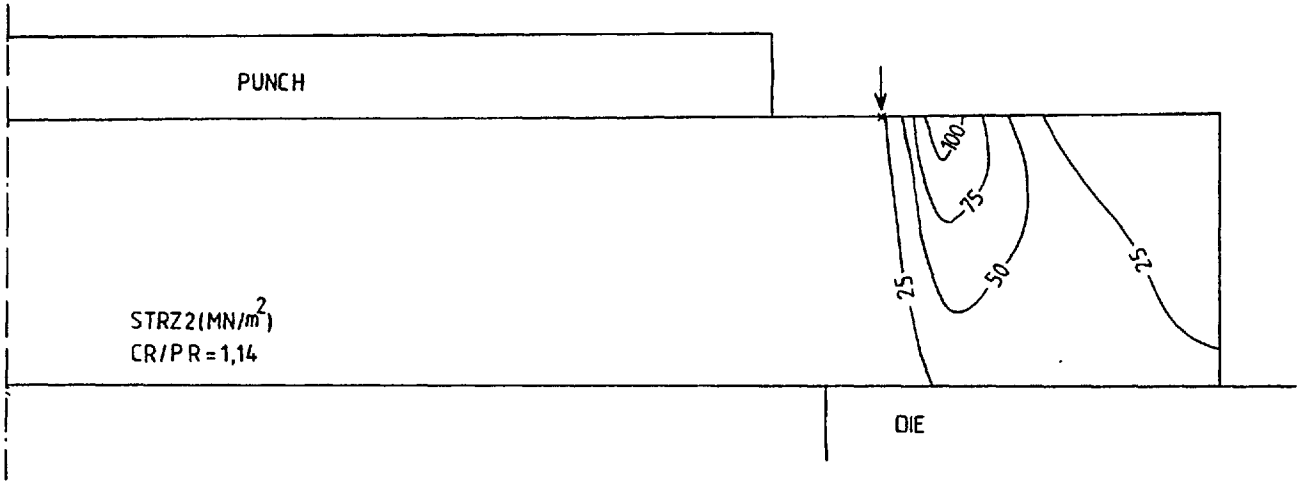

Fig. 5-133. Shear stress contours during blanking when a CF = 70 kN clamping force at a clamp/punch diameter ratio of (CR/PR = 1.14) was used.

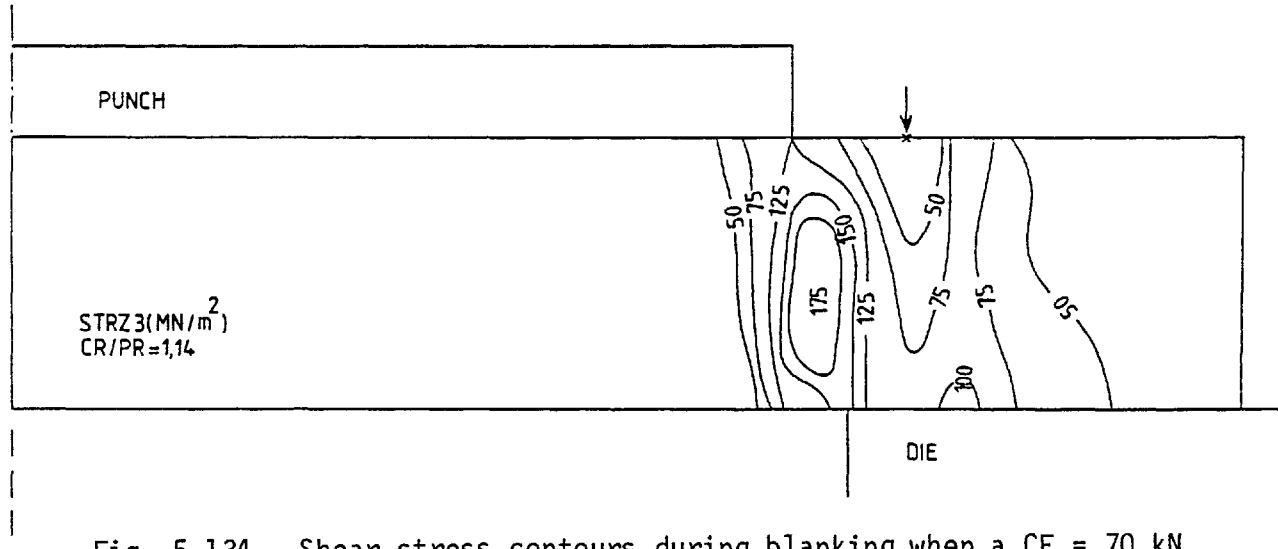

Fig. 5-134. Shear stress contours during blanking when a CF = 70 kN clamping force at a clamp/punch diameter ratio of (CR/PR = 1.14) was used.

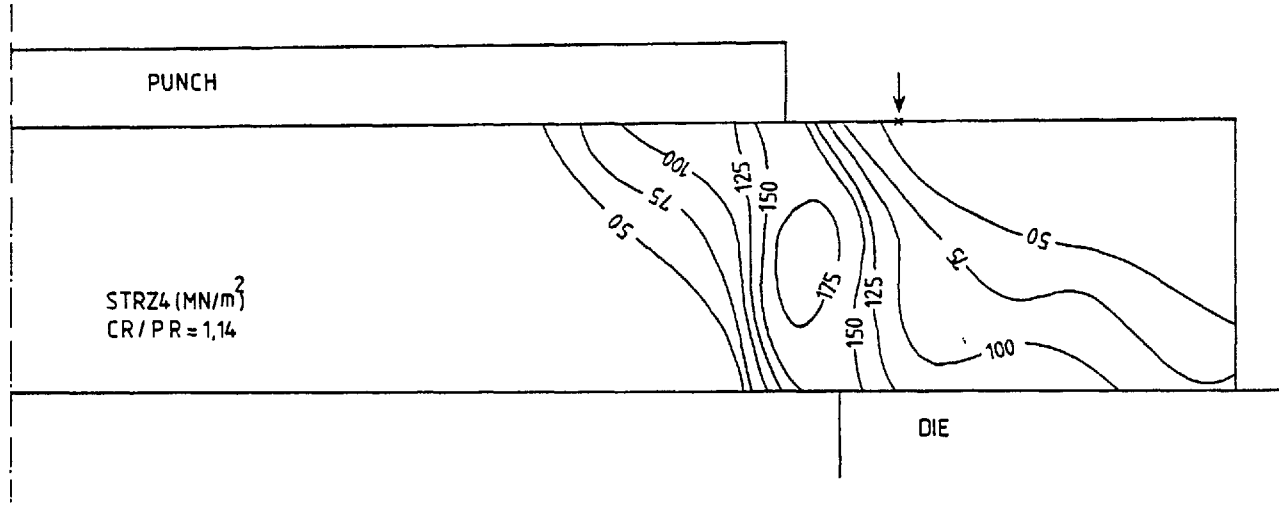

Fig. 5-135. Shear stress contours during blanking when a BP = 70 kN back-load and a CF = 70 kN clamping force, at a clamp/punch diameter ratio of (CR/PR = 1.14), were used.

The shear stress contours, when the blank-holder with minimum diameter (CR/PR = 1.14) was used during blanking, are shown in Fig. 5-134. Comparing this figure with the corresponding case shown in Fig. 5-131 for a clamp with maximum diameter (CR/PR = 1.28), it becomes clear that when a smaller clamp diameter is used a higher concentration of stress contours around the shear line develops.

The shear stress contours when an equal value of back-load was used in addition to the clamping force are shown in Fig. 5-135. The addition of a back-load produces some increase in the intensity of the shear stress contours around the shear line.

5.15.6 Hydrostatic component of stress contours

The hydrostatic component of stress contours during blanking are shown in Fig. 5-136. The stress contours are concentrated around the shearing zone and particularly around the punch and die edges.

The hydrostatic component of stress contours when the specimen was indented by the blank-holder only, with maximum diameter (CR/PR = 1.28), at a clamping force of 70 kN are shown in Fig. 5-137. The stress field pattern is similar to those of hoop stress and radial stress shown in Figs. 5-116 and 5-123 respectively.

The hydrostatic component of stress contours, when the blank-hoder with maximum diameter (CR PR = 1.28) was used during blanking, are shown in Fig. 5-138. An increase in the concentration of stress contours around the shearing zone, compared to that of simple blanking shown in Fig. 5-136, is noticeable. This increase is more pronounced around the die edge.

The hydrostatic component of stress contours, when an equal value of back-load was used in addition to the clamping force during blanking, are shown in Fig. 5-139. The stress contour pattern on the right hand side of the shearing zone is nearly the same as that obtained during blanking when only the clamping force was present, Fig. 5-138. A spread of high stressed regions on the left hand side of the shear line and especially at the punch and die edges is noticeable.

The hydrostatic component of stress contours when the specimen was indented only by the blank- holder with minimum diameter (CR/PR = 1.14) at a clamping force of 70 kN is shown in Fig. 5-140. This stress field is almost the same as the corresponding case shown in Fig. 5-137, when the blank-holder with maximum diameter was used.

The hydrostatic component of stress contours, when the blank-

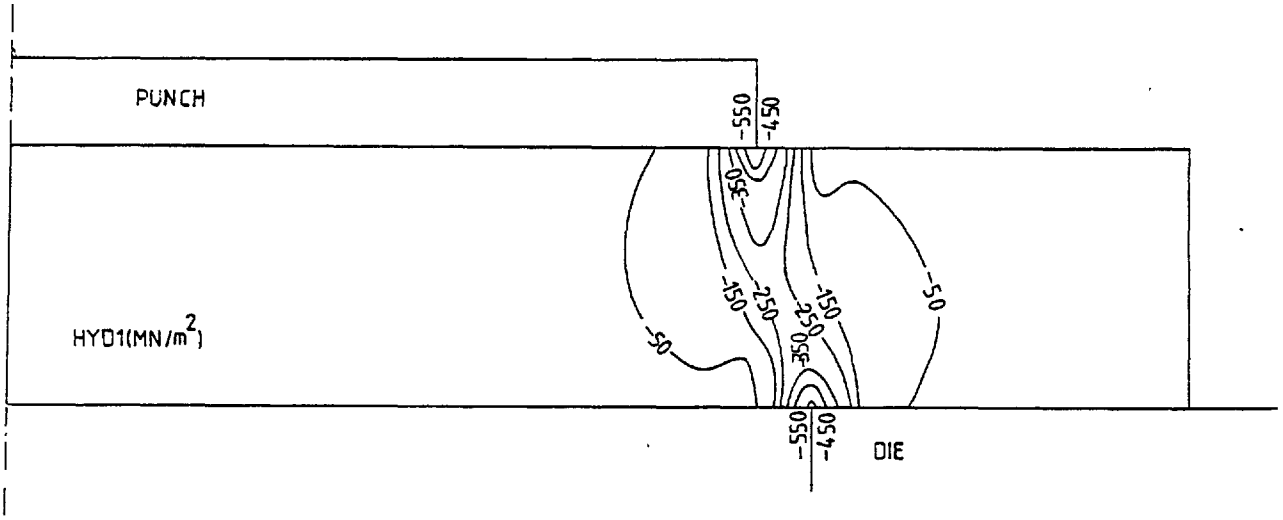

Fig. 5-136. Hydrostatic component of stress contours during blanking, without clamping force and back-load (CF = BP = 0).

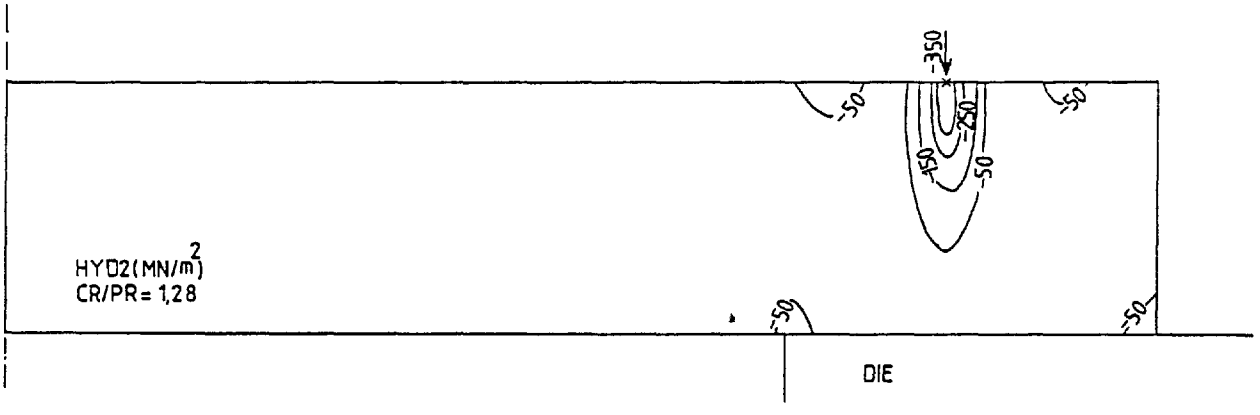

Fig. 5.137. Hydrostatic component of stress contours when the specimen was indented by a CF = 70 kN clamping force at a clamp/ punch diameter ratio of (CR/PR = 1.28).

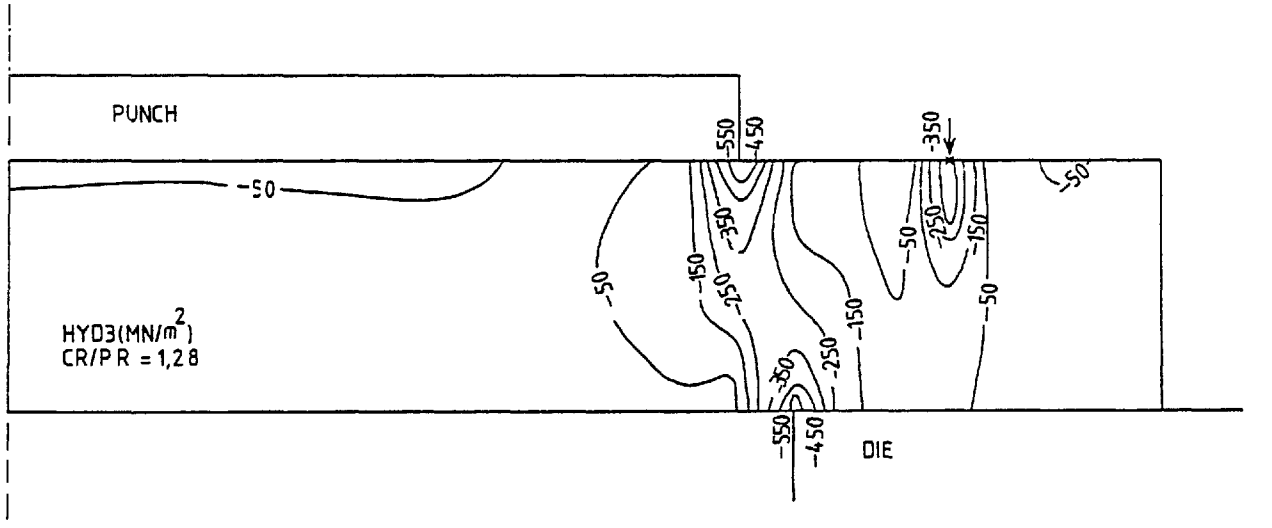

Fig. 5-138. Hydrostatic component of stress contours during blanking when a CF = 70 kN clamping force at a clamp/punch diameter ratio of (CR/PR = 1.28) was used.

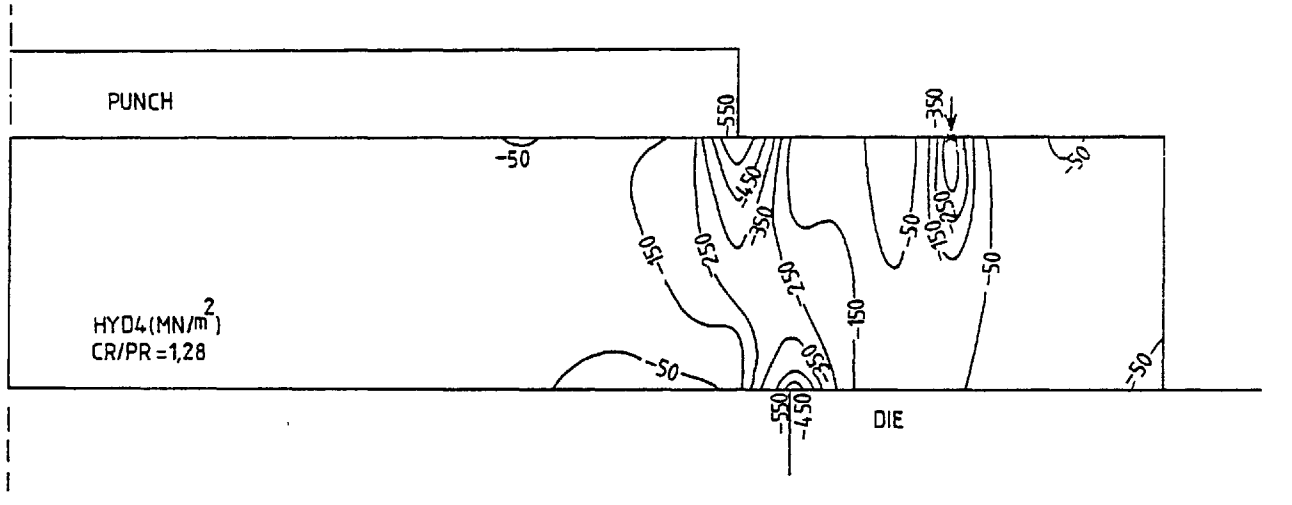

Fig. 5-139. Hydrostatic component of stress contours during blanking when a BP = 70 kN back-load and a CF = 70 kN clamping force, at a clamp/punch diameter ratio of (CR/PR = 1.28), were used.

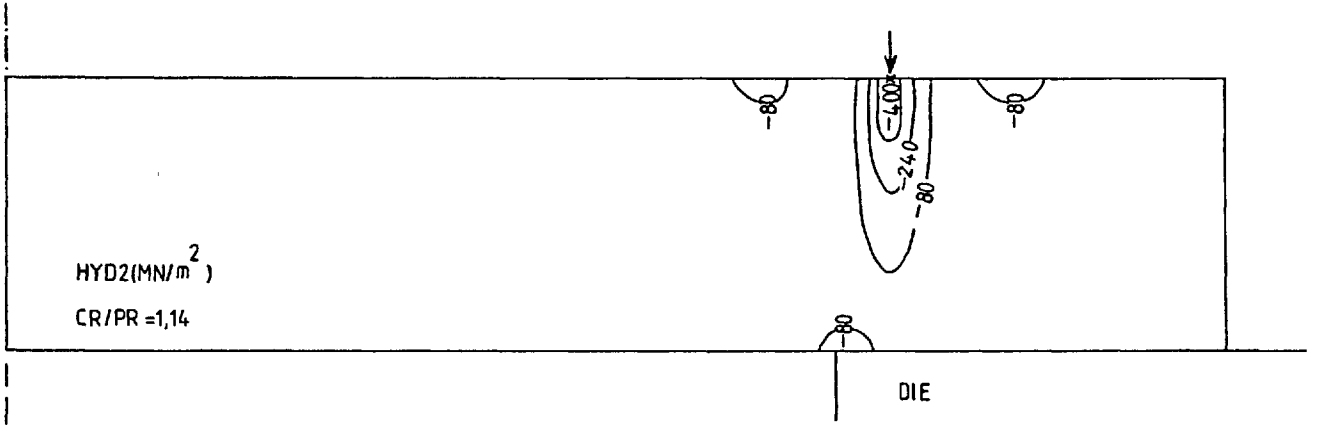

Fig. 5.140. Hydrostatic component of stress contours when the specimen was indented by a CF = 70 kN clamping force at a clamp/punch diameter ratio of (CR/PR = 1.14).

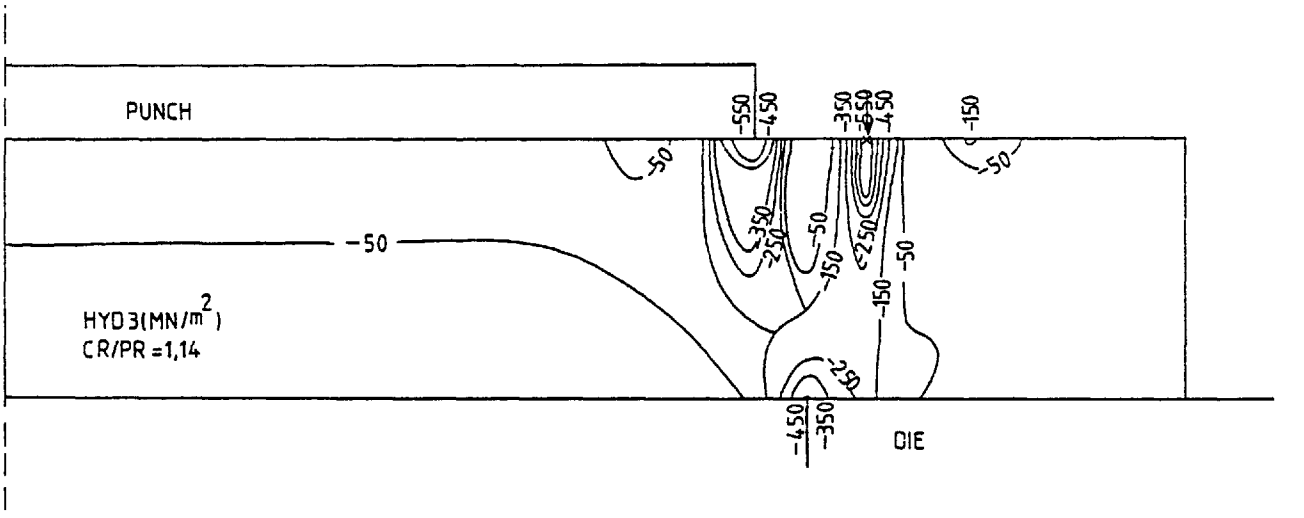

Fig. 5-141. Hydrostatic component of stress contours during blanking when a CF = 70 kN clamping force at a clamp/punch diameter ratio of (CR/PR = 1.14) was used.

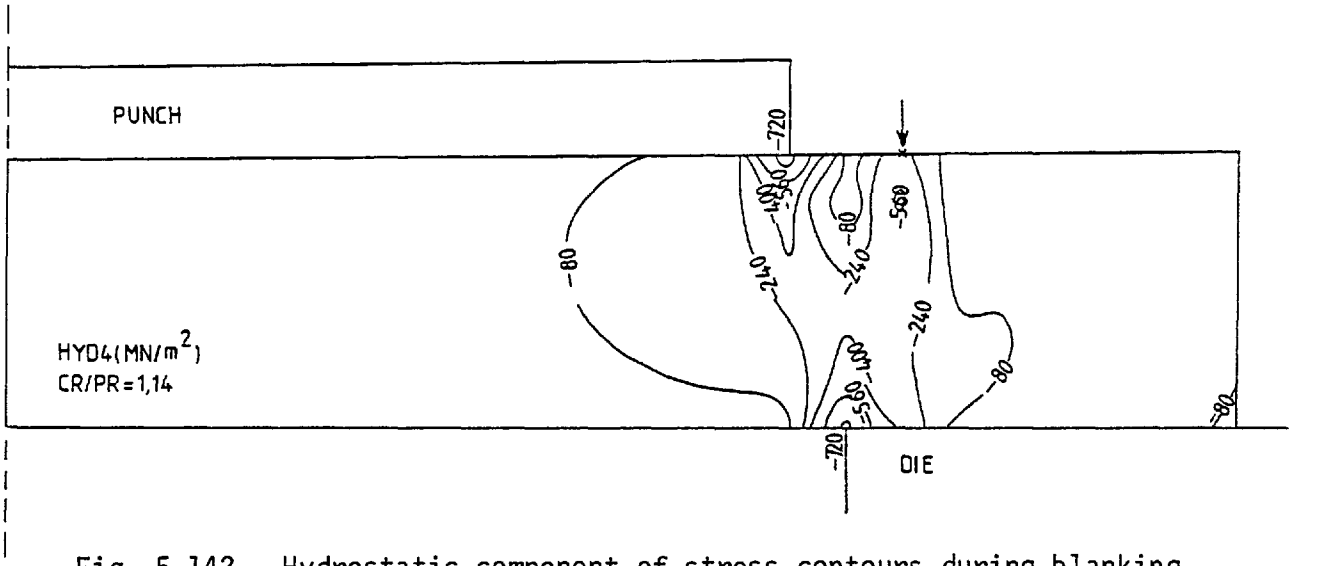

Fig. 5-142. Hydrostatic component of stress contours during blanking when a BP = 70 kN back-load and a CF = 70 kN clamping force, at a clamp/punch diameter ratio of (CR/PR = 1.14), were used.

holder with minimum clamp diameter was used during blanking, are shown in Fig. 5-141. Comparing this stress field with that of simple blanking shown in Fig. 5-136, it becomes clear that the region with high stress level at the punch edge is smaller and a considerable reduction in the stress concentration around the die edge, similar to the corresponding hoop stress and radial stress fields explained earlier in sections 5.15.3 and 5.15.4, is quite noticeable.

The hydrostatic component of stress contours when an equal value of back-load was used in addition to the clamping force are shown in Fig. 5-142. Here again, similar to the hoop and radial stresses an addition of a back-load with minimum clamp diameter, a sudden increase in the concentration of stress contours occurs at the die edge compared to the previous case shown in Fig. 5-141. As was mentioned previously, this sudden increase in the stress contours concentration at the die edge must be due to the prevention of excessive bending of the specimen by the application of a back-load. The harmful effect of excessive bending on the concentration of stress contours in the shearing zone will be discussed later in section 5.16.

An increase in the concentration of stress contours around the shearing zone and especially at the punch and die edges, compared to the corresponding case shown in Fig. 5-139 is quite noticeable. In this case, for the same amount of punch penetration, higher stresses build up in the shearing zone, which must be due to a smaller volume of confined material. Shorter distance of the line of action of the clamping force from the die edge, when using a smaller clamp diameter, which restrains a smaller volume of the material for the same value of clamping force, compared to the case when using maximum clamp diameter, must have a significant effect on the stresses in this region.

5.16 Discussion

It is generally recognized that the maximum tensile principal stress has a critical effect on propagating cracks, and causing fracture. Both crack nucleation and propagation are favoured by high tensile stresses. Conversely, shear deformation requires high shear stresses. Shear deformation tends to relieve the stresses developed in the deforming material, and thus it is difficult to achieve large stresses when a metal deforms easily by shear. From these considerations it can be concluded that any stress system capable of producing a combination of large tensile stresses and small shear stresses favours fracture.

In simple uniaxial tension, the stress can be viewed as equivalent to a set of shear stresses oriented at 45^{o} to the tensile stress axis. This relationship is shown in Fig. 5-143, where the tensile stress in one case is assumed horizontal and in the other case vertical.

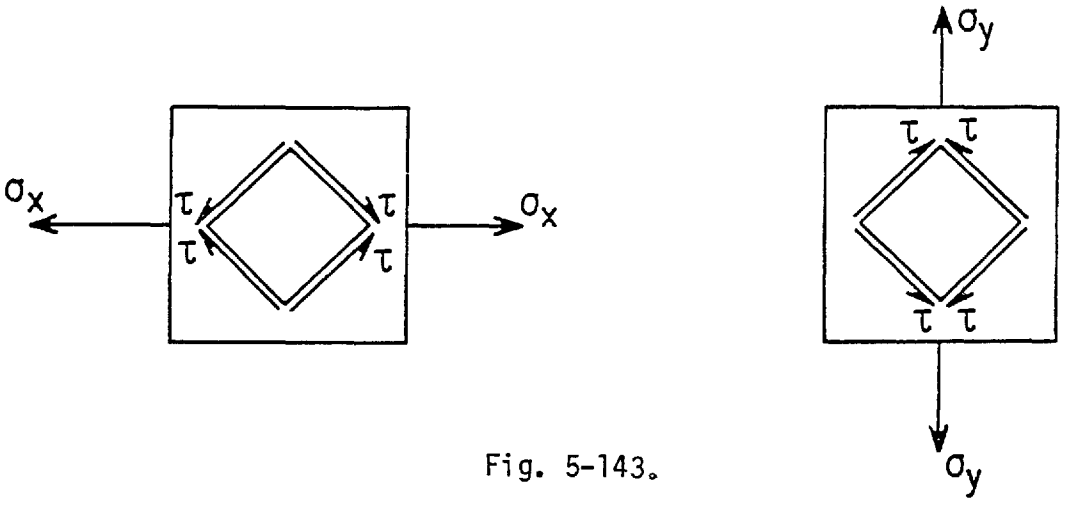

Fig. 5-143.

If the two tensile stresses (at 90^{o} to each other, as shown in these drawings) are applied simultaneously to the same specimen, the shear stress components will oppose each other. In the two dimensional case, it is clear that under a state of biaxial tension the shear stress in the material is reduced. Also, if a third tensile stress is applied

normal to the plane of the above two stresses, and all tensile stresses are assumed equal, a state of hydrostatic tension will occur in which the material experiences no shear stress whatsoever.

From the above it can be concluded that, whenever a metal specimen is tested under conditions of biaxial or triaxial tension, slip that requires shear stress will tend to be suppressed. Because of this, a high level of tensile stress can be attained and fibrous fracture can be promoted. Conversely, if a metal specimen is pulled in tension while immersed in a fluid under pressure, the above conditions will be radically altered. In this case, the applied tensile stress will be complemented by compressive stresses, having shear components in the same direction as those of the applied tensile stress. Deformation by slip in this case is highly favoured, and very high ductilities can be achieved.

The blanks obtained from the conventional blanking operation consist mainly of a bright burnished ring due to shear deformation and a rough fractured section caused by crack propagation, Fig. 4-45. At the early stages of the blanking operation the material undergoes a pure shear deformation. As the process continues, tensile stresses develop and micro cracks nucleate within the material. At a certain amount of punch penetration the developing tensile stresses in the shearing zone reach such a level so as to cause the cracks to open, which then propagate and result in fracture.

The foregoing considerations, and the studying of the effect of hydrostatic pressure on different metal forming processes, presented in section 5.12, suggest that the change of surface finish from fibrous to pure shear in fine blanking must be due to the additional compressive stresses caused in the shearing zone, through the application of clamping

force and back-load. The induced compressive stresses caused by the blank-holder and counter-punch reduce the maximum tensile principal stress in the shearing zone. The decrease in the maximum tensile principal stress favours deformation by slip and tends to suppress crack propagation and so also prevent fibrous fracture.

In the following, a general discussion concerning the effect of the punch/die clearance, blank-holder, counter-punch and blank-holder diameter on the state of stress in the shearing zone will be given. In addition, comparisons of some of the theoretical results and experimental findings will be made in support of the above argument, i.e., that by the application of clamping force and back-load, the hydrostatic component of stress which develops in the shearing zone suppresses crack propagation so also fracture, by reducing the maximum principal stress in that region. It will be shown that in all cases an increase in the hydrostatic component of stress accompanied by a decrease in the corresponding maximum principal stress in the shearing zone, corresponds in experiment to an improvement in the blank edge surface finish, under the same boundary conditions.

It has been found experimentally that for thin materials the blank surface finish improves as the clearance between the punch and die decreases. The theoretical results for different values of punch/die clearance, section 5.14.9, are in agreement with the experimental results. A decrease in the clearance between the punch and die causes an increase in the hydrostatic component of stress which is accompanied by a decrease in the corresponding maximum tensile principal stresses in the shearing zone.

Minimizing the clearance between the punch and die has a significant effect on the state of stress which develops in the shearing zone

during blanking. In the case of a large punch/die clearance the process of punch penetration leads to a material deficiency in the shearing zone which is directly proportional to the clearance between the punch and die, Fig. 5-144. It can be envisaged that when such a material

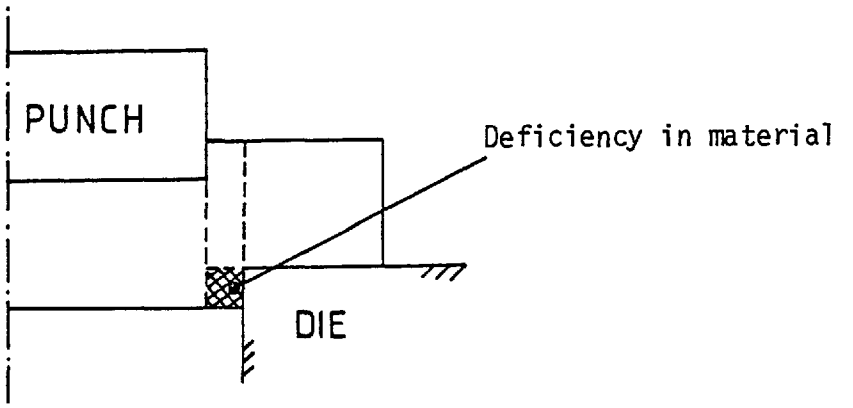

Fig. 5-144.

deficiency occurs, even a high hydrostatic component of stress caused by indentation with a blank-holder would be relieved and a condition of high tension would prevail in the shearing zone, leading to fracture. To perform a successful fine blanking operation it is thus imperative to provide minimum clearance between the punch and die. Bigger values of clearance not only lead to non accurate dimensional accuracy, which is contrary to one of the main requirements of a fine blanked product, but also reduce the effect of blank-holder and counter-punch. To obtain blanks with a smooth surface finish much higher values of clamping force and back-load would probably now be required to make up for the deficiency of material occuring in the shearing zone due to the excessive clearance.

The inefficiency of the blank-holder in the case of large punch/die clearances, cannot be analyzed by the theoretical method. This is due to the limitation of the type of element used in the analysis, in which the boundary of the elements remain as straight lines during

the deformation. In the actual blanking operation an excessive clearance between the punch and die affects the stresses in the shearing zone causing the material to flow into the volume shown by the shaded area in Fig. 5-144. However, in the case of quadrilateral isoparametric elements, which were used in the computer program, owing to the limitation mentioned above concerning the boundary of the elements, the material flow cannot be modelled to fill this gap and thus the stresses will not be affected to a great extent, Fig. 5-145(a). Higher order elements which can deform into curved boundaries would be more suitable to study this particular effect, since in this case the element boundaries can deform and the deforming material could be modelled to fill the gap, Fig. 5-145(b).

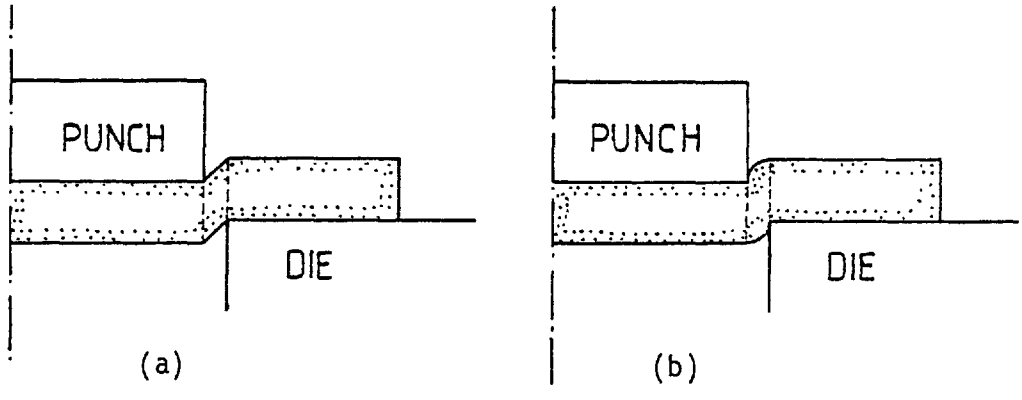

Fig. 5-145

It has been assumed for sometime, that in fine blanking the material on the die face moves away from the shear line. The provision of a blank-holder not only compresses the material towards the shear line, thereby causing high compressive stresses in the shearing zone, but also contributes to an increase in the compressive stresses in that region by blocking the outward flow of material.

In this work by the use of the finite element method, the tangential forces applied to the die face through the specimen were calculated

and by finding the direction of these forces the movement of the material away from the shear line was verified, section 5.11.2. This substantiates the idea that the provision of bank-holder during blanking increases the compressive stresses in the shearing zone, in the manner mentioned above.

The experimental results in section 4.8.4 showed that the increase in clamping force resulted in an increase in the crack free surface portion of the blank. The experimental works performed by Johnston(36) and Maeda (37) also prove this point. This increase in the crack free surface portion of the blank due to the increase in the clamping force was now theoretically analyzed and it was found that, for a certain blank-holder diameter, an increase in the clamping force causes an increase in the hydrostatic component of stress and a decrease in the corresponding maximum principal stress prevailing in the shearing zone. This must be the cause for a higher percentage of smooth surface finish of the blank observed in the experiment. The decrease in the maximum tensile principal stress shown in the theoretical results indicates that the deformation (shearing) can now continue further before the maximum principal stresses develop to such a level so as to cause fracture.

The increase in the compressive stresses in the shearing zone caused by increasing the clamping force is due to increased restraint of the material. Furthermore, the increased clamping force more efficiently blocks the outward flow of material.

The theoretical results indicated that, for equal values of clamping force and back-load, the clamping force resulted in a higher hydrostatic component of stress and lower values of maximum principal stress in the shearing zone than the back-load, indicating that the

clamping force is more effective than the back-load in producing blanks with better surface finish. The results showed that the back-load has little effect when it acts alone. The higher effect of the clamping force than the back-load on the blank edge surface finish has been experimentally verified by Maeda (37).

The inefficiency of the back-load in developing high compressive stresses in the shearing zone caused by the compression of the specimen between the punch and counter-punch, must be due to the, relatively limited restriction on the outward flow of material imposed by the rest of material situated outside the shear line, Fig. 5-146.

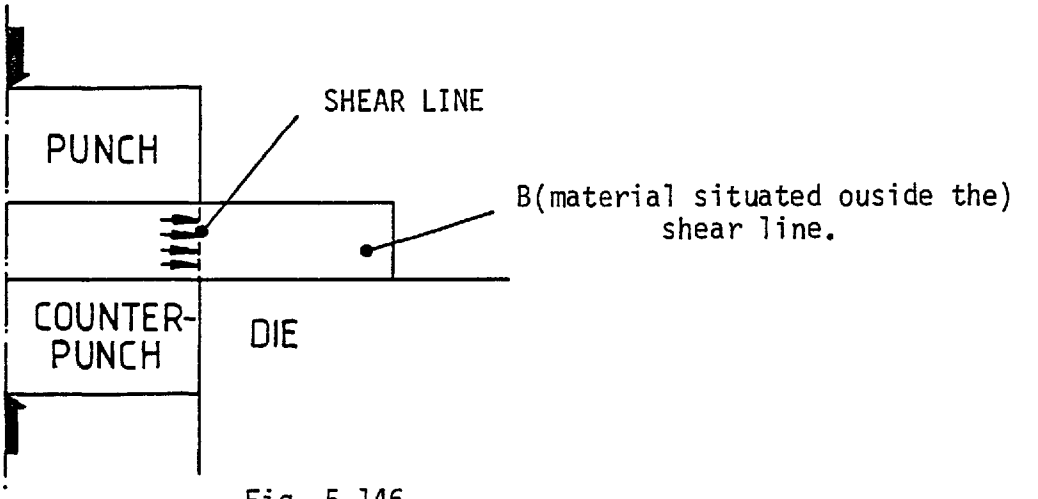

Fig. 5-146.

A high state of compression cannot build up in the shearing zone as the material 'B' situated outside the shear line can expand to relieve the stresses.

The experimental results presented in section 4.8.4 and observations indicate that the combination of clamping force and back-load result in higher crack free surface portion of the blank edge, compared to the cases when back-load or clamping force act alone. This has also been verified by the experimental work performed by Maeda (37). The theoretical

results are in complete agreement with the experimental results as it was found that, for any given value of clamp diameter, a clamping force together with a back-load produce the highest hydrostatic component of stress during blanking and also the lowest value of the maximum principal tensile stress in the shearing zone.

The experimental results in section 4.8.4 showed that an optimum clamp diameter exists for any given vlaue of clamping force when the fractured surface finish of the blank is at a minimum. This has also been verified by Maeda (37) in his experimental work on fine blanking. In the theoretical model an explanation for the existence of this optimum clamp diameter was sought through the study of the hydrostatic component of stress and maximum principal stress prevailing in the shearing zone. The theoretical results show that, when the clamping force is acting at the farthest distance from the punch edge, CR/PR = 1.28, the hydrostatic component of stress in the shearing zone increases slightly. The corresponding maximum principal stress then becomes smaller to some extent but, even with the addition of the maximum clamping force (CF = 70 kN) to an equal value of back-load, the maximum principal stress still remains tensile over most of the material thickness. This is due to the large distance between the line of action of the clamping force and the die edge, which allows some stress release, thus the blank-holder cannot effectively influence the state of stress in the shearing zone.

When a smaller clamp diameter is used, the theoretical results predict a higher hydrostatic component of stress and a lower value of maximum principal stress in the shearing zone. The maximum principal stress for the maximum value of clamping force (70 kN) decreases considerably and when an equal value of back-load is present, it becomes

zero or negative in most parts of the shearing zone. The increase in the smooth surface portion of the blank edge observed experimentally must be due to this increase in the hydrostatic component of stress and decrease in the corresponding maximum tensile principal stress, which, as was mentioned earlier, will allow a further shear deformation of the material before the developing tensile stresses reach a level sufficient to open up the cracks and cause them to propagate.

The increase in the hydrostatic component of stress caused by the decrease in the clamp diameter must be due to the fact that the line of action of the clamping force is now nearer to the die edge and thus the same clamping force restrains a smaller volume of the material than was the case for the larger clamp diameter, Fig. 5-147.

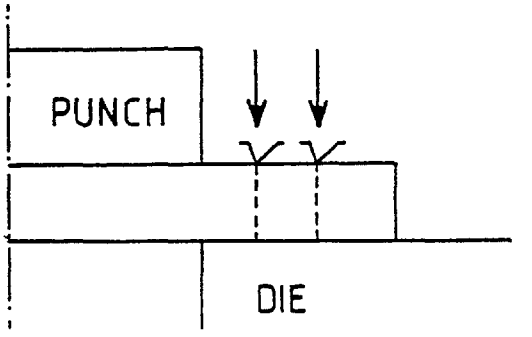

Fig. 5-147. By decreasing the clamp diameter, for the same value of clamping force, the clamp restrains a smaller volume of the material.

The theoretical results indicate that, as the clamp diameter is decreased further (CR/PR = 1.14), there is a sudden change in the trend of the hydrostatic component of stress and maximum principal stress curves. The curves take a strong wavy pattern, compared to the two previous cases (CR/PR = 1.21 and 1.28), and although the results show further improvement in one part of the shear line (i.e. higher value of the hydrostatic component of stress and lower value of maximum principal tensile stress in another part they continuously yield less desirable values, indicating that the blank-holder is not able to affect

the prevailing state of stress throughout the shear line to the same extent. The examination of the hydrostatic component of stress contours indicates that, when a blank-holder with a clamp/punch diameter ratio of (CR/PR = 1.14) is used i.e. closest to the punch edge, the hydrostatic component of stress in the vicinity of the die edge decreases dramatically, as distinct from the effect of a blank-holder with clamp/punch diameter ratio of (CR/PR = 1.28).

This sudden change of trend must be due to the excessive bending of the specimen as the clamp diameter decreases. A possible explanation is that the blank-holder produces a convex bending of the specimen when viewed from the die as a result of the larger transverse compression of the material on the punch side, see illustration below for definitions.

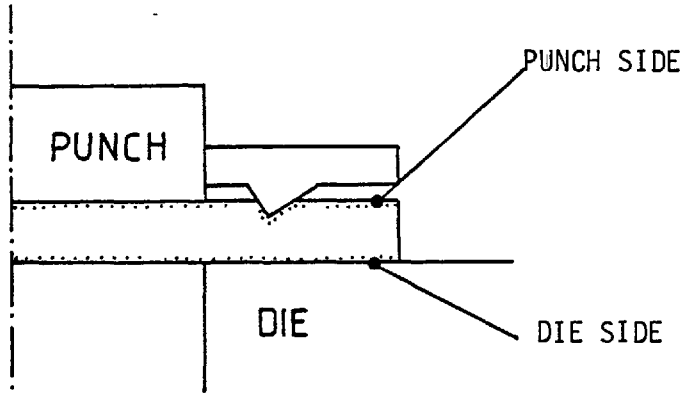

This bending effect increases with the increase of clamping force and the decrease of clamp diameter, the latter being due to the increase in the distance from the die edge of the force 'F' applied to the specimen by the blank-holder, as the clamp diameter decreases, Fig. 5-148.

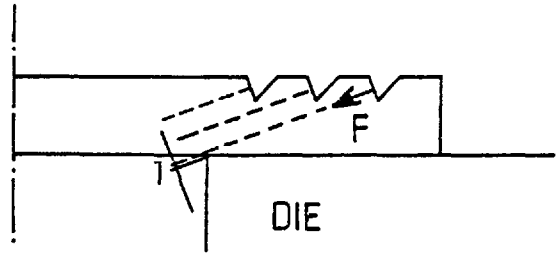

Fig. 5-148. The distance of force 'F' from the die edge decreases as the clamp diameter increases.

At large values of clamp diameter distance 'l' is small thus the bending moment of force'F' with respect to the die edge and the bending of the confined material, are small values. The application of clamping force at such clamp diameters will mainly act to compress the confined material towards the axis of symmetry rather than to bend the specimen, Fig. 5-149.

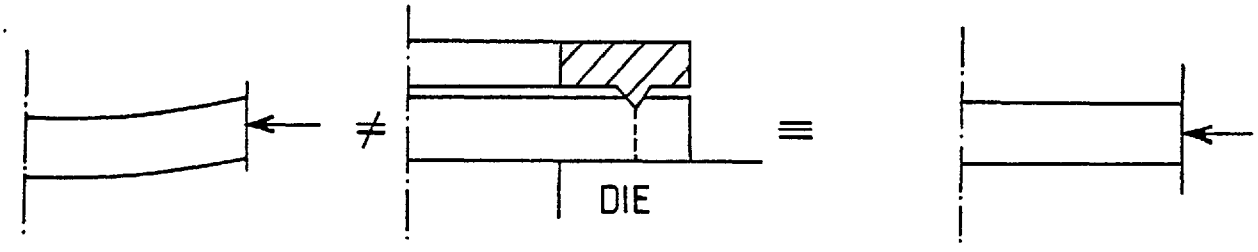

Fig.5-149. At large values of clamp diameter the specimen bends very little and the clamping force mainly acts to compress the confined material in a constrained manner rather than to bend the specimen.

As the clamp diameter decreases the distance'l' increases thus the bending moment of force 'F' with respect to the die edge also increases. For blank-holder diameters smaller than a certain value the bending moment with respect to the die edge of the force 'F' under high values of clamping force reaches such a level that the confined material mainly undergoes bending rather than a constrained compression, Fig. 5-150.

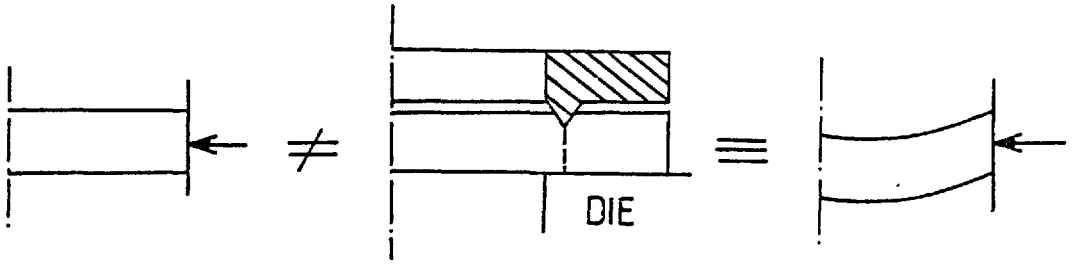

Fig. 5-150. At small values of clamp diameter the bending moment of the clamping force reaches such a level that the clamping force will mainly act to bend the specimen rather than to compress and constrain the material.

For this case the increase in clamping force does not affect the prevailing state of stress in the shearing zone significantly.

The results indicate that, by reducing the clamp diameter, the hydrostatic component of stress in the shearing zone increases with increasing clamping force, which has the desirable effect on the blank edge surface finish. When using a clamp diameter smaller than a certain value, by increasing the clamping force the state of stress in the shearing zone improves up to a limit i.e. higher hydrostatic component of stress and lower value of maximum tensile principal stress. After a certain limit, further increase in the clamping force will improve the state of stress in the shearing zone only to a very small extent, thus decreasing the efficiency of the blank-holder when its diameter is below a critical value.

The hydrostatic component of stress contours indicate that although a clamping force alone at a clamp/punch diameter ratio of (CR/PR = 1.14) results in a dramatic decrease in the hydrostatic component of stress at the die edge, the addition of back-load causes a substantial increase in the corresponding value in this region. This must be due to the prevention of the excessive bending of the specimen through the application of back-load, which once again causes the confined material to undergo a constrained compression rather than bending.

It must be emphasized that the finite element approach to the fine blanking process presented in this thesis was employed mainly as a tool to study the state of stresses within the material under different boundary conditions and thereby find an explanation for the effect of clamping force, clamp diameter, back-load, material thickness and punch/die clearance on the surface finish of the blank. In blanking mild steel strips of thickness t = 0.120 in. (3.04 mm),

the theoretical results indicate that 70 kN clamping force and the same back-load, when clamp/punch diameter ratios of (CR/PR = 1.14 or 1.21) are used, reduce the maximum principal stresses in the shearing zone to zero or negative values. The experimental results, when using optimum clamp diameter, indicate that the use of approximately 50 kN clamping force and back-load results in a blank with a crack free surface finish. Considering the theoretical prediction and experimental findings and bearing in mind that, to prevent fracture the maximum tensile principal stress must be lower than a critical value (not necessarily zero) it can be concluded that the extension of this work to fracture mechanics may lead to quantitative results so that conditions leading to any desired condition of the blank edge could be predicted theoretically. Furthermore, the calculation of clamping force, back-load and clamp diameter could be carried out with a much higher degree of accuracy, if a finer mesh is chosen throughout the whole specimen, and particularly around the shearing zone and clamp. This would not only lead to a much more accurate calculation of the stresses within the material but would provide the possibility of choosing narrower elements at the clearance between the punch and die resulting in a more realistic simulation of the actual process, as explained in the following.

It was previously mentioned that, to simulate the blanking operation, a configuration such as shown in Fig. 5-151 has to be used with the punch edge acting at point 'A' to provide zero or very small clearance

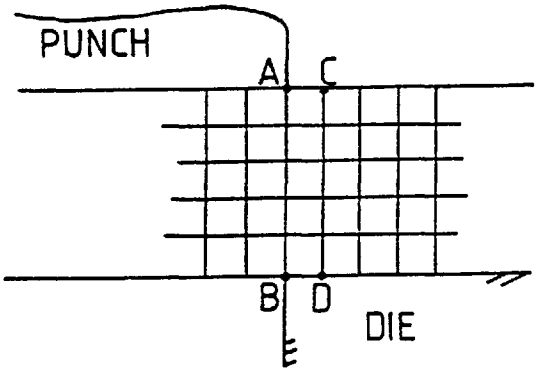

Fig. 5-151.

between the punch and die, as in the actual process. On the other hand this configuration cannot simulate the actual deformation process. The reason is that in the actual process the blanking load shears the material along the line AB as the punch penetrates it, Fig. 5-152(a). This results in a displacement of the material on the left of AB relative to that on the right. One possible way of modelling this process shown in Fig. 5-152(b) does not allow for this relative displacement of the material but instead the penetration of the punch is modelled by the compression of the material along AB, thus requiring a much higher value of blanking load to achieve the same punch penetration as in the actual process.

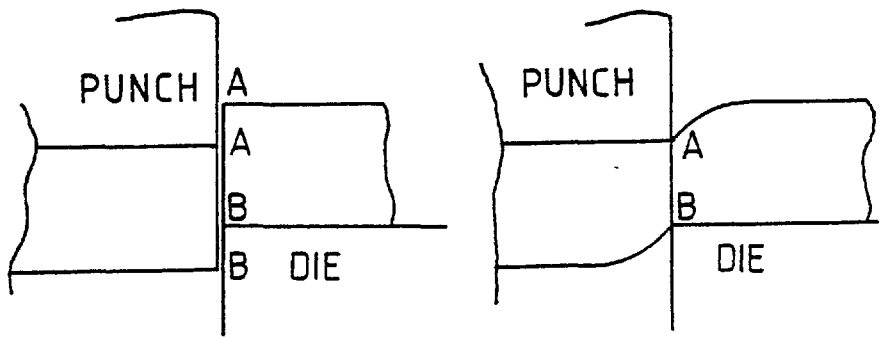

(a) Actual process (b) An improper model

Fig. 5-152.

To overcome this problem it was decided to release point 'B' so that it can have vertical displacement, Fig. 5-153. Referring to Fig. 5-151, the adoption of this method would result in a clearance between the punch and die equal to the width of one mesh element in this region.

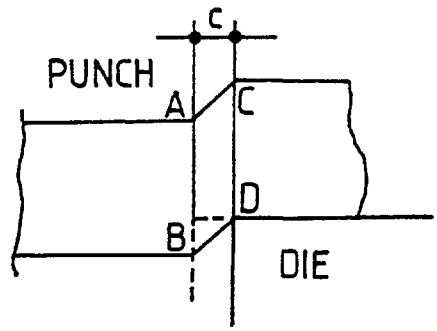

Fig. 5-153. More realistic model for blanking.

By choosing a very fine mesh the line CD can come very close to the line 'AB' and by following the procedure explained earlier a very small punch/die clearance would be introduced into the model.

As the punch die clearance decreases, the line MN, Fig. 5-154, approaches the shear line along which the hydrostatic component of stress and maximum principal stress calculations are carried out. Since MN is the line along which crack propagation is most likely to occur, a decrease in punch/die clearance not only brings the model

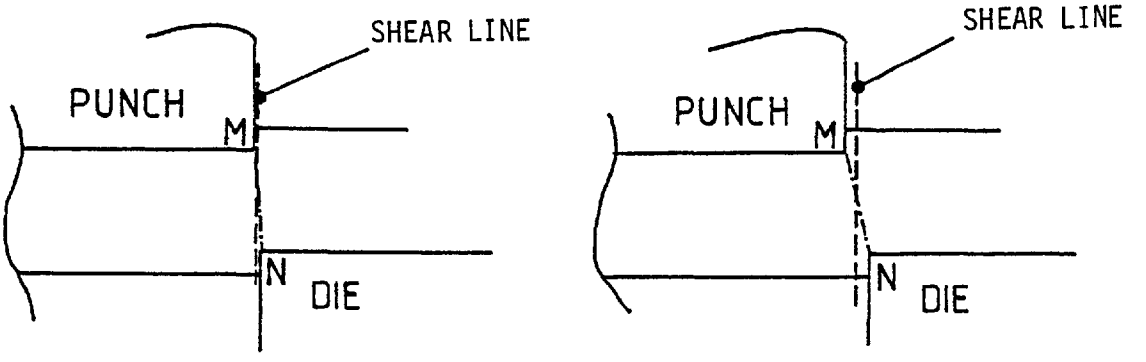

Fig. 5-154.

closer to the actual process but the hydrostatic component of stress and maximum principal stress calculations along the shear line would be more representative of the values corresponding to the most likely direction of crack propagation.

5.17 Conclusions

The final conclusions may be summarized as follows.

1) The blanking load obtained from the experimental results is almost independent of the clamping force and clamp diameter and, when the back-load is present, the curve is uniformly displaced by an amount equal to the back-load.

The finite element method predicts the blanking load up to the maximum value with a very good degree of accuracy for all the material thicknesses. It also predicts the experimental results concerning the effect of clamping force, clamp diameter and back-load on the load displacement characteristics of the material.

2) The hardness survey over a sectioned partially blanked specimen indicates that the hardness value is at its highest level on the shear line, and the maximum values occur at the punch and die edges, the higher value being at the die edge.

The theoretical equivalent stress contours indicate that the stresses increase towards the shear line and approach their highest level closer to it. As the equivalent stress and hardness values are both related to the amount of work hardening of the material, it can be concluded that the finite element approach predicts the same highly work hardened regions as the results obtained from experiments.

3) By the use of a blank-holder, there is no change in the position of the maximum hardness gradient over the sectioned partially blanked specimen. This is also verified by the equivalent stress contours obtained from the theoretical method, which is also an indication of the hardness values in the different regions.

This indicates that the smooth surface finish obtained in fine .

blanking by the application of a blank-holder must be due to suppression of cracks through the provision of high compressive stresses caused by the blank-holder. This is unlike finish piercing, where a smooth surface finish is due to the transfer of crack propagation from the work material to the waste material.

4) The theoretical method predicts a higher dishing effect for the blanks produced from thicker strips of material and also when the specimen remains clamped against the die using a blank-holder throughout the operation. These results are in agreement with experimental observations.

5) The theoretical results indicate a maximum distribution of load at the punch and die edges which decreases very rapidly away from them.

6) The theoretical method predicts an outward flow of material away from the shear line during blanking, which indicates the effect of the blank-holder in raising the compressive stresses in the shearing zone by blocking this outward flow.

7) The experimental results show that, by increasing the clamping force, the unfractured surface portion of the blank increases. The corresponding theoretical results prove that an increase in clamping force, irrespective of clamp diameter, results in an increase in the hydrostatic component of stress and a decrease in the maximum tensile principal stress in the shearing zone. It can be concluded that the effect of additional tooling is the production of crack-free blanks achieved by an increase in the hydrostatic component of stress and by decreasing the maximum tensile principal stresses in the shearing zone.

8) The theoretical results indicate that the clamping force is more effective than the back-load and the combined clamping force

and back-load has the greatest effect on the production of smooth blanks. These results were verified by existing experimental results.

9) An optimum clamp diameter was found to exist, experimentally, where, for any given value of the clamping force, the fractured region is at a minimum. This optimum clamp diameter was also predicted by the theoretical method. The theoretical results indicate that blank-holders of diameter greater than the optimum value could not act effectively owing to the large distance between the blank-holder projection and the shear line which permits stress release. For diameters smaller than the optimum value bending of the blank becomes predominant, which nullifies the effect of the blank-holder.

10) The theoretical results predict a higher hydrostatic component of stress and a lower value of the maximum tensile principal stress with decreasing punch/die clearance. This is in agreement with the improvement in the blank surface finish obtained experimentally.

APPENDIX 'A'

LISTING OF THE COMPUTER PROGRAMS USING TRIANGULAR AND ISOPARAMETRIC QUADRILATERAL ELEMENTS

Variables in COMMON BLANK	Definition (TRIANGULAR ELEMENTS)
FORCE	Nodal forces
D	Elasticity matrix
ESK	Element stiffness matrix
DSTZ	Axial stress increment
DSTR	Radial stress increment
DSTT	Hoop stress increment
DSTRZ	Shear stress increment
DEP	Plastic strain increment
TEP	Total plastic increment
DDIS	Nodal point displacement increments
DTST	Equivalent stress increments
DFORCE	Nodal point force increments
TSK	Matrix containing element stiffness matrices
PL	Status vector defining the elements state as plastic or elastic
STR	Radial stress
STZ	Axial stress
STT	Hoop stress
STRZ	Shear stress
TST	Equivalent stress
DSK	Element stiffness matrix increment
Y	Elements yield stress
TDIS	Nodal point total displacement
B	Strain displacement matrix
HP	Tangent modulus
G	Shear modulus of elasticity
NU	Poisson's ratio

E1	Modulus of elasticity
NELE	Number of elements
NEQ	Number of equations
NBAND	Overall stiffness matrix bandwidth
NOP	Element nodal point connections
SK	Overall stiffness matrix of the structure
DIS	Nodal point displacement
POINTR	Status vector defining the state of nodal points as suppressed or free surfaces

COMMON B1		Definition
NBC	NBC	Boundary nodal points that their status will be set in the program
Z,R	Z,R	Coordinates of nodal points

MAIN PROGRAM	Definition
CLAMP	Clamping force
BLANK	Blanking force

ESTIF SUBROUTINE	Definition
BJ, BM, CJ, CM	Local coordinates of elements
AREA	Element area
RBAR	Element centroid coordinate

```
      PROGRAM TRI(INPUT=113B,OUTPUT,
     6TAPE5=INPUT,TAPE6=OUTPUT,TAPE1=113B,TAPE2=113B)
      COMMON/ / FORCE(350),D(4,4),W(4,6),ESK(6,6),DSTZ(309),DSTR(309),DS
     6TT(309),DSTRZ(309),DEP(309),TEP(309
     6),DDIS(350),R1(350),DTST(309),DFORCE(350),TSTP2(309),TEMP(6),
     6TSK(309,6,6),PL(309),STR(309),STZ(309),STT(309),STRZ(309),TST(309)
     6,DSK(6,6),Y(309),TDIS(350),DB(4,6),B(4,6),
     6HP,G,NU,E1,NELE,NEQ,NB,NBAND,NOP(309,3),SK(350,28),DIS(35
     60),POINTR(350)
      COMMON/B1/NBC(20),Z(175),R(175)
      INTEGER P,Q,O,POINTR,PUNCH1,PL
      REAL NU
      DATA NBC/1,14,27,40,53,66,79,92,111,124,137,150,163,167,171,175,
     698,85,72,59/
      DATAR/7*2.2,6*2.15,7*2.1,6*2.05,7*2.,6*1.95,7*1.9,6*1.85,7*1.8,
     66*1.75,7*1.7,6*1.65,7*1.6,6*1.55,7*1.5,6*1.45,7*1.4,6*1.35,7*1.3,
     66*1.25,7*1.2,6*1.15,7*1.1,6*1.05,7*1.,4*.8,4*.4,4*.0/
      DATAZ/0.,0.1,0.2,0.3,0.4,0.5,0.6,0.05,.15,.25,.35,.45,.55,
     6.0,.1,.2,.3,.4,.5,.6,.05,.15,.25,.35,.45,.55,
     6.0,.1,.2,.3,.4,.5,.6,.05,.15,.25,.35,.45,.55,
     6.0,.1,.2,.3,.4,.5,.6,.05,.15,.25,.35,.45,.55,
     6.0,.1,.2,.3,.4,.5,.6,.05,.15,.25,.35,.45,.55,
     6.0,.1,.2,.3,.4,.5,.6,.05,.15,.25,.35,.45,.55,
     6.0,.1,.2,.3,.4,.5,.6,.05,.15,.25,.35,.45,.55,
     6.0,.1,.2,.3,.4,.5,.6,.05,.15,.25,.35,.45,.55,
     6.0,.1,.2,.3,.4,.5,.6,.05,.15,.25,.35,.45,.55,
     6.0,.1,.2,.3,.4,.5,.6,.05,.15,.25,.35,.45,.55,
     6.0,.1,.2,.3,.4,.5,.6,.05,.15,.25,.35,.45,.55,
     6.0,.1,.2,.3,.4,.5,.6,.05,.15,.25,.35,.45,.55,
     6.0,.1,.2,.3,.4,.5,.6,.0,.2,.4,.6,.0,.2,.4,.6,.0,.2,.4,.6/
      NCLAMP=20
      DO 1 I=1,309
      Y(I)=2000.
1     CONTINUE
      NU=0.291$E1=2.1E06$HP=2500.$G=E1/(2.*(1.+NU))
      NBAND=28$NELE=309$NODE=175
      READ(5,20)((NOP(I,J),J=1,3),I=1,NELE)
20    FORMAT(24I3)
      MK=16$LL=9$NB=15
      NEQ=2*NODE
      DO 11 I=1,NODE
      Z(I)=0.506*Z(I)
```

```
11    CONTINUE
      DO 13 I=1,NEQ
      POINTR(I)=1
      FORCE(I)=0.
      R1(I)=0.
      DIS(I)=0.
13    CONTINUE
      DO 14 I=1,NELE
      PL(I)=0
      STZ(I)=0.$STR(I)=0.$STT(I)=0.$STRZ(I)=0.$TST(I)=0.
      TEP(I)=0.$DTST(I)=0.
14    CONTINUE

C     *********FORM ELEMENT STIFFNESS MATRIX*****************

************************                          ********************************
      DO 60 I=1,NELE
      CALL BMATX(I)
      CALL DMATX(I)
      CALL DBE(DB,D,B)
      CALL ESTIF(I)
      DO 60 P=1,6
      DO 60 Q=1,6
60    TSK(I,P,Q)=ESK(P,Q)
************************                          ********************************
      DO 70 N=1,NEQ
      DO 70 M=1,NBAND
70    SK(N,M)=0.
      DO 120 N=1,NELE
      DO 110 JJ=1,3
      NROWB=(NOP(N,JJ)-1)*2
      DO 110 J=1,2
      NROWB=NROWB+1
      I=(JJ-1)*2+J
      DO 100 KK=1,3
      NCOLB=(NOP(N,KK)-1)*2
      DO 90 K=1,2
      L=(KK-1)*2+K
      NCOL=NCOLB+K+1-NROWB
      IF(NCOL)90,90,80
80    SK(NROWB,NCOL)=SK(NROWB,NCOL)+TSK(N,I,L)
90    CONTINUE
100   CONTINUE
110   CONTINUE
120   CONTINUE
************************                          ********************************
      POINTR(349)=0$POINTR(347)=0$POINTR(345)=0$POINTR(343)=0
      DO 21 I=1,8
      J=NBC(I)
      POINTR(2*J)=0$POINTR(2*J-1)=0
21    CONTINUE
      DO 2100 I=NCLAMP,NCLAMP
      J=NBC(I)
      POINTR(2*J-1)=0
      POINTR(2*J)=0
```

```
      DIS(2*J)=-1.$DIS(2*J-1)=-.6
2100  CONTINUE
************************                              ********************************
      CALL SOLVE

************************                              ********************************
      DO 130 L=1,NELE
      CALL BMATX(L)
      CALL DMATX(L)
      CALL DBE(DB,D,B)
      I=NOP(L,1)$J=NOP(L,2)$K=NOP(L,3)
      TEMP(1)=R1(2*I-1)
      TEMP(2)=R1(2*I)
      TEMP(3)=R1(2*J-1)
      TEMP(4)=R1(2*J)
      TEMP(5)=R1(2*K-1)
      TEMP(6)=R1(2*K)
      STZ(L)=0.$STR(L)=0.$STT(L)=0.$STRZ(L)=0.
      DO 125 II=1,6
      STZ(L)=STZ(L)+DB(1,II)*TEMP(II)
      STR(L)=STR(L)+DB(2,II)*TEMP(II)
      STT(L)=STT(L)+DB(3,II)*TEMP(II)
      STRZ(L)=STRZ(L)+DB(4,II)*TEMP(II)
125   CONTINUE
      TST(L)=SQRT(2.)/2.*SQRT((STR(L)-STZ(L))**2+(STZ(L)-STT(L))**2+(STT
     6(L)-STR(L))**2+6.*STRZ(L)**2)
130   CONTINUE

      SIGMAX=0.
      DO 150 I=1,NELE
      IF(TST(I).GE.SIGMAX) GO TO 140
      GO TO 150
140   SIGMAX=TST(I)
      P=I
150   CONTINUE
      ETA=Y(P)/SIGMAX
      DO 160 I=1,NELE
      STR(I)=ETA*STR(I)$STZ(I)=ETA*STZ(I)
      STT(I)=ETA*STT(I)$STRZ(I)=ETA*STRZ(I)$TST(I)=ETA*TST(I)
160   CONTINUE
      DO 170 I=1,NEQ
      FORCE(I)=ETA*DFORCE(I)
      TDIS(I)=ETA*R1(I)
170   CONTINUE
      WRITE(6,181)(I,TST(I),I=1,NELE)
181   FORMAT(10X,*NO*,I3,10X,*TST=*,E15.5)
      WRITE(6,182)(I,TDIS(2*I),FORCE(2*I),I=1,NODE)
182   FORMAT(10X,*COOR=*,I3,*DIS=*,F10.6,*FORCE=*,F10.2)
C     ******APPLY DISPLQCEMENT INCREMENT***************
      ITT=0
      CLAMP=0.
************************                              ********************************
      III=0
      DO 530 M=1,500
```

```
      DO 5030 I=1,8
      J=NBC(I)
      IF(FORCE(2*J).GE.0.) GO TO 5030
      POINTR(2*J)=1$POINTR(2*J-1)=1
      FORCE(2*J)=0.$FORCE(2*J-1)=0.
5030  CONTINUE
      IF(M.EQ.1) GO TO 5010
      IF(CLAMP.GE.-3000.) GO TO 210
      DO 1820 I=NCLAMP,NCLAMP
      J=NBC(I)
      POINTR(2*J)=1$POINTR(2*J-1)=1
1820  CONTINUE
      IF(III.EQ.1) GO TO 1900
      DISMAX=TDIS(350)
      DO 211 I=9,16
      J=NBC(I)
      IF(TDIS(2*J).GE.DISMAX) GO TO 212
      GO TO 211
212   DISMAX=TDIS(2*J)
      PUNCH1=2*J
211   CONTINUE
      III=1
      POINTR(PUNCH1)=0
      DIS(PUNCH1)=-0.0005
1900  DO 213 I=9,16
      J=NBC(I)
      IF(POINTR(2*J).EQ.0) GO TO 214
213   CONTINUE
214   JJJ=2*J
      DO 216 I=9,16
      J=NBC(I)
      IF(TDIS(2*J).GT.TDIS(JJJ)) GO TO 215
      GO TO 216
215   POINTR(2*J)=0
      DIS(2*J)=-.0005
216   CONTINUE
      DO 217 I=9,16
      J=NBC(I)
      IF(FORCE(2*J).LE.0.) GO TO 217
      POINTR(2*J)=1
      FORCE(2*J)=0.
217   CONTINUE
      GO TO 260
210   DO 2600 I=NCLAMP,NCLAMP
      J=NBC(I)
      DIS(2*J)=-.0005
      DIS(2*J-1)=-.0003
2600  CONTINUE
260   DO 350 I=1,NEQ
      R1(I)=0.
350   CONTINUE
**********                                  **********
      CALL SOLVE

**********                                  **********
```

```
      DO 380 L=1,NELE
      CALL DMATX(L)
      CALL BMATX(L)
      CALL DBE(DB,D,B)
      I=NOP(L,1)$J=NOP(L,2)$K=NOP(L,3)
      TEMP(1)=R1(2*I-1)
      TEMP(2)=R1(2*I)
      TEMP(3)=R1(2*J-1)
      TEMP(4)=R1(2*J)
      TEMP(5)=R1(2*K-1)
      TEMP(6)=R1(2*K)
      DSTZ(L)=0.$DSTR(L)=0.$DSTT(L)=0.$DSTRZ(L)=0.
      DO 360 II=1,6
      DSTZ(L)=DSTZ(L)+DB(1,II)*TEMP(II)
      DSTR(L)=DSTR(L)+DB(2,II)*TEMP(II)
      DSTT(L)=DSTT(L)+DB(3,II)*TEMP(II)
      DSTRZ(L)=DSTRZ(L)+DB(4,II)*TEMP(II)
360   CONTINUE
      STRP2=STR(L)+DSTR(L)
      STZP2=STZ(L)+DSTZ(L)
      STTP2=STT(L)+DSTT(L)
      STRZP2=S TRZ(L)+DSTRZ(L)
      TSTP2(L)=SQRT(2.)/2.*SQRT((STRP2-STZP2)**2+(STZP2-STTP2)**2+(
     6STTP2-STRP2)**2+6.*STRZP2**2)
380   CONTINUE

      DO 390 I=1,NEQ
      DDIS(I)=R1(I)
390   CONTINUE
      ETA=5.
************************                              *********************************
      DO 410 I=1,NELE
      IF(PL(I).EQ.1) GO TO 402
      A=(DSTR(I)-DSTZ(I))**2+(DSTT(I)-DSTZ(I))**2+(DSTR(I)-DSTT(I))**2
     6+6.*DSTRZ(I)**2
      C=2.*(TST(I)**2-Y(I)**2)
      X=(STR(I)-STZ(I))*(DSTR(I)-DSTZ(I))+(STR(I)-STT(I))*(DSTR(I)-
     6DSTT(I))+(STT(I)-STZ(I))*(DSTT(I)-DSTZ(I))+6.*DSTRZ(I)*STRZ(I)
      ETA1=(-X+SQRT(X**2-A*C))/A
      IF(ETA1.LE.ETA.AND.ETA1.GE.0.01) GO TO 400
      GO TO 410
400   ETA=ETA1
      GO TO 410
402   IF(TST(I).GE.3500.)GO TO 410
      A=(DSTR(I)-DSTZ(I))**2+(DSTT(I)-DSTZ(I))**2+(DSTR(I)-DSTT(I))**2
     6+6.*DSTRZ(I)**2
      C=2.*(TST(I)**2-3500.**2)
      X=(STR(I)-STZ(I))*(DSTR(I)-DSTZ(I))+(STR(I)-STT(I))*(DSTR(I)-
     6DSTT(I))+(STT(I)-STZ(I))*(DSTT(I)-DSTZ(I))+6.*DSTRZ(I)*STRZ(I)
      ETA1=(-X+SQRT(X**2-A*C))/A
      IF(ETA1.LE.ETA.AND.ETA1.GE.0.01) GO TO 408
      GO TO 410
408   ETA=ETA1
410   CONTINUE
************************                              *********************************
```

```
      IF(ETA.GT.1.) ETA=1.
      DO 460 I=1,NELE
      DSTR(I)=ETA*DSTR(I)$DSTZ(I)=ETA*DSTZ(I)
      DSTT(I)=ETA*DS TT(I)$DSTRZ(I)=ETA*DSTRZ(I)
      TS TP2(I)=SQRT(2.)/2.*S QRT((S TR(I)+DS TR(I)-STZ(I)-DSTZ(I))**2+
     6(STR(I)+DSTR(I)-STT(I)-DSTT(I))**2+(STZ(I)+DSTZ(I)-S TT(I)-DSTT(I)
     6)**2+6.*(STRZ(I)+DSTRZ(I))**2)
      IF(PL(I).EQ.1.AND.(TSTP2(I)-TST(I)).LT.0.) GO TO 440
      GO TO 450
440   PL(I)=0
      CALL DMATX(I)
      CALL BMATX(I)
      CALL DBE(DB,D,B)
      MM=NOP(I,1)$J=NOP(I,2)$K=NOP(I,3)
      TEMP(1)=ETA*R1(2*MM-1)
      TEMP(2)=ETA*R1(2*MM)
      TEMP(3)=R1(2*J-1)*ETA
      TEMP(4)=ETA*R1(2*J)
      TEMP(5)=R1(2*K-1)*ETA
      TEMP(6)=R1(2*K)*ETA
      DSTZ(I)=0.$DSTR(I)=0.$DSTT(I)=0.$DSTRZ(I)=0.
      DO 445 II=1,6
      DSTZ(I)=DSTZ(I)+DB(1,II)*TEMP(II)
      DSTR(I)=DSTR(I)+DB(2,II)*TEMP(II)
      DSTT(I)=DSTT(I)+DB(3,II)*TEMP(II)
      DSTRZ(I)=DSTRZ(I)+DB(4,II)*TEMP(II)
445   CONTINUE
450   STR(I)=S TR(I)+DSTR(I)
      STZ(I)=STZ(I)+DSTZ(I)
      STT(I)=STT(I)+DS TT(I)
      STRZ(I)=STRZ(I)+DSTRZ(I)
      TSTP2(I)=SQRT(2.)/2.*SQRT((STR(I)-STZ(I))**2+(STR(I)-STT(I))**2+
     6(STZ(I)-STT(I))**2+6.*STRZ(I)**2)
460   CONTINUE
**********                                  **********
      DO 461 I=1,NEQ
      TDIS(I)=TDIS(I)+ETA*R1(I)
      FORCE(I)=FORCE(I)+ETA*DFORCE(I)
      R1(I)=ETA*R1(I)
461   CONTINUE
      DO 501 I=1,NELE
      HP=30000.
      IF(TST(I).GE.3500.)HP=3000.
      IF(PL(I).EQ.0) GO TO 480
      IF(TSTP2(I).GE.TST(I)) GO TO 470
      DEP(I)=0.
      GO TO 500
470   DEP(I)=(TSTP2(I)-TST(I))/ HP
      TEP(I)=TEP(I)+DEP(I)
      GO TO 500
480   IF(TSTP2(I).GT.Y(I)) GO TO 490
      DEP(I)=0.
      GO TO 500
490   DEP(I)=(TSTP2(I)-Y(I))/ HP
      TEP(I)=TEP(I)+DEP(I)
```

```
500   DTST(I)=TSTP2(I)-TST(I)
      TST(I)=TSTP2(I)
      IF(TST(I).GT.Y(I))Y(I)=TST(I)
501   CONTINUE
**********                                  **********
5010  DO 503 I=1,NELE
      IF(DTST(I).LT.0.) GO TO 62
      IF(TST(I).GE.0.998*Y(I)) GO TO 61
      GO TO 503
61    PL(I)=1
      CALL BMATX(I)
      CALL DMATX(I)
      CALL DBE(DB,D,B)
      CALL ESTIF(I)
      CALL SKINCR(I)
      GO TO 503
62    IF(PL(I).EQ.1) GO TO 63
      GO TO 503
63    PL(I)=0
      CALL BMATX(I)
      CALL DMATX(I)
      CALL DBE(DB,D,B)
      CALL ESTIF(I)
      CALL SKINCR(I)
503   CONTINUE
      IF(M.EQ.1) GO TO 530
C*************************************************************************************
      BLANK=0.$CLAMP=0.
      DO 5000 I=LL,MK
      J=NBC(I)
      BLANK=BLANK+FORCE(2*J)
5000  CONTINUE
      CLAMP=0.
      DO 5100 I=NCLAMP,NCLAMP
      J=NBC(I)
      CLAMP=CLAMP+FORCE(2*J)
5100  CONTINUE
      D116=TDIS(222)
      WRITE(6,4500)M,ETA,BLANK,CLAMP,D116
4500  FORMAT(1X,*LOADING STEP=*,I3,*ETA=*,E15.5,*BLANK=*,E15.5,10X,
     6*CLAMP=*,E15.5,*TDIS(66)=*,E15.5)
1010  DO 1004 I=99,104
      S8=R(I)
      S9=Z(I)
      S10=R1(2*I)
      S11=R1(2*I-1)
      S12=TDIS(2*I)
      S13=TDIS(2*I-1)
      NO=0
      S1=0.$S2=0.$S3=0.$S4=0.$S5=0.$S6=0.$S7=0.
      DO 1005 N=1,NELE
      IF(NOP(N,1).EQ.I)GO TO 1006
      IF(NOP(N,2).EQ.I) GO TO 1006
      IF(NOP(N,3).EQ.I) GO TO 1006
      GO TO 1005
```

```
1006  NO=NO+1
      S1=S1+TST(N)
      S2=S2+TEP(N)
      S3=S3+STZ(N)
      S4=S4+STR(N)
      S5=S5+STT(N)
      S6=S6+STRZ(N)
      S7=S7+(STR(N)+STZ(N)+STT(N))/3.
1005  CONTINUE
      S1=S1/FLOAT(NO)$S2=S2/FLOAT(NO)$S3=S3/FLOAT(NO)
      S4=S4/FLOAT(NO)$S5=S5/FLOAT(NO)$S6=S6/FLOAT(NO)$S7=S7/FLOAT(NO)
      WRITE(6,601)I,S1,S2,S3,S4,S5,S6,S7
601   FORMAT(I4,7(E10.3))
1004  CONTINUE
      IF(MOD(M,50).NE.0) GO TO 16000
      DO 2650 I=1,20
      J=NBC(I)
      WRITE(6,182)(J,TDIS(2*J),FORCE(2*J))
2650  CONTINUE
       TT=0.0
      IF(BLANK.LE.-4000.) GO TO 535
530   CONTINUE
535   STOP
      END
      SUBROUTINE ESTIF(L)
      COMMON/ / FORCE(350),D(4,4),W(4,6),ESK(6,6),DSTZ(309),DSTR(309),DS
     6TT(309),DSTRZ(309),DEP(309),TEP(309
     6),DDIS(350),R1(350),DTST(309),DFORCE(350),TSTP2(309),TEMP(6),
     6TSK(309,6,6),PL(309),STR(309),STZ(309),STT(309),STRZ(309),TST(309)
     6,DSK(6,6),Y(309),TDIS(350),DB(4,6),B(4,6),
     6HP,G,NU,E1,NELE,NEQ,NB,NBAND,NOP(309,3),SK(350,28),DIS(35
     60),POINTR(350)
      COMMON/B1/NBC(20),Z(175),R(175)
      INTEGER P,Q,O
      REAL NU
      I=NOP(L,1)$J=NOP(L,2)$M=NOP(L,3)
      BJ=Z(M)-Z(I)
      BM=Z(I)-Z(J)
      CJ=R(I)-R(M)
      CM=R(J)-R(I)
      AREA=(BJ*CM-BM*CJ)/2.
      RBAR=(R(I)+R(J)+R(M))/3.
      DO 4 P=1,6
      DO 4 Q=1,6
      ES K (P,Q)=0.
      DO4 O=1,4
4     ESK(P,Q)=ESK(P,Q)+2.*3.1415*B(O,P)*DB(O,Q)*RBAR*AREA
      RETURN
      END
      SUBROUTINE DMATX(L)
      COMMON/ / FORCE(350),D(4,4),W(4,6),ESK(6,6),DSTZ(309),DSTR(309),DS
     6TT(309),DSTRZ(309),DEP(309),TEP(309
     6),DDIS(350),R1(350),DTST(309),DFORCE(350),TSTP2(309),TEMP(6),
     6TSK(309,6,6),PL(309),STR(309),STZ(309),STT(309),STRZ(309),TST(309)
     6,DSK(6,6),Y(309),TDIS(350),DB(4,6),B(4,6),
```

```
     6HP,G,NU,E1,NELE,NEQ,NB,NBAND,NOP(309,3),SK(350,28),DIS(35
     60),POINTR(350)
      COMMON/B1/NBC(20),Z(175),R(175)
      INTEGER PL
      REAL NU
      IF(PL(L).EQ.1) GO TO 5
      C1=E1*(1.-NU)/((1.+NU)*(1.-2.*NU))$C2=NU/(1.-NU)
      D(1,1)=C1$D(1,2)=C1*C2$D(1,3)=C1*C2$D(1,4)=0.
      D(2,1)=D(1,2)$D(2,2)=C1$D(2,3)=C1*C2$D(2,4)=0.
      D(3,1)=D(1,3)$D(3,2)=D(2,3)$D(3,3)=C1$D(3,4)=0.
      D(4,1)=D(1,4)$D(4,2)=D(2,4)$D(4,3)=D(3,4)
      D(4,4)=C1*(1.-2.*NU)/(2.*(1.-NU))
      GO TO 10
5     T=(STR(L)+STZ(L)+STT(L))/3.
      STPR=STR(L)-T$STPZ=STZ(L)-T$STPT=STT(L)-T
      HP=30000.
      IF(TST(L).GE.3500.) HP=3000.
      S=2./3.*TST(L)**2*(1.+HP/(3.*G))
      W1=1.-NU$W2=1.-2.*NU$W5=E1/(1.+NU)
      D(1,1)=W5*(W1/W2-STPZ**2/S)
      D(1,2)=W5*(NU/W2-STPZ*STPR/S)
      D(1,3)=W5*(NU/W2-STPZ*STPT/S)
      D(1,4)=W5*(-STPZ*STRZ(L)/S)
      D(2,1)=D(1,2)
      D(2,2)=W5*(W1/W2-STPR**2/S)
      D(2,3)=W5*(NU/W2-STPR*STPT/S)
      D(2,4)=W5*(-STPR*STRZ(L)/S)
      D(3,1)=D(1,3)
      D(3,2)=D(2,3)
      D(3,3)=W5*(W1/W2-STPT**2/S)
      D(3,4)=W5*(-STPT*STRZ(L)/S)
      D(4,1)=D(1,4)$D(4,2)=D(2,4)$D(4,3)=D(3,4)
      D(4,4)=W5*(1./2.-STRZ(L)**2/S)
10    RETURN
      END
      SUBROUTINE BMATX(L)
      COMMON/ / FORCE(350),D(4,4),W(4,6),ESK(6,6),DSTZ(309),DSTR(309),DS
     6TT(309),DSTRZ(309),DEP(309),TEP(309
     6),DDIS(350),R1(350),DTST(309),DFORCE(350),TSTP2(309),TEMP(6),
     6TSK(309,6,6),PL(309),STR(309),STZ(309),STT(309),STRZ(309),TST(309)
     6,DSK(6,6),Y(309),TDIS(350),DB(4,6),B(4,6),
     6HP,G,NU,E1,NELE,NEQ,NB,NBAND,NOP(309,3),SK(350,28),DIS(35
     60),POINTR(350)
      COMMON/B1/NBC(20),Z(175),R(175)
      I=NOP(L,1)$J=NOP(L,2)$M=NOP(L,3)
      BI=Z(J)-Z(M)
      BJ=Z(M)-Z(I)
      BM=Z(I)-Z(J)
      CI=-R(J)+R(M)
      CJ=R(I)-R(M)
      CM=R(J)-R(I)
      RBAR=(R(I)+R(J)+R(M))/3.
      AREA=(BJ*CM-BM*CJ)/2.
      B(1,1)=0.$B(1,2)=CI/(2.*AREA)
      B(1,3)=0.$B(1,4)=CJ/(2.*AREA)
```

```
      B(1,5)=0.$B(1,6)=CM/(2.*AREA)
      B(2,1)=BI/(2.*AREA)$B(2,2)=0.
      B(2,3)=BJ/(2.*AREA)$B(2,4)=0.
      B(2,5)=BM/(2.*AREA)$B(2,6)=0.
      B(3,1)=1./(3.*RBAR)$B(3,2)=0.
      B(3,3)=1./(3.*RBAR)$B(3,4)=0.
      B(3,5)=1./(3.*RBAR)$B(3,6)=0.
      B(4,1)=CI/(2.*AREA)$B(4,2)=BI/(2.*AREA)
      B(4,3)=CJ/(2.*AREA)$B(4,4)=BJ/(2.*AREA)
      B(4,5)=CM/(2.*AREA)$B(4,6)=BM/(2.*AREA)
      RETURN
      END
      SUBROUTINE DBE(DB,D,B)
      DIMENSION DB(4,6),D(4,4),B(4,6)
      DO 10 I=1,4
      DO 10 J=1,6
      DB(I,J)=0.
      DO 10 JJ=1,4
      DB(I,J)=DB(I,J)+D(I,JJ)*B(JJ,J)
10    CONTINUE
      RETURN
      END
      SUBROUTINE SKINCR(I)
      COMMON/ / FORCE(350),D(4,4),W(4,6),ESK(6,6),DSTZ(309),DSTR(309),DS
     6TT(309),DSTRZ(309),DEP(309),TEP(309
     6),DDIS(350),R1(350),DTST(309),DFORCE(350),TSTP2(309),TEMP(6),
     6TSK(309,6,6),PL(309),STR(309),STZ(309),STT(309),STRZ(309),TST(309)
     6,DSK(6,6),Y(309),TDIS(350),DB(4,6),B(4,6),
     6HP,G,NU,E1,NELE,NEQ,NB,NBAND,NOP(309,3),SK(350,28),DIS(35
     60),POINTR(350)
      COMMON/B1/NBC(20),Z(175),R(175)
      INTEGER P,Q,O,POINTR,PUNCH1,PL
      DO 270 P=1,6
      DO 270 Q=1,6
      DSK(P,Q)=ESK(P,Q)-TSK(I,P,Q)
270   TSK(I,P,Q)=ESK(P,Q)
C     **********ADD THE INCREMENT TO OVERALL STIFFNSESS
      DO 330 JJ=1,3
      NROWB=(NOP(I,JJ)-1)*2
      DO 330 J=1,2
      NROWB=NROWB+1
      II=(JJ-1)*2+J
      DO 320 KK=1,3
      NCOLB=(NOP(I,KK)-1)*2
      DO 310 K=1,2
      IL=(KK-1)*2+K
      NCOL=NCOLB+K+1-NROWB
      IF(NCOL)310,310,300
300   SK(NROWB,NCOL)=S K(NROWB,NCOL)+DSK(II,IL)
310   CONTINUE
320   CONTINUE
330   CONTINUE
       RETURN
      END
      SUBROUTINE SOLVE
```

```
      DIMENSION VSK(350,28)
      COMMON/ / FORCE(350),D(4,4),W(4,6),ESK(6,6),DSTZ(309),DSTR(309),DS
     6TT(309),DSTRZ(309),DEP(309),TEP(309
     6),DDIS(350),R1(350),DTST(309),DFORCE(350),TSTP2(309),TEMP(6),
     6TSK(309,6,6),PL(309),STR(309),STZ(309),STT(309),STRZ(309),TST(309)
     6,DSK(6,6),Y(309),TDIS(350),DB(4,6),B(4,6),
     6HP,G,NU,E1,NELE,NEQ,NB,NBAND,NOP(309,3),SK(350,28),DIS(35
     60),POINTR(350)
      COMMON/B1/NBC(20),Z(175),R(175)
      INTEGER POINTR
      DO 490 I=1,NEQ
      DO 490 J=1,NBAND
      VSK(I,J)=SK(I,J)
490   CONTINUE
      DO 50 I=1,175
      NROWB=(I-1)*2
      DO 49 M=1,2
      NROWB=NROWB+1
      IF(POINTR(NROWB).EQ.1) GO TO 49
      R1(NROWB)=(10.E08)*VSK(NROWB,1)*DIS(NROWB)
      VSK(NROWB,1)=(10.E08)*VSK(NROWB,1)
49    CONTINUE
50    CONTINUE
      DO 300 N=1,NEQ
      I=N
      DO 290 L=2,NBAND
      I=I+1
      IF(VSK(N,L)) 240,290,240
240   C=VSK(N,L)/VSK(N,1)
      J=0
      DO 270 K=L,NBAND
      J=J+1
      IF(VSK(N,K)) 260,270,260
260   VSK(I,J)=VSK(I,J)-C*VSK(N,K)
270   CONTINUE
      VSK(N,L)=C
      R1(I)=R1(I)-C*R1(N)
290   CONTINUE
300   R1(N)=R1(N)/VSK(N,1)
      N=NEQ
350   N=N-1
      IF(N)500,500,360
360   L=N
      DO 400 K=2,NBAND
      L=L+1
      IF(VSK(N,K))370,400,370
370   R1(N)=R1(N)-VSK(N,K)*R1(L)
400   CONTINUE
      GO TO 350
500   DO 20 I=1,NEQ
      IF(POINTR(I).EQ.1) GO TO 30
      R1(I)=DIS(I)
      A1=0.
      DO 5 J=1,NBAND
      IF( SK(I,J).EQ.0.) GO TO 5
```

```
      A1=A1+ SK(I,J)*R1(I+J-1)
5     CONTINUE
      A2=0.
      K=I
      DO 10 II=2,NBAND
      K=K-1
      IF(K.EQ.0) GO TO 15
      A2=A2+ SK(K,II)*R1(K)
10    CONTINUE
15    DFORCE(I)=A1+A2
      GO TO 20
30    DFORCE(I)=0.
20    CONTINUE
      RETURN
      END
```

Variables in COMMON B1	Definition (ISOPARAMETRIC QUADRILATERAL ELEMENTS)
Y	Yield stress of sampling points
NBC	Boundary nodal points with defined conditions in the program
Z, R	Nodal point coordinates

COMMON BLANK	Definition
FORCE	Nodal point forces
D	Elasticity matrix
ESK	Element stiffness matrix
DSTZ	Axial stress increment
DSTR	Radial stress increment
DSTT	Hoop stress increment
DSTRZ	Shear stress increment
DEP	Plastic strain increment
TEP	Total plastic strain
DTST	Equivalent stress increment
SHAP	Shape function
DFORCE	Nodal force increment
TSK	Matrix containing element stiffness matrices
DSK	Element stiffness matrix increment
TDIS	Nodal points total displacements
ELDIS	Element nodal points displacements
ELCOD	Element nodal points coordinates
B	Strain displacement matrix
GPCOD	Gauss points coordinates

G	Shear modulus
NU	Poison's ratio
E1	Modulus of elasticity
CARTD	Cartesian derivaties
ZETA, ETAA	Natural coordinates of Gauss points

Main program	Definition
NELE	Number of elements
NEQ	Number of equations
NBAND	Overall stiffness matrix band width
SK	Overall stiffness matrix
DIS	Nodal points displacements
POINTR	Status vector defining nodal point status as suppressed or free surfaces
PL	Status vector defining sampling points status as plastic or elastic
NOP	Element nodal point connections
STR	Radial stress
STT	Hoop stress
STRZ	Shear stress
TST	Equivalent stress

```
 PROGRAM ISO(INPUT,OUTPUT,TAPE5=INPUT,TAPE6=OUTPUT,TAPE3)
 COMMON/B1/Y(616),NBC(62),Z(190),R(190)
 COMMON/ /FORCE(380),D(4,4),ESK(8,8),DSTZ(616),DSTR(616),DSTT(616)
6,DSTRZ(616),DEP(616),TEP(616),R1(380),DTST(616),SHAP(4)
6,DFORCE(380),TSK(154,8,8),DSK(8,8),TDIS(380),ELDIS(8),ELCOD(2,4),
6RGAUS(4),DB(4,8),B(4,8),GPCOD(2,4),CARTD(2,4),DERIV(2,4),G,NU,E1
6,NELE,NEQ,NBAND,SK(380,44),DIS(380),POINTR(380),PL(616),NOP(154,4)
6,ZETA(4),ETAA(4),STZ(616),STR(616),STT(616),STRZ(616),TST(616),
6VSK(380,44),XJACM(2,2),XJACI(2,2),S,T,DJACB
 DIMENSION RR(616),ZZ(616),NODAL(48)
 INTEGER P,Q,O,POINTR,PL,PUNCH1
 REAL NU
 DATA NODAL/310,309,306,305,302,301,298,297,294,293,290,289,286,
6285,282,281,278,277,274,273,270,269,266,265,312,311,308,307,304,
6303,301,299,296,295,292,291,288,287,284,283,280,279,276,275,272,
6271,268,267/
 DATA NBC/1,6,11,16,21,26,33,43,53,63,77,90,111,116,121,126,131,136,
6,141,146,151,156,161,166,171,176,181,186,186,187,188,189,190,
6190,185,180,175,170,165,160,155,150,145,140,135,130,125,120,115,
6102,76,68,62,60,58,52,50,48,42,40,38,32/
 DATA Y/616*2000./
 DATAZ/0.,0.15,0.3,0.45,0.6,0.,0.15,0.3,0.45,0.6
6,0.,0.15,0.3,0.45,0.6,0.,0.15,0.3,0.45,0.6
6,0.,0.15,0.3,0.45,0.6,0.,0.15,0.3,0.45,0.6
6,0.575,0.6,0.,.15,.3,.45,.55,.6,.575,.6,.575,.6
6,.0,.15,.3,.45,.55,.6,.575,.6,.575,.6,.0,.15,.3,.45,.55,.6
6,.575,.6,.575,.6,.0,.15,.3,.45,.55,.6,.05,.1,.2,.25,.35,.4,.575,.6
6,0.,0.05,0.1,.15,.2,.25,.3,.35,.4,.45,.5,.55,.6
6,0.,0.05,0.1,.15,.2,.25,.3,.35,.4,.45,.5,.55,.6
6,0.05,0.1,0.2,0.25,0.35,0.4,0.5,0.55
6,0.,0.15,0.3,0.45,0.6,0.,0.15,0.3,0.45,0.6
6,0.,0.15,0.3,0.45,0.6,0.,0.15,0.3,0.45,0.6
6,0.,0.15,0.3,0.45,0.6,0.,0.15,0.3,0.45,0.6
6,0.,0.15,0.3,0.45,0.6,0.,0.15,0.3,0.45,0.6
6,0.,0.15,0.3,0.45,0.6,0.,0.15,0.3,0.45,0.6
6,0.,0.15,0.3,0.45,0.6,0.,0.15,0.3,0.45,0.6
6,0.,0.15,0.3,0.45,0.6,0.,0.15,0.3,0.45,0.6
6,0.,0.15,0.3,0.45,0.6,0.,0.15,0.3,0.45,0.6/
 DATAR/5*2.2,5*2.1,5*2.,5*1.9,5*1.8,5*1.7,2*1.66,6*1.65,2*1.64,
62*1.61,6*1.6,2*1.59,2*1.56,6*1.55,2*1.54,2*1.51,6*1.5,6*1.475,
62*1.49,13*1.45,13*1.4,8*1.375,5*1.35,5*1.3,5*1.25,5*1.2,5*1.1,
```

```
     65*1.,5*.9,5*.8,5*.7,5*.6,5*.5,5*.4,5*.3,5*.2,5*.1,5*.0/
      C=0.577350269189626
      ZETA(1)=-C$ZETA(2)=-C
      ZETA(3)=C$ZETA(4)=C
      ETAA(1)=-C$ETAA(2)=C
      ETAA(3)=-C$ETAA(4)=C
      NU=0.291$E1=2.1E06$G=E1/(2.*(1.+NU))
      N1=11$N2=17$N3=5$N4=17$N5=12
      BPFORCE=3000. $CLFORCE=-3000. $ICLAMP=52$NB=62
      KKK=1
      NBAND=44$NELE=154$NODE=190$LL=12$MK=28
      NEQ=2*NODE$NGAUS=4*NELE$TFACT=0.506$NCYCLE=400
      READ(5,10)((NOP(I,J),J=1,4),I=1,NELE)
10    FORMAT(24I3)
      DO 20 I=1,NODE
      Z(I)=TFACT*Z(I)
20    CONTINUE
      J=NBC(ICLAMP)
      IF(KKK.NE.1)Z(J)=Z(J)-0.02

C     *****SET THE INITIAL VALUES*************

      DO 30 I=1,NEQ
      POINTR(I)=1
      FORCE(I)=0.
      R1(I)=0.
      DIS(I)=0.
30    CONTINUE
      DO 40 I=1,NGAUS
      PL(I)=0
      TEP(I)=0.
      DTST(I)=0.
      STZ(I)=0.
      STR(I)=0.
      STT(I)=0.
      STRZ(I)=0.
      TST(I)=0.
40    CONTINUE

C     *****FORM OVER ALL STIFFNESS MATRIX*****

      DO 60 L=1,NELE
      CALL ELSTIF(L)
      DO 50 II=1,8
      DO 50 JJ=1,8
50    TSK(L,II,JJ)=ESK(II,JJ)
60    CONTINUE
      DO 70 I=1,NEQ
      DO 70 J=1,NBAND
70    SK(I,J)=0.
      DO 80 L=1,NELE
      CALL FORMK(L)
80    CONTINUE

C     ****SET BOUNDARY CONDITION******
```

```
      CALL BOUND1(KKK,N1,N2,N3,N4,N5,ICLAMP)
      CALL SOLVE

C     *****CALCULATE THE STRESSES*****

      M=0
      DO 130 L=1,NELE
      DO 100 I=1,4
      J=NOP(L,I)
      ELDIS(2*I-1)=R1(2*J-1)
      ELDIS(2*I)=R1(2*J)
      ELCOD(1,I)=R(J)
100   ELCOD(2,I)=Z(J)
      KGAUS=0
      DO 120 II=1,2
      DO 120 JJ=1,2
      KGAUS=KGAUS+1
      M=M+1
      CALL SDBE(KGAUS,M)
      DO 110 I=1,8
      STZ(M)=STZ(M)+DB(1,I)*ELDIS(I)
      STR(M)=STR(M)+DB(2,I)*ELDIS(I)
      STT(M)=STT(M)+DB(3,I)*ELDIS(I)
      STRZ(M)=STRZ(M)+DB(4,I)*ELDIS(I)
110   CONTINUE
      TST(M)=SQRT(2.)/2.*SQRT((STZ(M)-STR(M))**2+(STZ(M)-STT(M))**2+
     6(STR(M)-STT(M))**2+6.*STRZ(M)**2)
120   CONTINUE
130   CONTINUE

C     ****SET MAX STRESS AND ETA**************

      SIGMAX=0.
      DO 150 I=1,NGAUS
      IF(TST(I).GE.SIGMAX) GO TO 140
      GO TO 150
140   SIGMAX=TST(I)
      J=I
150   CONTINUE
      ETA=Y(J)/SIGMAX
      NN=N1+1$MM=N1+N2
      BP=0.
      DO 151 I=NN,MM
      J=NBC(I)
      BP=BP+ETA*DFORCE(2*J)
151   CONTINUE
      IF(BP.LE.BPFORCE) GO TO 152
      ETA=ETA*BPFORCE/BP

C     ********MULTIPLY BY ETA**********

152   DO 160 I=1,NGAUS
      STZ(I)=ETA*STZ(I)
      STR(I)=ETA*STR(I)
```

```
      STT(I)=ETA*STT(I)
      STRZ(I)=ETA*STRZ(I)
      TST(I)=ETA*TST(I)
160   CONTINUE
      DO 170 I=1,NEQ
      R1(I)=ETA*R1(I)
      DFORCE(I)=ETA*DFORCE(I)
       TDIS(I)=R1(I)
      FORCE(I)=DFORCE(I)
170   CONTINUE
      WRITE(6,190)(I,TST(I),I=1,NGAUS)
190   FORMAT(10X,*NO*,I3,10X,*TST=*,E15.5)
      WRITE(6,200)(I,TDIS(I),FORCE(I),I=1,NEQ)
200   FORMAT(10X,*COOR*,I3,*DIS=*,E15.5,*FORCE=*,E15.5)

C     *****APPLY THE LOAD INCREMENTS********

      DO 490 MMM=1,NCYCLE
      IF(MMM.EQ.1) GO TO 381

C     ****CHANGE BOUNDARY CONDITION OF THE SEPARATING POINTS******

      CALL BOUND2(KKK,N1,N2,N3,N4,N5,ICLAMP,CLFORCE,BPFORCE,BP)
241   DO 250 I=1,NEQ
      R1(I)=0.
250   CONTINUE
      CALL SOLVE

C     *****CALCULATE STREES INCREMENTS*********

      M=0
      DO 280 L=1,NELE
      DO 260 I=1,4
      J=NOP(L,I)
      ELDIS(2*I-1)=R1(2*J-1)
      ELDIS(2*I)=R1(2*J)
      ELCOD(1,I)=R(J)
260   ELCOD(2,I)=Z(J)
      KGAUS=0
      DO 270 II=1,2
      DO 270 JJ=1,2
      KGAUS=KGAUS+1
      M=M+1
      CALL SDBE(KGAUS,M)
      DSTZ(M)=0.
      DSTR(M)=0.
      DSTT(M)=0.
      DSTRZ(M)=0.
      DO 270 I=1,8
      DSTZ(M)=DSTZ(M)+DB(1,I)*ELDIS(I)
      DSTR(M)=DSTR(M)+DB(2,I)*ELDIS(I)
      DSTT(M)=DSTT(M)+DB(3,I)*ELDIS(I)
      DSTRZ(M)=DSTRZ(M)+DB(4,I)*ELDIS(I)
270   CONTINUE
280   CONTINUE
```

```
C      ****SET ETA*******

       ETA=1.
       DO 290 I=1,NGAUS
       IF(TST(I).GE.3490.) GO TO 290
       TT=Y(I)
       IF(PL(I).EQ.1) TT=3500.
       A=(DSTR(I)-DSTZ(I))**2+(DSTT(I)-DSTZ(I))**2+(DSTR(I)-DSTT(I))**2
      6+6.*DSTRZ(I)**2
       C=2.*(TST(I)**2-TT**2)
       X=(STR(I)-STZ(I))*(DSTR(I)-DSTZ(I))+(STR(I)-STT(I))*(DSTR(I)-
      6DSTT(I))+(STT(I)-STZ(I))*(DSTT(I)-DSTZ(I))+6.*DSTRZ(I)*STRZ(I)
       ETA1=(-X+SQRT(X**2-A*C))/A
       IF(ETA1.GE.ETA) GO TO 290
       ETA=ETA1
290    CONTINUE

C      *****MULTIPLY BY ETA*********

       DO 300 I=1,NEQ
       R1(I)=ETA*R1(I)
       DFORCE(I)=ETA*DFORCE(I)
       TDIS(I)=TDIS(I)+R1(I)
       FORCE(I)=FORCE(I)+DFORCE(I)
300    CONTINUE
       DO 350 I=1,NGAUS
       DSTZ(I)=ETA*DSTZ(I)
       DSTR(I)=ETA*DSTR(I)
       DSTT(I)=ETA*DSTT(I)
       DSTRZ(I)=ETA*DSTRZ(I)
       DTST(I)=SQRT(2.)/2.*SQRT((STZ(I)+DSTZ(I)-STR(I)-DSTR(I))**2+
      6(STZ(I)+DSTZ(I)-STT(I)-DSTT(I))**2+(STR(I)+DSTR(I)-STT(I)-DSTT(I))
      6**2+6.*(STRZ(I)+DSTRZ(I))**2)-TST(I)
       IF(PL(I).EQ.1.AND.DTST(I).LT.0.) GO TO 310
       GO TO 340

C      *****RECALCULATE STRESSES FOR UNLOADING ELEMENTS**********

310    PL(I)=0
       JJ=I-(I/4)*4
       L=(I/4)+1
       IF(JJ.EQ.0) L=I/4
       DO 320 II=1,4
       J=NOP(L,II)
       ELDIS(2*II-1)=R1(2*J-1)
       ELDIS(2*II)=R1(2*J)
       ELCOD(1,II)=R(J)
320    ELCOD(2,II)=Z(J)
       KGAUS=I-(I/4)*4
       IF(KGAUS.EQ.0) KGAUS=4
       CALL SDBE(KGAUS,I)
       DSTZ(I)=0.
       DSTR(I)=0.
       DSTT(I)=0.
```

```
      DSTRZ(I)=0.
      DO 330 II=1,8
      DSTZ(I)=DSTZ(I)+DB(1,II)*ELDIS(II)
      DSTR(I)=DSTR(I)+DB(2,II)*ELDIS(II)
      DSTT(I)=DSTT(I)+DB(3,II)*ELDIS(II)
330   DSTRZ(I)=DSTRZ(I)+DB(4,II)*ELDIS(II)
      DTST(I)=SQRT(2.)/2.*SQRT((STZ(I)+DSTZ(I)-STR(I)-DSTR(I))**2+
     6(STZ(I)+DSTZ(I)-STT(I)-DSTT(I))**2+(STR(I)+DSTR(I)-STT(I)-DSTT(I))
     6**2+6.*(STRZ(I)+DSTRZ(I))**2)-TST(I)
340   STZ(I)=STZ(I)+DSTZ(I)
      STR(I)=STR(I)+DSTR(I)
      STT(I)=STT(I)+DSTT(I)
      STRZ(I)=STRZ(I)+DSTRZ(I)
350   CONTINUE

C     *****SET PLASTIC STRAIN*********

      DO 380 I=1,NGAUS
      HP=30000.
      IF(TST(I).GE.3490.) HP=3000.
      IF(PL(I).EQ.0) GO TO 370
      IF(DTST(I).GE.0.) GO TO 360
      GO TO 370
360   DEP(I)=DTST(I)/HP
      TEP(I)=TEP(I)+DEP(I)
370   TST(I)=SQRT(2.)/2.*SQRT((STZ(I)-STR(I))**2+(STZ(I)-STT(I))**2+
     6(STR(I)-STT(I))**2+6.*STRZ(I)**2)
380   CONTINUE

C     ****SET PL=1 IF POINT IS PLASTIC*********
C     *****FORM SK FOR PLASTIC OR UNLOADING ELEMENTS*********

381   M=0
      DO 430 L=1,NELE
      III=0
      DO 410 II=1,2
      DO 410 JJ=1,2
      M=M+1
      IF(TST(M).GT.Y(M)) Y(M)=TST(M)
      IF(PL(M).EQ.1) GO TO 390
      IF(TST(M).GE.0.998*Y(M)) GO TO 400
      GO TO 410
390   IF(DTST(M).LT.0.) PL(M)=0
      III=1
      GO TO 410
400   PL(M)=1
      III=1
410   CONTINUE
      IF(III.EQ.0) GO TO 430
411   CALL ELSTIF(L)
      DO 420 II=1,8
      DO 420 JJ=1,8
      DSK(II,JJ)=ESK(II,JJ)-TSK(L,II,JJ)
420   TSK(L,II,JJ)=ESK(II,JJ)
      CALL SKINCR(L)
```

```
430   CONTINUE
      NN=N1+1
      MM=N1+N2
      BP=0.
      DO 431 I=NN,MM
      J=NBC(I)
      BP=BP+FORCE(2*J)
 431   CONTINUE
      BLANK=0.
      NN=N1+N2+N3+1
      MM=N1+N2+N3+N4
      DO 440 I=NN,MM
      J=NBC(I)
      BLANK=BLANK+FORCE(2*J)
440   CONTINUE
      J=NBC(ICLAMP)
      CLAMP=FORCE(2*J)
      WRITE(6,450)MMM,ETA,BLANK,CLAMP,BP,TDIS(126)
450   FORMAT(*LOAD STEP*,I3,*ETA*,E15.5,*BLANK*,E15.5,*CLAMP*,E15.5,
     6*BP*,E15.5,*TDIS*,E15.5)
453   IF(MOD(MMM,50).NE.0) GO TO 480
      DO 452 I=1,NB
      J=NBC(I)
      WRITE(6,451)I,TDIS(2*J),FORCE(2*J)
      WRITE(6,451)I,TDIS(2*J-1),FORCE(2*J-1)
451   FORMAT(5X,*I=*,I4,5X,*TDIS=*,E15.5,5X,*FORCE=*,E15.5)
452   CONTINUE
      WRITE(6,469)
469   FORMAT(6X,*NODE*,12X,*TST*,12X,*TEP*,12X,*STZ*,12X,*STR*,12X,*STT*
     6,11X,*STRZ*,12X,*HYD*,8X,*TENSILE*)
      DO 472 I=1,48
      J=NODAL(I)
      HYD=(STZ(J)+STR(J)+STT(J))/3.
      TENSILE=(STR(J)+STZ(J))/2.+SQRT(((STZ(J)-STR(J))/2.)**2+STRZ(J)**2
     6)
      WRITE(6,471)(J,TST(J),TEP(J),STZ(J),STR(J),STT(J),STRZ(J),HYD,
     6TENSILE)
471   FORMAT(5X,I5,5X,8(E10.3,5X))
472   CONTINUE
      DO 470 I=1,NGAUS
      WRITE(6,460)(I,TST(I),TEP(I),STR(I),STT(I),STZ(I),STRZ(I))
460   FORMAT(I4,6(9X,E12.5))
470   CONTINUE
480   TT=0.
490   CONTINUE
      STOP
      END


      SUBROUTINE BOUND1(KKK,N1,N2,N3,N4,N5,ICLAMP)
      COMMON/B1/Y(616),NBC(62),Z(190),R(190)
      COMMON/ /FORCE(380),D(4,4),ESK(8,8),DSTZ(616),DSTR(616),DSTT(616)
     6,DSTRZ(616),DEP(616),TEP(616),R1(380),DTST(616),SHAP(4)
     6,DFORCE(380),TSK(154,8,8),DSK(8,8),TDIS(380),ELDIS(8),ELCOD(2,4),
     6RGAUS(4),DB(4,8),B(4,8),GPCOD(2,4),CARTD(2,4),DERIV(2,4),G,NU,E1
```

```
     6,NELE,NEQ,NBAND,SK(380,44),DIS(380),POINTR(380),PL(616),NOP(154,4)
     6,ZETA(4),ETAA(4),STZ(616),STR(616),STT(616),STRZ(616),TST(616),
     6VSK(380,44),XJACM(2,2),XJACI(2,2),S,T,DJACB
      INTEGER P,Q,O,POINTR,PL,PUNCH1
      REAL NU
      DO 5 I=1,N1
      J=NBC(I)
      POINTR(2*J)=0
      POINTR(2*J-1)=0
5     CONTINUE
      NN=N1+N2+1
      MM=N1+N2+N3
      DO 10 I=NN,MM
      J=NBC(I)
      POINTR(2*J-1)=0
10    CONTINUE
      IF(KKK.EQ.2) GO TO 15
      IF(KKK.EQ.3) GO TO 20
      NN=N1+N2+N3+N4
      J=NBC(NN)
      POINTR(2*J)=0$DIS(2*J)=-1.
      GO TO 40
15    I=NBC(ICLAMP-1)
      J=NBC(ICLAMP)$K=NBC(ICLAMP+1)
      POINTR(2*I-1)=0$POINTR(2*K-1)=0$POINTR(2*J-1)=0$POINTR(2*J)=0
      DIS(2*J)=-1.$DIS(2*I-1)=-.57735$DIS(2*K-1)=0.57735
      GO TO 40
 20    NN=N1+1
      MM=N1+N2
      DO 25 I=NN,MM
      J=NBC(I)
      POINTR(2*J)=0$POINTR(2*J-1)=0
25    CONTINUE
      NN=N1+N2+N3+1$MM=N1+N2+N3+N4
      DO 30 I=NN,MM
      J=NBC(I)
      POINTR(2*J)=0$POINTR(2*J-1)=0$DIS(2*J)=-1.
30    CONTINUE
40    RETURN
      END
      SUBROUTINE BOUND2(KKK,N1,N2,N3,N4,N5,ICLAMP,CLFORCE,BPFORCE,BP)
      COMMON/B1/Y(616),NBC(62),Z(190),R(190)
      COMMON/ /FORCE(380),D(4,4),ESK(8,8),DSTZ(616),DSTR(616),DSTT(616)
     6,DSTRZ(616),DEP(616),TEP(616),R1(380),DTST(616),SHAP(4)
     6,DFORCE(380),TSK(154,8,8),DSK(8,8),TDIS(380),ELDIS(8),ELCOD(2,4),
     6RGAUS(4),DB(4,8),B(4,8),GPCOD(2,4),CARTD(2,4),DERIV(2,4),G,NU,E1
     6,NELE,NEQ,NBAND,SK(380,44),DIS(380),POINTR(380),PL(616),NOP(154,4)
     6,ZETA(4),ETAA(4),STZ(616),STR(616),STT(616),STRZ(616),TST(616),
     6VSK(380,44),XJACM(2,2),XJACI(2,2),S,T,DJACB
      INTEGER P,Q,O,POINTR,PL,PUNCH1
      REAL NU
      IF(KKK.EQ.2) GO TO 25
      IF(KKK.EQ.3) GO TO 46
      DO 5 I=1,N1
      J=NBC(I)
```

```
      IF(FORCE(2*J).GE.0.) GO TO 5
      POINTR(2*J)=1$POINTR(2*J-1)=1
      FORCE(2*J)=0.$FORCE(2*J-1)=0.
5     CONTINUE
      NN=N1+N2+N3+1$MM=N1+N2+N3+N4
      DO 10 I=NN,MM
      J=NBC(I)
      IF(POINTR(2*J).EQ.1) GO TO 10
      DIS(2*J)=-.0005$JJJ=2*J
10    CONTINUE
      DO 15 I=NN,MM
      J=NBC(I)
      IF(TDIS(2*J).LE.TDIS(JJJ)) GO TO 15
      POINTR(2*J)=0$DIS(2*J)=-.0005
15    CONTINUE
      DO 20 I=NN,MM
      J=NBC(I)
      IF(FORCE(2*J).LE.0.) GO TO 20
      POINTR(2*J)=1$POINTR(2*J-1)=1
      FORCE(2*J)=0.$FORCE(2*J-1)=0.
20    CONTINUE
      GO TO 80
25    I=NBC(ICLAMP-1)
       J=NBC(ICLAMP)$K=NBC(ICLAMP+1)
      IF(FORCE(2*J).LE.CLFORCE) GO TO 30
      DIS(2*J)=-.0005$DIS(2*I-1)=-.0002886$DIS(2*K-1)=.0002886
      GO TO 80
30    POINTR(2*J)=1$DIS(2*J)=0.
      POINTR(2*I-1)=1$DIS(2*K-1)=0.
      NN=N1+N2+N3+N4
       J=NBC(NN)
      POINTR(2*J)=0$POINTR(2*J-1)=0$DIS(2*J)=-.0005
      NN=N1+N2+N3+1$MM=N1+N2+N3+N4
      DO 31 I=NN,MM
      J=NBC(I)
      IF(POINTR(2*J).EQ.1) GO TO 31
      DIS(2*J)=-.0005
31    CONTINUE
      NN=N1+N2+N3+1$MM=N1+N2+N3+N4-1
      DO 35 I=NN,MM
      J=NBC(I)
      JJ=NBC(MM+1)
      IF(TDIS(2*J).LE.TDIS(2*JJ)) GO TO 35
      POINTR(2*J)=0$POINTR(2*J-1)=0$DIS(2*J)=-.0005
35    CONTINUE
       NN=N1+N2+N3+1$MM=N1+N2+N3+N4
       DO 40 I=NN,MM
       J=NBC(I)
       IF(FORCE(2*J).LE.0.) GO TO 40
      POINTR(2*J)=1$POINTR(2*J-1)=1
      FORCE(2*J)=0.$FORCE(2*J-1)=0.
 40    CONTINUE
       DO 45 I=1,N1
      J=NBC(I)
      IF(FORCE(2*J).GE.0.) GO TO 45
```

```
      POINTR(2*J)=1$POINTR(2*J-1)=1
      FORCE(2*J)=0.$FORCE(2*J-1)=0.
45    CONTINUE
      GO TO 80
46    IF(BP.GE.0.998*BPFORCE) GO TO 51
      NN=N1+N2+N3+1$MM=N1+N2+N3+N4
      DO 50 I=NN,MM
      J=NBC(I)
      DIS(2*J)=-.0005
50    CONTINUE
      GO TO 80
51    NN=N1+1
      MM=N1+N2
      DO 55 I=NN,MM
      J=NBC(I)
      POINTR(2*J)=1$POINTR(2*J-1)=1
55    CONTINUE
      I=NBC(ICLAMP-1)$J=NBC(ICLAMP)$K=NBC(ICLAMP+1)
      IF(FORCE(2*J).LE.CLFORCE) GO TO 52
      POINTR(2*J-1)=0$POINTR(2*J)=0$POINTR(2*I-1)=0$POINTR(2*K-1)=0
      DIS(2*J)=-.0005$DIS(2*I-1)=-.0002886$DIS(2*K-1)=.0002886
      NN=N1+N2+N3+1$MM=N1+N2+N3+N4
      DO 53 I=NN,MM
      J=NBC(I)
      DIS(2*J)=0.
53    CONTINUE
      GO TO 80
52    I=NBC(ICLAMP-1)$J=NBC(ICLAMP)$K=NBC(ICLAMP+1)
      POINTR(2*J)=1$POINTR(2*I-1)=1$DIS(2*K-1)=0.
      NN=N1+N2+N3+1$MM=N1+N2+N3+N4
      DO 60 I=NN,MM
      J=NBC(I)
      DIS(2*J)=-.0005
60    CONTINUE
      DO 65 I=NN,MM
      J=NBC(I)
       IF(FORCE(2*J).LE.0.) GO TO 65
       POINTR(2*J-1)=1$POINTR(2*J)=1
       FORCE(2*J-1)=0.$FORCE(2*J)=0.
65    CONTINUE
      DO 70 I=1,N1
      J=NBC(I)
      IF(FORCE(2*J).GE.0.) GO TO 70
      POINTR(2*J-1)=1$POINTR(2*J)=1
      FORCE(2*J-1)=0.$FORCE(2*J)=0.
70    CONTINUE
80    RETURN
      END
      SUBROUTINE SDBE(KGAUS,INGAUS)
      COMMON/B1/Y(616),NBC(62),Z(190),R(190)
      COMMON/ /FORCE(380),D(4,4),ESK(8,8),DSTZ(616),DSTR(616),DSTT(616)
     6,DSTRZ(616),DEP(616),TEP(616),R1(380),DTST(616),SHAP(4)
     6,DFORCE(380),TSK(154,8,8),DSK(8,8),TDIS(380),ELDIS(8),ELCOD(2,4),
     6RGAUS(4),DB(4,8),B(4,8),GPCOD(2,4),CARTD(2,4),DERIV(2,4),G,NU,E1
     6,NELE,NEQ,NBAND,SK(380,44),DIS(380),POINTR(380),PL(616),NOP(154,4)
```

```
     6,ZETA(4),ETAA(4),STZ(616),STR(616),STT(616),STRZ(616),TST(616),
     6VSK(380,44),XJACM(2,2),XJACI(2,2),S,T,DJACB
      INTEGER P,Q,O,POINTR,PL,PUNCH1
      REAL NU
      S=ZETA(KGAUS)
      T=ETAA(KGAUS)
      CALL SHAPFU
      RGAUS(KGAUS)=0.
      DO 10 I=1,4
      RGAUS(KGAUS)=RGAUS(KGAUS)+ELCOD(1,I)*SHAP(I)
10    CONTINUE
      CALL JACOB2(KGAUS)
      CALL DMATX(INGAUS)
      CALL BMATX(KGAUS)
      CALL DBE
      RETURN
      END


      SUBROUTINE ELSTIF(L)
      COMMON/B1/Y(616),NBC(62),Z(190),R(190)
      COMMON/ /FORCE(380),D(4,4),ESK(8,8),DSTZ(616),DSTR(616),DSTT(616)
     6,DSTRZ(616),DEP(616),TEP(616),R1(380),DTST(616),SHAP(4)
     6,DFORCE(380),TSK(154,8,8),DSK(8,8),TDIS(380),ELDIS(8),ELCOD(2,4),
     6RGAUS(4),DB(4,8),B(4,8),GPCOD(2,4),CARTD(2,4),DERIV(2,4),G,NU,E1
     6,NELE,NEQ,NBAND,SK(380,44),DIS(380),POINTR(380),PL(616),NOP(154,4)
     6,ZETA(4),ETAA(4),STZ(616),STR(616),STT(616),STRZ(616),TST(616),
     6VSK(380,44),XJACM(2,2),XJACI(2,2),S,T,DJACB
      INTEGER P,Q,O,POINTR,PL,PUNCH1
      REAL NU
      DO 10 I=1,4
      J=NOP(L,I)
      ELCOD(1,I)=R(J)
10    ELCOD(2,I)=Z(J)
      DO 20 I=1,8
      DO 20 J=1,8
20    ESK(I,J)=0.
      KGAUS=0
      INGAUS=4*(L-1)
      DO 50 II=1,2
      DO 50 JJ=1,2
      KGAUS=KGAUS+1
      INGAUS=INGAUS+1
      S=ZETA(KGAUS)
      T=ETAA(KGAUS)
      CALL SHAPFU
      RGAUS(KGAUS)=0.
      DO 30 I=1,4
      RGAUS(KGAUS)=RGAUS(KGAUS)+ELCOD(1,I)*SHAP(I)
30    CONTINUE
      CALL JACOB2(KGAUS)
      DVOLU=DJACB*RGAUS(KGAUS)
      CALL DMATX(INGAUS)
      CALL BMATX(KGAUS)
      CALL DBE
```

```
      DO 40 I=1,8
      DO 40 J=1,8
      DO 40 K=1,4
40    ESK(I,J)=ESK(I,J)+8.*ATAN(1.)*B(K,I)*DB(K,J)*DVOLU
50    CONTINUE
      RETURN
      END


      SUBROUTINE SKINCR(L)
      COMMON/B1/Y(616),NBC(62),Z(190),R(190)
      COMMON/ /FORCE(380),D(4,4),ESK(8,8),DSTZ(616),DSTR(616),DSTT(616)
     6,DSTRZ(616),DEP(616),TEP(616),R1(380),DTST(616),SHAP(4)
     6,DFORCE(380),TSK(154,8,8),DSK(8,8),TDIS(380),ELDIS(8),ELCOD(2,4),
     6RGAUS(4),DB(4,8),B(4,8),GPCOD(2,4),CARTD(2,4),DERIV(2,4),G,NU,E1
     6,NELE,NEQ,NBAND,SK(380,44),DIS(380),POINTR(380),PL(616),NOP(154,4)
     6,ZETA(4),ETAA(4),STZ(616),STR(616),STT(616),STRZ(616),TST(616),
     6VSK(380,44),XJACM(2,2),XJACI(2,2),S,T,DJACB
      INTEGER P,Q,O,POINTR,PL,PUNCH1
      REAL NU
      DO 40 JJ=1,4
      NROWB=(NOP(L,JJ)-1)*2
      DO 40 J=1,2
      NROWB=NROWB+1
      II=(JJ-1)*2+J
      DO 30 KK=1,4
      NCOLB=(NOP(L,KK)-1)*2
      DO 20 K=1,2
      IL=(KK-1)*2+K
      NCOL=NCOLB+K+1-NROWB
      IF(NCOL)20,20,10
10    SK(NROWB,NCOL)=SK(NROWB,NCOL)+DSK(II,IL)
20    CONTINUE
30    CONTINUE
40    CONTINUE
      RETURN
      END


      SUBROUTINE FORMK(L)
      COMMON/B1/Y(616),NBC(62),Z(190),R(190)
      COMMON/ /FORCE(380),D(4,4),ESK(8,8),DSTZ(616),DSTR(616),DSTT(616)
     6,DSTRZ(616),DEP(616),TEP(616),R1(380),DTST(616),SHAP(4)
     6,DFORCE(380),TSK(154,8,8),DSK(8,8),TDIS(380),ELDIS(8),ELCOD(2,4),
     6RGAUS(4),DB(4,8),B(4,8),GPCOD(2,4),CARTD(2,4),DERIV(2,4),G,NU,E1
     6,NELE,NEQ,NBAND,SK(380,44),DIS(380),POINTR(380),PL(616),NOP(154,4)
     6,ZETA(4),ETAA(4),STZ(616),STR(616),STT(616),STRZ(616),TST(616),
     6VSK(380,44),XJACM(2,2),XJACI(2,2),S,T,DJACB
      INTEGER P,Q,O,POINTR,PL,PUNCH1
      REAL NU
      DO 40 JJ=1,4
      NROWB=(NOP(L,JJ)-1)*2
      DO 40 J=1,2
      NROWB=NROWB+1
      I=(JJ-1)*2+J
```

```
      DO 30 KK=1,4
      NCOLB=(NOP(L,KK)-1)*2
      DO 20 K=1,2
      LL=(KK-1)*2+K
      NCOL=NCOLB+K+1-NROWB
      IF(NCOL)20,20,10
10    SK(NROWB,NCOL)=SK(NROWB,NCOL)+TSK(L,I,LL)
20    CONTINUE
30    CONTINUE
40    CONTINUE
      RETURN
      END


      SUBROUTINE BMATX(KGAUS)
      COMMON/B1/Y(616),NBC(62),Z(190),R(190)
      COMMON/ /FORCE(380),D(4,4),ESK(8,8),DSTZ(616),DSTR(616),DSTT(616)
     6,DSTRZ(616),DEP(616),TEP(616),R1(380),DTST(616),SHAP(4)
     6,DFORCE(380),TSK(154,8,8),DSK(8,8),TDIS(380),ELDIS(8),ELCOD(2,4),
     6RGAUS(4),DB(4,8),B(4,8),GPCOD(2,4),CARTD(2,4),DERIV(2,4),G,NU,E1
     6,NELE,NEQ,NBAND,SK(380,44),DIS(380),POINTR(380),PL(616),NOP(154,4)
     6,ZETA(4),ETAA(4),STZ(616),STR(616),STT(616),STRZ(616),TST(616),
     6VSK(380,44),XJACM(2,2),XJACI(2,2),S,T,DJACB
      INTEGER P,Q,O,POINTR,PL,PUNCH1
      REAL NU
      N=0
      DO 10 I=1,4
      M=N+1
      N=M+1
      B(1,M)=0.
      B(1,N)=CARTD(2,I)
      B(2,M)=CARTD(1,I)
      B(2,N)=0.
      B(3,M)=SHAP(I)/RGAUS(KGAUS)
      B(3,N)=0.
      B(4,M)=CARTD(2,I)
      B(4,N)=CARTD(1,I)
10    CONTINUE
      RETURN
      END


      SUBROUTINE JACOB2(KGAUS)
      COMMON/B1/Y(616),NBC(62),Z(190),R(190)
      COMMON/ /FORCE(380),D(4,4),ESK(8,8),DSTZ(616),DSTR(616),DSTT(616)
     6,DSTRZ(616),DEP(616),TEP(616),R1(380),DTST(616),SHAP(4)
     6,DFORCE(380),TSK(154,8,8),DSK(8,8),TDIS(380),ELDIS(8),ELCOD(2,4),
     6RGAUS(4),DB(4,8),B(4,8),GPCOD(2,4),CARTD(2,4),DERIV(2,4),G,NU,E1
     6,NELE,NEQ,NBAND,SK(380,44),DIS(380),POINTR(380),PL(616),NOP(154,4)
     6,ZETA(4),ETAA(4),STZ(616),STR(616),STT(616),STRZ(616),TST(616),
     6VSK(380,44),XJACM(2,2),XJACI(2,2),S,T,DJACB
      INTEGER P,Q,O,POINTR,PL,PUNCH1
      REAL NU
      DO 10 I=1,2
      GPCOD(I,KGAUS)=0.
```

```
      DO 10 J=1,4
      GPCOD(I,KGAUS)=GPCOD(I,KGAUS)+ELCOD(I,J)*SHAP(J)
10    CONTINUE
      DO 20 I=1,2
      DO 20 J=1,2
      XJACM(I,J)=0.
      DO 20 II=1,4
      XJACM(I,J)=XJACM(I,J)+DERIV(I,II)*ELCOD(J,II)
20    CONTINUE
      DJACB=XJACM(1,1)*XJACM(2,2)-XJACM(1,2)*XJACM(2,1)
      XJACI(1,1)=XJACM(2,2)/DJACB
      XJACI(2,2)=XJACM(1,1)/DJACB
      XJACI(1,2)=-XJACM(1,2)/DJACB
      XJACI(2,1)=-XJACM(2,1)/DJACB
      DO 40 I=1,2
      DO 40 J=1,4
      CARTD(I,J)=0.
      DO 40 JJ=1,2
      CARTD(I,J)=CARTD(I,J)+XJACI(I,JJ)*DERIV(JJ,J)
40    CONTINUE
      RETURN
      END


      SUBROUTINE SHAPFU
      COMMON/B1/Y(616),NBC(62),Z(190),R(190)
      COMMON/ /FORCE(380),D(4,4),ESK(8,8),DSTZ(616),DSTR(616),DSTT(616)
     6,DSTRZ(616),DEP(616),TEP(616),R1(380),DTST(616),SHAP(4)
     6,DFORCE(380),TSK(154,8,8),DSK(8,8),TDIS(380),ELDIS(8),ELCOD(2,4),
     6RGAUS(4),DB(4,8),B(4,8),GPCOD(2,4),CARTD(2,4),DERIV(2,4),G,NU,E1
     6,NELE,NEQ,NBAND,SK(380,44),DIS(380),POINTR(380),PL(616),NOP(154,4)
     6,ZETA(4),ETAA(4),STZ(616),STR(616),STT(616),STRZ(616),TST(616),
     6VSK(380,44),XJACM(2,2),XJACI(2,2),S,T,DJACB
      INTEGER P,Q,0,POINTR,PL,PUNCH1
      REAL NU
      SHAP(1)=(1.-T-S+S*T)/4.
      SHAP(2)=(1.-T+S-S*T)/4.
      SHAP(3)=(1.+T+S+S*T)/4.
      SHAP(4)=(1.+T-S-S*T)/4.
      DERIV(1,1)=(T-1.)/4.
      DERIV(1,2)=-(T-1.)/4.
      DERIV(1,3)=(T+1.)/4.
      DERIV(1,4)=-(T+1.)/4.
      DERIV(2,1)=(S-1.)/4.
      DERIV(2,2)=-(S+1.)/4.
      DERIV(2,3)=(S+1.)/4.
      DERIV(2,4)=-(S-1.)/4.
      RETURN
      END


      SUBROUTINE DMATX(I)
      COMMON/B1/Y(616),NBC(62),Z(190),R(190)
      COMMON/ /FORCE(380),D(4,4),ESK(8,8),DSTZ(616),DSTR(616),DSTT(616)
     6,DSTRZ(616),DEP(616),TEP(616),R1(380),DTST(616),SHAP(4)
```

```
     6,DFORCE(380),TSK(154,8,8),DSK(8,8),TDIS(380),ELDIS(8),ELCOD(2,4),
     6RGAUS(4),DB(4,8),B(4,8),GPCOD(2,4),CARTD(2,4),DERIV(2,4),G,NU,E1
     6,NELE,NEQ,NBAND,SK(380,44),DIS(380),POINTR(380),PL(616),NOP(154,4)
     6,ZETA(4),ETAA(4),STZ(616),STR(616),STT(616),STRZ(616),TST(616),
     6VSK(380,44),XJACM(2,2),XJACI(2,2),S,T,DJACB
      INTEGER P,Q,O,POINTR,PL,PUNCH1
      REAL NU
      IF(PL(I).EQ.1) GO TO 5
      C1=E1*(1.-NU)/((1.+NU)*(1.-2.*NU))$C2=NU/(1.-NU)
      D(1,1)=C1$D(1,2)=C1*C2$D(1,3)=C1*C2$D(1,4)=0.
      D(2,1)=D(1,2)$D(2,2)=C1$D(2,3)=C1*C2$D(2,4)=0.
      D(3,1)=D(1,3)$D(3,2)=D(2,3)$D(3,3)=C1$D(3,4)=0.
      D(4,1)=D(1,4)$D(4,2)=D(2,4)$D(4,3)=D(3,4)
      D(4,4)=C1*(1.-2.*NU)/(2.*(1.-NU))
      GO TO 10
5     T=(STR(I)+STZ(I)+STT(I))/3.
      STPR=STR(I)-T$STPZ=STZ(I)-T$STPT=STT(I)-T
      HP=30000.
      IF(TST(I).GE.3490.)HP=3000.
      S=2./3.*TST(I)**2*(1.+HP/(3.*G))
      W1=1.-NU$W2=1.-2.*NU$W5=E1/(1.+NU)
      D(1,1)=W5*(W1/W2-STPZ**2/S)
      D(1,2)=W5*(NU/W2-STPZ*STPR/S)
      D(1,3)=W5*(NU/W2-STPZ*STPT/S)
      D(1,4)=W5*(-STPZ*STRZ(I)/S)
      D(2,1)=D(1,2)
      D(2,2)=W5*(W1/W2-STPR**2/S)
      D(2,3)=W5*(NU/W2-STPR*STPT/S)
      D(2,4)=W5*(-STPR*STRZ(I)/S)
      D(3,1)=D(1,3)
      D(3,2)=D(2,3)
      D(3,3)=W5*(W1/W2-STPT**2/S)
      D(3,4)=W5*(-STPT*STRZ(I)/S)
      D(4,1)=D(1,4)$D(4,2)=D(2,4)$D(4,3)=D(3,4)
      D(4,4)=W5*(1./2.-STRZ(I)**2/S)
10    RETURN
      END


      SUBROUTINE SOLVE
      COMMON/B1/Y(616),NBC(62),Z(190),R(190)
      COMMON/ /FORCE(380),D(4,4),ESK(8,8),DSTZ(616),DSTR(616),DSTT(616)
     6,DSTRZ(616),DEP(616),TEP(616),R1(380),DTST(616),SHAP(4)
     6,DFORCE(380),TSK(154,8,8),DSK(8,8),TDIS(380),ELDIS(8),ELCOD(2,4),
     6RGAUS(4),DB(4,8),B(4,8),GPCOD(2,4),CARTD(2,4),DERIV(2,4),G,NU,E1
     6,NELE,NEQ,NBAND,SK(380,44),DIS(380),POINTR(380),PL(616),NOP(154,4)
     6,ZETA(4),ETAA(4),STZ(616),STR(616),STT(616),STRZ(616),TST(616),
     6VSK(380,44),XJACM(2,2),XJACI(2,2),S,T,DJACB
      INTEGER P,Q,O,POINTR,PL,PUNCH1
      REAL NU
      DO 490 I=1,NEQ
      DO 490 J=1,NBAND
      VSK(I,J)=SK(I,J)
490   CONTINUE
      NODE=190
```

```
      DO 50 I=1,NODE
      NROWB=(I-1)*2
      DO 49 M=1,2
      NROWB=NROWB+1
      IF(POINTR(NROWB).EQ.1) GO TO 49
      R1(NROWB)=(10.E08)*VSK(NROWB,1)*DIS(NROWB)
      VSK(NROWB,1)=(10.E08)*VSK(NROWB,1)
49    CONTINUE
50    CONTINUE
      DO 300 N=1,NEQ
      I=N
      DO 290 L=2,NBAND
      I=I+1
      IF(VSK(N,L)) 240,290,240
240   C=VSK(N,L)/VSK(N,1)
      J=0
      DO 270 K=L,NBAND
      J=J+1
      IF(VSK(N,K)) 260,270,260
260   VSK(I,J)=VSK(I,J)-C*VSK(N,K)
270   CONTINUE
280   VSK(N,L)=C
      R1(I)=R1(I)-C*R1(N)
290   CONTINUE
300   R1(N)=R1(N)/VSK(N,1)
      N=NEQ
350   N=N-1
      IF(N)500,500,360
360   L=N
365   DO 400 K=2,NBAND
      L=L+1
      IF(VSK(N,K))370,400,370
370   R1(N)=R1(N)-VSK(N,K)*R1(L)
400   CONTINUE
      GO TO 350
500   DO 20 I=1,NEQ
      IF(POINTR(I).EQ.1) GO TO 30
      R1(I)=DIS(I)
      A1=0.
      DO 5 J=1,NBAND
      IF( SK(I,J).EQ.0.) GO TO 5
      A1=A1+ SK(I,J)*R1(I+J-1)
5     CONTINUE
      A2=0.
      K=I
      DO 10 II=2,NBAND
      K=K-1
      IF(K.EQ.0) GO TO 15
      A2=A2+ SK(K,II)*R1(K)
10    CONTINUE
15    DFORCE(I)=A1+A2
      GO TO 20
30    DFORCE(I)=0.
20    CONTINUE
      RETURN
```

```
      END
      SUBROUTINE DBE
      COMMON/B1/Y(616),NBC(62),Z(190),R(190)
      COMMON/ /FORCE(380),D(4,4),ESK(8,8),DSTZ(616),DSTR(616),DSTT(616)
     6,DSTRZ(616),DEP(616),TEP(616),R1(380),DTST(616),SHAP(4)
     6,DFORCE(380),TSK(154,8,8),DSK(8,8),TDIS(380),ELDIS(8),ELCOD(2,4),
     6RGAUS(4),DB(4,8),B(4,8),GPCOD(2,4),CARTD(2,4),DERIV(2,4),G,NU,E1
     6,NELE,NEQ,NBAND,SK(380,44),DIS(380),POINTR(380),PL(616),NOP(154,4)
     6,ZETA(4),ETAA(4),STZ(616),STR(616),STT(616),STRZ(616),TST(616),
     6VSK(380,44),XJACM(2,2),XJACI(2,2),S,T,DJACB
      INTEGER P,Q,O,POINTR,PL,PUNCH1
      REAL NU
      DO 10 I=1,4
      DO 10 J=1,8
      DB(I,J)=0.
      DO 10 JJ=1,4
      DB(I,J)=DB(I,J)+D(I,JJ)*B(JJ,J)
10    CONTINUE
      RETURN
      END
```

REFERENCES

1. Finish blanking of aluminium and copper, P.E.R.A. report No.27, April 1956.
2. Finish blanking of steel, P.E.R.A. report No. 57, April 1958.
3. Application of finish blanking, P.E.R.A. report No. 64, April 1959.
4. Anthony, G.C. Pressure recording indicator for punching machinery, Trans. A.S.M.E. 33, 369 (1911).
5. Blanking and piercing - Preliminary investigation into punch speed and punch and die clearance. P.E.R.A. research report, 1951.
6. Blanking and piercing - Part II. P.E.R.A. report No. 22, November 1955.
7. Crasemann, H.J., Der Offene Scnitt Von Grob-blechen, Mitt. Forsch - Ges. Blechverarb. Nr. 14/15, 5, 193-211 (1962) (in German).
8. Timmerbeil, F.W., Untersuchung des Schneid - Vorganges bei Blech, insbesondere beim geschlossenen Schnitt, Werkstattstechn. U. Masch - Bau. Nr. 5, S 231/239 (1957) (in German).
9. Noble, C.F. and Oxley, P.L.B., Crack formation in blanking and piercing. Intern. J. Prod. Res., 265, Dec. 1963, Vol. 2 No.4.
10. Chang, T.M., Shearing of metal blanks., J. Inst. Metals., 78, 393, (1950-51).
11. Maeda, T. and Tamura, K. Influence of size of blanking diameter in shearing operation of sheet metals. Bull. Jap. S. M. E., 3, No.11, 312, (1960).
12. Johnson, W. and Slater, R.A.C. A comparison of the energy required for slow speed and dynamic blanking using an improved linear motor. Proc. Inst. Mech. Engs., 179, (Pt. 1), 257, (1964-65).

13. Cockcroft, M.G. The metal forming symposium in Czechoslovakia, September 1960, N.E.L. report No.6 (1961).

14. Zener, C. and Holloman, C. Effect of strain-rate upon plastic flow of steel. J. Appl. Phys., 15, 22 (1944).

15. Zener, C. Fracturing of metals, 1948, 3. Amer. Soc. Metals., (New York).

16. Davies, R. and Dhawan, S.M. A preliminary investigation of high-speed blanking and piercing of metals. Paper 20, Applied Mechanics Convention (Cambridge) 1966, (Inst. Mech. Engs., London).

17. Johnson, W. and Slater, R.A.C. Further experiments in quasi-static and dynamic blanking of circular discs from various materials. Proc. Inst. Mech. Engs., 180 (Pt.31), (1965-66).

18. Johnson, W. and Travis, F.W. High speed blanking of copper. Paper 16, Applied Mechanics Convention (Cambridge) 1966, (Inst. Mech, Engs., London).

19. Goldsmith, W. Impact, 1962 (Edward Arnold, London).

20. Davies, R. and Dhawan, S.M. Further developments in high-speed blanking of metals. Advances in machine tool design and research. Proc. 7th International M.T.D.R. Conf. University of Birmingham, Sept. 1966.

21. Slater, R.A.C. and Johnson, W. The effect of temperature, speed and strain-rate on the force and energy required in blanking. J. Inst. Mech. Sci. 1967, Vol.9, pp 271-305.

22. Davies, R. and Dhawan, S.M. Comparison of some strain-rate effects in slow and high-speed blanking. Advances in Machine Tool Design and Research. Proc. 9th International M.T.D.R. Conference., Sept. 1968, pp 135-148.

23. Tilsley, R. and Howard, F. Recent investigations into the blanking and piercing of sheet materials. Paper 16, Conf. on Techniques of Engineering Manufacture, Inst. Mech. Engs. London, (1958).

24. Finish blanking of medium and high carbon steels. P.E.R.A. report No. 120 (November, 1963).

25. Blanking and piercing - A metallographic study of the mechanism of constrained shear. P.E.R.A. report No.93, Dec. 1961.

26. Shinji Fukui, Kazuyoshi Kondo, Katsutoshi Maeda. Smooth shearing by stepped profile tool. Annals of the C.I.R.P., Vol.20/1 1971, pp 57-58.

27. Kondo, K. and Maeda, K. Development of a new precision shearing process. Proc. 12th International Machine Tool Design and Research Conference, 15-17 Sept. 1971, pp 61-67.

28. Maeda, T. Reciprocating blanking method. Science of Machine, Vol. 10, No. 1 (1958), p. 140.

29. Jimma, T. Theoretical research on the blanking of sheet material. Bull. J.S.M.E., 568, (1962).

30. Haag, R. Sheet Metal Ind., 37, 352 (1960).

31. Guidi, A. Fine blanking saves finishing costs. Metalworking Production. October 3rd, 1962, pp 75-82.

32. Bösch, F. and Stäger, A. Werkstatt Betrieb, 96, 607, 843 (1963).

33. Hedges, J.F. Metalworking Production. 107, No. 50, P. 45 (1963).

34. Freeman, J.S. Sheet Metal Ind. 41, 19 (1964).

35. Meyer, M. and Kienzle, E.H.O. C.I.R.P. Annalen, 11, 111 (1962-3).

36. Johnston, R., Fogg, B. and Chisholm, A.W.J. An investigation into the fine blanking process. (1968) Proc. 9th International Machine Tool Design Research Conference. Pergamon.

37. Maeda, T. and Nakagawa, T. Experimental investigation of fine blanking. Scientific Papers of the Inst. Physical and Chemical Research. Vol. 62, No.2, 65-80, June 1968, Tokyo, Japan.

38. Lubrication eases the pressures of fine blanking. Metalworking Production, May 1979, p. 178.

39. Turner, J.L., Clough, R.W., Martin, H.C. and Topp, L.J. Stiffness and deflection analysis of complex structures. J. Aero. Sci., Vol. 23, No.9., Sept. 1956, pp 805-825.

40. Mendelson, A. and Manson, S.S. Practical solution of plastic deformation problems in the elastic-plastic range. N.A.S.A. TR R28, 1959.

41. Gallagher, R.H., Padlog, J. and Bijlaard, P.P. Stress analysis of heated complex shapes. A.R.S. Journal, May 1962, pp 700-707.

42. Argyris, J.H. Elasto-plastic matrix displacement analysis of three dimensional continua. J. Royal Aero. Soc. 69, pp 633-635, 1965.

43. Zienkiewicz, O.C., Valliappan, S. and King, I.P. Elasto-plastic solutions of engineering problems. Initial stress, finite element approach. J. Inst. Num. Meth. in Eng., 1, 75-100, 1969.

44. Pope, G. A discrete element method for anlaysis of plane elastic plastic stress problems. Royal Aeronautical Establishment, TR 65028, 1965.

45. Swedlow, J.L. and Yang, W.H. Stiffness analysis of elastic-plastic plates. Graduate Aeronautical Laboratory, California Institute of Technology, SM 65-10, 1965.

46. Marcal, P.V. and King, I.P. Elastic-plastic analysis of two dimensional stress systems by the finite element method. International Journal of Mech. Sci., Vol. 9, No.3, 1967, pp 143-155.

47. Yamada, Y., Yoshimura, N. and Sakurai, T. International Journal of Mech. Sci., Vol. 10, 1968, pp 343-354.

48. Marcal, P.V. Elastic-plastic analysis of pressure vessel components. Proc. 1st. Pressure Vessel and Piping Conference, A.S.M.E., Sept. 1968.

49. Akyuz, F.A. and Merwin, J.E. A.I.A.A. Journal 6, 1825 (1968).

50. Nagamatsu, A., Murota, T. and Jimma, T. On the non-uniform deformation of material in axially symmetric compression caused by friction. Bull. of the J.S.M.E., pp. 339-347, Vol.14 1971.

51. Nagamatsu, A. Murota, T. and Jimma, T. On the non-uniform deformation of material in axially symmetric compression caused by friction. Bull. of the J.S.M.E., No.89, 1972.

52. Nagamatsu, A., Murota, T. and Jimma, T. On the non- uniform deformation of a block in plane-strain compression caused by friction. Vol. 14, No.70, 1971 Bull. of the J.S.M.E.

53. Gordon, J.L. and Weinstein, A.S. A finite element analysis of the plane-strain drawing problem. Proceedings 2nd North American Metalworking Research Conf., 194-208, University of Wisconsin, Madison 1974.

54. Wata, I, Osakada, K. and Fujino, S. Analysis of hydrostatic extrusion by the finite element method. J. Eng. Ind. (trans. A.S.M.E.) Vol. 94, pp 697-703, May 1972.

55. Odell, E.I. A study of wall ironing by the finite element technique. J. Eng. Ind. Vol. 100, pp 31-36, Feb.(1978).

56. Shah, S.N. and Kobayashi, S. Rigid plastic analysis of cold heading by the matrix method. Proc. 15th Int. M.T.D.R. Conf. Birmingham 1974, pp 603-610.

57. Price, J.W.H. A study of dieless drawing and isothermal forming. PhD Thesis, London University (1977).

58. Matsumoto, H., Oh, S.I. and Kobayashi, S. Proc. 18th Int. M.T.D.R. Conf. Imperial College, London (1977).

59. Hartley, P. PhD Thesis, Birmingham University (1979).

60. Hartley, P., Sturgess, C.E.N. and Rowe, G.W. Friction in finite element analysis of metal forming process. J. Inst. Mech. Sci., Vol. 21, pp. 301-311, 1979.

61. Turner, M.J., Dill, E.H., Martin, H.C. and Melosh, R.J. Large deflections of complex structures subjected to heating and external loads. J. Aerospace Sciences, Vol.27, 1960, pp 97-106.

62. Argyris, J.H., Kelsey, S.K. and Kamel, H. Matrix methods of structural analysis. pp 105-120, Pergamon Press (1964).

63. Gallagher, R.H., Gellatly, R.A., Padlog, J. and Mallett, R.H. Discrete element procedure for thin shell instability analysis. A.I.A.A. Journal, 5, pp 138-144 (1967).

64. Kapur, K.K. and Hartz, B.J. Stability of plates using the finite element method. J. Eng. Mech. Div. Am. Soc. Civ. Engs. 92, 177-195 (1966).

65. Martin, H.C. Derivation of stiffness matrices for the analysis of large deflection and stability problems. Proc. 1st Conf. on matrix methods in struct. Mech. pp 607-75 (1966).

66. Marcal, P.V. The effect of initial displacement on problems of large deflection and stability. Division of Engineering, Brown University. A.R.P.A. E54 (1967).

67. Purdy, D.M. and Przemieniecki, I.S. Influence of higher order terms in the large deflection analysis of frameworks. Proc. A.S.C.E. Joint Spec. Conf. Optimization and non-linear problems. pp 142-152 (1968).

68. Mallett, R.H. and Marcal, P.V. Finite element analysis of non-linear structures. J. Stuct. Div. Am. Soc. Civ. Engs. 94. 2081-2105 (1968).

69. Murray, D.W. and WIlson, E.L. Finite element post buckling analysis of thin elastic plates. Proc. 2nd Conf. Matrix Methods in Struct. Mechs. (1968).

70. Felippa, C.A. Refined finite element analysis of linear and non-linear two dimensional structures. PhD Thesis, University of California (1966).

71. Oden, J.T. and Kubitza, W.K. Numerical analysis of non-linear pneumatic structures. Proc. 1st. Int. Colloq. Pneumatic structures, Stuttgart (1967).

72. Kawai, T. Finite element analysis of the geometrically non-linear problems of elastic plates. United States -Japan Seminar on Matrix Methods of Structural Analysis and Design. Tokyo, 1969, pp 383-414.

73. Marcal, P.V. Finite element analysis of combined problems of non-linear material and geometric behaviour. Proc. A.S.M.E. Joint Computer Conf. on Computational approach to applied mechanics. pp 133-149, Chicago (1969)

74. Hofmeister, L.D., Greenbaum, G.A. and Evensen, D.A. Large strain elasto-plastic finite element analysis. J. A.I.A.A. Vol.9, No.7, pp 1248-1254, July 1971.

75. Hibitt, H.D., Marcal, P.V. and Rice, J.R. A finite element formulation for problems of large strain and large displacement. Int. J. Solids. Structures., 1970, Vol.6, pp 1068-1086.

76. McMeeking, R.M. and Rice, J.R. Finite element formulation for problems of large elastic-plastic deformation. Int. J. Solids. Structures., 1975, Vol.11, pp 601-616.

77. Needleman, A. A numerical study of necking in circular cylindrical bars. J. Mech. Phys. Solids. 20, pp 111-127 (1972).

78. Hill, R. Some basic principles in the mechanics of solids without a natural time. J. Mech. Phys. Solids. 7, pp 209 (1959).

79. Felippa, C.A. and Sharifi, P. Computer implementation of non-linear finite element analysis in numerical solution of non-linear structural problems. (Edited by R.F. Hartung), A.S.M.E., p 31, New York (1973).

80. Gunasekara, J.S. Matrix analysis of large deformation elastic-plastic problems. PhD Thesis, University of London (1972).

81. Lee, C.H. and Kobayashi, S. Elasto-plastic analysis of plane strain and axisymmetric flat punch indentation by the finite element method. Int. J. Mech. Sci. 1970, Vol.12, pp 349-370.

82. Lee, C.H. and Kobayashi, S. Analysis of axi-symmetric upsetting and plane strain side-pressing of solid cylinders by the finite element method. J. Eng. for Ind., May 1971, pp 445-454.

83. Blass. A. A finite element approach in metalworking and its application to the radial upsetting process. PhD Thesis, University of London (Feb. 1976).

84. Johnson, W. and Mellor, P.B. Engineering plasticity. Van Nostrand Reinhold Co., London. pp 316-320.

85. Bridgman, P.W. Studies in large plastic flow and fracture. McGraw-Hill, London and New York, 1952.

86. Bridgman, P.W. J. Appl. Phys. 1953, 24(5), 560.

87. Pugh, H.L.I.D. and Gunn, D.A. Physics and Chemistry of high pressure. Soc. Chem. Ind. 1962.

88. Karman, Von Th. Zeitschrift v.d.i. 55 , No.42, pp 1749-1757, 1911.

89. Crossland, B. and Dearden, W.H. Proc. Inst. Mech. Engs., 172, No.26, 1958.

90. Bridgman, P.W. Reviews of modern physics. 17, 3, 1945.

91. Crossland, B. Proc. Inst. Mech. Engs., 168 (40), 1954.

92. Pugh, L.L.I.D. and Green, D. Progress report on the behaviour of materials under hydrostatic pressure. M.E.R.L. Plasticity Report No.147, 1958. National Engineering Laboratory, East Kilbride, Glasgow.

93. Hayes, A.E. and Yoblin, J.A. New concepts for fabricating Beryllium through advanced forging and powder-metallurgy techniques. Inst. Metals Conference on Metallurgy of Beryllium, London, 1961.

94. Cogan, R.M. Forging against back pressure. American Machinist, 107 (21), 105, Oct. 1963.

95. Cogan, R.M. Hydrodynamic forming. J. Eng. for Indust. p 105, May 1965.

96. Alexander, J.M. and Lengyel, B. J. Inst. Metals, 93(5), p 137-144, 1965.

97. Fuchs, Jr., F.J. Production metal forming with hydrostatic pressure. Paper 65-prod-17 presented at Metals Engineering and Production Engineering Conference, Berkeley, California, 1965.

98. Fuchs, Jr., F.J. Hydrostatic pressure - its role in metal forming. Mech. Engng., April 1966, p.34.

99. Bobrowsky, A., Stack, E.A., and Austen, A. Extrusion and drawing using high pressure hydraulics. Paper No. SP65-33, A.S.T.M.E. Conference, 1964.

100. Komoly, T.J. Contribution to discussion of the effect of hydrostatic pressure on the plastic flow and fracture of matals by Pugh, H.L.I.D., and Green, D. Proc. Inst. Mech Engs, 179(1), 1964-65.

101. British Patent 1040804 : September 1966.

102. Mott, N.F. Proc. Roy. Soc. (A) 223, 1953, 1.

103. Stroh, A.N. Proc. Roy. Soc. (A) 223, 1954, 404.